TECTONIC MORPHOLOGY OF NEOGENE–QUATERNARY STRUCTURES IN THE EASTERN BETICS

MORFOLOGÍA TECTÓNICA DE ESTRUCTURAS NEÓGENO–CUATERNARIAS EN LAS BÉTICAS ORIENTALES

FLAVIO GIACONIA

PhD Thesis – Thesis Doctoral 2013

ugr Universidad de Granada
CSIC Consejo Superior de Investigaciones Científicas
IACT
Barcelona CSI Center for Subsurface Imaging

Instituto Andaluz de Ciencias de la Tierra
Universidad de Granada
&
Consejo Superior de Investigaciones Científicas

TECTONIC MORPHOLOGY OF NEOGENE–QUATERNARY STRUCTURES IN THE EASTERN BETICS

MORFOLOGÍA TECTÓNICA DE ESTRUCTURAS NEÓGENO–CUATERNARIAS EN LAS BÉTICAS ORIENTALES

FLAVIO GIACONIA

PhD Thesis – Thesis Doctoral

Memoria de Tesis Doctoral presentada por el Licenciado en Geologia D. Flavio Giaconia para aportar al Grado de Doctor por la Universidad de Granada

Esta Tesis Doctoral ha sido dirigida por el Dr. Guillermo Booth Rea, Profesor Titular de la Universidad de Granada, el Dr. José Miguel Azañón Hernández, Catedrático de la Universidad d Granada, y el Dr. José Miguel Martínez Martínez, Catedrático de la Universidad de Granada.

5 de julio de 2013

Granada, Spain

Editor: Editorial de la Universidad de Granada
Autor: Flavio Giaconia
D.L.: GR 224-2014
ISBN: 978-84-9028-743-9

El doctorando Flavio Giaconia y los directores de la tesis Guillermo Booth Rea, José Miguel Azañón Hernández y José Miguel Martínez Martínez garantizamos, al firmar esta tesis doctoral, que el trabajo ha sido realizado por el doctorando bajo la dirección de los directores de la tesis y hasta donde nuestro conocimiento alcanza, en la realización del trabajo, se han respetado los derechos de otros autores a ser citados, cuando se han utilizado sus resultados o publicaciones.

Granada, 5 de julio 2013

Directores de la Tesis

Doctorando

Fdo. Guillermo Booth Rea

Fdo. Flavio Giaconia

Fdo. José Miguel Azañón Hernández

Fdo. José Miguel Martínez Martínez

Abstract

This thesis provides a detailed onshore-offshore structural analysis of Neogene–Quaternary tectonic structures in the southeastern Betics and their control on bathymetry, landscape and drainage evolution. The extensional processes that led to the development of the southeastern Betic basins (Sorbas–Tabernas, Vera and Níjar basins) in the core of the Gibraltar subduction-collisonal system produced important Tortonian marine depocenters coeval to arc and backarc magmatic accretion offshore along the Palomares margin. Unconformities related to this extension occur up to the latemost Tortonian (~8 Ma) affecting the Azagador member temperate limestones. This extension was strongly heterogeneous and partitioned by large transfer faults like the Carboneras sinistral and North Cabrera dextral faults.

The contractive inversion of the basins initiated during the latemost Tortonian with the development of the E–W Sierra Alhamilla–Polopos and NE–SW Cabrera anticlinoria and associated reverse faults, together with the E–W to ESE–WNW Polopos dextral and NNE-SSW Palomares sinistral conjugate transcurrent faults. This thesis provides a new morpho-structural map (fault segmentation, fluvial terraces and alluvial fans) defining the ~30 km length Polopos fault zone and highlighting its Quaternary to recent activity. This fault zone is formed by the North Alhamilla reverse fault and the North and South Gafarillos dextral-reverse faults, all segments active from the latemost Tortonian (≈ 7 Ma) up to the late Pleistocene (≥ 70 ky) except the North Gafarillos one that is sealed by the Messinian Cantera member reef carbonates. The helicoidal geometry of the fault zone permits to shift SE-directed displacement along the South Cabrera reverse fault to NW-directed shortening along the North Alhamilla reverse fault via vertical Gafarillos fault segments, in between.

Structural field-based and morphometric GIS-based studies show that dextral transpressive and reverse displacement along the Polopos fault zone conditioned the relief in the Sierra Alhamilla northern slope producing a set of fault-related geomorphic features congruent with the tectonic uplift of its hanging-wall (e.g. rectilinear mountain fronts, deeply dissected basins and valleys, immature drainage basins, and stream "rejuvenation" process in the proximity of faults). The morphometric GIS-based and tectonic data set in the Sierra Cabrera anticlinorium highlights the occurrence of an active pop-up formed between the North and the South Cabrera reverse faults. The pop-up developed in a constrictional domain of the large-scale Polopos and Palomares conjugate strike-slip faults. Meanwhile, extension in the Níjar basin perpendicular to the present maximum shortening axis occurs in the extensional domain of the large-scale conjugate strike-slip fault system. The high-angle normal fault system occurring in the Níjar basin conditioned the relief in the Sierra Alhamilla southern slope producing a set of fault-related geomorphic evidence congruent with the tectonic uplift of their footwall (e.g. rectilinear mountain fronts, deeply dissected basins and valleys, immature drainage basins, fault-related knickpoints).

Once the North Gafarillos fault segment was sealed by Messinian limestones, a new dextral-reverse fault segment developed to the south of Sierra de Polopos (South Gafarillos fault) that shifted the main mountain front from the north to the south of the mountain range. This process together with the uplift and westward propagation of the North Alhamilla reverse fault favored the incision of the Alias river and its affluent the Rambla de Lucainena that captured the Sorbas basin centripetal drainage during the middle Pleistocene. Continued tectonic uplift of the Sierra Alhamilla–Polopos and Cabrera anticlinoria and local subsidence associated to the Palomares fault zone in the Vera basin promoted the headward erosion of the Aguas river drainage and the late Pleistocene capture of the Sorbas basin.

Offshore deep reflection seismic lines, parametric profiles, and bathymetry at the Palomares margin, together with GPS geodetic data available and focal mechanisms indicate that the inversion of the Palomares margin resulted in NE–SW reverse faults and folds and NNE–SSW sinistral strike-slip faults. These structures are comparable to the ones observed onshore and consistent with the NW–SE present stress field and presently active as inferred by seafloor features (e.g. submarine canyon deflections and submarine fault escarpments) and focal mechanisms in the area. The set of Palomares margin structures, both onshore and offshore, fit in an oblique convergence model where NW–SE shortening is partitioned between en-echelon reverse faults and associated folds, and strike-slip faults along a NNE–SSW margin. Inversion of the Palomares margin occurred during the latemost Tortonian–Messinian up to the present day and is coeval to the inversion of the Algerian margin. The late Miocene to present compressional inversion of the western Mediterranean is developing a new transpressive plate boundary at the southern margins of the Algero–Balearic and Alborán basins. This plate boundary has propagated westwards from the Algerian margin approximately 7 Ma ago to the Alborán Ridge about 5 Ma ago, ending along the southern margin of the Western Alborán basin.

Keywords:Tectonic inversion, active tectonics, morpho-tectonics, geomorphic indices; fault segmentation, multichannel seismic, western Mediterranean, eastern Betics, Palomares margin, Sierra Alhamilla, Sierra Cabrera, Gafarillos fault, Palomares fault zone, Polopos fault zone, Abubacer anticline.

Resumen

Esta tesis proporciona un análisis detallado, en tierra y en mar, de las estructuras tectónicas Neógeno–Cuaternarias en las Béticas orientales y su influencia en la batimetría y en la evolución del paisaje y la red de drenaje. Los procesos extensionales que llevaron a la formación de las cuencas sedimentarias de las Béticas surorientales (cuencas de Sorbas–Tabernas, Vera y Níjar) en el interior del sistema orogénico del Arco de Gibraltar produjeron importantes depocentros marinos Tortonienses coetáneos con la acreción magmática de arco y de retro-arco a lo largo del margen de Palomares. Discordancias relacionadas con esta extensión, que afectan a las calizas templadas del miembro Azagador, ocurren hasta el Tortoniense terminal (~8 Ma). La extensión fue extremadamente heterogénea y segmentada por grandes fallas de transferencia como la falla sinistrorsa de Carboneras y la falla dextrorsa de Sierra Cabrera Norte.

En el Tortoniense terminal se inició la inversión contractiva de las cuencas con la formación de los anticlinorios E–O de Sierra Alhamilla–Polopos y NE–SO de Sierra Cabrera y fallas inversas asociadas. Otras estructuras resultado de la inversión son la fallas dextrorsa de Polopos, de dirección E–O/ESE–ONO, y su conjugadas, la falla sinistrorsa de Palomares, de dirección NNE–SSO.

En esta tesis se realizó un nuevo mapa morfo-estructural de la zona de falla de Polopos que tiene aproximadamente 30 km de longitud con énfasis en su actividad Cuaternario hasta el presente. Esta zona de falla está formada por la falla inversa de Sierra Alhamilla Norte y las fallas transpresivas dextrorsas Gafarillos Norte y Gafarillos Sur, todas activas desde el Trotoniense terminal (≈ 7 Ma) hasta el Pleistoceno superior (≥ 70 ky) excepto la falla Gafarillos Norte, que está sellada por las calizas arrecifales del miembro Cantera. La geometría helicoidal de la zona de falla permite la transferencia desde un desplazamiento hacia el SE a lo largo de la falla inversa de Sierra Cabrera Sur hasta un desplazamiento hacia el NO asociado a la falla inversa de Sierra Alhamilla Norte por medio de segmentos de falla verticales dextrorsos de Gafarillos.

Los estudios estructurales de campo y morfométricos (basados en SIG) indican que el desplazamiento transpresivo dextrorso a lo largo de la zona de falla de Polopos condicionó el relieve de la ladera norte de Sierra Alhamilla produciendo un conjunto de rasgos geomorfológicos relacionados con fallas, congruentes con el levantamiento tectónico de sus bloques de techo (ej. frentes montañosos rectilíneos, cuencas y valles profundamente erosionados, cuencas de drenaje inmaduras, y procesos de rejuvenecimiento de los cauces en la inmediación de las fallas). El conjunto de datos tectónicos y morfométricos en el anticlinorio de Sierra Cabrera pone en manifiesto una estructura de *"pop-up"* activa formada por las fallas inversas de Sierra Cabrera Norte y Sierra Cabrera Sur. El *"pop-up"* se formó en dominio constrictivo entre las fallas conjugadas de salto en dirección de Polopos y Palomares. Mientras tanto, en la cuenca de Níjar tuvo lugar extensión perpendicular a la dirección del esfuerzo máximo

compresivo horizontal actual en el dominio extensional de las fallas conjugadas de salto en dirección. Las fallas normales de alto ángulo de la cuenca de Níjar condicionaron el relieve en la ladera sur de la Sierra Alhamilla produciendo un conjunto de rasgos geomorfológicos relacionados con fallas, congruentes con el levantamiento tectónico de sus bloques de muro (ej. frentes montañosos rectilíneos, cuencas y valles profundamente erosionados, cuencas de drenaje inmaduras, y "knickpoints" relacionados con fallas).

Una vez que el segmento Norte de la falla de Gafarillos fue sellado por calizas Messinienses, un nuevo segmento de falla transpresiva dextrorsa se desarrolló al sur de la Sierra de Polopos (la falla de Gafarillos Sur) que desplazó el principal frente montañoso del norte al sur de la sierra. Este proceso junto con el levantamiento y la propagación hacia el oeste de la falla inversa de Sierra Alhamilla Norte favoreció la incisión del río Alias y de su afluente la rambla de Lucainena que capturó la red de drenaje centrípeta de la cuenca de Sorbas en el Pleistocene medio. El continuo levantamiento de los anticlinorios de Sierra Alhamilla–Polopos y Sierra Cabrera y la subsidencia local asociada con la zona de falla de Palomares en la cuenca de Vera promovió la erosión en la cabecera del río Aguas y la captura de la cuenca de Sorbas en el Pleistoceno superior.

Líneas sísmicas de reflexión profunda, perfiles paramétricos, y mapas batimetrícos a lo largo del margen de Palomares, en mar, junto con los datos geodésicos de GPS y mecanismos focales disponibles en el área indican que la inversión del margen de Palomares produjo fallas inversas y pliegues de dirección NE–SO y fallas sinistrorsas de dirección NNE–SSO. Estas estructuras son comparables con las que se observan en tierra y consistentes con la dirección actual, NE–SO, del esfuerzo horizontal máximo y son activas hoy en día como indican los rasgos del fondo marino (ej. deflexiones de cañones submarinos y escarpes de fallas submarinas) y los mecanismos focales en el área. El conjunto de estructuras del margen de Palomares, tanto en tierra como en mar, es congruente con un modelo de convergencia oblicua donde el acortamiento NO–SE se reparte entre fallas inversas *"en-echelon"* y pliegues asociados, y fallas de salto en dirección a lo largo de un margen orientado NNE–SSO. La inversión del margen de Palomares ocurrió desde el Tortoniense terminal–Messiniense hasta el presente y es coetánea con la inversión del margen de Argelia. La inversión compresiva del Mediterráneo occidental desde el Mioceno superior hasta el presente, está produciendo un nuevo límite de placas transpresivo a lo largo del margen sur de las cuencas Argelino-Balear y de Alborán. Este límite de placas se ha propagado hacia el oeste desde el margen de Argelia aprox. hace 7 Ma hasta la Cresta del Alborán aprox. 5 Ma, terminando a lo largo del margen sur de la cuenca del Alborán Occidental.

Palabras claves: Inversión tectónica, tectónica activa, morfo-tectónica, índices geomorfológicos, segmentación de fallas, sísmica multicanal, Mediterráneo occidental, Béticas orientales, margen de Palomares, Sierra Alhamilla, Sierra Cabrera, falla de

Gafarillos, zona de falla de Palomares, zona de falla de Polopos, anticlinal de Abubacer.

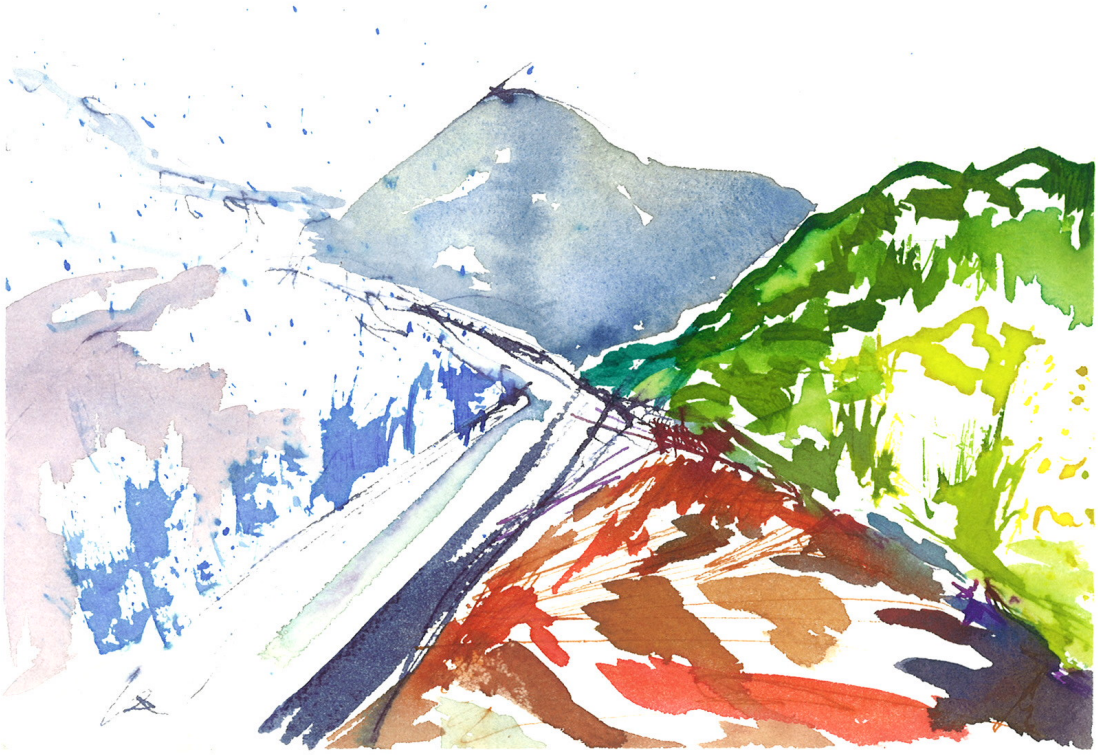

A mio Nonno per il suo inaspettato Grazie del 31 di Ottobre 2006,
e a mia Nonna per non smettere di credermi bambino.

Ringraziamenti - Agradecimientos - Acknowledgments

Mis profundos agradecimientos a todas aquellas personas que directamente o indirectamente han participado y me han suportado en la realización de esta tesis. Especialmente a mi director por la motivación y el apoyo recibido a lo largo de estos años, que me han presentado como Guillermo y he acabado conociendo como Bill.

Quiero agradecer el fundamental y fructífero aporte a esta tesis recibido por José Miguel Azañón, José Miguel Martínez Martínez, Vicente Pérez Peña, Cesar Ranero, Eulalia Gràcia, Fabrizio Storti y Andrea Artoni.

I thank in advance the evaluation commission for their constructive contribution to my thesis and my future research.

Además quiero dar las gracias a mis compañeros de Granada y de Barcelona sobre todos a las personas que han contribuido directamente con su ayuda humana y profesional a esta tesis, como Alejandra, Montse, Claudio, Manuel, Hector, Alcinoe, Sergio y Ben.

Un agradecimiento especial lo doy a Nuria por su duradera y fiel amistad y los fines de semanas gastronómicos en Bascanó.

Un infinito gracias a mis compañeros de bajadas de la muerte y de paisajes *"maravillosos"*, Juan y Erwin, aun que algunos de ellos se dopaba con constancia.

Agradezco de todo corazón a mi familia granadina por no permitirme de sentirme solo en Graná, Mara y Andrei (y su terraza también), Vanesa y Javi por su "alegría" y positividad, Conchi, Jugrena, Juan y Ulyses, y claro Stefania por sus panelle especialmente.

Ringrazio tutte le persone che per decadi mi hanno sostenuto, come Sergio e Nino, che malgrado gli *"aggaddi"* restano le persone che meglio mi conoscono al mondo, e Tancredi compagno di troppe cose per scriverle qui di seguito.

Un ringraziamento speciale a tutta la mia Famiglia, sopratutto mia Madre per insegnarmi l'arte della determinazione ed a mio Padre per insegnarmi a fare solo le cose che mi piacciono ed in cui credo.

Niente di tutto ció sarebbe stato possibile senza di te Alice per il tuo continuo sostegno, la tua infinita pazienza e per mantenermi in contatto con la vita che relamente ci importa, grazie!

TABLE OF CONTENTS

0.0 Resumen extendido

El principal objetivo de esta tesis es la caracterización de las estructuras tectónicas Neógeno–Cuaternarias en la Béticas orientales desde el punto de vista estructural, analizando su geometría y segmentación, y desde una perspectiva morfo-tectónica, analizando el control tectónico de estas estructuras sobre la evolución del relieve. Se ha prestado una especial atención a las estructuras formadas desde el Mioceno superior en el marco de la inversión tectónica de las cuencas de Alborán y Argelino–Balear y de sus márgenes en las Béticas y el Rif en relación con la convergencia entre África e Iberia. Se han analizado las estructuras responsables de los últimos eventos extensionales que dieron lugar a las cuencas sedimentarias de las Béticas surorientales y del margen de Palomares durante el Tortoniense superior y las estructuras formadas con posterioridad representadas por fallas de salto en dirección e inversas y pliegues asociados.

El análisis geomorfológico y morfo-tectónico ha tenido un enfoque cualitativo y cuantitativo basado en la cartografía de rasgos geomorfológicos como terrazas y abanicos fluviales y el cálculo de índices geomorfológicos, en áreas claves de las Béticas surorientales. El análisis estructural integra datos marinos y del margen emergido de Palomares, incluyendo: a) la cartografía de los sistemas de fallas y su caracterización estructural; b) cortes geológicos construidos con la ayuda de sondeos y tomografía eléctrica 2D; c) cortes balanceados; d) interpretación y procesado de datos geofísicos marinos (sísmica multicanal, perfiles paramétricos y batimetría). Finalmente, el conjunto del análisis ha sido integrado con una recopilación de datos publicados por otros autores, como desplazamientos geodésicos de GPS, mecanismos focales, campos de esfuerzos, y datos de cartografía estructural tanto en tierra como en mar. A continuación, se resumen los distintos capítulos correspondientes a publicaciones o manuscritos que han resultado de esta Tesis Doctoral.

0.1 Influencia de la tectónica extensional de las fallas transfer en las cuencas de las Béticas surorientales (Sorbas y Níjar)

Este apartado corresponde al capítulo 6 de la tesis y presenta el análisis estructural de dos depocentros controlados por fallas extensionales en la cuenca de Sorbas, situándolos en el contexto más amplio de la extensión que desde el Mioceno medio afectó a las Béticas orientales. La falla dextrorsa del Norte de la Sierra Cabrera, junto con otras fallas E–O/NE–SO de salto en dirección, es una falla de transferencia que acomoda la extensión SO-NE entre el Serravalliensey elTortoniense. Estas fallas “tranfer” y las fallas normales asociadas forman los principales bordes de dos depocentros sedimentarios activos desde el Mioceno medio hasta el Tortoniense. El depocentro más antiguo, situado al norte de Sierra Cabrera, fue activo entre el Serravalliensey elTortoniense inferior (aprox. de 13.8 a 10 Ma), mientras que el depocentro más joven (depocentro de Gacía) se formó por un nuevo pulso extensional en el Tortoniense, entre

9 y 7.5 Ma. El depocentro de Gacía se formó al oeste del depocentro del norte de Sierra Cabrera a favor de un sistema de fallas normales lístricas, con dirección de transporte hacia el SO, que se unen en un despegue de bajo ángulo. Un corte geológico balanceado a través del depocentro de Gacía indica que el despegue se enraíza dentro del complejo Nevado–Filábride aproximadamente a una profundidad de 0.8 km, basculando el despegue extensional previo entre los complejos Alpujárride y Nevado–Filábride. Esta extensión es coetánea y está cinemáticamente vinculada a la falla sinistrorsa de Carboneras, más al sur en la cuenca de Níjar. Esta extensión, con dirección de transporte hacia el oeste,tiene un carácter heterogéneo y produce"core-complexes" extensionales en los que se distinguen bloques basculados al norte de la falla de Carboneras. Este mismo proceso extensional es el causante de la acreción magmática sobre corteza continental adelgazada al sur de esta región. La extensión y el magmatismo representan la manifestación superficial de la rotura de la litosfera del Tetis y la delaminación, con una fuerte componente lateral, a lo largo de un límite de entidad litósférica debajo de la rama norte del orógeno Bético-Rifeño.

0.2 Evidencias geomorfológicas de actividad tectónica compresiva Cuaternaria asociada a la zona de falla de Polopos y su conjugada, la zona de falla de Palomares

En este apartado, que corresponde a los capítulos 7 y 8 de la tesis, se presentan las características estructurales de la zona de falla dextrorsa transpresiva ESE–ONO de Polopos y el condicionamiento que ésta ejerce sobre la evolución reciente del relieve. Este apartado se compone de dos partes, una primera centrada en la parte más occidental de la falla de Polopos y su relación con el anticlinorio de Sierra Alhamilla–Polopos, y una segunda que se centra en el anticlinorio de Sierra Cabrera, que se situa entre la terminación oriental de esta falla y la terminación meridional de la falla de Palomares, una falla sinistrorsa de orientación NNE–SSO que se ha interpretado como una conjugada del sistema de Polopos.

En Sierra Alhamilla se ha realizado un mapa en el que se tiene en cuenta la segmentación de la zona de falla de Polopos en función, entre otros parámetros, de los abanicos aluviales asociados y se han calculado los siguientes índices geomorfológicos: la sinuosidad de los frentes montañosos, la relación anchura-altura del fondo de valle, el factor de asimetría en cuencas de drenaje, curva e integral hipsométrica, perfiles longitudinales de los cauces, y el índice del gradiente longitudinal de río normalizado respecto a la pendiente graduada de río (índice SLk). Los datos morfo-estructurales confirman, contrariamente a lo previamente publicado por diversos autores, que hay deformación tectónica activa en la Sierra Alhamilla. Esta deformación es de carácter transpresivo dextro en su borde norte (falla inversa Norte Alhamilla al borde norte de la sierra) y de salto en dirección dextrorsa en su borde oriental (falla de Sur Gafarillos). Estas fallas afectan a la red de drenaje en la vertiente norte de Sierra Alhamilla

produciendo deflexiones de los cauces fluviales. Además, las fallas normales activas condicionan la geometría de los depósitos aluviales de la vertiente sur de esta sierra.

El mapa de SLk indica dos conjuntos de anomalías positivas: a) una orientada E–O relacionada con la falla transpresiva dextrorsa de Polopos en el flanco norte del anticlinorio; b) un grupo de anomalías con orientación NNO–SSE relacionadas con fallas normales NO–SE y NNO–SSE que cortan el flanco sur de la sierra. En el borde norte de Sierra Alhamilla, la sinuosidad del frente montañoso y la relación anchura-altura del fondo de los valles han permitido estimar tasas de levantamiento Cuaternario moderadas (entre 0.05 y 0.5 m ka-1). La falla de Gafarillos corta las terrazas fluviales de las ramblas de Lucainena y de los Feos, en las que se reconocen depósitos del Pleistoceno superior que transicionan a techo a depósitos coluviales Holocenos. Esta falla induce desviaciones en los cauces fluviales. Por otra parte, las curvas hipsométricas de las subcuencas de esa vertiente presentan una forma convexa hacia arriba, característica de zonas con un levantamiento tectónico muy reciente.

El relieve del flanco sur de la terminación occidental de Sierra Alhamilla está controlado por fallas normales de alto ángulo. Estas fallas son las responsables de los bajos valores de la sinuosidad de este frente montañoso y de la baja relación anchura-altura del fondo de los valles de este flanco sur.

Al igual que en la Sierra Alhamilla, se ha investigado la actividad cuaternaria de las fallas de Polopos y Palomares y su incidencia en la evolución del relieve de la Sierra Cabrera. El análisis morfológico indica que los principales frentes montañosos del anticlinorio de Sierra Cabrera están condicionados por las fallas inversa Norte y Sur de Cabrera que se unen lateralmente con las fallas de Palomares y Polopos, respectivamente. La actividad de estas fallas ha dado lugar a knickpoints, desviaciones de cauces, cuencas con curvas hypsométricas complejas, anomalías positivas de SLk y un fuerte encajamiento de la red de drenaje. La red fluvial de esta sierra presenta un patrón en forma de S que refleja una rotación progresiva en sentido sinistrorso asociado con la falla sinistrorsa de Palomares. Las tasas de levantamiento, determinadas por medio de la integración entre el índice de sinuosidad de frente montañoso y la relación anchura-altura del fondo de valle, son más altas que los observadas en las fallas de salto de dirección en la Béticas orientales. Estas mayores tasas de levantamiento indican que el relieve topográfico de la Sierra Cabrera está controlado por fallas inversas que forman una estructura de pop-up inducido por la componente compresiva de las fallas conjugadas de salto en dirección de Polopos y Palomares. Además, datos geodésicos de GPS sugieren que las fallas inversa Norte y Sur de la sierra de Cabrera acomodan una parte importante de la convergencia entre África e Iberia en la región.

0.3 Migración de frentes montañosos y capturas fluviales asociadas con la segmentación de las fallas del sistema transpresivo dextro de Polopos

En este apartado, que correspondería al capítulo 9 de la tesis, se presenta la evolución y crecimiento de los segmentos de la zona de falla transpresiva dextrorsa de Polopos y su relación con la evolución del relieve en las Béticas surorientales durante el Cuaternario. Este trabajo ha permitido relacionar los procesos de enlace y crecimiento de segmentos de la falla con la migración de los frentes montañosos asociados y las capturas que han ocurrido en la región de las cuencas de Sorbas–Tabernas y Níjar. La zona de falla de Polopos está formada por la falla inversa Norte Alhamilla de orientación E–O y por las fallas dextrorsas Norte y Sur Gafarillos de orientación ESE–ONO. Esta zona de falla de aproximadamente 30 km de longitud es un sistema conjugado a la falla NNE–SSO sinistrorsa de Palomares, activa desde el ultimo Tortoniense terminal (≈ 7.5 Ma) hasta el tardo Pleistoceno superior (≥ 70 ka). La geometría helicoidal de la zona de falla permite la transferencia de desplazamiento hacia el SE a lo largo de la falla inversa Sur Cabrera a desplazamiento hacia el NO asociado a la falla inversa Norte Alhamilla por medio de segmentos verticales dextros de Gafarillos en medio. Desde el Messiniense la actividad de la falla ha migrado hacia el sur formando la falla Sur Gafarillos y desplazando el frente montañoso asociado con la falla del norte al sur de la Sierra de Polopos, mientras que la actividad reciente de la falla Norte Alhamilla ha migrado hacia el oeste. La falla de Polopos ha determinado el levantamiento diferencial entre la Sierra Alhamilla y la cuenca de Sorbas–Tabernas promoviendo la captura que ocurrió en el Pleistoceno medio en el margen sur de la cuenca de Sorbas. El continuo levantamiento de los anticlinorios de Sierra Alhamilla–Polopos y Cabrera y la subsidencia local de la cuenca de Vera, promovida por el funcionamiento a la falla de Palomares, induce el retroceso de la cabecera de la subcuenca del río Aguas provocando la captura de la cuenca de Sorbas en el Pleistoceno superior (ca. 70 ka).

0.4 Convergencia oblicua en el margen de Palomares desde el Mioceno superior hasta la actualidad en el contexto de la inversión tectónica compresiva de la cuenca Argelino-Balear (Mediterráneo occidental)

En este apartado, que corresponde al capítulo 10 de la tesis, proporcionan datos sobre la inversión tectónica en las Béticas orientales y más concretamente, sobre su incidencia en el margen de Palomares desde el Mioceno superior hasta la actualidad, situándolos en el contexto más amplio de la inversión del Mediterráneo occidental (cuencas Argelino–Balear y de Alborán). Este modelo se ha obtenido a partir de la integración de datos estructurales, geodésicos, deformación de sondeos profundos realizados en tierra y datos geofísicos marinos del margen de Palomares (sísmica de reflexión profunda, perfiles acústicos paramétricos y batimetría). Los perfiles de sísmica de reflexión multicanal muestran que el margen de Palomares, que marca la transición entre corteza continental adelgazada con abundantes intrusiones de rocas volcánicas de arco (cuenca del Alborán oriental) y corteza oceánica de retroarco (cuenca Argelino–Balear), se ha formado durante la apertura de la cuenca Argelino–Balear en el Mioceno

Superior. Sin embargo, los principales altos batimétricos observados en el margen se han producido en relación con una inversión contractiva posterior a la formación del margen. Al igual que en el margen emergido, las estructuras contractivas del margen de Palomares están formadas por fallas inversas y pliegues asociados de orientación ~N50ºE, como los anticlinales de Sierra Cabrera y el alto de Abubacer, y fallas de salto en dirección de orientación N10-20ºE, como las fallas de Palomares y Terreros. Los perfiles paramétricos en mar, la deformación de sondeos, la deformación de sedimentos cuaternarios en tierra y en mar, los datos de desplazamientos geodésicos de GPS disponibles, los mecanismos focales de terremotos y la batimetría indican que la inversión tectónica del margen de Palomares es activa. El margen de Palomares presenta un patrón estructural comparable con el de los márgenes del norte de Marruecos y Argelia donde la convergencia entre las placas de Africa y Eurasia se acomoda por fallas inversas de orientación NE–SO, fallas NNO–SSE sinistrorsas y fallas ONO–ESE dextrorsas. Las estructuras contractivas de este margen contribuyen a la inversión tectónica general del Mediterráneo occidental desde hace aproximadamente 7 Ma, coetáneamente con la inversión del margen Argelino. El acortamiento a lo largo de las fallas de Al-Idrisi y las de la cresta de Alborán se producen con posterioridad (desde hace 5 Ma), indicando una propagación hacia el oeste de la inversión contractiva del Mediterráneo occidental.

Outline of the Thesis

The thesis is subdivided into five major parts:

In **PART I**, the Introduction (Chapter 1) provides some introductory notions to present the main subject of the thesis to the reader and illustrate the aims and motivations behind this work. The chapter summarizes the processes that determine the landscape evolution, presenting its control factors and focusing on the influence of tectonics. Tectonics controls the landscape evolution through both local fault structures and epeirogenic uplift. Then, qualitative and quantitative geomorphic analyses by geomorphic indices are presented as a useful tool to define and quantify the landscape features and the tectonic control on them. Finally, we illustrate the main objectives and the methodology adopted of these thesis briefly in the Introduction (Chapter 1) and fully in the Aims of this thesis (Chapter 2). This section is followed by the Tectonic setting (Chapter 3) that illustrates the Gibraltar subduction-collisonal system presenting the tectonic domains of the Betic–Gibraltar–Rif arched orogenic system. Further topics presented in this section are the crustal types of the Alborán and Algero–Balearic basins, Neogene extensional basins and Neogene–Quaternary and active tectonic structures of the southeastern Betics. Chapter 4 provides a detailed Lithostratigraphy of the region illustrating the metamorphic basement rocks and the Neogene to Quaternary sedimentary rocks of the study area, and focusing on the Quaternary fluvial terraces and drainage pattern evolution. Chapter 5 describes the Methodology adopted in this thesis, including the structural field-based and morphometry GIS-based methods and the seismic data processing flow.

PART II presents the main Results of this thesis and is subdivided into five chapters. Except the first one that is a paper in preparation and the last one that is a submitted paper, all these chapters have been published in top ranked scientific journals in the field of structural geology, tectonics and geomorphology. Chapter 6 deals with the importance of the late Miocene extensional tectonics in the evolution of the eastern Betics and Neogene–Quaternary sedimentary basins. This chapter provides an example from the Sorbas basin where a Tortonian extensional fault system segmented by transfer faults determines a large Tortonian sedimentary depocenter later inverted under the present NW–SE compressive stress field. Chapter 7 and Chapter 8 present two morpho-tectonic studies in two adjacent areas of the eastern Betics, the Sierra Alhamilla–Polopos and Cabrera anticlinoria together with nearby basins, the Sorbas–Tabernas and Níjar basins. In these chapters we present the geomorphic evidence of active to recent tectonic activity in the region associated to the Palomares and the Polopos conjugate strike-slip fault zones and the constructional domain in between. In Chapter 9 we present a structural study about mountain front migration and drainage captures in the Sorbas–Tabernas and Níjar basins related to fault segment linkage and growth of the Polopos fault zone together with the Palomares fault zone and the epiorogenic uplift documented in the area. In Chapter 10 we analyse multichannel seismic, parametric

profiles and bathymetry offshore at the Palomares margin. This work is integrated with the previous morpho-structural data set providing an offshore onshore kinematic model for the late Miocene to present tectonic inversion of the Palomares margin and eastern Betics in the context of the western Mediterranean.

In **PART III** we present the Conclusions (Chapter 11) in a synthetic way referring to the results chapters. The References cited in this thesis are reported in **PART IV** (Chapter 12).

Part I – Introduction, Aims of the thesis, Tectonic setting, Litostratigraphy of the region and Methodology

1.0 Introduction

Landscape evolution occurs by geomorphic processes, both fluvial and alluvial that are influenced by topography, climate, sea level fluctuations, lithology, tectonics and epeirogenic uplift. These factors must be taken into account when tectonically oriented conclusions are deduced *(e.g. Ollier, 1981; Jackson and Leeder, 1994; Schumm et al., 2000; Burbank and Anderson, 2001; Azor et al., 2002; Keller and Pinter, 2002)*. Tectonics competes with, and influences, the geomorphic processes during landscape evolution, both locally, in response to tectonic structures that affect the topography, and regionally, in response to epeirogenic or fault-block uplift *(e.g. Jackson et al., 1996; Goldsworthy and Jackson, 2000; Booth-Rea et al., 2004a; Pérez-Peña et al., 2010)*. Strike-slip fault displacement, for example, generates horizontal topographic alterations and important topographic gradients forming both uplifted ranges and sedimentary depocenters in antidilational and dilational jogs, respectively *(Sibson, 1986; Sylvester, 1988)*.Furthermore, growth and migration of fault and fold systems by the development of new fault segments and folds determine topographic modifications but also variations in the position of active sedimentary depocenters *(Ollier, 1981; Walker and Jackson, 2002; Booth-Rea et al., 2003a)*. Faulting related topographic and sedimentary changes induce local-base level variations that in turn produce dissection or aggradation processes and drainage adjustments like fluvial captures, river deflection, headward erosion and stream head- or foot-rejuvenation processes *(Holbrook and Schumm, 1999; Snyder et al., 2000; Burbank and Anderson, 2001; Lave and Avouac, 2001; Hilley and Arrowsmith, 2008)*. Thus, fluvial and alluvial systems should reflect the fault activity migration and mountain front evolution in time and space *(e.g. Keller and Pinter, 2002)*.

Epeirogenic uplift influences the landscape evolution in a wider manner controlling the general topographic gradient in large uplifted regions and plateaus, and thus, influencing the drainage pattern, its flow direction and the general dissection grade. Epeirogenic uplift can result from lithospheric delamination, a mechanism that has been invoked for the Late Neogene evolution of the Betic–Rif orogeny *(Duggen et al., 2003; Martínez-Martínez et al., 2006; Lis Mancilla et al., 2013)*. Sustained early Pliocene–Quaternary epeirogenic uplift produced repeated river incision episodes since the middle Pleistocene onward in the eastern Betics *(Harvey and Wells, 1987; Mather, 1993; Braga et al., 2003)*. Typically, this uplift was higher in the antiformal ridges than in the Neogene–Quaternary basins (of about 100 m Ma-1; *Weijermars et al., 1985; Braga et al., 2003*).

Local tectonic structures together with the epeirogenic uplift control most of the landscape evolution in the eastern Betics, both concurring with and conditioning the alluvial and fluvial processes (e.g. fluvial captures, drainage adjustments and mountain front migration; *Mather, 1993, 2000b; Stokes and Mather, 2000; Mather et al., 2002; Maher et al., 2007*). The regional uplift, associated river incision episodes and generalized erosion has resulted in few outcrops of Quaternary sediments in the eastern

Betics, which are limited to fluvial strath and bedrock terraces and dissected alluvial fans.

Where the Quaternary geomorphic or geological markers are insufficient to detect and characterize recent or active tectonics, the qualitative and quantitative geomorphic analyses provide a useful tool to define and quantify the landscape features and the tectonic control on them. This approach has been broadly applied to identify and characterize sectors deformed by active faults with low to moderate deformation rates *(e.g. Bull and McFadden, 1977; Rockwell et al., 1984; Wells et al., 1988; Merrits and Vincent, 1989)*. The results of this methodology is particularly productive in semiarid zones like SE Spain, where landforms related to active tectonics are preserved for long periods *(Silva et al., 2003)*. Active tectonic structures have been evaluated using quantitative geomorphic analyses in regions of the central and eastern Betics, for example in Sierra Nevada and the Granada basin *(Pérez-Peña et al., 2009c, 2010)* or at the southern limb of the Sierra de las Estancias antiform *(Pedrera et al., 2009b)*.

We carried out both structural field-based and geomorphic analyses in selected areas of the eastern Betics in order to detect and define active or recent tectonics, the landscape evolution and the tectonic control on it, both local and regional. First, we selected the region identified by the Sierra Alhamilla and the Sierra de Polopos antiformal ridges, including the Sorba–Tabernas and Níjar basins. We focus our research especially on tectonic-driven mountain front migration and fluvial captures. Secondly, we selected the region coinciding with the Sierra Cabrera and Sierra de Polopos antiformal ridges, including the Vera and Níjar basins. Our analyses in this area were addressed to discern the tectonic contribution on the landscape/relief provided by the strike-slip and reverse tectonics, respectively.

Finally, to characterize the active tectonic processes occurring in areas offshore of the eastern Betics we obtained and processed marine geophysical data (deep reflection seismics, parametric sub-bottom profiles and bathymetry) from the Palomares margin. We integrated this data with the previous onshore data. The integration of onshore and offshore structural, geomorphic and bathymetric data in the southeastern Betics and the Palomares margin with available work by previous authors in the Algero–Balearic and Alborán basins permits us to propose a revised model for the tectonic inversion of the Western Mediterranean since the latemost Tortonian until present.

2.0 Aims of the thesis

The main aim of this thesis is to contribute consistently to the definition of the main tectonic structures (both their kinematics and timing) that control the landscape evolution of the southeastern Betics and the Palomares margin offshore since the late Miocene to present. We focus on fluvial captures and mountain front migration and the tectonic control on them, both local and regional. This objective is achieved by

structural field- and morphometry GIS-based studies exhaustively explained in chapters 6, 7 8 and 9.

The final aim of this thesis is to provide a synthetic morpho-tectonic and structural model that could explain the landscape evolution and the recent to present tectonic setting of the southeastern Betics and the Palomares margin. Furthermore, we set this study area in the wider context of the late Miocene to present tectonic inversion of the westernmost Mediterranean proposing a revised model. This aim is achieved by the integration of structural field- and morphometry GIS-based onshore data with marine geophysical data (two deep reflection seismic and parametric sub-bottom profiles and bathymetry), as illustrated in chapters 9 and 10. Furthermore, we integrate our onshore-offshore data set with a recompilation of geophysical available in the area (e.g. GPS geodetic displacement data, earthquake focal mechanisms, borehole and fault inversion, heat flow, thermal conductivity, radiogenic heat production, crustal thickness and rheological profile).

Finally, this thesis provides a multidisciplinary approach using methodologies based on the integration of different data sets that could solve and explain complex tectonic scenarios as the eastern Betics and the Palomares margin in the context of the wider Eurasia–Africa boundary plate.

3.0 Tectonic setting

The Betic and Rif belts belong to the Gibraltar arc orogenic system that formed by combined subduction and oblique collision mechanisms (Fig. 1). Early to late Miocene subduction of Mesozoic oceanic crust of the Thethys Ocean occurred under central areas of the Gibraltar arc resulting in an accretionary wedge that is preserved in the Gulf of Cádiz *(e.g. Gutscher et al., 2001; Iribarren et al., 2007; Sallarès et al., 2011; Gutscher et al., 2012)*, a volcanic arc in the Eastern Alborán basin and back-arc extension that lead to the opening of the Algero–Balearic basin during the middle to late Miocene *(e.g. Lonergan and White, 1997; Duggen et al., 2003, 2004a; Mauffret et al., 2004; Duggen et al., 2005; Booth-Rea et al., 2007)*. Simultaneous to this subduction, oblique collision of the Iberian and the North Maghrebian passive margins beneath the Alborán domain orogenic wedge occurred in the northern and southern branches of the Gibraltar arc *(e.g. Balanyá and García-Dueñas, 1987; Martínez-Martínez and Azañón, 1997; Durand-Delga et al., 2000; Faccenna et al., 2004; Booth-Rea et al., 2005; Luján et al., 2006; Platt et al., 2006; Balanyá et al., 2007; Booth-Rea et al., 2007)*. The Gibraltar arc formed in the context of NW–SE Nubia–Iberia convergence during the Alpine orogeny *(e.g. Dewey et al., 1989; Mazzoli and Helman, 1994; McClusky et al., 2003; Nocquet and Calais, 2004)*, however, the mechanisms driving the tectonic evolution of the system have been strongly debated. These include mantle convective removal *(Platt and Vissers, 1989)*, slab rollback *(Lonergan and White, 1997)*, slab

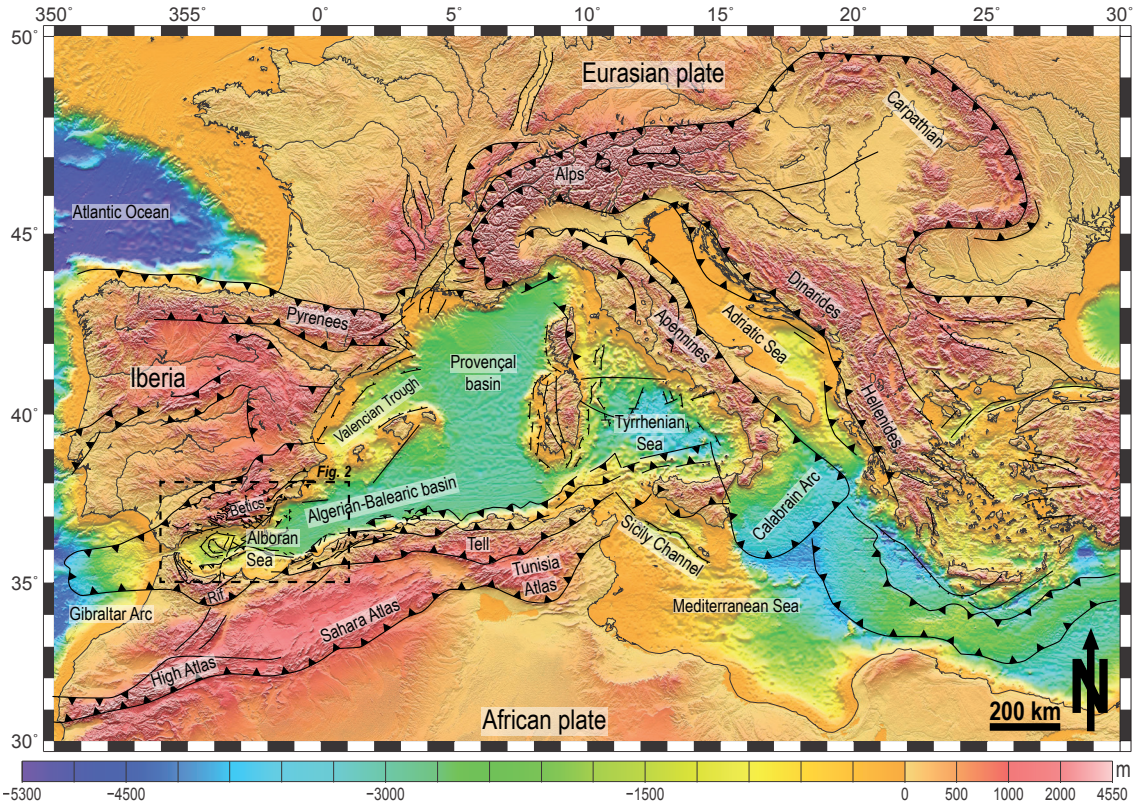

Fig. 1: Tectonic map of the western Mediterranean region (modified from, Faccenna et al., 2004; Mauffret, 2007; Billi et al., 2011).

tearing or breakoff *(Zeck, 1996; Carminati et al., 1998; Zeck, 1999)*, lithospheric delamination *(García-Dueñas et al., 1992; Martínez-Martínez and Azañón, 1997; Faccenna et al., 2004; García-Castellanos and Villasenor, 2011)* or a combination of subduction beneath central areas of the Alborán basin and edge-delamination beneath the Betic–Rif margins *(Duggen et al., 2003; Martínez-Martínez et al., 2006; Booth-Rea et al., 2007, 2012b)*.

Thrusting and folding of the South–Iberian Mesozoic to Tertiary passive margin sedimentary cover during the early to late Miocene was coeval to extensional processes in the core of the Betics. Middle to late Miocene extensional tectonics along WSW-directed core-complex type detachments exhumed HP metamorphic rocks and markedly attenuated the previous metamorphic nappe stack *(García-Dueñas and Martínez-Martínez, 1988; Galindo-Zaldívar et al., 1989; Platt and Vissers, 1989; García-Dueñas et al., 1992; Martínez-Martínez and Azañón, 1997; Martínez-Martínez et al., 1997; Booth-Rea et al., 2005)*. This extension resulted in the development of internal Betic Neogene extensional basins and the E–W spreading of the Alborán and Algero–Balearic basins in the core of the orogeny, involving the formation of oceanic crust *(García-Dueñas et al., 1992; Comas et al., 1999; Mauffret et al., 2004; Booth-Rea et al., 2007; Pesquer et al., 2008)*.

Ongoing NW–SE convergence between Africa and Eurasia produced the tectonic inversion of the eastern Betic–Rif extensional basins and of the Alborán and Algero–Balearic basins *(Bourgois et al., 1992; Campos et al., 1992; Comas et al., 1992; Mauffret et al., 1992; Morel and Meghraoui, 1996; Martínez-Martínez and Azañón,*

1997; Comas et al., 1999; Soto et al., 2000; Martínez-Martínez et al., 2002; Booth-Rea et al., 2005; Déverchère et al., 2005; Domzig et al., 2006; Mauffret, 2007; Billi et al., 2011; Booth-Rea et al., 2012b). This compressional tectonic inversion resulted in the development of several large strike-slip and reverse faults since the late Miocene, most of which continue active until the Plio–Quaternary or the present *(Bousquet and Montenat, 1974; Bousquet, 1979; Weijermars et al., 1985; de Larouzière et al., 1988; Montenat and Ott d´Estevou, 1990; Booth-Rea et al., 2004a; Stich et al., 2006)*.

3.1 Tectonic domains of the Gibraltar Arc orogenic system

The Gibraltar Arc orogenic system has been traditionally subdivided into four major tectonic domains: a) the South–Iberian passive continental palaeomargin; b) the Maghrebian passive continental palaeomargin; c) the Flysh Trough units; d) and the Alborán domain (Fig. 2). Furthermore, the orogen includes several Neogene–Quaternary extensional basins.

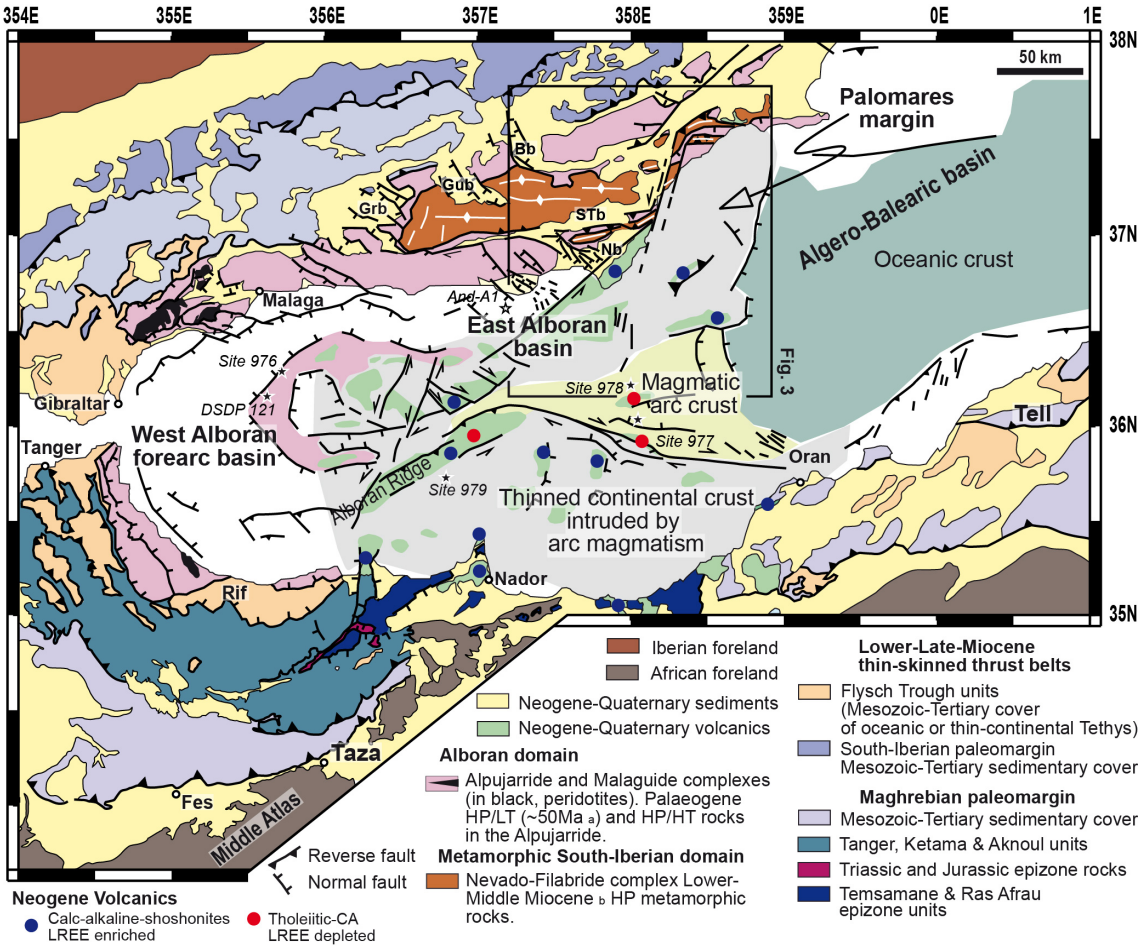

Fig. 2: Simplified geological map showing the tectonic domains of the Gibraltar Arc and the Alborán and Algero–Balearic basins (modified from, Comas et al., 1999; Booth-Rea et al., 2007; Martínez-García et al., 2013). Igneous geochemistry data acquired from El Bakkali et al. (1998), Coulon et al. (2002), Duggen et al. (2004a; 2005). Age of metamorphism: (a) Platt et al. (2005) and (b) Platt et al (2006). Scientific drill sites (DSDP and ODP) and commercial wells in the Alborán Basin are also located. See Fig. 1 for its location.

3.1.1 The South–Iberian and Maghrebian passive continental palaeomargins (external zone)

These domains are foreland thrust and fold belts formed by Mesozoic and Tertiary sediments deposited at the South–Iberian and Maghrebian rifted palaeomargins (Fig. 2).

The South–Iberian paleomargin sediments deposited during the Mesozoic and part of the Cenozoic upon the Hercynian basement in shelf and deep basin environments *(Vera, 2001)*. These sediments, non-metamorphosed or poorly metamorphosed, were detached from their Hercynian basement and deformed by thin-skinned tectonics *(Crespo-Blanc and de Lamotte, 2006)*. This domain has been traditionally subdivided into a Prebetic Zone to the north and a Subbetic Zone to the south, that have both tectonic and stratigraphic substantial differences *(García-Hernández et al., 1980)*. The Prebetic units deposited mostly in shallower marine conditions with continental exposure including locally erosion, whilst the Subbetic units show dominant pelagic facies *(Vera, 2001)*. The Prebetic tectonic style varies from imbricate thrust sheets to large folds with subordinated thrusts. Meanwhile the Subbetic formed a thrust-and-fold-belt that was highly extended during the late Miocene *(Rodríguez-Fernández et al., In Press)*.

The Mesozoic and Tertiary Maghrebian paleomargin sediments, namely the External Rif units, deposited in deeper marine environments on the rifted African margin and locally over exhumed mantle *(Michard et al., 1997)*. These units are formed by evaporitic deposists of Triassic Germanic facies (evaporites, pelites, dolomites and some volcanics in a sabkha environment), by a lower to middle Jurassic carbonate sequence (transgressive carbonate platform deposits and shallow to deep marine limestones and dolomites), by upper Jurassic detritic series and a lower Cretaceous olistostromic unit *(Favre et al., 1991; Azdimousa et al., 2007)*. These rocks were detached from their basement from early Miocene onwards, deformed by thin-skinned tectonics as fold-and-thrust belt and metamorphosed during subduction. Metamorphic grade increases eastward from diagenesis in the west, to anchizone in the central Rif (Ketama unit), and reaching IP–LT conditions and a penetrative foliation in the eastern Rif (Temsamane units) *(Azdimousa et al., 1998, 2007; Negro et al., 2007; Booth-Rea et al., 2012b; Vázquez et al., In press)*.

3.1.2 The Flysh Trough units

The Flysch Trough units are formed by deep-water or oceanic siliciclastic turbidites and abyssal plain sediments deposited along an elongated trough between the African and Iberian paleomargins during the lower Cretaceous to lower Miocene (Fig. 2). The Flysch Trough basin was floored by thinned-continental or oceanic basement *(Dercourt et al., 1986; Durand-Delga et al., 2000; Luján et al., 2006)*. These units were detached from their basements and deformed without metamorphism by thin-skinned tectonics overriding the underlying Subbetic units essentially during the early to middle Miocene *(Luján et al., 2003, 2006)*.

3.1.3 The Alborán domain (internal zone)

The Alborán domain includes three poly-metamorphic nappe complexes of variable metamorphic grade that are, in ascending order, the Nevado–Filabride, Alpujarride, and Malaguide complexes (Fig. 2) *(Balanyá et al., 1997)*. These complexes are made up manlyof Palaeozoic and Mesozoic rocks that underwent low to high-grade metamorphism and penetrative deformation during the late Cretaceous to Paleogene or Miocene. The Nevado–Filabride complex is formed by Paleozoic to Cretaceous rocks that suffered a polyphase Alpine metamorphism with an early HP/LT metamorphism, followed by high-greenschist facies in the two lower tectonic units and almandine-amphibolite facies in the uppermost one, and later by an decompression and exhumation *(Nijhuis, 1964; Gómez-Pugnaire and Fernández-Soler, 1987; García-Dueñas et al., 1988; Bakker et al., 1989; Soto, 1991; Johnson, 1997; Johnson et al., 1997)*. The Alpujarride complex is formed by Paleozoic metapelites and Triassic carbonate rocks that underwent Alpine metamorphism with a first HP/LT event followed by isothermal decompression inducing low and intermediate pressure metamorphism *(Goffé et al., 1989; Tubía et al., 1992; Azañón et al., 1997; Balanyá et al., 1997)*. The Malaguide complex is formed by the remnants of a stack of at least six thrust sheets formed by a Palaeozoic basement and a Permo–Triassic sedimentary cover. The base of the basement underwent low-grade metamorphism during the Hercynian orogeny *(Chalouan and Michard, 1990)*. The Triassic cover reached anchizonal metamorphic conditions in the structurally lowest Malaguide thrust sheets during the Alpine orogeny *(Nieto et al., 1994; Lonergan and Platt, 1995; Abad et al., 2003; Booth-Rea et al., 2004c)*. This metamorphism resulted from nappe stacking during the underthrusting of the Alpujarride complex *(Lonergan and Platt, 1995; Balanyá et al., 1997)*.

The Alpujarride complex HP/LT metamorphism occurred during the Palaeogene (40-50 Ma) and is interpreted as originated after crustal stacking under the Malaguide complex *(Balanyá et al., 1997; Platt et al., 2005)*. The following near isothermal decompression is interpreted as the response to ductile regional thinning *(Balanyá et al., 1993)* that led to the exhumation of the Alpujarride complex during the early Miocene (19 Ma, *Lonergan and Johnson, 1998; Esteban et al., 2004*). Extension of the Malaguide complex and associated tholeiitic and calc-alkaline volcanism initiated earlier during the Oligocene *(Duggen et al., 2004b; Garrido et al., 2011; Marchesi et al., 2012)*. The Nevado–Filabride complex underwent HP metamorphism (both –LT and –HT) during the early–middle Miocene (14-18 Ma) from Lu-Hf dating of garnetin eclogite *(Platt et al., 2006)* and U-Pb of zirconin piroxenite *(López Sánchez-Vizcaíno et al., 2001)* by continental subduction and crustal stacking under the Alpujarride and Malaguide complexes. Coeval to the extension and exhumation of both Malaguide and Alpujarride complexes and their stacking over the Nevado–Filabride complex, the Flysch Trough units underwent to imbricate thrust stacking in the early Miocene. Finally, extensional denudation of the Nevado–Filabride complex occurred between

the middle and late Miocene according to fission-track analyses (12-6 Ma, *Johnson, 1997; Johnson et al., 1997; Vázquez et al., 2011*). The extension has continued during the Quaternary to present denudating the Nevado–Filabride complex at the western Sierra Nevada mountain front *(e.g. Galindo-Zaldívar et al., 1996; Martínez-Martínez et al., 2004; Pérez-Peña et al., 2010)*. The superposition of extensional events (early to middle Miocene for the Malaguide and Alpujarride complexes), and middle Miocene to present for the Nevado–Filabride complex) have determined that most of the boundaries between the Alborán domain units are ductile, ductile-brittle or brittle extensional shear zones *(García-Dueñas et al., 1992; Crespo Blanc et al., 1994; Azañón et al., 1997; Martínez-Martínez et al., 2004)*.

The Alpujarride and Malaguide complexes share a common orogenic evolution since the Palaeogene *(e.g. Lonergan and Platt, 1995; Azañón et al., 1997; Balanyá et al., 1997; Booth-Rea et al., 2004a; Platt et al., 2004)*, however, the Nevado–Filabride complex entered the orogenic wedge at a later stage, during the early to middle Miocene *(López Sánchez-Vizcaíno et al., 2001; Platt et al., 2006)*. Considering these different tectono-metamorphic evolutions, the Alborán domain includes two different terrains, on one hand, the Alpujarride and Malaguide complexes and, on the other hand, the Nevado–Filabride complex. The Alpujarride and Malaguide complexes represent the remnants of an earlier orogenic wedge that underwent crustal staking and HP/LT metamorphism *(Goffé et al., 1989; Tubía and Gil Ibarguchi, 1991; Azañón et al., 1997; Booth-Rea et al., 2002)* associated to Eocene continental collision *(Lonergan, 1993)* prior to the evolution of the Gibraltar Arc (about 50 Ma, *Balanyá et al., 1997; Azañón and Crespo Blanc, 2000; Platt et al., 2005*). In contrast, the Nevado–Filabride complex underwent a later HP metamorphism and represents the Paleozoic basement and Permo–Triassic cover of the south Iberian passive margin that subducted beneath the Alpujarride and Malaguide complexes during the formation of the Gibraltar arc between the early to middle Miocene (14-18 Ma, *López Sánchez-Vizcaíno et al., 2001; Platt et al., 2004; Booth-Rea et al., 2005; Platt et al., 2005; Platt et al., 2006; Booth-Rea et al., 2007*).

3.1.4 The Neogene extensional basins

The early to late Miocene extension of the orogen hinterland produced the Neogene Alborán and Algero–Balearic basins together with other minor internal Neogene basins that showed marine continuity with the previous ones during the late Neogene and are currently emerged in the Betics *(Platt and Behrmann, 1986; Galindo-Zaldívar et al., 1989; Platt and Vissers, 1989; García-Dueñas et al., 1992; Lonergan and Platt, 1995; Martínez-Martínez and Azañón, 1997; Comas et al., 1999; Martínez-Martínez et al., 2002; Booth-Rea et al., 2005)*. Examples from the western and central Betics are the Granada and Guadix-Baza basins related to late Miocene to Quaternary extensional tectonics (Fig. 2, *Fernández et al., 1996; Azañón et al., 2004a; Rodríguez-Fernández and Sanz de Galdeano, 2006; Azañón et al., 2007; Pedrera et al., 2007, 2009b; Pérez-*

Peña et al., 2009c). The Sorbas–Tabernas, Níjar–Carboneras and Vera basins in the eastern Betics underwent important extension in their origin but were tectonically inverted since the late Miocene by strike-slip faults and associated reverse faults and folds (Fig. 2, *Weijermars et al., 1985; Montenat and Ott d´Estevou, 1990; Booth-Rea et al., 2004a*).

3.2 Crustal types of the Alborán and Algero–Balearic basins (fore-arc and back-arc basins)

The Alborán and Algero–Balearic basins lie above de part of the Gibraltar Arc that underwent subduction and thus show a different structure than the regions where oblique collision occurred. In the Alborán and Algero–Balearic basins three main crustal domains can be defined: the continental crust of the West Alborán fore-arc basin, the thinned continental crust intruded by arc magmatism of the East Alborán basin, and oceanic crust of the Algero–Balearic basin, progressively eastwards (Fig. 2, *Comas et al., 1999; Booth-Rea et al., 2007; Mauffret, 2007*). The West Alborán basin represents the fore-arc basin of the magmatic arc (*Booth-Rea et al., 2007; Mauffret et al., 2007*) and corresponds to the major sedimentary depocenter of the Alborán basin that is infilled by up to 7-8 km of early to middle Miocene sediments (*Comas et al., 1999*). This basins is floored by metamorphic rocks of the Alborán crustal domain that reach the maximum crustal thickness of about 18 km in the western sector (decreasing to less than 12 km in the East Alboran basins, *Comas et al., 1999*). This basin was affected by a post-Messinian subsidence of thermal *(Watts et al., 1993)* or flexural origin *(Docherty and Banda, 1995)*, and later, since the middle Miocene until the Pliocene extensive diapirism occurred *(Comas et al., 1999)*.

The East Alborán basin is floored by thinned continental crust heavily intruded by arc volcanism during the Serravallian to Messinian (as recent as ≈6 Ma), in the western part, and by magmatic arc crust (belonging both to the tholeiitic and calc-alkaline series) older than ≈8 Ma in the eastern part *(Comas et al., 1997; Turner et al., 1999; Hoernle et al., 2003; Duggen et al., 2004a; Gill et al., 2004; Duggen et al., 2005; Booth-Rea et al., 2007; Duggen et al., 2008)*. In the back-arc region, the Algero–Balearic basinspread in an E–W direction between 16 and 8 Ma *(Mauffret et al., 2004; Booth-Rea et al., 2007)* involving the formation of oceanic crust *(Pesquer et al., 2008)* probably older than 10–12 Ma in its eastern part.

3.3 Neogene–Quaternary and active tectonic structures of the southeastern Betics

The main sinistral strike-slip faults associated to the late Miocene compressional tectonic inversion in the southeastern Betics are the Palomares, Terreros, Carboneras and Alhama de Murcia fault zones (Fig. 3, *Bousquet and Montenat, 1974; Bousquet,*

1979; Weijermars et al., 1985; de Larouzière et al., 1988; Montenat and Ott d´Estevou, 1990; Booth-Rea et al., 2004a; Stich et al., 2006). Furthermore, both folding and dextral and reverse faulting occurred during this tectonic inversion, for example, at the Sierra Alhamilla–Polopos and Cabrera anticlinoria and the Gafarillos dextral fault *(Stapel et al., 1996; Huibregtse et al., 1998; Jonk and Biermann, 2002; Martínez-Martínez et al., 2002; Martín et al., 2003; Martínez-Martínez, 2006; Martínez-Martínez et al., 2006)*.

The sinistral Carboneras fault zone was active at least since the Serravallian until the QuateQuaternary. The Miocene activity of this fault was essentially strike-slip *(Bousquet, 1979; Montenat and Ott d´Estevou, 1990; Stapel et al., 1996; Huibregtse et al., 1998; Jonk and Biermann, 2002; Rutter et al., 2012)*. On the contrary, its Plio–Quaternary activity appears to be transpressive rather than strike-slip *(Bell et al., 1997; Reicherter and Reiss, 2001; Rutter et al., 2012)*. New field data give evidence for shortening in the Plio–Quaternary along the Carboneras fault zone and folding in the Sierra Cabrera, such as folding-related unconformities in the latemost Messinian to Pliocene sedimentary rocks *(Rutter et al., 2012)*. Similarly, along the Sierra Cabrera northern mountain front, reverse faulting- and folding-related unconformity in the latemost Tortonian–Messinian sediment (8–7.24 Ma) marks the initial growth of the Sierra Cabrera anticlinorium (together with the Sierra Alhamilla–Polopos one) and the following reverse faulting *(Martínez-Martínez et al., 2002; Booth-Rea et al., 2003a; Martín et al., 2003; Booth-Rea et al., 2004a, 2005; Martínez-Martínez, 2006; Martínez-Martínez et al., 2006)*. Nevertheless, reverse faulting during the Plio–Quaternary is not documented yet nor solved.

The Palomares fault zone was characterized by a pure sinistral strike-slip kinematic during the Tortonian–Messinian meanwhile during the Plio–Quaternary the fault zone lengthened and widened eastwards evolving in an transtensional oblique-slip regime *(Booth-Rea et al., 2004a)*. The present activity of this fault zone is confirmed by its influence on the drainage network and topography (e.g. higher drainage density in the uplifted fault-block, stream deflections, *Booth-Rea et al., 2004a*).

Dextral transpressive or reverse faulting along the Gafarillos trough the Sierra Alhamilla–Polopos anticlinoria northern mountain fronts (Fig. 3) probably initiated its activity in the Tortonian and locally was sealed by latemost Tortonian and early Messinian temperate limestones (between 8 and 6.4–5.9 Ma; *Platt et al., 1983; Weijermars et al., 1985; Ott d'Estevou and Montenant, 1990; Stapel et al., 1996; Huibregtse et al., 1998; Jonk and Biermann, 2002*). Furthermore, to the west of the Sierra Alhamilla, *Sanz de Galdeano et al. (2010)* documented the existence of active E–W-striking dextral faults that cross the Tabernas basin (Fig. 3).

Finally, a Pliocene–Quaternary NW–SE- to NNW–SSE-striking high-angle normal fault system occurs in the Níjar–Almeria basin with a SW-toward extension direction and sub-parallel to the present sub-horizontal maximum shortening direction (Fig. 3;

Martínez-Martínez and Azañón, 1997; Martínez-Díaz and Hernández-Enrile, 2004; Marín-Lechado et al., 2005; Pedrera et al., 2006). The present activity if this fault system is confirmed by extensional focal mechanisms in the area (e.g. the Mw 4.8 2002

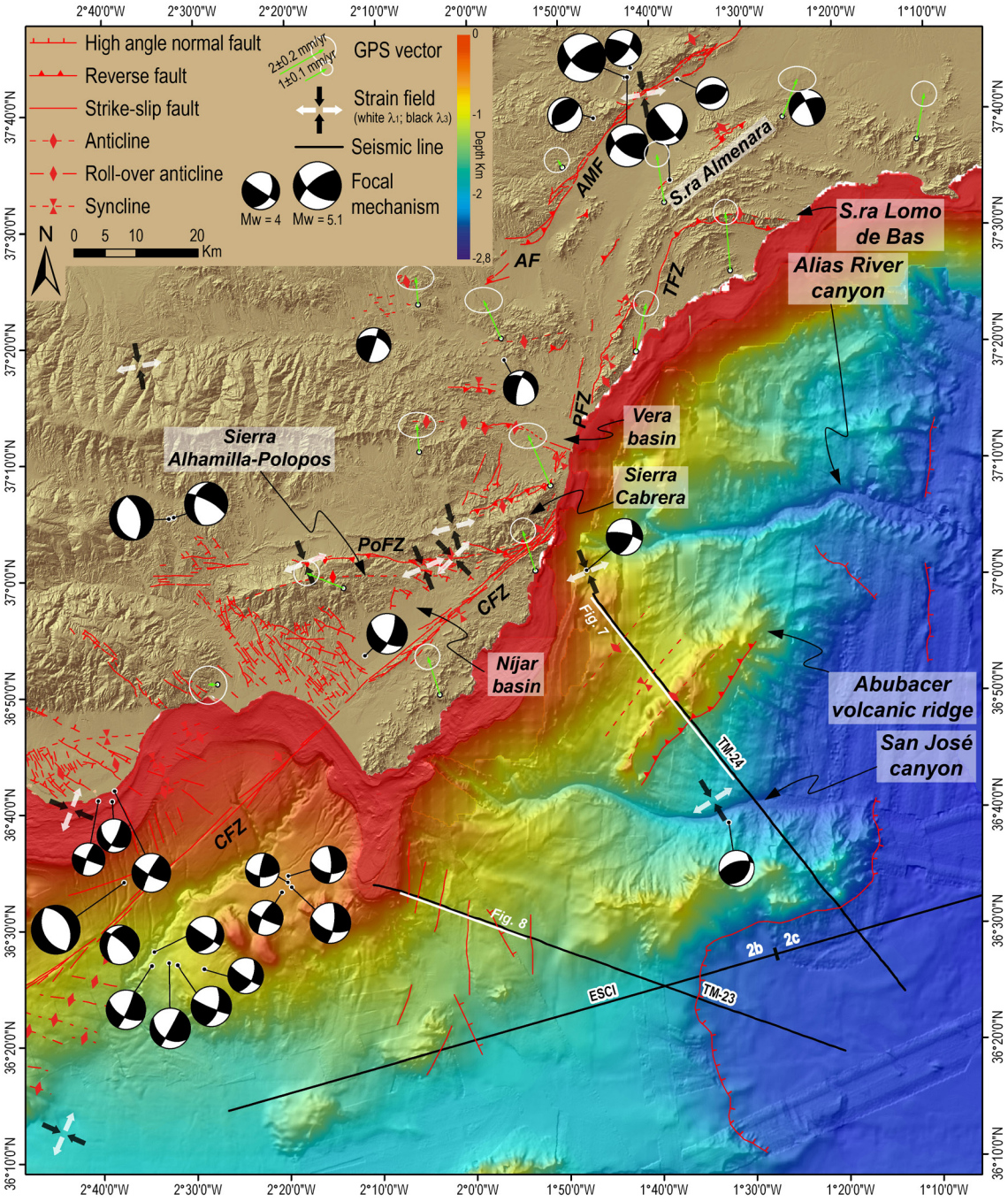

Fig. 3: Structural map where the main tectonic structures active during the Quaternary are shown: the Albox fault (AF), the Alhama de Murcia fault (AMF), the Carboneras fault zone (CFZ), the Palomares fault zone (PFZ) and the Polopos fault zone (PoFZ) (see Fig. 2 for location, Booth-Rea et al., 2004a, 2004c; Masana et al., 2004; Marín-Lechado et al., 2005; Masana et al., 2005; Gràcia et al., 2006; Pedrera et al., 2006, 2009a; Sanz de Galdeano et al., 2010; Booth-Rea et al., 2012a; Giaconia et al., 2012a, 2012b; Pedrera et al., 2012; Giaconia et al., 2013a). Furthermore, focal mechanisms, local stress tensor (both from focal mechanisms and fault slicken-line inversion data, Stich et al., 2003a; Fernández-Ibáñez et al., 2007; Giaconia et al., 2013a) and GPS geodetic data (Khazaradze et al., 2008; Echeverria et al., 2011) are shown. Topographic and bathymetric map (100 m grid) of the study area from digital grids released by SRTM-3, IEO bathymetry (Ballesteros et al., 2008; Muñoz et al., 2008), CSIC bathymetric dataset (Gràcia et al., 2012) and MEDIMAP multibeam compilation (MEDIMAP GROUP et al., 2008) at 90m grid-size.

Gergal and the Mw 6.1 1910 Adra earthquakeas; *Stich et al., 2003b; Béjar et al., 2006*).

All these structures are oriented well fitting to the present NW–SE compressive stress field between Africa and Eurasia (Fig. 3). This stress field is supported by earthquakes, focal mechanisms and GPS geodetic displacement data available both in the Betics and the Alborán and Algero–Balearic basins *(Buforn et al., 1995; Morel and Meghraoui, 1996; Buforn et al., 2004; Gràcia et al., 2006; Stich et al., 2006; Fernández-Ibáñez et al., 2007; Serpelloni et al., 2007; Khazaradze et al., 2008; Echeverria et al., 2011)*.

4.0 Lithostratigraphy of the southeastern Betics

4.1 Metamorphic basement rocks of the study area

The exhumed crustal section of the Nevado–Filabride complex is completely exposed in the Sierra Nevada and Sierra de los Filabres and partially crops out in the Sierra Alhamilla–Cabrera anticlinorium. This metamorphic complex is formed by three major tectonic units separated by two ductile shear zones subparallel to both the main foliation and the litological contacts (Fig. 4, *Martínez-Martínez et al., 2004*). These tectonic units are the Ragua, Calar Alto, and Bédar–Macael units, in ascending order. All these units except the Ragua unit crop out in the study area at the Sierra Alhamilla, Polopos and Cabrera antiformal ridges. The Ragua unit consists of low-grade, albite-rich, graphite Palaeozoic mica-schist with numerous metapsammite rocks interlayered at the top. The Calar Alto unit is formed by metasedimentay sequence including chloritoid-rich, graphite mica-schist of Palaeozoic protholith (Montenegro

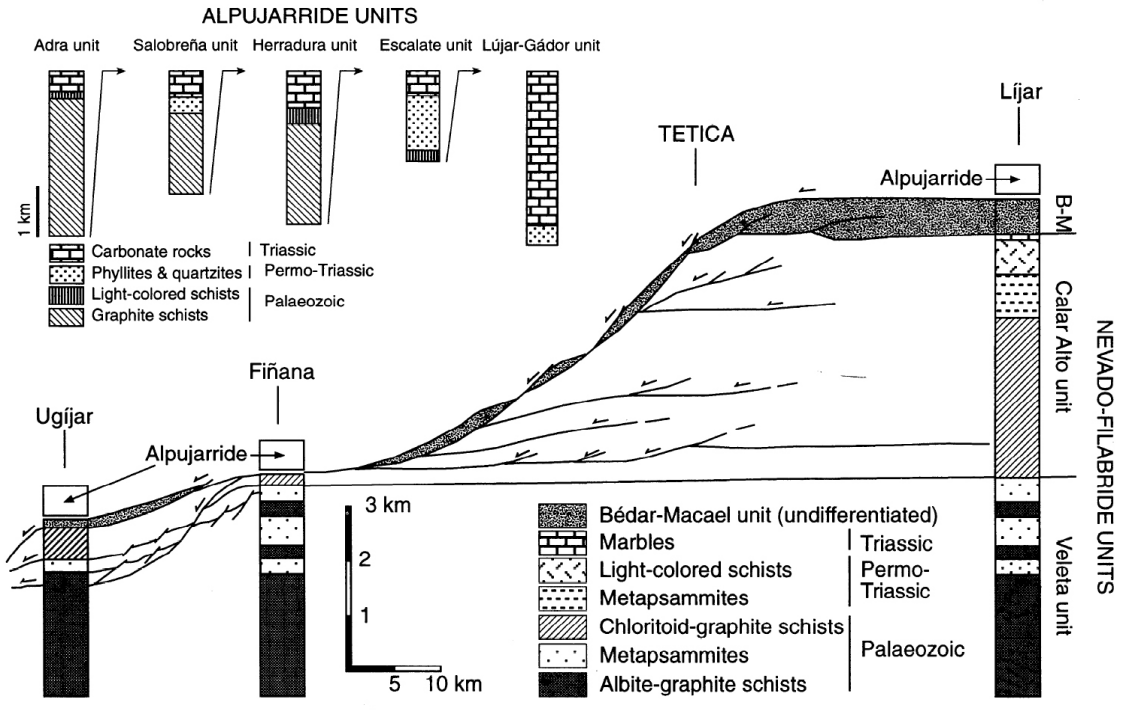

Fig. 4: Nevado–Filabride tectono stratigraphic columns beneath the detachment surface at the base of the Alpujarrides. Standard lithostratigraphic columns in the different Alpujarride units are also shown. Figure from Martínez-Martínez and Azañón (1997).

formation) with orthogneisses derived from late Carboniferous granites, light-colored schist derived from Permo–Triasic pelites (Tahal formation), and marble and meta-evaporites of Triassic protholith. Serpentinites and metamorphosed Jurassic metabasites are also included. This unit underwent variable metamorphic conditions from eclogites to greenschist facies. In the study area only the Tahal formation of the Calar–Alto unit is missing. The Bédar–Macael unit includes staurolitestaurolite graphite mica-schist, tourmaline gneiss, light-colored schist, serpentinite, amphibolites, and marbles *(Martínez-Martínez et al., 2004)*. Available thermobarometric data indicate a metamorphic thermal peak of 550 ºC and over 12 kbar for the Bédar–Macael unit *(Bakker et al., 1989; Soto, 1991)*. The Calar–Alto unit eclogites and serpentinites reached higher pressure of up to 2.0 Gpa and temperature above 600ºC, however, the exhumation P–T path evolved under lower temperature conditions (450 ºC, *Martínez-Martínez, 1986; Soto, 1991; González-Casado et al., 1995; Platt et al., 2006; Padrón-Navarta et al., 2011*). Although the metamorphic evolution of the Ragua unit is not well constrained, the unit was metamorphosed under greenschist and albite-epidote amphibolites metamorphic conditions (<450 ºC) and is assumed to have lower pressure conditions than the other two overlying units *(Martínez-Martínez, 1986; de Jong, 1993; Puga et al., 2002)*. More recent data indicate HP–LT metamorphic conditions of 320º-450 ºC and 1.2-1.6 GPa for the Ragua and Calar–Alto units from graphite schists *(Booth-Rea et al., 2003b, 2004b; Augier et al., 2005; Booth-Rea et al., 2005)*.

The Alpujarride complex comprises three major tectonic units in the study area, in ascending order, the Lower unit *(Martínez-Martínez and Azañón, 1997)*, Intermediate unit (Variegato unit, *Booth-Rea et al., 2005*) and the Upper unit (Fig. 5). These units crop out mostly in the core of antiformal ridges in the southeastern Betics (e.g. the Sierra de los Filabres, Sierra Cabrera, Sierra Almagrera and Sierra de Almagro) bounded by extensional ductile and brittle shear zones. The Lower unit is formed by a medium-grade metamorphic tectonostratigraphic sequence that includes, from bottom to top, calcite-dolomite marbles, kyanite phyllites and quartzites, light-colored chloritoid-garnet schists, and sturolite-kyanite-garnet graphite schists. This unit is overturned, as indicated by an inverted metamorphic zonation and age, that is Triassic for the marbles and Palaeozoic for the graphite schists *(Platt et al., 1983; Martínez-Martínez and Azañón, 1997)*. This unit has been correlated to the Herradura unit in the central Betics *(Azañón et al., 1994; Martínez-Martínez and Azañón, 1997)*. The Intermediate unit corresponds to the low-grade metamorphic Variegato unit defined by *Simon (1963)* and revised by *Booth-Rea et al. (2005)*. This unit comprises at least three second-order imbrications: the two lowest are formed by fine-grained schists of Permo–Triassic age and by Triassic carbonate rocks, and the structurally highest one also includes graphite schists at its base with garnet and biotite. The Upper unit only crops out locally between segments of the Carboneras fault in Sierra Cabrera. It is formed by K-feldespar gneises, sillimanite schist that gradually pass to lower-grade metapelites and then to metapelites with staurolite, garnet, andalusite and chloritoid. The staurolite schists usually show

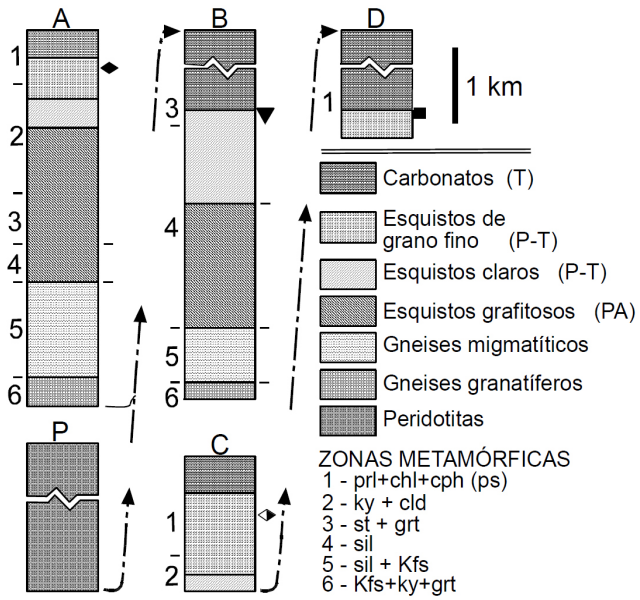

Metamorfismo bajo gradiente (evento 1)

Unidad	Roca	Paragenesis	kbar	ºC
◆ A	Esquistos grano fino	cph+ky ky+cld+chl	10	440
▼ B	Esquistos claros	grt+ky+pl	11	570
◆ C	Esquistos grano fino	cph+prl+chl	8	400
■ D	Esquistos grano fino	sud+prl+chl	<7	340

Metamorfismo de gradiente intermedio (evento 2)

Unidad	Roca	Paragenesis	ºC
▼ B	Esquistos grano fino	sil+st+ky+grt	>550
☆ A,B	Esquistos oscuros	sil+st+ky+grt	>550
★ A,B	gneis migmatítico	sil+Kfs	>550
▲ A,B	gneis granatífero	ky+cpx+opx+grt	>700

Fig. 5: Lithological sequences and metamorphic zonation of the Alpujarride Units cropping out in the central and eastern Betics, with their position in the Alpujarride nappe and the mineralogical paragenesis used for their distinction. Figure from Balanyá et al. (1998).

kyanite relicts that disappear upwards *(García-Casco et al., 1993; García-Casco and Torrés-Roldán, 1999)*.

The Malaguide complex in the study area comprises a Lower Malaguide unit that underwent low-grade metamorphism (anchizonal) during the Alpine orogeny, and the non-metamorphosed post-Triassic sedimentary cover *(Lonergan, 1993; Lonergan and Mangerajetzky, 1994; Nieto et al., 1994; Lonergan and Platt, 1995)*. The Lower Malaguide unit comprises several imbricate thrust sheets formed by, from bottom to top, Permo–Triassic quartz-pelitic rocks (red quartzite, red slate, micro-conglomerates and some gypsum levels) and Triassic carbonate rocks (calc-phyllite, massive black dolomites, gypsum, tabular dolomites and limestone). The post-Triassic sedimentary rocks comprise conglomerates and limestones of Palaeogene age resulted from the exhumation and dismantlement of the Malaguide complex.

4.2 Neogene to Quaternary sedimentary rocks of the study area (Sorbas–Tabernas and Níjar basins)

4.2.1 Pre-Tortonian (Burdigalian–Serravallian) sedimentary units

The older sediments in the Sorbas–Tabernas and Níjar basins are early to middle Miocene in age (Fig. 6, Burdigalian–Serravallian). The lower Burdigalian unit is formed by pelagic limestone, marly limestone and marls of pelagic facies that became shallower upwards of Burdigalian age. In ascending order, red conglomerates, sandstones with echinoderm and lamellibranchia, platform limestones, turbiditic marls, and continental conglomerates of late Burdigalian to Langhian age overlay the previous unit. The middle Miocene sequence is capped by a Serravallian unit that includes several

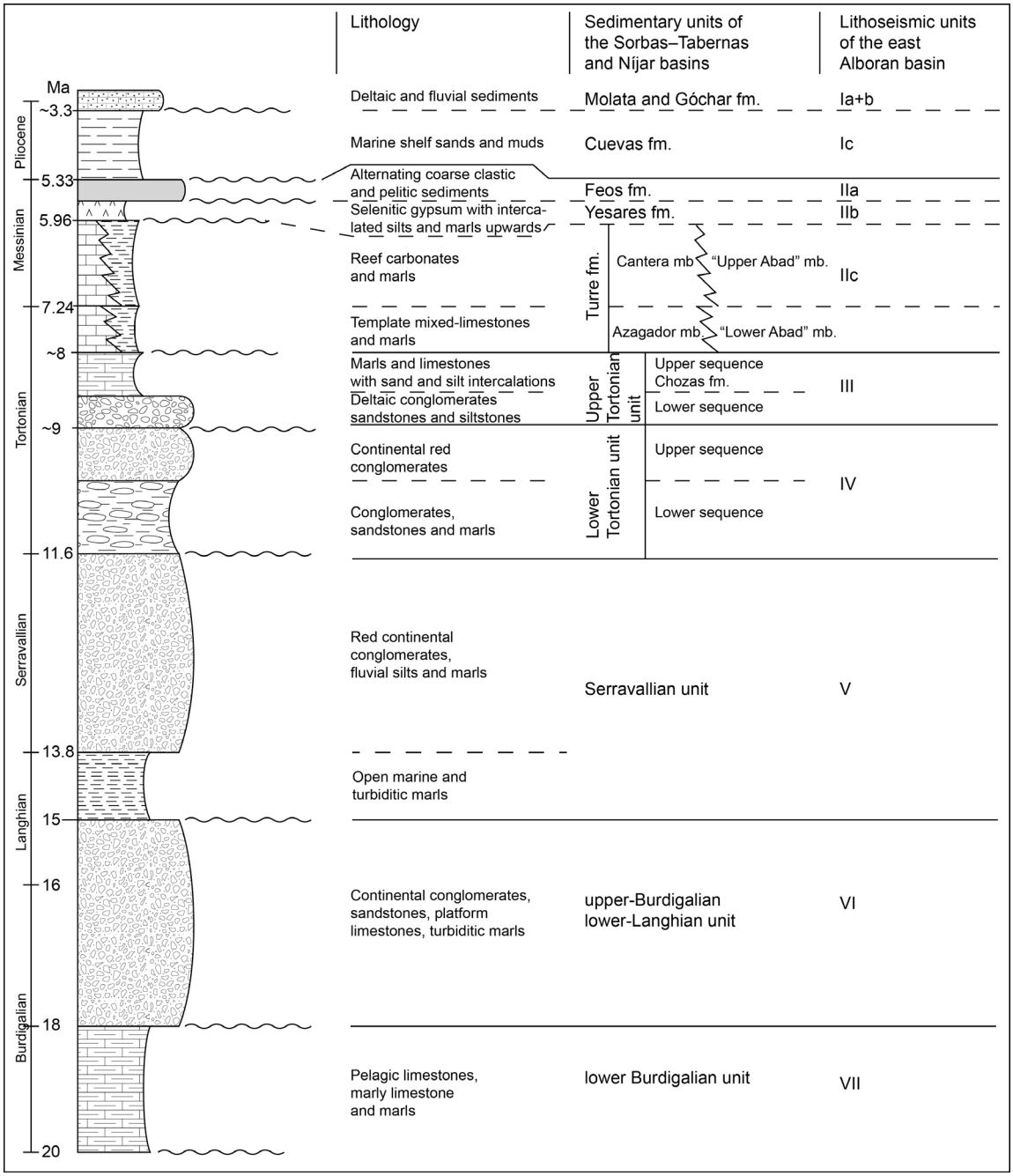

Fig. 6: Synthetic stratigraphic column of the Neogene–Quaternary sediments of the Sorbas-Tabernas and Níjar basins that were correlated with the lithoseismic units differentiated in the eastern Alborán following the seismo-stratigraphic correlation proposed by Booth-Rea et al. (2007).

facies from open marine turbiditic to continental conglomeratic with Alpujarride and Malaguide clasts *(Völk, 1966; Barragán, 1997; Booth-Rea et al., 2004a)*.

4.2.2 Tortonian sedimentary units

The lower Tortonian unit comprises two depositional sequences and is probably equivalent to lithoseismic unit IV in the east Alborán (Fig. 6). The lower sequence is formed by conglomerates, calcareous sandstones and marls deposited in transitional marine environments. The upper sequence is formed by red continental conglomerates with Nevado–Filabride boulders *(Barragán, 1997)*. The upper Tortonian unit is formed by two depositional sequences, the lower one defines an erosional angular unconformity on both sediments and metamorphic basement (intra-Tortonian unconformity),

whilst the upper one shows a sedimentary continuity with the previous one. This unit probably is equivalent to lithoseismic unit III in the east Alborán basin (Fig. 6). The first sequence comprises deltaic conglomerates with Nevado–Filabride boulders, sandstones and siltstones of transitional and marine facies. The second is formed by marls and limestones with sand and silt intercalations of the Chozas formation (Fig. 6, *Ruegg, 1964*).

4.2.3 Messinian sedimentary units

The Messinian sedimentary units comprise, from bottom to top, the pre Messinian salinity crisis Turre formation (latemost Tortonian–early Messinian), the evaporitic Yesares formation (Messinian) and finally the post crisis Feos formation (Figs. 6 and 7, late Messinian). All these units are probably equivalent to lihoseismic unit II in the east Alborán basin (Fig. 6). The Turre formation (~lithoseismic subunit IIc) is formed by the Azagador, the Cantera and Abad members (Figs. 6 and 7). The latemost Tortonian temperate carbonates of the Azagador member (8-7.24 Ma; *Völk, 1966; Martín et al., 2003*) are composed of bioclastic calcarenites and sandstones, locally mixed with conglomerates, with abundant bryozoans, bivalves, coralline algae and benthic foraminifera, and minor brachiopods, solitary corals, barnacles and gastropods *(Wood, 1966)*. The Azagador member shows progressive unconformities related both to the initial growth of the Sierra Alhamilla–Polopos and Cabrera anticlinoria *(Alvado, 1986; Ott d'Estevou and Montenant, 1990; Booth-Rea et al., 2004a)* and to Tortonian SW-directed extension at the western termination of Sierra Cabrera *(Giaconia et al., 2013b)*. The distal equivalent of the Azagador member are the open marine marls of the "Lower Abad" member that are characterized by a cyclic pattern of alternating whitish marly chalks and beige marls *(Fortuin and Krijgsman, 2003)* intercalated with diatomites and contain abundant calcareous nanoplankton and planktonic foraminifera of Messinian age *(Sierro et al., 2001)*.

Messinian reef carbonates of the Cantera member overlie the Tortonian sediments (7.24-5.96 Ma; *Völk, 1966; Sierro et al., 2001*) sealing part of the folding in the Sierra Alhamilla *(Weijermars et al., 1985)*, although they themselves define an open fold. This member is composed of tropical platform carbonates, locally mixed with siliciclastics, that pass upward to prograding fringing reefs composed of corals encrusted by stromatolites *(Braga et al., 1996)*. The top of these reefs is an erosional surface with signs of subareal exposure.

The distal equivalent of the Cantera member are the Messinian marls of the "Upper Abad" member that confirm the open marine conditions in the then connected Níjar and Sorbas–Tabernas basins until the occurrence of the Messinian salinity crisis *(Hsü et al., 1973, 1977)*. The "Upper Abad" member deposited during increasing restriction of marine conditions and includes sapropelitic laminites, marls and chalks that mark an upward shoaling *(Fortuin and Krijgsman, 2003)*.

The Messinian evaporites of the Yesares formation (~lithoseismic subunit IIb, Fig. 6) deposited in both the Níjar and Sorbas–Tabernas basins over the basin-scale Messinian erosional unconformity at the top of both Cantera and Abad members (5.96-5.67 Ma; *Martín and Braga, 1994; Krijgsman et al., 2001*). The Yesares formation predominantly consists of selenitic gypsum that are intercalated upwards with beds of marine silts and marls containing benthic and planktonic foraminifera of Messinian age *(Riding et al., 1998)*. At the final stage of the crisis, during the late Messinian, basin differential uplift closed the connection between the two basins producing different lithostratigraphic sequences since then *(Braga et al., 2003; Booth-Rea et al., 2005)*. In the Níjar basin the marine environment was restored during the late Messinian as confirmed by the Lago Mare facies sediments of the Feos formation (5.67-5.33 Ma; *Fortuin and Krijgsman, 2003*). This formation (~lithoseismic subunit IIa, Fig. 6) is formed by alternating coarse clastic and pelitic sediments reflecting strongly fluctuating environmental conditions during its deposition *(Fortuin and Krijgsman, 2003)*. The Miocene–Pliocene boundary is an erosive unconformity in the marginal part of the basin *(Aguirre and Sánchez-Almazo, 2004)*, whereas in the basin center, it is characterized by a conformable, bioturbated contact *(Fortuin and Krijgsman, 2003)*.

The post-evaporitic Feos formation (~lithoseismic subunit IIa, Fig. 6) is subdivided, from bottom to top, in the Sorbas and Zorreras members in the Sorbas basin (Fig. 7). The costal sequence of the Sorbas member is formed by whitish coated to entirely oolithic sandstones, siliciclastic sands and conglomerates, with local oolitic carbonates and coral patch reefs, changing basinwards to silts and marls *(Martín et al., 1993; Fortuin and Krijgsman, 2003)*. The continental sequence of the Zorreras member contains only two brackish Lago Mare incursions (lacustrine limestones containing a so-called caspibrackish fauna) on a total of eight sedimentary cycles of alternating reddish silts and yellowish sands that correlates very well with the eight sedimentary cycles of the Feos formation in the Níjar basin *(Krijgsman et al., 2001; Fortuin and Krijgsman, 2003)*. Thus, since the late Messinian the Sorbas–Tabernas basin had emerged.

4.2.4 Pliocene sedimentary units

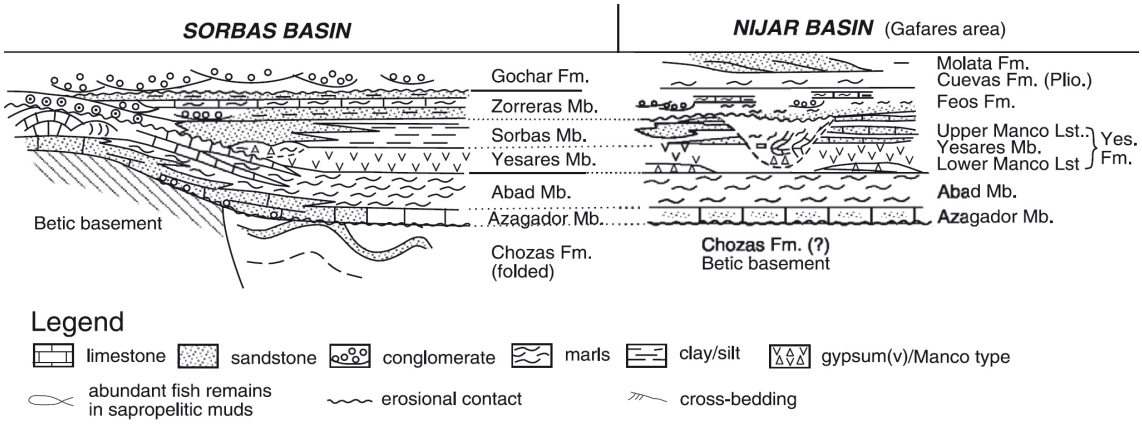

Fig. 7: Lithostratigraphic overview of the Messinian–Pliocene successions in the northern Nijar Basin (Gafares area) and correlation with the (partly equivalent) units in the Sorbas Basin. Figure from Fortuin and Krijgsman (2003).

Marine conditions persisted longer in the Níjar basin, between the early Pliocene when marine shelf sands and muds of the Cuevas formation deposited (~lithoseismic subunit Ic), and the beginning of the late Pliocene, as inferred by the fan delta deposits of the Molata formation (~lithoseismic subunit Ib, Fig. 6) *(Mather, 1993; Stokes and Mather, 2000)*. In contrast, the late Pliocene aggrading fluvial sediments of the Góchar formation (~lithoseismic subunit Ib) confirms the final emersion of the Sorbas–Tabernas basin until present (Fig. 6, *Mather, 1993; Aguirre, 1998*).

4.3 Quaternary fluvial terraces and drainage pattern evolution of the study area (Sorbas–Tabernas and Níjar basins)

During the early Pleistocene the Sorbas drainage was centripetal toward the Lobos axial system in the basin center, meanwhile, southwards the drainage system incised through the Sierra Alhamilla–Polopos and Cabrera anticlinoria *(Mather, 2000b)*. This system drained the Sorbas–Tabernas basin into the Alias river in the Níjar basin by means of the Rambla de los Feos that connected both basins (Fig. 8, *Harvey and Wells, 1987; Mather, 2000b; Maher et al., 2007*). This connection is inferred by the alluvial sediments from the base of the Góchar formation that feed the late Pliocene (3.2 Ma, *Aguirre, 1998*) fan deltas of the Molata formation *(Mather, 1993)* southwards across the Sierra Alhamilla–Polopos and Cabrera anticlinoria. During the late Pliocene and the early Pleistocene a continuous alluvial aggradational system developed in the Sorbas basin.

Since the middle Pleistocene onward repeated river incision episodes and strath-terrace development spread out in the Sorbas basin mainly triggered by changes in

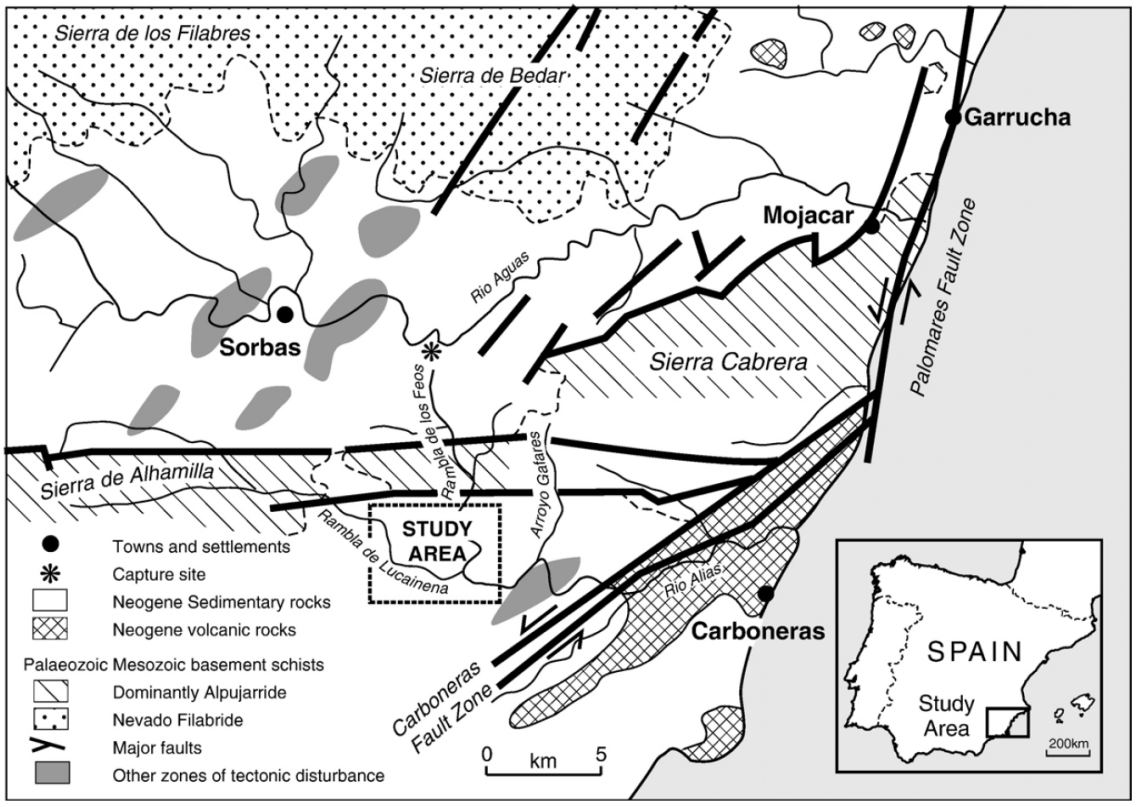

Fig. 8: Simplified geological scheme and drainage system of the southeastern Betics. Figure from Maher et al. (2007).

regional gradients associated to sustained early Pliocene–Quaternary uplift in the region *(Harvey and Wells, 1987; Mather, 1993; Braga et al., 2003)*. Five tearraces (A-E) have been defined in the area from previous authors *(Harvey and Wells, 1987; Mather, 1993; Maher et al., 2007; Whitfield and Harvey, 2012)*. Terraces A-C overly unconformably the Neogene basin fill sediments and basement rocks whilst the base of the aggradational event linked to terrace D is below the level of the modern channel (Fig. 9). Terrace E is an extremely patchy remnant throughout the area often associated with the modern floodplain. Fluvial conglomerates associated with terraces A-C are usually well-cemented both by pedogenically-derived carbonate and groundwater-borne carbonate, whilst the younger terrace deposits (D-E) have very little, if any, cementation developed. Terraces A-C are mainly sourced by the Sierra de los Filabres metamorphic rocks, including marbles, granitic gneiss and amphibole schists, and to a lesser extent by Neogene basin fill sediments, evaporitic gypsum and Góchar formation conglomerates. In contrast terrace E-D are mainly sourced by the Sierra Alhamilla and Cabrera low grade metamorphic rocks, including graphite mica schists with small amounts of garnet mica schist, metacarbonates and vein quartz, and the Neogene basin fill sediments that comprises marl, calcareous sandstone, dolomitic and reef limestones, and subordinately gypsum *(Harvey and Wells, 1987; Mather, 1993; Maher et al., 2007)*.

The highest and oldest terrace A is formed by heavily cemented channelized fluvial gravels that are poorly preserved in the area. This terrace marks the aggradational-incision transition in the basin and has been dated at 304 ± 26 ka, although it should be older than 400 ka since the dated calcretes at the top of the terraces formed post

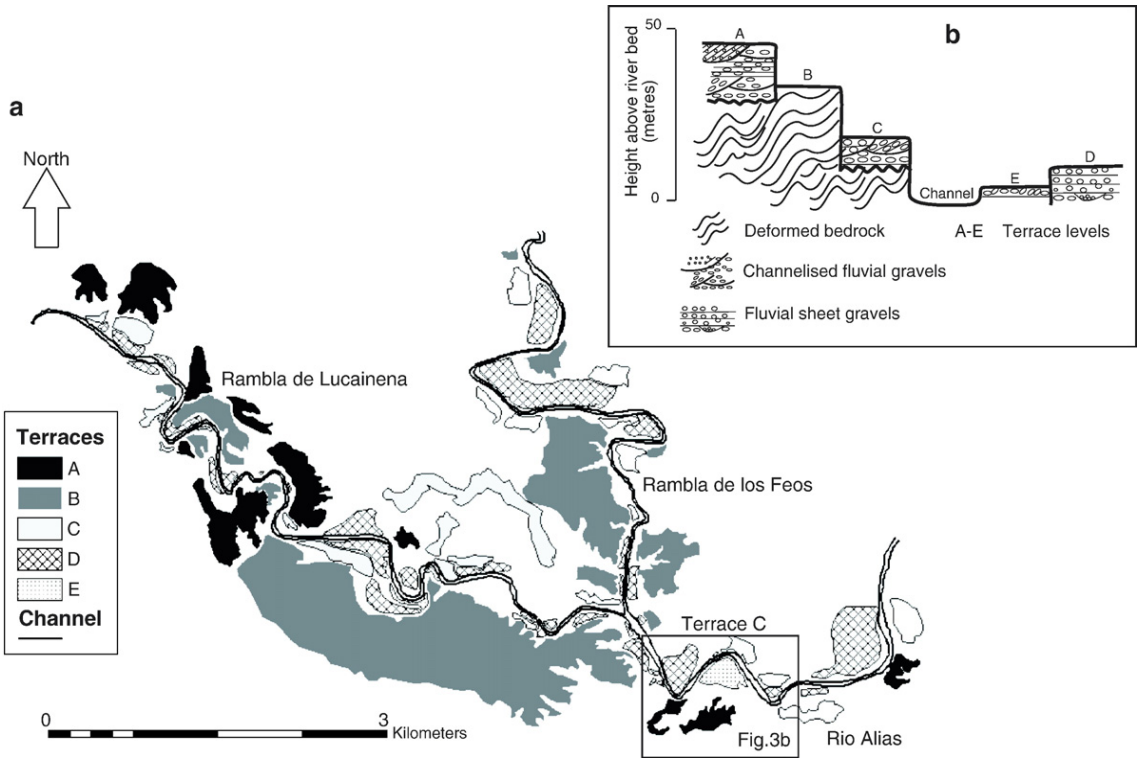

Fig. 9: a) Map of fluvially derived terraces on the Rio Alias, Rambla de los Feos and the Rambla Lucainena. b) Idealised terrace cross section on the Rio Alias immediately downstream of the Feos junction. Figure from Maher et al. (2007).

abandonment of the surfaces *(Candy et al., 2005; Candy and Black, 2009)*. These river terraces post date the first capture operated by the Alias river in the middle Pleistocene. This capture re-routed 15% of the original Sorbas basin drainage into the Alias river drainage basin (Níjar basin) to the south through the Rambla de Lucainena *(Mather, 2000a, 2000b)*. This capture isolated the northeastern mountain front area of Sierra Alhamilla from the Sorbas basin forming the Rambla de Lucainena.

Post-capture terrace B is formed by cemented coarse fluvial gravels with channel structures that usually overlie the metamorphic basement culminating with carbonate-accumulating red soils dated at 207± 11 ka *(Candy et al., 2005; Whitfield and Harvey, 2012)*. Terrace C deposits contain planar cross-stratified conglomerates, horizontally stratified conglomerates (and subordinate sands) and large palaeo-channel structures. The conglomerates are texturally mature (rounded clasts) and the amphibole schist amount reaches the 15% of the total clast assemblage. Preserved calcretes on terrace C show an higher degree of rubification and pedogenic carbonate accumulation compared with the terrace D ones *(Maher et al., 2007)*. Terrace C calcretes have been dated at 77 ± 4 ka *(Candy et al., 2005)*.

The second capture operated by the Aguas river occurred in the late Pleistocene (≈ 70 ka) re-routing 73% of the original Sorbas basin drainage into the Vera basin to the east. This capture disconnected the Rambla de los Feos from the Sorbas basin and expanded the area of the Aguas river drainage system (capture site in Fig. 9, *Mather, 2000b; Maher et al., 2007*). Terrace D, dated between 12.8 ± 1 ka to 8.7 ± 0.5 ka *(Candy et al., 2005)*, provides evidence of source material and a sedimentary environment shift inferring and postdating the late Pleistocene capture. Terrace D deposits are formed by dominant sheet gravel beds alternating with horizontally laminated sands and silts. Small channels are associated with limited amounts of planar cross-stratification or massive sand plugs. These deposits are texturally fairly mature (clasts varying between sub-angular and rounded) indicating that a significant proportion of the sediments have travelled only short distances. The amphibole schist amount is lower than 2% of the total clast assemblage, thus indicating a dramatic loss of source material with respect to the terrace C. Terraces D culminates with immature brown soils with little if any carbonate development *(Maher et al., 2007)*. The modern terrace E is formed by horizontally laminated silts and sands with dispersed flattened fine clasts. The essential source material of these deposits is formed by the graphite schists that confer the characteristic dark appearance to terrace E.

5.0 Methodology

In this chapter I describe the methodology adopted for the development of the thesis research objectives. Since these aims involve various geologic disciplines I carried out a multidisciplinary approach mainly founded on the integration of different data sets. I employed structural field- and morphometry GIS-based methods and tools in order to

define the kinematics and timing of recent to present tectonic structures and their control on the landscape, respectively. Furthermore, I processed two deep seismic reflection lines acquire during the TOPOMED seismic survey at the BCSI (Barcelona Center for Subsurface Imaging).

5.1 Structural field-based methods and tools

We collected structural data and mapped the main fault segments, obtaining geological cross-sections with the aid of drill holes and electrical tomography in order to define the kinematics, fault linkage and growth evolution of the Polopos fault zone. Furthermore, I calculated net and vertical fault slips and displacement rates taking into account the elevation differences of geological or geomorphic surfaces across fault segments, their age, the fault plane orientation and the slickenlines (fault displacement vector). I inverted the slip structural data (using the DAISY3 software, *Salvini et al., 1999*) in order to define the strain orientation along the fault system and to verify its congruence with the present stress field (obtained from GPS geodetic displacement data, earthquake focal mechanisms, borehole deformation available in the area). Finally, we mapped the present geomorphic elements (e.g. fluvial terraces, alluvial fans and mountain fronts) to define qualitatively the influence of these tectonic structures on the landscape (e.g. topography and the drainage system).

5.2 Morphometry GIS-based methods and tools

I carried out both qualitative and quantitative geomorphic analyses using geomorphic indices to define and quantify the tectonic control on the geomorphic process and the landscape evolution. The qualitative analyses are focused on topographic profiles, longitudinal river profiles, ridge-line profiles (Fig. 10a), pattern of the drainage network, spatial distribution of drainage basins and their geometric relationships *(Ouchi, 1985; Whipple and Tucker, 1999; Azor et al., 2002; van der Beek et al., 2002; Wegmann and Pazzaglia, 2002; Clark et al., 2004; Zhang et al., 2004; Korup, 2006)*. The quantitative geomorphic analyses were conducted using geomorphic indices that allow characterizing quantitatively the geomorphic features of a landscape to evaluate its relative level of tectonic activity *(Seeber and Gornitz, 1983; Brookfield, 1998; Keller and Pinter, 2002; Chen et al., 2003; Kobor and Roering, 2004)*. Thus, the final aim of this kind of analyses is to describe a landscape and possibly associate a set of geomorphic features to a detected tectonic structure or other geologic control factors (e.g. erodibility contrasts, capture processes or sea-level changes).

The quantitative analyses were conducted calculating the following geomorphic indices: mountain-front sinuosity (S_{mf}, Fig. 10b), valley floor width-to-height ratio (V_f, Fig. 10c), drainage basin asymmetry factor (Fig. 10d), basin hypsometric curve and integral

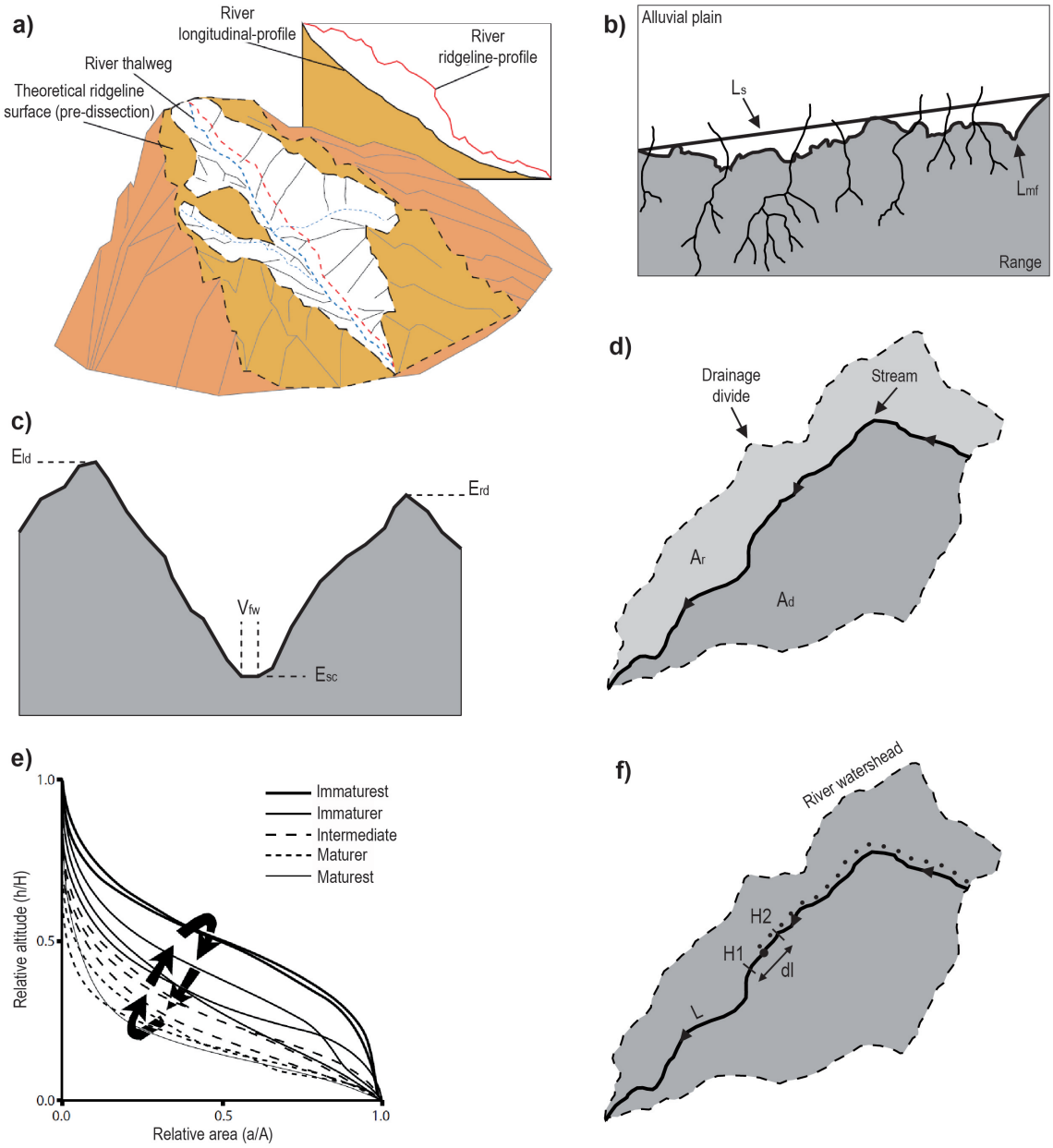

Fig. 10: Synthetic scheme of the geomorphic used in this thesis: a) stream and ridge-line profiles, b) the mountain-front sinuosity (S_{mf}), c) the valley floor width-to-height ratio (V_f), d) the drainage basin asymmetry factor, e) basin hypsometric curve and integral, f) and the stream-length gradient index normalized by the graded river gradient (SLk index).

(Fig. 10e), and stream-length gradient index (Fig. 10f) normalized by the graded river gradient (*SLk* index). Further details of the morphometry GIS-based methodology are explained in the Chapter 7.

5.3 Seismic data processing flow

I processed two deep seismic reflection lines in order to explore how the studied tectonic structures continue offshore and, overall, to redefine tectonically the Palomares margin and the southeastern Betics in the wider context of the tectonic inversion of the westernmost Mediterranean. I employed a typical seismic data processing flow of the deep seismic reflection lines that included the following steps (Fig. 11a): data quality control to verify the continuity of the seismic imaging; definition of the line geometry and shots-to-CMP conversion (Fig. 11b) to obtain the first stack; velocity analysis to

achieve a velocity model congruent with the geologic and structural features imaged by the first stack (useful for the Normal Moveout Correction, Fig. 11c); compensation of the spherical divergence to correct the amplitude loss in depth (Fig. 11d); picking of the external and internal "mutes" in order to remove the non acceptable seismic energy (Fig. 11e); predictive deconvolution to suppress multiple reflections (Fig. 11f); pre-stack Radon and symmetric FK filters in order to remove the dipping and flat multiples; time migration to move dipping reflections to a more correct location (Fig. 11g) and space conversion to obtain a more correct geological interpretation of the deep seismic reflection lines. Further details of the seismic data processing flow are explained in the Chapter 10.

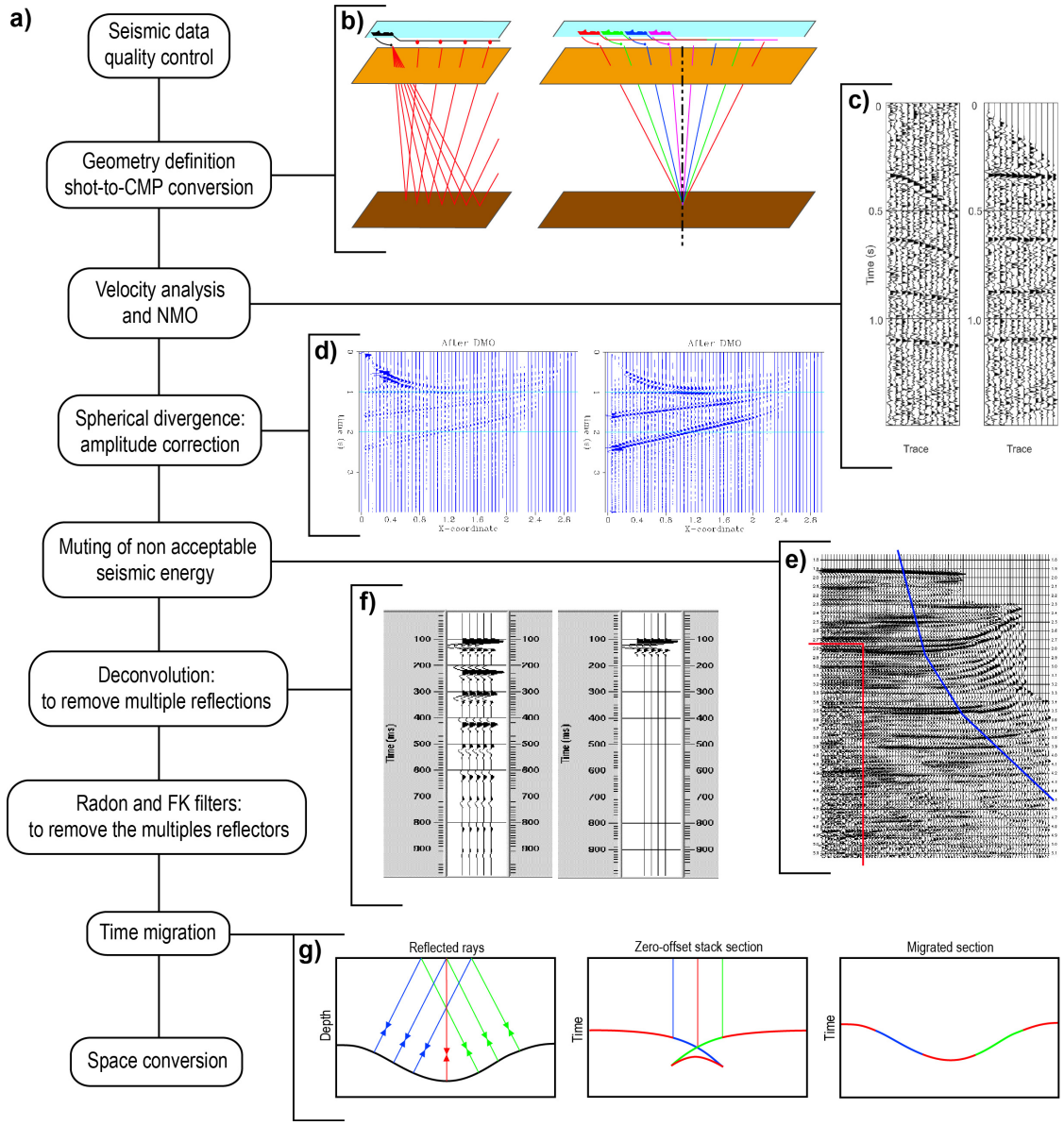

Fig. 11: a) Synthetic scheme of the processing flow applied on the multichannel reflection seismic data in this thesis: b) definition of the line geometry for the shots-to-CMP conversion, c) Normal Moveout Correction of the CMP gathers for the stack, d) compensation of the spherical divergence to correct the amplitude loss in depth, e) external and internal "mutes" to remove the non acceptable seismic energy, f) predictive deconvolution to suppress multiple reflections, g) and time migration to move dipping reflections to a more correct location.

Part II – Results

Paper in preparation for the Journal of Structural Geology

6.0 Heterogeneous extension and the role of transfer faults in the development of the southeastern Betic basins (SE Spain)

F. Giaconia [a, *], G. Booth-Rea [a], J.M. Martínez-Martínez [a], J.M. Azañón [a], F. Storti [b], A. Artoni [b]

[a] Dpto. Geodinámica, Instituto Andaluz de Ciencias de la Tierra (CSIC-UGR), Campus Fuentenueva S/N, 18002, Granada, Spain
[b] Dipartimento di Fisica e Scienze della Terra "Macedonio Melloni", Università degli Studi di Parma, Campus Universitario, Parco Area delle Scienze 157/A, 43124, Parma, Italy
[*] Corresponding author. E-mail address: flavio@ugr.es, flavio@iact.ugr-csic.es (F. Giaconia)

Abstract: The north Cabrera dextral fault and other E–W to NE–SW strike-slip faults active during the Serravallian to Tortonian in the Sorbas basin were transfer faults produced under SW–NE extension. These transfer faults, together with related normal faults form the main boundaries of two sedimentary depocenters active between the middle Miocene and the Tortonian. The older, north Cabrera depocenter, was active between the Serravallian and the lower Tortonian (approx. 13.8 to 9 Ma), whilst the younger Gacía depocenter formed in response to a new extensional pulse during the Tortonian, between 9 to 7.5 Ma. The Gacía depocenter formed to the west of the north Cabrera depocenter by the development of a listric fan of normal faults with SW-directed transport that detach on a low-angle detachment. A balanced cross-section across the Gacía depocenter shows that the detachment cuts into the Nevado–Filabride complex at approximately 0.8 km depth tilting a previous extensional detachment between the Alpujarride and Nevado–Filabride complexes. This extension was temporal and kinematically linked to sinistral displacement along the Carboneras fault further south in the Níjar basin. Westward-directed heterogeneous extension in the region produced elongated core-complexes and tilted-blocks to the north of the Carboneras fault and magmatic accretion upon thinned continental crust to the south. This extension and magmatism represents the superficial manifestation of the rupture of the Tethyan slab and associated edge delamination along a lithospheric transform fault beneath the northern branch of the Betic–Rif orogen.

Keywords: strike-slip fault, extensional tectonics, SE Betics, Carboneras fault zone, delamination

6.1 Introduction

Strike-slip faults can be found in all tectonic settings, developed in transcurrent tectonic regimes as dynamic structures or in both compressional and extensional regimes as transfer and transform faults that are kinematic structures formed in response to deformation heterogeneities among fault segments *(e.g. Dahlstro, 1970; Gibbs, 1984; Sylvester, 1988; Martínez-Martínez et al., 2006)*. The fundamental difference between these faults is that transcurrent faults strike obliquely to the principal regional stress axes (normally ~30º), whereas transfer faults are subparallel to the direction of shortening or extension. Furthermore, transfer faults can show variable transport sense and amount of slip along them, depending on the kinematics of the faults that they link *(e.g. Duebendorfer and Black, 1992; Faulds and Varga, 1998; Martínez-Martínez et al., 2006)*. Transfer faults in extensional regime are transverse structures that link spatially separated loci of extension. They show "hard linkage" with the faults they connect, allowing slip to be transferred *(Walsh and Watterson, 1991; McClay and Khalil, 1998; Martínez-Martínez et al., 2006)*.

The tectonic evolution of the eastern Betics has been strongly influenced by strike-slip tectonics during the middle–late Miocene to present. The main eastern Betic Neogene–Quaternary basins occur in synclines among E/W- to ENE/WSW-elongated antiformal ridges that are related to or cut by large-scale transcurrent faults like the Palomares, Terreros and Alhama de Murcia sinistral faults or the Polopos dextral fault *(e.g. Bousquet and Montenat, 1974; Ott d´Estevou and Montenat, 1985; Hernandez et al., 1987; Weijermars, 1987; Larouzière et al., 1988; Coppier et al., 1990; Montenat and Ott d´Estevou, 1990; Martínez-Díaz, 2002; Booth-Rea et al., 2004a; Masana et al., 2004)*. These faults formed in response to NW–SE convergence between Africa and Iberia. Moreover, large strike-slip faults occur parallel to the folds axes, bounding the margins of some of the main basins, like the Alpujarras fault or or the Cantona and North Cabrera the strike-slip faults described in the southern margin of the Sorbas, Tabernas and Vera basins *(Sanz de Galdeano et al., 1985; Sanz de Galdeano, 1987; Rodriguez-Fernandez et al., 1990; Haughton, 2001; Hodgson and Haughton, 2004; Martínez-Martínez, 2006; Martínez-Martínez et al., 2006)*. Thus, most literature in the area has related the development and evolution of the southeastern Betic Neogene–Quaternary basins in a transcurrent tectonic setting. However, other works have shown the great importance of extensional tectonics in the development and evolution of these basins during the Miocene *(Platt and Vissers, 1989; Martínez-Martínez and Azañón, 1997; Martínez-Martínez et al., 2002; Booth-Rea et al., 2005)*. Furthermore, the transcurrent model for the development of the eastern Betic basins fails to explain the exhumation of early to middle Miocene HP rocks in the core of all the outcropping basement highs *(e.g. López Sánchez-Vizcaíno et al., 2001; Platt et al., 2006; Behr and Platt, 2012)*.

In order to differentiate between transcurrent and transfer faults, and to define their

role in the origin and evolution of the southeastern Betic basins during late Miocene extensional tectonics, we have carefully mapped a key area in the Sorbas basin where a set of dextral transcurrent faults have been described previously *(e.g. Sanz de Galdeano, 1987; Montenat and Ott d´Estevou, 1990; Stapel et al., 1996; Huibregtse et al., 1998; Jonk and Biermann, 2002)*. We analyzed the age, segmentation, linking and crosscutting relationships between normal and strike-slip fault segments, differentiating between transfer and transcurrent faults in the area. Later, we analyzed the geometry of the main middle and late Miocene sedimentary depocenters in the area and their relations to the mapped faults. Finally, we constructed a balanced cross section transversely to the main Tortonian sedimentary depocenter with the aid of drill holes and electrical tomography to evaluate the importance of late Tortonian extension in the development of the Sorbas basin and its significance in the evolution of the eastern Betic basins.

6.2 Structural framework

The Betics and Rif together with the Gulf of Cádiz accretionary wedge form the Gibraltar Arc orogenic system that developed by combined subduction and oblique collision during the Alpine orogeny. Subduction of the Mesozoic oceanic crust of the Tethys Ocean occurred under the central areas of the arc during the early to late Miocene, whilst oblique collision of the Iberian and the North Maghrebian passive margins beneath the Alborán domain orogenic wedge occurred in the northern and southern branches of the Gibraltar Arc *(e.g. Balanyá and García-Dueñas, 1987; Martínez-Martínez and Azañón, 1997; Durand-Delga et al., 2000; Faccenna et al., 2004; Booth-Rea et al., 2005; Luján et al., 2006; Platt et al., 2006; Balanyá et al., 2007; Booth-Rea et al., 2007, 2012b)*. This subduction-collisional system comprises an accretionary wedge presently preserved in the Gulf of Cádiz *(e.g. Gutscher et al., 2001; Iribarren et al., 2007; Sallarès et al., 2011; Gutscher et al., 2012)*, a volcanic arc in the Eastern Alborán basin and a back-arc region coinciding with the Algero–Balearic basin *(e.g. Lonergan and White, 1997; Duggen et al., 2003, 2004a; Mauffret et al., 2004; Duggen et al., 2005; Booth-Rea et al., 2007)*. The mechanisms driving the tectonic evolution of the system have been strongly debated including mantle convective removal *(Platt and Vissers, 1989)*, slab rollback *(Lonergan and White, 1997)*, slab tearing or breakoff *(Zeck, 1996; Carminati et al., 1998; Zeck, 1999)*, lithospheric delamination *(García-Dueñas et al., 1992; Martínez-Martínez and Azañón, 1997; Faccenna et al., 2004; García-Castellanos and Villasenor, 2011)* or a combination of subduction beneath central areas of the Alborán basin and edge-delamination beneath the Betic–Rif margins *(Duggen et al., 2003; Martínez-Martínez et al., 2006; Booth-Rea et al., 2007, 2012b)*.

Thrusting and folding of the South–Iberian Mesozoic to Tertiary passive margin sedimentary cover in the external zone was coeval to extensional processes in the Betic

hinterland during the early–late Miocene. This extension resulted in the development of the Alborán and Algero–Balearic basins in the core of the orogeny, involving the formation of oceanic crust *(García-Dueñas et al., 1992; Comas et al., 1999; Mauffret et al., 2004; Booth-Rea et al., 2007; Pesquer et al., 2008)*. Extension started before the Burdigalian, when the Alpujarride metamorphic complex was denudated (19 Ma, *Lonergan and Johnson, 1998; Esteban et al., 2004*), and continued through the Serravallian (13.6 Ma) until the present, when the Nevado–Filabride metamorphic complex was exhumed *(Johnson et al., 1997; Martínez-Martínez et al., 2002, 2006)*. The main extension occurred along WSW-directed core-complex detachments that exhumed HP metamorphic rocks of the Nevado–Filabride complex and markedly attenuated the previous metamorphic nappe stack *(García-Dueñas and Martínez-Martínez, 1988; Galindo-Zaldívar et al., 1989; Platt and Vissers, 1989; García-Dueñas et al., 1992; Martínez-Martínez and Azañón, 1997; Martínez-Martínez et al., 1997; Booth-Rea et al., 2005)*. The SW-directed extensional exhumation of the Nevado–Filabride complex propagated westwards in the Sierra de Filabres and Sierra Nevada elongated domes *(Johnson et al., 1997)*. At the Sierra de Filabres, apatite fission tracks young from about 13-11.5 Ma to the east to 7-8 Ma to the west of the dome *(Johnson et al., 1997; Vázquez et al., 2011)*.

WSW-directed extension in the Betics and Rif belts was heterogeneous in style including core-complex structures like the Sierra Nevada elongated dome in the central Betics *(e.g. Martínez-Martínez et al., 2002, 2004; Negro et al., 2007; Booth-Rea et al., 2012b)* and upper crustal extension characterized by tilted block domains *(e.g. García-Dueñas et al., 1992; Martínez-Martínez and Azañón, 1997; Booth-Rea et al., 2003c, 2004c; Martínez-Martínez, 2006)*. Moreover, crustal thinning offshore at the east Alborán and Algero–Balearic basins was accommodated by magmatic accretion between the middle and late Miocene. These domains with different styles of extension were separated by extensional transfer faults like the ENE–WSW Alpujarras dextral fault in the central Betics *(Martínez-Martínez, 2006; Martínez-Martínez et al., 2006)* orthe sinistral NE –SW Carboneras fault in the eastern Betics *(Rutter et al., 2012)*.

The heterogeneity of the early–late Miocene extension in the Betics includes changes in direction of extension both in time and space. Extension started with a N–S displacement during the early Miocene and continued with a W to SW displacementfrom the middle Miocene until present in the central Betics *(e.g. García-Dueñas et al., 1992; Martínez-Martínez et al., 2002)*. Meanwhile, SE-directed extensional faults like the Almenara detachment contributed to the exhumation of the Nevado–Filabride complex in the eastern Betics during the late Miocene *(Booth-Rea et al., 2012a)*. Eastwards directed extension during the late Miocene also occurred east of the Alborán magmatic arc in the Algero–Balearic back-arc basin *(Booth-Rea et al., 2007)*.

Many basins developed on the hanging-walls of the extensional system that showed

marine continuity with the Alborán and Algero–Balearic basins during the late Miocene *(Platt and Behrmann, 1986; Galindo-Zaldívar et al., 1989; Platt and Vissers, 1989; García-Dueñas et al., 1992; Lonergan and Platt, 1995; Martínez-Martínez and Azañón, 1997; Comas et al., 1999; Martínez-Martínez et al., 2002; Booth-Rea et al., 2005)*. The Granada and Guadix–Baza basins are examples from the western and central Betics of sedimentary basins produced by extensional tectonics during the late Miocene to Quaternary (*Fernández et al., 1996; Azañón et al., 2004a; Rodríguez-Fernández and Sanz de Galdeano, 2006; Azañón et al., 2007; Pedrera et al., 2007, 2009b; Pérez-Peña et al., 2009c; Fernández-Ibánez et al., 2010; Pérez-Peña et al., 2010*). Other examples are the Sorbas–Tabernas, Níjar–Carboneras and Vera basins in the eastern Betics that underwent important extension in their origin during the middle–late Miocene but were tectonically inverted in contraction since the late Miocene (Fig. 1, *Weijermars et al., 1985; Montenat and Ott d´Estevou, 1990; Booth-Rea et al., 2004a*). During the late Miocene to present tectonic inversion, both normal and transfer fault of the extensional system were reused as strike-slip faults or inverted as reverse faults depending on their orientation with respect to the stress field *(e.g. Martínez-Martínez, 2006; Meijninger and Vissers, 2006)*.

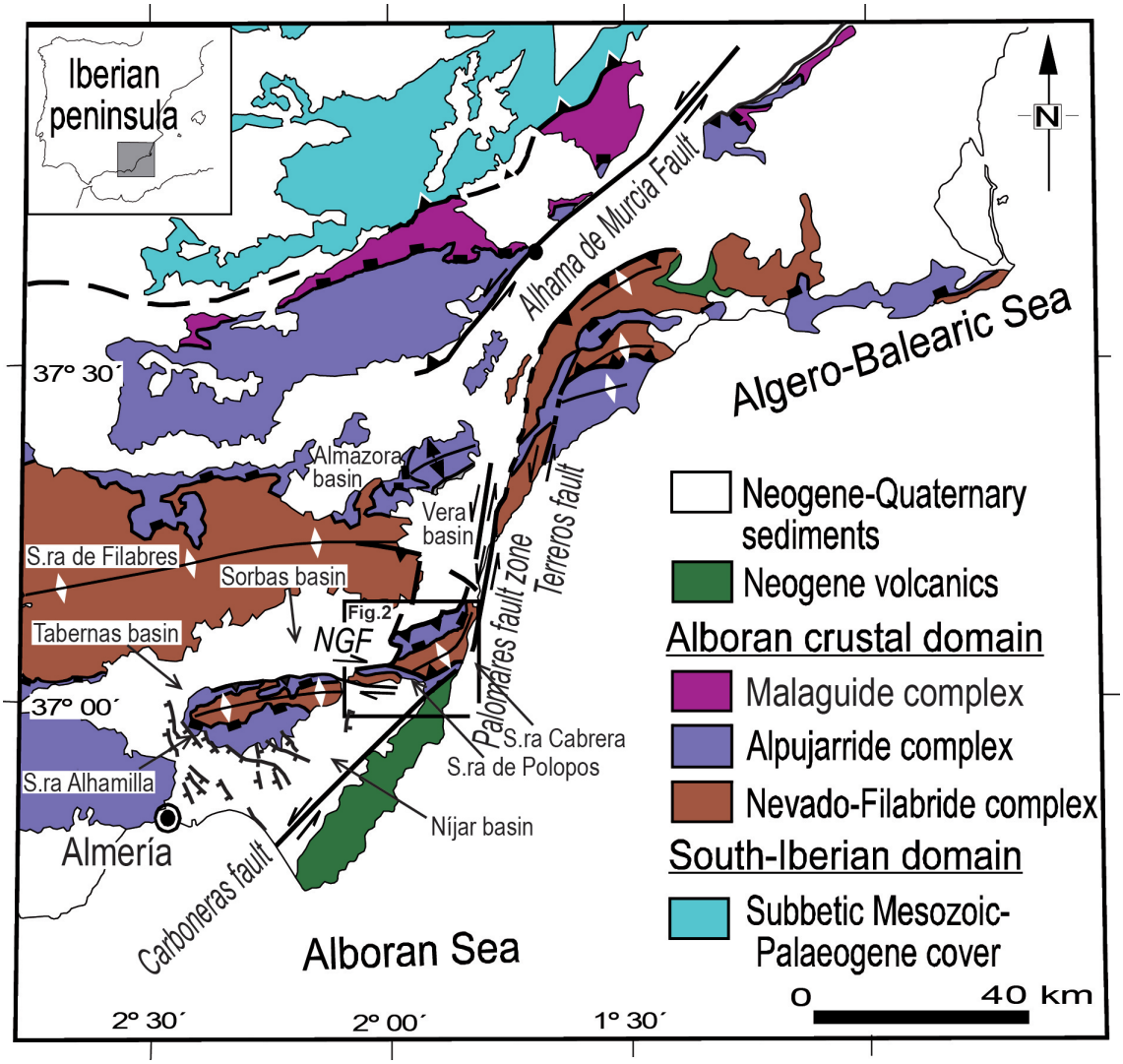

Fig.1 Geological sketch of the southeastern Betics highlighting the studied area modified after Giaconia et al. (2012b). NGF: North Gafarillos fault.

The main examples of these inversion shortening structures in the southeastern Betics are large strike-slip faults like the sinistral Palomares and Terreros fault zones, the dextral Polopos fault zone and other structures as the Sierra Cabrera and Alhamilla–Polopos anticlinoria and associated reverse faults (Fig.1, *Bousquet, 1979; Weijermars et al., 1985; Montenat and Ott d´Estevou, 1990; Montenat et al., 1990; Ott d´Estevou et al., 1990; Booth-Rea et al., 2004a, 2005; Giaconia et al., 2012b, 2013a*).

6.3 Balanced cross section method

We constructed a NE–SW oriented balanced cross section parallel to the direction of extension following the inclined-shear construction technique proposed by *Dula (1991)* that assumes the inclined-shear model as the dominant deformation mechanism for the hanging-wall. The assumption of the inclined-shear model was widely checked by clay-model analog experiments and both forward inclined-shear construction and inverse fault-to-bed construction on subsurface examples and seismic records. This technique allows reconstructing the master fault geometry of a listric fault system from sub-superficial geometry of the hanging-wall roll-over-anticline. The control factor that determines both the roll-over-anticline geometry and the master fault geometry and depth is the shear angle. The shear angle can be estimated by iterative modeling varying the shear angle systematically. The resultant fault and roll-over-anticline shape is compared to the shallow geometry of the master fault segments and the roll-over-anticline until a best fit is obtained.

In order to obtain the balanced cross section we extrapolated our mapping information at depth with the aid of drill holes with continuous depth sampling and taking into account the strata dips, the shallow geometry of the extensional faults and the stratigraphic contacts. Later, we input our preliminary shallow cross section into the 2DMOVE software and tested different shear angles in order to obtain the master fault geometry that best fitted the shallow geometry of the roll-over-anticline.

6.4. Lithostratigraphy of the study area

6.4.1 Metamorphic basement rocks

The metamorphic rocks that form the basement in the study area belong to the Albóran domain that is composed of three poly-metamorphic nappe complexes that are, in ascending order, the Nevado–Filabride, Alpujarride, and Malaguide complexes (Fig. 2, B*alanyá et al., 1997*). The Nevado–Filabride metamorphic complex is formed by three major tectonic units separated by two ductile shear zones subparallel to both the main foliation and the litological contacts *(Martínez-Martínez et al., 2004)*. These tectonic units are the Ragua, Calar Alto, and Bédar–Macael units, in ascending order.

All these units except the Ragua unit crop out at the Sierra Alhamilla, Polopos and Cabrera antiformal ridges. The Calar Alto unit is formed by a metasedimentay sequence including chloritoid-rich, graphite mica-schist of Palaeozoic protholith (Montenegro formation) with orthogneisses derived from late Carboniferous granites and light-colored schist (Tahal formation), marble and meta-evaporites of Permo–Triassic protholith. Serpentinites and metamorphosed Jurassic metabasites are also included. This unit underwent variable metamorphic conditions, reaching HP eclogite facies between 17 and 15 Ma *(López Sánchez-Vizcaíno et al., 2001; de Jong, 2003; Platt et al., 2006)*, followed by greenschist facies metamorphism before its exhumation that started at 13 Ma, age of the oldest zircon fission-track data *(Johnson et al., 1997; Vázquez et al., 2011)*. The Bédar–Macael unit includes staurolite graphite mica-schist, tourmaline gneiss, light-colored schist, serpentinite, amphibolites, and marbles *(Martínez-Martínez et al., 2004)*.

The Alpujarride complex comprises three major tectonic units bounded by extensional ductile and brittle shear zones, the Lower unit *(Martínez-Martínez and Azañón, 1997)*, Intermediate unit (Variegato unit, *Booth-Rea et al., 2005*) and the Upper unit (Fig. 2). The Lower unit is formed by a medium-grade tectono-metamorphic sequence that includes, from bottom to top, calcite-dolomite marble, kyanite bearing phyllite and quartzite, chloritoid-garnet graphite schist, and sturolite-kyanite-garnet graphite schist. This unit is overturned, showing an inverted metamorphic zonation and age that is Triassic for the marbles and Palaeozoic for the graphite schist *(Platt et al., 1983; Martínez-Martínez and Azañón, 1997)*. The Intermediate unit corresponds to the low-grade metamorphic Variegato unit *(Simon, 1963; Booth-Rea et al., 2005)* and comprises at least three second-order imbrications. The two lowest are formed by fine-grained schist of Permo–Triassic age and by marble of Triassic protholith. The structurally highest Variegato nappe also includes graphite schist at its base with garnet and biotite. The Upper unit only crops out locally between segments of the Carboneras fault in Sierra Cabrera. It is formed by K-feldespar gneises, sillimanite schist that gradually pass to lower-grade metapelites and then to metapelites with staurolite, garnet, andalusite and chloritoid.

The Malaguide complex in the study area comprises a Lower Malaguide unit that underwent low-grade metamorphism (anchizonal) during the Alpine orogeny, and some small outcrops of the Palaeogene limestones of the post-Triassic sedimentary cover *(Lonergan, 1993; Lonergan and Mangerajetzky, 1994; Nieto et al., 1994; Lonergan and Platt, 1995)*. The Lower Malaguide unit comprises several imbricate thrust sheets formed by, from bottom to top, Permo–Triassic quartz-pelitic rocks (red quartzite, red slate, micro-conglomerates and some gypsum levels) and Triassic carbonate rocks (calc-phyllite, massive black dolomite, gypsum, tabular dolomite and limestone).

6.4.2 Neogene sedimentary rocks

The sediments in the eastern Betic basins have been traditionally divided in older and recent Neogene. The older Neogene is formed by early to middle Miocene sediments and the recent Neogene by late Miocene sediments. The main difference between these sedimentary sequences is that the recent Neogene sediments registered the extensional denudation of the Nevado–Filabride complex rocks *(Völk, 1967; Ott d'Estevou et al., 1990)*. The older sediments in the Sorbas–Tabernas basin are early to middle Miocene in age (Fig. 3, Burdigalian–Serravallian). The lower Burdigalian unit is formed by a shallowing upwards sequence of pelagic limestone, marly limestone and marls. In ascending order, red conglomerates, sandstones with echinoderm and lamellibranchia, platform limestones, turbiditic marls, and continental conglomerates of late Burdigalian to Langhian age form the overlaying unit. A Serravallian unit that includes open marine

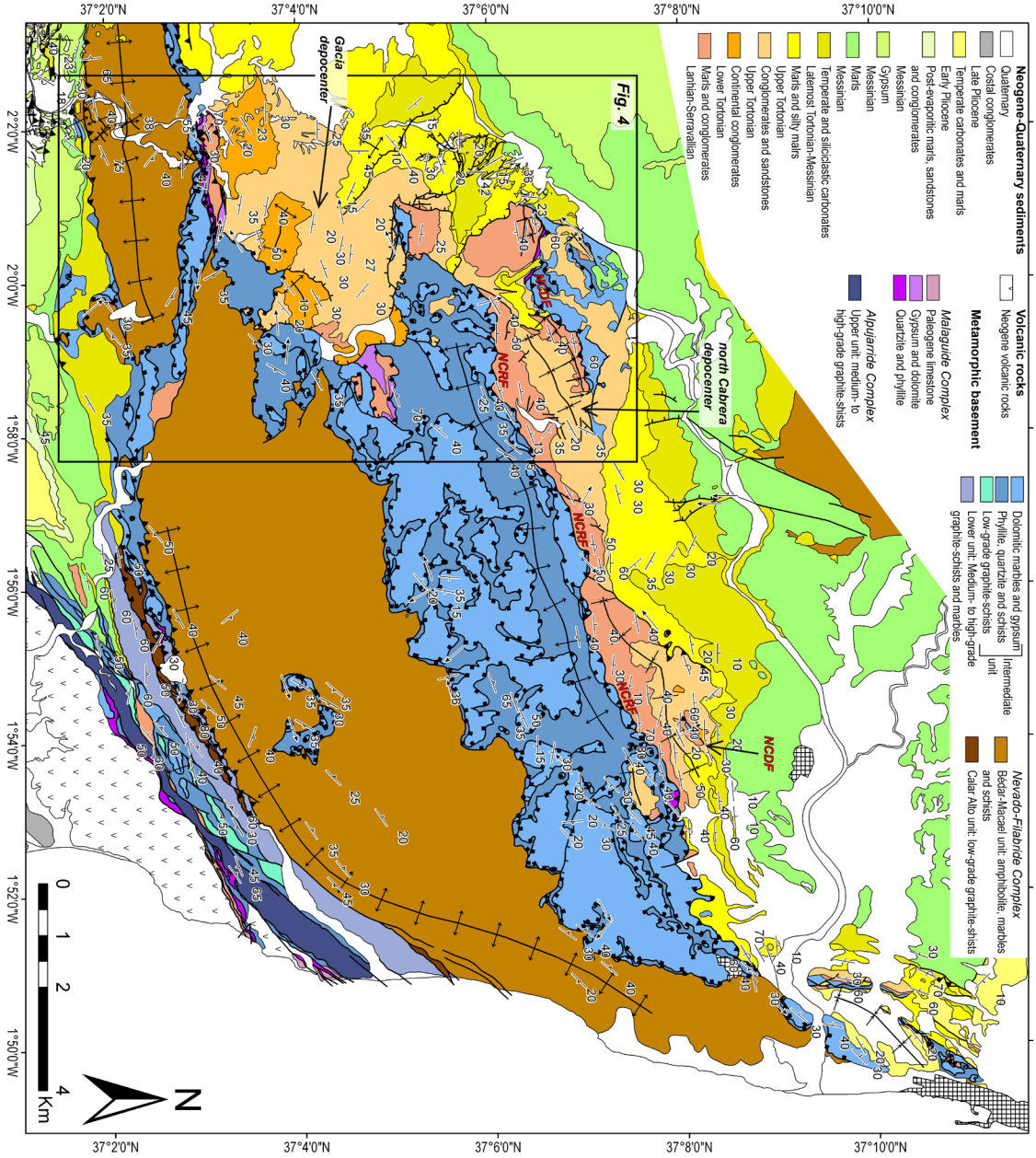

Fig. 2. Geological map of the Sierra Cabrera ridge and surrounding Neogene sedimentary basins: the Sorbas and Vera basins, to the north, and the Nijar basin, to the south. NCRF: North Cabrera reverse fault; NCDF: north-Cabrera dextral fault. See Fig. 1 for its location.

turbidites to continental conglomerates with Alpujarride and Malaguide clasts above, capes the older Neogene sequence *(Völk, 1966; Barragán, 1997; Booth-Rea et al., 2004a)*.

Tortonian to Pliocene sediments form the recent Neogene sedimentary sequence. Two sedimentary units deposited during the Tortonian. The lower Tortonian unit comprises two depositional sequences. The lower sequence is formed by conglomerates,

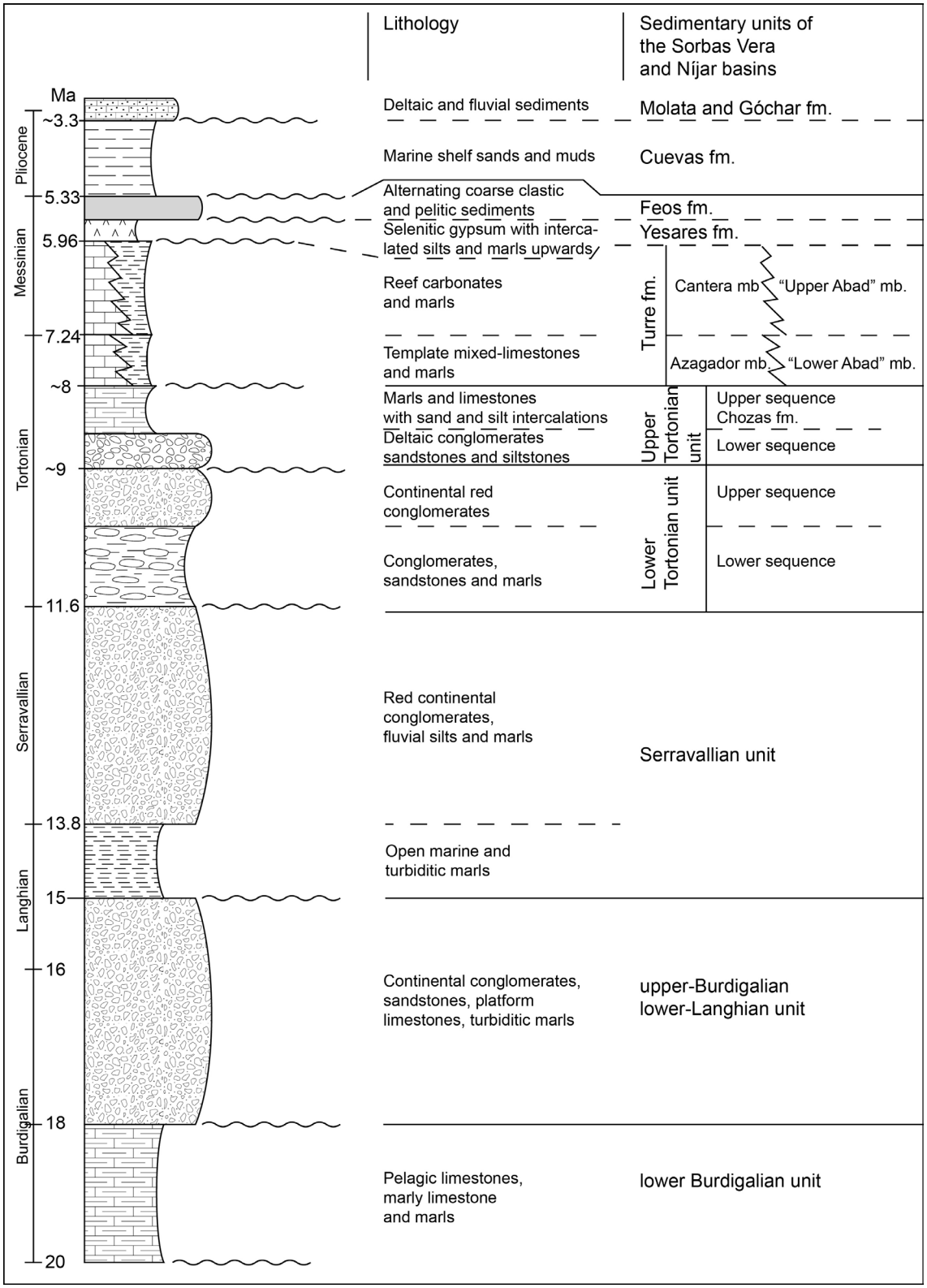

Fig. 3. Synthetic stratigraphic column of the Neogene–Quaternary sediments of the Sorbas, Vera and Níjar basins (Barragán, 1997; Fortuin and Krijgsman, 2003; Piller et al., 2007).

calcareous sandstones and marls deposited in transitional marine environments. The upper sequence is formed by red continental conglomerates with Nevado–Filabride boulders *(Barragán, 1997)*. The upper Tortonian unit is formed by two depositional sequences. The lower sequence defines an erosional angular unconformity on both sediments and metamorphic basement (intra-Tortonian unconformity) and comprises deltaic conglomerates with Nevado–Filabride boulders, sandstones and siltstones of transitional and marine facies. The upper sequence shows a sedimentary continuity with the previous one and is formed by marls and limestones with sand and silt intercalations of the Chozas formation (Fig. 3, *Ruegg, 1964*).

The latemost Tortonian to Messinian sedimentary units comprise, from bottom to top, the pre Messinian salinity crisis Turre formation (latemost Tortonian–early Messinian), the evaporitic Yesares formation (Messinian) and finally the post crisis Feos formation (Fig. 3, late Messinian). The Turre formation is formed by the Azagador, the Cantera and Abad members (Fig. 3). The latemost Tortonian temperate calcarenites of the Azagador member (8-7.24 Ma; *Völk, 1966; Martín et al., 2003*) are composed of bioclastic calcarenites and sandstones, locally mixed with conglomerates, with abundant bryozoans, bivalves, coralline algae and benthic foraminifera, and minor brachiopods, solitary corals, barnacles and gastropods *(Wood, 1966)*. The Azagador member shows progressive unconformities related both to the initial growth of the Sierra Alhamilla–Polopos and Cabrera anticlinoria *(Alvado, 1986; Ott d'Estevou and Montenant, 1990; Booth-Rea et al., 2004a)* and to Tortonian SW-directed extension at the western termination of Sierra Cabrera *(Giaconia et al., 2013b)*. The distal equivalent of the Azagador member are the open marine marls of the "Lower Abad" member that are characterized by a cyclic pattern of alternating whitish marly chalks and beige marls *(Fortuin and Krijgsman, 2003)* intercalated with diatomites and contain abundant calcareous nanoplankton and planktonic foraminifera of Messinian age *(Sierro et al., 2001)*.

Messinian reef carbonates of the Cantera member overlie the Tortonian sediments (7.24-5.96 Ma; *Völk, 1966; Sierro et al., 2001*) sealing part of the folding in the Sierra Alhamilla *(Weijermars et al., 1985)*, although they themselves define an open fold. This member is composed of tropical platform limestones, locally mixed with siliciclastics, that pass upward to prograding fringing reefs composed of corals encrusted by stromatolites *(Braga et al., 1996)*.

The distal equivalent of the Cantera member are the Messinian marls of the "Upper Abad" member that confirm the open marine conditions in the then connected Níjar and Sorbas–Tabernas basins until the occurrence of the Messinian salinity crisis *(Hsü et al., 1973, 1977)*. The "Upper Abad" member deposited during increasing restriction of marine conditions and includes sapropelitic laminites, marls and chalks that mark an upward shoaling *(Fortuin and Krijgsman, 2003)*.

The Messinian evaporites of the Yesares formation (Fig. 3) deposited in both the Níjar and Sorbas–Tabernas basins over the basin-scale Messinian erosional unconformity at the top of both Cantera and Abad members (5.96-5.67 Ma; *Martín and Braga, 1994; Krijgsman et al., 2001)*. The Yesares formation predominantly consists of selenitic gypsum that are intercalated upwards with beds of marine silts and marls containing benthic and planktonic foraminifera of Messinian age *(Riding et al., 1998)*. At the final stage of the crisis, during the late Messinian, basin differential uplift closed the connection between the two basins producing different lithostratigraphic sequences since then *(Braga et al., 2003; Booth-Rea et al., 2005)*. In the Níjar and Vera basins the marine environment was restored during the late Messinian as confirmed by the Lago Mare facies sediments of the Feos formation (5.67-5.33 Ma; *Fortuin and Krijgsman, 2003*) and persisted until the Pliocene as inferred by marine shelf sands and muds of the Cuevas formation (early Pliocene, Fig. 3, *Mather, 1993; Stokes and Mather, 2000*).

6.5 Results

The main faults in the studied region were active and produced important tectonic subsidence during the deposition of Neogene marine and continental sedimentary units in the Sorbas basin. Two well-differentiated sedimentary depocenters occur in the eastern part of the Sorbas basin related to the activity of strike-slip and normal faults during the middle to late Miocene.

The older sedimentary depocenter here named north Cabrera depocenter has an ENE–WSW orientation and runs parallel to northern limb of the Sierra Cabrera anticline into the Vera basin to the east (Fig. 2). It contains late Burdigalian to early Tortonian sediments that are bounded to the north by different ENE–WSW segments of the north–Cabrera dextral strike-slip fault zone that turns to a WNW–ESE orientation towards the west *(Sanz de Galdeano, 1987),* and to the south by the latemost–Tortonian to Quaternary North Cabrera reverse fault *(Giaconia et al., 2012b)*. Many NW–SE normal faults occur with both NE- and SW-directed extension along the southern boundary of the north Cabrera depocenter (Fig. 4).

The younger sedimentary depocenter, namely the Gacía depocenter, occurs at the western termination of the Sierra Cabrera with a WNW to ESE orientation and is bounded by NW–SE normal faults with SW-directed extension and by both dextral and sinistral oblique strike-slip faults of E–W to NE–SW orientation (Fig. 4). These fault segments form a strongly curved brittle fault zone that separates the metamorphic basement from the Tortonian sediments and shows consistent W to SW-directed extensional displacement. This basement bounding fault zone merges or is cut at

Fig. 4. Geological map of the eastern margin of the Sorbas basin where the north–Cabrera and Gacía sedimentary depocenters occur. Drill holes, structural stations, cross sections and photo sites (in Figs. 6 and 8) are located.

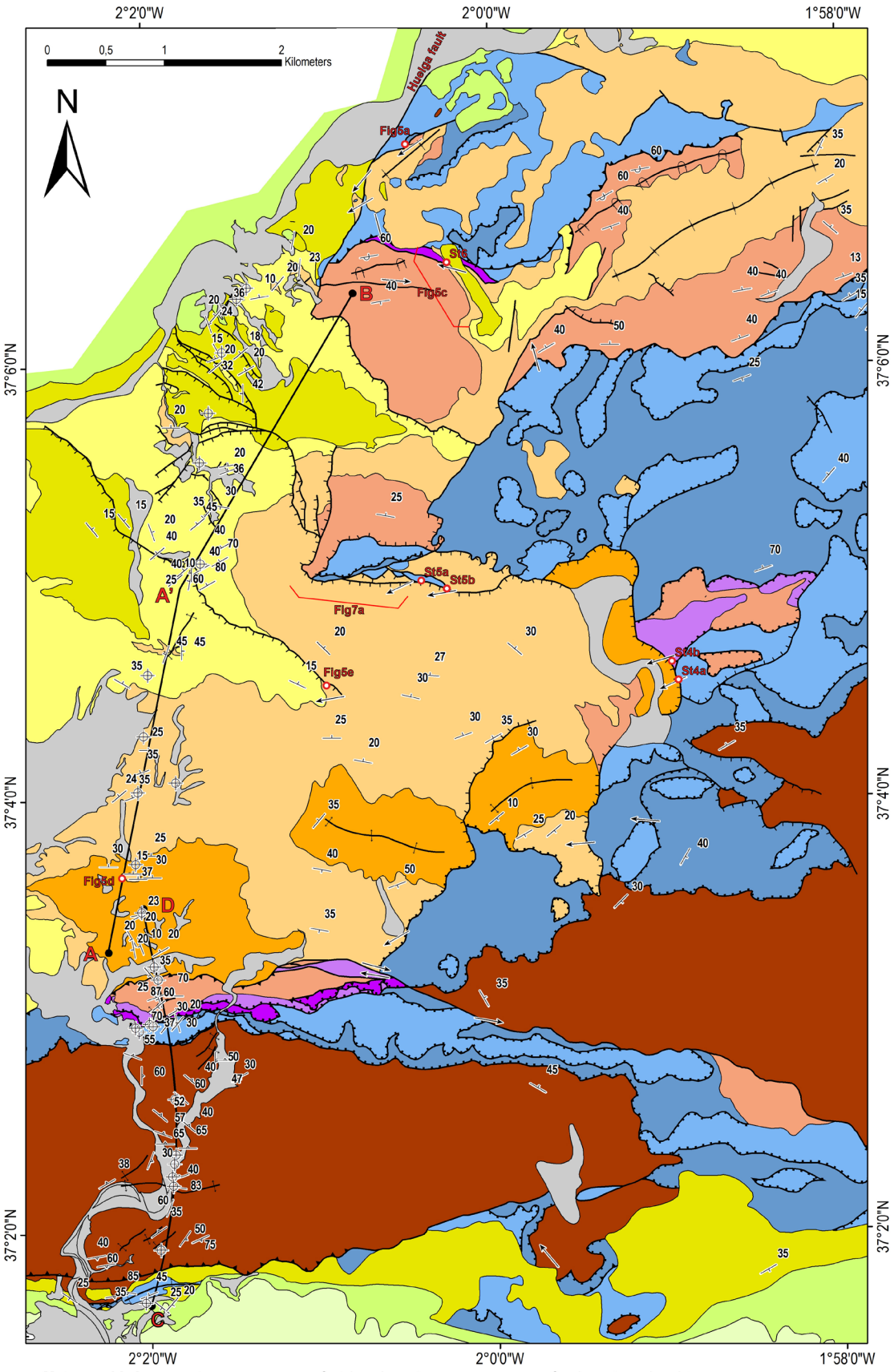
2°2'0"W
2°0'0"W
1°58'0"W
37°6'0"N
37°4'0"N
37°2'0"N
0 0,5 1 2 Kilometers
N
Huelga fault
Flg5a
Flg5c
Flg7a
Flg5e
Flg3d
St5
St5a
St5b
St4b
St4a
A
A'
B
C
D
Metamorphic basement
Malaguide Complex
Gypsum and dolomite
Quartzite and phyllite
Alpujarride Complex
Dolomitic marbles and gypsum
Phyllite, quartzite and schists
Nevado-Filabride Complex
Bédar-Macael unit: amphibolite, marbles and schists
Neogene-Quaternary sediments
Quaternary
Costal conglomerates Late Pliocene
Temperate carbonates and marls Early Pliocene
Post-evaporitic marls, sandstones and conglomerates Messinian
Gypsum Messinian
Marls Messinian
Temperate and siliciclastic carbonates Latemost Tortonian-Messinian
Marls and silty malrs Upper Tortonian
Conglomerates and sandstones Upper Tortonian
Continental conglomerates Lower Tortonian
Marls and conglomerates Lanhian-Serravallian
Normal bedding
Overturned bedding
Foliation
Slickenslines
Anticline
Syncline
Overturned syncline
Thrust
Strike-slip fault
Normal fault
Extensional detachment
Cross section
Drill holes

its intersection with the dextral North Gafarillos fault zone at the south of the Gacía depocenter (Fig. 4). The Gacía depocenter contains two thick Tortonian sedimentary units that are tilted and fan out towards the NE. Towards the NW the greatest thickness of Messinian and Pliocene sediments of the Sorbas basin seal the faults that bound the Gacía depocenter.

6.5.1 Serravallian to Tortonian extensional system and the north Cabrera depocenter

Segments of the north–Cabrera dextral fault zone crop out discontinuously along the northern foothills of the Sierra Cabrera. Most of these segments separate metamorphic rocks of the Alpujarride and Malaguide complexes in the northern block from middle Miocene and Tortonian sediments in the southern one. The main dextral strike-slip fault segments mapped show ENE–WSW orientation with subhorizontal striae. However, some of these segments presently show reverse kinematics. Locally, vertical fault segments with dextral kinematics and E–W to WNW–ESE orientation occur to the NW of the Sierra Cabrera (Fig. 4). Most of the observed dextral fault segments cut and are sealed by the deltaic conglomerates of the upper-Tortonian lower-sequence, whilst the Tortonian Chozas marls seal them (Figs. 5b and c). Many NW–SE normal faults occur with both NE- and SW-directed extension along the southern boundary of the north Cabrera depocenter affecting up to the upper-Tortonian lower-sequence deltaic conglomerates.

The sedimentary sequence in the north Cabrera depocenter shows a progressive unconformity within late-Serravallian conglomerates that has an ENE–WSW hinge parallel to the western termination of the north–Cabrera dextral strike-slip fault zone (Fig. 4 and 5a). This unconformity can be observed at several localities to the north of Sierra Cabrera. Furthermore, an angular unconformity occurs at the base the lower Tortonian unit. This data indicate a Serravallian to Tortonian age (13,8 to approximately 9 Ma) for the north-Cabrera dextral fault zone and extensional faults within the north Cabrera depocenter.

The north Cabrera depocenter is affected by later compressive structures, being folded in a syncline and cut by the North Cabrera reverse fault that has been active during the Quaternary (Figs. 2 and 4, *Booth-Rea et al., 2004a; Giaconia et al., 2012b*). Furthermore, at the western termination, the depocenter is bounded and cut by the NE–SW sinistral Huelga fault and by a NW–SE normal fault with SW transport that cuts up to the latemost Tortonian to Messinian Turre formation (Fig. 4).

6.5.2 Early–latemost Tortonian extensional system and the Gacía depocenter

The extensional system that bounds and cuts the Gacía depocenter is formed by normal faults that strike N140º-160ºE, dipping about 40º southwestwards and showing an

Fig. 5. a) a) A western segment of the north-Cabrera dextral strike-slip fault showing a progressive unconformity within the late Serravallian conglomerates (on the right) that has an ENE-WSW hinge

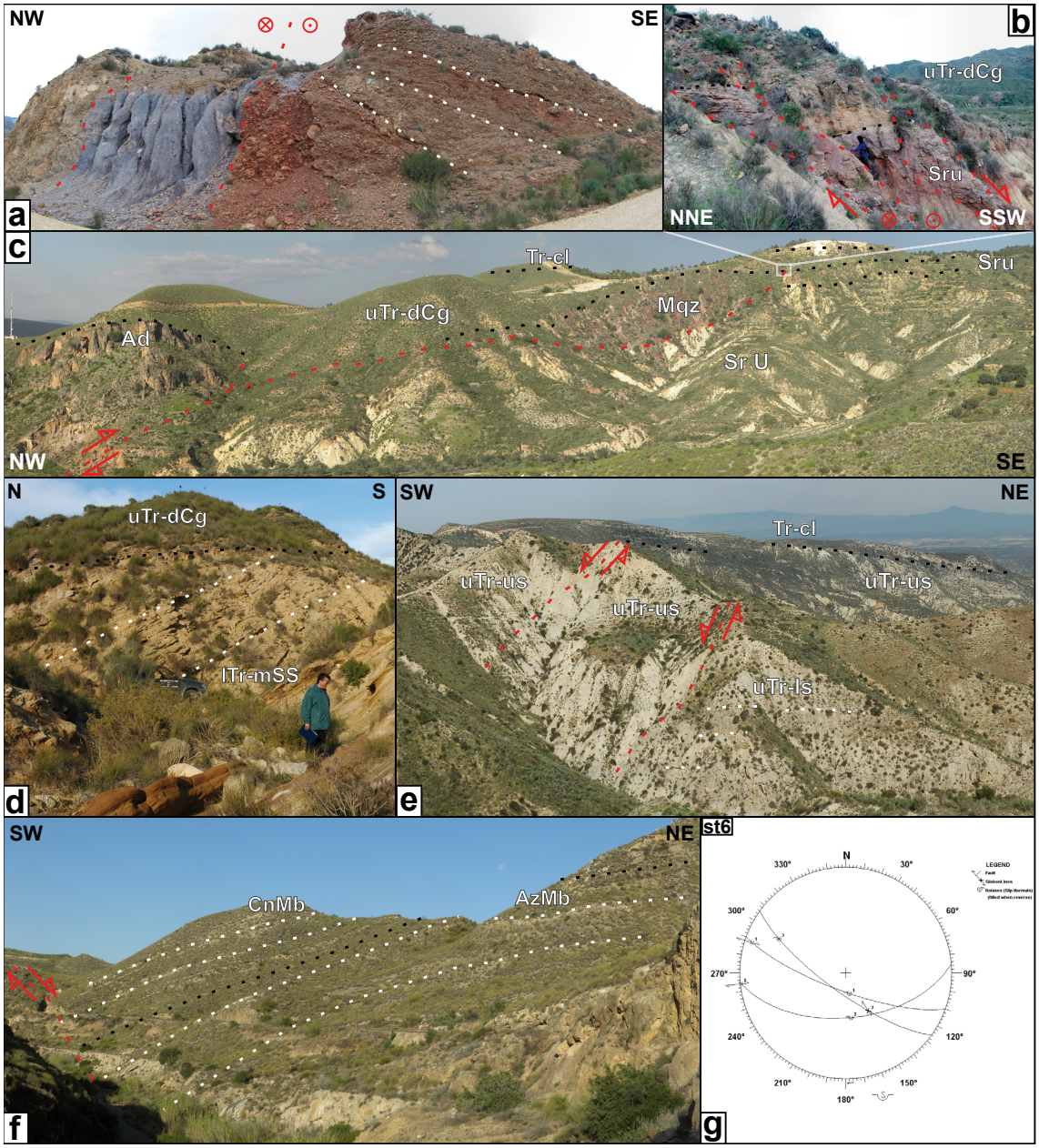

parallel to the fault zone (see Fig. 4 for its location). b) A north-Cabrera dextral fault segment that cuts and is sealed by the deltaic conglomerates of the uppe-Tortonian lower-sequence (see station 6 in Fig. 4 for its location). c) Panoramic view of the dextral strike-slip fault sealed by the latemost Tortonian–Messinian temperate calcarenites (see Fig. 4 for its location). d) Intra-Tortonian unconformity that separates marine sandstones and siltstones of the lower Tortonian unit from deltaic conglomerates of the upper Tortonian unit occurred at approximately 10 Ma (Fig. 4 for its location). e) Fault-related facies changes in the Tortonian sequences, which deepen in the hanging-walls towards the SW (Fig. 4 for its location). f) Progressive unconformity in the Azagador member related to a normal fault with NE-directed extension between the Sierra Alhamilla and the Sierra de Polopos at the northern margin of the Nijar basin. g) Stereonet collecting structural data of the dextral fault in Fig 5b (see Fig. 4 for its location). Ad: Alpujarride dolomites; AzMb: latemost Tortonian–Messinian temaplate mixed-limestones of the Azagador member; CnMb: latemost Tortonian–Messinian tropical platform limestones of the Cantera member; Mqz: Malaguide quartzite; lTr-mSS: marine sandstones and siltstones of the lower Tortonian unit; Sru: open marine turbidites to continental conglomerates with Alpujarride and Malaguide clasts of the Serravallian unit; Tr-cl: latemost Tortonian–Messinian temperate calcarenites of the Azagador member (Turre formation); uTr-dCg: deltaic conglomerates with Nevado–Filabride boulders of the lower sequence of the upper Tortonian unit; uTr-ls: sandstones and siltstones of transitional and marine facies of the upper-Totonian lower-sequence; uTr-us: marls and limestones with sand and silt intercalations (Chozas formation) of the upper-Tortonian upper-sequence.

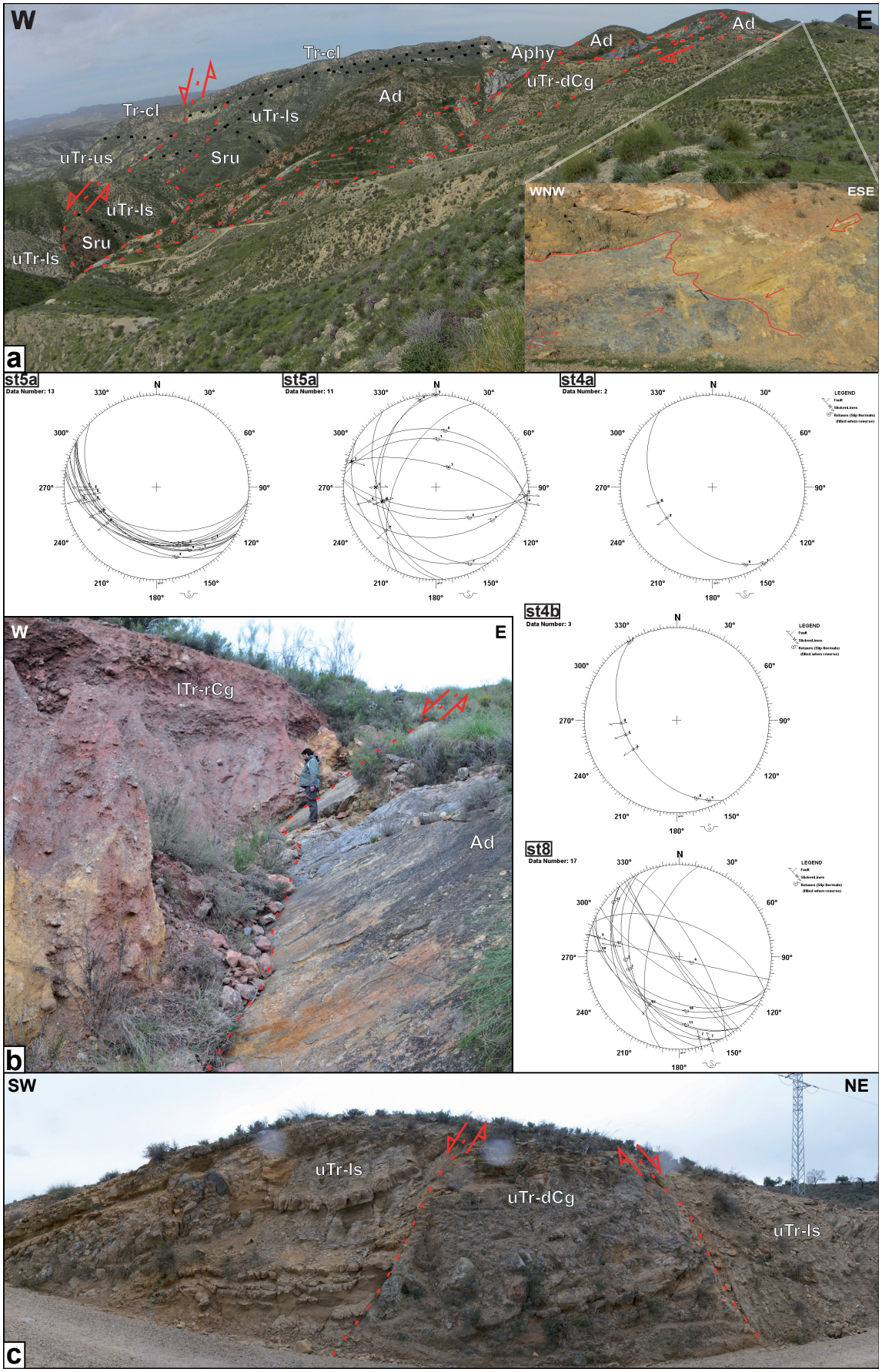

Fig. 6. a). Panoramic view of the a dextral lateral ramp that evolve to the left to a normal fault of the Tortonian extensional system, see structural stations st5a and 5b and Fig. 4 for its location. In the white inset a photo of the dextral lateral ramp is shown b). Frontal ramp of the Tortonian extensional system, see structural stations st4a and 4b and Fig. 4 for its location. c) Normal fault affecting the upper Tortonian unit (see Fig. 4 for its location). St8. Stereonet collecting structural data of the Tortonian

extension displacement towards N240-270ºE. These faults in the basin, link with a brittle fault zone with variable orientation that separates the metamorphic basement from the Tortonian sediments and shows consistent W to SW-directed displacement (Fig. 4). This strongly curved fault zone is formed by both N150ºE normal and N70-90ºE oblique strike-slip fault segments that dip about 50-70º both north- and southwards (Figs. 4 and 6). The oblique strike-slip segments show dextral-normal kinematics when they produce sinistral apparent offset of the normal faults they link and dip towards the south (Figs. 4, 6a and b). Meanwhile, they show sinistral-normal kinematics when they produce dextral apparent offset of the normal faults they link and dip towards the north. All the fault segments that define the main sediment-basement bounding fault zone are continuous between each other; thus, no crosscutting relationship can be established between them. The basement bounding fault zone merges or is cut at its intersection with the dextral North Gafarillos fault zone at the south of the Gacía depocenter (Fig. 4).

The balanced cross section across the Gacía depocenter was obtained using a shear angle of 80º and indicates a listric fault fan that roots in a basal detachment at 0.8 km depth (Fig.7). Gravimetric data available in the area *(Li et al., 2012)* indicate that the Nevado–Filabride/Alpujarride contact in the section is located at a depth of about 0.6 km, thus indicating that the extensional system cuts into the Nevado–Filabride complex. This extensional system produced a 1.2 km depth depocenter, reaching about a 39 % amount of extension during the Tortonian. The Tortonian sedimentary rocks show a progressive decrease of the dip of their strata upwards, describing a growth-strata structure toward the main extensional fault segments. Furthermore, within each unit the strata shows a decrease in dip angle away from the main faults, defining a hanging-wall roll-over-anticline (Fig. 7).

The two Tortonian sedimentary units that fill the Gacía depocenter show strong thickness changes between the outcrops located in the footwall of the normal fault system to the NE where they reach approximately 150 m thick and the center of the depocenter where 800-900 m of Tortonian sediments occur. Furthermore, across each normal fault strong changes occur in the sedimentary facies of the Tortonian sequences, which deepen in the hanging-walls, towards the SW (Fig. 5e).

Two angular-unconformities were recognized in the Tortonian sediments of the Gacía depocenter. The first one, namely the intra-Tortonian unconformity, occurred

extensional system affecting the lower Tortonian unit (see Fig. 4 for its location). Ad: Alpujarride dolomites; Aphy: Alpujarride phyllite; lTr-rCg: red continental conglomerates with Nevado–Filabride boulders of the late-Tortonian upper-sequence; Sru: open marine turbidites to continental conglomerates with Alpujarride and Malaguide clasts of the Serravallian unit; Tr-cl: latemost Tortonian–Messinian temperate calcarenites of the Azagador member (Turre formation); uTr-dCg: deltaic conglomerates with Nevado–Filabride boulders of the lower sequence of the upper Tortonian unit; uTr-ls: sandstones and siltstones of transitional and marine facies of the upper-Totonian lower-sequence; uTr-us: marls and limestones with sand and silt intercalations (Chozas formation) of the upper-Tortonian upper-sequence.

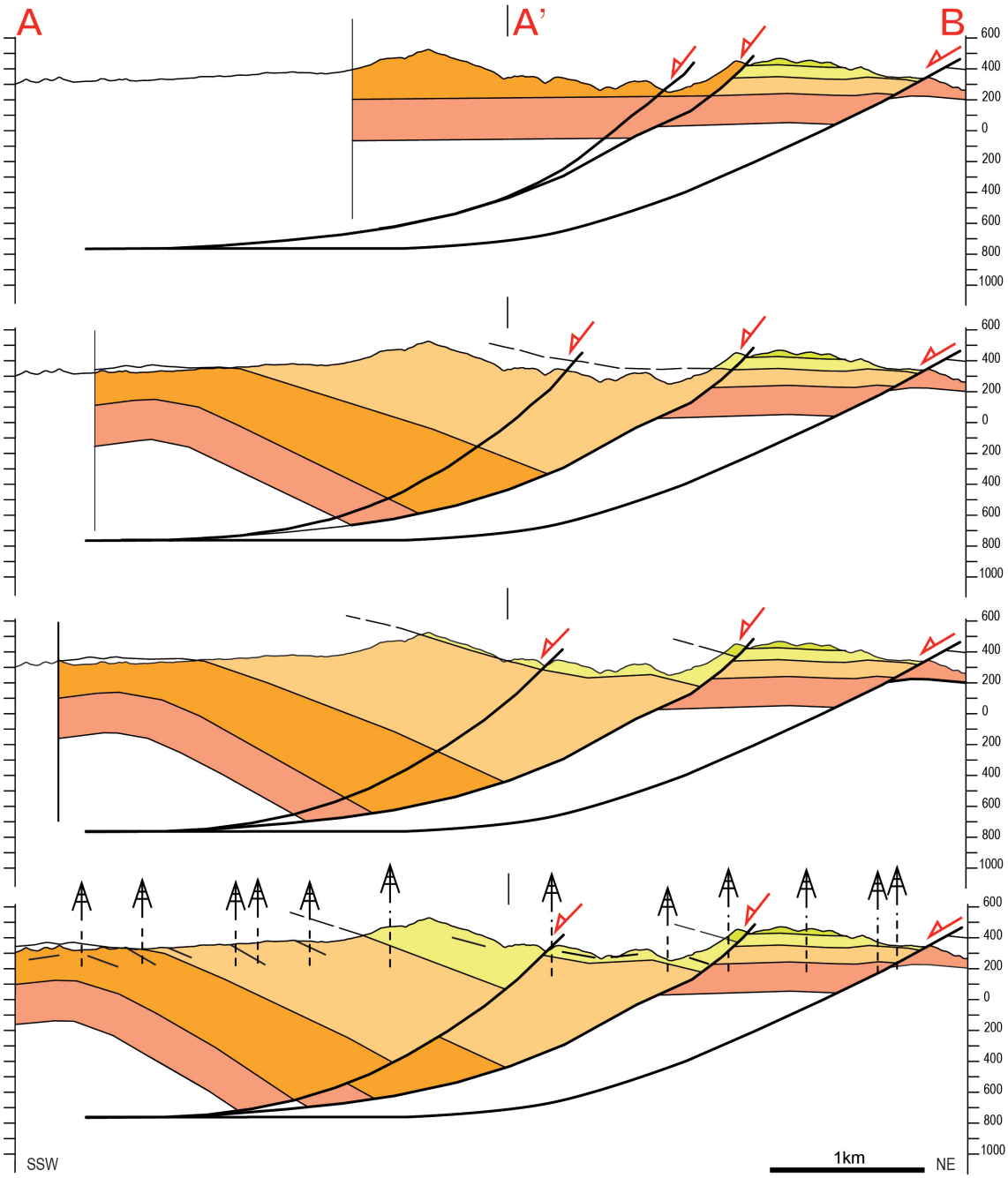

Fig. 7. Restored balanced cross section thought the Gacía sedimentary depocenter, see Fig. 4 for its location.

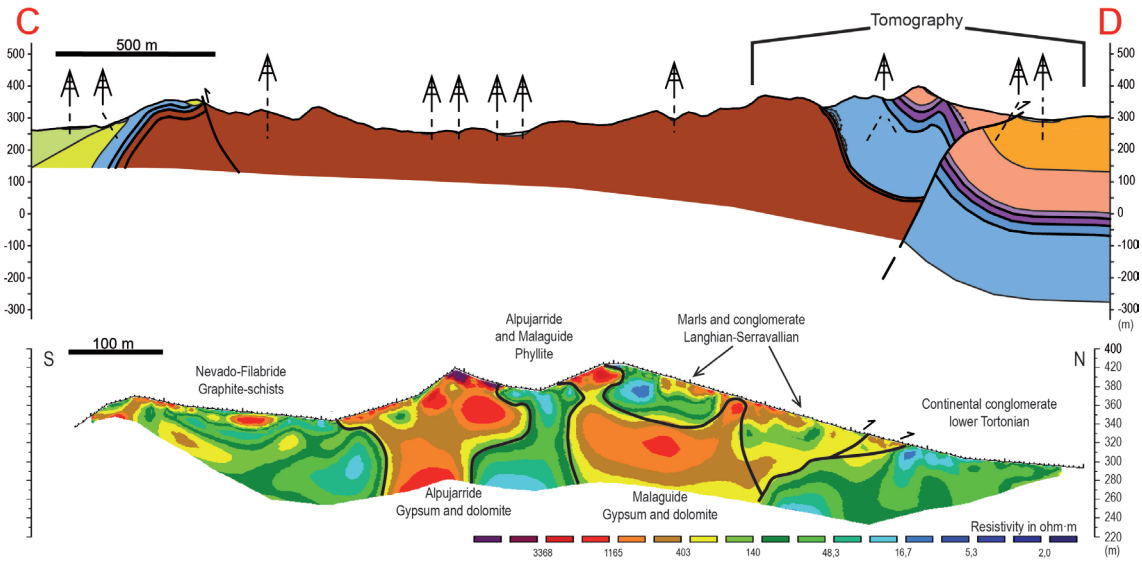

at approximately 9 Ma and separates marine sandstones and siltstones of the lower Tortonian unit from deltaic conglomerates of the upper Tortonian unit (Fig. 5d). The second one occurred at approximately 8 Ma between the late Tortonian Chozas formation marls and the template mixed-limestones of the Azagador member. Both unconformities are related to the NE-directed tilting produced by the NW–SE normal faults that defines the northeastern margin of the depocenter (Fig. 4). Finally, a further extension-related progressive unconformity occurred within the latemost Tortonian–Messinian Azagador member between ~8 and 7.24 Ma, whilst the Messinian Abad marls seal the fault system (Fig. 4). A progressive unconformity in the Azagador member related to a normal fault with NE-directed extension has been observed further west between the Sierra Alhamilla and the Sierra de Polopos at the northern margin of the Nijar basin (Fig. 5f).

The southern boundary of the Gacía depocenter is defined by the North Gafarillos fault that shows WNW–ESE orientation and dextral kinematics at the east and curves towards an ENE–WSW orientation to the west where it has reverse kinematics *(Giaconia et al., 2013a)*. To the west, the reverse segment of the North Gafarillos fault separates Langhian conglomerates or metamorphic basement of the northern limb of the Polopos anticline from Tortonian sediments of the Gacía depocenter (Fig. 4). An electric tomography section across the northern limb of the Polopos anticline shows that the North Gafarillos reverse fault segment dips gently at the surface (aprox. 15º) towards the south (Fig. 8). Although the North Gafarillos fault shows dextral-reverse kinematics the uplifted fault block that forms the Polopos anticline lies at a lower structural level than the western termination of the Sierra Cabrera anticline. Moreover, a middle Miocene sedimentary depocenter is preserved in the southern fault block that is tilted NE-wards against Nevado–Filabride graphite schist in the Sierra Cabrera fault block.

6.6 Discussion

This work shows that the Sorbas basin underwent important normal faulting during the Serravallian to Tortonian coinciding with the tectonic denudation of the HP Nevado-Filabride complex between 13,8 and 7,5 Ma.. The extensional system was strongly segmented with both NW–SE oriented normal faults and E–W to ENE–WSW strike-slip faults. The fact that the strike-slip faults link with the normal faults and that both structures were coeval suggests that they generated in a common extensional setting. Thus, the strike-slip faults are transfer faults developed under regional extension. This is further demonstrated by the fact that the apparent offset these faults produce is contrary to their kinematics and that faults with approximately the same orientation can show contrary kinematics. Two main sedimentary depocenters formed in the studied area

Fig. 8. Corss section and electrical resistivity tomography thought the Polopos anticline and the North Gafarillos reverse fault (see Fig. 4 for its location).

during this Serravallian to late Tortonian extension (approx. 13.8 to 7.5 Ma) that were strongly influenced by the transfer faults.

The older North Cabrera depocenter is strongly compartmented by segments of the north–Cabrera dextral transfer fault zone and by normal faults with both NE and SW transport that were active between the Serravallian and the Tortonian (approx. 13.8 to 9 Ma). The normal and transfer faults related to the north Cabrera depocenter cut and were finally sealed by upper Tortonian deltaic conglomerates and the Chozas marls. Meanwhile, the progressive unconformity observed within Serravallian conglomerates and the angular unconformity at the base of the lower Tortonian unit probably are both related to the activity of this fault zone. The dextral kinematics of the north–Cabrera transfer fault zone suggests that eastward-directed extension was probably dominant towards the east, in the Vera basin.

The Gacía depocenter in the western termination of the Sierra Cabrera formed in relation to a later extensional pulse between approximately 9 and 7.5 Ma that supposed a westward propagation of extension and the abandonment of the north–Cabrera dextral fault zone. This second depocenter was also controlled by a strongly segmented extensional system with both N140-160ºE normal faults and N70-90ºE transfer faults and W- to SW-directed extension. The normal faults cut the Gacía depocenter defining a listric fan that coalesces in a low-angle detachment. Both published gravity data and the construction of a balanced-cross section across the Gacía depocenter indicate that the main detachment cuts into schist of the Nevado–Filabride complex at approximately 0.8 km depth. Thus, this fault system cuts and tilts an older extensional system that detached at the contact between the Nevado–Filabride and Alpujarride complexes *(e.g. Platt and Vissers, 1989; Martínez-Martínez and Azañón, 1997; Booth-Rea et al., 2005; Behr and Platt, 2012)*. The normal faults controlled the upper Tortonian sedimentary facies shifting from continental and deltaic conglomerates in the footwall to silts and basin marls in the main depocenter. Tortonian to Messinian SW and NE directed extension occurred also at the Níjar basin, this work, and further south in the Cabo de Gata region *(Brachert et al., 2002; Krautworst and Brachert, 2003)*.

The westward migration of the locus of extension from the north Cabrera depocenter during the Serravallian–lower Tortonian to the Gacía depocenter during the Tortonian follows very closely the apatite fission track cooling ages obtained from Nevado–Filabride samples from the Sierra de Filabres to the north. The samples to the north of the north Cabrera depocenter cooled between 15 to 11 Ma, whilst at the N to NW of the Gacía depocenter the apatite FT ages young to 9.5-7.5 Ma *(Johnson et al., 1997; Vázquez et al., 2011)*. Furthermore, this hypothesis is supported by the position of the Tortonian detachment within the Nevado–Filabride complex, indicating that it cut the previous Alpujarride–Nevado Filabride detachment that presently crops out tilted in the

Fig. 9. Synthetic tectonic model for the Serravallian to Tortonian extension (a) and the later compressive tectonic inversion (b) in the southeastern Betics. In white inactive fault are shown.

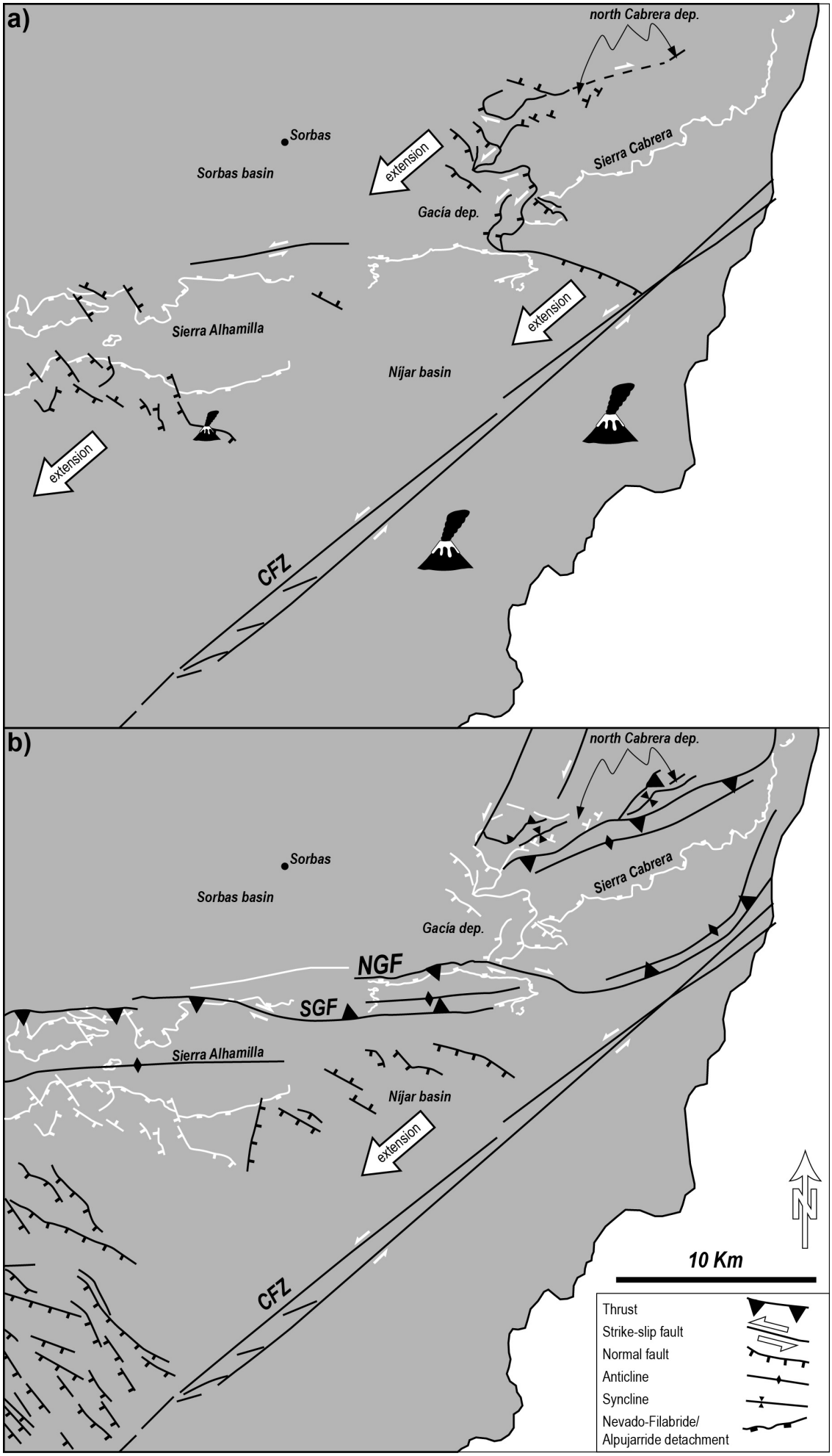
a)
north Cabrera dep.
Sorbas
Sorbas basin
extension
Sierra Cabrera
Gacía dep.
extension
Sierra Alhamilla
Níjar basin
extension
CFZ
b)
north Cabrera dep.
Sorbas
Sorbas basin
Sierra Cabrera
Gacía dep.
NGF
SGF
Sierra Alhamilla
Níjar basin
extension
CFZ
10 Km
Thrust
Strike-slip fault
Normal fault
Anticline
Syncline
Nevado-Filabride/
Alpujarride detachment

Sierra de Polopos to the south of the Gacía depocenter.

The North Gafarillos dextral-reverse fault overthrusts the folded metamorphic basement of the Sierra de Polopos antiform upon Tortonian sediments at the south of the Gacía depocenter. However, this fault zone does not manage to displace the metamorphic basement in the hanging-wall of the Sierra de Polopos at a higher structural position with respect to the footwall of the Sierra Cabrera. Thus, suggesting that the North Gafarillos fault has inverted a normal fault with SW-directed extension, but not undone its previous extensional displacement. The North Gafarillos fault shows a hard-linkage relationship with the Carboneras sinistral transfer fault that was active since the middle Miocene *(Keller et al., 1995; Rutter et al., 2012)*. Thus, extension in the Gacía depocenter during the Tortonian continued along the North Gafarillos fault and was transferred to sinistral displacement along the Carboneras fault to the south. This fault configuration results in a strongly heterogeneous extensional system with short normal frontal ramps linked by long dextral and sinistral transfer faults that separate regions with different styles of extension during the Tortonian. Core-complex type extension exhumed the Sierra de Filabres elongated dome to the north of the Sorbas basin (*Martínez-Martínez et al., 2002, 2004)*, tilted-block extension produced the main depocenters in the Sorbas and Nijar basins, and magmatic accretion with normal faulting upon thinned continental crust occurred to the south of the Carboneras transfer fault (Fig. 9, *Krautworst and Brachert, 2003; Booth-Rea et al., 2007; Giaconia et al., Submitted*).

Serravallian to late Tortonian extension probably occurred in a transtensional setting above a lithospheric transform fault that permitted the westward propagation of the Thethyan oceanic slab beneath the Albóran basin producing edge delamination beneath the Betics *(Duggen et al., 2003; Martínez-Martínez et al., 2006; Booth-Rea et al., 2007)*. Slab tearing beneath the Betics probably induced a transtensional setting characterized by the development of elongated core complexes, predicted theoretically by le *Pourhiet et al. (2012)*. Furthermore, both the observed SKS and Pn seismic anisotropy *(Buontempo et al., 2008; Díaz et al., 2010; Bokelmann et al., 2011)* and mantle xenolith fabrics support the existence of a vertical ENE–WSW foliation in the lithospheric mantle formed in a transtensional setting during the late Miocene *(Konc, 2013; Konc et al., Submitted)*. Thus, the superficial manifestation of a lithospheric transform fault in the Betics would be a region with heterogeneous extension characterized by elongated core-complexes, tilted blocks and magmatic accretion, segmented by long transfer faults like the Alpujarras, the north-Cabrera and the Carboneras faults. Slab tearing probably took advantage of the continental-oceanic transition to the south of Iberia that would explain the contrast between the clear oceanic subduction signal in the Alboran and Algero-Balearic basins to the south of the transform and continental collision features to the north in the central and eastern Betics.

6.7 Conclusions

The Sorbas basin underwent important normal faulting during the Serravallian to Tortonian producing two extensional-related sedimentary depocenters in the region. The older North Cabrera depocenter is strongly compartmented by segments of the north–Cabrera dextral transfer fault zone and by normal faults with both NE and SW transport that were active between the Serravallian and the Tortonian (approx. 13.8 to 9 Ma). A normal-fault listric fan with SW-directed extension that rooted in a detachment within the Nevado–Filabride complex formed the Gacía depocenter between approximately 9 and 7.5 Ma. This system tilted the previous Nevado-Filabride/Alpujarride detachment, produced a westward migration of SW-directed extension and the abandonment of the north-Cabrera dextral fault zone.

Extension in the Gacía depocenter was coeval and probably linked with sinistral displacement along the Carboneras fault to the south, producing a strongly heterogeneous extensional system with short normal frontal ramps linked by long dextral and sinistral transfer faults. Westward directed heterogeneous extension in the region resulted in different styles of extension, producing tilted-block domains and metamorphic core-complexes to the north of the Carboneras sinistral transfer fault and magmatic accretion upon previously thinned continental crust to the south of the fault. Serravallian to latemost Tortonian extension probably occurred in a transtensional setting above a lithospheric transform fault that permitted the westward propagation of the Thethyan oceanic slab beneath the Albóran basin producing edge delamination under the Betics.

Acknowledgments: The authors were supported by research projects CGL2011-29920 and CSD2006-00041 TOPOIBERIA CONSOLIDER-INGENIO2010 from the Spanish Ministry of Science and Innovation.

Geomorphology 145–146 (2012) 90–106, doi:10.1016/j.geomorph.2011.12.043
Received 22 December 2010 / Available online 4 January 2012

7.0 Geomorphic evidence of active tectonics in the Sierra Alhamilla (eastern Betics, SE Spain)

F. Giaconia [a,*], G. Booth-Rea [a], J. M. Martínez-Martínez [a], J. M. Azañón [a] , J. V. Pérez-Peña [a] , J. Pérez-Romero [b] and I. Villegas [c]

[a] Dpto. Geodinámica, Instituto Andaluz de Ciencias de la Tierra (CSIC-UGR), Campus Fuentenueva s/n, 18002, Granada, Spain
[b] ETS Arquitectura, University of Málaga, Campus del Ejido s/n, 29071, Málaga, Spain
[c] CEMOSA, C\Benaque, 9, 29004, Málaga, Spain
[*] Corresponding author. E-mail address: flavio@ugr.es, flavio@iact.ugr-csic.es

Abstract: Active tectonic deformation influencing the streams and hillslopes of the Sierra Alhamilla ridge (anticlinorium) in southeast Spain is related to the dextral-reverse Polopos Fault Zone to the north and east of the ridge and to normal faulting in the southern side of the ridge. A fault segmentation and fluvial terrace mapping is presented in this paper. The following geomorphic indices were calculated in the area: the mountain-front sinuosity, valley floor width-to-height ratio, drainage basin asymmetry factor, basin hypsometric curve and integral, longitudinal river profile and the stream-length gradient index normalized by the graded river gradient (*SLk* index). The *SLk* map shows two sets of high anomalies: a) an E–W-striking anomaly, due to the dextral-reverse Polopos Fault Zone located in the northern limb of the anticlinorium; b) a group of NNW–SSE-striking anomalies, associated with Pliocene–Quaternary NW–SE- to NNW–SSE-striking high-angle normal faults that cut the southern limb. Late Pleistocene–Holocene activity occurred along the North Alhamilla Reverse Fault and the dextral transpressive South Gafarillos Fault; two segments in the Polopos Fault Zone. The former fault produces rejuvenation of the streams at the base of the northern slope. In this area, mountain-front sinuosity and valley floor width-to-height ratio suggest Quaternary uplift rates between 0.05 and 0.5 m ky^{-1}. Holocene to present-day activity of the South Gafarillos Fault is demonstrated by faulted late Pleistocene terraces and Holocene colluvial deposits and suggested by deflected streams that have complex or convex hypsometric curves. Pliocene–Quaternary high-angle normal faults control the relief in the southern limb and the western end of the Sierra Alhamilla. These faults produce low mountain-front sinuosity and valley floor width-to-height ratio indices typical of uplift rates quite higher than field based rates from some other studies.

Keywords: Active tectonics; Geomorphic indices; Eastern Betics; Sierra Alhamilla; Gafarillos fault

7.1 Introduction

Studies of Quaternary and present-day tectonic activity are mainly based on geomorphologic, geologic, geodetic and seismologic data. In regions affected by low/ moderate tectonic deformation rates, geomorphologic and geologic data provide some of the best approaches to detect and characterize active tectonics *(Molin et al., 2004; Dumont et al., 2005; Necea et al., 2005)*.

Recent and active tectonics may affect geomorphic processes and landscape evolution. For example, tectonic activities producing differential uplift and/or tilting and local base-level variations may control the development of alluvial fans *(Mather, 2000b; Mather et al., 2000; 2002; Stokes et al., 2008)*. Tectonic uplift induces erosion that usually turns into the main driving factor of channel incision, river deflection, headward erosion, stream head- or foot-rejuvenation processes and eventually piracy processes *(Holbrook and Schumm, 1999; Snyder et al., 2000; Burbank and Anderson, 2001; Lave and Avouac, 2001; Hilley and Arrowsmith, 2008)*. However, geomorphic processes are also controlled by topographic, climatic, and lithologic factors that must be taken into account when tectonically oriented conclusions are deduced *(Jackson and Leeder, 1994; Schumm et al., 2000; Burbank and Anderson, 2001; Keller and Pinter, 2002)*.

Qualitative and quantitative geomorphic analyses are useful tools to investigate the impact of tectonic activity on geomorphic processes and landscape development. Qualitative analyses usually study topographic and longitudinal river profiles, drainage networks, spatial distribution of drainage basins and their geometric relationships, having the aim to define controlling factors and reconstruct the evolution of landscapes *(Ouchi, 1985; Whipple and Tucker, 1999; Azor et al., 2002; van der Beek et al., 2002; Wegmann and Pazzaglia, 2002; Clark et al., 2004; Zhang et al., 2004; Korup, 2006)*. Quantitative geomorphic analyses are conducted using geomorphic indices, which help to assess the relative level of tectonic activity in an area and to characterize quantitatively the geomorphic features of a landscape *(Seeber and Gornitz, 1983; Brookfield, 1998; Keller and Pinter, 2002; Chen et al., 2003; Kobor and Roering, 2004)*. Geomorphic indices have been broadly used as a tool to identify and characterize sectors deformed by active faults *(Keller and Pinter, 2002; Pedrera et al., 2009a; Pérez-Peña et al., 2010)*. Thus, the final aim of the quantitative analyses is to describe a landscape in detail and possibly associate a set of geomorphic features to a detected tectonic structure. These kind of studies are appropriate in semiarid zones like SE Spain, where landforms related to active tectonics such as fault-generated mountain fronts are preserved for long periods (>100 ky, *Mayer, 1986; Silva et al., 2003*).

Furthermore, in strike-slip fault systems, like those found in the eastern Betics, displacement may generate important topographic gradient associated with uplift and subsidence in antidilational and dilational jogs, respectively *(Sibson, 1986)* forming both uplifted blocks and sedimentary depocenters *(Sylvester, 1988)*. Temporal variations

in the position of active fault segments together with creation of new segments lead to migration of active sedimentary depocenters and changes in the topography and drainage pattern *(Ollier, 1981; Walker and Jackson, 2002; Booth-Rea et al., 2004a)*.

Here, we explore the presence of active structures in the Sierra Alhamilla ridge (anticlinorium) and surrounding Neogene basins (Sorbas–Tabernas and Níjar–Almería basins), using both qualitative and quantitative geomorphologic analyses, in order to provide evidence of the present activity of these structures and characterize the geomorphic features associated with them. Qualitative analyses focused on topographic profiles, longitudinal river profiles, and ridge-line profiles, pattern of the drainage network, and spatial distribution of drainage basins and their geometric relationships. Quantitative analyses were conducted calculating the following geomorphic indices: the mountain-front sinuosity, the valley floor width-to-height ratio, drainage basin asymmetry factor, basin hypsometric curve and integral, and the stream-length gradient index normalized by the graded river gradient (*SLk* index). The main structures in this area are the Sierra Alhamilla ridge, with associated reverse faults in its northern limb, and the Gafarillos dextral fault in the northeastern termination of the ridge *(Weijermars et al., 1985; Ott d'Estevou and Montenant, 1990; Stapel et al., 1996; Huibregtse et al., 1998)*. A late Pliocene to Quaternary extensional regime *(Stapel et al., 1996)* and related high-angle normal faults have also been described in the Níjar–Almería basin to the south of the Sierra Alhamilla *(Pedrera et al., 2006)*.

Both the reverse fault and the Gafarillos dextral strike-slip fault in the northern side of the Sierra Alhamilla are locally truncated by Messinian sediments, and thus, inactive *(Ott d'Estevou and Montenant, 1990; Stapel et al., 1996; Huibregtse et al., 1998; Jonk and Biermann, 2002)*. However, seismicity in the region indicates the presence of active reverse and strike-slip faults (*Stich et al., 2003a; Marín-Lechado et al., 2005)*. This evidence, together with the new geological and geomorphologic data we present here, indicate that reverse faulting in the northern side of the Sierra Alhamilla and dextral strike-slip deformation in its eastern termination are presently active, affecting local topography and the drainage network.

7.2 Regional setting

The southeastern Betics are characterized by the presence of Neogene to Quaternary sedimentary basins that occur in synclines among E/W- to ENE/WSW–elongated antiformal ridges, where the metamorphic basement occurs bounded by folded extensional detachments. This basement is made up of several metamorphic complexes belonging to the Alborán domain, a terrain that collided with the South Iberian and Maghrebian passive margins during the Miocene, forming the Gibraltar Arc and the Betic and Rif ranges *(Balanyá and García-Dueñas, 1987; Martínez-Martínez and Azañón, 1997; Martínez-Martínez et al., 2002; Platt et al., 2003; Booth-Rea et al.,*

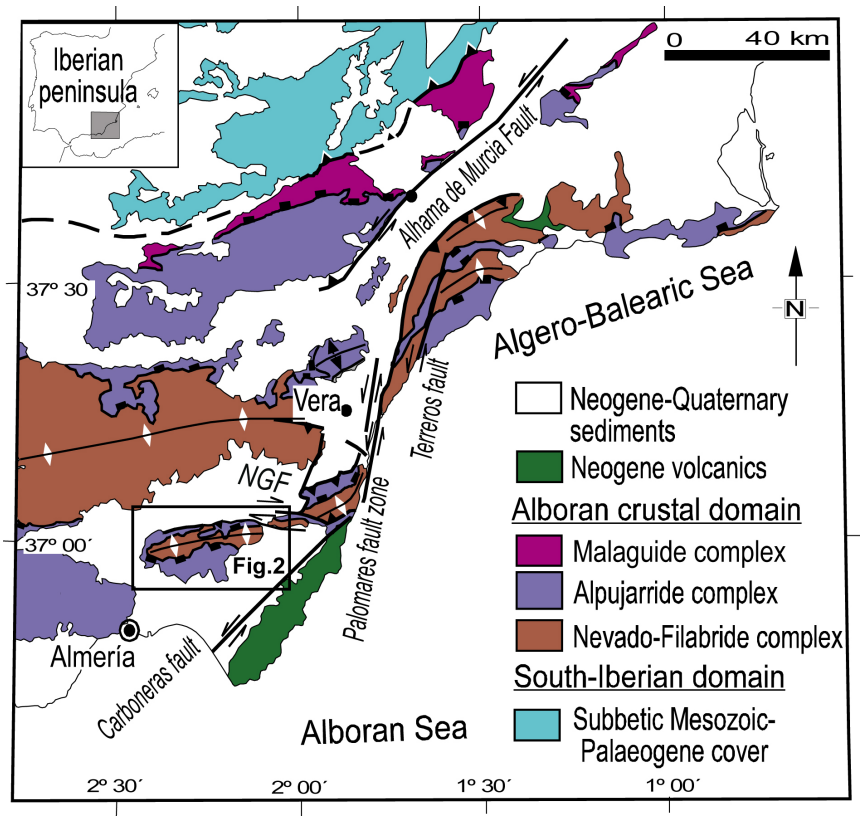

Fig. 1. Geological sketch of the southeastern Betics highlighting the studied area. NGF: North Gafarillos fault.

2005; 2007).

The Neogene sedimentary basins in the internal Betics formed during Miocene extensional tectonics, which markedly attenuated the previous pile of metamorphic units of the Alborán domain. The ultimate result of this severe extensional tectonics was the formation of the Alborán Sea and the Algero–Balearic basin in the core of the Betic–Rif orogen, coeval to thrusting in the external domains *(García-Dueñas et al., 1992; Martínez-Martínez and Azañón, 1997; Comas et al., 1999; Booth-Rea et al., 2005; 2007)*. Ongoing late Miocene to present-day convergence between Northern Africa and Iberia *(Dewey et al., 1989; McClusky et al., 2003; Serpelloni et al., 2007)* has resulted in tectonic inversion of the Miocene extensional basins and the development of folds and strike-slip fault systems including dextral and sinistral faults *(Weijermars et al., 1985; Montenat and Ott d´Estevou, 1990; Comas et al., 1999; Booth-Rea et al., 2004a)*.

The most important sinistral strike-slip faults active during the latest Miocene and Quaternary are the Carboneras *(Bell et al., 1997; Gràcia et al., 2006)*, Alhama de Murcia *(Martínez-Díaz, 2002; Masana et al., 2004)*, Palomares *(Bousquet, 1979; Booth-Rea et al., 2004a)*, and Terreros sinistral fault-zones, all of them with a NNE/SSW to NE/SW trend. Conjugate dextral faults are not as long and show a dominant WNW/ESE orientation, like the North Gafarillos fault zone that bounds the western end of the Sierra Cabrera (Fig. 1, *Ott d'Estevou and Montenant, 1990; Stapel et al., 1996; Barragán, 1997; Huibregtse et al., 1998; Jonk and Biermann, 2002*). Large regional uplift of south Iberia has been related either to this recent convergence *(e.g. Jolivet et*

al., 2006) or alternatively, to deep mantle processes associated with subcontinental-mantle lithosphere edge delamination *(Duggen et al., 2003; Booth-Rea et al., 2007*).

7.2.1 Structural framework

The Sorbas–Tabernas and Níjar–Almería basins, to the north and to the south of the Sierra Alhamilla, respectively (Fig. 2), are examples of extensional Miocene basins that have later evolved into a transpressive late Miocene to Quaternary tectonic scenario *(Weijermars et al., 1985; Martínez-Martínez and Azañón, 1997)*. Late Miocene transpression resulted in the development of the Sierra Alhamilla anticlinorium and associated reverse and strike-slip faults *(Weijermars et al., 1985; Ott d'Estevou and Montenant, 1990; Stapel et al., 1996; Huibregtse et al., 1998; Jonk and Biermann, 2002; Booth-Rea et al., 2004a)*.

The main active or recent tectonic structures in the study area are the transpressive dextral Gafarillos Fault to the east of the Sierra Alhamilla ridge and its western prolongation as a reverse fault (here called North Alhamilla reverse fault, NARF) in the northern limb of the Alhamilla anticlinorium (Fig. 2, *Ott d'Estevou and Montenant, 1990; Stapel et al., 1996; Huibregtse et al., 1998; Jonk and Biermann, 2002*); whereas to the south in the Níjar–Almería basin Pliocene–Quaternary high-angle normal faults occur with an NW–SE to NNW–SSE strike (Fig. 2, *Martínez-Martínez and Azañón, 1997; Marín-Lechado et al., 2005; Pedrera et al., 2006; Sanz de Galdeano et al., 2010*). Finally, to the west of the Sierra Alhamilla, *Sanz de Galdeano et al. (2010)* documented the existence of active E–W-striking dextral faults, which cross the Tabernas basin (Fig. 2).

Both fault segmentation mapping and geomorphic analysis of the area (presented below) show the existence of active dextral fault segments to the south of the Polopos–Cabrera antiformal ridge, here called South Gafarillos Fault (SGF). It is a highly segmented strike-slip fault system with several parallel and oblique fault segments that cut through the Messinian to Quaternary sedimentary cover of the Níjar basin and fan out towards the SE as they get close to the Carboneras sinistral strike-slip fault zone.

The South Gafarillos Fault (SGF) connects with the North Alhamilla Reverse Fault (NARF) that runs along the northern mountain front of the Sierra Alhamilla. The NARF locally shows splays that cut through early Tortonian turbidites and offset Quaternary

Fig. 3. Geological sketch where the North Alhamilla Reverse Fault affects the Quaternary alluvial fan in the Sierra Alhamilla northern front. a) Detail of the northern limb of the Sierra Alhamilla anticline and the North Alhamilla Reverse Fault (see Fig. 2 for location), with examples of drainage divide profiles coinciding with middle to late Pleistocene alluvial fan surfaces that show the displacement and topographic uplift produced by the fault. LANF: low angle normal fault; HANF: high angle normal fault. b) Topographic profiles #5 and #6 of Quaternary alluvial fans (see a) for location) showing displacement and slope increase in the intersection with the North Alhamilla Reverse Fault. c) Late Pleistocene calcrete cut by a North Alhamilla Reverse Fault segment. See a) and d) for location. d) Panoramic view of the North Alhamilla Reverse Fault located at the foot of the northern slope of the ridge. At this site, the mountain front is developed within highly erodible Tortonian marls.

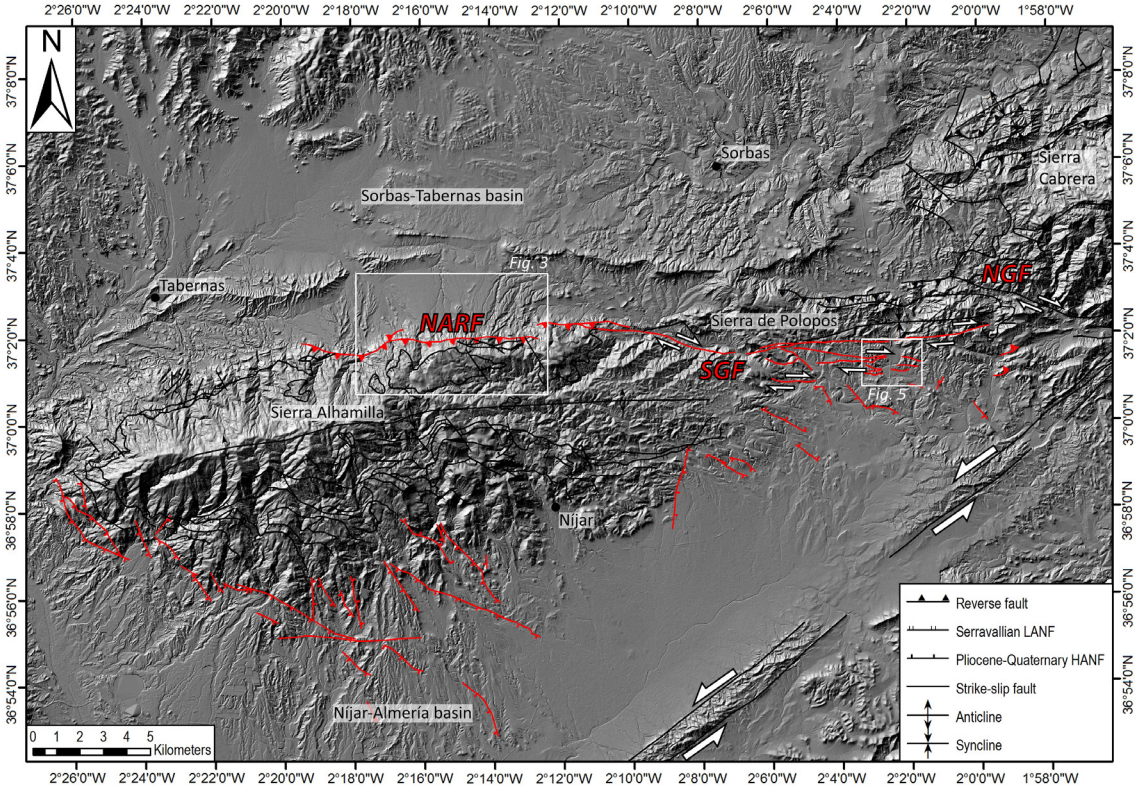

Fig. 2. Structural map of the study area (see Fig. 1 for its location) where the main tectonic structures of the Sierra Alhamilla are shown: the North Alhamilla Reverse Fault (NARF), the North and the South Gafarillos faults (NGF and SGF, respectively), after Martínez-Martínez and Azañón (1997). Faults with Quaternary activity are shown in red.

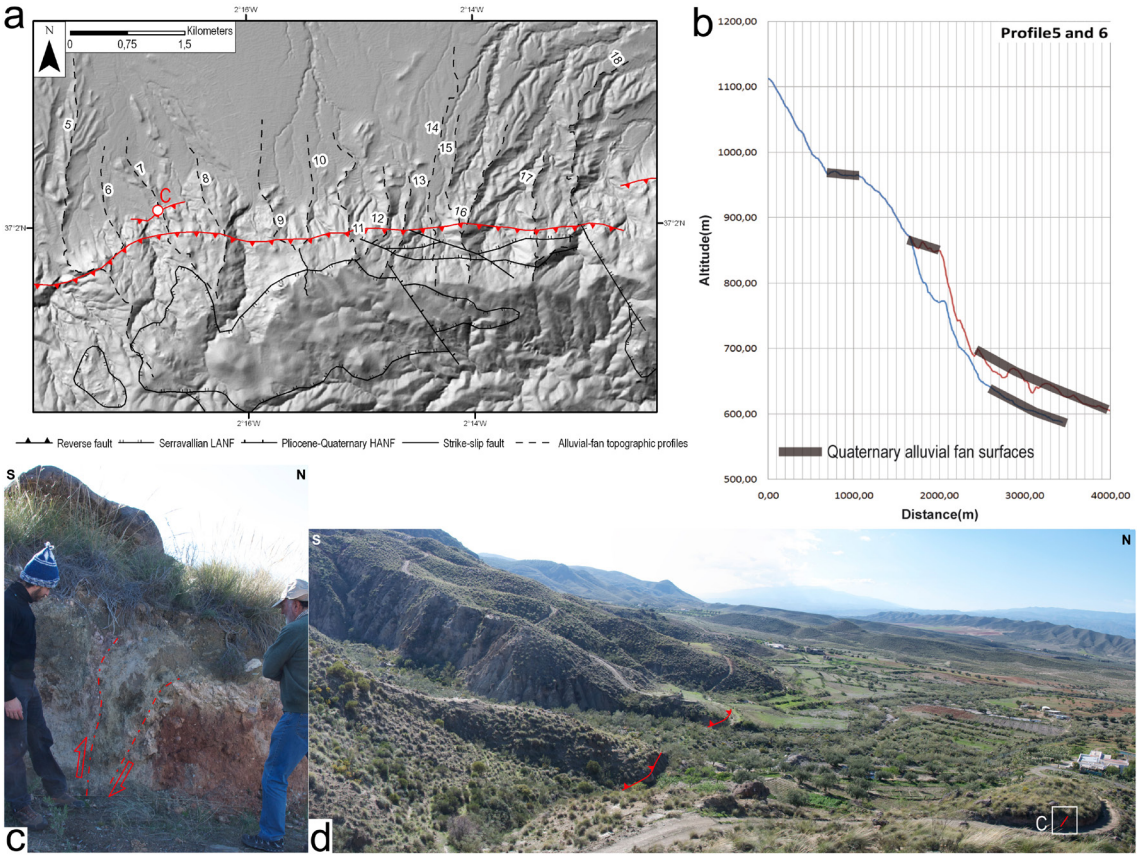

alluvial fans defining the present mountain front within these highly erodible sediments. *Harvey et al. (2003)* described two alluvial-fan units and related them to dated terraces in the Sorbas basin. The oldest one is formed by debris-flow dominated deposits and several palaeosol and calcrete horizons of middle Pleistocene age. The youngest unit is formed by sheet and channel gravels and culminates at the fan surface with a well developed pedogenic calcrete. This unit has been correlated by these authors with terrace C in the Sorbas basin that includes calcretes dated between 70 and 100 ky *(Harvey et al., 1995; Maher et al., 2007)*. These calcretes are locally faulted by the NARF, indicating a post-late Pleistocene activity of this structure (Fig. 3c and d). These alluvial fans define a Quaternary palaeo-topographic surface that has been cut by the reverse fault (Fig.3a). This surface with an age between 400 and 70 ky *(Harvey et al., 1995; Harvey et al., 2003; Candy et al., 2005)* has been displaced approximately 100 m by reverse faulting after 400- 70 ky with a slip rate ranging between 0.25 and 1.4 mm yr^{-1} (Fig. 3b). The NARF and the SGF together define a fault system 28 km long here called Polopos fault zone (Fig. 2) conjugate to the Palomares sinistral strike-slip fault zone.

The Pliocene–Quaternary NW–SE- to NNW–SSE-striking high-angle normal fault system affects Quaternary alluvial fan sediments deposited above dated late Pliocene coastal sediments (about 3.2 Ma, *Aguirre, 1998*) in the Níjar–Almería and produces fault scarps in the southern and southwestern mountain fronts of the ridge and associated Quaternary alluvial fans (Fig. 2, *Martínez-Martínez and Azañón, 1997; Martínez-Díaz and Hernández-Enrile, 2004; Marín-Lechado et al., 2005; Pedrera et al., 2006; Sanz de Galdeano et al., 2010*). These faults generally dip to the SW and sometimes show evidence of synsedimentary activity and, moreover, produce seismicity in nearby areas where extensional focal mechanisms have been determined, for example, the Mw 4.8 2002 Gérgal earthquake *(Béjar et al., 2006)* or the Mw 6.1 1910 Adra earthquake *(Stich et al., 2003b)*.

7.2.2 Geomorphologic features

The study area is characterized by the Sierra Alhamilla ridge bounded by the Sorbas–Tabernas and Níjar–Almería basins, to the north and to the south, respectively. The Sierra Alhamilla shows an E–W elongated shape and a mean altitude between 1200 and 1300 m.a.s.l., reaching a maximum height of 1387 m.a.s.l.. This ridge topographically contrasts with the low-lying Sorbas–Tabernas and Níjar–Almería basins, whose heights range between 300 and 500 m.a.s.l. and from 0 to 200 m.a.s.l., respectively (Fig. 4). The region is characterized by a semi-arid climate, with a mean annual rainfall of around 200 mm y^{-1} *(Harvey and Wells, 1987)*.

The Sorbas basin fill is dissected by two drainage systems, the NNE-wards Rio Aguas drainage system, to the north, and the SSE-wards Rio Alias drainage system, to the south. The latter drains the southern area of the basin across the Sierra Alhamilla and

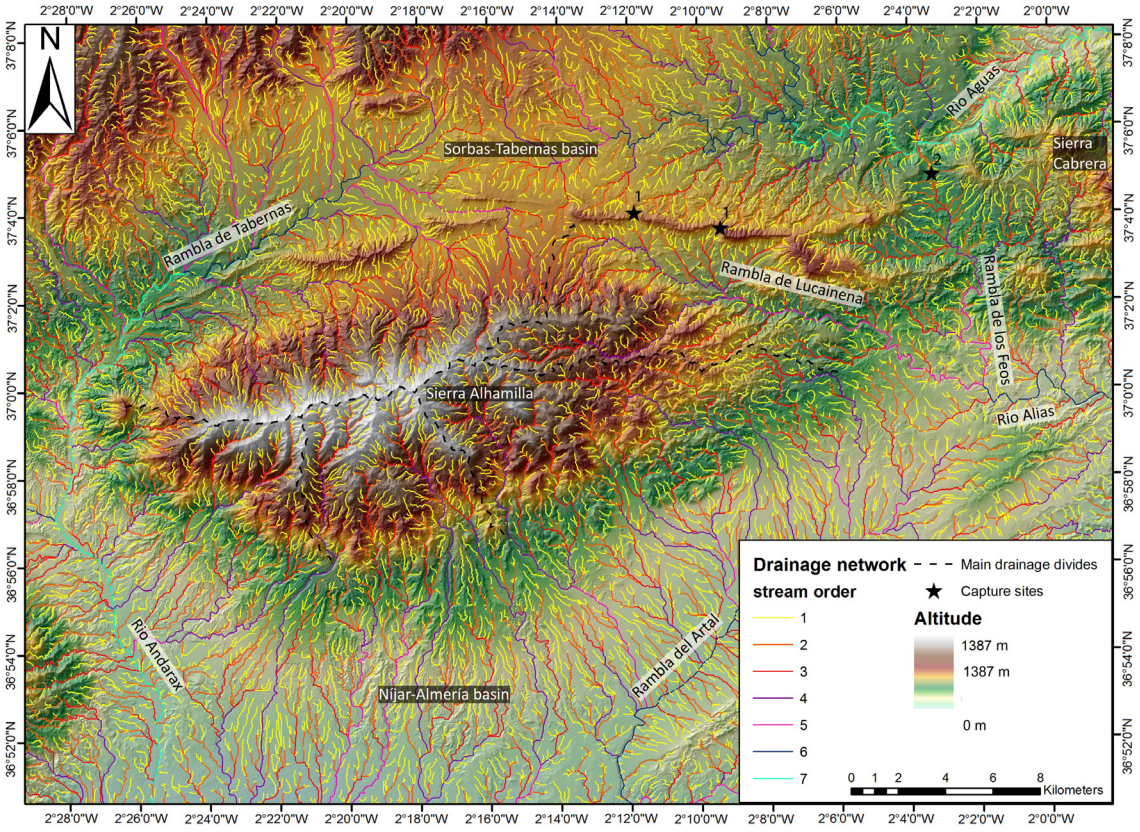

Fig. 4. Topographic map of the study area (see Fig. 1 for location) where the drainage network, the main drainage divides of the Sierra Alhamilla and capture sites are shown.

Cabrera into the Níjar–Almería basin, by means of the Rambla de los Feos and Rambla de Lucainena streams (Fig. 4). In the southern part of the Sorbas basin two regionally significant captures occurred, both triggered by changes in regional gradients associated with sustained Quaternary uplift in the region (160 m Ma^{-1} over the Plio/Pleistocene, *Mather, 2000b*).

The initial drainage was centripetal towards the Sorbas basin until the early Pleistocene. The first capture occurred in the early to middle Pleistocene and re-routed 15% of the original drainage in the Sorbas basin across the Alhamilla and Cabrera ridges, into the Níjar–Almería basin to the south via the Rio Alias (*Mather, 2000b*). This capture disconnected the northeastern mountain front area from the Sorbas basin and gave rise to the Rambla de Lucainena (capture site 1 in Fig. 4).

The second capture occurred in the late Pleistocene and re-routed 73% of the original Sorbas Basin drainage into the Rio Aguas to the east, so isolating the Rambla de los Feos from the Sorbas basin and expanding the area of the Rio Aguas drainage system (capture site 2 in Fig. 4, *Mather, 2000b; Maher et al., 2007*). The fluvial terraces related to these captures, both strath and fill terraces, have been dated using calcretes and palaeosols. Their ages range between 400 and 70 ky and *(Harvey and Wells, 1987; Mather, 2000b; Candy et al., 2005; Maher et al., 2007)*. The inversion of the Sorbas basin since the early Pleistocene produced a long-term trend of fluvial incision with episodic periods of aggradation, recording increased sediment supply to the catchment during the cold/dry climates experienced during glacial stages. This long-term fluvial-

incision was controlled also by short-term climatic oscillations relating to Europe glacial/interglacial periods *(Harvey and Wells, 1987)*. During glacial aggradation episodes fluvial terraces and alluvial fans developed, whereas during interglacial warm phases incision prevailed forming calcretes and palaeosols *(Candy and Black, 2009)*. However, not only climate has influenced the geomorphic features occurring in the area but also tectonics producing different regional uplift rates between the ranges and Neogene basins and also between the various basins. Pliocene to recent regional uplift-rates are between 80 and 150 m Ma^{-1} for the Sierra Alhamilla *(Weijermars et al., 1985)* and higher than 170 m Ma^{-1} for the Sierra Cabrera, meanwhile they are typically much lower for the Neogene basins, 70 and 100 ± 20 m Ma^{-1} for the Sorbas basin, up to 120 ± 20 m Ma^{-1} for the Tabernas basin, and between 53 and 76 ± 20 m Ma^{-1} for the Níjar–Almería basin *(Braga et al., 2003)*. During the Quaternary, the differential regional tectonic uplift among ranges and basins disconnected the Sorbas basin from the sea and changed local base-levels causing ponding and lake development in the basin center, followed by dissection propagating up the system *(Harvey et al., 2003)*. Furthermore, in the SE part of the Sorbas basin in the Rambla de Lucainena, a fault-related drainage-captures followed by incision was documented in relation with the NARF *(Mather, 2000b)*. The mountain-piedmont junction in the Sierra Alhamilla has either a lithological or a fault origin. The mountain fronts defined by lithological contacts occur mostly in the southern slope of the Sierra Alhamilla and developed on the previously folded most resistant rocks, like Messinian carbonates or metamorphic basement. Whilst mountain fronts coinciding with faults, sometimes occur within the same lithology, for example, Tortonian marls in some segments of the NARF, and others between different lithologies juxtaposed by the faults.

The Tabernas basin fill is dissected by the SW-wards Rambla de Tabernas drainage system that flows into the Rio Andarax and drains the entire western termination of the ridge and the Níjar–Almería basin (Fig. 4). The main geomorphologic features of the Tabernas basin are deeply eroded badlands to the west and coalescent aggrading alluvial fans to the east linked by entranced canyons whose origin have been strongly influenced by the Pliocene–Quaternary uplift in the eastern part of the basin. This uplift produced a considerable incision and the development of steep regional gradients. The incised Tabernas drainage falls 260 m in less than 16 km from Tabernas Town to the Rio Andarax *(Nash and Smith, 1998)*. Similarly, the Rio Andarax incision history, which constitutes the axial stream of the eastern Alpujarras valley, was controlled largely by the propagation of an incision wave induced by tectonic uplift *(García et al., 2003; 2004)*.

Finally, the Níjar–Almería basin fill is drained by the SW-wards Rambla del Artal drainage system that flows parallel to the Carboneras fault zone (Fig. 4). In the northeastern part of the basin the Pliocene–Quaternary high-angle normal fault system, together with the differential regional uplift between the Níjar–Almería basin and the

Sierra Alhamilla, as well as the Sorbas–Tabernas basin, generates the Sierra Alhamilla southern mountain front and the associated Quaternary alluvial fans.

7.3 Material and methods

Present tectonic activity in the study area has been documented by fault-segment and fluvial-terrace mapping in selected areas, as presented below. Furthermore, qualitative and quantitative geomorphic analyses were conducted. Qualitative observations were carried out on the drainage network, spatial distribution of drainage basins and their geometric relationships, and on topographic profiles perpendicular to the Sierra Alhamilla and longitudinal river profiles. Quantitative geomorphic analyses were carried out employing several geomorphic indices that are indicated below.

Mountain-front sinuosity (S_{mf}) has been employed to evaluate tectonic activity along mountain fronts, apart from its dependence of climate and lithology *(Bull, 1977; Keller and Pinter, 2002; Silva et al., 2003; Bull, 2007)*. It was defined by *Bull (1977)* as;

$$S_{mf} = L_{mf}/L_S \quad (1)$$

where L_{mf} is the length of the mountain front along the foot of the mountain, e.g. the topographic break in the slope, and LS is the length of the mountain front measured along a straight line. In active mountain fronts, uplift will prevail over erosional processes, producing straight fronts with low S_{mf} values. Whereas, in less active fronts the erosional processes, overcoming the tectonic ones, will generate sinuous fronts with high S_{mf} values. Some studies have proposed that S_{mf} values lower than 1.4 are typical of tectonically active fronts *(Keller, 1986; Silva et al., 2003; Pérez-Peña et al., 2010)*.

In order to discriminate between V-shaped and U-shaped flat-floored valleys the valley floor width-to-height ratio (V_f) has been calculated for the selected mountain fronts. This index has been previously applied to several mountain fronts located in the eastern and central Betics *(Silva et al., 2003; Pedrera et al., 2009b; Pérez-Peña et al., 2010)* and was defined by *Bull and McFadden (1977)* as:

$$V_f = (2V_{fw}) / [(E_{ld} - E_{sc}) + (E_{rd} - E_{sc})] \quad (2)$$

where V_f is the valley floor width-to-height ratio, V_{fw} is the width of the valley floor, E_{ld} and E_{rd} are elevations of the left and right valley divides, and E_{sc} is the elevation of the valley floor.

Deep V-shaped valleys ($V_f < 1$) are associated with downcutting streams distinctive of areas subjected to active uplift, whilst flat-floored valleys ($V_f > 1$) are characteristic of sectors with major lateral erosion in response to relatively tectonic quiescence *(e.g. Keller and Pinter, 2002)*.

In order to assign tectonic activity ranges to the mountain fronts analyzed in this work,

we integrated the S_{mf} index with the V_f of the main rivers of each mountain front.

Tectonically active fronts are characterized by low values of both indices and inactive fronts by high values. Intermediate values are assigned to the moderate tectonically active fronts class typically controlled by low displacement rates *(Silva et al., 2003; Bull, 2007)*.

The basin asymmetry factor (*AF*) was applied to identify possible tectonic tilting, as well as fold propagation, at the scale of the whole range. The *AF* is defined as *(Keller and Pinter, 2002)*:

$$AF = 100(A_r / A_t) \quad (3)$$

where A_r is the area of the basin to the right (facing downstream) of the trunk stream, and A_t is the total area of the drainage basin. Values of *AF* above or below 50 indicate that the basin is asymmetric. Following *Pérez-Peña et al. (2010)* we express *AF* as the absolute value minus 50 and added an arrow indicating the asymmetry direction. Subsequently we defined four asymmetry classes: $AF < 5$ (symmetric), $AF = 5–10$ (slightly asymmetric), $AF = 10–15$ (moderately asymmetric), and $AF > 15$ (strongly asymmetric).

The fourth geomorphic index we used is the drainage basin hypsometric curve that represents the distribution of area and altitude within the selected basins *(Strahler, 1952)*. This curve is obtained by plotting the proportion of the total basin height (relative height) against the proportion of total basin area (relative area, *Strahler, 1952; Keller and Pinter, 2002*). The shape of the hypsometric curve is related to the degree of dissection of the basin (e.g. its erosional stage), and moreover allows the comparison among basins with different sizes *(Keller and Pinter, 2002; Walcott and Summerfield, 2008; Pérez-Peña et al., 2009a)*. Convex hypsometric curves characterize "young" weakly eroded basins; S-shaped curves are typically associated with moderately eroded basins; and, finally, highly eroded basins show concave curves. This index is highly dependent of lithology and structure.

The hypsometric integral (*HI*) is defined as the area below the hypsometric curve and it varies from 0 to 1. Highly eroded and weakly eroded basins show *HI* values close to 0 and 1, respectively. Obviously, these two geomorphic indices are controlled by lithological and tectonic factors. The hypsometric curve and integral were calculated applying the CalHypso ARCgis tool developed by *Pérez-Peña et al. (2009b*).

The fifth geomorphic index consists of the longitudinal river profiles that are influenced by balance between erosion and uplift rates. Concave profiles represent long-term equilibrium between uplift and erosion rates. Concave-convex profiles with erosion steps in the middle reaches indicate long-term predominance of erosional processes. Convex profiles are typical of areas where uplift is dominant *(Hovius, 2000; Menéndez et al., 2008)*.

Useful information can also be obtained from "ridge-line profiles" drawn by projecting rivers onto their theoretical pre-incision surface *(Menéndez et al., 2008)*. This surface is obtained by interpolating the altitude from present-day lateral divides of the basins. However, this interpolated surface cannot be considered to be the precise pre-incision surface because basin divides themselves are affected by erosional processes *(Brocklehurst and Whipple, 2002)*. Thus, these profiles give the minimum bulk erosion for each basin, allowing relative comparisons of bulk erosion among the different basins and thus their relative erosional stage.

In order to facilitate the reading and interpretation of these data a "minimum bulk erosion map" was produced. This is a raster map where each cell results from the subtraction between the cell value on the theoretical pre-incision surface and the one on the DEM. We obtained this map with the aid of ArcGIS software, using the raster calculator and executing a subtraction between the DEM and the rasterized theoretical pre-incision surface. Thus, this map shows spatial variations in minimum bulk erosion expressed in eroded-rock column and allows discerning weakly eroded areas from highly eroded ones.

The sixth geomorphic index is the stream-length gradient index (*SL* index). In a river reach it is defined as follows *(Hack, 1973)*:

$$SL = (\mathrm{d}h/\mathrm{d}l)\, L \qquad (4)$$

where d*h*/d*l* is the slope or gradient of the reach and *L* is the channel length upstream from the midpoint of the reach to the river head.

The *SL* index shows the variation in stream power along the river reaches and it is very sensitive to changes in channel slope *(Pérez-Peña et al., 2009c)*. For this reason it allows the evaluation of recent tectonic activity and/or rock resistance.

In order to compare *SL* values of rivers with different lengths and, finally, obtain an *S*L map, a normalization factor must be used. We used the graded river gradient of the equilibrium profile (*K*) to normalize the *SL* index, obtaining the *SLk* index. With this normalization it is possible to compare the *SLk* index between rivers of different lengths *(Pérez-Peña et al., 2009c)*.

To conduct the *SLk* analysis we extracted the drainage network from a digital elevation model with 10-m spatial resolution using the D8 method (0.5 km^2 as threshold of the flow accumulation, *O'Callaghan and Mark, 1984*). To perform the *SLk* analysis, 200 channels were selected from the drainage network. To obtain the *SLk* values along the selected channels we used the *SLk* ARCgis tool developed by *Pérez-Peña et al. (2009c)*. This tool calculates the index for a fixed d*l* value. In order to determine the optimum spacing for the study area, three dl values were used (150, 250 and 350 m) to obtain the *SLk* data.

To obtain *SLk* maps, the ordinary kriging method was applied with the aid of the ArcGIS geostatistical analyst tool. Subsequently, these maps were compared, taking into account their statistical errors and congruence with the geological and tectonic features present in the study area. Finally, the *SLk* map obtained from the dataset with a d*l* of 150 m was selected.

7.4 Results

7.4.1 Fault activity: timing and kinematic constraints from mapping

Fault segmentation in the SGF zone is characterized by reverse and reverse-oblique strike-slip kinematics producing both dilatational and antidilational jogs and associated folds (Fig. 5). This fault zone affects Neogene and Quaternary sediments of the Níjar and Sorbas basins. Recent activity is manifested by cut and folded Quaternary terraces and by the tectonic control exerted on the drainage pattern. The SGF produces large deflections in the Rambla de los Feos congruent with E–W-strike-slip faulting (southern area of the map in Fig. 5). Furthermore, deformed Quaternary alluvial terraces provide useful time constraints for the SGF activity. The characteristics of these terraces are strongly influenced by two capture events in the area *(Maher et al., 2007)*; the oldest one occurred between the early and middle Pleistocene (>400 ky) according to *Mather (2000b)* and *Candy et al. (2005)*. The youngest capture has been dated using pedogenic carbonates between 70 and 100 ky *(Harvey and Wells, 1987; Candy et al., 2005)*. Terrace mapping by *Maher et al. (2007)* in the Rambla de los Feos identified terraces A to C that developed after the first capture event, and are thus of middle Pleistocene age, and terraces D and E of late Pleistocene age. The 70 ky capture produced a shift in deposition-facies in the Rambla de los Feos from coarse channelized fluvial gravels, typical of the C pre-capture terrace, to fine fluvial sheet gravels in terraces D and E developed after the capture. The southern SGF segments cut and deform all terraces (SW sector of Fig. 5). The middle Pleistocene A terrace shows clear syn-tectonic stratigraphic architecture with internal progressive unconformities/cumulative wedge-outs in outcrops with synformal geometry (see cross-section in Fig. 5). Holocene colluvial silts are cut and/or associated with the southernmost segments of the SGF, meanwhile the Rambla de los Feos show an example of large stream deflection congruent with E–W strike-slip faulting (Fig. 5). Since SGF segments produce stream deflections and affect Holocene colluvial silts it is most likely that their activity continued up to the present.

7.4.2 Results from qualitative geomorphic analysis

Focusing on the main drainage divides an extreme northwards asymmetry of the entire ridge is observed and confirmed by perpendicular topographic profiles (Fig. 4). This asymmetry is characterized by a steeper and narrower northern slope and a wider gently

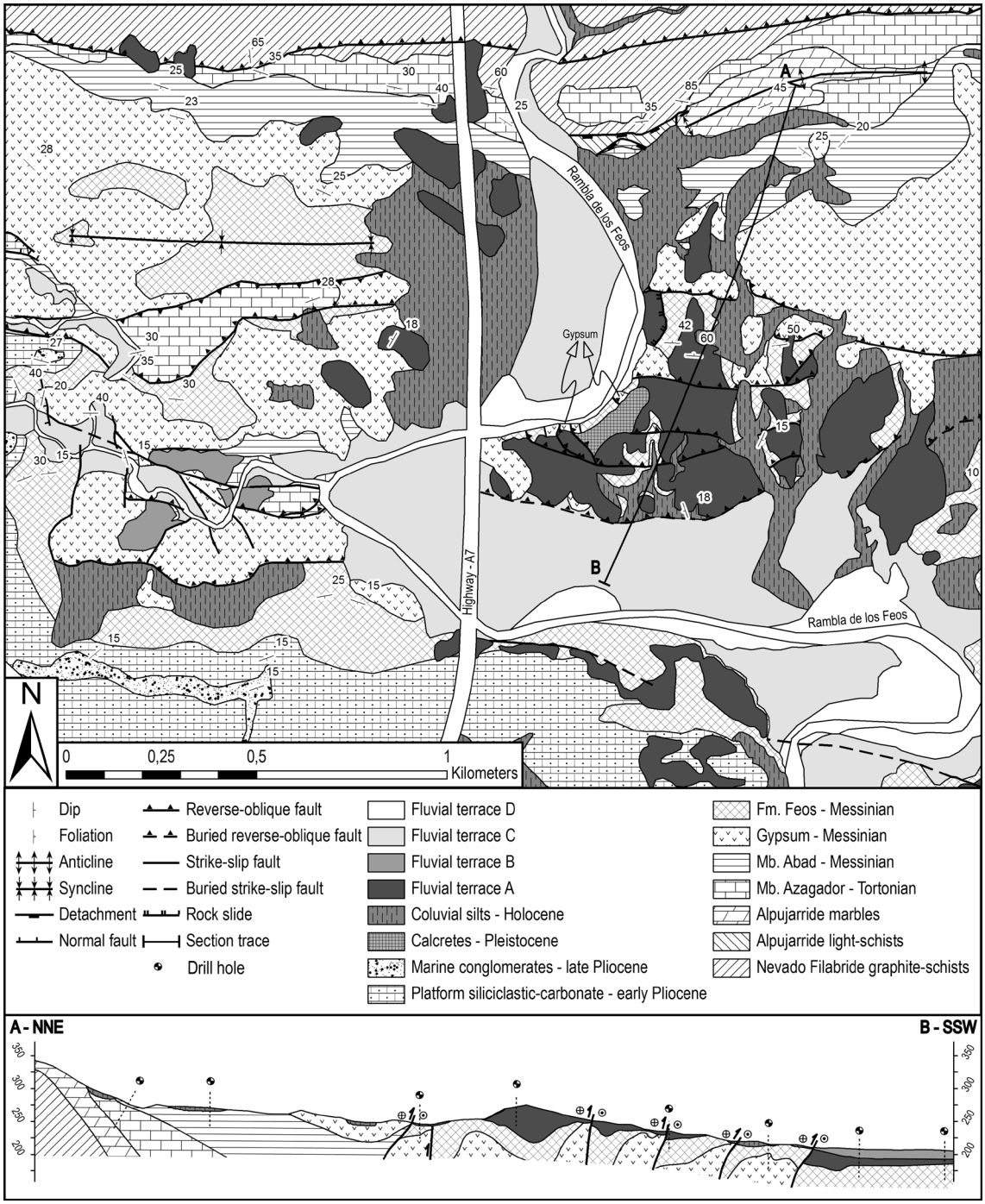

Fig. 5. Fault segments and fluvial terraces in a key area of the South Gafarillos Fault. See Fig. 2 for location. Fault segmentation is characterized by dextral and dextral-reverse kinematics affecting Neogene and Quaternary sediments and terraces of the Níjar basin. This fault zone controls the drainage pattern producing large deflections in the Rambla de los Feos congruent with E–W strike-slip faulting (southern area of the map). The middle Pleistocene C terrace shows clear syn-tectonic stratigraphic architecture with cumulative wedge-outs in outcrops with synformal geometry (see the cross section).

dipping southern slope coinciding with the fore limb and the back limb of the anticline, respectively.

The Sierra Alhamilla shows a dendritic drainage pattern with an elongated centripetal radial geometry because of its E–W ridge shape. This kind of drainage network is well manifested in the central part of the southern slope of the ridge. Also in its western part, where the same drainage pattern occurs, locally displaced according to a WNW–ESE direction.

The southern edge of the Sorbas–Tabernas basin, especially at the western and eastern terminations of the Sierra Alhamilla, is affected by an asymmetric dendritic drainage pattern extremely developed at the Rambla de Lucainena head (Fig. 4). This drainage network is characterized by a main set of axial E–W- to NW–SE-oriented streams (of orders 5 and 4) that drain the foot of the hillslope east and westward throughout the ridge terminations. From these streams come up near N–S-oriented streams (of orders 1 to 3) that drain the northern hillslope. They are shorter to the north and longer and more evolved to the south of the main axial streams. Such a drainage pattern should be produced by a recent E–W drainage system that is capturing a previous N–S one, in response to tectonic activity and/or geologic control factors occurring in the Rambla de Lucainena. This valley originated from an early Pleistocene capture driven by reverse displacement along the NARF to the south, and differential erosion between the Tortonian silty-marls and late Tortonian to Messinian temperate carbonates and reefs to the north *(Mather, 2000b)*.

The spatial distribution analysis and geometric relationships among the basins of the central part of the southern limb of the anticlinorium, both at the watershed and at the foot, indicate that they are advancing northwards by headward erosion. Indeed southern slope basins are steeper than the northern slope ones (Fig. 6). Furthermore, the E–W main drainage divide does not follow a straight line but shows an irregular trend characterized by a near northward convexity (Fig. 7a). Thus, a northward erosional trend seems likely for the basins of the southern limb. In the eastern termination, basins proceed both north- and westwards, and the main streams become progressively sub-parallel (near E–W) to the South Gafarillos Fault close to it (Figs. 7a and 9). However, the ridge asymmetry and the different slopes between the northern and southern hillslopes could be related with the asymmetry of the anticline and in particular with the different dips for its fore limb and back limb.

7.4.3 Mountain front sinuosity (S_{mf})

With respect to the mountain front sinuosity, the Sierra Alhamilla shows a quite continuous linear E–W-trending northern front, whilst the southern one is less continuous because of the development of alluvial fans, embayments and the presence of normal faults oblique to the ridge (Fig. 6). Two sectors can be differentiated in the southern front, a quite regular western front with a WNW–ESE main strike, and a less continuous eastern front that shows NNW–SSE-trending segments.

S_{mf} index values were calculated for 16 mountain fronts here named with a first letter representing the main front they belong to (N for the northern one, S for the southern one, W and E for the western and eastern terminations, respectively, Table 1) and the second one increasing progressively eastward. The northern mountain front, with S_{mf} index values lower than 1.4, indicates active tectonics especially in its eastern part (Fig. 6). The tectonic structures that produce this front are the NARF and the SGF,

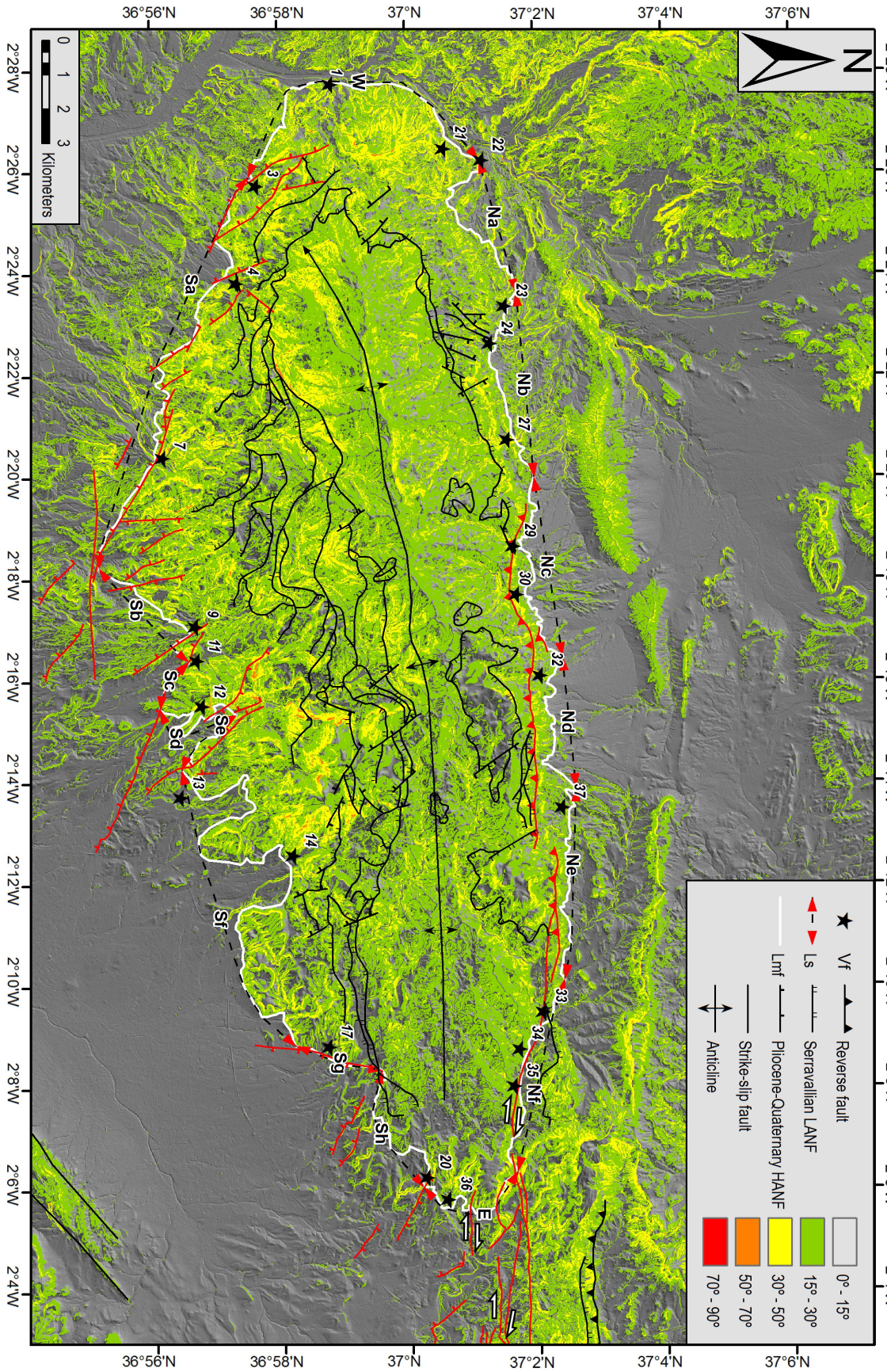

Fig. 6. Slope map of the Sierra Alhamilla showing the mountain fronts and main tectonic structures of the Sierra Alhamilla (after Martínez-Martínez and Azañón 1997). L_{mf} (the length of the mountain front) and L_S (its length measured along a straight line) employed to calculate S_{mf} values (mountain front sinuosity index values), and V_f values (valley floor width-to-height ratio) are also shown.

to the west and to the east, respectively. On the contrary the southern mountain front is characterized by at least two segments showing S_{mf} index values higher than 1.4 coinciding with the basin fill-metamorphic basement contact where alluvial fans occur (Fig. 6). The remaining segments to the south show values lower than this threshold in response to the NW–SE- to NNW–SSE-striking high-angle normal faulting. The western and the eastern ridge terminations are characterized by S_{mf} index values lower than 1.4. The eastern one induced steep regional gradients probably because of the SGF presence, whilst the western one could be related to the marked incision operated by the Rio Andarax system in response to uplift *(Nash and Smith, 1998; García et al., 2003; 2004)*.

7.4.4 Valley floor width-to-height ratio (V_f)

The V_f index was calculated for the main streams 300 m upstream from the mountain front (Fig. 6 and Table 2). Since the DEM is insufficient to accurately measure valley

Front	S_{mf}	*Front*	S_{mf}
Sa	*1.20*	*W*	*1.06*
Sb	*1.30*	*Na*	*1.47*
Sc	*1.01*	*Nb*	*1.22*
Sd	*1.70*	*Nc*	*1.44*
Se	*1.14*	*Nd*	*1.40*
Sf	*1.96*	*Ne*	*1.23*
Sg	*1.01*	*Nf*	*1.10*
Sh	*1.30*	*E*	*1.38*

Table 1. Mountain-front sinuosity values (S_{mf}) for fronts shown in Fig. 6.

Basin	*HI*	V_f	*Basin*	*HI*	V_f
1	*0.37*	*0.59*	*20*	*0.40*	*0.27*
2	*0.30*	*–*	*21*	*0.36*	*0.22*
3	*0.44*	*0.25*	*22*	*0.36*	*0.92*
4	*0.56*	*0.90*	*23*	*0.47*	*1.22*
5	*0.48*	*–*	*24*	*0.42*	*1.22*
6	*0.50*	*–*	*25*	*0.46*	*–*
7	*0.58*	*0.87*	*26*	*0.40*	*–*
8	*0.47*	*–*	*27*	*0.53*	*1.22*
9	*0.57*	*0.34*	*28*	*0.45*	*–*
10	*0.32*	*–*	*29*	*0.44*	*1.44*
11	*0.36*	*0.14*	*30*	*0.48*	*1.44*
12	*0.54*	*0.46*	*31*	*0.61*	*–*
13	*0.35*	*0.78*	*32*	*0.64*	*1.40*
14	*0.52*	*1.08*	*33*	*0.56*	*1.10*
15	*0.04*	*–*	*34*	*0.54*	*1.10*
16	*0.42*	*–*	*35*	*0.57*	*1.10*
17	*0.41*	*0.84*	*36*	*0.50*	*1.38*
18	*0.40*	*–*	*37*	*0.29*	*1.23*
19	*0.48*	*–*			

Table 2. Hypsometric integral and valley floor width-to-height ratio values (V_f) for basins and streams shown in Figs. 7 and 9.

widths, especially for narrow stream valleys, the V_{fw} parameter was obtained by measuring widths directly from aerial photographs *(Pedrera et al., 2009b; Pérez-Peña et al., 2010)*.

In the northern and southern slope of the Sierra Alhamilla, streams present V-shaped valleys ($V_f < 1$), with only two streams with slightly higher V_f values (streams 23 in the northern front and 14 in the southern one). Moreover, some of the streams in both fronts present particularly low V_f values ($V_f < 0.5$), thus suggesting highly active fronts (Fig. 6).

By integrating mountain front sinuosity and valley floor width-to-height ratio, we are able to assign different tectonic activity classes to each mountain front *(Rockwell et al., 1984; Silva et al., 2003)*. The mountain fronts of the eastern and western terminations belong to the tectonically active front class, showing low values of both S_{mf} and V_f. The northern mountain fronts are divided between tectonically highly active fronts (Nb, Nf, and Ne) and moderately active fronts (Na, Nc and, Nd) that present low V_f and over-threshold S_{mf} values. The southern mountain fronts, Sa, Sb, Sc, Se, Sg, and Sh have been defined as tectonically active, whereas fronts Sd and Sf present characteristics of moderately and low activity, respectively (Fig. 6). Thus, for both highly and moderately active fronts, streams downcut producing V-shaped valleys upstream from the fault. Nevertheless, the western termination shows low S_{mf} and V_f values probably related to the marked incision operated by the Rio Andarax system *(Nash and Smith, 1998; García et al., 2003; 2004)*.

Some authors have proposed uplift-rate ranges for each tectonic activity class: rates of >0.5 m ky^{-1} for class 1; 0.5–0.05 m ky^{-1} for class 2; and <0.05 m ky^{-1} for class 3 *(Rockwell et al., 1984; Mayer, 1986; Silva et al., 2003; Bull, 2007)*. Taking into account these uplift-rate ranges as a reference, we are able to assign a tectonic uplift rate from 0.05 m ky^{-1} to at least 0.5 m ky^{-1} to the entire Alhamilla northern front. However, we cannot assign any uplift rate to the whole southern front because the fault system here is extremely segmented by faults with different strikes. We use these ranges because it is very difficult to constrain the uplift-rates with field data since morpho-stratigraphic markers are not continuous, for example in the Sierra Alhamilla northern front the youngest Pleistocene alluvial unit is missing in the hanging-wall fault block where only the oldest one crops out.

7.4.5 Basin asymmetry factor (AF)

Three sectors with similar basin asymmetry factor can be recognized: a) the eastern termination shows a clear southwards asymmetry; b) the northern slope shows a common westward asymmetry; and c) the western termination and the southern slope show roughly a common eastwards asymmetry (Fig. 7a). Based on the asymmetry classes, basins of the western termination show the lower asymmetry values, belonging to the first and second classes, in contrast to those of the eastern termination that belong

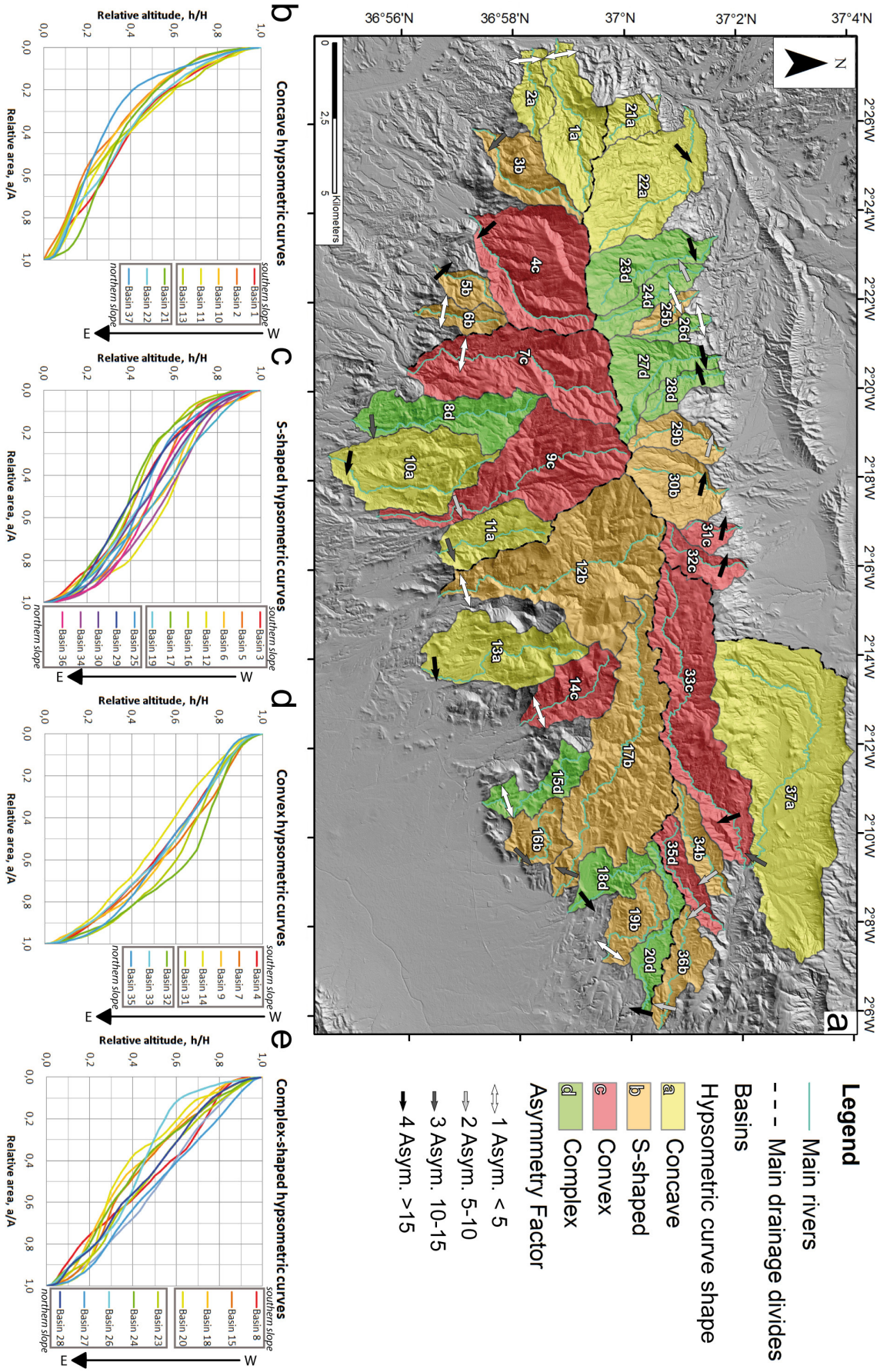

Fig. 7. Maturity drainage-basin map of the Sierra Alhamilla. a) Drainage basins distribution map where the main drainage divides, streams, drainage basins (classified depending on their hypsometric curve shapes) with their asymmetry factor are shown. b) Hypsometric curves associated with mature and highly eroded basins. c) Hypsometric curves associated with moderately eroded basins. d) Hypsometric curves associated with "younger" and weakly eroded basins. e) Hypsometric curves associated with stream "rejuvenation" processes, at the foot or head of the streams.

to the second and forth classes. Basins of the northern slope show the highest values of asymmetry belonging commonly to the fourth class, whereas the southern slope ones show more variable values (Fig. 7a).

7.4.6 Hypsometric curves and integral (HI)

Basins with concave hypsometric curves, and so more mature, occur in the western termination of the ridge and at the foot of the southern slope (Fig. 7a and b). Basins with S-shaped hypsometric curves, and so intermediately mature, are located mainly in the eastern part of the ridge, both at the foot of the northern slope and in its eastern termination (Fig. 7a and c). The less mature basins with convex hypsometric curves are found in the western part of the southern slope at the main watershed, and locally, in the eastern part of the northern slope (Fig. 7a and d).

Some basins show quite irregular hypsometric curves that cannot be classified within the previous shapes. The irregular form of these curves might be due to "rejuvenation" processes at the foot or head of the streams and/or piracy events, probably related to active tectonics together with litho-geological control factors. Thus, here we propose the term "complex hypsometric curves" to distinguish them from the previous curves.

Basins with complex hypsometric curves are recognized in the western part of the northern slope and also locally at the foot of the southern hillslope (Fig. 7a and e). Typically, basins in the southern slope show a convex shape in the upper part of their hypsometric curves indicating a lower grade of maturity with respect to their lower part and thus head-rejuvenation processes. Nevertheless, the hypsometric curve shape of basin 20 could be related to a piracy event caused by an E–W-drainage that captured an N–S previous one (Fig. 7a and e). On the other side, basins of the northern slope show evidence of foot-rejuvenation processes responsible for a convex trend in the lower part of the curves. However, the shapes of the curves of basins 27 and 28 could be related to a piracy event produced by stream 27 at the head of stream 28.

It is important to underline the occurrence of basins with convex and S-shaped curves continuously from the eastern termination to the central part of the northern slope (Fig. 7a). Basins with complex curves are found farther west, along the northern slope, and locally at the foot of the southern hillslope. The previous observations were confirmed by the calculated *HI* values, reported in the Table 2.

7.4.7 Longitudinal stream profiles

Three sectors with similar longitudinal stream profiles can be recognized: a) streams at the eastern termination of the ridge show concave profiles; b) those at the southern slope are characterized by both concave and concave-convex profiles; and c) streams with convex and concave-convex profiles occur both at the western termination and northern slope of the ridge.

The most important results from the longitudinal stream profiles concern the streams of the central and eastern parts of the northern slope. Longitudinal stream profiles 31, 32, 34 and 35 are characterized by convex geometries, thus suggesting areas affected by an uplift-incision ratio higher than 1. The stream profiles 34 and 35 (Fig. 8) are associated with uplift (south to the SGF) caused by the SGF, which is characterized by dextral transpressive kinematics. Similarly, the stream profiles 31 and 32 (Fig. 8) seem to be related to the NARF that produces an important uplift of its southern block in this sector of the northern slope. Both streams show a knickpoint at the foot of their profile coinciding with the fault scarp of the NARF, meanwhile the other ones are the result of either an older fault scarp that has migrated upstream (stream 31) or a lithologic control (Alpujarride–Nevado Filabride complexes contact, for stream 32).

Longitudinal stream profiles in the southern slope locally show concave-convex profiles, with knickpoints probably associated with the NW–SE- to NNW–SSE-striking high-angle normal faults, like streams 3 and 12 (Fig. 8). Both stream profiles show two knickpoints associated with these high-angle normal faults that produce a local base-level fall downstream. The other knickpoints are probably the result of the lithological contrast across the extensional detachment between the Alpujarride and the Nevado Filabride complexes. These results evidence that most streams in the study area, showing both fault- and lithologic-related knickpoints, cannot be considered as continuous systems but as subsystems in the evolution of both stream profiles and drainage divides. Indeed both streams and drainage basins affected by faults have to remove the fault-related geomorphic anomaly before they can equilibrate themselves (as a continuous system), reaching a concave stream profile and hypsometric curve. This geomorphic action is accomplished when the sub-portions of the same basin reach the same geomorphic evolutionary stage.

7.4.8 Ridge-line profiles and minimum bulk erosion map

The minimum bulk erosion map shows that basins occurring in the southern slope of the ridge, especially in its central part, are the most eroded in the area. These basins are numbered 4, 7, 9 and 12 (Fig. 9). The maximum bulk erosion value of 390 m (eroded-rock column) is reached by stream 12, meanwhile the average in the south is between 200 and 300 m (eroded-rock column). The basins occurring in the eastern termination of the ridge are the less eroded, indeed their streams show a mean bulk erosion value between 20 and 80 m (eroded-rock column, Fig. 9). Basins of the northern slope of the

Fig. 8. Representative longitudinal stream and ridge-line profiles (×10 vertical scale, see Fig. 7a for location). Solid lines are stream profiles; dotted lines are ridge-line profiles. Triangles indicate fault-related knickpoints. Profiles 3 and 12 are examples of streams from the southern slope of the Sierra Alhamilla affected by the Pliocene–Quaternary high-angle normal fault system (HANF) that produces knickpoints in their profiles. Profiles 31, 32, 34, and 35 are examples of streams from the northern slope of the Sierra Alhamilla where the North Alhamilla Reverse Fault–South Gafarillos Fault system produces "foot-rejuvenation" processes (NARF in profiles 31 and 32) or convex profile shapes (profiles 34 and 35). Profiles 3 and 32 show knickpoints produced by the Serravallian low angle normal fault system (LANF).

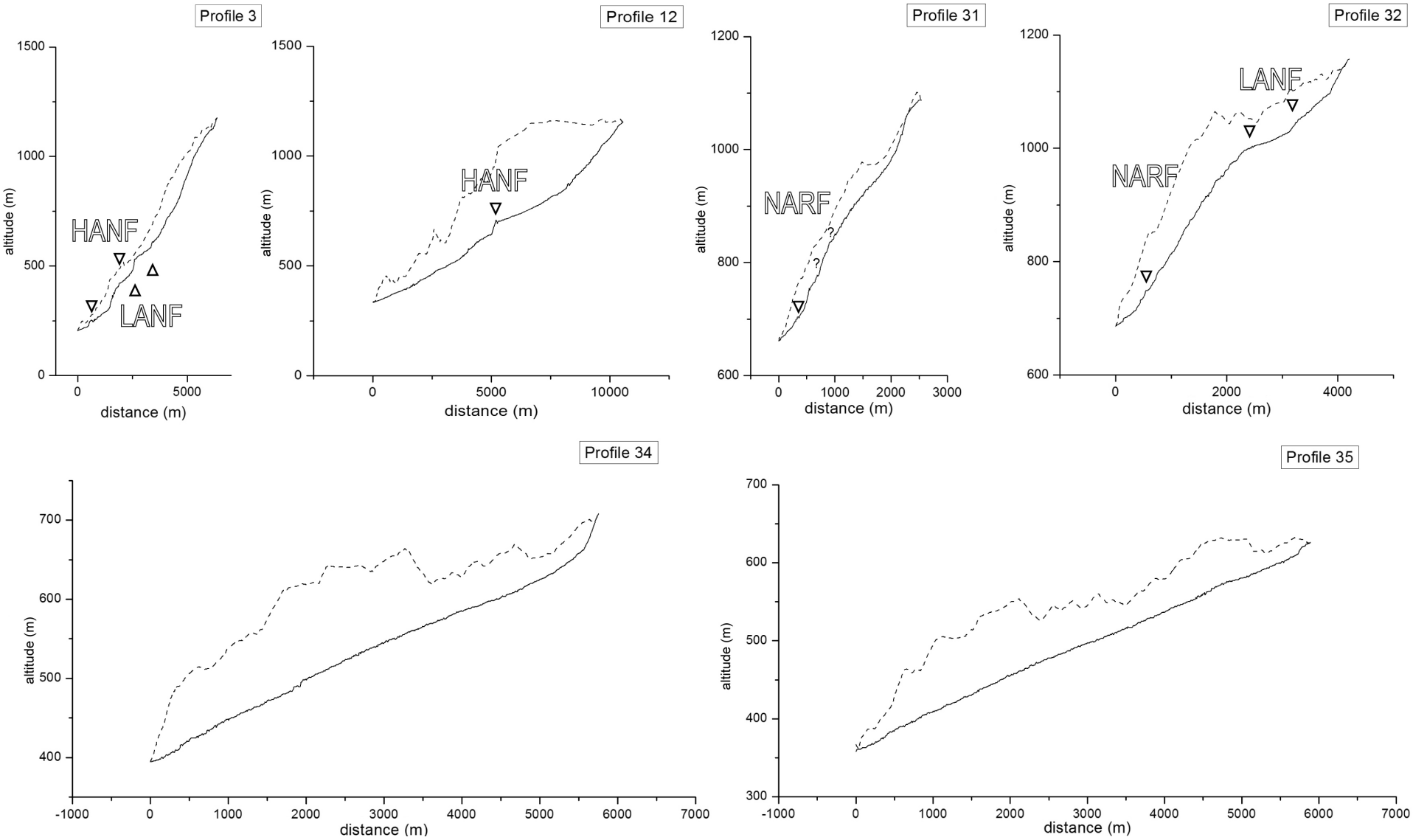
Profile 3
HANF
LANF
altitude (m)
distance (m)
Profile 12
HANF
altitude (m)
distance (m)
Profile 31
NARF
?
altitude (m)
distance (m)
Profile 32
LANF
NARF
altitude (m)
distance (m)
Profile 34
altitude (m)
distance (m)
Profile 35
altitude (m)
distance (m)

ridge, especially in its central part, show the highest bulk erosion values relative to this slope (basins 27 to 30, and 33, Fig. 9). Bulk erosion values in these streams are between 60 and 150 m, reaching a maximum value of 173 m (eroded-rock column). Summing up, the highest erosion bulks occur in the central part of the southern slope, whereas the lowest bulks are located in the eastern termination of the ridge (Fig. 9).

7.4.9 SLk map and anomalies

The *SLk* map discerns areas with low slope from areas with high slope along the stream channel, thus allowing detecting anomalies that may be related to recent tectonic activity and/or gradients of rock resistance. The *SLk* map obtained shows at least five high *SLk* anomalies (Fig. 10). Two of them are located on the topographic break of the northern slope of the ridge and show an E–W elongated shape (1 and 2 in Fig. 10). The length of these anomalies is 8 and 13 km, respectively; both are 2 km wide. The other anomalies (3 to 5 in Fig. 10) are located on the southern slope having an NNW–SSE main strike, although their shape is quite irregular. It is important to remark that a good correspondence between most of the high *SLk* anomalies and the highest bulk erosion values is observed, as in the case of anomaly 4 in basin 12 (Figs. 9 and 10).

7.5 Discussion

In addition to local and regional tectonic activity, geomorphic processes are also controlled by topographic, climatic, and lithologic factors that must be taken into account when tectonically oriented conclusions are deduced *(Jackson and Leeder, 1994; Schumm et al., 2000; Burbank and Anderson, 2001; Keller and Pinter, 2002)*. Thus, in this section we will discern the tectonic control on the conducted geomorphic analyses from the other controlling factors. Subsequently we will try to associate these geomorphic features with the tectonic structures present in the study area.

The North Gafarillos Fault probably initiated its activity in the Tortonian, in response to NW–SE Nubia–Iberia convergence, and was sealed both by latest Tortonian and early Messinian temperate carbonates and by Messinian reefs in the northern limb of the Sierra Alhamilla, thus staying active between 8 and 6.4–5.9 Ma *(Ott d'Estevou and Montenant, 1990; Stapel et al., 1996; Huibregtse et al., 1998; Jonk and Biermann, 2002; Booth-Rea et al., 2004a)*. Dextral displacement along the North Gafarillos Fault was transferred to the North Alhamilla reverse fault located in the northern limb of the Sierra Alhamilla–Polopos anticline *(Platt et al., 1983; Weijermars et al., 1985)*.

Although some of these fault segments are sealed, the qualitative and quantitative geomorphic analyses carried out here, together with the fluvial terrace mapping and the epicenter position of reverse and strike-slip focal mechanisms *(Stich et al., 2003a)*, testify that other fault segments of the system have been active during and after the Pleistocene, which control the present geomorphologic features in the area. This

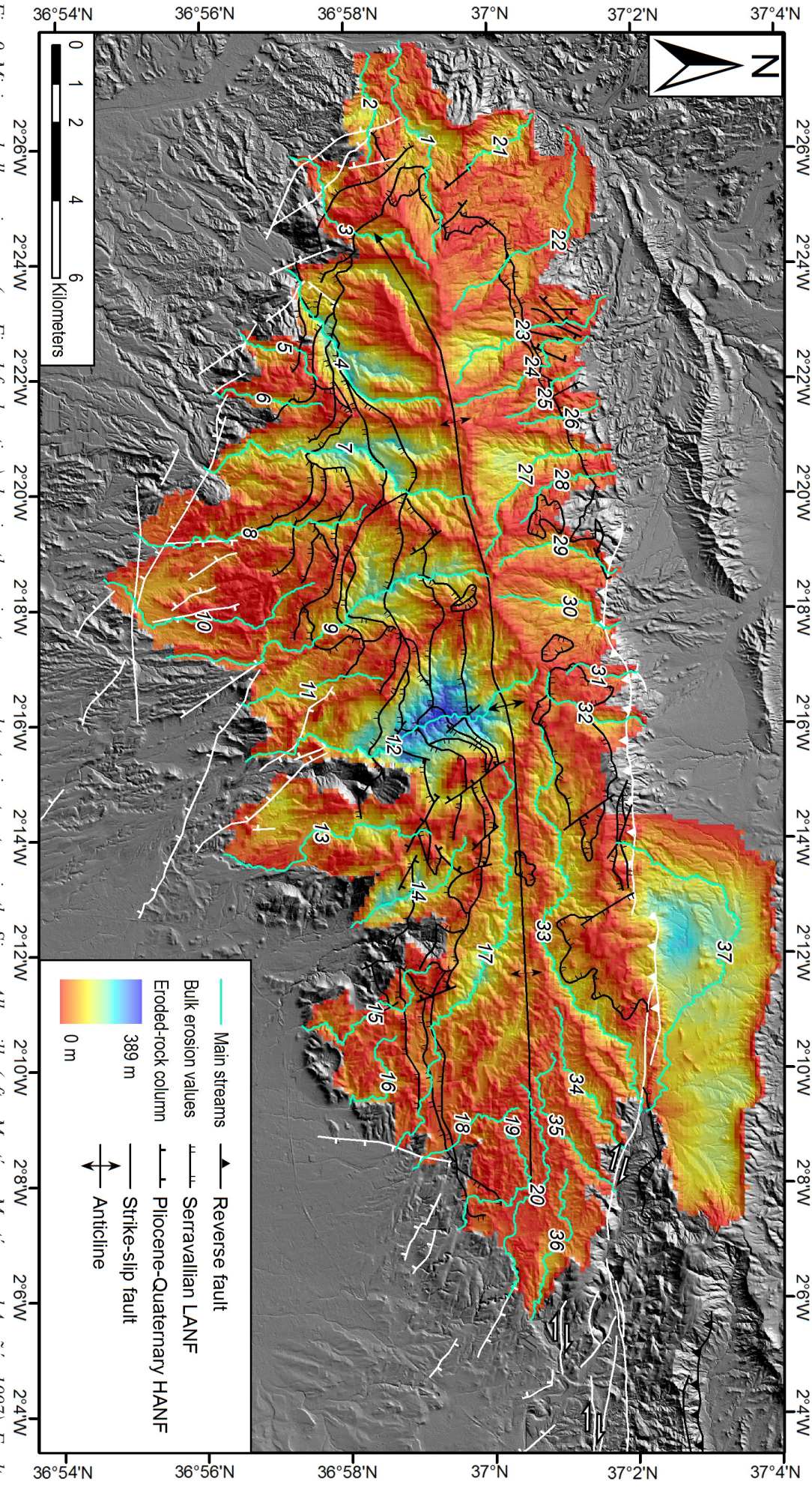

Fig. 9. Minimum bulk erosion map (see Fig. 1 for location) showing the main streams and tectonic structures in the Sierra Alhamilla (after Martínez-Martínez and Azañón 1997). Faults with Quaternary activity are shown in white.

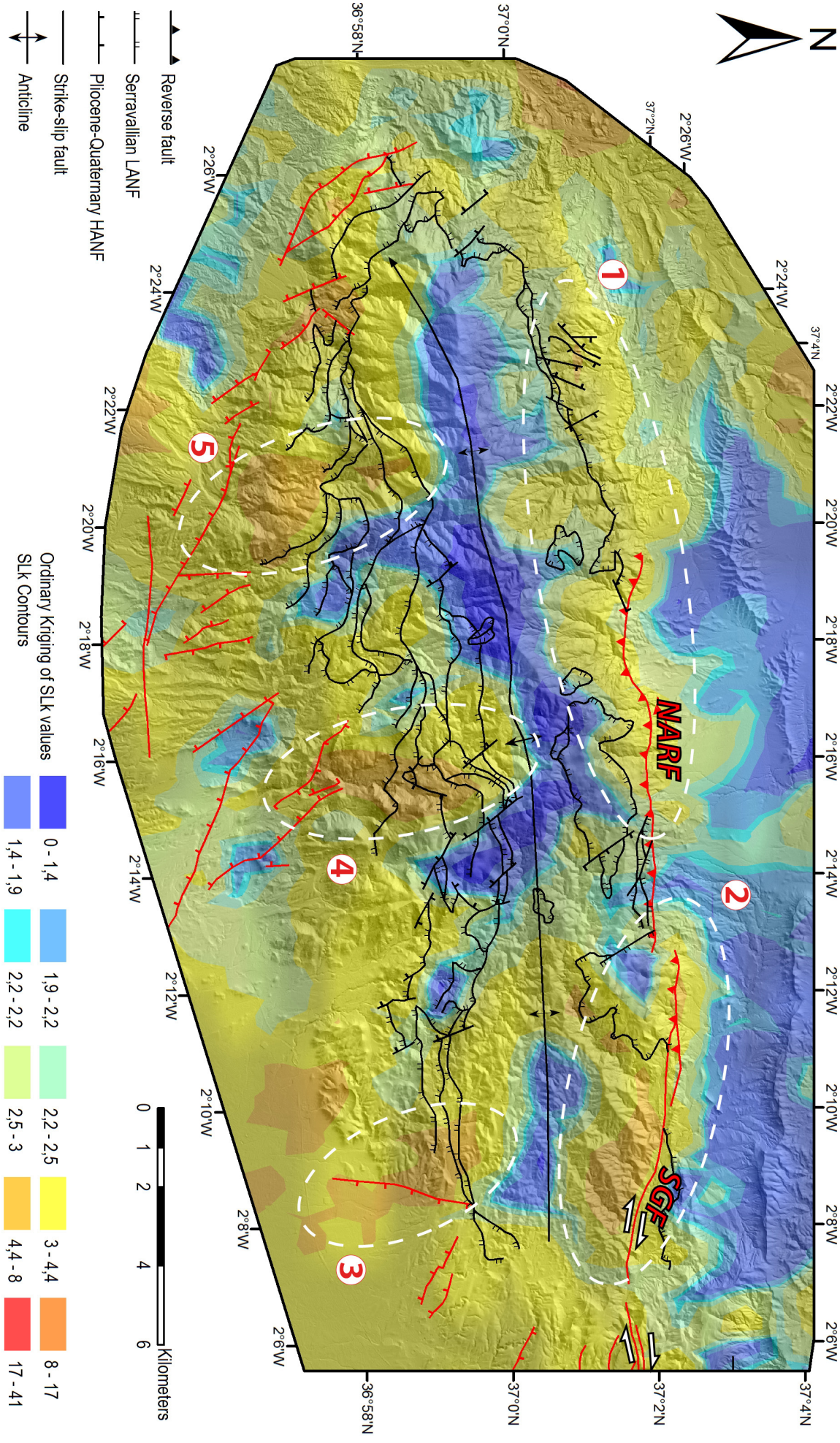
N
Reverse fault
Serravallian LANF
Pliocene-Quaternary HANF
Strike-slip fault
Anticline
Ordinary Kriging of SLk values
SLk Contours
0 - 1,4
1,4 - 1,9
1,9 - 2,2
2,2 - 2,5
2,2 - 2,2
2,5 - 3
3 - 4,4
4,4 - 8
8 - 17
17 - 41
0 1 2 4 6 Kilometers
NARF
SGF
1
2
3
4
5
37°4'N
37°2'N
37°0'N
36°58'N
2°26'W
2°24'W
2°22'W
2°20'W
2°18'W
2°16'W
2°14'W
2°12'W
2°10'W
2°8'W
2°6'W

is the case of the North Alhamilla reverse fault and the South Gafarillos Fault, to the southeast.

Finally, geomorphic analyses show the occurrence of Pliocene–Quaternary high-angle normal faulting in the southern slope and western termination of the Sierra Alhamilla, congruent with the structures documented in literature *(Martínez-Martínez and Azañón, 1997; Martínez-Díaz and Hernández-Enrile, 2004; Marín-Lechado et al., 2005; Pedrera et al., 2006; Sanz de Galdeano et al., 2010)*.

7.5.1 The NARF-SGF fault system

The low S_{mf} index values obtained for the Sierra Alhamilla northern front seem to be related to the occurrence of an E–W-anticline that forms the entire ridge (Na and Nb in Fig. 6). In the eastern part of this front, the tectonic control on topography is accentuated by the NARF occurrence. Indeed the low S_{mf} index values occurring here support the late Pleistocene activity of the NARF that ends westward (Nc, Nd and Ne in Fig. 6). The high *SLk* anomaly 1 in Fig. 10 seems to be related to the NARF that produces a significant uplift of its hanging-wall block, coinciding with the northern slope of the ridge. The uplift rate deduced from the integration between the S_{mf} and the V_f indices ranges between 0.5 and 0.05 m ky^{-1} in the Quaternary. In addition, the occurrence of basins showing high bulk erosion values at the foot of northern slope of the ridge, especially in its central part (Fig. 9), support the uplift of the NARF southern block. Indeed a continuous fault activity lowers the local base-level of streams, allowing the occurrence of high bulk erosion and high *SLk* anomalies. Thus, to obtain such a geomorphic output a prolonged fault activity is necessary.

Fault segmentation and fluvial-terrace mapping shows that the SGF has been active until the Holocene (probably up to the present) in the eastern part of the Sierra Alhamilla northern front (Nf in Fig. 6). Moreover, the southward basin asymmetries recognized here (Fig. 7a) seem to be associated with the uplift of the southern block of the NARF–SGF system, which in this sector is characterized by an NW-ward displacement of the hanging-wall in response to a dextral-transpressive regime. This uplift is supported also by the high *SLk* anomaly 2 in Fig. 10 that is located just to the south of this fault system. The uplift rate assigned to this fault from the integration of the S_{mf} and the V_f indices is more than 0.5 m ky^{-1} in the Quaternary. Contrary to the expected occurrence of highly eroded basins south of this fault system, the minimum bulk erosion map shows the less eroded basins here (Fig. 9). This is most likely due to the more pure strike-slip displacement component of the SGF verified in the field.

These hypotheses are confirmed also by the occurrence of streams with convex and

Fig. 10. SLk map and main tectonic structures of the Sierra Alhamilla. NARF: North Alhamilla Reverse Fault. SGR: South Gafarillos Fault. In the legend LANF stands for low angle normal fault, and HANF for high angle normal fault. Faults with Quaternary activity are shown in red. Modified after Martínez-Martínez and Azañón (1997).

concave–convex longitudinal profiles and basins with S-shaped, convex and complex hypsometric curves in the entire northern slope (Fig. 7a). The relative uplift of the southern block of NARF–SGF fault system changes local base-levels causing the occurrence of less mature basins. In addition, in response to reverse displacement along this fault system, foot-rejuvenation processes should occur in basins above the fault trace, thus generating complex hypsometric curve shapes.

Furthermore, a progressive gradient is observed from completely rejuvenated basins to the east (basins 31 to 33), passing through basins showing S-shaped hypsometric curves in the center (29 and 30) towards basins with complex curves in the western end of the NARF (26 to 28 in Fig. 7a). This gradient can reflect both the westward propagation of the fault system along time and/or a progressive decrease of net slip towards the tip line, in our case the west one. The westward asymmetry of basins in the central part of the northern front confirms the existence of fault displacement gradient increasing towards the east, with maximum uplift being localized close to the junction between the NARF and the SGF. This net slip gradient, which in turn produces a differential uplift, would have promoted tilting towards the west, away from the area of maximum uplift, located at the head of stream 33. Furthermore, the occurrence of a fault displacement gradient along the NARF is supported by the eastward increasing S_{mf} index values (Nc to Nf mountain fronts in Fig. 6).

7.5.2 The Pliocene–Quaternary high-angle normal fault system

The low S_{mf} index values obtained for the Sierra Alhamilla southern front (Sa, Sc and Se in Fig. 6) support the recent to present activity of the NW–SE- to NNW–SSE-striking high-angle normal fault system that affects the southern slope of the ridge and the Níjar–Almería basin. The uplift rate assigned to the faults, coinciding with theses fronts (Sa, Sc and Se in Fig. 6) from the integration between the S_{mf} and the V_f indices is more than 0.5 m ky^{-1} in the Quaternary, values quite different from displacement rates documented in the area from other authors (between 0.23 and 0.48 m ky^{-1} for the western part of the system, *Martínez-Díaz and Hernández-Enrile, 2004*). These observations are confirmed by the occurrence of basins with S-shaped, convex and complex hypsometric curve shape at the southern slope (Fig. 7a). In response to SW-wards normal displacement, the relative uplift of southern slope sectors, especially westward, has changed the streams local base-level thus producing younger drainage basins. In addition, stream head-rejuvenation processes should occur in basins above the fault traces, generating complex hypsometric curve shapes. Congruently with these observations, longitudinal stream profiles in the southern slope locally show concave-convex profiles with knickpoints (Fig. 8). Finally, the relative uplift of the respective high-angle normal fault footwalls in the southern front is further confirmed by the occurrence of high *SLk* anomalies 5 and 4 (Fig. 10).

In the eastern part of the Sierra Alhamilla southern slope the occurrence of basins with

S-shaped and complex hypsometric curve shapes (Fig. 7a) seems to be related to a Pliocene–Quaternary high-angle normal fault having an N–S strike and a down to the east normal displacement (Fig. 2). The Quaternary activity of this fault is also suggested by the low S_{mf} index value associated with the Sg mountain front (Fig. 6). Furthermore, this fault, producing a relative uplift of its western block, seems to be the cause of the high *SLk* anomaly 3 shown in Fig. 10.

Finally, the occurrence of the most eroded basins in the southern slope of the ridge, especially in its central part (Fig. 9), should be related also to the high-angle normal fault system together with differential uplift between the Sorbas–Tabernas and Níjar–Almería basins *(Braga et al., 2003)*.

Although the tectonic displacement rate of this fault system is relatively low (between 0.23 and 0.48 m ky^{-1} for the western part of the system, *Martínez-Díaz and Hernández-Enrile, 2004*) geomorphic indicators of the fault activity, such as the sinuosity of the fault-related mountain fronts, are preserved because of the semi-arid climate and the strength contrast between the Neogene sediments and the metamorphic basement.

7.5.3 Western and eastern terminations

The low S_{mf} index values obtained for the western and eastern terminations of the Sierra Alhamilla (E and W in Fig. 6) seem to be related in the western end with the occurrence of the peri-anticlinal closure and in the eastern one by the presence of the SGF cutting the fold. Basins with concave hypsometric curve shape (Fig. 7a), together with the absence of a high *SLk* anomaly at the western termination (Fig. 10) should prove a quiescent activity of the Sierra Alhamilla anticlinorium in its westernmost end; whereas, the occurrence of low S_{mf} index values (Fig. 6), could be related to the marked incision operated by the Rio Andarax system and its Rambla de Tabernas tributary in response to uplift induced steep regional gradients *(Nash and Smith, 1998; 2003; García et al., 2004)*.

7.6 Conclusions

The qualitative and quantitative geomorphic analyses suggest that the Sierra Alhamilla is tectonically active during the Pleistocene and Holocene, and probably up to the present. The high *SLk* anomaly 1 in Fig. 10 seems to be related to the North Alhamilla Reverse Fault (NARF) that produces an uplift of the northern slope of the ridge with rates ranging between 0.05 and 0.5 m ky^{-1} in the Quaternary. The results from the geomorphologic analyses together with the field data support the Pleistocene activity along the NARF. These include the northwards asymmetry of the entire ridge, low S_{mf} and V_f values of the northern front, the "foot-rejuvenation" of the northern slope streams, characterized by convex and concave-convex profiles, and finally, the occurrence of basins with high bulk erosion values that show convex and S-shaped

hypsometric curves.

The high *SLk* anomaly 2 in Fig. 10 is likely produced by the fault system formed by the junction between the NARF and the South Gafarillos Fault (SGF), which is characterized by a dextral transpressive regime. These segments of the Polopos Fault Zone have also been active in the Pleistocene and the Holocene producing uplift of the southern block with respect to the NARF and SGF with rates above 0.5 m ky^{-1} in the Quaternary. This activity is supported by both fluvial terrace mapping and geomorphologic analyses, which show low S_{mf} and V_f values of the northern front, southwards migration and asymmetry of the basins, stream "rejuvenation" and reorientation close to the SGF and convex stream longitudinal profiles.

The NARF–SGF system is characterized by a progressive decrease of net slip towards its tip line at the west. This observation is supported by a progressive eastward "rejuvenation gradient" of basins along the NARF together with an eastward increasing S_{mf} index value of the northern mountain front. In turn this tectonic transport gradient causes an eastward increase in uplift of the southern block producing westward asymmetric basins in the central part of the northern slope of the ridge.

The high *SLk* anomalies 3, 4 and 5 in Fig. 10 are probably due to the Pliocene–Quaternary high-angle normal fault system that affects the entire southern slope of the Sierra Alhamilla and the Níjar–Almería basin. Uplift rates in the southern mountain fronts that coincide with high-angle normal faults are higher than 0.5 m ky^{-1} in the Quaternary. The geomorphic evidence of such a tectonic control are: a) low S_{mf} and *V*f values in southern mountain front segments that are congruently oriented with respect to the normal faults; b) the northwards asymmetry of the entire ridge; c) the northwards advance and stream "head-rejuvenation" of the basins located in the central part of the southern slope; d) longitudinal stream profiles in the southern slope that locally show concave-convex profiles with knickpoints; and e) maximum bulk erosion values of basins occurring in the southern slope.

Acknowledgments: This study was supported by research projects CGL2008-03249/BTE, CGL-29920, TOPOIBERIA CONSOLIDER-INGENIO2010 and CTM2007-66179-C02-01/MAR from the Spanish Ministry of Science and Innovation and MMA083/2007 from the Spanish Ministry of Environment.

Tectonophysics 580 (2012) 27–42, doi:10.1016/j.tecto.2012.08.028
Received 7 May 2012 / Available online 3 September 2012

8.0 Geomorphic analysis of the Sierra Cabrera, an active pop-up in the constrictional domain of conjugate strike-slip faults: the Palomares and Polopos fault zones (eastern Betics, SE Spain)

Flavio Giaconia [a,*], G. Booth-Rea [a, b], J. M. Martínez-Martínez [a, b], J. M. Azañón [a, b], J. V. Pérez-Peña [b]

[a] Dpto. Geodinámica, Instituto Andaluz de Ciencias de la Tierra (CSIC-UGR), Campus Fuentenueva S/N, 18002, Granada, Spain
[b] Dpto. Geodinámica, Universidad de Granada (UGR), Campus Fuentenueva S/N, 18002, Granada, Spain
[*] Corresponding author. E-mail address: flavio@ugr.es, flavio@iact.ugr-csic.es (F. Giaconia)

Abstract: The NNE–SSW sinistral Palomares and the conjugate dextral WNW–ESE striking Polopos fault zones terminate in the Sierra Cabrera antiform. In order to test the Quaternary activity and topographic relief control in the termination of these fault zones, here we present new qualitative and quantitative geomorphic analyses supported by a new structural map of the region. The main mountain fronts of the Cabrera antiform are formed by the North and South Cabrera reverse faults that merge laterally into the Palomares and Polopos faults, respectively. These faults produce knickpoints, stream deflections, complex basin hypsometric curves, high *SLk* anomalies and highly eroded basins in their proximity. Furthermore, the drainage network shows an S-shaped pattern reflecting progressive anticlockwise rotation related to the sinistral Palomares fault zone. The estimated uplift rates determined by the integration between mountain front sinuosity index and valley floor width to height ratio are larger than those obtained for strike-slip faults in the eastern Betics. These larger uplift rates with our geomorphic and structural dataset indicate that the topographic relief of the Sierra Cabrera antiform is controlled by reverse faults that form a pop-up structure in the constrictional domain between the larger Palomares–Polopos conjugate strike-slip faults. Existing GPS geodetic data suggest that the North and South Cabrera reverse faults probably accommodate a large part of Africa–Iberia convergence in the region.

Keywords: Active tectonics; Geomorphic indices; Eastern Betics; Polopos fault zone; Palomares fault zone

8.1 Introduction

Geomorphic analyses are very productive in semiarid zones like SE Spain, where landforms related to active tectonics are preserved for long periods *(Silva et al., 2003)*. Furthermore, geomorphic indices are tools to characterize sectors deformed by active faults with low to moderate deformation rates *(Keller and Pinter, 2002; Gràcia et al., 2006; Pedrera et al., 2009b; Pérez-Peña et al., 2010)*. In regions affected by strike-slip faults, like the eastern Betics, displacement generates important topographic gradients forming both uplifted ranges and sedimentary depocenters in antidilational and dilational jogs, respectively *(Sibson, 1986; Sylvester, 1988)*. Similarly, thrust systems and associated folds control the development and evolution of alluvial and fluvial systems in response to tectonically induced local base-level variations, together with fault linkage and time-space migration of folds *(Ramsey et al., 2008; Pedrera et al., 2009b)*. Furthermore, creation of new fault segments produces migration of active sedimentary depocenters and variations in the topography and drainage network *(Ollier, 1981; Walker and Jackson, 2002; Booth-Rea et al., 2004a)*. In the southeastern Betics the main positive topographic reliefs coincide either with antidilational jogs related to strike-slip faults or with antiformal structures that define the Sierras in the area *(e.g. Montenat and Ott d´Estevou, 1990)*.

Sierra Cabrera is a key area to evaluate the nature of active tectonics in the eastern Betics because three of the main active faults in SE Spain, the Carboneras, the Palomares and the Polopos fault zones, converge and terminate there. Contrasting with the pure strike-slip Neogene activity of these faults *(Bousquet, 1979; Montenat et al., 1990; Ott d´Estevou et al., 1990; Faulkner et al., 2003; Gràcia et al., 2006)*, the Quaternary activity of the Carboneras and the Palomares fault zones appears to be oblique-slip along their terminations *(Buforn et al., 1988; 1995; Bell et al., 1997; Reicherter and Reiss, 2001; Booth-Rea et al., 2003a; Booth-Rea et al., 2004a; Buforn et al., 2004)*.

The N90-100ºE dextral Polopos fault zone, conjugate of the Palomares fault zone, bounds the southwestern termination of the Sierra Cabrera antiform and has been active during the Pleistocene with a global transpressive regime *(Giaconia et al., 2012a)*. This fault zone merges into N50-60ºE reverse fault segments, here named the South Cabrera reverse faults, in the southeastern corner of the Sierra Cabrera. The Carboneras fault is a sinistral strike-slip fault active during the Neogene to Quaternary *(Bousquet, 1979; Montenat et al., 1990; Ott d´Estevou et al., 1990; Faulkner et al., 2003; Gràcia et al., 2006)*. This fault worked as a transform fault system accommodating differential extension between the Níjar and other postorogenic basins to the NW of it and the volcanic Cabo de Gata terrain to the SE *(Rutter et al., 2012)*. Its Plio–Quaternary activity appears to be oblique-slip according to the field data *(Buforn et al., 1988; 1995; Bell et al., 1997; Reicherter and Reiss, 2001; Buforn et al., 2004; Rutter et al., 2012)*. The Plio–Quaternary activity of the Palomares Fault Zone is characterized by a sinistral-

normal displacement that uplifts its eastern block, represented by the Sierra Almagrera. Toward the south, Palomares fault segments turn and splay out into reverse faults in the northern limb of the Sierra Cabrera antiform *(Booth-Rea et al., 2003a; 2004a)*. In this paper we refer to these faults as North Cabrera reverse faults. GPS geodetic studies in the southeastern Betics show deformation rates of 1-1.5 mm yr^{-1} on the coast, roughly parallel to the NW–SE direction of the Africa–Eurasia plate convergence, while the stations inland exhibit insignificant motion with respect to the stable part of the Eurasian plate *(Echeverria et al., 2011)*. This indicates that the majority of the convergence between Africa and Eurasia in the area is accommodated along structures located near the coast, like the Sierra Cabrera antiform and associated structures.

In this paper we carry out a thorough geomorphic analysis of the Sierra Cabrera ridge supported by a new geological and structural map inferring that strike-slip displacement along the Polopos and Palomares fault zones has been accommodated by reverse faulting in the southern and northern hillslopes of the ridge by the South and North Cabrera reverse faults, respectively. This reverse tectonic regime in the Sierra Cabrera antiform, together with the epeirogenic uplift of the southern Betics *(Braga et al., 2003)*, results in a strong dissection of its hillslopes by the Aguas and Alias river systems, to the north and to the south, respectively. Because of this morphotectonic context the Quaternary alluvial and fluvial deposits are missing at the foot of the hillslopes impeding the timing of faulting and fault slip-rate determination. Thus, the objective of this paper is to test the presence of active or recent reverse faults that may control the topographic relief of the Sierra Cabrera antiform and surrounding Neogene basins (e.g. Vera and Níjar basins), using both qualitative and quantitative geomorphic analyses. Quantitative analyses were conducted calculating the following geomorphic indices: mountain-front sinuosity, valley floor width-to-height ratio, drainage basin asymmetry factor, basin hypsometric curve and integral, and the stream-length gradient index normalized by the graded river gradient (*SLk* index).

8.2 Structural framework

The southeastern Betics are characterized by the occurrence of Neogene basins formed during Miocene extensional tectonics *(Martínez-Martínez and Azañón, 1997; Booth-Rea et al., 2004c; 2005)*. Later, late Miocene to present convergence between Africa and Iberia *(Dewey et al., 1989; McClusky et al., 2003; Serpelloni et al., 2007)* produced tectonic inversion of the Miocene extensional basins and development of folds, reverse and strike-slip fault systems *(Weijermars et al., 1985; Montenat and Ott d´Estevou, 1990; Comas et al., 1999; Booth-Rea et al., 2004a)*. Thus, most of the sedimentary cover occurs in synclines among E–W- to ENE–WSW-elongated antiformal ridges, where the metamorphic basement crops out bounded by folded extensional detachments (Fig. 1). This basement is formed by several metamorphic complexes belonging to the

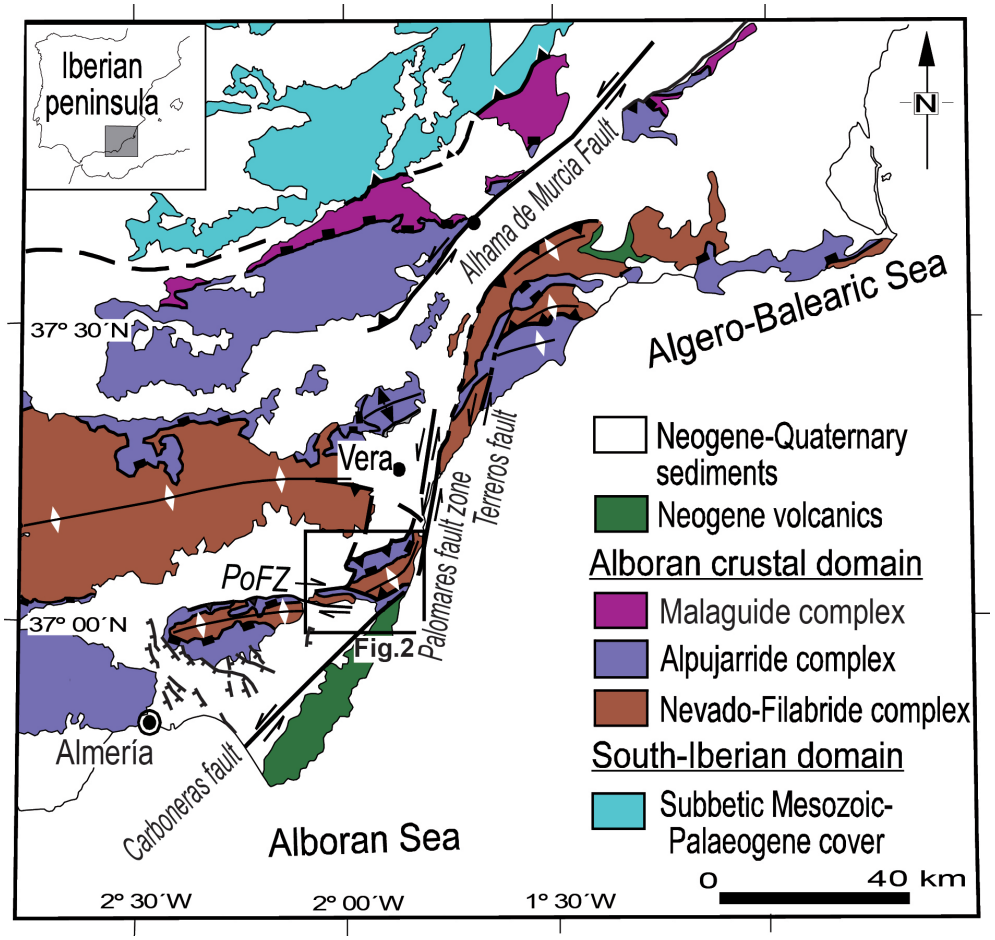

Fig. 1. Geological sketch of the southeastern Betics highlighting the studied area after Giaconia et al. (2012a). PoFZ: Polopos Fault Zone.

Alborán domain, a terrain that collided with the South Iberian and Maghrebian passive margins during the Miocene, forming the Gibraltar Arc and the Betic and Rif cordilleras *(Balanyá and García-Dueñas, 1987; Martínez-Martínez and Azañón, 1997; Platt et al., 2003; Booth-Rea et al., 2007)*. The Sierra Cabrera antiform is an example of these elongated antiformal ridges where metamorphic rocks crop out, surrounded by Miocene to Quaternary sediments of the Sorbas–Tabernas, Vera and Níjar basins (Fig. 1).

The Sierra Cabrera antiform is located in the termination of three strike-slip faults developed in the NW–SE late Miocene to present convergent setting (Fig. 2). These are the sinistral Carboneras *(Bell et al., 1997; Gràcia et al., 2006)* and Palomares *(Bousquet, 1979; Booth-Rea et al., 2004a)* fault zones that end in the eastern termination of the antiform, and the dextral Polopos fault zone that bounds the southwestern end of the Sierra Cabrera *(Giaconia et al., 2012a)*. The Polopos fault zone includes several fault segments, some of which have been described in the literature, like the Gafarillos fault (Fig. 1, *Ott d'Estevou and Montenant, 1990; Stapel et al., 1996; Barragán, 1997; Huibregtse et al., 1998; Jonk and Biermann, 2002*).

The Palomares fault zone initiated its activity during the Tortonian–Messinian with sinistral strike-slip displacement. Subsequently, during the Plio–Quaternary, the fault zone lengthened and widened eastwards evolving in an oblique-slip regime *(Booth-Rea et al., 2004a)*. Deformation along this fault zone migrated toward the east,

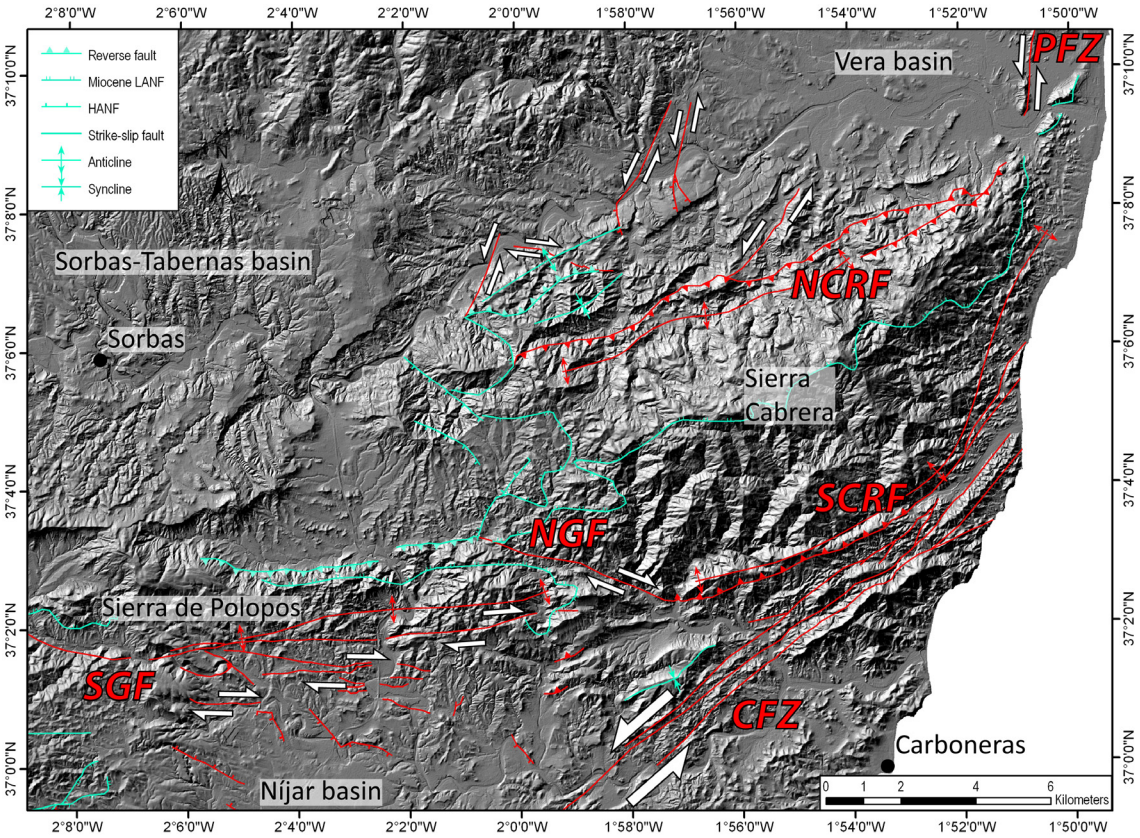

Fig. 2. Structural map of the study area (see Fig. 1 for its location) where the main tectonic structures of the Sierra Cabrera are shown: the Carboneras fault zone (CFZ), the Palomares fault zone (PFZ), the North and the South Cabrera reverse faults (NCRF and SCRF, respectively), and the North and the South Gafarillos faults (NGF and SGF, respectively). LANF: low angle normal faults; HANF: high angle normal fault. Faults and folds with Quaternary activity are shown in red, meanwhile those with a Miocene activity are in blue.

from the Palomares segment, with its main activity during the Upper Tortonian and Messinian, toward the Arteal fault, active during the Pliocene and Quaternary *(Booth-Rea et al., 2003a)*. Present drainage network and topography give evidence of fault segmentation and migration of deformation related to the Palomares fault zone. Indeed drainage density is higher in the uplifted eastern block of the Palomares fault zone showing stream deflections, meanwhile recent activity of fault segments has increased topographic gradients inducing headward erosion of streams transverse to active segments *(Booth-Rea et al., 2004a)*.

The sinistral Carboneras fault zone was active at least since the Serravallian and its activity is documented until the Pliocene *(Rutter et al., 2012)*. The Miocene activity of this fault was essentially strike-slip in response to a NW–SE compressive regime *(Bousquet, 1979; Montenat et al., 1990; Stapel et al., 1996; Huibregtse et al., 1998; Jonk and Biermann, 2002; Rutter et al., 2012)*. On the contrary, the Plio–Quaternary activity of this fault appears to be transpressive rather than strike-slip *(Bell et al., 1997; Reicherter and Reiss, 2001; Rutter et al., 2012)*. New filed data give evidence for shortening along the Carboneras fault zone and folding of basement rocks of the Sierra Cabrera, such as folding-related unconformities in the latemost Messinian to Pliocene sedimentary rocks *(Rutter et al., 2012)*. The Carboneras fault zone shows a

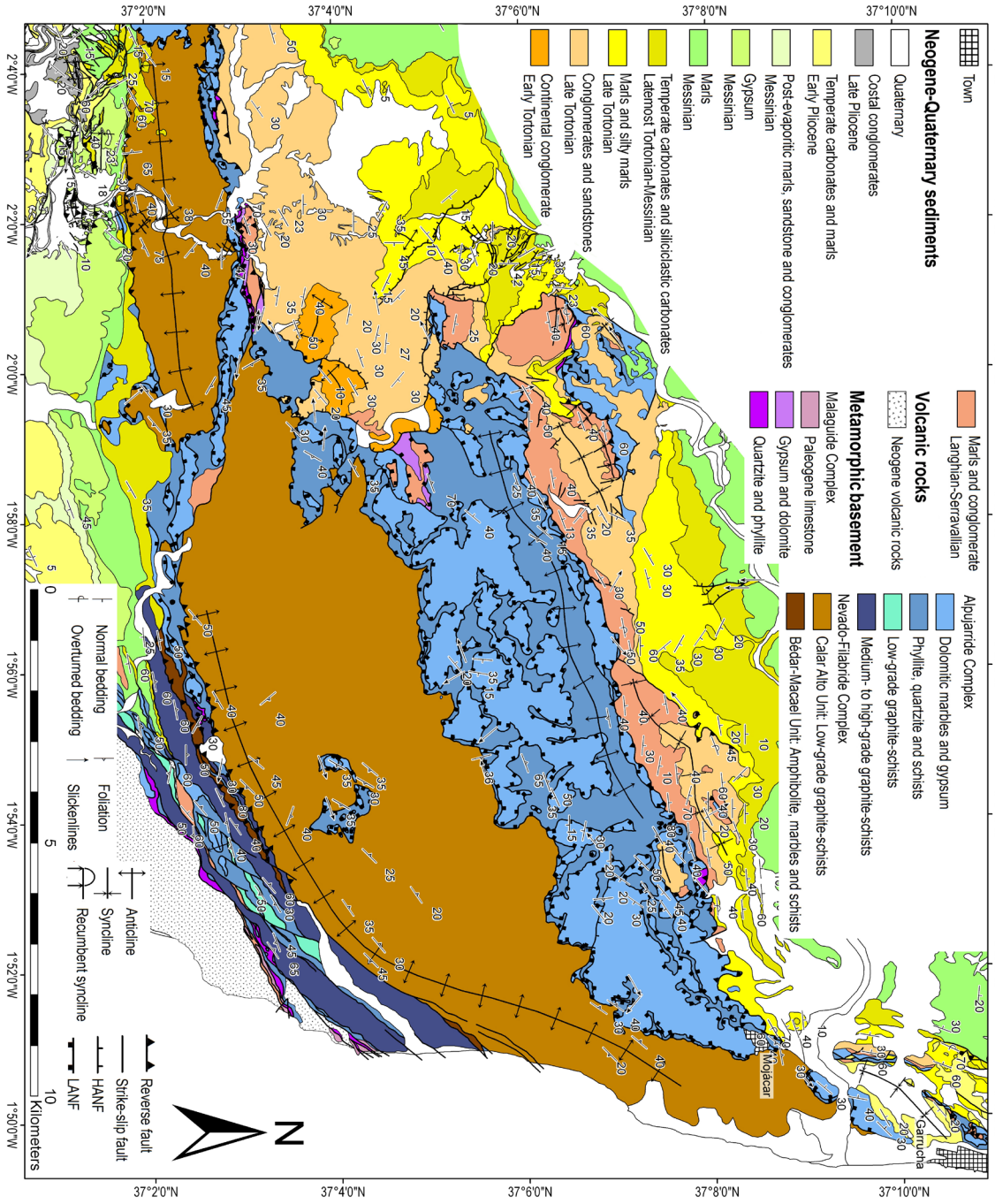

Fig. 3. Geological map of the Sierra Cabrera ridge and surrounding Neogene sedimentary basins: the Sorbas and Vera basins, to the north, and the Níjar basin, to the south.

width slightly larger than 1 km in its northernmost outcrops, where it includes several parallel fault segments. These segments run close by and slightly oblique to the South Cabrera reverse fault in the southern slope of the Sierra Cabrera. Longitudinal valleys like Rambla de Sopalmo have developed parallel to the Carboneras fault segments most probably related to the strong comminution of the basement rock produced by the fault zone (Fig. 3).

The dextral-oblique Polopos fault zone is formed by three main fault segments, the North and South Gafarillos strike-slip faults, and the North Alhamilla reverse fault. The North and South Gafarillos faults bound the northern and the southern Sierra de Polopos range-fronts, respectively, meanwhile the North Alhamilla reverse fault occurs at the northern Sierra Alhamilla one. This fault zone, conjugate to the Palomares sinistral fault

zone, was probably active from the Tortonian to present, although, some of its fault segments were sealed by Messinian sediments (Fig. 2, *Ott d'Estevou and Montenant, 1990; Stapel et al., 1996; Huibregtse et al., 1998; Jonk and Biermann, 2002; Giaconia et al., 2012a*).

8.3 Geomorphic features

The Sierra Cabrera and Polopos ridges are bounded by the Vera and Sorbas–Tabernas basins, to the north, and the Níjar basin, to the south. The Sierra Cabrera ridge shows an E–W elongated shape and an average altitude between 700 and 900 masl, reaching a maximum height of about 1,000 masl. This ridge emerges topographically between the coastline and the Vera, Níjar and Sorbas–Tabernas basins, whose heights range between 0 and 200 masl for the first two, and from 300 to 500 masl for the later (Fig. 4). The study area is characterized by a semi-arid climate, with a mean annual rainfall of around 200 mm yr^{-1} *(Harvey and Wells, 1987)*.

The Vera basin is drained by a series of macro-scale external drainage systems; the Almanzora, Antas and Aguas Rivers. These drainage systems and associated Plio–Pleistocene landforms (river terraces, pediments, erosional straths and badlands) record up to 200 m of dissected topographic relief in the mountain front areas. The magnitude of dissection decreases from central basin areas, eastwards toward the coast, culminating in a low topographic relief coastal plain region in the shoreline area of the modern Mediterranean Sea *(Stokes, 2008)*.

Two drainage systems dissect the Sorbas basin infill, the NNE-directed Rio Aguas drainage-system to the north, and the SSE-directed Rio Alias drainage-system to the south. The first one incises into the sediments of the Vera basin and flows parallel to the northern mountain front of the Sierra Cabrera ridge. The Rio Alias drainage system drains the southern area of the Sorbas basin across the Sierra Alhamilla and Cabrera into the Níjar basin, through the Rambla de los Feos and Rambla de Lucainena streams (Fig. 4).

Two regional-scale significant captures occurred in the southern part of the Sorbas basin, both prompted by the sustained Quaternary uplift of the basin (160 m Ma^{-1} over the Plio/Pleistocene, *Mather, 2000b*). The initial drainage system (early Pleistocene) had a centripetal network toward the center of the Sorbas basin. The first capture (capture site 1 in Fig. 4) occurred in the early to middle Pleistocene and deflected 15% of the original Sorbas basin drainage system into the Níjar basin to the south *(Mather, 2000b)*. The second capture occurred in the late Pleistocene and deflected 73% of the original Sorbas basin drainage system into the Vera basin to the east by the Rio Aguas. This later capture isolated the Rambla de los Feos from the Sorbas basin and expanded the drainage area of the Rio Aguas (capture site 2 in Fig. 4, *Mather, 2000b; Maher et al.,*

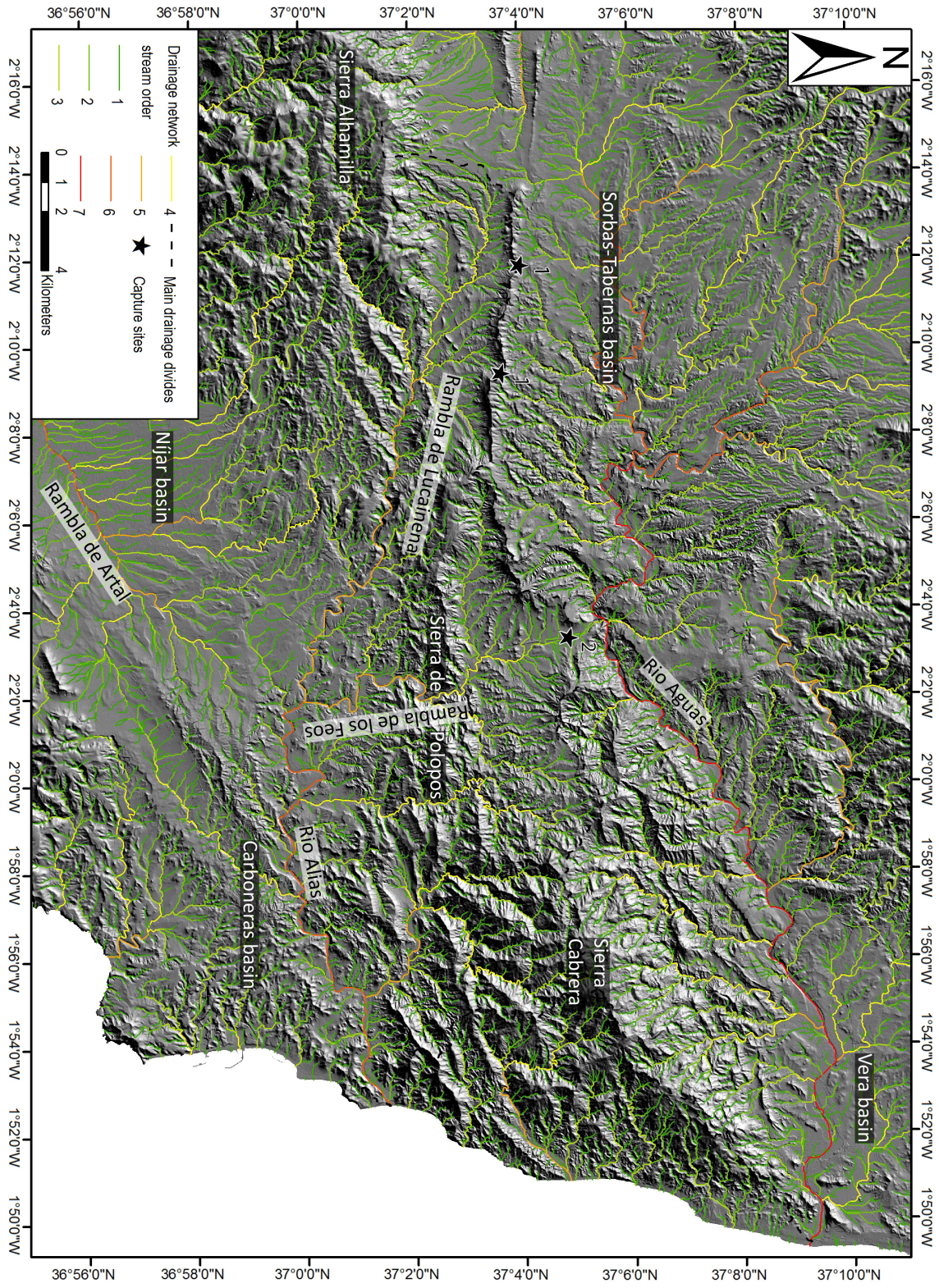

Fig. 4. DEM of the study area (see Fig. 1 for its location) where the drainage network, the main drainage divides of the Sierra Cabrera and capture sites are shown.

2007). The ages of fluvial terraces related to these captures (strath and fill terraces) range between 400 and 70 ky *(Harvey and Wells, 1987; Mather, 2000b; Candy et al., 2005; Maher et al., 2007)*.

The sustained Quaternary uplift of the Sorbas basin produced a long-term fluvial-incision phase with episodic periods of aggradation controlled by short-term climatic oscillations related to Europe glacial/interglacial periods *(Harvey and Wells, 1987)*.

Fluvial terraces and alluvial fans developed during glacial aggradation periods, whereas incision prevailed during interglacial warm phases forming calcretes and palaeosols *(Candy and Black, 2009)*. In addition, also tectonics influenced the geomorphic features in the area producing different regional uplift-rates between ranges and Neogene basins and also between the various basins. Typically, Pliocene to recent regional uplift-rates are higher in the ranges (Sierra Alhamilla and Cabrera) than in the Neogene basins *(Weijermars et al., 1985)* and higher in the northern basins (Tabernas and Sorbas basins) than in the Níjar basin *(Braga et al., 2003)*.

8.4 Methodology

In order to evaluate the topographic relief response to active tectonics in the area we carried out qualitative and quantitative geomorphic analyses. Qualitative observations were focused on the drainage-network geometry, the geometric relationships between drainage basins, and on topographic profiles. Quantitative geomorphic analyses employed several geomorphic indices.

Mountain-front sinuosity (S_{mf}) has been employed in several works to evaluate tectonic activity along mountain fronts. Since this index expresses the relation-factor between the length of the mountain front and its length measured along a straight line, commonly, is less than 3 and approaches the minimum value of 1.0 where steep mountains raised rapidly along a range-bounding fault or fold *(Bull, 1977; Keller and Pinter, 2002; Silva et al., 2003; Bull, 2007; Pérez-Peña et al., 2010)*. In this work mountain-fronts were defined with the aid of a slope map where a topographic break of the slope higher than 15º occurs systematically, later the existence of these fronts was verified in the field. This index evaluates the sinuosity of a mountain front, which is controlled through the balance between erosion and tectonics. Tectonically active fronts, where tectonics prevails over erosional processes, are characterized by linear segments that typically show low S_{mf} values ($S_{mf} < 1.4$, *Keller and Pinter, 2002; Silva et al., 2003; Bull, 2007; Pérez-Peña et al., 2010*).

The valley floor width-to-height ratio index (V_f) has been calculated for the selected mountain fronts *(Bull and McFadden, 1977)* allowing to discriminate between V-shaped and U-shaped valleys. The height of the valley divides was calculated from a river-perpendicular topographic profile obtained from the DEM and the valley floor width from aerial photographs. Deep V-shaped valleys ($V_f < 1$) are associated with linear active-downcutting in areas subjected to active uplift, while flat-floored valleys ($V_f > 1$) are typical of sectors with major lateral erosion in response to relative tectonic quiescence *(e.g. Keller and Pinter, 2002; Silva et al., 2003; Pedrera et al., 2009b; Pérez-Peña et al., 2010)*. We calculated the V_f of the main rivers at a distance of 300 m upstream from the mountain fronts, as well as the S_{mf} index of each front, in order to establish different tectonic activity classes; used to determine relative uplift-rate ranges

as proposed on empirical basis by other authors *(Rockwell et al., 1984; Silva et al., 2003; Bull, 2007)*. These authors proposed rates above 0.5 m ky^{-1} for tectonically active fronts (class 1); between 0.5 and 0.05 m ky^{-1} for moderately active fronts (class 2); and finally down to 0.05 m ky^{-1} for inactive fronts (class 3). In this paper we use the term uplift as rock uplift.

The basin asymmetry factor (*AF*) expresses the area of the drainage basin to the right of the trunk stream with respect the total area in order to identify possible tectonic tilting at the scale of the whole range *(Keller and Pinter, 2002)*. We calculated the asymmetry of the main basins of the study area following the classification proposed by *Pérez-Peña et al. (2010)* where the index is expressed as the absolute value of *A*F minus 50, with an arrow indicating the asymmetry direction. This classification defines the sense and the magnitude of the basin asymmetry in four classes; symmetric basins ($AF < 5$), gently asymmetric basins ($5 < AF < 10$), moderately asymmetric basins ($10 < A\text{F} < 15$), and strongly asymmetric basins ($AF > 15$).

The hypsometric curve represents the degree of dissection of the basin. This curve is obtained by plotting the proportion of the total basin height (relative height) against the proportion of total basin area (relative area, *Strahler, 1952*). Its shape is related to the degree of dissection of the basin (e.g. its erosional stage); convex hypsometric curves characterize immature weakly eroded basins; S-shaped curves are typically associated to moderately eroded basins; and concave curves depict highly eroded basins *(Keller and Pinter, 2002; Pérez-Peña et al., 2009a)*. Hypsometric curves for the study area were calculated applying the CalHypso ARCgis tool developed by Pérez-Peña et al. *(2009a; 2009b)*.

Longitudinal river topographic-profiles can be interpreted as the result of the present-day balance between erosion and uplift rates. River ridgeline-profiles can be considered as proxies of pre-incision conditions, and they can be obtained by projecting rivers onto their theoretical pre-incision surface obtained by interpolating the altitude from present-day lateral divides of each individual basin *(Menéndez et al., 2008; Pérez-Peña et al., 2010)*. The comparison between longitudinal river topographic-profiles and ridgeline-profiles gives a relative estimation of the bulk erosion within a basin if geological evidence is are available to demonstrate that ridgelines are pre-incision surfaces *(Small and Anderson, 1995)*. When this evidence is missed this surface cannot be considered to be the precise pre-incision surface because basin divides themselves are affected by weathering erosional and gravitational processes *(Brocklehurst and Whipple, 2002)*. However, the comparison between these profiles represents minimum bulk erosion for each basin that allows the relative comparison in terms of erosion among different basins giving information about the grade of dissection *(Pérez-Peña et al., 2010)*.

In order to facilitate the reading and interpretation of these data a “minimum bulk erosion map” is presented. This map represents the elevation differences between the

whole theoretical surface (calculated for all the basins in the study area) and the present-day topography (obtained from a 10m DEM). This map allows discerning between areas with different degrees of erosion in terms of eroded-rock column.

The last geomorphic index used in this work is the normalized stream-length gradient index (*SLk* index, *Hack, 1973; Pérez-Peña et al., 2009c*) that shows the variation in stream power along the river reaches. This index is very sensitive to changes in channel slope, thus allowing the evaluation of recent tectonic activity and/or rock resistance *(Chen et al., 2003; Pedrera et al., 2009b; Pérez-Peña et al., 2009c; Giaconia et al., 2012a)*. We followed the methodology proposed by *Perez-Peña et al. (2009c)* in order to obtain the *SLk* anomaly map. We used 204 channels of the drainage basin, a fixed d*l* of 150 m and the geostatistical kriging-interpolator (see methodology section in *Pérez-Peña et al., 2009c* for further details).

8.5 Results

The Sierra Cabrera ridge shows a dendritic drainage network with an elongated centripetal radial geometry coherent with its ENE–WSW-striking antiformal geometry (Fig. 4). Focusing on the NE–SW-oriented main drainage divides, both to the north and to the south, the 1st and 2nd order streams are NW–SE-oriented meanwhile those of 3rd and 4th orders have a N–S orientation (Fig. 4). This double stream set, perpendicular and oblique to the main drainage divides, gives an S-shape to the drainage network in this area indicating an anticlockwise-rotation of the ridge.

The entire southern slope of the Sierra Cabrera and the adjacent margin of the Níjar basin are dissected by an asymmetric dendritic drainage network characterized by a main set of major WSW–ENE-oriented streams (of 4th and 5th orders), which located at the base of the ridge drain eastwards into the Mediterranean Sea (Fig. 4). Most of the 4th and 5th order streams show ENE–WSW to E–W deflections suggesting active tectonic structures with sub-parallel strike (Figs. 2 and 4). The N–S to NW–SE-oriented drainage system is perpendicular to the Sierra Cabrera anticline axis. The deflection toward the WSW–ENE of the 4th and 5th order streams is probably produced by the joint activity of the South Cabrera reverse fault that deflects the streams around the foot of the uplifted fault-block and the Carboneras fault that produces relative uplift of its southern block to the south of the streams (Figs. 2 and 4). Further west where the reverse displacement of the South Cabrera reverse fault is transferred to the dextral branch of the North Gafarillos fault streams flow subparallel to it (Fig. 5). Meanwhile, south of the Sierra de Polopos, meanders in the Ramblas de los Feos and de Lucainena appear strongly controlled by the dextral South Gafarillos fault segments (Fig. 5).

The entire northern slope of the Sierra Cabrera and the adjacent margin of the Vera basin are dissected by two stream sets: a main SW–NE-oriented one (of 5th and 4th

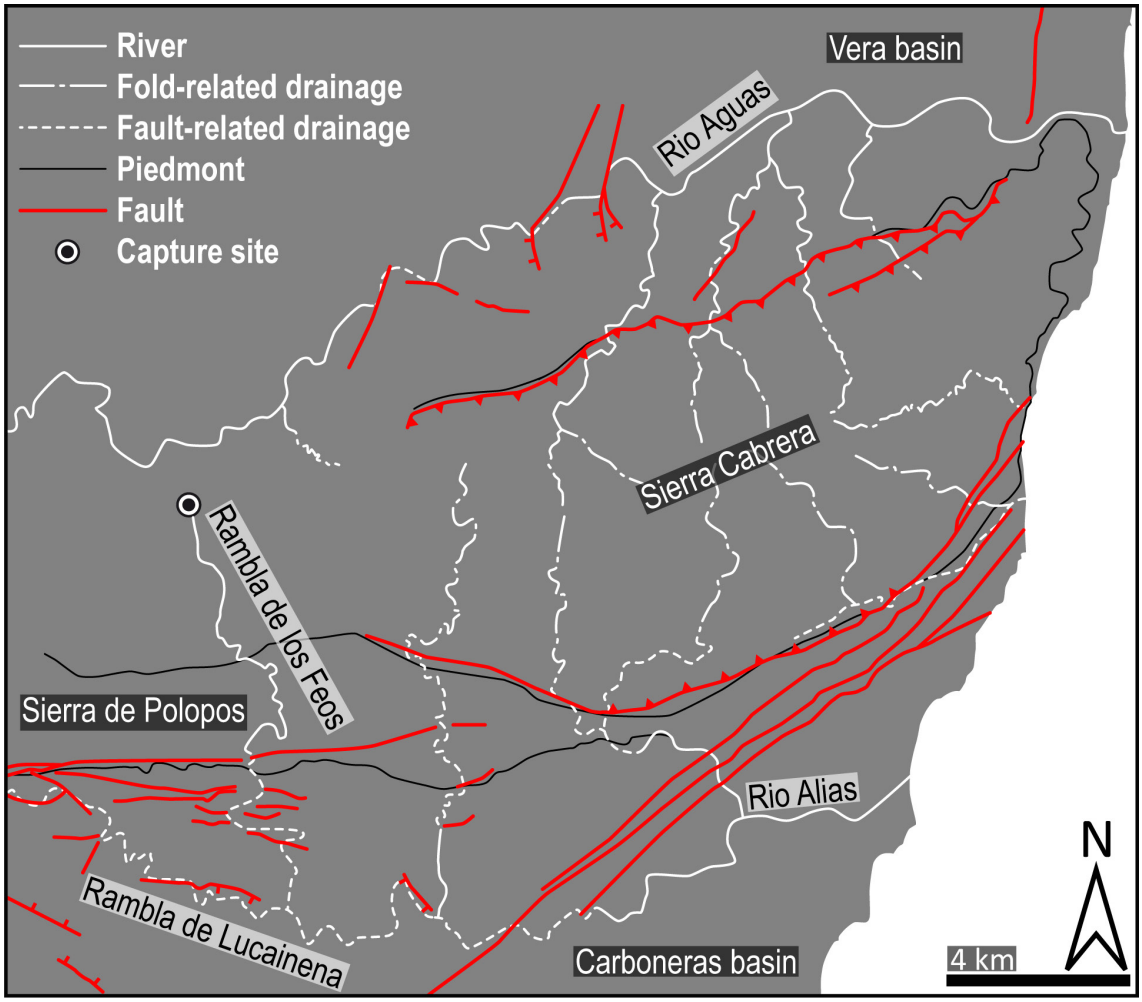

Fig. 5. Simplified sketch of the drainage network of the study area showing its relation to the main tectonic structures.

orders) occurring at the slope foot and basin margin; and a minor SE–NW-oriented one (up to 3rd order) occurring in the upper part of the hillslope (Figs. 4 and 5). The SW–NE-oriented streams flow to the E–W Aguas axial-system and their orientation is influenced by the lithological contrast between folded Messinian marls and latemost Tortonian temperate carbonates in the center of the basin and between late Tortonian marls and Serravallian or Tortonian conglomerates in the southern margin of the basin (Fig. 3). The SW–NE streams are related to the northern limb of the Sierra Cabrera anticline. Meanwhile, the sharp connection between the two stream sets is reasonably related to and coincides with the North Cabrera reverse fault.

Ridge-perpendicular topographic profiles show a northward asymmetry of the entire ridge (Fig. 6). This asymmetry results from a steeper and narrower northern slope and from a wider gently dipping southern slope. This is reasonably due to the geometry of the fold and to the timing of thrusting and associated uplift between the southern and northern mountain fronts, having started earlier in the northern side *(e.g. Jackson et al., 1996)*. In the western termination of the ridge the main drainage divide is driven toward the north in the head region of the present Alias River drainage system. This is related to the presence of highly erodible Tortonian marls in the area and to the importance of this drainage system before its capture by the Aguas River in the late Pleistocene (Fig. 5,

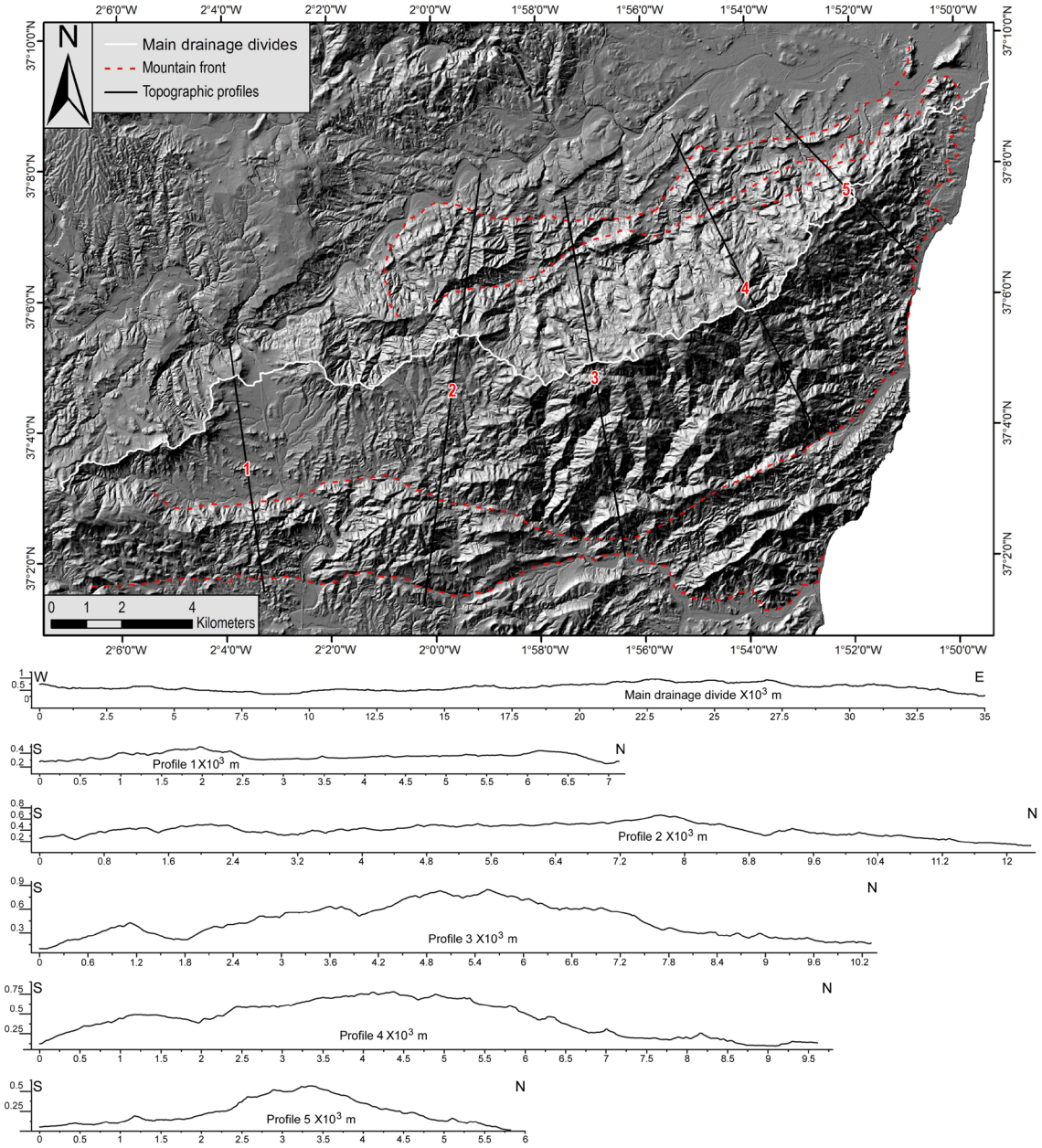

Fig. 6. Topographic profiles across the Sierra Cabrera ridge, their location is shown in the map at the top of the figure where the main drainage divides and the mountain fronts are shown. The first topographic profile is along the main drainage divide of the ridge, meanwhile the other ones are perpendicular to the ridge advancing eastwards.

Harvey and Wells, 1987; Mather, 2000b; Maher et al., 2007). Actually, in this area the presently more vigorous Aguas drainage system is advancing toward the west cutting into the late Pleistocene main drainage divide between the Sorbas and the Vera basins.

8.5.1 Mountain front sinuosity (S_{mf})

The Sierra Cabrera shows several generations of mountain fronts having a common E–W to NE-SW trend. These fronts seem to be congruently oriented with the main tectonic structures present in the area, e.g. the North and South Gafarillos faults, and the North and South Cabrera reverse faults.

S_{mf} index values were calculated for 10 mountain fronts (shown in Table 1), here named with a first letter representing the main front they belong to (N for the northern one,

S for the southern one) and the second one incrementing progressively eastwards. The northern mountain fronts, showing S_{mf} index values lower than 1.4, indicate active tectonics especially at the inner mountain front that appears branched (Nd and Ne in Fig. 7). The tectonic structures that produce these fronts are sinistral faults parallel to the Palomares fault zone and a conjugate dextral one (Na and Nb in Fig. 7) together with the North Cabrera reverse faults that bound the entire Sierra Cabrera northern slope (Nd and Ne in Fig. 7). Meanwhile, the Nc mountain front has a lithological origin, formed by the contact between the folded latemost Tortonian and Messinian members of the Turre formation, the Azagador mixed-platform carbonates and the Abad marls, respectively (Fig. 5, *Völk, 1967*). The southern mountain fronts also seem related to active structures, having S_{mf} index values lower than 1.4 (Fig. 7). The structures that control the evolution of these mountain fronts are the North and South Gafarillos faults, which produce the Sa and the Sd fronts (Fig. 7), respectively, together with the South Cabrera reverse fault and the Palomares fault segments that generate the Sb and Sc fronts, respectively (Fig. 7). The Se front is probably produced by incision of the Alias stream in the resistant Neogene Cabo de Gata volcanics (Figs. 3 and 7).

8.5.2 Valley floor width-to-height ratio (V_f)

The V_f index was calculated for 27 streams 300 m upstream from the mountain front, obtaining the V_f values shown in Table 2. In the northern and southern slopes of the Sierra Cabrera, streams present V-shaped valleys ($V_f < 1$), with only four streams with slightly higher V_f values (streams 1 and 4 in the northern front and 22 and 23 in the southern one). Moreover, some of the streams in both fronts present particularly low $V_f$values ($V_f < 0.5$), thus indicating highly active fronts (Fig. 7).

We assigned different tectonic activity classes to each mountain front by integrating mountain front sinuosity and valley floor width-to-height ratio *(Rockwell et al., 1984; Silva et al., 2003)*. The mountain fronts of the northern slope of the Sierra Cabrera belong to the tectonically active front class, showing both S_{mf} and V_f low values. Only the Nc front differs from them being a moderate to tectonically active front with V_f values higher than 1 (stream 22 in Fig. 7). The southern mountain fronts belong both to tectonically active fronts (Sb and Sc) and moderate active fronts (front Sa and Sd in Fig. 7). Actually, the latter ones belong to an intermediate class because they show one of the V_f values higher than 1 (V_f values 1b and 4a for the Sa and Sd fronts, respectively). Similarly, the Sc front shows S_{mf} and V_f values that are quite near to the threshold allowing to consider it as tectonically active.

In the absence of geomorphic markers useful to determine uplift-rates for these fault-related mountain-fronts we used uplift-rate ranges proposed by some authors for each tectonic activity class *(Rockwell et al., 1984; Mayer, 1986; Silva et al., 2003; Bull, 2007)*. Rates above 0.5 m ky^{-1} were proposed for class 1 (tectonically active fronts); between 0.5 and 0.05 m ky^{-1} for class 2 (moderately active fronts); and finally down

to 0.05 m ky^{-1} for class 3 (inactive fronts). Referring to these uplift-rate ranges, we are able to assign an uplift-rate higher than 0.5 m ky^{-1} for the northern fronts, excepting the Nc front (0.5-0.05 m ky^{-1}). The Sa and Sd fronts in the southern hillslope of the Sierra Cabrera are related to uplift ranges between 0.5 and 0.05 m ky^{-1}. Meanwhile, an uplift rate higher than 0.5 m ky^{-1} would be associated to the Sb and Sc fronts.

8.5.3 Basin asymmetry factor (AF)

In the Sierra Cabrera three sectors with similar basin asymmetry factor can be identified: a) the central and eastern parts of the northern slope show a clear westward asymmetry; b) the easternmost part of the southern slope shows a common southward asymmetry; c) and the central part of the southern slope shows roughly a common eastward asymmetry (Fig. 8a). In terms of the asymmetry classes, basins of the southern slope show the lower asymmetry values, belonging to the first and second classes (symmetric and gently asymmetric basins, respectively), in contrast to those of the northern slope that belong mainly to the third and fourth classes (moderate asymmetric and strong asymmetric basins, respectively). Basins showing the highest asymmetry values occur in the eastern termination of the ridge and in the central part of its northern slope (Fig.8a).

Mountain front	S_{mf}	*Mountain front*	S_{mf}
Na	*1.01*	*Sa*	*1.05*
Nb	*1.04*	*Sb*	*1.00*
Nc	*1.13*	*Sc*	*1.20*
Nd	*1.08*	*Sd*	*1.06*
Ne	*1.03*	*Se*	*1.10*

Table 1. Mountain-front sinuosity values (S_{mf}) are shown for fronts in Fig. 7, here named with a first letter representing the main front they belong to (N for the northern one, S for the southern one) and the second one incrementing progressively eastwards.

Stream	V_f	*Stream*	V_f
1a	*0.88*	*16*	*0.49*
1b	*1.67*	*17*	*0.67*
2	*0.32*	*18a*	*0.29*
3a	*0.48*	*18b*	*0.31*
3b	*0.16*	*19a*	*0.26*
3c	*0.14*	*19b*	*0.26*
4a	*1.59*	*20a*	*0.41*
4b	*0.34*	*20b*	*0.34*
8	*0.30*	*21a*	*0.32*
9	*0.66*	*21b*	*0.25*
10	*0.87*	*21c*	*0.21*
11	*0.85*	*22*	*1.43*
14	*0.22*	*23*	*1.04*
15	*0.51*		

Table 2. Valley floor width-to-height ratio values (V_f) are shown for streams in Fig. 7 here named with a first number representing the stream they belong to and the letter increasing progressively.

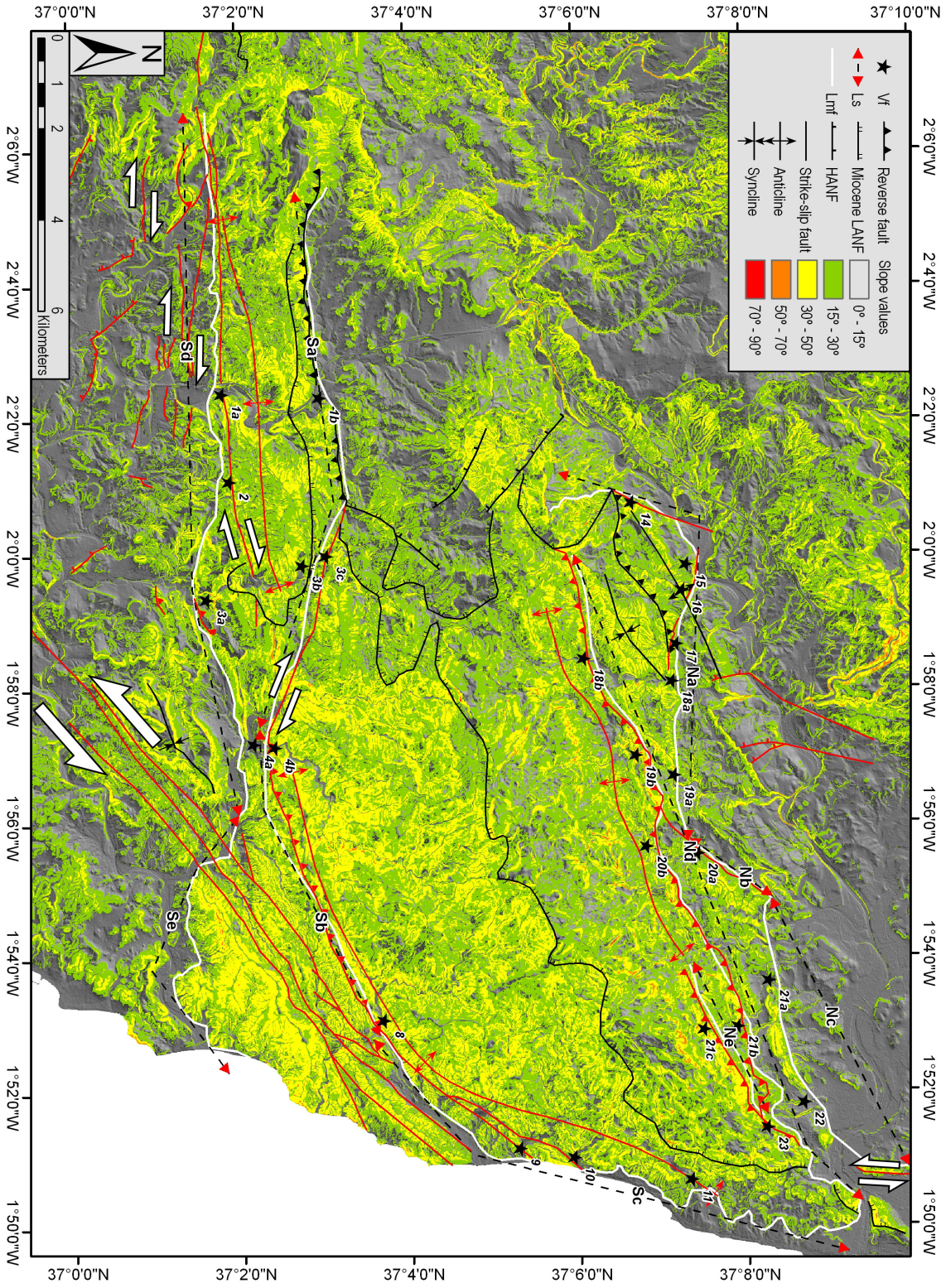

Fig. 7. Slope map of the Sierra Cabrera showing the mountain fronts and main tectonic structures. LANF: low angle normal faults; HANF: high angle normal fault. Faults and folds with Quaternary activity are shown in red, meanwhile those with a Miocene activity are in black. Furthermore, L_{mf} (the length of the mountain front) and L_s (its length measured along a straight line) employed to calculate S_{mf} values (mountain front sinuosity index values), and V_f values (Valley floor width-to-height ratio) are shown.

8.5.4 Hypsometric curves

Basins showing concave hypsometric curves, and so mature, are located in the western and eastern terminations of the ridge (Fig. 8a and b). Basins with S-shaped hypsometric curves, and so in an intermediate stage of maturity, occur widely in the eastern and central parts of the southern slope of the ridge, and in the western part of the northern slope (Fig. 8a and c). The less mature basins with convex hypsometric curves are locally found in the northern and southern slopes of the ridge, both at the slope foot (Fig. 8a and d). Basins with complex hypsometric curves are recognized only in the northern slope of the Sierra Cabrera (Fig. 8a and e). These basins show a convex trend in the lower part of the curves indicating stream foot-rejuvenation processes. Furthermore, the hypsometric curve of basin 19 gives evidence of two sites of foot-rejuvenation.

The most important result from basin hypsometric curves is the occurrence of basins with complex and S-shaped curves in the northern slope of the ridge, and basins with S-shaped curves in the eastern part of the southern slope (Fig. 8a).

8.5.5 Longitudinal stream profiles

Three sectors with the same longitudinal stream profile shape can be recognized: a) streams in the northern slope and at the western termination of the ridge are characterized by concave-convex profiles; b) streams at the eastern termination show concave profiles; c) those in the southern slope of the ridge show both concave and concave-convex profiles. Streams with convex profiles occur locally in the northern slope of the ridge. These results indicate: a) long-term predominance of erosional processes at the northern slope and the western termination of the ridge where Miocene extensional structures bound the sediment-basement contact *(Booth-Rea et al., 2004a; 2005)*; b) long-term equilibrium between uplift and erosion rates at the eastern termination of the ridge; c) and finally from long-term equilibrium to erosion predominance at the southern slope.

The most important result from the longitudinal stream profiles is the occurrence of knickpoints normally related with active fault segments. Most of the streams located at the southern slope of the ridge show knickpoints at their foot, locally very sharp (streams 3 and 7 in Fig. 9). Stream 3 shows a knickpoint at the foot of its profile coinciding with a South Gafarillos fault scarp, whereas in streams 7 and 9 knickpoints coincide with fault scarps of the Carboneras and the southern Palomares fault segments, respectively (Figs. 9 and 10). Similarly, streams occurring in the northern slope show knickpoints both at the foot and the head, in some cases several knickpoints occur (e.g. streams 19 and 21 in Fig. 9). In the case of streams 19, 20 and 21 knickpoints occur at the foot of their profile corresponding to the fault traces of the North Cabrera reverse faults, whereas in stream 14 the knickpoint is probably related to a western sinistral segment of the Palomares fault zone (Figs. 9 and 10).

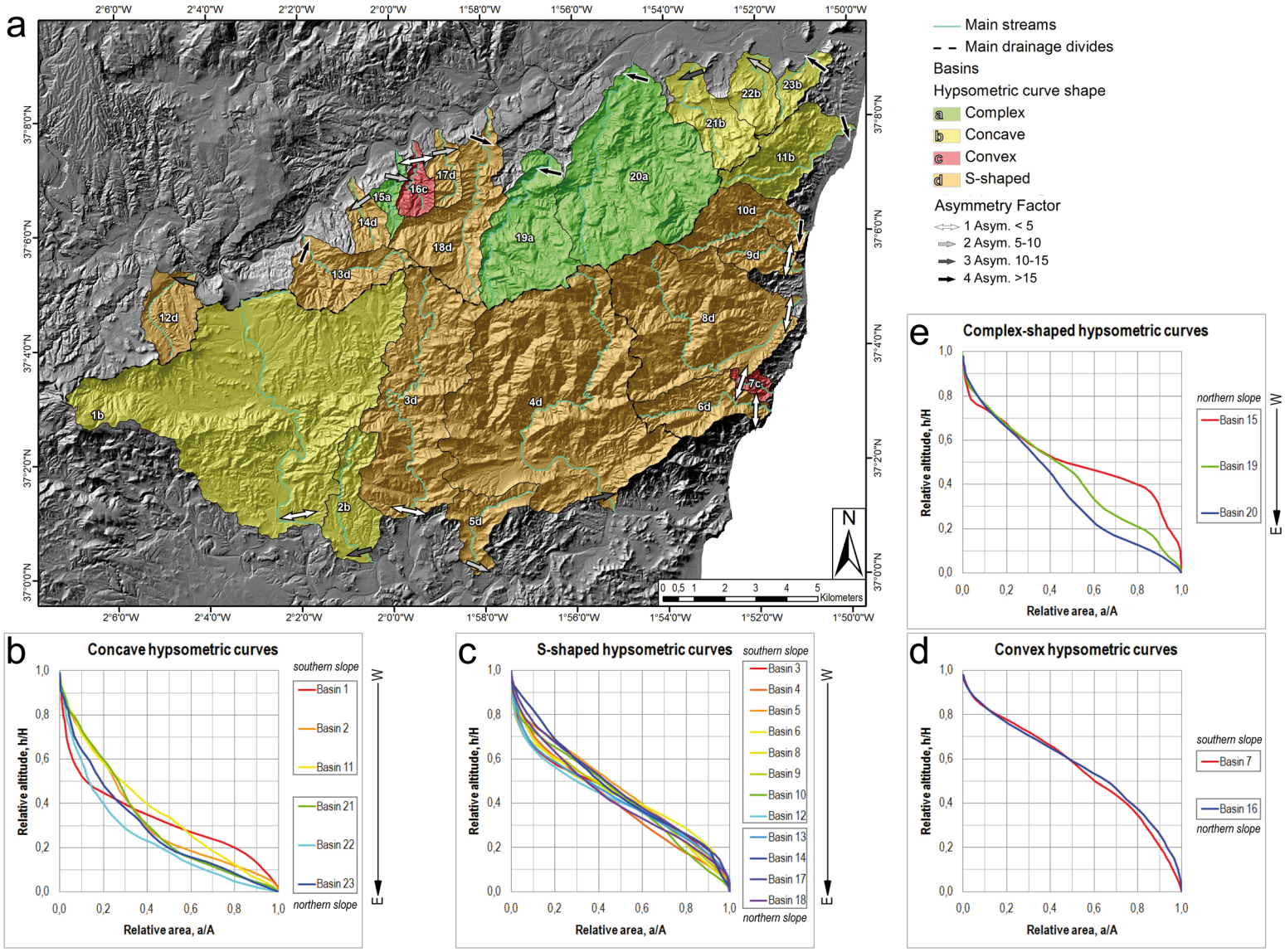

Fig. 8. Drainage-basins and hypsometric diagrams of the Sierra Cabrera. a) Map of drainage basin distribution (see Fig. 1 for its location), where the main drainage divides, streams, drainage basins (classified depending on their hypsometric curve shapes) and basin asymmetry factors are shown. b) Hypsometric curves associated with highly eroded basins. c) Hypsometric curves associated with moderately eroded basins. d) Hypsometric curves associated with weakly eroded basins. e) Hypsometric curves associated with stream "rejuvenation" processes, at the foot or head of the streams.

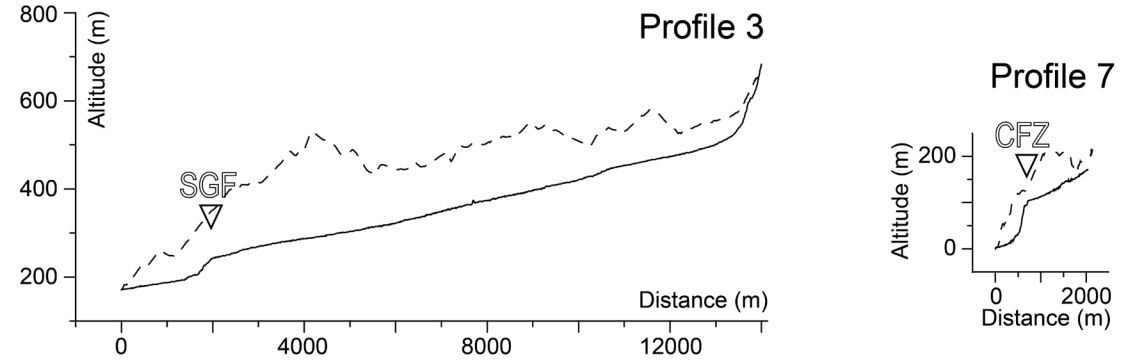
Profile 3
Altitude (m)
800
600
400
200
SGF
Distance (m)
0
4000
8000
12000

Profile 7
Altitude (m)
200
0
CFZ
0
2000
Distance (m)

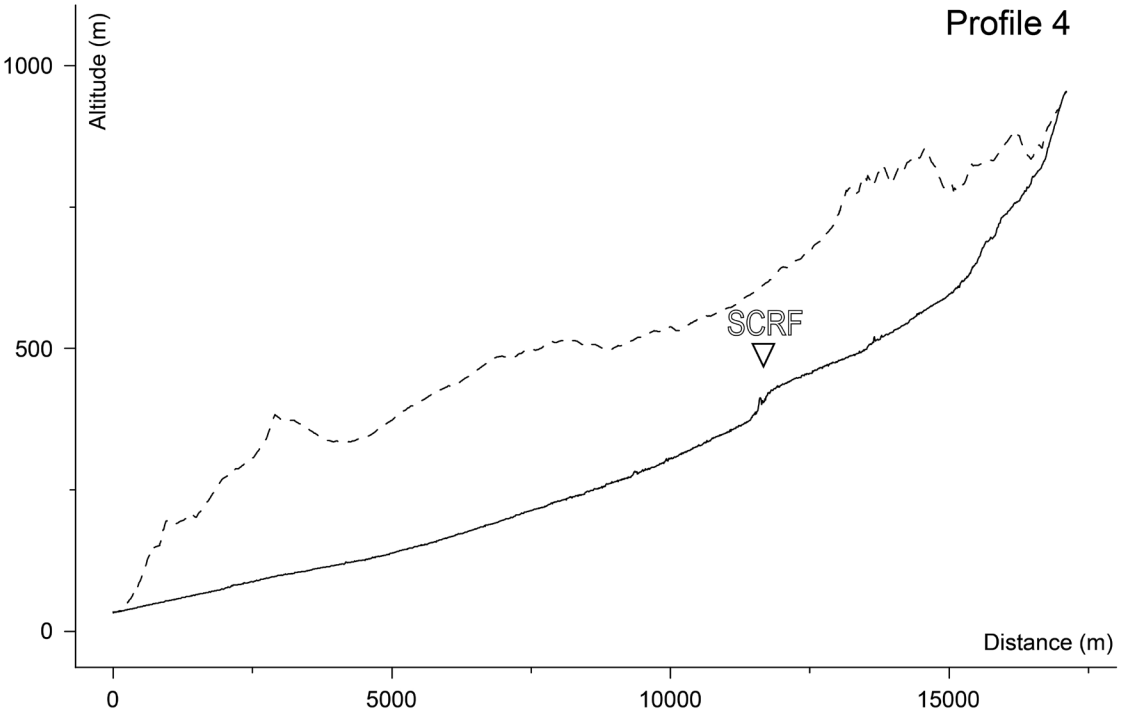
Profile 4
Altitude (m)
1000
500
0
SCRF
Distance (m)
0
5000
10000
15000

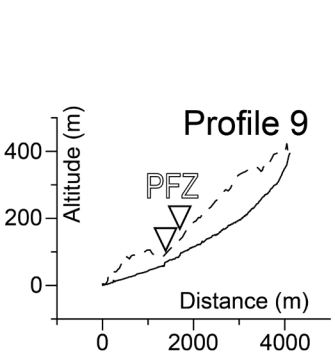
Profile 9
Altitude (m)
400
200
0
PFZ
Distance (m)
0
2000
4000

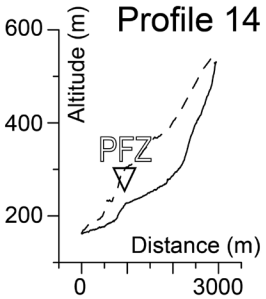
Profile 14
Altitude (m)
600
400
200
PFZ
Distance (m)
0
3000

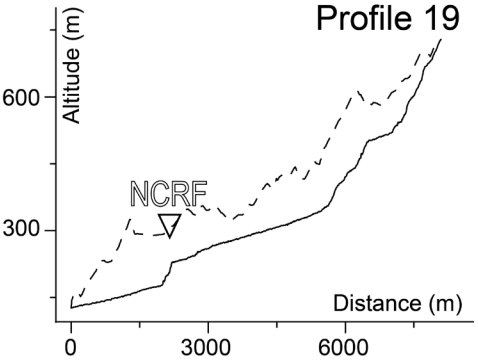
Profile 19
Altitude (m)
600
300
NCRF
Distance (m)
0
3000
6000

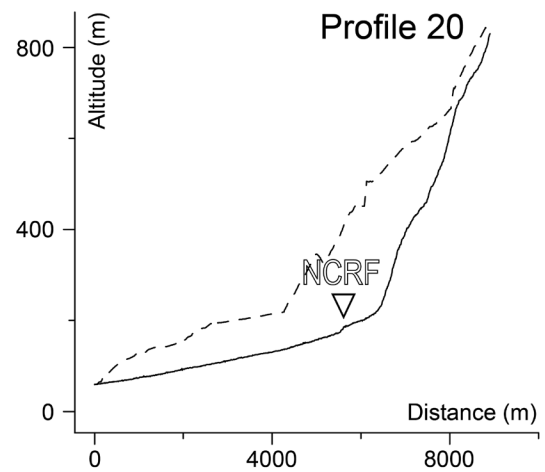
Profile 20
Altitude (m)
800
400
0
NCRF
Distance (m)
0
4000
8000

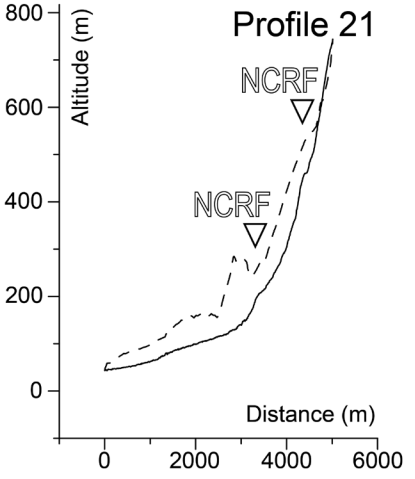
Profile 21
Altitude (m)
800
600
400
200
0
NCRF
NCRF
Distance (m)
0
2000
4000
6000

8.5.6 Ridge-line profiles and minimum bulk erosion map

Basins occurring in the southern slope of the ridge, both in its central and eastern parts, are the most eroded in the area, as shown by the minimum bulk erosion map where these basins are numbered 1, 4, and 8 (Fig. 10). The maximum bulk erosion value of 315 m (eroded-rock column) is reached by stream 8, meanwhile the average is between 150 and 250 m. Also basins occurring in the northern slope, especially in its eastern part, show the highest bulk erosion values relative to this slope (basins 13, 18 and 20 in Fig. 10). Bulk erosion values in these streams are between 100 and 200 m (eroded-rock column), reaching a maximum value of 300 m in basin 20.

The basins occurring in the eastern termination of the ridge are the least dissected; indeed their streams show a minimum bulk erosion value between 20 and 60 m (eroded-rock column Fig. 10). Resuming, the most incised basins occur in the southern slope, whereas the least dissected basins are located in the eastern termination of the ridge (Fig. 10).

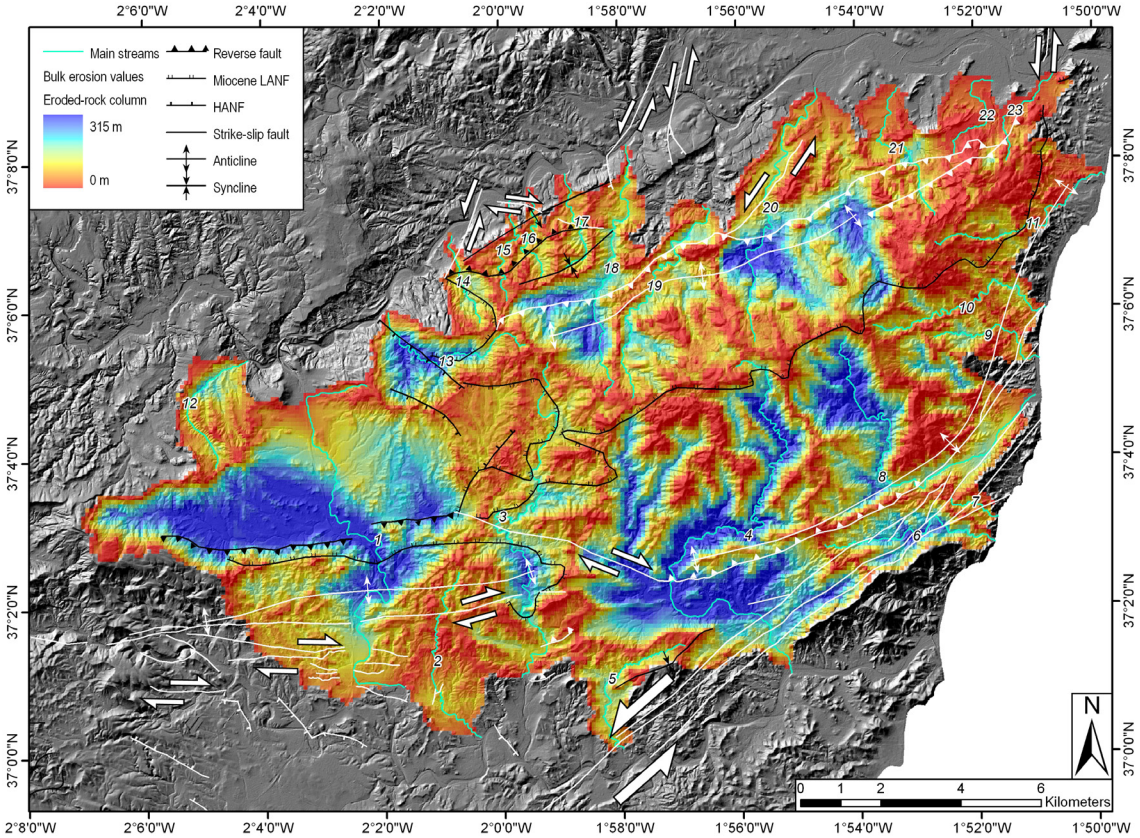

Fig. 10. Minimum bulk erosion map of the Sierra Cabrera (see Fig. 1 for its location) showing the main streams and tectonic structures. LANF: low angle normal faults; HANF: high angle normal fault. Faults and folds with Quaternary activity are shown in white.

Fig. 9. Representative longitudinal stream and ridge-line profiles (×10 vertical scale, (see Figs. 8 and 10 for its location). Stream profiles are shown in black lines; dotted lines are ridge-line profiles. Triangles indicate fault-related knickpoints. Profile 3 is an example of streams at the southern slope of Sierra Cabrera affected by the South Gafarillos oblique dextral fault that produces knickpoints at their foot. Profiles 7 shows examples of knickpoints related to the Carboneras fault zone oblique-sinistral segments. Profile 9 show knickpoints related to the Palomares fault segments. Profiles 19, 20 and 21 are examples of streams in the northern slope of Sierra Cabrera affected by the North Cabrera reverse faults that produce several knickpoints.

8.5.7 SLk map and anomalies

The *SLk* map allows us to distinguish areas with low slope from areas with high slope along streams, thus detecting anomalies associated with recent tectonic activity and/or differences in rock resistance. We recognized at least four positive anomalies of the *SLk* index value, fixing the threshold at 3 and taking into account the tectonic structures occurring in the area. Anomaly 1 bounds the foot of the Sierra Cabrera northern slope having an ENE–WSW main strike (Fig. 11). This anomaly is 12 km long and 2.5 km wide. Anomalies 2 and 3 are located on the southern slope of the ridge and show a NE–SW irregular elongated shape (Fig. 11). The length of these anomalies is 9 km and 20 km, respectively; both are 2.5 km wide. Finally, anomaly 4, 5.5 km long and 1.5 km wide, occurs at the western termination of the Sierra Cabrera with a near E–W strike.

8.6 Discussion

The geomorphic analyses performed in this paper evidence the Quaternary active tectonics in the Sierra Cabrera region. The most interesting results are given by the minimum bulk erosion map and the *SLk* map. Indeed in both cases fault-related anomalies occur topographically just above the fault traces. This analysis highlights that the topographic relief records uplift in response to displacement along reverse faults located in the northern and southern hillslopes of the ridge (e.g. the North and the South Cabrera reverse faults). Uplift in the lateral terminations of the ridge is transferred to segments of the Polopos and Palomares conjugate strike-slip faults that merge into the South and North Cabrera reverse faults, respectively. The Polopos fault follows westwards bounding the southern limb of the Sierra de Polopos antiform (e.g. the South Gafarillos faults) meanwhile, the Palomares fault runs parallel to the coast in the eastern part of the Sierra Cabrera southern hillslope. In the following subchapters we will associate geomorphic features of landscape obtained from qualitative and quantitative analyses to the tectonic structures occurring in the study area.

8.6.1 The North Cabrera reverse faults

The low S_{mf} and V_f values obtained for the Sierra Cabrera northern front are related to the occurrence of the North Cabrera reverse faults that bound the entire northern slope of the ridge (Nd and Ne in Fig. 7). These low S_{mf} and V_f values confirm the Quaternary activity of these faults. The uplift-rate for these fault-related mountain fronts obtained from the integration of S_{mf} and V_f indices and the assignation to the tectonically active front class is higher than 0.5 m ky^{-1}. The high *SLk* anomaly 1 in Fig. 11 seems to be associated to the North Cabrera reverse faults that uplift its southern block. In addition, the occurrence of basins showing high bulk erosion values in the northern slope of the ridge, just to the south of these faults (Fig. 10), supports this uplift.

The tectonic activity of the northern Cabrera front is confirmed by the occurrence of

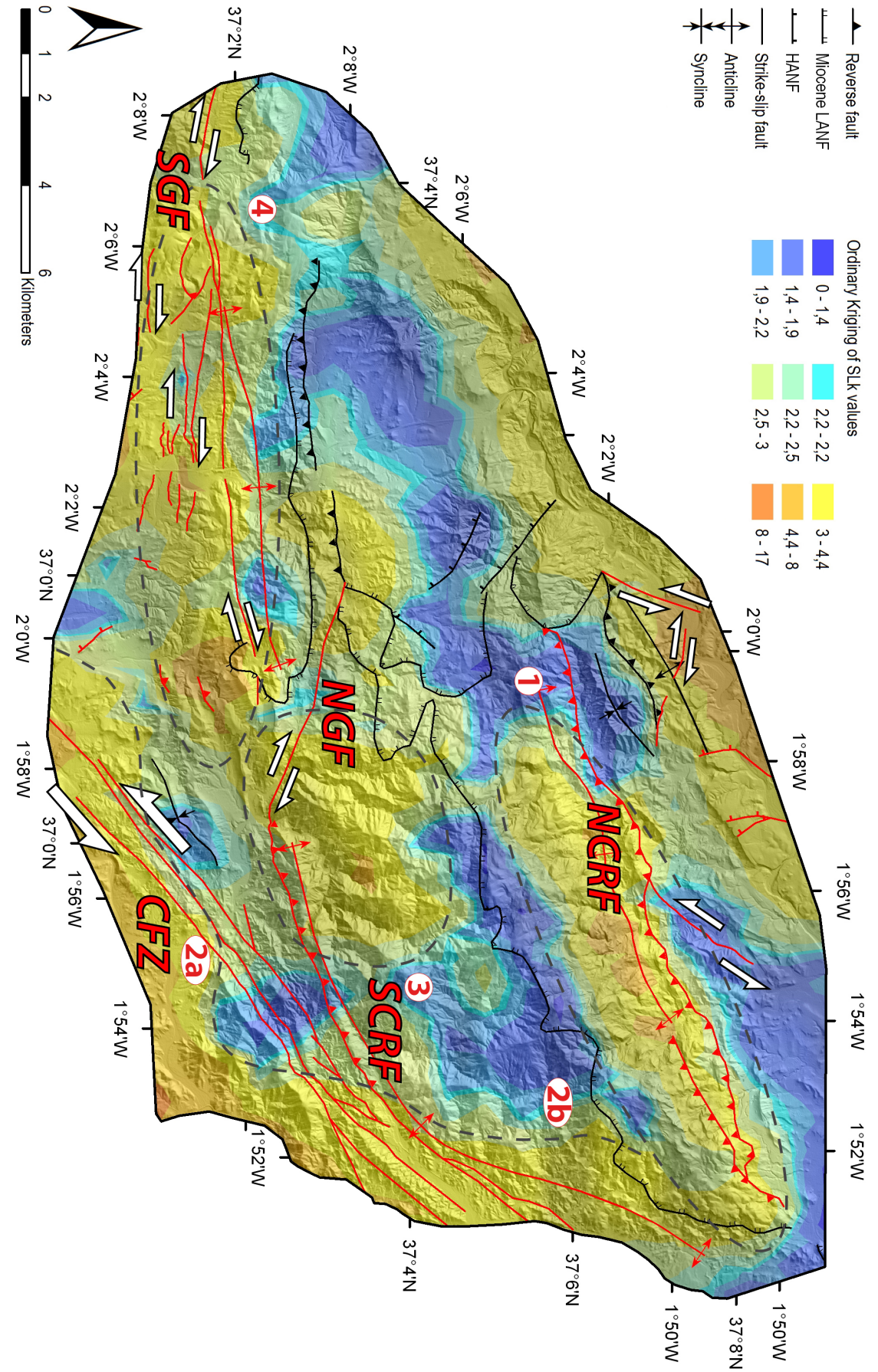

Fig. 11. SLk map and main tectonic structures of the Sierra Cabrera: the Carboneras fault zone (CFZ), The Palomares fault zone (PFZ), the North and the South Cabrera reverse faults (NARF and SCRF, respectively), the North and the South Gafarillos faults (NGF and SGF, respectively). LANF: low angle normal faults; HANF: high angle normal fault. Faults and folds with Quaternary activity are shown in red.

drainage basins in the central part of the northern front that have complex hypsometric curves indicative of stream foot-rejuvenation processes (Fig. 8a and e). In addition, streams that transect the North Cabrera reverse faults show deflections congruently oriented with an ENE–WSW direction and knickpoints both at the foot and the head (streams 18, 19, 20, 21 and 23 in Fig. 9). Finally, the northwestern directed basin asymmetry factor in central areas of the Sierra Cabrera northern slope is compatible with active uplift along the North Cabrera reverse faults (Fig. 8a). Uplift at the northern Cabrera front is probably related both to the reverse kinematics of the faults that bound it and to the associated anticline that probably determines the general north asymmetry of the Sierra Cabrera ridge (Fig. 3).

8.6.2 The South Cabrera reverse fault

The Quaternary activity of the South Cabrera reverse fault is widely inferred from stream features in the area. Indeed streams become sub-parallel to the fault close to it and are affected by deflections congruently oriented with an ENE–WSW to E–W main direction (Fig. 5), and most of them show knickpoints at their foot (streams 4, 8 in 9) fitting with a reverse component of displacement along the South Cabrera reverse fault. The low S_{mf} and V_f values obtained for the Sierra Cabrera southern front allow us to assign this front to the tectonically active fronts class inferring its Quaternary activity (Sb in Fig. 7), this front seems to be related to the occurrence of the South Cabrera reverse fault. Since this front belongs to the tectonically active front class we can assign an uplift-rate higher than 0.5 m ky^{-1}. The high *SLk* anomaly 3 in Fig. 11 seems to be related to the uplift produced by the South Cabrera reverse fault together with the dextral branch of the North Gafarillos fault, further westwards (Figs. 2 and 3). This uplift is confirmed by the occurrence of high minimum bulk erosion just north of the fault system (Fig. 10).

The fact that the southern slope of the Sierra Cabrera is wider than the northern one but has higher bulk erosion values probably indicates that the South Cabrera reverse fault developed later once the northern fold asymmetry had been established (Figs. 8a and 10). This is supported also by the longitudinal stream profiles at the southern slope that show long-term equilibrium to erosion predominance processes and S-shaped hypsometric curves typical of moderately eroded basins in an intermediate stage of maturity (Fig. 8a).

8.6.3 The Palomares fault zone

The low S_{mf} and V_f values obtained for the western part of the Sierra Cabrera northern front are caused by short sinistral Palomares fault segments (N20-30ºE) (Na and Nb in Fig. 7). Similarly, the eastern termination of the Sierra Cabrera antiform shows low S_{mf} and V_f values most likely related to the main Palomares fault segments (Sc in Fig. 7), suggesting their Quaternary activity. The V_f values and the minimum bulk erosion map show variations that relate to the orientation of the faults, and thus, probably to their

tectonic regime as expected from a present NW–SE shortening stress field *(Fernández-Ibáñez et al., 2007)* and present GPS determined geodetic displacements *(Echeverria et al., 2011)*. The segments that have a N50-60ºE strike (e.g. the South Cabrera reverse fault) show lower V_f and larger minimum bulk erosion values than the ones that have a N30ºE strike (e.g. the Palomares sinistral fault segments). Thus, the uplift rates associated to both these segments differ depending on their orientation; the N50-60ºE segments have associated uplift rates higher than 0.5 m ky^{-1}, while the N30ºE segments would have uplift rates close to 0.5 m ky-1. This assessment was obtained by the integration of S_{mf} and V_f data for the Sb and Sc fronts (Fig. 7).

The Palomares sinistral fault segments produce the *SLk* high anomaly 2b related to the uplift of the northwestern fault block in relation to oblique-slip along the Palomares fault segments (Fig. 11). Meanwhile, anomaly 2a should be related to the uplift of the southeastern Carboneras fault block in the Níjar basin (0.05 to 0.1m ky^{-1} since the late Pleistocene, *Bell et al., 1997*; or 0.03-0.05 m ky^{-1} since the early Pliocene, *Martín et al., 2003*), Resuming, the N50-60ºE faults probably have mostly reverse kinematics while the N30ºE ones are strike-slip.

8.6.4 The South Gafarillos Fault

The Quaternary activity of the dextral South Gafarillos fault is inferred from stream features in the area. These streams show deflections congruently oriented with the strike of the fault system (Fig. 5), and knickpoints at the foot of their longitudinal profiles (streams 2 and 3 in Fig. 9).

The low S_{mf} and V_f values obtained along the Sc front (Fig. 7) seem to be related to the occurrence of the South Gafarillos fault. Furthermore, the integration between these two geomorphic indices allows us to assign this fault related-mountain front to the moderately active front and consequently an uplift-rate that ranges between 0.05 and 0.5 m ky^{-1} for the northern fault block. The high *SLk* anomaly 4 in Fig. 11 occurs in the uplifted block of this fault system that is formed mostly by oblique dextral-reverse fault segments. This fault system is highly segmented with both dilational and antidilational jogs that produce locally uplifted and sunken blocks, thus providing an irregular *SLk* anomaly. The *SLk* anomaly map shows at least two uplifted blocks in the central and eastern part of anomaly 4 (Fig. 11) coinciding with local restraining bends.

The low uplift rates obtained for the South Gafarillos fault activity support that the kinematics of this fault zone is essentially strike-slip. However, the large minimum bulk erosion obtained for the Rambla de los Feos (Fig. 10) together with concave hypsometric curve of its basin (basin 1 in Fig. 8) indicates a sustained uplift of the northern South Gafarillos (the Sierra de Polopos) fault block since the early-middle Pleistocene, age when the Alias-Feos drainage system captured the Sorbas basin centripetal system *(Mather, 2000b; Candy et al., 2005; Maher et al., 2007)*. This timing also coincides with the age of the oldest synkinematic sediments associated to

these fault segments *(Giaconia et al., 2012a)* and with folding of the Sierra de Polopos Anticline documented by folded paleo-profiles of the Rambla de los Feos *(Harvey and Wells, 1987)*.

8.6.5 The North Gafarillos Fault

The North Gafarillos Fault is sealed by Messinian sediments *(Ott d'Estevou and Montenant, 1990; Stapel et al., 1996; Huibregtse et al., 1998; Jonk and Biermann, 2002)*, nevertheless any recent tectonic-related geomorphic-results would have been erased by the strong dissection of the Rambla de los Feos transverse basin *(Mather, 2000b)*, driven by the early-middle Pleistocene uplift of the southern Sierra de Polopos mountain front *(Harvey and Wells, 1987)*. Thus, geomorphic analyses performed here cannot confirm the geomorphic-effects of a North Gafarillos Fault Quaternary activity. The occurrence of the Sa mountain front with low S_{mf} value at the northern Sierra de Polopos fold limb seems to be related to the erosional contrast between the metamorphic basement, to the south, and the late Tortonian marls and silty-marls, to the north (Fig. 3). However, the occurrence of the high *SLk* anomaly 3 and the presence of drainage basins with S-shaped hypsometric curves, together with the present stress field orientation and GPS measured displacements in the area *(Fernández-Ibáñez et al., 2007; Echeverria et al., 2011, respectively)* support the present activity of the dextral branch of the North Gafarillos fault, whereas its reverse branch seems inactive.

8.6.6 Drainage-network evolution in response to folding and faulting

Progressive unconformities in latemost Tortonian sediments of the Azagador member (8-7.24 Ma) of the Turre formation mark the initial growth of the Sierra Cabrera fold structures in response to the North Cabrera reverse fault activity *(Booth-Rea et al., 2004a; Booth-Rea et al., 2005)*. This developed an initial northward asymmetry of the anticlinal ridge that is still observed in the present topographic relief. Part of the folding of the Cabrera anticline is sealed by the Messinian Yesares gypsum formation (5,96-5,67 Ma; *Krijgsman et al., 2001*). However, folding, strike-slip faulting and thrusting continued in the southern limb of the Polopos–Cabrera anticline producing synsedimentary unconformities and folds in early–middle Pleistocene alluvial sediments and strath-terraces *(Harvey and Wells, 1987; Giaconia et al., 2012a)*. This tectonic activity produced a second fold hinge at the southern hillslope of the ridge and the present box-fold geometry of the Cabrera anticline *(Booth-Rea et al., 2005)* and activated deep dissection of the wider and longer southern drainage basins. At the same time stream deflections along the South Cabrera reverse and the South Gafarillos dextral faults occurred.

The S-shaped drainage network in the main drainage divide area (Fig. 12) testifies an anticlockwise rotation of the Sierra Cabrera in response to the recent activity of the Palomares strike-slip fault zone. Paleomagnetic data measured in the Vera basin attest the importance of Neogene rotations associated to segments of the Palomares fault

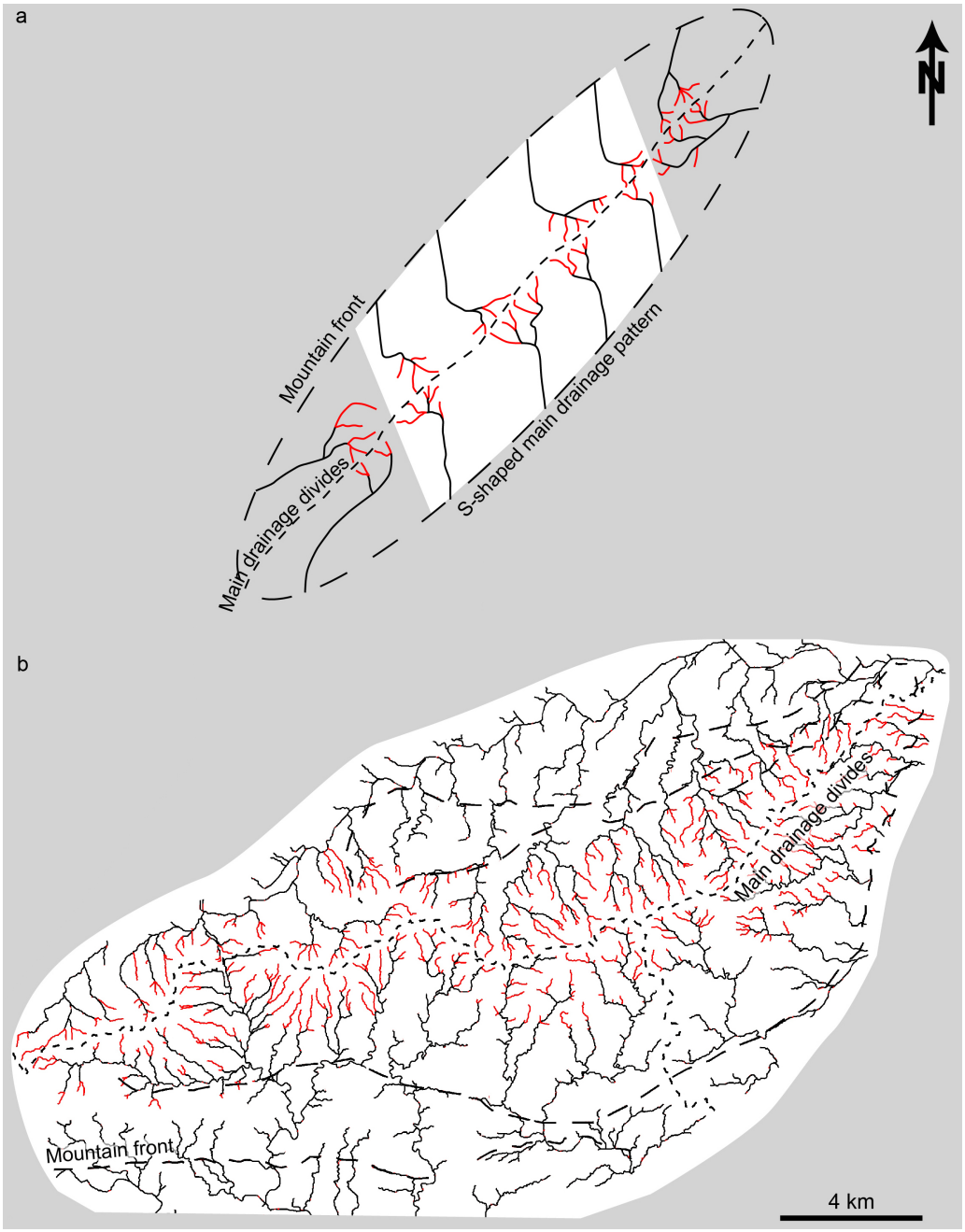

Fig. 12. Simplified sketch showing the S-shaped drainage network in the area around the main divide of the Sierra Cabrera antiform that testifies for the anticlock-wise rotation of the ridge in response to the Palomares fault zone activity. a) Simplified sketch of the drainage network; b) real drainage network of the Sierra Cabrera. The 1st order streams are shown in red and the rest in black.

zone *(Calvo et al., 1997)*. During the Tortonian to Messinian sinistral displacement along the Palomares fault zone was accommodated along the North Cabrera and the North Gafarillos reverse faults. Meanwhile, we have not observed evidence of reverse displacement related to the Polopos fault zone in the southern hillslope during this time. During the early-middle Pleistocene faulting along the Polopos fault zone jumped from the North to the South Gafarillos faults that propagated eastwards forming the South Cabrera reverse fault. At this time the present pop-up structure of Sierra Cabrera developed between the North and the South Cabrera reverse faults in the constructional domain between the conjugate Polopos and Palomares strike-slip fault zones.

8.7 Conclusions

The qualitative and quantitative geomorphic analyses conducted suggest that the main tectonic structures controlling the topographic relief and drainage network of the Sierra Cabrera and Polopos antiforms are both reverse and oblique-slip faults. These structures are the North and the South Cabrera reverse faults, the sinistral Palomares fault segments, at the eastern termination of the Cabrera ridge, and the dextral oblique-slip South Gafarillos faults, which bound the southern slope of the Polopos antiform. All these faults have been active during the Quaternary. The topographic relief is very sensitive to variations in the tectonic regime of the faults that depends on their orientation relative to the present stress field. The reverse fault segments show a N50-60ºE strike (e.g. The North and the South Cabrera reverse faults), perpendicular to the present NW–SE convergent stress regime *(Fernández-Ibáñez et al., 2007)*, and have associated uplift rates larger than 0.5 m ky^{-1}. Fault segments with a N20-30ºE strike show a sinistral oblique strike-slip regime that results in lower uplift rates, between 0.05 and 0.5 m ky^{-1} (e.g. the Palomares fault segments). These last uplift rates are comparable to the ones obtained for the dextral conjugate N110ºE striking faults (e.g. the South Gafarillos fault). This observation is translatable to a larger scale in the southeastern Betics where uplift rates associated to strike-slip faults are in the range of 0.1 to 0.05 m ky^{-1}, for example, those related to the Palomares strike-slip fault segments *(Booth-Rea et al., 2004a)* or to the southern Carboneras fault segments *(Bell et al., 1997; Martín et al., 2003)*.

The transpressive or reverse regime related to the main faults bounding the southern and northern mountain fronts of the Sierra Cabrera inferred from the geomorphic analyses is supported by the present stress field in the area *(Fernández-Ibáñez et al., 2007)* and the GPS geodetic studies, which show that the displacement in the area is parallel to the NW–SE convergence between Africa and Eurasia and is accommodated close to the southeastern Betics coastline *(Echeverria et al., 2011)*. The geomorphic data and the tectonic scenario depicted here highlight the occurrence in the Sierra Cabrera antiform of an active pop-up formed between the North and the South Cabrera reverse faults. The pop-up developed in a constrictional domain of the large-scale Polopos and Palomares conjugate strike-slip faults.

The shortening and important uplift observed in the Sierra Cabrera region contrasts with areas nearby where local extension has dominated during the Quaternary, for example in the Níjar basin to the south *(Pedrera et al., 2006)* or locally in the Vera basin to the north *(Booth-Rea et al., 2004a; Stokes, 2008)*. These data, apparently contrasting, fit well considering that the Níjar basin is located in the extensional domain of the aforementioned large-scale conjugate strike-slip fault system. Extension in the Vera basin is related to small releasing bends of the Palomares fault zone *(Booth-Rea et al., 2004a)*. Finally, the sinistral Carboneras fault segments that run with a N40ºE strike to the southeast of the Sierra Cabrera do not seem to contribute much to the uplift

observed in the mountain range as they produce relative uplift in the opposite, Cabo de Gata, fault block *(Bell et al., 1997; Reicherter and Reiss, 2001; Martín et al., 2003)*, which probably remains fixed while the Carboneras fault zone works as transfer a fault of Quaternary extension in the Níjar basin.

This paper highlights that qualitative and quantitative geomorphic analyses, based on the study of the drainage network and on the use of several geomorphic indices, and its integration with the geological and structural field data can consistently constrain the fault- and fold-related control on topographic relief. Furthermore, this methodology permits to infer the Quaternary tectonic activity in those regions where useful geological markers, such as alluvial fan or fluvial terraces, are missing by erosion or where geochronological ages are not available yet. Finally, the use of geomorphic indices, in a semi-quantitative way, can give useful information about, the erosional stage of a landform, the erosion suffered by a region, and the uplift rates of fault-related mountain fronts and consequently an order of magnitude of the fault slip rates if field data such as fault-plane and slicken-line orientations are not available.

Acknowledgments: This Study was supported by research projects CGL2008-03249/BTE, CGL2011-29920, CSD2006-00041 TOPOIBERIA CONSOLIDER-INGENIO2010, CTM2007-66179-C02-01/MAR and the CTM2011-30400-C02-01 Hades Project from the Spanish Ministry of Science and Innovation.

Journal of Structural Geology 46 (2013) 76–91, doi: 10.1016/j.jsg.2012.10.005
Received 30 May 2012 / Available online 23 October 2012

9.0 Mountain front migration and drainage captures related to fault segment linkage and growth: the Polopos transpressive fault zone (southeastern Betics, SE Spain)

F. Giaconia [a,*], G. Booth-Rea [a], J. M. Martínez-Martínez [a], J. M. Azañón [a], J. Pérez-Romero [b] and I. Villegas [c]

[a] Dpto. Geodinámica, Instituto Andaluz de Ciencias de la Tierra (CSIC-UGR), Campus Fuentenueva S/N, 18002, Granada, Spain
[b] ETS Arquitectura, University of Málaga, Campus del Ejido s/n, 29071, Málaga, Spain
[c] CEMOSA, C\Benaque, 9, 29004, Málaga, Spain
[*] Corresponding author. E-mail address: flavio@ugr.es, flavio@iact.ugr-csic.es (F. Giaconia)

Abstract: The Polopos E–W- to ESE–WNW-oriented dextral-reverse fault zone is formed by the North Alhamilla reverse fault and the North and South Gafarillos dextral faults. It is a conjugate fault system of the sinistral NNE–SSW Palomares fault zone, active from the latemost Tortonian (≈ 7 Ma) up to the late Pleistocene (≥ 70 ky) in the southeastern Betics. The helicoidal geometry of the fault zone permits to shift SE-directed movement along the South Cabrera reverse fault to NW-directed shortening along the North Alhamilla reverse fault via vertical Gafarillos fault segments, in between. Since the Messinian, fault activity migrated southwards forming the South Gafarillos fault and displacing the active fault-related mountain-front from the north to the south of Sierra de Polopos; whilst recent activity of the North Alhamilla reverse fault migrated westwards. The Polopos fault zone determined the differential uplift between the Sierra Alhamilla and the Tabernas–Sorbas basin promoting the middle Pleistocene capture that occurred in the southern margin of the Sorbas basin. Continued tectonic uplift of the Sierra Alhamilla–Polopos and Cabrera anticlinoria and local subsidence associated to the Palomares fault zone in the Vera basin promoted the headward erosion of the Aguas river drainage that captured the Sorbas basin during the late Pleistocene.

Keywords: Strike-slip faults; Morpho-tectonics; Fault segmentation; Polopos fault zone; eastern Betics; Sierra Alhamilla.

9.1 Introduction

Tectonic structures strongly control the morphology and evolution of topography and drainage at a given area *(e.g. Jackson et al., 1996; Goldsworthy and Jackson, 2000; Booth-Rea et al., 2004a; Pérez-Peña et al., 2010; Giaconia et al., 2012a)*. In strike-slip fault systems, as in the case of the Palomares fault zone in the eastern Betics, displacement along offset fault segments generates important topographic gradients with associated uplift and subsidence in antidilational and dilational jogs, respectively *(Sibson, 1986)*, forming both uplifted ranges and sedimentary depocenters *(Sylvester, 1988; Booth-Rea et al., 2004a)*. In these fault systems, migration of activity by the creation of new fault segments determines topographic modifications and variations in the position of active sedimentary depocenters *(e.g. Ollier, 1981; Walker and Jackson, 2002; Booth-Rea et al., 2004a)*. Faulting related morphologic and sedimentary changes induce drainage adjustments, like fluvial captures, drainage deviation and dissection or aggradation associated to local-base level variations *(Booth-Rea et al., 2004a)*. Thus, fluvial and alluvial systems should reflect the fault activity migration and mountain front evolution in time and space *(e.g. Keller and Pinter, 2002)*.

Two different tectonic mechanisms have been proposed to explain the uplift in the Betics and Rif that drove the closure of the Atlantic–Mediterranean gateways producing the Messinian salinity crisis and ongoing uplift of the Betic–Rif margins since then. On one side, late Miocene edge delamination, slab tearing and associated asthenospheric upwelling beneath the Betics and Rif *(Duggen et al., 2003, 2005; Booth-Rea et al., 2007; García-Castellanos and Villasenor, 2011)* and on the other side the development of late Miocene to present contractive structures in both the Betics and Rif *(Weijermars et al., 1985; Krijgsman et al., 1999; Jolivet et al., 2006)*. Both these mechanisms have been proposed as exclusive, however, both could have contributed to uplift in the Betic–Rif margins, the first producing large wave-length epeirogenic uplift of the margins and the second one contributing with localized uplift associated to local structures like folds and reverse faults or strike-slip restraining bends *(e.g. Weijermars et al., 1985; Montenat and Ott d´Estevou, 1990; Booth-Rea et al., 2004a)*. A third mechanism responsible for the most important localized uplift recorded in the Betics, and probably also in the Rif, is core-complex type extension coeval with orthogonal shortening related to the ongoing convergence between Iberia and Africa. In this mechanism the unloading and uplift of the detachment footwalls is isostatically compensated by lower-middle crustal flow and folding creating important domal structures like the Sierra Nevada elongated dome in the Betics *(Martínez-Martínez et al., 2002, 2004)* or the Temsamane massif in the Rif *(Negro et al., 2007; Booth-Rea et al., 2012b)*. Uplift associated to core-complex type extension in the Betics is probably responsible for differential elevation between sedimentary basins located in the footwall and hanging-wall of the extensional system, respectively. For example, between the Guadix–Baza and Granada basins in the Central Betics *(Pérez-Peña et al., 2010; Booth-Rea et al.,*

2012b) or between the Sorbas and Níjar–Almería basins in the southeastern Betics (Fig. 1). These three mechanisms together with geomorphic processes like river captures and climatic changes have contributed to the present topography and drainage in the Betics *(e.g. Harvey and Wells, 1987; Mather, 2000b)*.

Here we analyze the influence that a large dextral transpressive fault system (the Polopos fault zone) and associated folds (e.g. Sierra Alhamilla–Polopos and Cabrera anticlinoria) had in the evolution of topography and drainage in the Sorbas–Tabernas–Vera and Níjar basins in the southeastern Betics (Fig. 1). Furthermore, we attempt to separate the influence of the differential regional uplift from the tectonic contribution to the evolution of topography and drainage within a context of differential uplift derived from previous extension and nearly simultaneous orthogonal shortening, later reworked by strike-slip and shortening tectonics. We choose the southeastern Betics because the drainage evolution of the Sorbas–Vera and Níjar basins since the late Pliocene is well known *(Harvey and Wells, 1987; Harvey et al., 1995; Mather, 2000b; Mather et al., 2000; Maher et al., 2007)* and dated since the early–middle Pleistocene *(Candy et al., 2005)*. Furthermore, in these basins two capture events occurred in the middle and late Pleistocene reorganizing the drainage network and inducing an erosion-wave up the fluvial system *(Harvey et al., 1995; Mather, 2000b; Maher et al., 2007)*. The stratigraphy and the ages of the strath fluvial terraces that mark the fluvial captures are sufficiently documented, but the role of tectonics in these captures is still weakly defined, having been related to epeiorogenic uplift and local tectonics in a general sense *(Harvey and Wells, 1987; Mather, 2000b)*.

In order to define the kinematics, fault linkage and growth evolution of the Polopos fault zone, and its influence on topography and the drainage system, we present new structural data, fault segmentation mapping and cross-sections obtained with the aid of drill holes and electrical tomography. Furthermore, we calculate net and vertical fault slips and displacement rates and finally we invert the slip structural data in order to define the strain orientation along the fault system. We have integrated this structural data with fluvial terrace and alluvial fan mapping in order to determine the role of active tectonics on the fluvial captures and the mountain front migration related to the fault segmentation and growth.

9.2 Geological setting

The Betic Rif orogen resulted from the oblique collision between the Alborán domain and the South Iberian passive margin during the Miocene *(e.g. Balanyá and García-Dueñas, 1987; Martínez-Martínez and Azañón, 1997; Booth-Rea et al., 2005; Platt et al., 2006; Balanyá et al., 2007)*. The hinterland of this orogen underwent Miocene extensional tectonics, which markedly attenuated the previous metamorphic nappe stack *(García-Dueñas et al., 1992; Martínez-Martínez and Azañón, 1997; Booth-Rea*

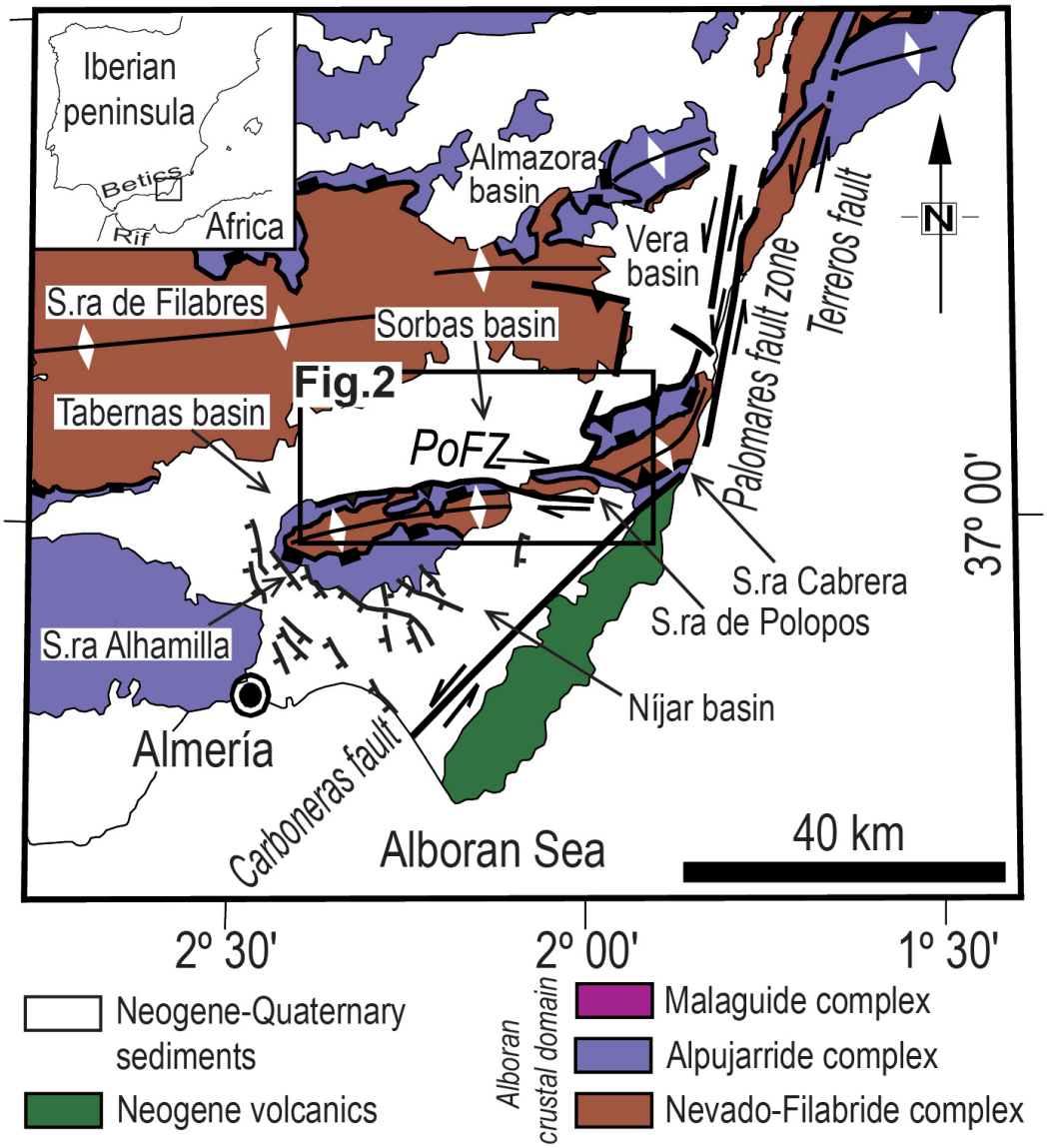

Fig. 1. Geological sketch of the southeastern Betics highlighting the studied area after Giaconia et al. (2012b). PoFZ: Polopos Fault Zone.

et al., 2005). The ultimate result of this extension was the development of the Alborán and Algero–Balearic basins in the core of the Betic–Rif orogen and other internal Betic Neogene extensional basins. These basins developed coeval to thrusting in the external domains *(García-Dueñas et al., 1992; Comas et al., 1999; Booth-Rea et al., 2007)*. Some of these basins occur in synclines among E/W- to ENE/WSW-elongated antiformal ridges, where the metamorphic basement is exhumed at the footwall of folded Miocene extensional detachments (Fig. 1, *García-Dueñas et al., 1992; Martínez-Martínez and Azañón, 1997; Martínez-Martínez et al., 2002; Booth-Rea et al., 2004c; Martínez-Martínez et al., 2004*).

The Sorbas–Tabernas–Vera and Níjar–Almeria basins are examples of these Neogene extensional basins, which showed marine continuity with the Alborán and Algero–Balearic basins during the late Neogene *(Braga et al., 2003)*. Although the Sorbas–Tabernas–Vera and Níjar–Almeria basins are different drainage/sedimentary basin domains, in this paper we use this Neogene basins nomenclature in a geographic sense because they are located to the north and to the south of the main ridge in the area,

respectively (e.g. the Sierra Alhamilla–Polpos and Cabrera anticlinoria). Furthermore, they show a geographic continuity being located in different major fault blocks of the Polopos fault zone, as inferred in this work. The Sorbas–Tabernas–Vera basins crop out between the Sierra de Filabres to the north and the Sierra Alhamilla–Polopos and Cabrera ENE–WSW anticlinoria to the south; whilst the Níjar–Almeria basin crops out to the south of the Sierra Alhamilla–Polopos and Cabrera anticlinoria (Fig. 1).

The main tectonic processes driving topography and drainage evolution in the southeastern Betics have changed since the late Miocene. The earlier Tortonian sediments in the basins (11.6 to 8 Ma) record the denudation of the Nevado–Filabride complex *(Völk, 1967; Johnson et al., 1997)*, the deepest metamorphic complex in the Betics. Core-complex type extension and coeval orthogonal shortening influenced the drainage by the development of large domal structures in the footwall and sedimentary basins in the hanging-wall during the Tortonian 11-8 Ma ago *(Martínez-Martínez et al., 2002, 2004)*. During this time large delta systems fed from the Sierra de Filabres dome developed to the south and north of it in the Sorbas–Tabernas–Vera basins and the Almanzora basin (Fig. 1), respectively *(Völk, 1966; Barragán, 1997; Booth-Rea, 2001; Haughton, 2001)*. Moreover, since the latemost Tortonian until present continued NW–SE convergence between Africa and Iberia *(Dewey et al., 1989; Rosenbaum et al., 2002)* led to the development of large NE–SW to NNE–SSW sinistral strike-slip faults like the Palomares, Terreros and Alhama de Murcia faults *(Bousquet, 1979; Weijermars et al., 1985; Booth-Rea et al., 2004a)* and the E–W to ENE–WSW conjugate Polopos fault zone (Fig. 1, *Giaconia et al., 2012a*). Furthermore, ongoing Africa–Iberia convergence led to the further growth of E–W and ENE–WSW folds. These structures configure the main topographic features and geologic grain in the southeastern Betics, together with the NE–SW Carboneras sinistral fault zone that has a more complex and older evolution *(e.g. Keller et al., 1995; Scotney et al., 2000; Rutter et al., 2012)*.

Progressive unconformities in latemost Tortonian sediments of the Azagador member (8-7.24 Ma; *Martín et al., 2003*), belonging to the Turre formation *(Völk, 1966)*, mark the initial growth of the Sierra Alhamilla–Polopos and Cabrera fold structures related to NW–SE convergence between Africa and Iberia *(Alvado, 1986; Ott d´Estevou et al., 1990; Booth-Rea et al., 2004a)*. Messinian reef carbonates of the overlying Cantera member (7.24-5.96 Ma, *Völk, 1966; Sierro et al., 2001*) seal the major part of the folding in the Sierra Alhamilla *(Weijermars et al., 1985)*, although they themselves define an open fold.

Before the occurrence of the Messinian salinity crisis *(Hsü et al., 1973; 1977)*, open marine conditions prevailed in the then-connected Níjar and Sorbas–Tabernas–Vera basins (Abad member and the upper Abad lateral equivalent, the Cantera reef member). Since the late Messinian differential uplift induced the closure of the connection between the two basins *(Braga et al., 2003; Booth-Rea et al., 2005)*. At this time the Messinian salinity crisis was occurring in both basins (Yesares formation, 5,96-5,67

Ma, *Krijgsman et al., 2001*), but at the final stage of the crisis, while Lago Mare facies sediments were still depositing in the Níjar basin (Feos formation, 5,67-5,33 Ma, *Fortuin and Krijgsman, 2003*), the Sorbas basin had emerged (Zorreras member). The Sorbas basin was briefly invaded again by a shallow marine sea (top level Zorreras member) during the early Pliocene after the restoration of open marine conditions in the western Mediterranean. The evapotitic and post-evaporitic Messinian units (Yesares and Feos formations, respectively) of these basins have been inferred to represent the final marine reflooding of the Western Mediterranean after the deep desiccation corresponding to the Messinian salinity crisis *(Braga et al., 2006)*.

Final emersion of the Sorbas basin took place in the late Pliocene (Góchar formation) and has continued until present. In contrast, marine conditions persisted longer in the Níjar basin between the earlier Pliocene (Cuevas formation) and the beginning of the late Pliocene (Molata formation). Alluvial sediments from the base of the Góchar formation feed the late Pliocene (3.2 Ma, *Aguirre, 1998*) fan deltas of the Molata formation *(Mather, 1993)* southwards across the Sierra Alhamilla–Polopos and Cabrera anticlinoria. This transverse drainage incised into the anticlinorium by antecedence forming the Rambla de los Feos that drains the Sorbas–Tabernas basin into the Alias river since the early Pleistocene (Fig. 2, *Harvey and Wells, 1987; Mather, 2000b; Maher et al., 2007*).

The first river terrace (Terrace A), which marks the transition in the Sorbas and Níjar basins from continuous alluvial aggradation to repeated river incision and terrace development episodes, includes calcretes at the top of the strath-terraces with an age of 304±26 ka that formed post abandonment of the terrace surfaces *(Candy et al., 2005; Candy and Black, 2009)*, although, these authors interpret that it should be older than 400 ka. Later terraces formed during the middle and late Pleistocene–Holocene (Terrace B, 207±11 ka, Terraces C, 77±4 ka; Terraces D, 12.8±1 ka to 8.7±0.5 ka; all of them dated by pedogenic calcrete formed after the deposition and abandonment of the terrace surface, *Candy et al., 2005*).

In the southern part of the Sorbas basin two regionally significant captures occurred, both were triggered by changes in regional gradients associated to sustained early Pliocene–Quaternary uplift in the region *(Harvey and Wells, 1987)*, between 70 and 100 ± 20 m Ma^{-1} for the Sorbas basin since the early Pliocene *(Braga et al., 2003)* or 160 m Ma^{-1} over the Plio/Pleistocene *(Mather, 1993)*. The initial drainage was centripetal toward the Lobos axial system in the Sorbas basin center until the early Pleistocene *(Mather, 2000b)*.

The first capture occurred in the middle Pleistocene re-routing 15% of the original Sorbas basin drainage into the Alias river drainage basin (Níjar basin) to the south through the Rambla de Lucainena (Fig. 2, *Mather, 2000b, 2000a*) . This capture isolated the northeastern mountain front area of Sierra Alhamilla from the Sorbas basin forming

the Rambla de Lucainena (capture site 1 in Fig. 2). The second capture occurred in the late Pleistocene (≈70 ky) re-routing 73% of the original Sorbas basin drainage into the Vera basin to the east. This capture disconnected the Rambla de los Feos from the Sorbas basin and expanding the area of the Aguas river drainage system (capture site 2 in Fig. 2, *Mather, 2000b; Maher et al., 2007*).

9.3 Structure of the region

The Sorbas–Tabernas–Vera and Níjar–Almeria basins are separated by a large E–W trending ridge. This ridge is formed by the Sierra Alhamilla–Polopos and Sierra Cabrera en echelon anticlinoria (Fig. 2). The Sierra Alhamilla–Polopos anticlinorium is a double plunging fold showing a north-vergent asymmetric profile with a gentle south-dipping backlimb and a north steep-dipping forelimb *(Platt et al., 1983)*. The fold nucleated on a strongly heterogeneous basement formed by extensional wedges and tilted blocks, which determined the double plunging of its hinge *(Martínez-Martínez et al., 1997)*. The fold shows a progressive decrease in its amplitude to the east toward the Sierra de Polopos terminating against the Sierra Cabrera where it is offset toward the North by the Polopos fault zone (Fig. 2). The forelimb is cut by the North Alhamilla reverse fault that separates the metamorphic basement in its hanging-wall from overturned steeply dipping middle Miocene to Tortonian sediments of the Sorbas–Tabernas basin in the footwall (Fig. 2, *Platt et al., 1983; Martínez-Martínez and Azañón, 1997*). The North Alhamilla reverse fault forms great part of the northern mountain front of the ridge and locally cuts Pleistocene fan conglomerates related to it *(Giaconia et al., 2012a)*. Toward the west the Alhamilla–Polopos anticlinorium terminates with a perianticlinal closure defined by Tortonian sediments in the Andarax river valley. The western termination of the fold and its southern limb are cut by a NW–SE normal fault system active during the Pliocene and Pleistocene that has strongly extended the western fold termination and the northern margin of the Níjar basin, defining the steepest mountain fronts at the south of Sierra Alhamilla (Fig. 1, *Martínez-Díaz and Hernández-Enrile, 2004; Pedrera et al., 2006; Giaconia et al., 2012a*). At the Sierra de Polopos both the northern and southern limbs of the anticlinorium are cut by slightly oblique N100-110ºE oriented transpressive dextral faults of the Polopos fault zone, the North and the South Gafarillos faults, respectively (Fig. 2, *Giaconia et al., 2012a*). These faults form the northern and southern mountain fronts of the Sierra de Polopos and the contacts between the metamorphic basement and the Neogene sediments of the Sorbas and Níjar basins, to the north and south, respectively.

Fig. 2. Structural map of the study area (see Fig. 1 for its location) where the main tectonic structures of the Sierra Cabrera are shown: The North Alhamilla reverse fault (NARF), the North and the South Gafarillos faults (NGF and SGF, respectively), the North and the South Cabrera reverse faults (NCRF and SCRF, respectively), and the Carboneras fault zone (CFZ). LANF: low-angle normal faults; HANF: high-angle normal fault. Faults and folds with Quaternary activity are shown in red, meanwhile those with a Miocene activity are in blue.

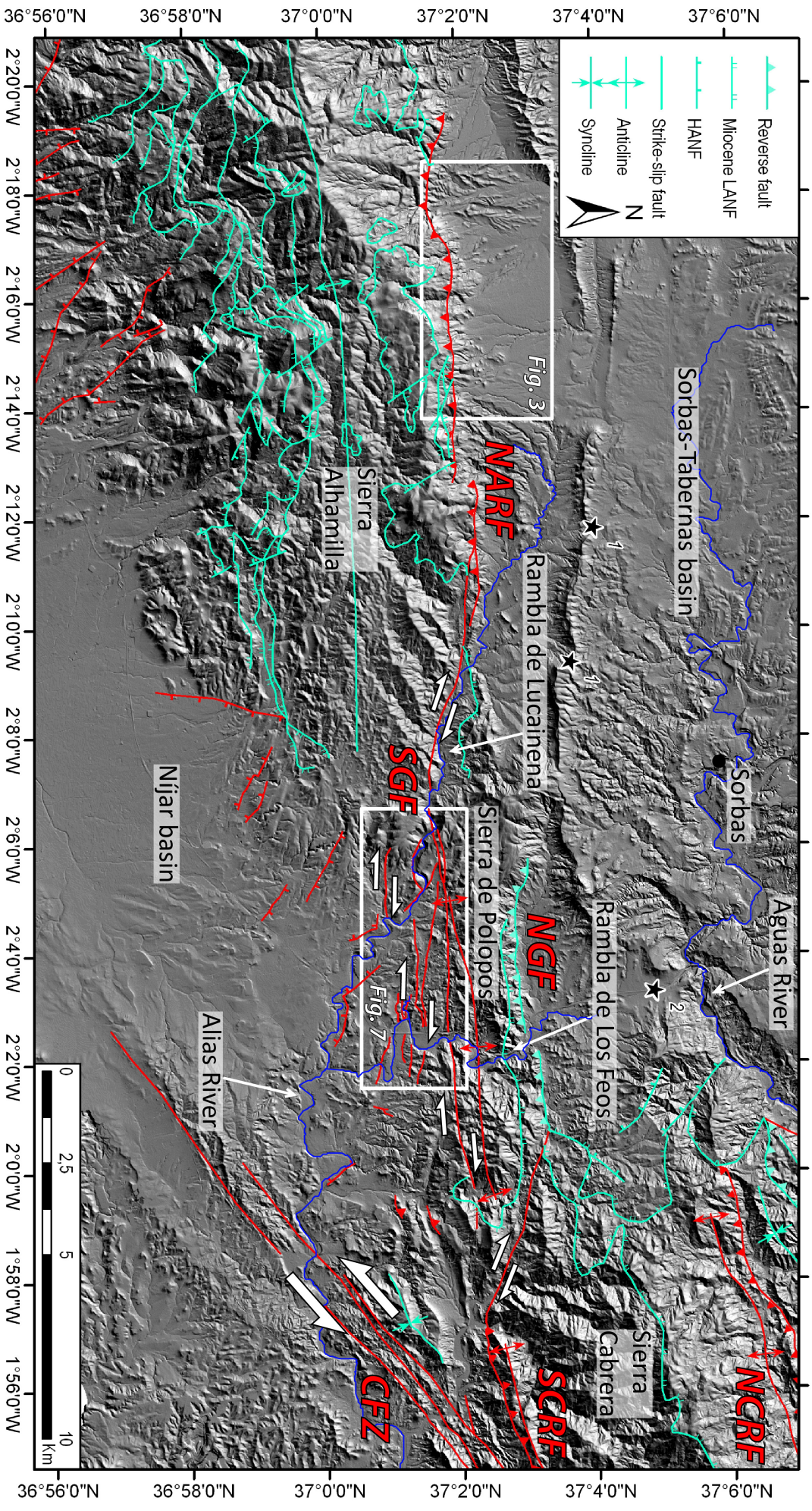
Reverse fault
Miocene LANF
HANF
Strike-slip fault
Anticline
Syncline
N
Fig. 3
NARF
Sierra Alhamilla
Rambla de Lucainena
Sorbas-Tabernas basin
Sorbas
Aguas River
Rambla de Los Feos
Sierra de Polopos
NGF
SGF
Fig. 7
Níjar basin
Alias River
Sierra Cabrera
NCRF
SCRF
CFZ
1
1
2
0
2,5
5
10
Km
36°56'0"N
36°58'0"N
37°0'0"N
37°2'0"N
37°4'0"N
37°6'0"N
2°20'0"W
2°18'0"W
2°16'0"W
2°14'0"W
2°12'0"W
2°10'0"W
2°8'0"W
2°6'0"W
2°4'0"W
2°2'0"W
2°0'0"W
1°58'0"W
1°56'0"W

The Sierra Cabrera has a box-fold geometry with two hinges to the north and south of the ridge where metamorphic basement rocks crop out *(Booth-Rea et al., 2005; Giaconia et al., 2012b)*. Both the northern and southern fold limbs are cut by reverse faults and by the Carboneras strike-slip fault zone to the southeast (Fig. 2). Meanwhile, the eastern termination of the Sierra Cabrera anticlinorium is cut by segments of the Palomares strike-slip fault zone (Fig. 1, *Weijermars, 1987; Coppier et al., 1990; Booth-Rea et al., 2004a*). Middle to late Miocene sediments of the Vera basin are overturned to the north of the fold forming the southern limb of a north-vergent asymmetric syncline *(Booth-Rea et al., 2004a)*. The Palomares fault zone bounds the eastern margin of the Vera basin where it shows sinistral-normal displacement and normal displacement in releasing bends, which produced important subsidence during the Quaternary *(Booth-Rea et al., 2004a; Stokes, 2008)*.

9.4 The Polopos fault zone

The Polopos fault zone is a N100-120ºE transpressive-dextral fault system developed in response to late Tortonian to Quaternary NNW–SSE shortening. This fault zone is formed by three main fault segments, the North and South Gafarillos dextral strike-slip faults, and the North Alhamilla reverse fault, to the east and the west, respectively (Figs. 1 and 2). This fault zone merges toward the East with the South Cabrera reverse fault along the Sierra Cabrera southern mountain front (Fig. 2, *Giaconia et al., 2012b*). The Polopos fault zone transfers southeast-directed oblique shortening along the South Cabrera reverse fault to northwest-directed shortening along the North Alhamilla reverse fault by the mean of dextral strike-slip South Gafarillos fault, in between. Thus, the fault zone shows helicoidal geometry, dipping toward the north and producing southeast-directed shortening to the east at the Sierra Cabrera southern mountain front and dipping toward the south with northwest-directed shortening at the Sierra Alhamilla northern mountain front.

The North Gafarillos fault at the western termination of Sierra Cabrera cuts the Sierra de Polopos with dextral kinematics and further west it turns toward a N80ºE trend, parallel to the northern limb of the Sierra Alhamilla–Polopos anticlinorium where it shows reverse kinematics and dips approximately 15º toward the south at the surface (Fig. 2). The reverse segment of the North Gafarillos fault is sealed by Messinian Cantera member reef carbonates toward the west *(Ott d'Estevou and Montenant, 1990; Stapel et al., 1996; Huibregtse et al., 1998; Haughton, 2001; Jonk and Biermann, 2002)*. However, both geomorphic analysis of the area and fault segmentation mapping show that the South Gafarillos fault and the North Alhamilla reverse fault have been active until the Holocene, affecting fluvial strath terraces, topography and the drainage network *(Giaconia et al., 2012a)*. The total length of the active Polopos fault zone, combining the North Alhamilla and the South Gafarillos faults, reaches about 30 km.

The N100-120ºE Polopos fault zone represents the transpressive-dextral conjugate-fault of the N10ºE oblique-sinistral Palomares fault zone since it makes an angle of about 60º with respect to the latter and an angle of about 30º with respect the NNW–SSE-oriented shortening direction.

9.4.1 The North Alhamilla reverse fault

The North Alhamilla reverse fault cuts the northern limb of the Sierra Alhamilla anticlinorium for about 17 km forming the contact between the metamorphic basement and the Neogene sedimentary cover of the Sorbas–Tabernas basin (Figs. 2 and 3). Globally the fault strikes N80ºE and dips 30-50º S showing SSE-plunging slickenlines that indicate a NNW hanging-wall displacement (Figs. 4 and 5).

Segments of the fault zone are linked by NW–SE transfer faults that permit the forward propagation of the main thrust front, for example just to the west of Turrillas village (Figs. 3 and 6c). Thrusts, lateral ramps and folds are consistent with a NNW–SSE-oriented sub-horizontal maximum principal stress (σ_1) and a sub-horizontal WSW–ENE-oriented intermediate principal stress (σ_2), as shown by the direct fault inversion (obtained by DAISY3 software, *Salvini et al., 1999*) of the collected structural data in the study area (Fig. 5).

This reverse fault system cuts through Serravallian–Tortonian conglomerate and sandstone and Quaternary alluvial fans and paleo-landslides associated with the northern mountain front of the Sierra Alhamilla (Figs. 3, 4 and 6a, b, d, e, f and g). These Quaternary landforms and sediments have been correlated with strath terraces of the Tabernas–Sorbas basin dated with the U/Th geochronological method on pedogenic calcretes that usually culminate the terrace and fan surfaces *(Harvey et al., 1995, 2003; Maher et al., 2007)*. The youngest alluvial fan unit, formed by sheet and channel gravels with pedogenic calcrete at the top, has been correlated, on the basis of the calcrete lithological characteristics (e.g. calcrete status and material source of the soil, *Harvey et al., 2003*), with strath terrace C in the center of the Sorbas basin that culminates with calcretes dated between 100 and 70 ky (late Pleistocene, *Harvey and Wells, 1987; Candy et al., 2005*, respectively). The older alluvial fan unit, formed by poorly-sorted clast-supported coarse- to very coarse- conglomerates and breccias of Nevado–Filabride origin, can be correlated according to *Maher et al. (2007)* with strath terrace A of the Sorbas basin, having a middle Pleistocene age (slightly older than 400 ky, *Harvey and Wells, 1987; Mather, 2000b*). Both alluvial fan units are cut and displaced by the North Alhamilla reverse fault, which was active after the late Pleistocene (70 ky) (Figs. 3, 4 and 6, *Giaconia et al., 2012a*).

The Pleistocene paleo-topographic surface formed by the alluvial fans (equivalent to fluvial strath terrace A) and landslides has been displaced vertically approximately 100 m by the North Alhamilla reverse fault *(Giaconia et al., 2012a)*. We have estimated net displacements in several locations along the cross sections (Fig. 4) taking into account

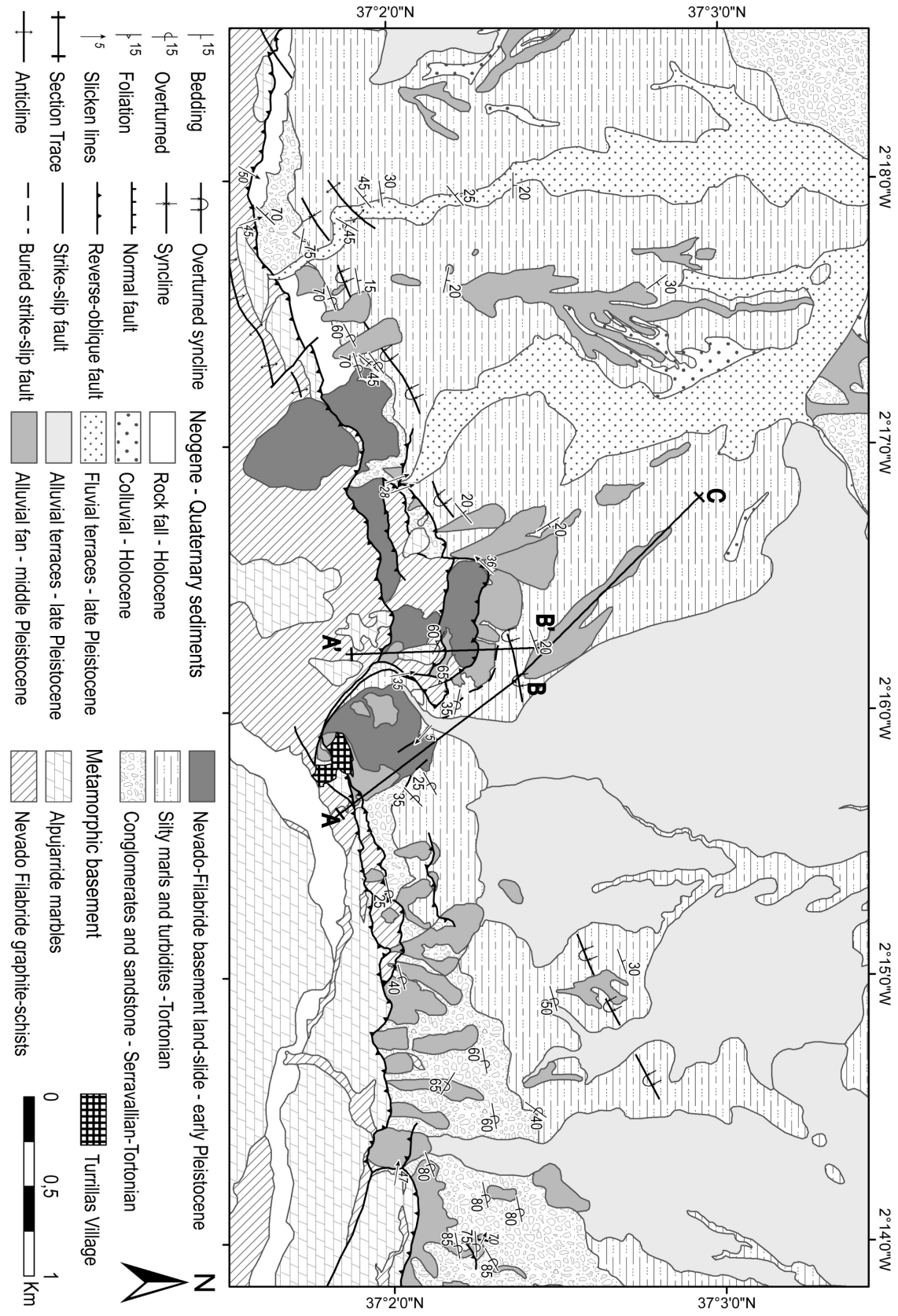

Fig. 3. Geological map of the western part of the North Alhamilla reverse fault (see Fig. 2 for its location). The fault system is characterized by reverse kinematics affecting Neogene and Quaternary sediments and alluvial fans of the Sorbas–Tabernas basin. The middle Pleistocene alluvial fans are cut and vertically displaced by segments of the North Alhamilla reverse fault (see the cross sections in Fig. 4).

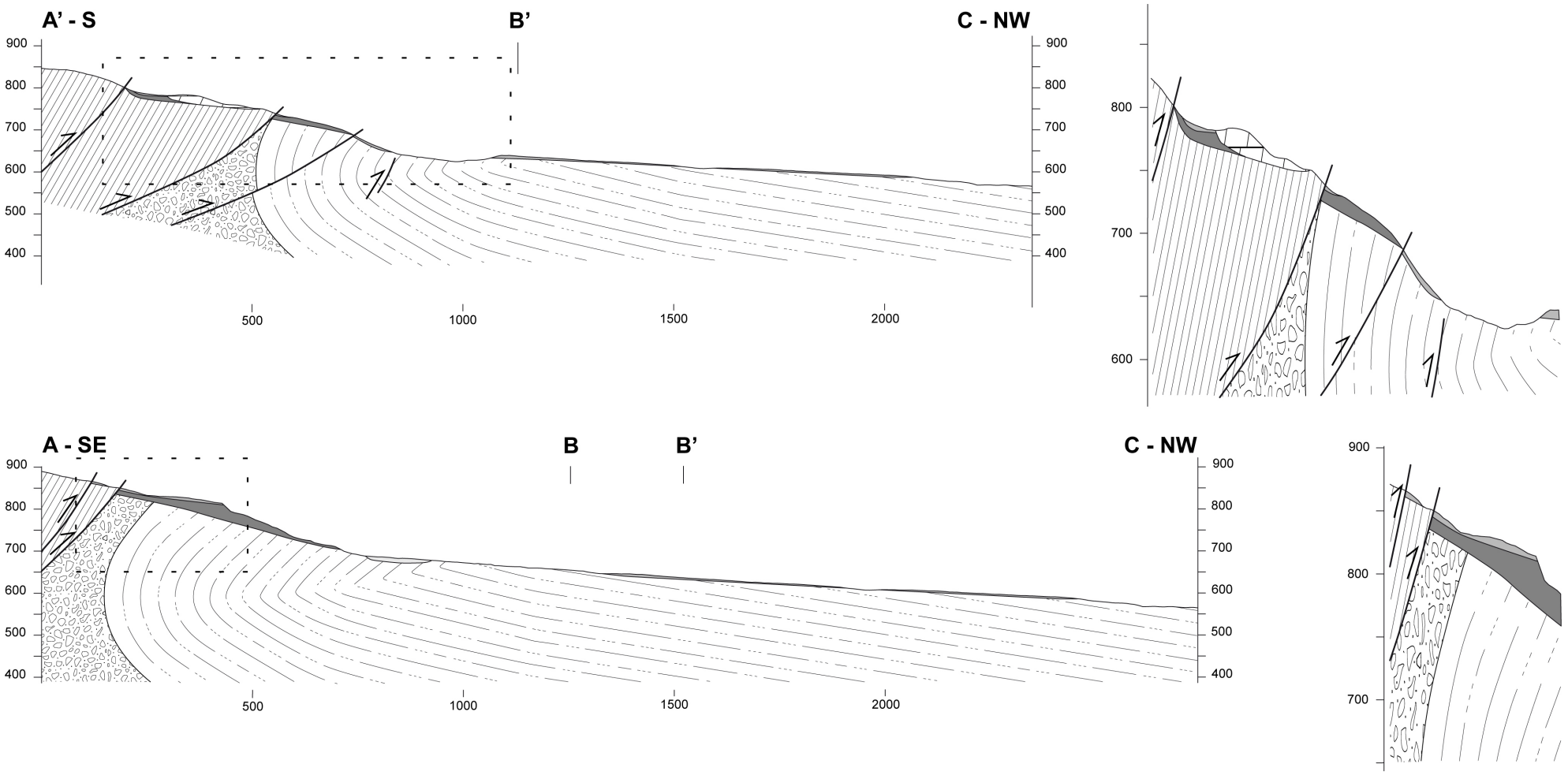

Fig. 4. Geological cross sections (see Fig. 3 for its location) across the North Alhamilla reverse fault and along middle Pleistocene alluvial fans in order to calculate vertical and net slip displacements (see the text in the Section 4.1). To the right zooms of cross sections show the late and middle Pleistocene alluvial fans cut by the fault system (vertical scale x 3).

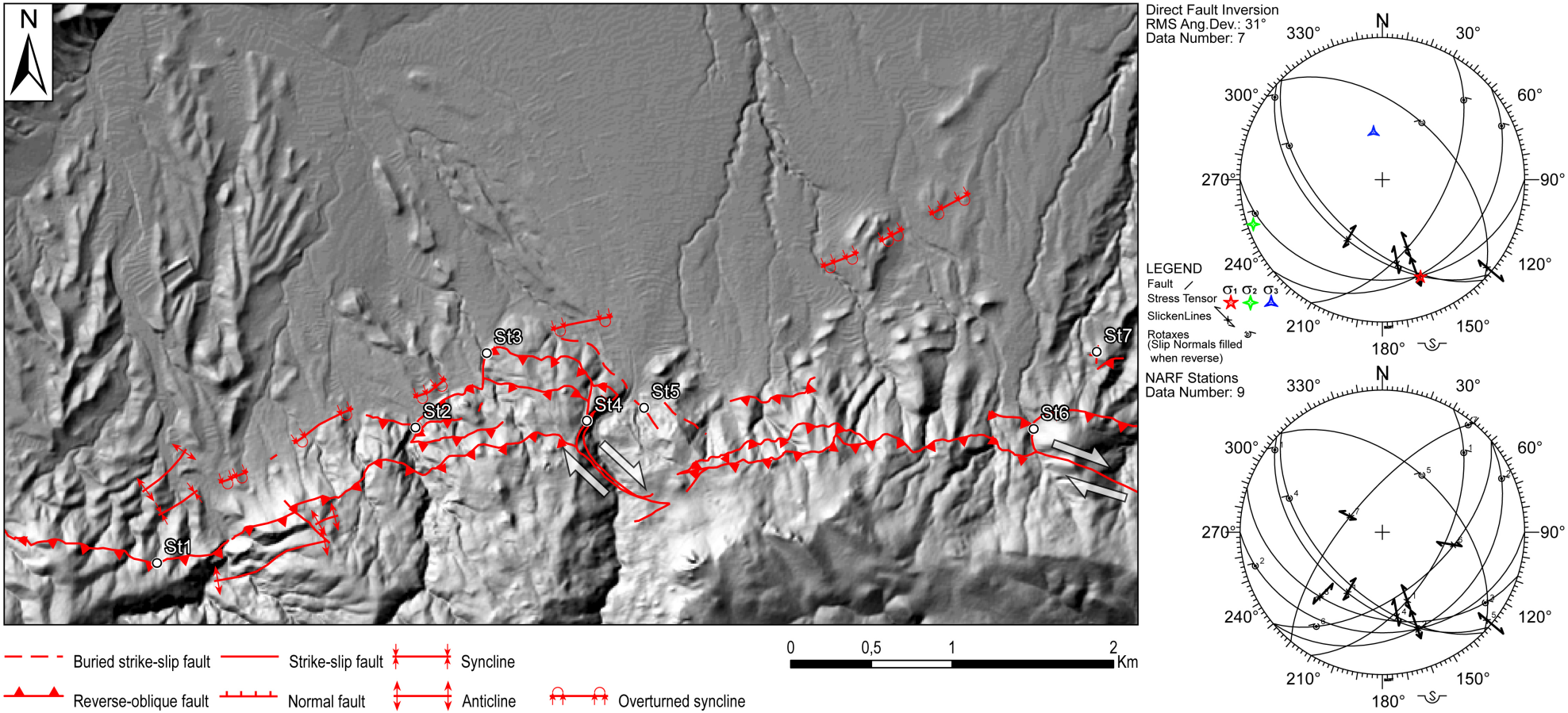

Fig. 5.Structural map and fault measurement stations of the North Alhamilla reverse fault (see Fig. 2 for its location) represented with a DEM in order to show the fault-related mountain fronts. Stereonets on the right show the structural data collected in the area and the direct inversion of them obtained by DAISY3 software, Salvini et al. (1999).

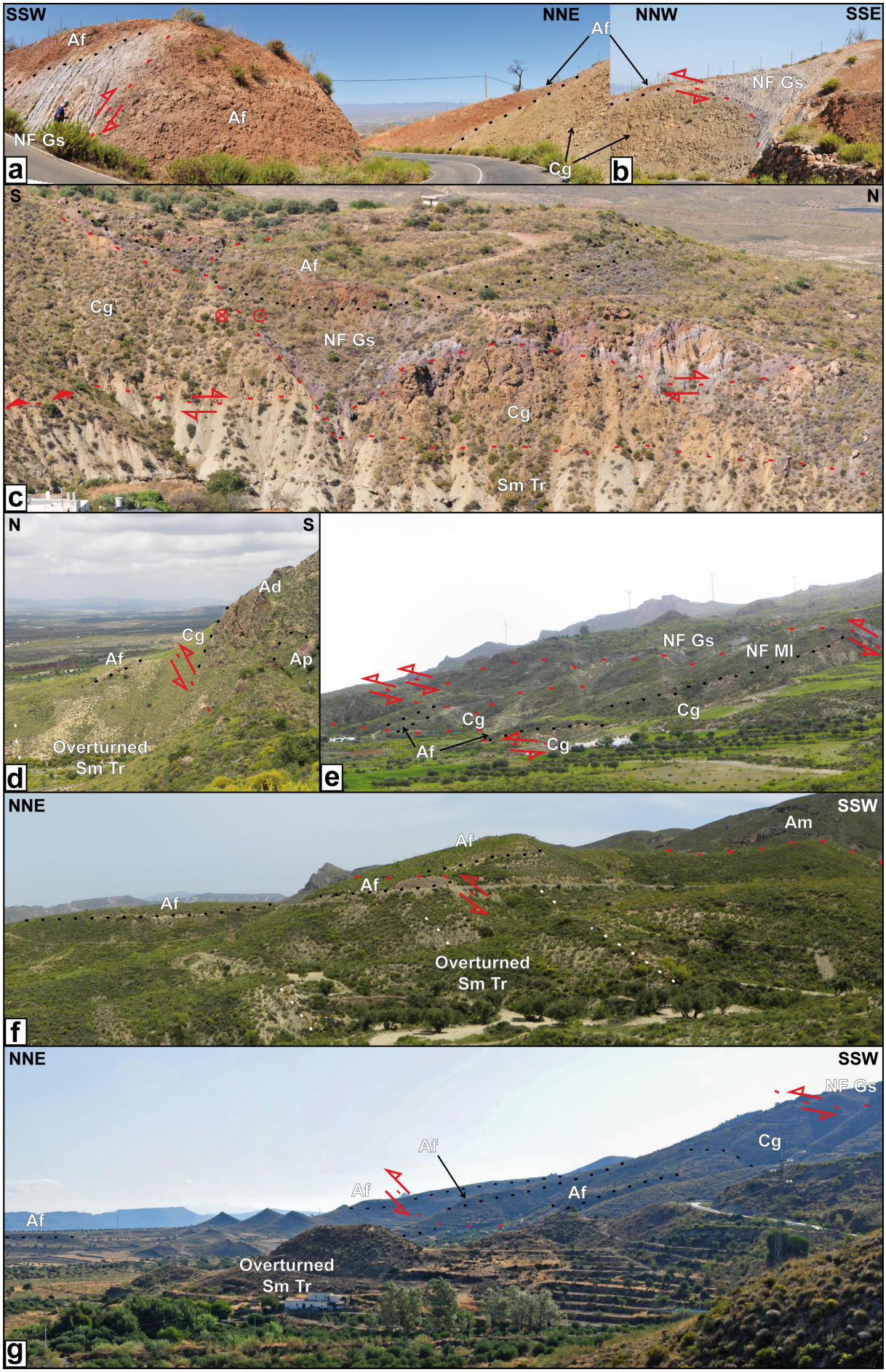
SSW
Af
NF Gs
Af
a
NNE
Af
Cg
NNW
SSE
NF Gs
b
S
N
Af
Cg
NF Gs
Cg
Sm Tr
c
N
S
Ad
Cg
Af
Ap
Overturned
Sm Tr
d
NF Gs
NF Ml
Cg
Cg
Af
Cg
e
NNE
SSW
Am
Af
Af
Af
Overturned
Sm Tr
f
NNE
SSW
NF Gs
Cg
Af
Af
Af
Af
Overturned
Sm Tr
g

the alluvial-fan profile, its extrapolation to the fault plane (dipping southwards 30º) and the slickenlines (showing a pitch of 73º W). Net displacements range between 80 and 125 m giving slip-rates 0.19 and 0.31 m ky^{-1}, during the last 400 ky. These slip-rate values are congruent with the ones previously obtained from geomorphic indices analysis that gave uplift rates between 0.05 and 0.5 m ky^{-1} *(Giaconia et al., 2012a)*.

9.4.2 The South Gafarillos fault

The South Gafarillos fault cuts the southern mountain front of the Sierra de Polopos for about 13 km in the northern margin of the Níjar basin (Fig. 2). The fault zone is a highly segmented dextral strike-slip system that includes several parallel and oblique segments with N90ºE to N120ºE strike that splay toward the SE as they approximate the Carboneras sinistral strike-slip fault zone and South Cabrera reverse fault (Fig. 2). The main fault segment separates the metamorphic basement (Alpujarride marbles and Nevado–Filabride graphite schist) from late Tortonian to Messinian sediments (Azagador and Abad members of the Turre formation). The southern fault segments cut through the whole sedimentary infilling of the Níjar basin, up to the Quaternary alluvial silts and gravels and fluvial strath terraces (Figs. 7 and 8).

Fault segmentation mapping and structural data show that the South Gafrillos fault zone is characterized by a dextral oblique strike-slip regime with both reverse and normal component of net displacement (Figs. 7-10). The oblique strike-slip regime of these faults produces syncline and anticline structures usually associated with positive flower structures (eastern part of the Fig.7, cross-section A-A' in Fig 8 and outcrops in Fig. 10a and h) or restraining bends (see the western part of the Fig. 7, cross-section B-B' in Fig. 8 and outcrops in Fig. 10d). Sinistral fault segments striking NE–SW to NNE–SSW typically occur within the fault zone (Fig. 11). At least 6 parallel fault segments have been mapped in the area where the Rambla de los Feos incises through the Sierra de Polopos (Fig. 7) that separate differentially uplifted fault-blocks showing increasing

Fig. 6. Photos of the most significant outcrops in the area of the North Alhamilla reverse fault. Ad: Alpujarride dolomite; Af: middle Pleistocene alluvial fan; Am: Alpujarride marbles; Ap; Alpujarride phyllite; Cg: Serravallian–Totonian conglomerates and sandstone; NF Gs: Nevado–Filabride graphite schists; NF Ml: early Pleistocene Nevado–Filabride basement land-slide; Sm Tr: Tortonian silty marls and turbidites. a) and b) North Alhamilla reverse fault segment that thrusts the metamorphic basement on the middle Pleistocene alluvial fan sediments (photo taken just at the start of the A-C cross section, see Figs. 3 and 4). c) Lateral ramp of the North Alhamilla main fault segment that thrusts the metamorphic basement on the Serravallian–Tortonian sediments, affecting also middle Pleistocene alluvial fan conglomerates (photo taken just to the west of the Turrillas village, see Fig. 3). d) Fold produced by the North Alhamilla reverse fault system (photo taken at the mountain-front mouth of the westernmost stream, see Fig. 3). e) View of the western part of the North Ahamilla reverse fault (just to the west of the cross sections, see Fig. 3) that thrusts metamorphic basement on the Serravallian–Tortonian sediments, whilst a northern branch cuts the middle Pleistocene alluvial fans. f) Middle Pleistocene alluvial fan sediments cut by a North Alhamilla reverse fault segment (photo taken in the westernmost part of the map of the northernmost reverse fault segment, see Fig. 3). g) View of the North Ahamilla reverse fault (just to the west of the Turrillas village, see Fig. 3) that thrusts metamorphic basement upon Serravallian–Tortonian sediments, whilst a northern splay cuts middle Pleistocene alluvial fans.

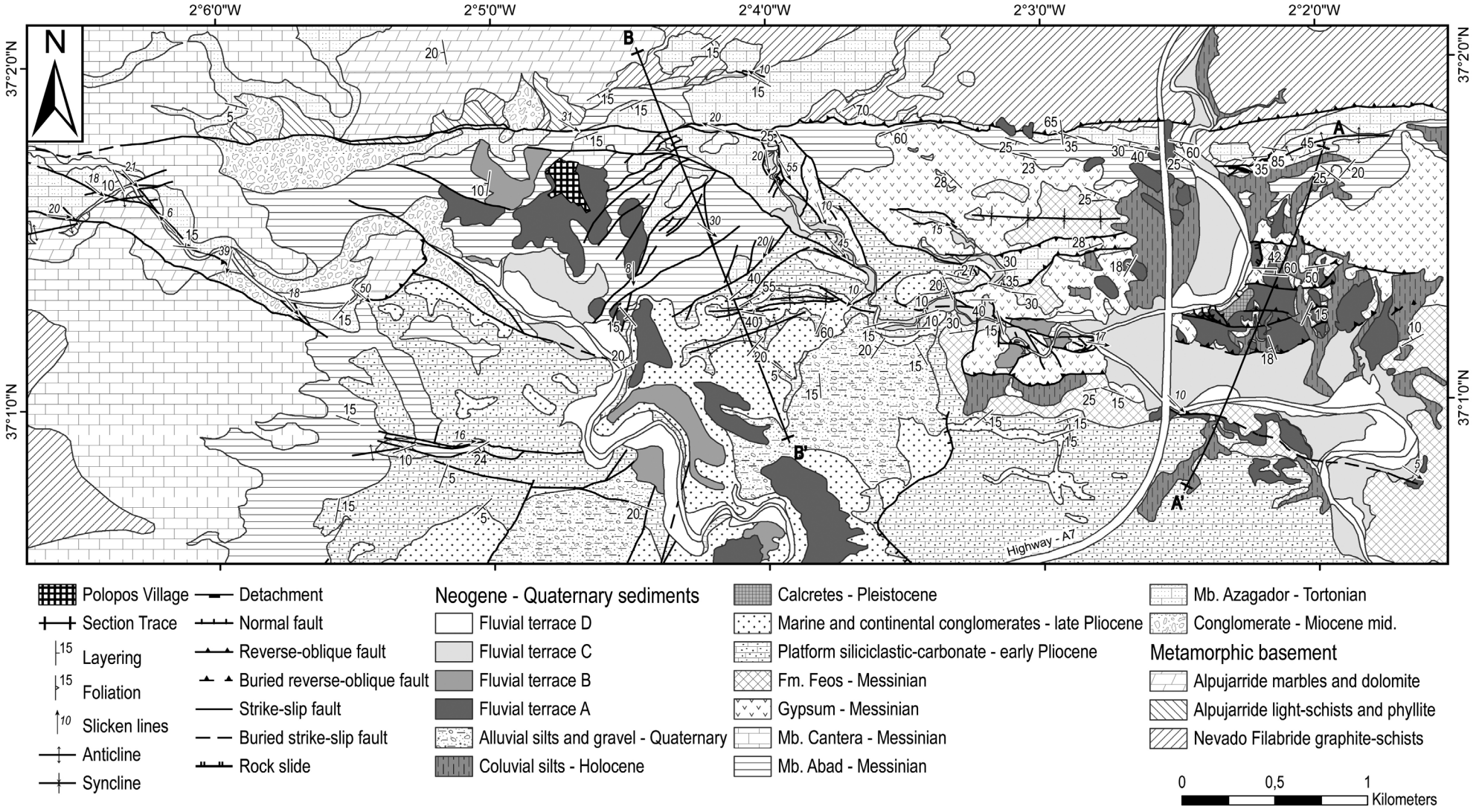

Fig. 7. Geological map of the South Gafarillos fault (see Fig. 2 for location). The fault system is characterized by dextral and dextral-reverse kinematics affecting Neogene and Quaternary sediments and terraces of the Nijar basin.

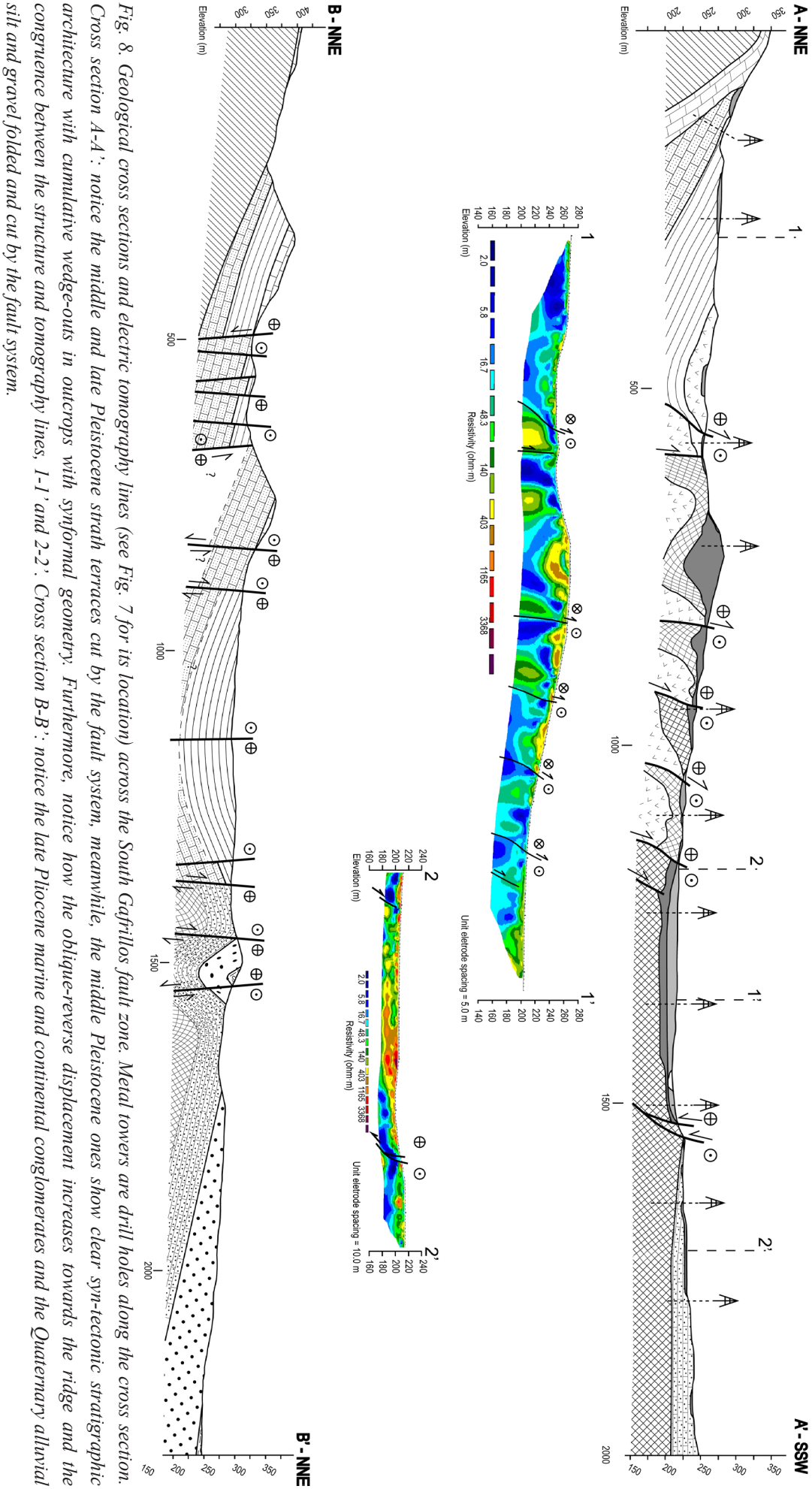

Fig. 8. Geological cross sections and electric tomography lines (see Fig. 7 for its location) across the South Gafrillos fault zone. Metal towers are drill holes along the cross section. Cross section A-A': notice the middle and late Pleistocene strath terraces cut by the fault system, meanwhile, the middle Pleistocene ones show clear syn-tectonic stratigraphic architecture with cumulative wedge-outs in outcrops with synformal geometry. Furthermore, notice how the oblique-reverse displacement increases towards the ridge and the congruence between the structure and tomography lines, 1-1' and 2-2'. Cross section B-B': notice the late Pliocene marine and continental conglomerates and the Quaternary alluvial silt and gravel folded and cut by the fault system.

uplift toward the North (cross section A-A' in Fig. 8 and Fig. 10a). All of them show dextral-reverse kinematics, except the southernmost one that shows dextral-normal kinematics (Fig. 7, cross section A-A' in Fig. 8 and Fig. 10c). This has lead to the development of a thick middle Pleistocene to Holocene sedimentary infilling (approx. 50 m) between the two fault segments beneath the Rambla de los Feos, revealed by drilling (cross section A-A' in Fig 8) and electric tomography (tomography line 2-2' in Fig. 8).

We inverted the slickenlines and fault plane data (by the rotaxes method using DAISY3 software, *Salvini et al., 1999*) obtaining a NNW–SSE-oriented sub-horizontal maximum principal stress (σ_1) and a sub-horizontal WSW–ENE-oriented intermediate principal stress (σ_2). Pervasive dextral and sinistral faults and folds in the study area are congruent with this stress tensor orientation and highlight a dextral shear zone where dextral faults striking about N120ºE correspond with the main Y faults. Dextral faults striking about N140ºE and N100ºE correspond to Riedel 1 (R_1) and P faults, respectively (Fig. 11). Meanwhile, sinistral faults striking about N190ºE and N230ºE correspond to Riedel 2 (R_2) and X faults, respectively (Fig. 11, *Davis et al., 2000; Faulkner et al., 2003*).

Quaternary alluvial silts and gravel and fluvial strath terraces provide a useful time constraint for the South Gafarillos fault activity because they are stratigraphically correlated with the strath terraces of the Aguas and Feos river systems *(Maher et al., 2007)* dated with U/Th geochronology on pedogenic calcretes (at the top of the strath terraces) in the Sorbas basin *(Harvey and Wells, 1987; Mather, 2000b; Candy et al., 2005)*. Strath terrace A with a typical coarse sediment assemblage was dated slightly older than 400 ky (middle Pleistocene, *Harvey and Wells, 1987; Mather, 2000b*), meanwhile strath terrace C includes calcretes dated between 70 and 100 ky (late Pleistocence, *Harvey and Wells, 1987; Candy et al., 2005*, respectively). Fault segmentation mapping (Fig. 7), cross-section A-A' and the electric tomography (Fig. 8) show that the southern South Gafarillos fault segments cut these two terraces (strath terrace A in Fig 10a and strath terrace C in Fig. 10h and f). Locally, strath terrace A shows internal progressive unconformities and soft-sediment deformation in outcrops with synformal geometry indicating a syn-tectonic stratigraphic architecture (Fig. 10a and b). Furthermore, Quaternary alluvial silts and gravels are clearly cut by a South Gafarillos fault segment and folded as shown in cross-section B-B' (at 1500 m from the origin in Fig. 8) and at the outcrop in Fig. 10g. Finally, the South Gafarillos fault provides an example of stream deflection and deviation in the Rambla de los Feos congruent with N90-110ºE strike-slip faulting and collected structural data (eastern part of Fig. 7, *Giaconia et al., 2012a*). Since Quaternary sediments and Pleistocene fluvial strath terraces (terrace A, slightly older than 400 ky, and C, between 70 and 100 ky) are cut and folded within the South Gafarillos fault zone, which also controls stream development, it is most likely that the fault zone activity continued up to present-

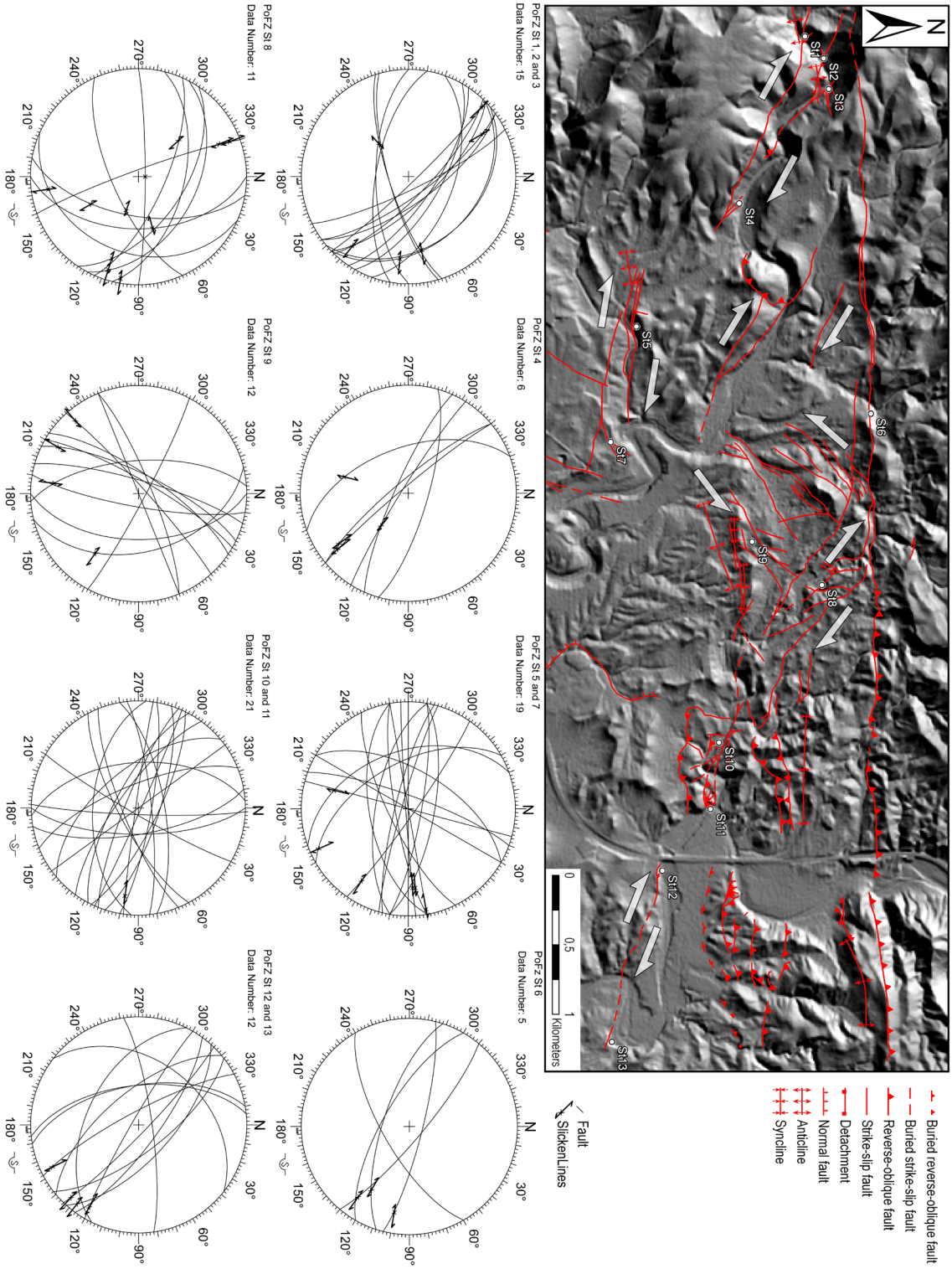

Fig. 9 .Structural map of the South Gafarillos fault (see Fig. 2 for its location) showing the structures and the structural stations. Stereonets of the data collected in the area show the occurence of dextral strike-slip faults with sub-horizontal slickenlines with both reverse and normal minor displacement, furthermore, sinitral strike-slip conjugate faults occur.

Fig. 10. Photos of the most significant outcrops in the area of the South Gafarillos fault system. Ad: Alpujarride dolomite; Am: Alpujarride marbles; At; Tortonian Azagador Mb.; Clc: Pleistocene calcretes; Fm: Messinina Feos Fm.; Gyp: Messinian gypsum; McCg: late Pliocene marine and continental conglomerates; Psc: early Pliocene platform siciclastic-carbonate; SgQt: Quaternary alluvial silt and gravel; Ta and Tc middle and late Pleistocene fluvial strath terraces, respectively. a) Dextral reverse-oblique faults affecting Messinian Feos formation and Gypsum up to middle Pleistocene fluvial strath terrace and Pleistocene calcretes (photo taken along the Rambla de los Feos at the midpoint of the cross-section A-A', see Fig. 7). b) Zoom of Figure a) showing the syn-tectonic stratigraphic architecture

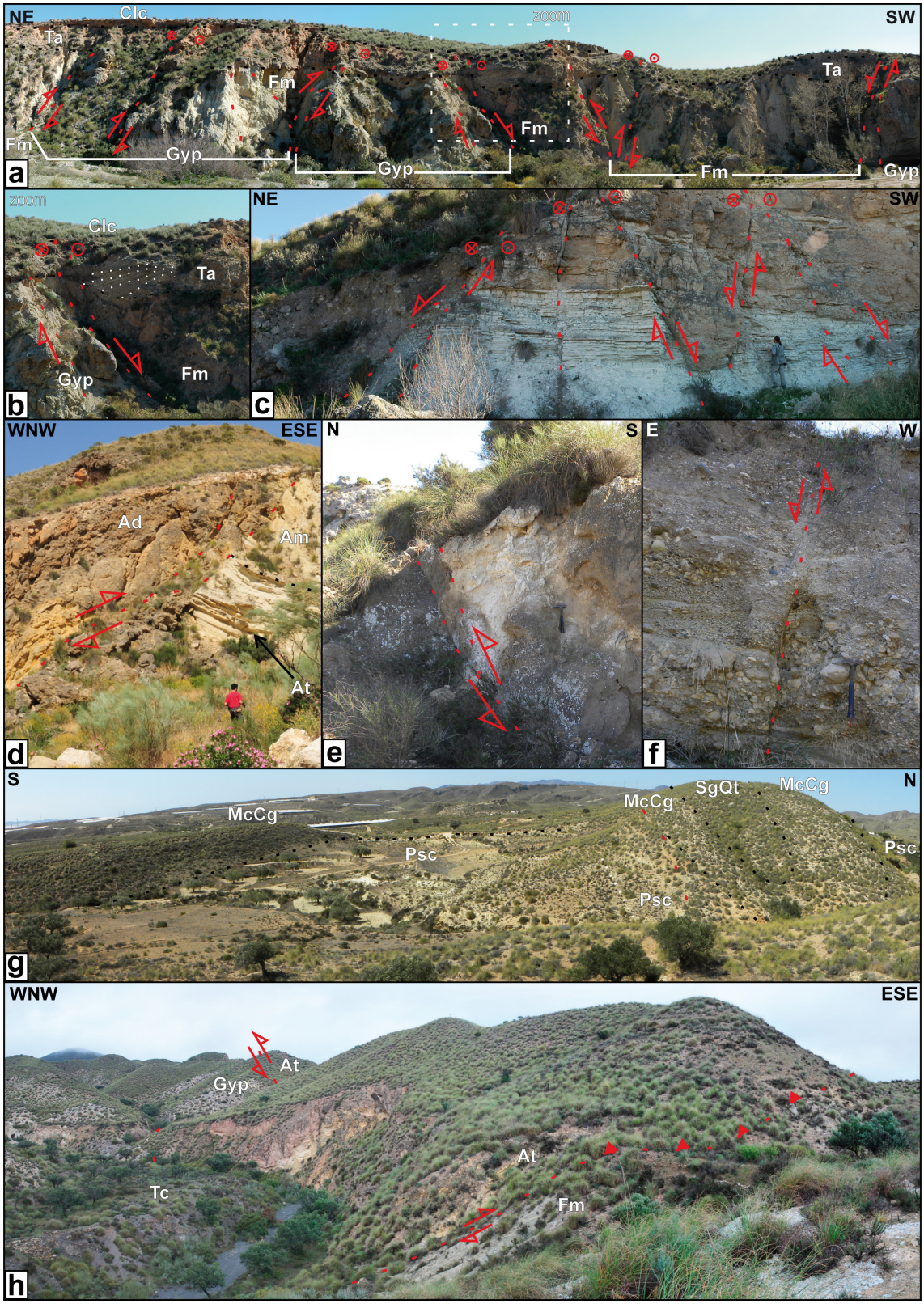

with cumulative wedge-outs of middle Pleistocene fluvial strath terrace. c) Dextral-normal fault system affecting the Messinian Feos formation and the late Pleistocene fluvial strath terrace (photo taken to the right of the highway near the A' point, see Fig. 7). d). Reverse fault in a restraining bend that thrusts Alpujarride dolomite on the Tortonian Azagador member (photo taken in the western part of the map, see Fig. 7). e) and f) faults affecting the late Pleistocene fluvial strath terrace (photo taken near the sharp closing of the meander of the Rambla de los Feos to the right of the highway, see eastern part of Fig. 7). g) Photo showing the Quaternary and late Pliocene sediments folded in a sinformal geometry and cut by the fault system (photo taken at the midpoint of cross-section B-B', see Fig. 7). h) Dextral positive flower structures that uplift the Tortonian Azagador member thrusting it on the Messinian Feos formation (photo taken at the eastern part of the map to the right of the highway, see Fig. 7).

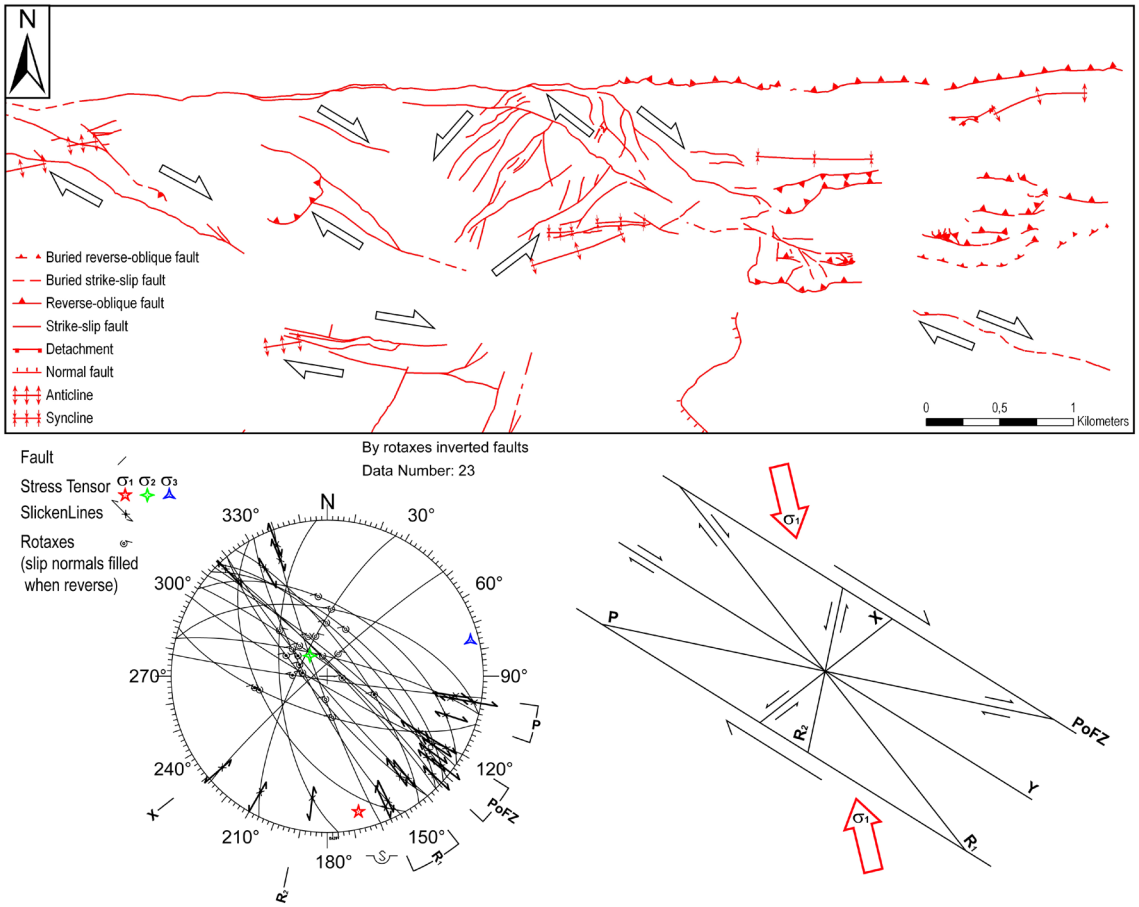

Fig. 11. Structural map of the fault zone and the slickenlines data inversion, obtained by the rotaxes method using DAISY3 software (Salvini et al., 1999). The stress field obtained shows a NNW–SSE-oriented sub-horizontal maximum principal stress (σ_1) and a sub-horizontal WSW–ENE-oriented intermediate principal stress (σ_2). Structural data highlights a dextral shear zone where the main dextral fault and Y faults strike about N120ºE, Riedel 1 (R1) and P dextral faults strike about N140ºE and N100ºE, respectively, meanwhile, Riedel 2 (R2) and X sinistral faults strike about N190ºE and N230ºE, respectively.

day. The oldest activity of the fault zone is difficult to determine, however, part of the angular unconformity between the Messinian gypsum (Yesares formation) and the underlying Azagador and Abad members of the Turre formation could be related to the fault activity. In addition, seismites and soft sediment deformation in sandstones from the Feos formation *(Fortuin and Dabrio, 2008)* were recognized in the study area and can be easily related to the South Gafarillos fault activity. This evidence implies that the dextral South Gafarillos fault segments have been active at least since the Messinian until present.

We calculated net displacements taking into account the elevation differences across fault segments of sub-horizontal geological surfaces, as the Azagador and Cantera members and the late Pliocene sediments, the fault plane orientation and the slickenlines (plunging between 5º and 15º both east- and westwards) that represent the fault displacement vector. Net displacements range usually between 30 and 100 m giving slip-rates of about 0.01 m ky^{-1} after the Messinian (5.96 Ma), and about 0.04 m ky^{-1} after the late Pliocene (3.2 Ma). Two net displacements differ strongly from the previous ones corresponding to 144 and 176 m in the western part of the map (Fig. 7

and structural station 3 in Fig. 9) and at the Rambla de los Feos sharp meanders (Fig. 7 and structural station 12 in Fig. 9), respectively. The corresponding slip rates are of 0.02 m ky^{-1}, after the Messinian (5.96 Ma), and 0.44 m ky^{-1}, during the last 400 ky. The vertical displacements are 0.0025 m ky^{-1} after the late Pliocene and 0.06 m ky^{-1} during the last 400 ky. Meanwhile, the vertical uplift estimated for the late Pliocene (3.2 Ma, *Aguirre 1998*) is about 0.10 m ky^{-1} taking into account its present altitude of about 300 m above the sea level and the sea level at that time (about 20 m below the present sea level, *Miller et al., 2011*).

9.5 Discussion

9.5.1 Fault linkage and growth

During the late Miocene the locus of dextral displacement occurred along the North Gafarillos fault segments that splayed into reverse fault segments to the north of the Sierra de Polopos (Fig. 2). Thus, the main mountain front in the Sierra de Polopos must have been in the northern limb of the Polopos anticlinorium until the early Messinian. The fault segments of the North Gafarillos fault and their associated mountain fronts were sealed by early Messinian temperate carbonates and by Messinian reefs in the northeastern Sierra Alhamilla and to the northwest of the Sierra de Polopos *(Ott d'Estevou and Montenant, 1990; Stapel et al., 1996; Huibregtse et al., 1998; Haughton, 2001; Jonk and Biermann, 2002)*. Since the Messinian, tectonic displacement in the area migrated southwards, as inferred by seismites in sandstones from the Feos formation *(Fortuin and Dabrio, 2008)*, forming the presently active South Gafarillos fault zone to the south of the Sierra de Polopos that linked with eastern segments of the North Alhamilla reverse fault (Fig. 2). The fact that uplift related to the South Gafarillos fault segments increases toward the Sierra de Polopos to the north and that the youngest faulted sediments occur southwards (Fig. 7) suggests that deformation has propagated toward the south, away from the ridge by the creation of new fault segments during the Pleistocene. These fault segments produced syn-depositional deformation in middle to late Pleistocene alluvial fans and terraces. Furthermore, the associated mountain front remains active until present day, as inferred from the fault segmentation map, strath-terrace ages cut by the fault system and morphotectonic analysis by *Giaconia et al. (2012a)*. This process enlarged the Polopos fault zone westwards linking the South Gafarillos fault with the North Alhamilla reverse fault up to the present tipline of the latter fault, located approximately at meridian 2º20'W (Fig. 2).

9.5.2 Mountain front migration and drainage captures

The geo-structural dataset presented in this paper shows that fault segment growth and migration shifted uplift from the northern side of Sierra de Polopos during the latemost Tortonian to early Messinian along the North Gafarillos fault to the southern side of

the ridge during the latemost Messinian to late Pleistocene along the South Gafarillos fault. Furthermore, fault segment growth and migration propagated the Polopos fault zone linking the South Gafarillos fault westwards with the North Alhamilla reverse fault reactivating the previous fold-related mountain front to the north of Sierra Alhamilla (Fig. 2).

During the Messinian to middle Pleistocene the mountain front shift controlled the development of new basins draining toward the south: the Feos drainage system across the Polopos ridge and the Lucainena one along the eastern termination of the Sierra Alhamilla, parallel to the South Gafarillos fault (Fig. 12a and b). In the Quaternary the first capture that affected the Sorbas basin occurred during the middle Pleistocene (>> 400 ky, although, poorly constrained by dating of calcretes at the top of terrace A performed by *Candy et al., 2005*) just to the north of the eastern part of the Sierra Alhamilla northern mountain front, along the contact between Tortonian silty-marls (to the south) and late Tortonian to Messinian temperate carbonates and reefs (to the north, Figs. 2 and 12b), producing the Rambla de Lucainena valley *(Mather, 2000b, 2000a)*. However, not only the erodibility contrast between these rocks favored the capture, but also another mechanism is needed. Differential uplift between ranges and Neogene to Quaternary basins played a key role at this time in the area. Indeed, Pliocene to recent regional uplift rates for the Sierra Alhamilla were calculated between 80 and 150 m Ma^{-1} by *Weijermars et al. (1985)*, sufficiently higher than those of the Sorbas basin, between 70 and 100±20 m Ma^{-1} *(Braga et al., 2003)*. However, the key data is the lower uplift rate of the Níjar basin, between 53 and 76±20 m Ma^{-1} *(Braga et al., 2003)*, with respect to the Sorbas one (Figs. 2 and 12b). This lower uplift rate could be related to the Pliocene–Quaternary NW–SE- to NNW–SSE-striking high-angle normal-fault system with southwestward directed extension that affects the northern margin of the Níjar basin (Fig. 12b, *Martínez-Martínez and Azañón, 1997; Martínez-Díaz and Hernández-Enrile, 2004; Marín-Lechado et al., 2005; Pedrera et al., 2006; Sanz de Galdeano et al., 2010*). This differential uplift between the Sorbas and Níjar basin together with the uplift produced at the southern limb of the Sierra de Polopos by the South Gafarillos fault segments favored headward erosion of the Lucainena drainage system parallel to the faults (Fig. 12b). This drainage system advanced trough the highly erodible Tortonian silty marls in the southern margin of the Sorbas basin, isolating the center of the basin from sediments of the Sierra Alhamilla. Propagation of the Lucainena drainage toward the center of the Sorbas basin was probably hindered by the presence of a strong erodibility contrast between Tortonian silty marls and latemost Tortonian Azagador temperate carbonates that dip toward the center of the basin (Figs. 2 and 12b). In this context the North Alhamilla reverse fault worked as a catalyzer of this process producing a positive relief just to the south of the Lucainena valley, causing a higher stream erosion-energy that favored its development and individualization.

The second capture suffered by the Sorbas basin occurred during the late Pleistocene

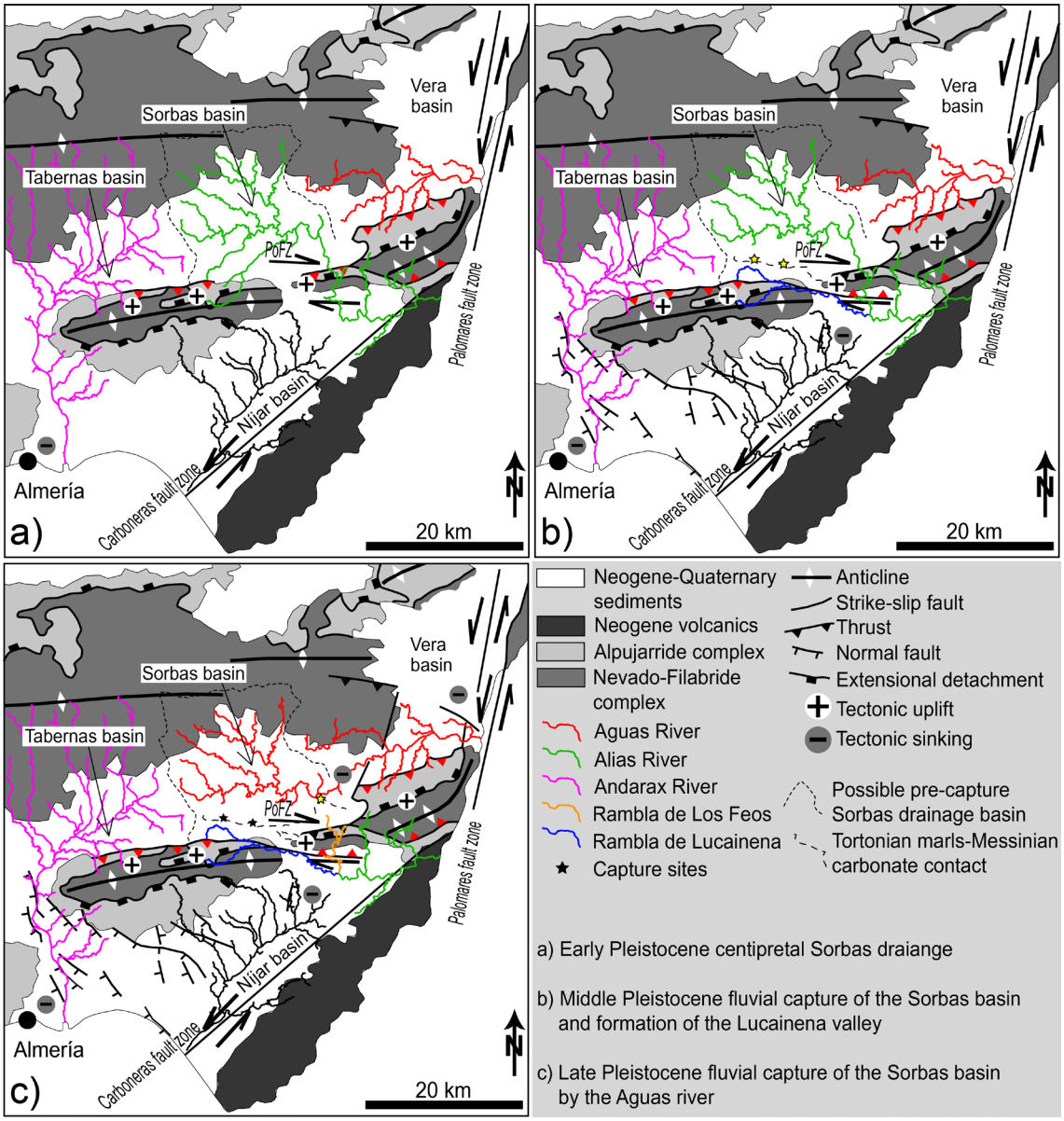

Fig. 12: Structural sketch of the southeastern Betics highlighting the evolution of the drainage systems and the fault-related mountain fronts (in red when active). Furthermore, capture sites (in yellow when active), the Tortonian marls–Messinian carbonate contact, the possible pre-capture Sorbas basin and the tectonic uplift and sinking related to the Polopos and the Palomares fault zones are shown.

(100-70 ky) to the north of the Sierra de Polopos at the lithological contact between the Tortonian silty-marls, to the south, and late Tortonian to Messinian temperate carbonates and reefs, to the north (Figs. 2 and 12c, *Mather, 2000b*). Also in this case, the differential uplift rate between ranges and the Neogene basins played a critical role in the capture and in particular the difference between the Sorbas basin and the Sierra Alhamilla–Polopos and Cabrera anticlinoria (higher than 170 m Ma^{-1} for Sierra Cabrera, *Weijermars et al., 1985*). The tectonic uplift of the entire Sierra Alhamilla–Cabrera anticlinorium promoted headward dissection of the Aguas river that advanced westwards as an axial valley capturing the Sorbas centripetal drainage and the Feos–Aguas transverse drainage across the Sierra de Polopos (Figs. 2 and 12c). The westward advance of the Aguas river headward dissection is congruent with the decrease of fault displacement and vertical uplift along the North Alhamilla reverse fault toward its western tipline *(Giaconia et al., 2012a)*. Furthermore, the Palomares fault zone played

a key role on the late Pleistocene (100-70 ky) capture controlling the topography and drainage system of the Vera basin during the Quaternary (Fig. 12c). Indeed, the Palomares fault zone, having oblique sinistral-normal kinematics during the Pliocene–Quaternary, produced the relative sinking and extension of the Vera basin in its western hanging-wall fault block *(Booth-Rea et al., 2003a; 2004a; Stokes, 2008)*. The relative sinking of the Vera basin caused an increase of the stream erosion-energy in the head region of the Aguas river drainage promoting its headward dissection and westwards advance, and finally the late Pleistocene (100-70 ky) capture of the Sorbas and the Feos–Aguas transverse drainage (Fig. 12c). At the same time further westwards, the Andarax drainage system, in the Tabernas basin, captured the north and south of the Sorbas basin margins probably before the deposition of terrace A, as inferred by preserved sediment in the northern margin *(Mather, 1991)*. However this incision wave did not hit the more central basin parts from the west due to greater distances that had to be covered.

9.5.3 Geomorphological evolution in response to different uplift mechanisms

The present geomorphologic features of the Betics are influenced by the summed effect of at least three different tectonic processes driving uplift since the late Neogene; asthenospheric upwelling, core-complex type extension with orthogonal shortening and later strike-slip and reverse faulting. The main difference among these three processes is the wave-length of their related uplift. Late Miocene asthenospheric upwelling produced large wave-length epeirogenic uplift in both the Betics and Rif, which caused the generalized dissection character of drainage systems since the Messinian until present *(Braga et al., 2003; Duggen et al., 2003; Martín et al., 2003; García-Castellanos and Villasenor, 2011)*. Core-complex type extension and coeval orthogonal shortening resulted in the development of large E–W elongated dome structures that grew westwards, toward the direction of extension, between 12 and 6 Ma ago *(Johnson et al., 1997; Martínez-Martínez et al., 2002, 2004; Vázquez et al., 2011)*. These elongated domes (e.g. Sierra de Filabres–Sierra Nevada) determined a centripetal drainage system away from its axial culmination toward the surrounding basins.

Late Miocene core-complex type extension in the studied region promoted the differential uplift between the Sierra de Filabres anticlinorium and the Tabernas–Sorbas–Vera basin. This ridge emerged during the Serravallian *(Braga et al., 2003)* generating the global southward directed drainage system in that basin, until the later Tortonian. The presence of large boulders originated from the Sierra de Filabres in Tortonian deltaic sediments on the top of the Sierra Cabrera testify the inexistence of this topographical relief during the Tortonian. Further west toward the Sierra Alhamilla, the E–W sinistral Cantona strike-slip fault formed an uplifted submarine fault-block producing contained Tortonian turbidites in the Sorbas basin *(Haughton, 2001)*. Both dextral and sinistral E–W strike-slip faults like the Cantona fault, active during the Tortonian, were probably transfer faults linking offset uplifting extensional loci

(Martínez-Martínez, 2006; Martínez-Martínez et al., 2006). Since folding nucleated in the uplifted footwalls of the extensional domes *(Martínez-Martínez et al., 2002)*, this would explain the delay in the timing of folding between the Filabres and Alhamilla–Cabrera elongated domes. Once the rolling-hinge produced by core-complex extension passed through the footwall of the elongated domes, extension ceased and the domes were further folded and cut by reverse and transcurrent faults. This occurred in the Alhamilla–Cabrera dome since the latemost Tortonian when progressive unconformities started to develop defining the northern fold limb in the Azagador member *(Booth-Rea et al., 2004a)*. This folding generated a large E–W axial valley along the Tabernas–Sorbas basins fed by a perpendicular drainage system across the fold limbs. Once the basins emerged in the Pliocene, the axial valleys flowed out of the system through the east and west terminations of the Alhamilla anticlinorium *(Mather et al., 2002)*. Since then, transcurrent faulting and associated shortening structures have produced localized uplift controlling the Pleistocene drainage adjustment and river captures described above.

9.6 Conclusions

The Polopos fault zone is a N100-120ºE dextral transpressive fault zone developed under Tortonian to Quaternary NNW–SSE shortening. The fault zone is conjugate to the coeval sinistral Palomares fault zone. This fault zone is formed by the North and South Gafarillos dextral-transpressive fault and the North Alhamilla reverse fault. Activity along the fault zone probably initiated in the latemost Tortonian (≈ 7 Ma) and continued up to the late Pleistocene (≥70 ky), at least. Deformation along this fault zone and the associated mountain fronts migrated southwestwards between the Messinian and Quaternary. The North Gafarillos fault was active until the Messinian, whilst the South Gafarillos fault and its westward continuation in the North Alhamilla reverse fault have been active since then and, at least, until the late Pleistocene affecting the topography, the drainage network and alluvial terrace deposition (of middle and late Pleistocene ages) along their length. The South Gafarillos and North Alhamilla reverse fault segments together produce a 30 km active mountain front connecting the Sorbas and Níjar basins (Fig. 2).

The reverse displacement along the North Alhamilla reverse fault and the dextral-transpressive one along the South Gafarillos fault together with the southwestwards extension along Pliocene–Quaternary normal faults in the Níjar basin have determined the differential uplift between Sierra Alhamilla and the Sorbas and Níjar basins. This differential uplift in turn promoted the middle Pleistocene capture occurred in the southern margin of the Sorbas basin and the formation of the Rambla de Lucainena valley parallel to the Polopos fault zone (Fig. 12). Later, continued displacement along the Polopos fault zone and associated tectonic uplift of the Sierra Alhamilla–Polopos

and Cabrera anticlinoria, together with local subsidence associated to transtensional kinematics of the Palomares fault zone in the Vera basin, promoted the headward erosion of Aguas river drainage and its late Pleistocene capture of the Sorbas basin and Feos–Aguas transverse drainage (Fig. 12).

The present geomorphic setting in the Betics results from Neogene to present uplift that is controlled by three different tectonic processes; asthenospheric upwelling, core-complex type extension with orthogonal shortening and later strike-slip and reverse faulting. The first one determined a large wave-length epeirogenic uplift that caused the generalized dissection of drainage systems in Betics since the Messinian until present. Core-complex type extension and coeval orthogonal shortening caused smaller wave-length and more localized uplift determining elongated radial drainage systems associated with E–W extensional domes. Finally strike-slip and reverse faulting produced localized tectonic uplift related to fault segmentation, geometry, growth and linkage producing mountain front migration and fluvial captures.

Acknowledgments: This Study was supported by research projects CGL2011-29920, CSD2006-00041 TOPOIBERIA CONSOLIDER-INGENIO2010, CTM2007-66179-C02-00 MEDOC Project, CGL2008-03474-E/BTE TOPOMED Project and the CTM2011-30400-C02-01 HADES Project from the Spanish Ministry of Science and Innovation. We thank Anne Mather and the anonymous referees for their constructive contribution to improving the paper.

Submitted to *Tectonics*, 10 May 2013

10.0 Compressional tectonic inversion of the Algero–Balearic basin: latemost Miocene to present oblique convergence at the Palomares margin (western Mediterranean)

F. Giaconia [a,*], G. Booth-Rea [a], C. R. Ranero [b], E. Gràcia [c], R. Bartolome [c], A. Calahorrano [c], C. Lo Iacono [d], M. G. Vendrell [c], A. L. Cameselle [c], S. Costa [c], L. Gómez de la Peña [c], S. Martínez-Loriente [c], H. Perea [c], M. Viñas [c]

[a] Dpto. Geodinámica, Instituto Andaluz de Ciencias de la Tierra (CSIC-UGR), Campus Fuentenueva s/n, 18071, Granada, Spain
[b] Barcelona-Center for Subsurface Imaging, ICREA at CSIC, Institut de Ciències del Mar, Passeig Marítim de la Barceloneta 37-49, 08003, Barcelona, Spain
[c] Barcelona-Center for Subsurface Imaging, CSIC, Institut de Ciències del Mar, Passeig Marítim de la Barceloneta 37-49, 08003, Barcelona, Spain
[d] Marine Geoscience, National Oceanographic Centre, European Way, SO143ZH Southamton, United Kingdom
[*] Corresponding author. E-mail address: flavio@ugr.es, flavio@iact.ugr-csic.es

Abstract: Multichannel seismic reflection profiles show that the Palomares margin formed by volcanic accretion during middle to late Miocene opening of the Algero–Balearic basin. The margin marks the transition between thinned continental crust intruded by arc volcanism and back-arc oceanic crust. Deformation produced during the later inversion of the margin and onshore is partitioned between ~N50ºE striking reverse faults and associated folds like the Sierra Cabrera and Abubacer anticlines, and N10-20ºE sinistral strike-slip faults like the Palomares and Terreros faults. Parametric sub-bottom profiles, borehole and recent onshore-offshore sediment deformation together with available GPS geodetic displacement data, earthquake focal mechanisms and bathymetry indicate that tectonic inversion of the Palomares margin is currently active. The Palomares margin shows a comparable structural pattern to the north Maghrebian margins where Africa–Eurasia plate convergence is accommodated by NE–SW reverse faults, NNW–SSE sinistral faults and WNW–ESE dextral ones. Contractive structures at this margin contribute to the general inversion of the western Mediterranean since approximately 7 Ma ago, coeval to inversion at the Algerian margin. Shortening at the Alborán ridge and Al–Idrisi faults occurred later, since 5 Ma, indicating a westward propagation of the compressional inversion of the western Mediterranean.

Keywords: Active tectonics, Tectonic inversion, Western Mediterranean, Multichannel seismic, Abubacer anticline, Palomares fault zone.

10.1 Introduction

Continued NW–SE convergence between the African and European plates is leading to tectonic inversion of Oligocene to Miocene back-arc basins in the western Mediterranean Sea *(Bourgois et al., 1992; Comas et al., 1992; Mauffret et al., 1992; Comas et al., 1999; Billi et al., 2011)*. Reverse and strike-slip faults related to this tectonic inversion develop in the onshore-offshore margins of these basins (Fig. 1, *Bourgois et al., 1992; Mauffret, 2007; Kherroubi et al., 2009; Strzerzynski et al., 2010; Billi et al., 2011; Martínez-García et al., 2013*). Inversion structures are found along the northern and southern margins of the Algero–Balearic to Alborán basins (Fig. 1). Reverse fault systems in the Algerian continental slope, the dextral Yusuf fault, and reverse faulting of the Alborán Ridge, are major active structures related to late Miocene to present-day inversion *(Bourgois et al., 1992; Campos et al., 1992; Comas et al., 1992, 1999; Déverchère et al., 2005; Domzig et al., 2006; Yelles et al., 2009; Billi et al., 2011; Martínez-García et al., 2013)*.

The Palomares margin extends from thinned continental crust intruded by arc magmatism in the west to back-arc oceanic crust of the Algero–Balearic basin to the east (Fig. 2, *Booth-Rea et al., 2007*). The overall structure of the margin and individual geological elements, like the Abubacer volcanic ridge (offshore), the Carboneras fault zone and the Sierra Cabrera anticlinorium (onshore), strike N40-50ºE sub-perpendicular to the present NW–SE shortening stress field (Fig. 3). The present NW–SE shortening direction (about N140ºE) is confirmed by in situ strain measurement (from boreholes),

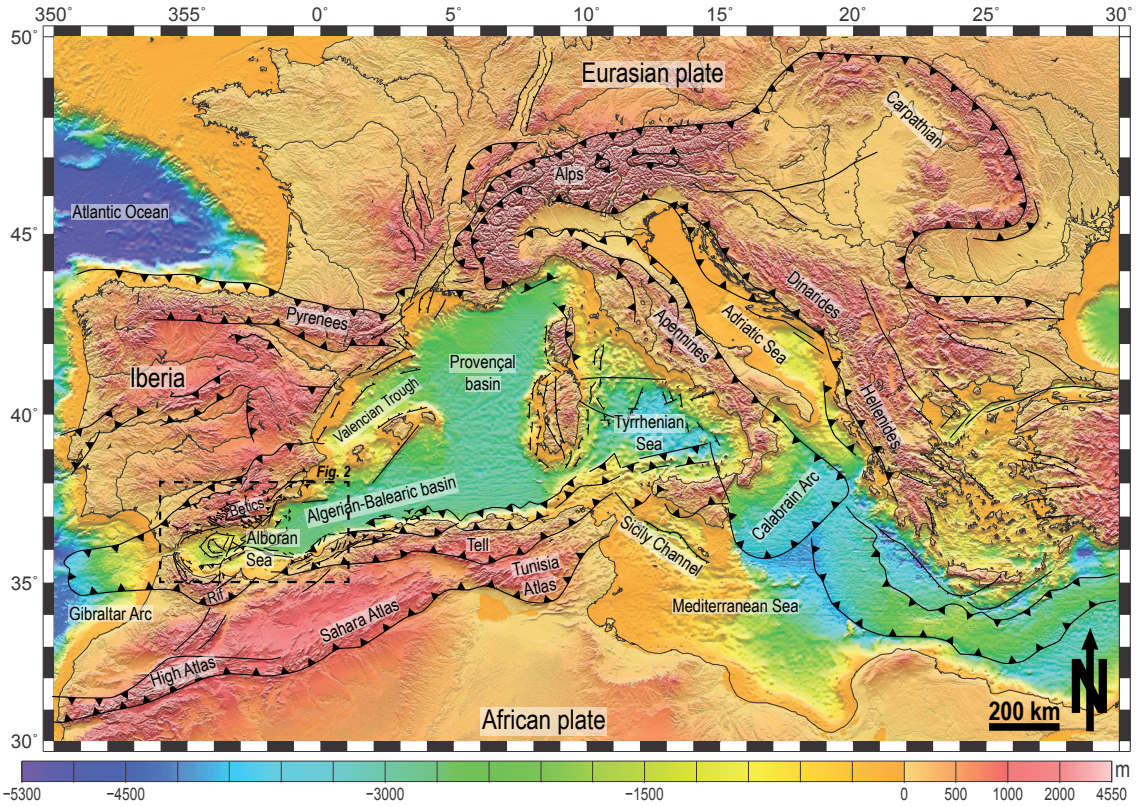

Fig. 1: Tectonic map of the western Mediterranean region (modified from, Faccenna et al., 2004; Mauffret, 2007; Billi et al., 2011).

fault slicken-line inversion data, GPS geodetic displacement data, and focal mechanisms in the area that show transpressive and reverse kinematics for the associated faults (Fig. 3, *Fernández-Ibáñez et al., 2007; Khazaradze et al., 2008; Echeverria et al., 2011; Giaconia et al., 2013a*). In contrast, the margin has been initially interpreted as formed by large tilted blocks developed during eastward extension *(Mauffret et al., 1992)*, and later as a transpressive strike-slip structure related to the occurrence of sinistral fault zones on land (e.g Terreros, Palomares and Carboneras fault zones in Fig. 3) in the eastern Betics *(Soto et al., 2000)*.

This incongruence between geodetic data and previous structural interpretations requires revision taking into consideration both onshore and offshore data. For this reason, we collected two multichannel seismic reflection lines across two contrasting areas of the Palomares margin. One line runs across the Abubacer volcanic ridge and is roughly parallel to the present maximum shortening direction. The second line is located in the transition to the East Alborán basin (Fig. 3). Simultaneously we acquired parametric sub-bottom profiles and swath-bathymetric data to analyze the most recent sedimentary/tectonic events and relate images of tectonic structures to seafloor relief.

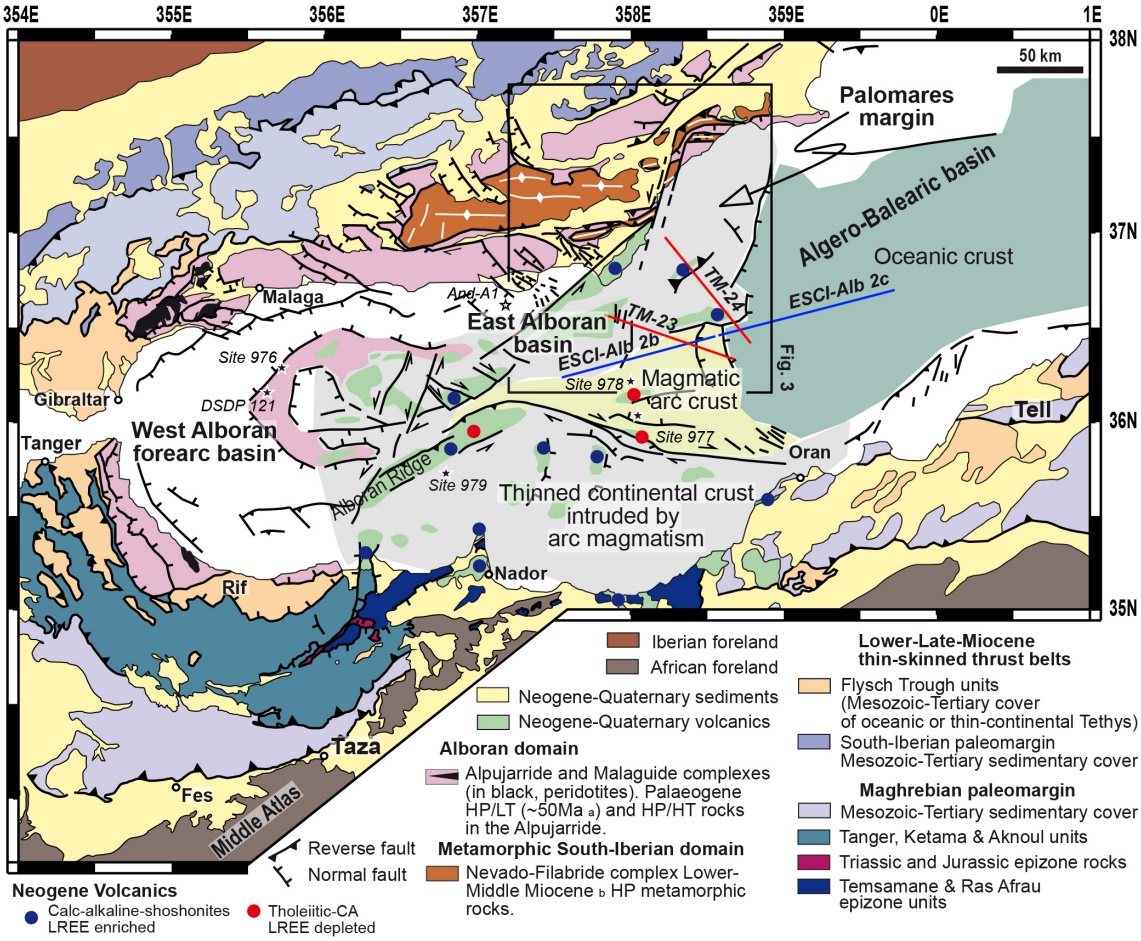

Fig. 2: Simplified geological map showing the tectonic domains of the Gibraltar Arc and the Alborán and Algero–Balearic basins (modified from, Comas et al., 1999; Booth-Rea et al., 2007; Martínez-García et al., 2013). Igneous geochemistry data acquired from El Bakkali et al. (1998), Coulon et al. (2002), Duggen et al. (2004a; 2005). Age of metamorphism: (a) Platt et al. (2005) and (b) Platt et al (2006). The new seismic profiles presented in this work (TM) are depicted as thick red lines whereas the pre-existing seismic profiles (ESCI) are as thick blue lines. Scientific drill sites (DSDP and ODP) and commercial wells in the Alborán Basin are also located. See Fig. 1 for its location.

The data were acquired on board the Spanish research vessel (R/V) Sarmiento de Gamboa in the frame of the European Science Foundation TopoEurope TOPOMED project *(Gràcia et al., 2011)* and processed at the Barcelona Center for Subsurface Imaging. Furthermore, in order to define the seismo-stratigraphy and calibrate their age

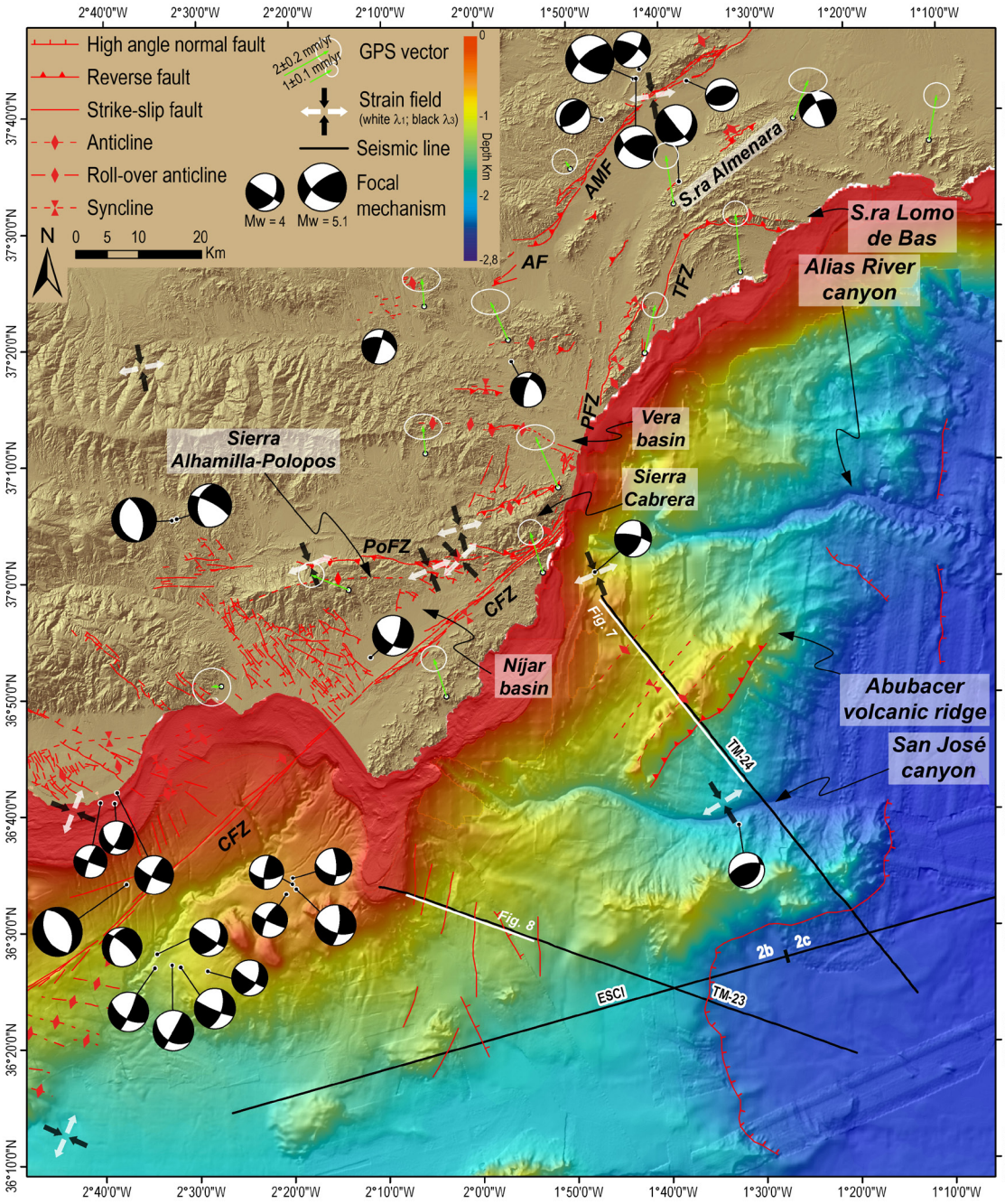

Fig. 3: Structural map where the main tectonic structures active during the Quaternary are shown: the Albox fault (AF), the Alhama de Murcia fault (AMF), the Carboneras fault zone (CFZ), the Palomares fault zone (PFZ) and the Polopos fault zone (PoFZ) (see Fig. 2 for location, Booth-Rea et al., 2004a, 2004c; Masana et al., 2004; Marín-Lechado et al., 2005; Masana et al., 2005; Gràcia et al., 2006; Pedrera et al., 2006, 2009a; Sanz de Galdeano et al., 2010; Booth-Rea et al., 2012a; Giaconia et al., 2012a, 2012b; Pedrera et al., 2012; Giaconia et al., 2013a). Furthermore, focal mechanisms, local stress tensor (both from focal mechanisms and fault slicken-line inversion data, Stich et al., 2003a; Fernández-Ibáñez et al., 2007; Giaconia et al., 2013a) and GPS geodetic data (Khazaradze et al., 2008; Echeverria et al., 2011) are shown. Topographic and bathymetric map (100 m grid) of the study area from digital grids released by SRTM-3, IEO bathymetry (Ballesteros et al., 2008; Muñoz et al., 2008), CSIC bathymetric dataset (Gràcia et al., 2012) and MEDIMAP multibeam compilation (MEDIMAP GROUP et al., 2008) at 90m grid-size.

we performed a correlation between the two new profiles and the published ESCI-Alb-2b and ESCI-2c profiles *(Booth-Rea et al., 2007)*, that ties the two lines (Fig. 3). To compare offshore and onshore tectonic regimes and timing, we correlated the seismo-stratigraphy units with the stratigraphic sequence of the Vera and Níjar Neogene basins as proposed by *Booth-Rea et al. (2007)*. Finally, we compare the interpretation of seismic images with two onshore geological cross-sections that cross the Sierra Cabrera anticlinorium parallel to the seismic lines.

10.2 Geological setting

The Algero–Balearic basin represents the back-arc region of the Gibraltar Arc, an arched orogenic belt formed during the Miocene oblique collision between the Alborán domain and the Iberian and Maghrebian passive margins during westward roll-back or delamination of the Tethyan slab in a general context of NW–SE Africa–Iberia convergence (Fig. 2 , *e.g. Lonergan and White, 1997; Martínez-Martínez and Azañón, 1997; Faccenna et al., 2004; Platt et al., 2006; Balanyá et al., 2007; Booth-Rea et al., 2007*). The Alborán domain has traditionally been defined as formed by three poly-metamorphic terrains, the Malaguide, Alpujarride and Nevado–Filabride complexes in descending structural order (Fig. 2, *Balanyá et al., 1997*). Recent work, however, shows that the Nevado–Filabride complex is formed by basement rocks of subducted South Iberian margin *(Booth-Rea et al., 2005; Platt et al., 2006; Booth-Rea et al., 2007)*. Thus, following this later interpretation, the Alborán domain may be formed by Alpujarride and Malaguide complexes rocks, which represent the remnants of an earlier orogenic wedge that underwent crustal stacking and HP metamorphism *(Goffé et al., 1989; Tubía and Gil Ibarguchi, 1991; Azañón et al., 1997; Booth-Rea et al., 2002)* associated to Eocene continental collision (Lonergan, 1993) dated about 50 Ma *(Platt et al., 2005)*. In contrast, the Nevado–Filabride complex underwent a later HP metamorphism during the Lower to middle Miocene representing the Paleozoic basement of the south Iberian passive margin (Fig. 2, *López Sánchez-Vizcaíno et al., 2001; Platt et al., 2004; Booth-Rea et al., 2005; Platt et al., 2005; Booth-Rea et al., 2007*).

The collision of the Alborán domain with the African and Iberian continental margins occurred during the early to late Miocene after the subduction of the ‘‘Flysch Trough’’ basement formed by oceanic or very thin continental crust (Fig. 2, *Durand-Delga et al., 2000; Luján et al., 2006*). Collision and tectonic inversion of both continental margins resulted in a fold-and-thrust belt formed mainly by the detached Mesozoic sedimentary covers of both margins that migrated progressively westwards *(Platt et al., 1995; Crespo-Blanc and Campos, 2001; Luján et al., 2003; Platt et al., 2003; Luján et al., 2006)*. During the middle to late Miocene, extension occurred in the hinterland of the collisional system along WSW-directed core-complex detachments that exhumed the

Nevado–Filabride complex *(García-Dueñas and Martínez-Martínez, 1988; Galindo-Zaldívar et al., 1989; Platt and Vissers, 1989; García-Dueñas et al., 1992; Martínez-Martínez and Azañón, 1997)*. Between 16 and 8 Ma the Algero–Balearic basin spread in an E–W direction *(Mauffret et al., 2004; Booth-Rea et al., 2007)* creating new oceanic-like crust *(Pesquer et al., 2008)*.

More recent NW–SE convergence between Africa and Eurasia produced the tectonic inversion of the Betic–Rif internal zones and structures of the Alborán and Algero–Balearic basins with the development of several large strike-slip and reverse faults since the late Miocene and active until the Plio–Quaternary or the present *(Bousquet, 1979; Weijermars et al., 1985; de Larouzière et al., 1988; Montenat and Ott d´Estevou, 1990; Bourgois et al., 1992; Mauffret et al., 1992; Morel and Meghraoui, 1996; Booth-Rea et al., 2004a; Giaconia et al., 2013a; Martínez-García et al., 2013)*. Tectonic inversion at the Algero–Balearic basin along the Algerian margin possibly started about 5-7 Ma and has continued during Plio–Quaternary times at N-verging thrusts that consist laterally of several fault strands *(Déverchère et al., 2005; Domzig et al., 2006; Mauffret, 2007; Kherroubi et al., 2009; Yelles et al., 2009; Strzerzynski et al., 2010)*.

10.3 Tectonics of the Palomares margin and the eastern Betics

The Palomares margin bounds the NW end of the Algero–Balearic basin with a NNE–SSW main orientation. The continental margin is formed by thinned continental crust intruded by arc volcanism that transits to oceanic crust to the east *(Comas et al., 1997; Booth-Rea et al., 2007)*. Volcanic rocks sampled in basement highs in the East Alborán and Algero–Balearic basins belong both to the tholeiitic and calc-alkaline series with Serravallian to Messinian ages ranging between 12.1–8.7 Ma and 10.1–6.1 Ma, respectively *(Comas et al., 1997; Turner et al., 1999; Duggen et al., 2004a, 2005)*. The arc-type origin of these rocks is confirmed by sampled volcanic highs in the East Alborán basin (Yusuf and Mansour) and the Alborán ridge that are formed by Light Rare Earth Elements (REE) depleted rocks of the tholeiitic series, characteristic of immature oceanic arcs (Fig. 2, *Duggen et al., 2004a; Gill et al., 2004*). Furthermore, in the thicker crustal domains near the ESCI-Alb lines LREE-enriched calc-alkaline and shoshonitic rocks have been sampled bearing a continental crust contamination of subduction-related magma *(Hoernle et al., 2003; Duggen et al., 2004a, 2005)*. The magmatic character of the East Alborán basin basement was interpreted in ESCI-Alb 2b line (Fig. 2) that shows a seismic structure that resembles the structure of oceanic crust formed at intermediate- to fast-spreading mid-ocean ridges, although thicker, as expected in a volcanic arc environment *(Booth-Rea et al., 2007)*. Further east, the eastern half of ESCI Alb 2c line (Fig. 2) shows a crustal thickness and structure similar to oceanic crust *(Booth-Rea et al., 2007)*. The sediment onlaping the basement indicate a minimum age of 10–12 Ma for the oceanic crust, and 8-10 Ma in the magmatic-arc

influenced region (Fig. 2, *Booth-Rea et al., 2007*). The westernmost segment of line ESCI-Alb 2b (Fig. 2) may have imaged magmatically-modified thin continental crust, where arc magmatism could be ≈6 Ma *(Duggen et al., 2004a)*,with magmatic accretion coeval to crustal extension *(Booth-Rea et al., 2007)*.

Onshore, the central and eastern Betics underwent middle to late Miocene WSW-directed extension that markedly attenuated the previous pile of staked metamorphic units of the Alborán domain *(García-Dueñas et al., 1992; Martínez-Martínez and Azañón, 1997; Booth-Rea et al., 2005, 2007)*. This extension was heterogeneous in its style developing metamorphic core complexes, like the Sierra Nevada elongated dome, and tilted-block domains separated by ENE–WSW extensional transfer faults like the Alpujarras dextral fault *(Martínez-Martínez et al., 2002; Martínez-Martínez, 2006; Martínez-Martínez et al., 2006)*.

The boundary between core complex domains onshore and extended region with magmatic additions in the East Alborán basin may correspond to extensional transfer faults like Carboneras sinistral fault along onshore segment of the Palomares margin *(Rutter et al., 2012)*. The Carboneras fault zone has been active at least since Serravallian until recent. The Miocene activity of this fault was essentially strike-slip *(Bousquet, 1979; Montenat and Ott d´Estevou, 1990; Stapel et al., 1996; Huibregtse et al., 1998; Jonk and Biermann, 2002; Rutter et al., 2012)*. In contrast, the Plio–Quaternary activity is locally transpressional, as indicated by folding-related unconformities in the latemost Messinian to Pliocene sediments in the Sierra Cabrera *(Bell et al., 1997; Reicherter and Reiss, 2001; Rutter et al., 2012)*. The adjacent region onshore and the Palomares margin underwent late Miocene to Quaternary inversion with thrusting, and strike-slip faulting with both dextral and sinistral kinematics *(Montenat and Ott d´Estevou, 1990; Comas et al., 1999; Booth-Rea et al., 2004a)*. The main sinistral strike-slip faults in the eastern Betics are from north to south: the Alhama de Murcia, Terreros, Palomares, and Carboneras fault zones (Fig. 3, *Montenat and Ott d´Estevou, 1990; Booth-Rea et al., 2004a; Masana et al., 2004; Stich et al., 2006; Moreno et al., 2008*). The Palomares fault zone was pure sinistral during Tortonian–Messinian times, and lengthened and widened eastwards evolving into a transtensional oblique-slip regime during the Plio–Quaternary *(Booth-Rea et al., 2004a)*. Latemost Tortonian (8-7.24 Ma) progressive unconformities mark the initial growth of the main folds of Sierra Alhamilla–Polopos and Cabrera anticlinoria (Fig. 3). Dextral transpressive and reverse faults bounding Sierra Alhamilla–Polopos and Cabrera anticlinoria have a late Miocene–Quaternary age (Fig. 3, *Giaconia et al., 2012b, 2012a*). Field data and geomorphic analysis indicate that the dextral transpressive Polopos fault zone bounding the northern Alhamilla mountain front and both the northern and southern Polopos ones (Fig. 3) started in latemost Tortonian and remained active until late Pleistocene *(Giaconia et al., 2012a, 2013a)*. Similar geomorphic analysis indicates recent reverse faults bounding the northern and southern mountain fronts of the Sierra

Cabrera anticlinorium (Fig. 3, *Giaconia et al., 2012b, 2013a*).

10.4 Methods

10.4.1 Data acquisition and processing

During the TOPOMED-GASSIS cruise, multichannel seismic (MCS) profiles, swath-bathymetry and parametric echosounder profiles were acquired with R/V "Sarmiento de Gamboa" in September-October 2011 *(Gràcia et al., 2011)*. The MCS data were acquired with a 50.15 l (3060 c.i.) air-gun source and a 5100 m-long active section Sentinel Sercel SEAL streamer with 408 active sections (12.5 m channel interval). The source array was composed by 8 G-GUN-II guns deployed at 7.5 m depth, in a single cluster. MCS data were recorded at 2 ms sample rate and 14 s two-way travel time (TWTT) record length. Air-gun shots were fired every 50 m distance providing a nominal maximum 56 common-mid-point (CMP) fold. We processed lines TM23 and TM24 using GLOBE Claritas software. Processing steps include shot and streamer geometry correction and 12.5 meter binning, velocity analysis every 100 CMP (625 m), spherical divergence, predictive deconvolution, normal-move-out correction, parabolic Radon filter to attenuate multiple energy, stretching mute, inner mute to further attenuate multiple energy in near offsets, and stack. Post stack cosmetics used frequency-wavenumber (F/K) to attenuate remaining coherent noise and finite differences time migration using a smooth velocity model. Finally, the lines were depth converted using velocities extracted from a model of a wide-angle seismic velocity profile coincident with ESCI line *(Leuchters et al., 2011)*. This depth conversion was done to balance the cross-section interpretation of the seismic lines. Swath-bathymetry was acquired with the hull mounted system ATLAS Hydrosweep DS echosounder, with a frequency between 14.5 to 16 kHz. The data were processed using CARIS software and integrated with existing data to produce digital terrain models of 50 m grid size. High-resolution narrow beam parametric sub-bottom profiler data were acquired using the ATLAS Parasound P.35. This system uses a primary frequency of 18-20 kHz, and a secondary frequency of 1.5 to 4 kHz. During the TOPOMED-GASSIS cruise a continuous wave single pulse was used, with frequencies of 4 kHz. The pulse length was 0.50 ms and pulse interval of 300 ms, with a maximum vertical resolution of 0.6 ms. These data show detailed stratigraphic information of the uppermost few tens of meters of sub-seafloor structure.

10.4.2 Balanced cross section

The structural analysis to calculate the detachment depth of the fault propagation fold recognized in the TM24 line was carried out applying the excess-area graphical technique proposed by *Epard and Groshong (1993)*. This method predicts the detachment depth of a fault propagation fold plotting a set of geological horizons in

an excess-area vs. depth diagram. The depth coordinates of this diagram are obtained by an arbitrary horizontal reference. Whilst, the excess-area coordinates are obtained calculating the area comprised between the folded geological horizon and the horizontal line that joins points of the geological horizons considered as undeformed/unfolded. This set of coordinates define a straight line with a slope that is the fault displacement meanwhile its intersection with the depth axis is the depth of the detachment with respect to the arbitrary horizontal reference.

10.5 Results

The main result obtained from the MCS lines and parametric sub-bottom profiles is the characterization of the shortening and transpressional structures of the Palomares margin. These structures strike NNE–SSW to NE–SW and are congruent with the present NW–SE shortening stress field indicated by in situ tensor strain data obtained from boreholes in the region (Fig. 4). Furthermore, these shortening structures are consistent with the timing of eastern Betic structures between latemost Tortonian–Messinian to the Quaternary. Line TM24 shows a fault propagation fold affecting Neogene volcanic basement of the Abubacer ridge, in response to a SE-ward displacing thrust, and a major syncline at the back of the structure (Fig. 5). Furthermore, line TM24 and 23 shows that the crust thins progressively eastwards, to find oceanic crust of the Algero–Balearic basin without a major tectonic boundary marking the transition (Fig. 5). Finally, line TM23 shows that major Palomares-type strike-slip faults extend southwards of the Sierra Cabrera anticlinorium across the coast line (Fig. 5).

10.5.1 Seismic stratigraphy of the margin

We used the seimostratigraphy defined in ESCI-Alb seismic lines, which tie lines TM23 TM24, and calibrated the sequence using the stratigraphy of Vera and Níjar basins proposed by *Booth-Rea et al. (2007)* (Fig. 6). This correlation defined lithoseismic units and their age. The comparison between offshore and onshore basins shed light on the tectonic regime and timing of deformation.

The sedimentary cover in profiles TM23 and TM24 thickens from slightly less than 1 s TWTT (≈1 km) in the western part of the lines to 1.5-2 s TWTT (≈1.5-2.0 km) in the central and eastern part of the lines (Fig. 6). We use previously defined lithoseismic units (I to IV) in the East Alborán basin formed by late Miocene to Quaternary sediments that onlap Neogene (Serravallian–Tortonian) volcanic basement *(Comas et al., 1992; Booth-Rea et al., 2007)*.

Unit I: The uppermost Pliocene to Quaternary unit has three sub-units (Ia, Ib and Ic) *(Alvarez-Marrón, 1999)*. In lines TM23 and 24, Unit Ia+b has a continuous high-frequency reflectivity and a maximum thickness of ~0.3 s TWTT (≈230m assuming a 1.55 km/s velocity) with good lateral continuity, except at basement highs (Figs. 5

and 6). The base of subunit Ia+b appears erosive in the western part of line TM24, infilling channels, meanwhile to the east it evolves to a paraconformity defined mostly by one reflection. Subunit Ia+b is probably equivalent to continental late Pliocene and Quaternary conglomerates onshore in the Níjar and Vera basin *(Booth-Rea et al., 2007)*.

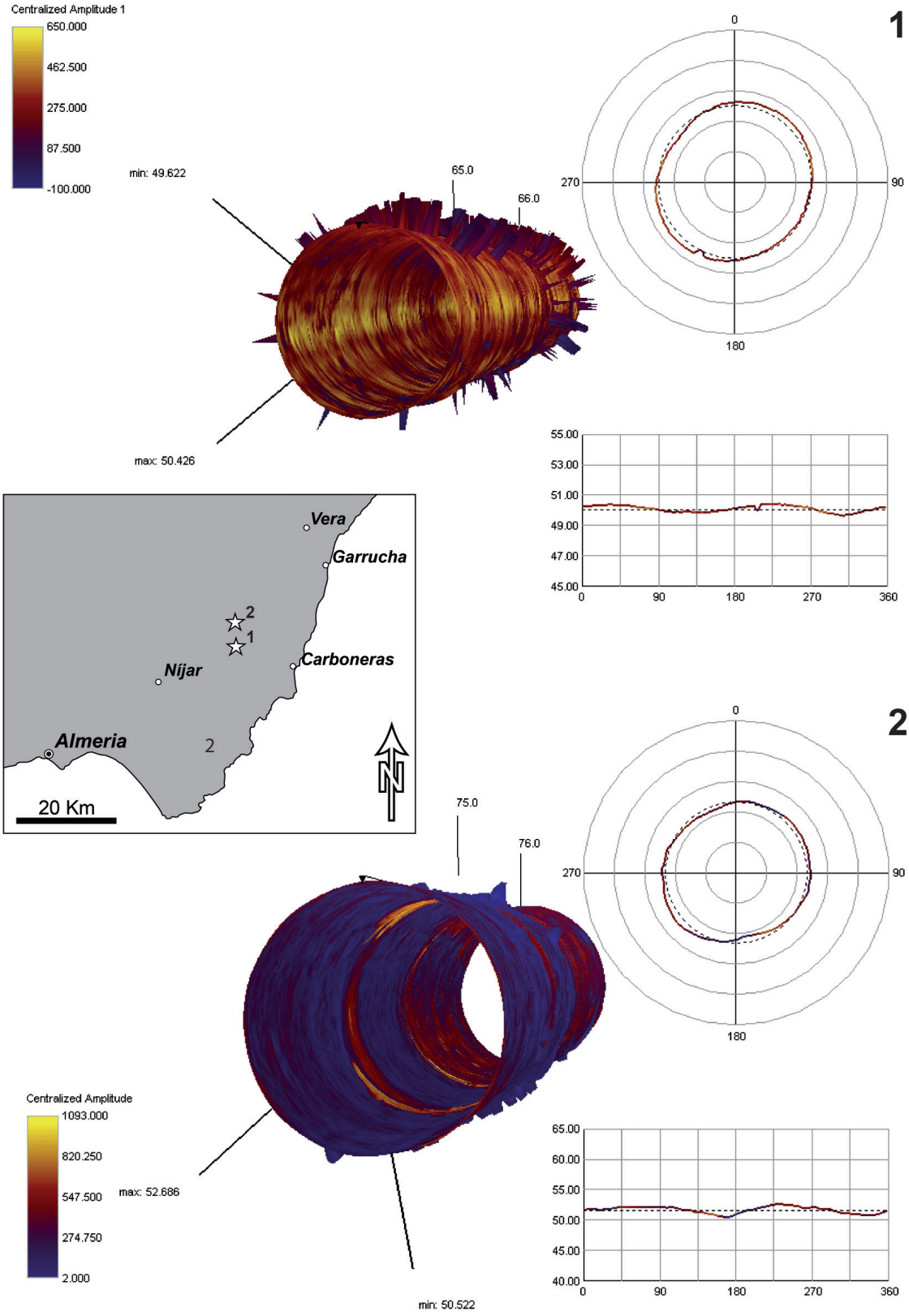

Fig. 4: Ovalization analysis from boreholes indicating the active local stress tensor and its maximum shortening axis. 1: Borehole at 64 m depth showing a maximum shortening axis oriented about N130ºE. 2: Borehole at 74 m depth showing a maximum shortening axis oriented about N150ºE. See inset for their location.

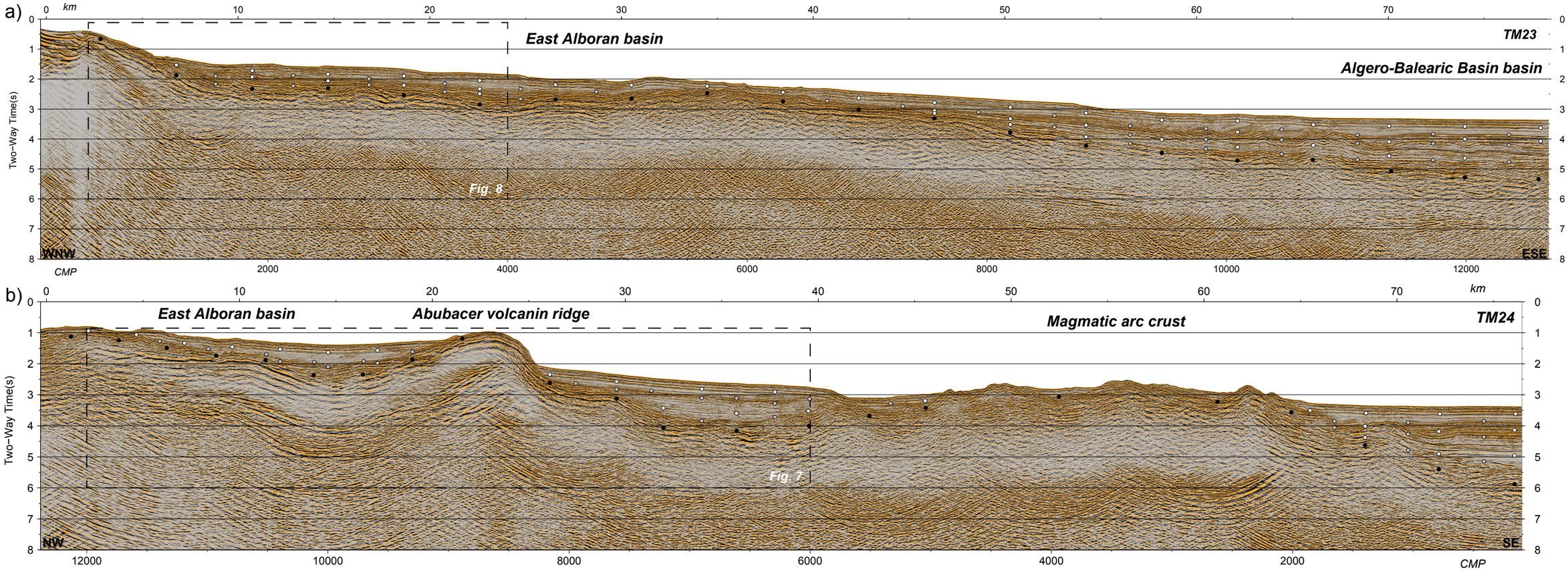

Fig. 5: Time migration of MCS profiles TM24 (a) and TM23 (b), with location of the main features (see Fig. 2 profile location). Rectangles correspond to the zooms of the seismic profiles presented in Figs 7 and Fig. 8, respectively.

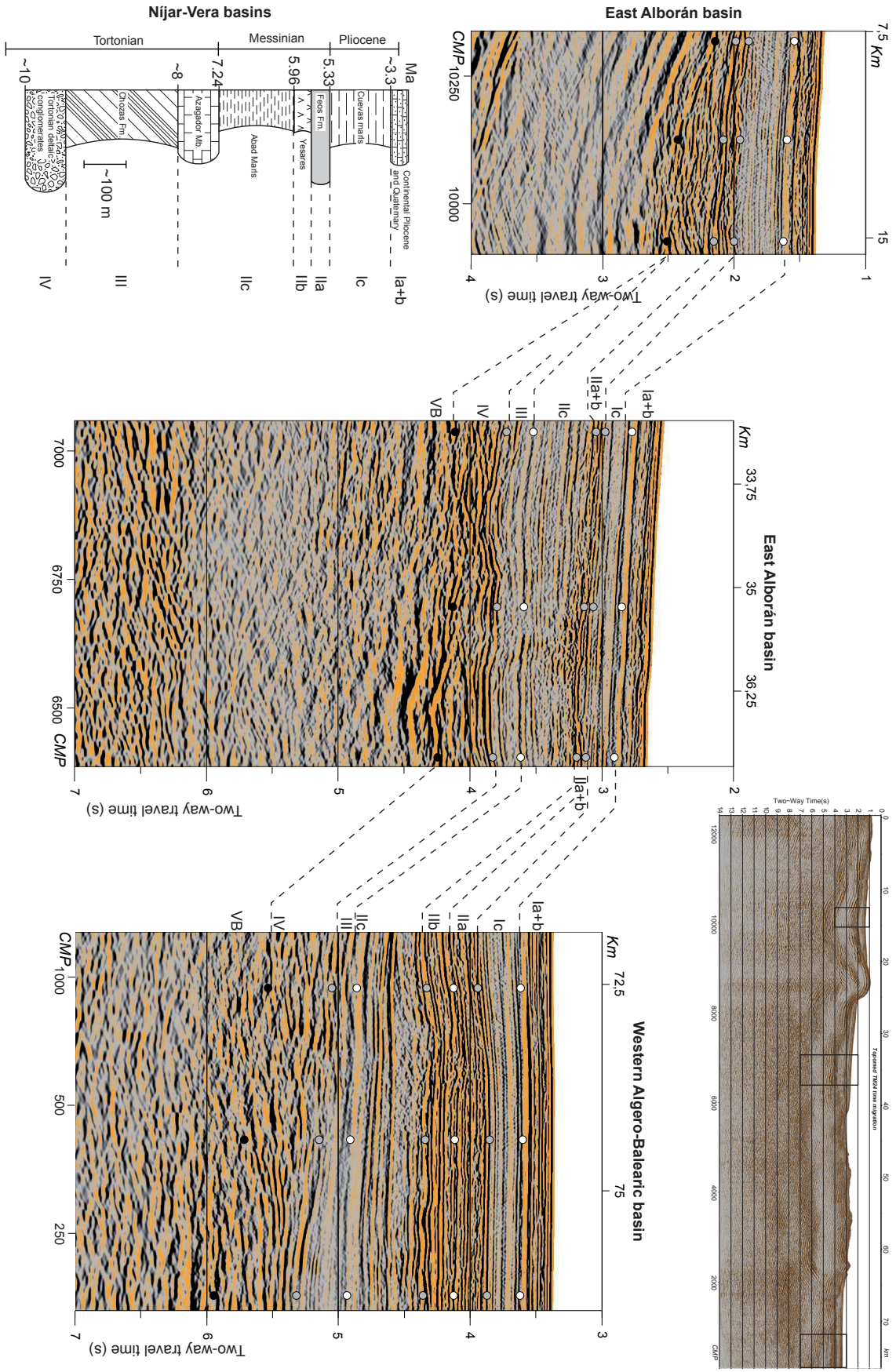

Fig. 6: Synthetic stratigraphic column of the late Neogene sediments of the Níjar–Vera basins that were correlated with the lithoseismic units differentiated in seismic profile TM24, following the seismo-stratigraphic correlation proposed by Booth-Rea et al. (2007). Unit I Plio–Quaternary: Ia +b, Quaternary–late Pliocene; Ic, early Pliocene; Unit II: Messinian; IIa, late Messinian upper evaporite; IIb, Messinian lower evaporite; IIc, Messinian pre-evaporitic; Unit III: Tortonian; Unit IV: Serravallian?–Tortonian unit; Unit VB: volcanic basement.

Subunit Ic reaches a maximum thickness of ~0.4 s TWTT (≈400 m assuming a 2.05 km/s velocity) and is characterized mostly by low-reflectivity facies typically bounded by two more reflective lithoseismic units (Figs. 5 and 6). It onlaps the unit below at the west and rests paraconformable at the east. This unit onlaps the Messinian erosional unconformity infilling possible fluvial-erosion channel in the western part of line TM24 (Figs. 5 and 6). Subunit Ic is probably equivalent to Pliocene Cuevas marls, deposited onshore at the Níjar and Vera basins between 5.3 and 3.2 Ma *(Aguirre, 1998; Booth-Rea et al., 2007)*.

Unit II: This unit has three sub-units (IIa, IIb and IIc) deposited between latemost Tortonian and Messinian *(Booth-Rea et al., 2007)*. Subunit IIa has been identified along the entire profile TM24 infilling synformal depressions with a maximum thickness of ~0.25 TWTT (≈300 m assuming a 2.4 km/s velocity). It shows high-amplitude reflections that onlap the Messinian erosive unconformity (Figs. 5 and 6). This subunit is probably equivalent to the Messinian Feos formation of the Níjar and Vera basins deposited during the Messinian salinity crisis between 5.6 and 5.3 Ma *(Krijgsman et al., 2001; Fortuin and Krijgsman, 2003; Booth-Rea et al., 2007)*. Subunit IIb occurs only locally in the eastern part of line TM24 where it is characterized mostly by high-amplitude continuous reflections overlying a high-amplitude reflection with negative polarity that indicates a decrease in seismic velocity in the underlying sedimentary unit (Figs. 5 and 6). This subunit is formed by evaporites deposited during the Messinian salinity crisis, bounded at the top by the M reflector, which is a local paraconformity above the evaporites and an erosive unconformity onlapped by subunits IIa or Ic westwards in most of the Alborán basin *(Comas et al., 1999)*. Subunit IIb reaches a maximum thickness of ~0.25 TWWT (≈300 m assuming a 2.4 km/s velocity) and is equivalent to the Messinian Yesares formation onshore (5.96-5-6 Ma, *Krijgsman et al., 2001*) in the Níjar and Vera basins *(Booth-Rea et al., 2007)*. Subunit IIc is characterized by discontinuous low-amplitude reflections in the eastern and central parts of line TM24 showing a decrease in seismic reflectivity compared to the overlying subunit IIb (Figs. 5 and 6). Toward the west in line TM24, subunit IIb shows different seismic facies characterized by higher reflectivity, probably related to a proximity to the sediment source and an increase in siliciclastic content. Furthermore, in this region subunit IIc appears onlapping the volcanic basement and infilling a syncline, showing discontinuous high-amplitude reflections that indicate its syn-tectonic deposit during fault propagation folding of the Neogene Abubacer volcanic ridge (Figs. 5 and 6). Reflections in subunit IIc are mostly parallel to those of the overlying unit, suggesting a paraconformity between both units in most of line TM24, except at the western end of line TM24 where continental facies of subunit IIb cut into or downlap subunit IIc. Subunit IIc reaches a maximum thickness of ~0.5 s TWTT (≈700 m assuming a 2.9 km/s velocity) and is equivalent to the Turre formation that includes latemost Tortonian Azagador member temperate carbonates (8-7.4 Ma, *Martín et al., 2003*) and the Messinian Abad marls in the Níjar and Vera basins, deposited before the Messinian

salinity crisis (~7.4 to 5.96 Ma, *Krijgsman et al., 2001*).

Unit III: This unit is characterized by low-amplitude facies with maximum thickness of ~0.25 s TWWT (≈350m assuming a 2.9 km/s velocity) in the central part of line TM24 (Figs. 5 and 6). It is absent in the western part of the lines, and is probably equivalent to Tortonian Chozas formation marls and silts in the Níjar and Vera basins (~8.5-7.4 Ma, *Rouchy et al., 1998; Rodríguez Fernández et al., 1999; Booth-Rea et al., 2007*).

Unit IV: It is characterized by discontinuous high-amplitude reflections and onlaps the volcanic basement along most of line TM24, except in the west where it is missing (e.g. TM23 seismic line, Figs. 5 and 6). The unit reaches a maximum thickness of ~0.5 s TWTT (≈700 m assuming a 2.9 km/s velocity) and probably is equivalent to Tortonian volcano-sedimentary breccias (Brèche rouge) or early Tortonian calcarenites or calcirudites that crop out onshore in Cabo de Gata, south of Níjar basin *(Montenat and Ott d´Estevou, 1990; Martín et al., 2003)*.

10.5.2 Shallow crustal structures and latemost Tortonian–Quaternary activity

Line TM24 shows a fault propagation fold affecting the volcanic basement that forms the Abubacer ridge (Fig. 7), where Neogene granodiorites have been dredged *(Duggen et al., 2008)*. The fault propagation fold involves mainly the volcanic basement, marked by its bright folded top and internal structure imaged as low-amplitude continuous reflections that could be related to volcanic flows. The main thrust, referred to as Abubacer Fault has a SE-wards sense of displacement, folding and uplifting the northwestern hanging-wall fault block. Minor thrusts affect the Abubacer anticline, including a NW-displacing back-thrust to the west of it (Fig. 7). The reverse faulting, and associated folding, produces approximately 700 m of vertical displacement of the acoustic basement (Fig. 7).

Westwards, between the Abubacer anticline and the coastline, a syncline is filled by possibly latemost Tortonian to Messinian syn-tectonic sediments corresponding to the subunit IIc (Figs. 6 and 7). In the footwall of the Abubacer Fault another syncline occurs filled by Messinian syn-tectonic sediments (Unit II, Figs. 6 and 7). Another minor SE-displacing thrust and associated fault propagation fold deforms the northwestern limb of this major syncline displacing the Neogene volcanic basement onto Unit IV (Fig. 7, *Booth-Rea et al., 2007*).

Line TM23 shows a positive strike-slip flower structure affecting the volcanic basement to the Quaternary sediments (Fig. 8). The southeastern fault block is uplifted and folded defining a transpressive strike-slip structure affecting a Plio–Quaternary depocenter (Fig. 8). Plio–Quaternary sediments appear syn-tectonic because they are folded and show growth geometry controlled by the transpressive structure.

Along line TM24 the parametric sub-bottom profile images anticlines and synclines deforming Quaternary sediments. Anticlines occur both near the coast in the

northwestern part and at Abubacer ridge, on either side of the main syncline (Fig. 9). Bathymetric data indicate a N40ºE strike for the anticlines and synclines of the Abubacer ridge and Plio–Quaternary sediments. The vertical displacement of the basement by reverse faulting and associated folding forms about 700 m relief at the seafloor (Fig. 9). The integration of MCS reflection lines, parametric sub-bottom profiles and bathymetric data shows a good congruence between structural and morphological features. The main submarine canyons dissecting the Palomares margin, the San José and Alias river are deviated by the fold and thrust system, trending slightly

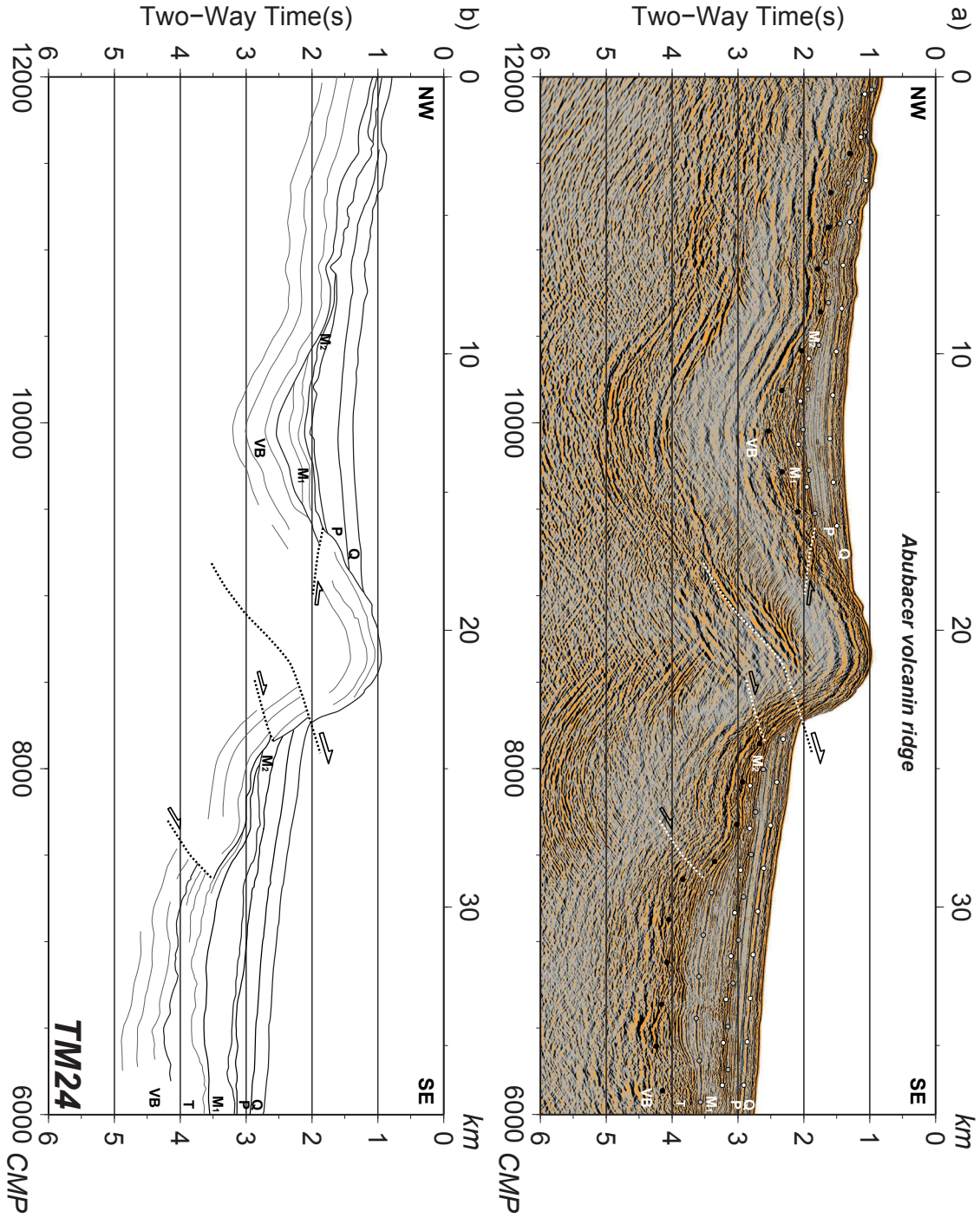

Fig. 7: Blow-up of the time migrated TM24 seismic profile (a) and line-drawing interpretation (b). The main features and lithoseismic units are located: Q, Quaternary–late Pliocene unit; P, Pliocene unit; M1 Messinian post-evaporitic unit; M2 Messinian pre-evaporitic unit, T, Tortonian unit; VB, volcanic basement. Notice the thrusts and associated fault propagation fold affecting the volcanic basement.

oblique to the synclines and cutting transverse to the Abubacer anticline (Fig. 3).

Parametric sub-bottom images on line TM23 together with the bathymetry show subvertical faults with both reverse and normal displacement affecting Quaternary sediments and the seafloor (Fig. 10). These faults strike N10-20ºE and may represent the offshore extension of the Palomares fault system south of the Sierra Cabrera anticlinorium (Fig. 3).

10.5.3 Depth conversion: Geometry of the Abubacer Fault and related structures

The depth conversion of seismic line TM24 (Fig. 11a) was carried out using velocities obtained from wide-angle velocity modeling of a profile coincident with ESCI-Alb 2

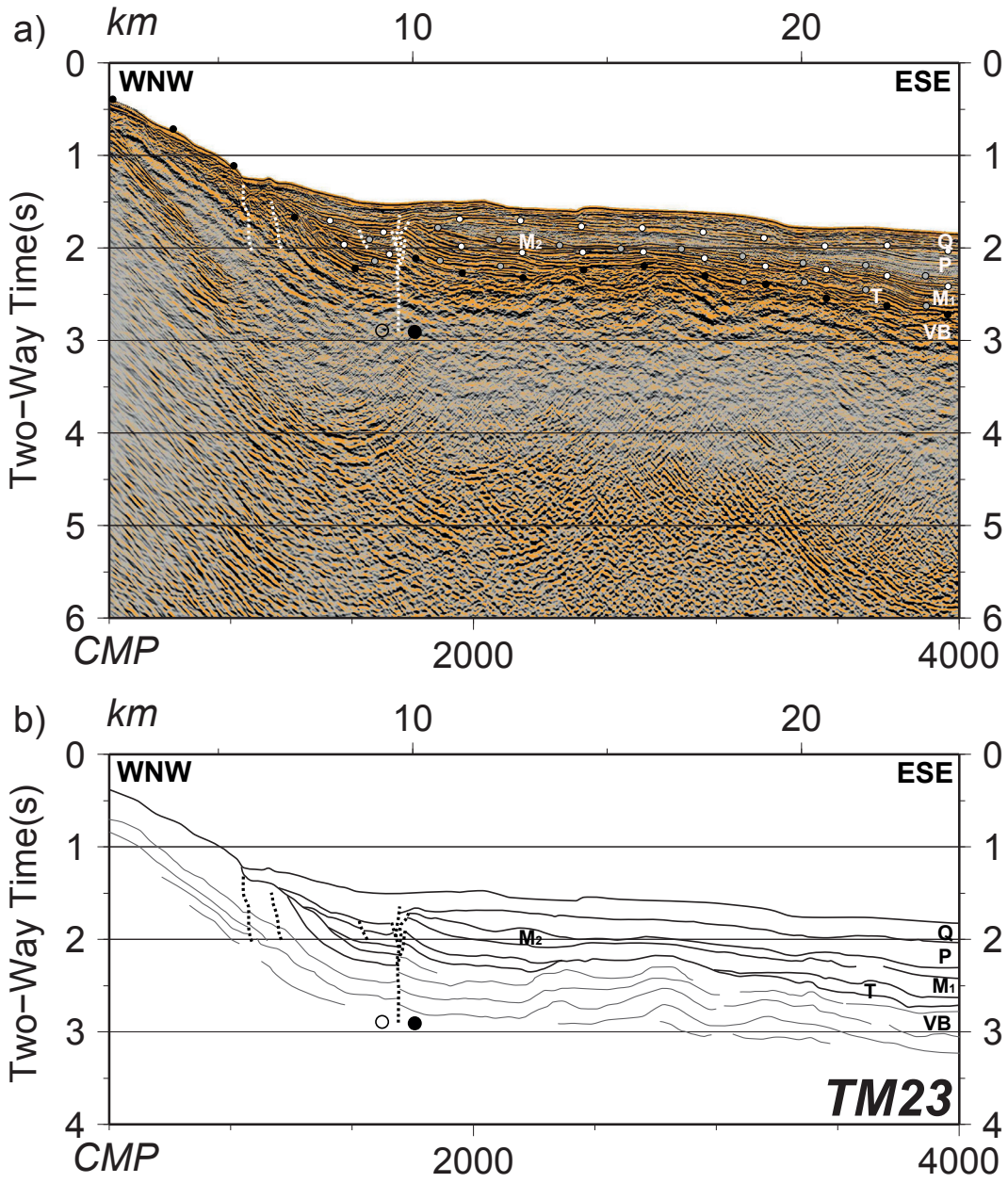

Fig. 8: Blow-up of the time migrated profile TM23 (a) and line-drawing interpretation (b). The main features and lithoseismic units are located: Q, Quaternary–late Pliocene unit; P, Pliocene unit; M1 Messinian post-evaporitic unit; M2 Messinian pre-evaporitic unit, T, Tortonian unit; VB, volcanic basement. Notice the positive strike-slip flower structure affecting the volcanic basement up to the Quaternary throughout the Tortonian–Messinian and Pliocene sediments.

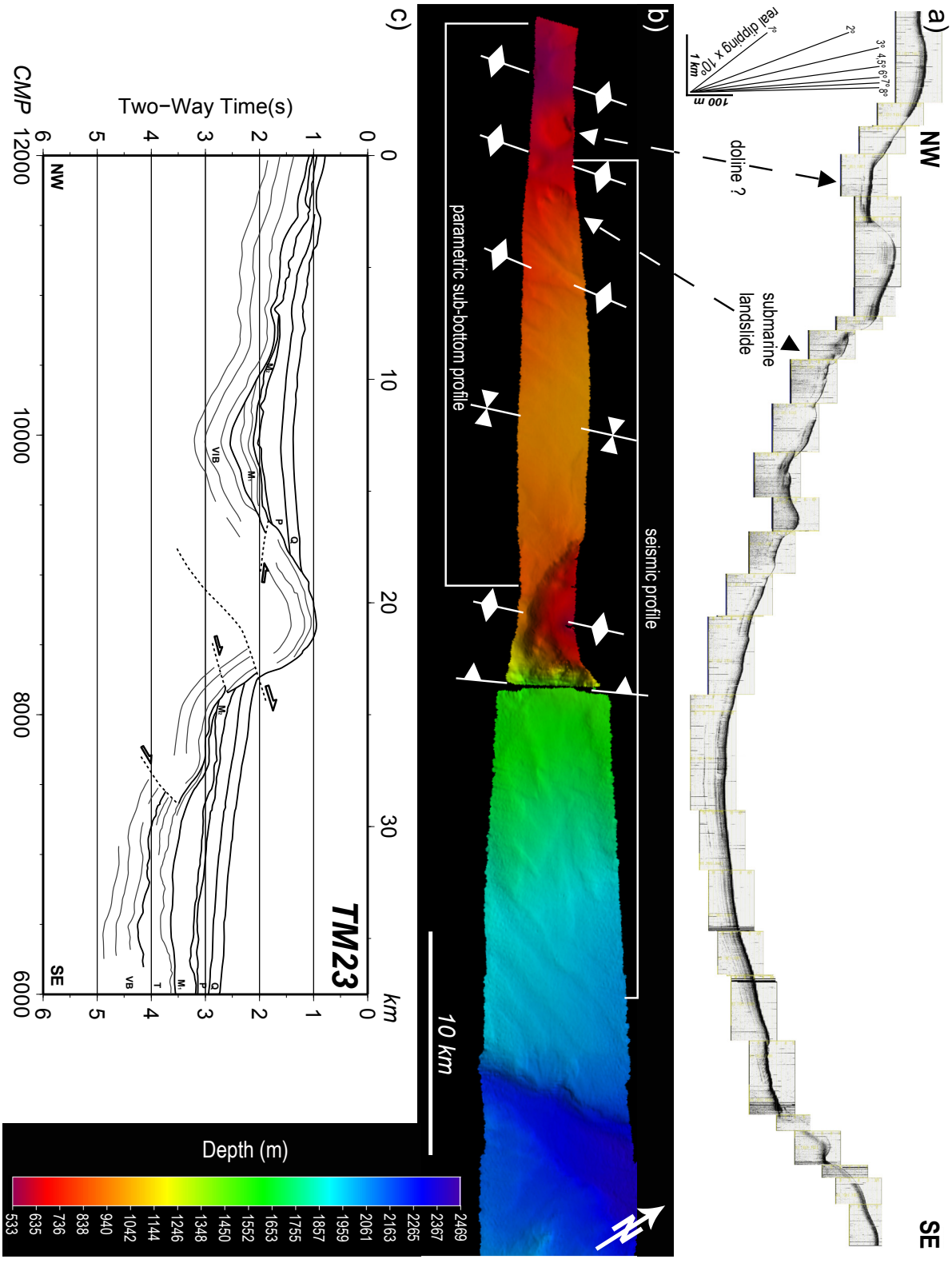

Fig. 9: a) Parametric sub-bottom profile along seismic line TM24 that shows anticlines and synclines affecting the Quaternary sediments. b) Bathymetric data indicate a N40 ºE strike for the anticlines and synclines detected both in the basement and in the Plio–Quaternary sedimentary cover and a vertical displacement of the acoustic basement of about 700 m produced by the reverse faulting, and associated folding. Finally, the line drawing of seismic line TM24 blow-up is shown (c) in order to integrate the parametric sub-bottom profile and the bathymetric data with the deep seismic reflection data.

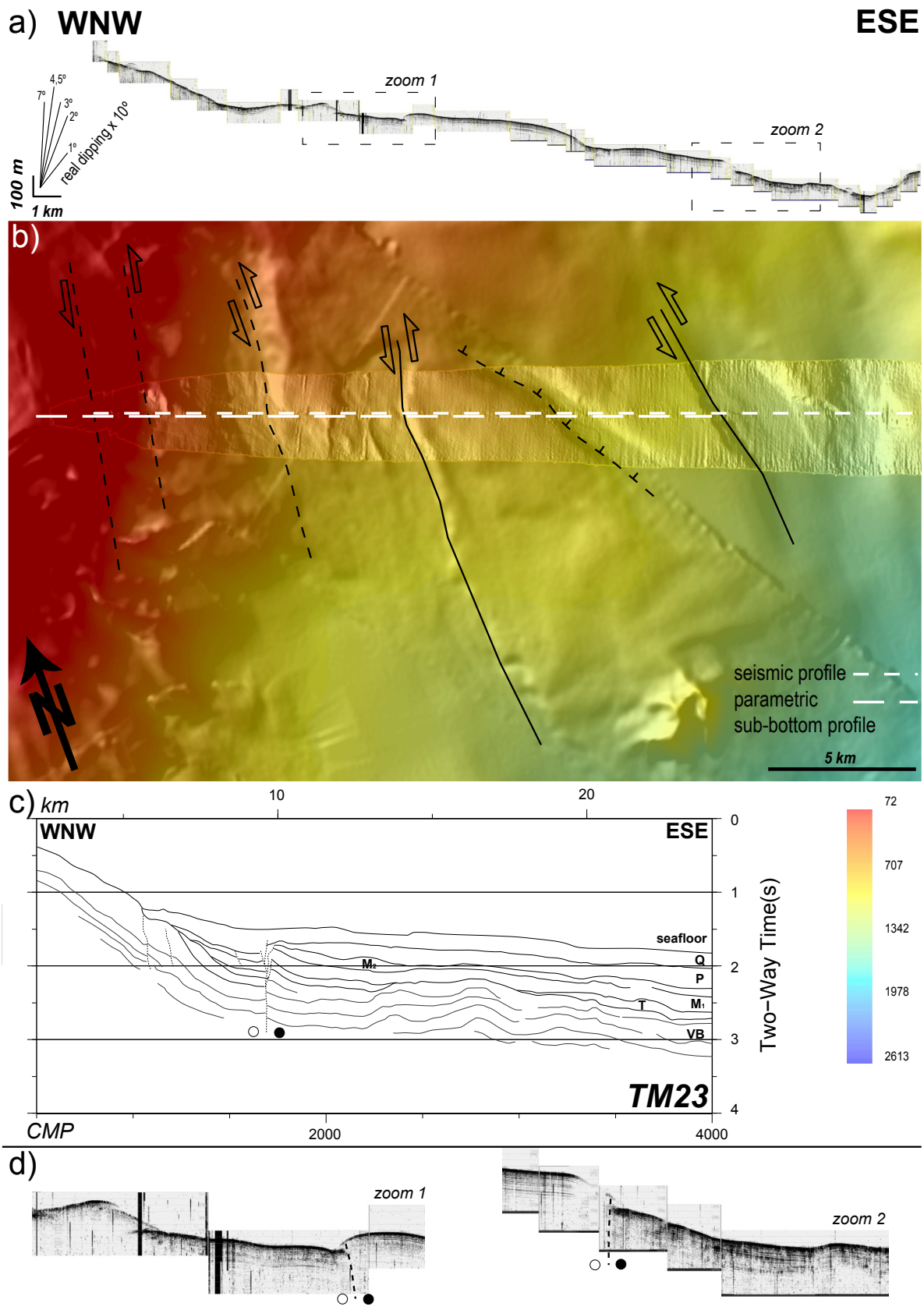

Fig. 10: a) Parametric sub-bottom profile along seismic line TM23 that shows subvertical faults with both reverse and normal displacement affecting the Quaternary sediments and the seafloor. b) Bathymetric data indicate a N10-20°E strike for these faults. c) The line drawing of seismic line TM23 blow-up is shown in order to integrate the parametric sub-bottom profile and the bathymetric data with the deep seismic reflection data. d) Blow-up of the faults imaged by the parametric sub-bottom profile.

line that crosses lines TM23 and TM24 *(Leuchters et al., 2011)*. The depth conversion provides a more realistic geometry and dimensions (both depth and fault plane/strata dipping angles) of the main fault-propagation fold. Globally the main thrust and the minor ones are relatively low angle, dipping 20-40º and displacing the basement up to 1 km (Fig. 11a).

Furthermore, the depth conversion allows constructing a balanced cross-section of the fault propagation fold (Fig. 11b). We applied the excess-area graphical technique proposed by *Epard and Groshong (1993)* to obtain the depth of the main detachment (see section 4). Using the balanced cross-section we have plotted a set of six geological horizons of the volcanic basement affected by the fault propagation fold in an excess-area vs. depth diagram (Fig. 12). The six points define in the diagram a linear equation ($y = a + b \cdot x$) that indicates a fault displacement of the entire fault system (except the southeastern thrust) of about 1.5 km and a detachment depth of about 10 km.

To constrain the rheological behavior of the rocks in the margin and obtain a depth

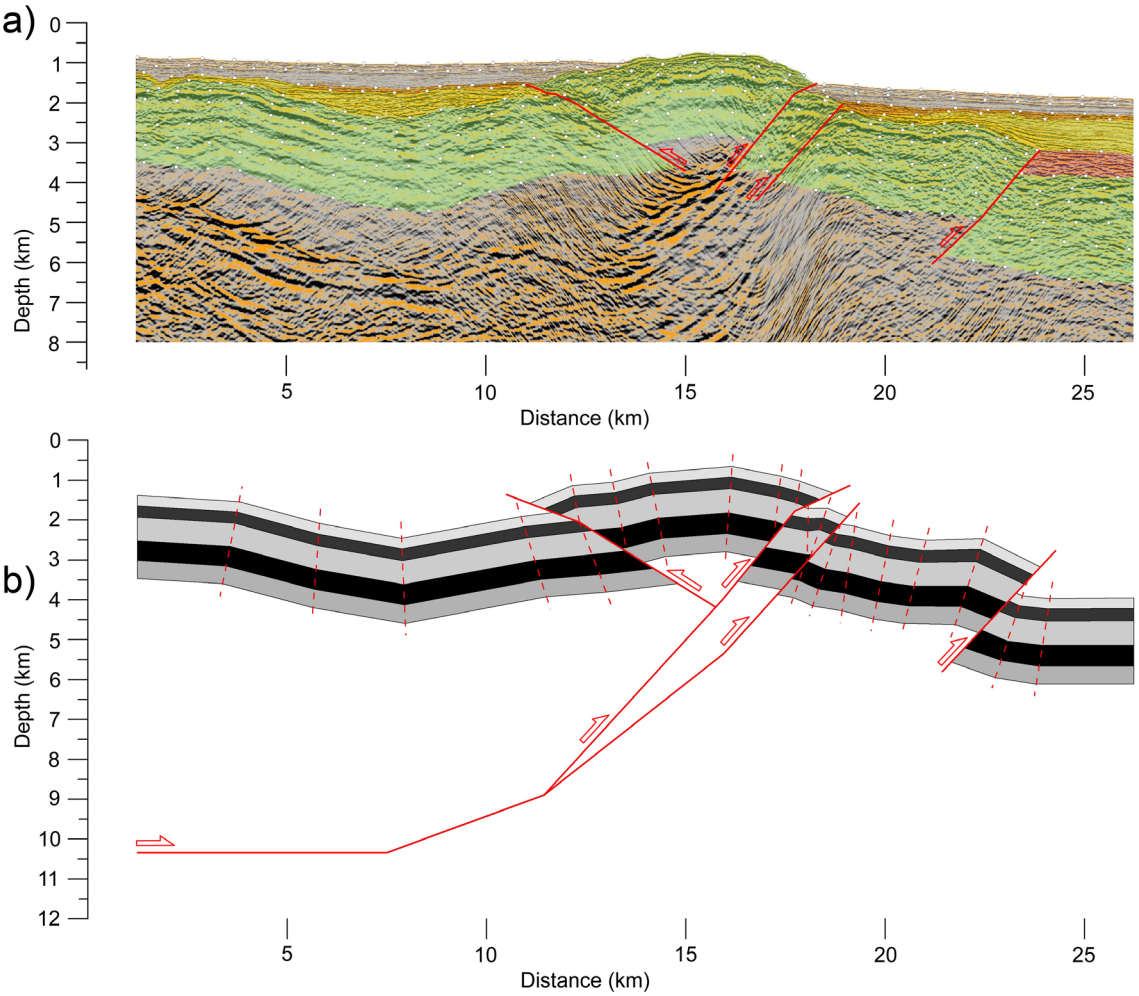

Fig. 11: a) Depth conversion of the blow-up of MCS profile TM-24 with the main lithoseismic units. In light gray the Quaternary–late Pliocene unit; in dark gray the Pliocene unit; in orange the Messinian post-evaporitic unit; in yellow the Messinian pre-evaporitic unit, in red the Tortonian unit; in green the volcanic basement. b) Balanced cross-section from MCS profile TM-24 for the pre-kinematic volcanic basement. The depth of the basal detachment of the fault propagation fold was calculated with the excess-area graphical technique proposed by Epard and Groshong (1993).

range for the brittle-ductile transition we calculated the geotherm and several strength envelopes using heat flow data available in the region *(Polyak et al., 1996; Soto et al., 2008)*. To determine the frictional deviatoric stress we used the equation given by the modified Anderson theory:

$$\sigma zz-\sigma xx = \alpha \rho g z(1-\lambda) \quad (1)$$

Where α is a numerical parameter depending on the type of faulting with values of 3.0, 1.2, and 0.75 for thrust, strike-slip and normal faults, respectively; ρ, g, z and λ are average density, gravity, depth and pore fluid factor *(Ranalli, 1995)*. We used a α value of 3.0 according to the thrust faulting regime at the margin. To evaluate qualitatively the contribution of pore fluid pressure to frictional sliding, we used both hydrostatical and elevated pore pressures (λ=0.4 and 0.8, respectively). For ductile flow we used the rheological model of dislocation creep proposed by *Ranalli (1995)*:

$$(\sigma zz-\sigma xx = (\varepsilon/A)^{1/n}\exp(E/nRT) \quad (2)$$

Where ε is the strain rate, A, n and *E* are Dorn parameter, stress exponent and creep activation energy, respectively. We used a common strain rate (2.5 *10-14) and several creep parameter sets (A, n, E) to account for a broad range of rock resistances. We calculated strength envelopes for weak rheologies like wet granite and granite, and stronger materials like plagioclase (An75) and quartz diorite, using creep parameters

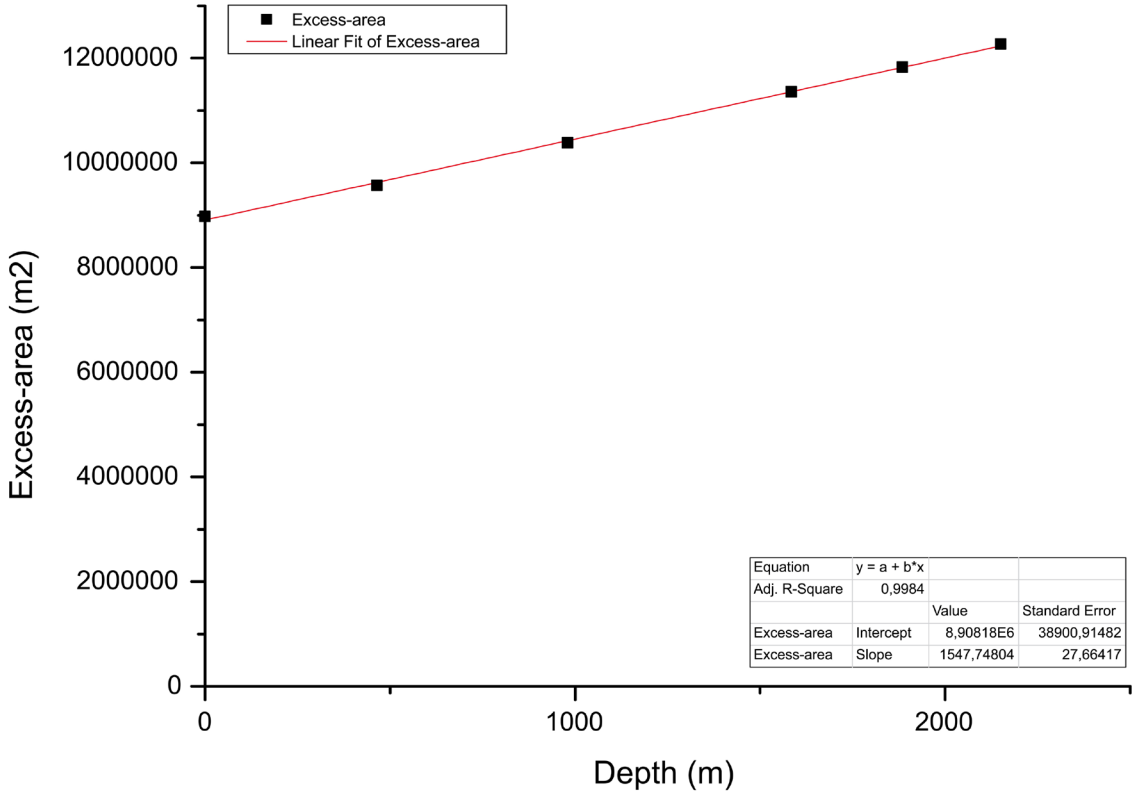

Fig. 12: Excess-area vs. depth diagram plotting six geological horizons from the balanced cross-section of the pre-kinematic volcanic basement of seismic profile TM24 (Fig. 11). The geological horizons define in the diagram a linear equation (y = a + b•x) that indicates a fault displacement of the entire fault system (except the southeastern thrust) of about 1.5 km (b = the line slope, with an error of ± 27.66 m) and a depth to the detachment of about 10 km (a = depth intercept of the line, with an error of ± 128.04 m).

proposed by *Ranalli (1995)* (Fig. 13). Using a granodiorite mineralogical composition (with an amount greater than 20% of quartz by volume where at least the 65% of feldspar is plagioclase, in the QAPF diagram) for the volcanic basement of the margin (like rocks sampled in the Abubacer ridge by *Duggen et al., 2008*) we can adopt a strength envelop intermediate between those of a granite and a plagioclase (An75). The strength envelope indicates that currently the brittle-ductile transition is at a depth range of 6.5-12.5 km and a temperature range of 225-375ºC (Fig. 13).

10.6 Discussion

10.6.1 Synthesis of the structures observed at the Palomares Margin

The MCS lines show the lack of a typical fault-block structure across the continent to ocean transition of the East Alborán basin to the Algero–Balearic basin at the Palomares margin. The data indicate that the crustal transition is formed by thinned continental crust that has been intruded pervasively by magma during the middle–late Miocene

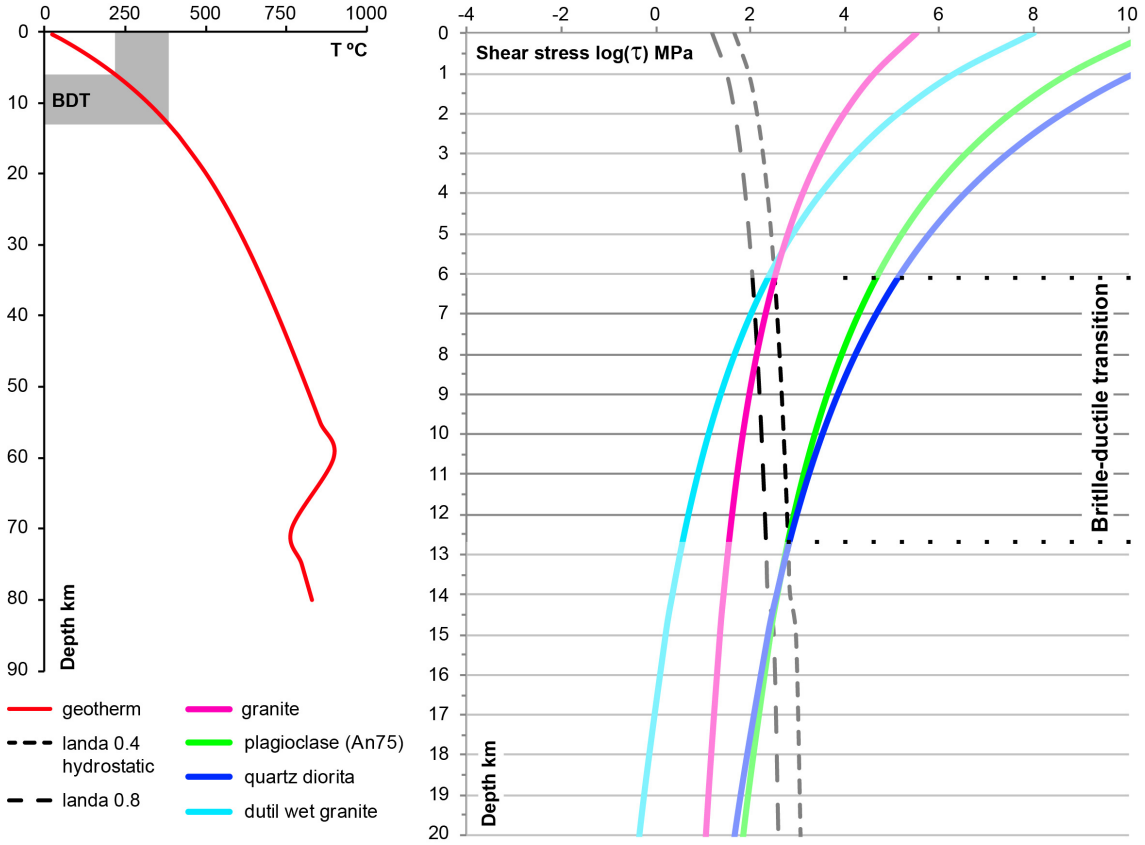

Fig. 13: Strength envelopes for a granodiorite mineralogical composition (the intermediate strength envelop between those of a granite and a plagioclase (An75)) for the volcanic basement of the Palomares margin (rocks sampled in the Abubacer ridge, Duggen et al., 2008) indicates a brittle-ductile transition at a depth between 6.5 km and 12.5 km and at a temperature between 225-375ºC. The frictional deviatoric stress was obtained using the equation given by the modified Anderson theory (σzz-σxx =αρgz(1-λ)) (Ranalli, 1995) with both hydrostatical and elevated pore pressures (λ=0.4 and 0.8, respectively). The ductile rheological behavior of the rocks was obtained using the rheological model of dislocation creep and creep parameters proposed by (Ranalli, 1995). The geotherm was obtained using heat flow data by Polyak et al.(1996) and Soto et al. (2008).

extension affecting the region as seen in the Cabo de Gata region onshore *(e.g. Turner et al., 1999; Duggen et al., 2008)*. The integrated interpretation of the MCS images, parametric sub-bottom profiles, and bathymetric data, indicates that the Palomares margin was affected by subsequent transpressive deformation that has produced inversion of the northern margin of the Algero–Balearic basin from late Tortonian until present-day. The structures that characterize this margin are a set of thrusts with a global SE-ward sense of displacement and related fault propagation folds (e.g. Abubacer anticline, Fig. 7). Other structures are transpressive strike-slip faults and associated positive flower structures (Fig. 8) that may indicate that the Palomares fault system continues southwards offshore (Figs. 3 and 10). Both pure shortening and transpressive strike-slip faults affect the volcanic basement and entire Tortonian to Plio–Quaternary sediment cover. Thrusts and folds strike N40ºE, whilst strike-slip faults strike N10ºE (Figs. 3, 9 and 10).

Pure shortening structures at the Palomares margin probably started in latemost Tortonian to Messinian (≈8-7 Ma), inferred from the syn-tectonic deposit of subunit IIc on the back of the fault propagation fold (Fig. 7). These shortening structures are presently active since they fold Plio–Quaternary sediments and produce pronounced seafloor relief that deflects submarine canyons (e.g. Alias River and San José submarine canyons, Fig. 3). Furthermore, a Mw 3.8 earthquake (30th/06/2005, Instituto Geográfico Nacional http://www.ign.es) produced a thrust focal mechanism at 11 ± 0.3km depth, about 50 km away from the coast (Fig. 3, *Fernández-Ibáñez et al., 2007*). The depth of this earthquake corresponds nearly to the detachment depth of the Abubacer ridge. According to our estimations the detachment occurs at the brittle-ductile transition. Timing of transpressive strike-slip structures imaged on line TM23 seems to be considerably younger, probably starting in the Pliocene and controlling Plio–Quaternary sedimentation. In contrast, Tortonian sediments, although disrupted by the fault, appear laterally continuous in thickness (Fig. 8). Sinistral focal mechanisms in the region and folded Quaternary sediments, indicate that transpressive faulting and related folding are currently active (Figs. 3 and 10, *Stich et al., 2006; Fernández-Ibáñez et al., 2007*).

10.6.2 Integration of onshore-offshore structural data

The Sierra Cabrera pop-up anticlinorium and sinistral Palomares and Terreros fault systems in the eastern Betics are structures similar to those mapped at the Palomares margin offshore (Fig. 3). Similarly to the Abubacer anticline, the Sierra Cabrera anticlinorium is bounded by north and south dipping reverse faults, all striking N40-50ºE, perpendicularly to present-day shortening stress field (Figs. 14 and 15). These structures affect the metamorphic and volcanic basement, and the Tortonian to early Pliocene sediments (Fig. 14 and 15). The initial growth of the Sierra Cabrera anticlinorium is shown by progressive unconformities in the latemost Tortonian Azagador member, corresponding to the base of subunit IIc *(Booth-Rea et al., 2007)*. The Quaternary activity of the North and South Cabrera reverse faults is indicated by

geomorphic analysis *(Giaconia et al., 2012b)*.

The Palomares sinistral fault zone striking N10ºE is parallel to transpressive faults of the Palomares margin offshore (e.g. positive flower structure imaged on line TM23) that initiated their activity during the latemost Tortonian. The transpressive structures of the Palomares margin offshore possibly represent the Plio–Quaternary southward propagation of the Palomares fault system.

Both onshore and offshore structures at the Palomares margin offshore fit an oblique convergence model, where NW–SE shortening deforms a NNE–SSW margin. This stress field generates NE–SW thrusts, anticlines and/or synclines (e.g. the N40-50ºE striking Abubacer anticline and Sierra Cabrera anticlinorium), NNE–SSW sinistral strike-slip faults (e.g. Nº 10 E striking Palomares and Terreros fault zones), WNW–ESE dextral strike-slip faults (e.g. the N110-120ºE Polopos fault zone) and NW–SE normal faults (e.g. the N140ºE Plio–Pleistocene high-angle normal fault system in the Níjar basin north of the Carboneras fault zone or the NW–SE Baza, Guadix and Granada basin faults Fig. 16, *Azañón et al., 2004b; Fernández-Ibánez et al., 2010; Sanz de Galdeano et al., 2012*).

During oblique convergence, shortening is mainly absorbed by en-echelon thrusts and folds connected by strike-slip faults that partition the deformation, as described in other more evolved systems like the Zagros thrust-fold belt *(Vernant and Chery, 2006; Malekzade et al., 2007)*. The Palomares and Terreros sinistral fault system transfer shortening at Sierra Almenara and Lomo de Bas to the north, to Sierra Cabrera to the south (Figs. 3 and 16). Whilst, the dextral Polopos fault zone transfers shortening at the Sierra Alhamilla to the west, to the Sierra Cabrera at the east (Figs. 3 and 16, *Giaconia et al., 2012a, 2012b, 2013a*). The GPS measured displacement vector at the Sierra Cabrera anticlinorium is significantly larger than measurements to the north, indicating that the reverse faults that bound the anticlinorium are absorbing an important amount of Africa–Iberia convergence in the region (Fig. 3). Similarly, further east the GPS displacement vectors decrease stepwise toward the north after the main active shortening structures, namely, the Lomo de Bas and Sierra Almenara reverse faults, and the Alhama de Murcia sinistral-reverse fault. The sinistral Palomares fault system partitions the deformation between the above shortening structures, having a smaller displacement vector that is oriented NNE-wards, congruent to the kinematics of the fault zone. Offshore, a large portion of the Africa–Iberia convergence is absorbed by a N40ºE thrust system and associated folds, and transfer occurs locally by sinistral strike-slip Palomares type faults.

Fig. 14: Geological map of the Sierra Cabrera anticlinorium and surrounding Neogene sedimentary basins: the Vera and the Níjar basins, to the north and to the south, respectively. Furthermore, two cross-sections subparallel to seismic line TM24 and to the main shortening direction in the region are located (Fig15).

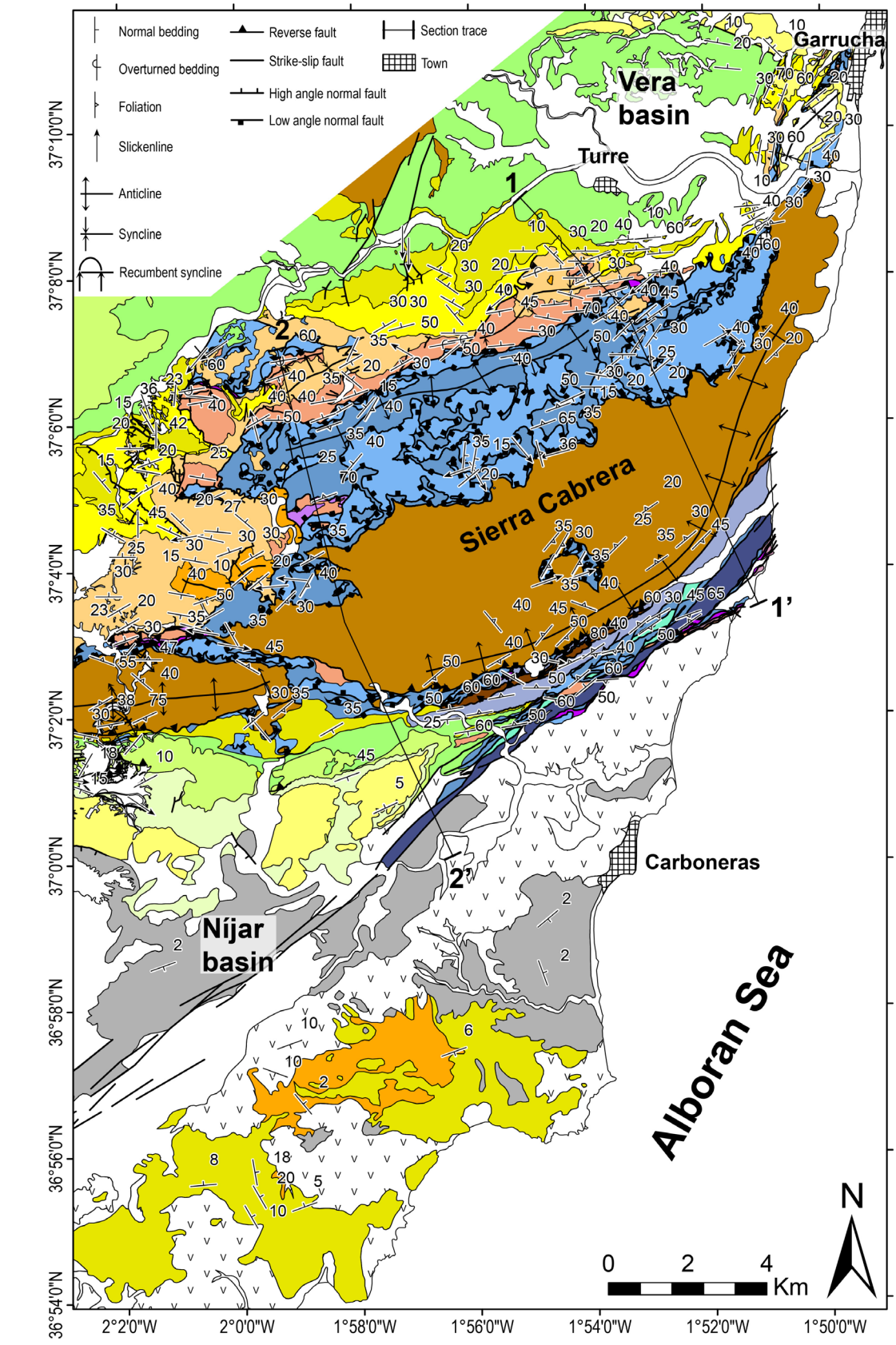

Neogene-Quaternary sediments
- Quaternary
- Costal conglomerates - Late Pliocene
- Temperate carbonates and marls - Early Pliocene
- Post-evaporitic marls, sandstone and conglomerates - Messinian
- Gypsum - Messinian
- Marls - Messinian
- Temperate carbonates and siliciclastic carbonates - Latemost Tortonian-Messinian
- Marls and silty marls - Late Tortonian
- Conglomerates and sandstones - Late Tortonian
- Continental conglomerate - Early Tortonian
- Marls and conglomerate - Langhian-Serravallian

Volcanics rocks
- Neogene volcanic rocks

Metamorphic basement

Malaguide Complex
- Paleogene limestone
- Gypsum and dolomite
- Quartzite and phyllite

Alpujarride Complex
- Upper Unit - Medium- to high-grade graphite-schists
- Dolomitic marbles and gypsum
- Phyllite, quartzite and schists
- Low-grade graphite-schists

Intermediate Unit

- Lower Unit - Medium-grade graphite-schist and marbles

Nevado-Filabride Complex
- Bédar-Macael Unit: Amphibolite, marbles and schists
- Calar Alto Unit: Low-grade graphite-schists

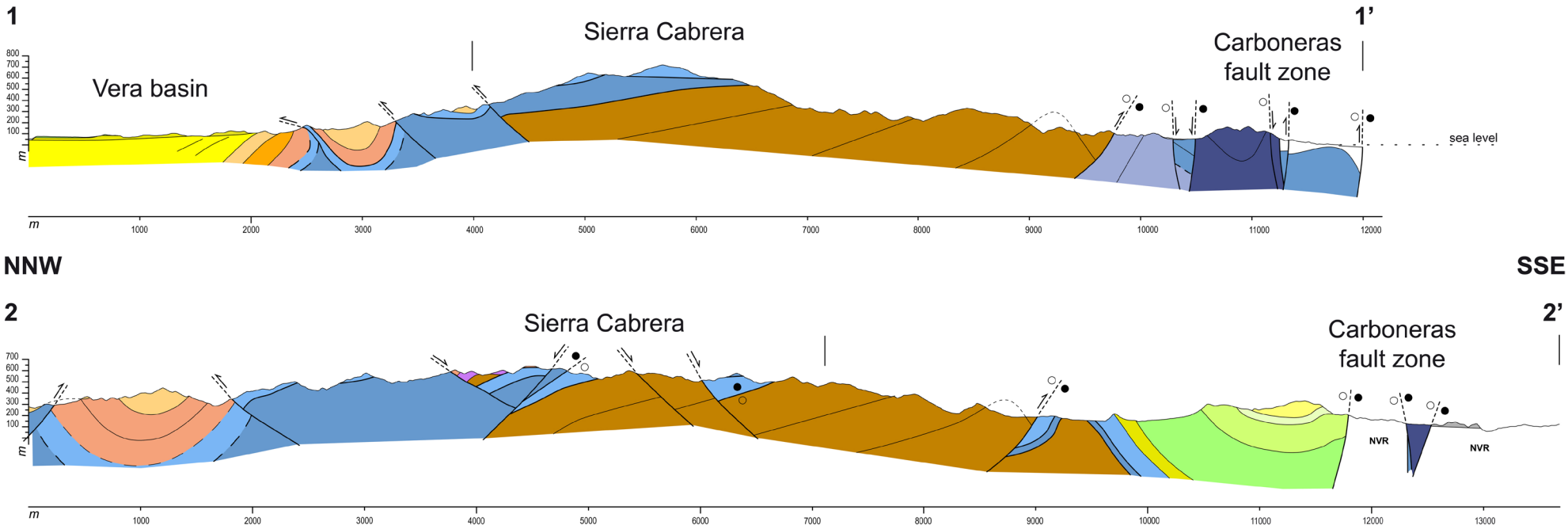

Fig. 15: Geological cross-sections through the Sierra Cabrera anticlinorium (see Fig. 15 for location) subparallel to seismic line TM24 and the main shortening direction in the region. Notice the congruence between the Abubacer anticline and the Sierra Cabrera anticlinorium in their tectonic regime (from pure shortening to transpressional regime) and timing of deformation (tectonic activity started in the latemost Tortonian and continued up to the Quaternary). See Figure 14 for the legend.

10.6.3 Neogene inversion of the western Mediterranean

Pure shortening and transpressive structures in the Palomares margin are consistent with structures mapped onshore in the southeastern Betics, and offshore in the Algerian margin, both in tectonic regime and timing. After middle–late Miocene E–W back-arc extension that generated the Algero–Balearic basin (16-8 Ma, *Mauffret et al., 2004*), inversion of the Algerian margin occurred during the late Miocene (about 5-7 Ma) and has continued to present time *(Déverchère et al., 2005; Domzig et al., 2006; Mauffret, 2007; Billi et al., 2011)*. The tectonic inversion reactivated S-verging thrusts onshore the Algerian margin (Fig. 16) and produced new N-verging thrusts near the continent to ocean transition *(Déverchère et al., 2005; Domzig et al., 2006; Mauffret, 2007; Kherroubi et al., 2009; Yelles et al., 2009; Strzerzynski et al., 2010)*. These structures cut and fold the basement and late Tortonian–Messinian sediments, and Plio–Quaternary sediments are tilted and show fold-onlapping growth strata indicating the recent activity *(Déverchère et al., 2005; Domzig et al., 2006; Kherroubi et al., 2009; Billi et al., 2011)*. The present activity is indicated by historical and instrumentally recorded thrust-mechanism earthquakes and GPS geodetic displacement data *(Mauffret, 2007; Serpelloni et al., 2007; Strzerzynski et al., 2010)*.

The Yusuf, Alborán ridge and Al–Idrisi faults in the East Alborán basin are structures kinematically equivalent to those of the Palomares margin. Although in this case, the origin or compressional inversion of these structures seems younger, after the Messinian (5.33 – 4,57 Ma, *Martínez-García et al., 2013*). Indeed, the N105ºE Yusuf dextral fault that merges westwards with the N60ºE Alborán ridge reverse fault (Fig. 16) cuts and folds the Plio–Quaternary sediments (e.g. the Yusuf and Alborán Ridge anticlines and the Yusuf Basin syncline). This fault system is cut by the N25ºE Al–Idrisi sinistral fault toward the west that also shows Plio–Quaternary growth strata (Fig. 16, *Martínez-García et al., 2013*). Thus, the present tectonic inversion of the western Mediterranean started about 7 Ma in the Palomares and Algerian margins and migrated westward toward the Moroccan margin by the development of the Alborán ridge and Al–Idrisi fault system about 5 Ma ago. Such a space-time evolution of the western Mediterranean inversion indicates the development of a new transpressional plate boundary along the southern margin of the Algero–Balearic and Alborán basins that is propagating westwards in response to the ongoing Eurasia–Africa plate convergence. The tipline of this newly developing plate boundary occurs along the Tofiño bank at the southern margin of the West Alborán basin.

10.7 Conclusions

The Palomares margin strikes NNE–SSW, with a direction oblique to the present NW–SE shortening stress field. Seismic reflection images indicate that middle to late Miocene extension in the region was accomplished mostly by magmatic accretion.

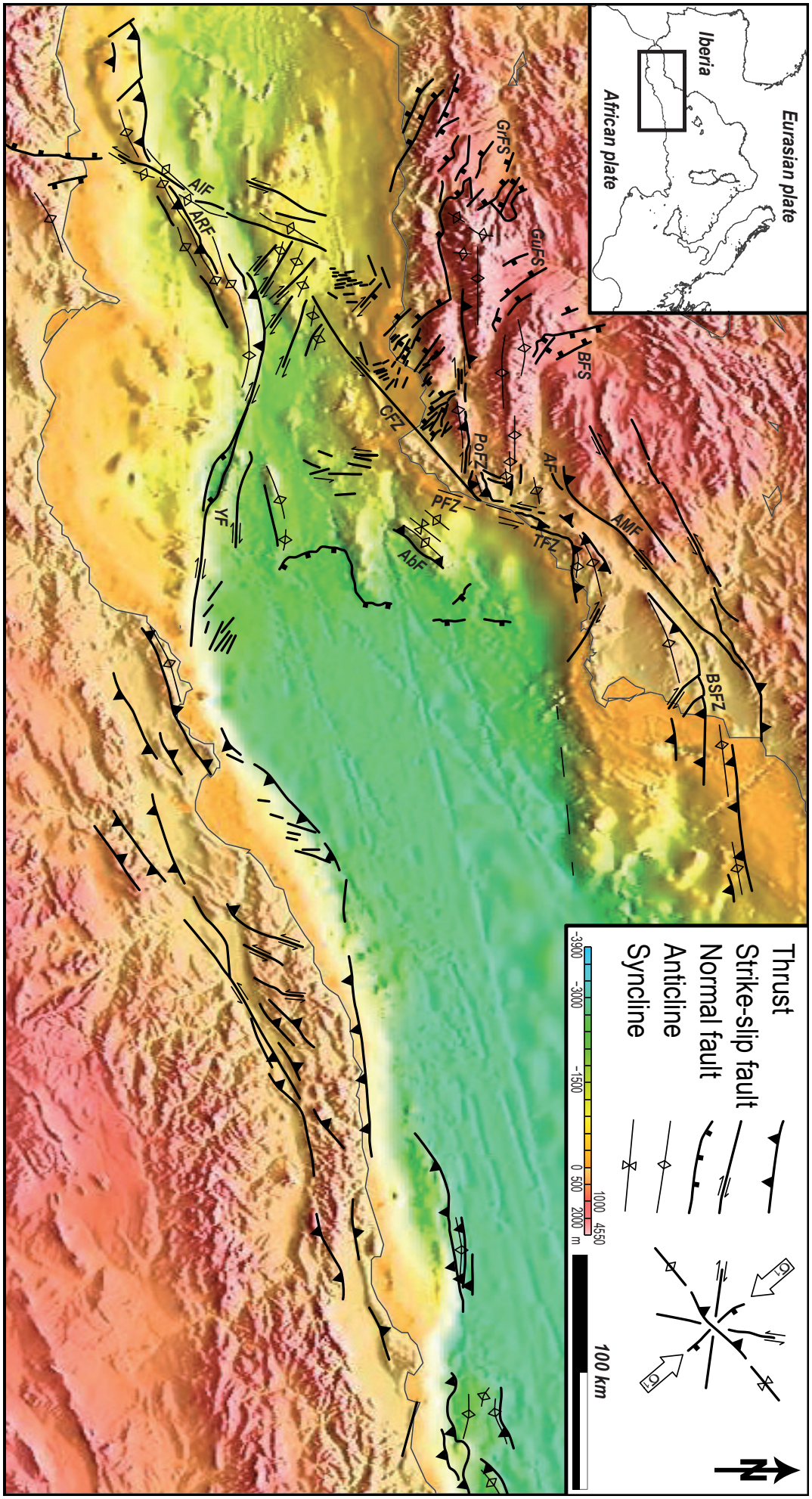
Eurasian plate
Iberia
African plate
GrFS
GuFS
BFS
CFZ
PoFZ
PFZ
AbF
AF
TFZ
AMF
BSFZ
AIF
ARF
YF
Thrust
Strike-slip fault
Normal fault
Anticline
Syncline
-3900
-3000
-1500
0
500
1000
2000
4550
m
100 km
N
σ1
σ3

The Palomares margin has been subsequently inverted by the development of N40ºE reverse faults and folds and N10ºE sinistral strike-slip faults that crop out both onshore and offshore. These structures are the Abubacer and Cabrera antiformal ridge and associated reverse faults together with segments of the Palomares sinistral fault system. The Abubacer reverse fault shows a planar geometry until its detachment at the brittle ductile transition at approximately 10 km depth and accommodates up to 1.5 km displacement. The tectonic structure and fault kinematics onshore and offshore of the Palomares margin are consistent with the NW–SE present stress field. The structures fit in an oblique convergence model where NW–SE shortening is partitioned between en-echelon reverse faults and associated folds, and strike-slip faults along a NNE–SSW margin. The strike-slip faults transfer deformation between shortening structures where most convergence is absorbed.

Tectonic inversion of the Palomares margin initiated during the latemost Tortonian to Messinian, coeval to structures observed onshore and along the Algerian margin and continues up to present day. The copressional inversion of the western Mediterranean is developing a new transpressive plate boundary at the southern margins of the Algero–Balearic and Alborán basins. This plate boundary has propagated westwards from the Algerian margin approximately 7 Ma ago to the Alborán Ridge about 5 Ma ago, ending along the Tofiño bank at the southern margin of the Western Alborán basin.

Acknowledgements: The seismic data were obtained in the frame of the CGL2008-03474-E European Science Fundation TopoEurope TOPOMED Project. The authors were supported by research projects CGL2011-29920, CSD2006-00041 TOPOIBERIA CONSOLIDER-INGENIO2010, CTM2007-66179-C02-01/MAR, CGL2011-30005-C02-02 SHAKE, and the CTM2011-30400-C02-01 HADES Project from the Spanish Ministry of Science and Innovation. We also acknowledge funding from the MICINN through the "Ramon y Cajal" program (R. Bartolome). Our grateful thanks to the captain, crew, and UTM-CSIC technical staff onboard the R/V Sarmiento de Gamboa, during the TOPOMED-GASSIS cruise.

Fig. 16: Main tectonic structures associated to the late Miocene (post-latemost Messinian) to present-day compressional tectonic inversion in the East Alborán and Algero–Balearic basins, both onshore and offshore, from recompilation of fault traces and kinematic data (Martínez-Díaz et al., 2002; Booth-Rea et al., 2004a, 2004c; Masana et al., 2004; Booth-Rea et al., 2005; Marín-Lechado et al., 2005; Masana et al., 2005; Domzig et al., 2006; Gràcia et al., 2006; Pedrera et al., 2006; Moreno et al., 2008; Pedrera et al., 2009a; Sanz de Galdeano et al., 2010; Gràcia et al., 2011; Alfaro et al., 2012; Pedrera et al., 2012; Perea et al., 2012; Sanz de Galdeano et al., 2012; Giaconia et al., 2013a; Maillard and Mauffret, 2013; Martínez-García et al., 2013). AbF, Abubacer fault; AlF, Al–Idrisi fault; AMF, Alhama de Murcia fault; ARF, Alborán Ridge fault, BFS, Baza basin fault system, BSFZ, Bajo Segura fault zone; CFZ, Carboneras fault zone; GrFS, Granada basin fault system, GuFS; Guadix basin fault system; PFZ, Palomaers fault zone; PoFZ, Polopos fault zone; TFZ; Terreros fault zone; YF, Yusuf fault. The set of structures is consistent with the NW–SE present stress field (see inset in the figure) and fits in an oblique convergence model where such a NW–SE trending shortening affects to the NNE–SSW oriented Palomares margin.

Part III – Conclusions

11.0 Conclusions

11.1 Heterogeneous extension and the role of transfer faults in the development of the southeastern Betic basins (SE Spain)

The Sorbas basin underwent important normal faulting during the Serravallian to Tortonian producing two extensional-related sedimentary depocenters in the region. The older North Cabrera depocenter is strongly compartmented by segments of the north–Cabrera dextral transfer fault zone and by normal faults with both NE and SW transport that were active between the Serravallian and the Tortonian (approx. 13.8 to 9 Ma). A normal-fault listric fan with SW-directed extension that rooted in a detachment within the Nevado–Filabride complex formed the Gacía depocenter between approximately 9 and 7.5 Ma. This system tilted the previous Nevado-Filabride/Alpujarride detachment, produced a westward migration of SW-directed extension and the abandonment of the north-Cabrera dextral fault zone.

Extension in the Gacía depocenter was coeval and probably linked with sinistral displacement along the Carboneras fault to the south, producing a strongly heterogeneous extensional system with short normal frontal ramps linked by long dextral and sinistral transfer faults. Westward directed heterogeneous extension in the region resulted in different styles of extension, producing tilted-block domains and metamorphic core-complexes to the north of the Carboneras sinistral transfer fault and magmatic accretion upon previously thinned continental crust to the south of the fault. Serravallian to latemost Tortonian extension probably occurred in a transtensional setting above a lithospheric transform fault that permitted the westward propagation of the Thethyan oceanic slab beneath the Albóran basin producing edge delamination under the Betics.

11.2 Geomorphic response to large-scale Polopos and Palomares conjugate strike-slip faults in the Sierra Alhamilla–Polopos and Cabrera anticlinoria

Tectonic structures at the Sierra Alamilla anticlinorium, as the North Alhamilla and Gafarillos faults, have been interpreted as inactive since the Messinian by previous authors. However, both qualitative and quantitative geomorphic analyses that we conducted in the Sierra Alhamilla indicate the occurrence of active tectonics during the Pleistocene and Holocene, and probably up to the present. These tectonic structures are the North Alhamilla Reverse Fault and the South Gafarillos Fault that together forms the post-Messinian active segments of the Polopos Fault Zone, as we named. Furthermore, a Pliocene–Quaternary high-angle normal fault system affects the entire southern slope of the Sierra Alhamilla and the Níjar–Almería basin.

Structural field-based and morphometric GIS-based analyses carried out in the Sierra Alhamilla area show that dextral transpressive and reverse displacement along the Polopos fault zone conditioned the relief in its northern slope producing a set of fault-related geomorphic features congruent with the tectonic uplift of its hanging-wall (e.g. rectilinear mountain fronts, deeply dissected basins and valleys, immature drainage basins, and "foot-rejuvenation" process). Similarly, the Pliocene–Quaternary high-angle normal fault system occurring in the Níjar basin conditioned the relief in the Sierra Alhamilla southern slope producing a set of fault-related geomorphic evidence congruent with the tectonic uplift of their footwall (e.g. rectilinear mountain fronts, deeply dissected basins and valleys, immature drainage basins, fault-related knickpoints). Geomorphic analyses carried out in the Sierra Cabrera and Polopos area indicate that the topographic relief and drainage network is controlled by both reverse and oblique-slip faults. These structures are the North and the South Cabrera reverse faults, the sinistral Palomares fault segments, at the eastern termination of the Cabrera ridge, and the dextral oblique-slip South Gafarillos faults, which bound the southern slope of the Polopos antiform. All these faults have been active during the Quaternary as inferred by the set of fault-related geomorphic features that they produced. The reverse fault segments (N50-60ºE North and the South Cabrera reverse faults) perpendicular to the present present maximum shortening axis have associated higher uplift rates than oblique strike-slip (N20ºE Palomares fault segments and the N110ºE dextral conjugate South Gafarillos fault). The geomorphic and tectonic dataset highlights the occurrence of an active pop-up formed between the North and the South Cabrera reverse faults in the Sierra Cabrera antiform. The pop-up developed in a constrictional domain of the large-scale Polopos and Palomares conjugate strike-slip faults. Meanwhile, extension in the Níjar basin perpendicular to the present stress regime occurs in the extensional domain of the large-scale conjugate strike-slip fault system, whilst extension in the Vera basin is related to small releasing bends of the Palomares fault zone.

11.3 Messinian to Pleistocene mountain-front migration and drainage captures related to the Polopos fault zone segment linkage and growth

The Polopos fault zone is a N100-120ºE dextral transpressive fault zone developed under Tortonian to Quaternary NW-SE shortening, mainly coeval to the conjugate sinistral Palomares fault zone. The fault zone is formed by the North and South Gafarillos dextral-transpressive fault and the North Alhamilla reverse fault. Faulting probably initiated in the latemost Tortonian (≈ 7 Ma) and continued up to the late Pleistocene (≥70 ky), at least. The fault zone affected the topography, the drainage network and alluvial terrace deposition (of middle and late Pleistocene ages). The North Alhamilla and the North Gafarillos faults (Gafarillos fault in bibliography) have been considered by previous authors as inactive since the Messinian. Our structural and mapping data indicate that the North Gafarillos fault was active until the Messinian,

whilst the South Gafarillos fault and its westward continuation, the North Alhamilla reverse fault, have been active since then and, at least, until the late Pleistocene. Thus, Deformation and fault-related mountain fronts migrated southwestwards between the Messinian and Quaternary.

The reverse to dextral-transpressive displacement along the Polopos fault zone and the southwestwards extension along Pliocene–Quaternary normal faults have determined the differential uplift between Sierra Alhamilla and the Sorbas and Níjar basins promoting the middle Pleistocene capture that occurred in the southern margin of the Sorbas basin. Later, the Sierra Alhamilla–Polopos and Cabrera anticlinoria tectonic uplift related to continued displacement along the fault zone, and local subsidence associated to transtensional kinematics of the Palomares fault zone in the Vera basin, promoted the late Pleistocene capture at the center of the Sorbas basin.

11.4 Neogene inversion of the Palomares margin and southeastern Betics (oblique convergence model)

The Palomares margin strikes NNE–SSW, with a direction oblique to the present NW–SE shortening stress field. Seismic reflection images indicate that magmatic accretion accommodated most of the middle to late Miocene extension in the region. Later compressional inversion of the Palomares margin resulted in N40ºE reverse faults and folds and N10ºE sinistral strike-slip faults that crop out both onshore and offshore. These structures are consistent with the NW–SE present stress field and presently active as inferred by seafloor features (e.g. submarine canyon deflections and submarine fault escarpments) and focal mechanisms in the area. The major structures are the Abubacer and Cabrera antiformal ridge and associated reverse faults together with segments of the Palomares sinistral fault system (both onshore and offshore). The Abubacer reverse fault accommodates most of the inversion offshore (up to 1.5 km displacement) showing a planar geometry until its detachment at the brittle ductile transition at approximately 10 km depth. The set of Palomares margin structures, both onshore and offshore, fit in an oblique convergence model where NW–SE shortening is partitioned between en-echelon reverse faults and associated folds, and strike-slip faults along a NNE–SSW margin.

11.5 Neogene inversion of the western Mediterranean

Tectonic inversion of the Palomares margin initiated during the latemost Tortonian to Messinian and continues up to present day. Inversion structures of the margin are coeval to those observed along the Algerian margin. The late Miocene to present compressional inversion of the western Mediterranean is developing a new transpressive plate boundary at the southern margins of the Algero–Balearic and Alborán basins. This plate

boundary has propagated westwards from the Algerian margin approximately 7 Ma ago to the Alborán Ridge about 5 Ma ago, ending along the southern margin of the Western Alborán basin.

12.0 Conclusiones

12.1 Extensión heterogénea y la influencia de fallas de transferencia en la evolución de las cuencas de las Béticas surorientales

La Cuenca de Sorbas sufrió una importante extensión desde el Serravalliense hasta el Tortoniense que produjo dos depocentros sedimentarios relacionados en la región. El depocentro más antiguo, situado al norte de Sierra Cabrera, se encuentra fuertemente compartimentado por falla normales con dirección de transporte hacia el NE y el SO que fueron activas desde el Serravalliense hasta el Tortoniense (aprox. 13.8 - 9 Ma). Un sistema de fallas normales lístricas, con dirección de transporte hacia el SO y que se unen en un despegue dentro del complejo Nevado–Filabride, produjo el depocentro de Gacía aproximadamente entre 9 y 7.5 Ma. Este sistema basculó el despegue extensional previo entre los complejos Alpujarride y Nevado–Filabride y produjo la migración hacia el oeste de la extensión, así como el abandono de la falla dextrorsa del Norte de la Sierra Cabrera.

La extensión en el depocentro de Gacía fue coetánea y probablemente relacionada con el desplazamiento sinistrorso de la falla de Carboneras al sur, produciendo un sistema extensional fuertemente heterogéneo con rampas frontales normales conectadas por largas fallas *"transfer"* sinistrorsas y dextrorsas. El carácter heterogéneo de esta extensión produjo dominios con bloques basculados y exhumación de domos metamórficos al norte de la falla *"transfer"* sinistrorsa de Carboneras y acreción magmática sobre corteza continental adelgazada al sur de la falla. La extensión Serravalliense–tardo Tortoniense probablemente ocurrió en un contexto transtensivo sobre una falla litosférica transformante que permitió la propagación hacia el oeste del *"slab"* de la litosfera del Tetis debajo de la cuenca del Alborán facilitando la delaminación con una fuerte compontente lateral debajo de la rama norte de la Cordillera Bético-Rifeña.

12.2 Evidencias morfológicas de la actividad de las fallas de salto en dirección conjugadas de Palomares y Polopos en los anticlinares de Sierra Alhamilla-Polopos y Sierra Cabrera

Las estructuras entorno al anticlinal de Sierra Alhamilla y las fallas que lo limitan por el norte (fallas del norte de Alhamilla y Gafarillos) han sido consideradas por diversos autores como inactivas desde el Mesiniense. Sin embargo, el análisis morfo-estructural realizado en esta región revela una actividad cuaternaria que parece extenderse hasta la actualidad. En la parte norte de la Sierra Alhamilla, las fallas inversas activas han sido agrupadas bajo la denominación de la zona de falla de Polopos mientras que en el borde sur de esta Sierra, fallas normales de alto ángulo afectan a los depósitos Plio-

cuaternarios de la cuenca de Níjar–Almería.

En este estudio se han recopilado abundantes datos estructurales que conjuntamente con los datos de carácter morfométrico (S_{mf}, V_f, *SLk*, rejuvenecimiento y captura de la red de drenaje, etc), obtenidos mediante el procesado de datos del relieve a partir de un sistema de información geográfica, permiten confirmar el funcionamiento transpresivo dextro de la zona de falla de Polopos. La actividad de esta falla en el borde norte y las fallas normales de alto ángulo en el borde sur promueven el levantamiento de la Sierra Alhamilla durante el Plio-Pleistoceno. Del mismo modo, el análisis morfo-estructural realizado en el área de la Sierra de Cabrera y Polopos indica que la topografía y la red de drenaje están controladas por fallas transpresivas. Estas estructuras son: las fallas inversas de norte y sur de Sierra Cabrera, la falla sinistra de Palomares y las fallas dextrorsas del sur de Gafarillos que limitan la vertiente sur del antiforme de Polopos. Todas estas fallas han sido activas a lo largo del Cuaternario como puede inferirse a partir del análisis de diversos rasgos morfológicos. Los segmentos que funcionan como fallas inversas puras N50-60ºE (ubicados al norte y sur de la Sierra de Cabrera), poseen una orientación perpendicular a la posición actual de $\sigma 1$ e inducen mayores tasas de elevación en el bloque de techo que los que presentan una componente lateral en el movimiento (el segmento N20ºE de la falla de Palomares y su conjugada N110ºE dextra, la falla del sur de Gafarillos). Los datos morfo-estructurales indican la existencia de un *"pop-up"* activo inducido por el funcionamiento de las fallas inversas que la limitan la Sierra de Cabrera. Esta estructura se desarrolla en el dominio compresivo limitado por las fallas de salto en dirección conjugadas de Polopos y Palomares. La extensión en la cuenca de Níjar es congruente con la situación de esfuerzos regional ya que estaría en el dominio extensional de este sistema de fallas conjugadas de salto en dirección, mientras que la extensión en la cuenca de Vera está relacionada con *"releasing bends"* producidos por la zona de falla de Palomares.

12.3 Migración de frentes montañosos y capturas fluviales inducidas por la activación de diferentes segmentos de la falla de Polopos entre el Mesiniense y el Pleistoceno

La zona de falla de Polopos, con una orientación N100-120ºE y carácter dextro transpresivo, es conjugada de la zona de falla sinistra de Palomares. Ambos conjuntos de estructuras se forman acomodando el acortamiento regional NW–SE entre el Tortoniense y el Cuaternario. La zona de falla de Polopos está constituida por las fallas transpresivas dextrorsas Gafarillos norte y Gafarillos sur y por la falla inversa del Norte de la Sierra Alhamilla. Estas fallas se inician probablemente al final del Tortoniense (aprox. 7 Ma) y su actividad continúa, como mínimo, hasta el Pleistoceno Superior. La zona de falla condiciona la topografía actual, produce deflexiones en la red de drenaje y corta a las terrazas fluviales de edad Pleistoceno medio y superior. Estas

fallas habían sido consideradas inactivas desde el Mesiniense por autores precedentes. Los datos morfo-estructurales ponen de manifiesto que la falla Gafarillos norte solo fue activa hasta el Mesiniense, mientras la falla Gafarrillos sur y su continuación hacia el oeste, la falla inversa del norte de Sierra Alhamilla, son activas entre el Mesiniense y el Pleistoceno superior. De este modo, la deformación y los frentes montañosos ligados a la actividad de estas fallas migran hacian el suroeste entre el Mesiniense y el Cuaternario.

La captura fluvial de la vertiente meridional de la cuenca de Sorbas está inducida por un levantamiento diferencial, durante el Pleistoceno medio, de la Sierra Alhamilla con respecto a las cuencas que la limitan. El desplazamiento, de inverso a transpresivo dextro, en la zona de falla de Polopos en el norte de la Sierra Alhamilla y las fallas normales con extensión hacia el suroeste constituyen los límites tectónicos que facilitan este levantamiento relativo. La continuación de este proceso durante el cuaternario permite la migración de la actividad hacia el Este, produciendo una cinemática transtensiva en la zona de falla de Palomares en su borde con la cuenca de Vera. Estos procesos inducen la captura, durante el Pleistoceno superior, del interior de la cuenca de Sorbas.

12.4 Inversión neógena del margen de Palomares y del margen suroriental de la Cordillera Bética (modelo de convergencia oblicua)

El margen de Palomares tiene una orientación NNE–SSW que es oblicua a la dirección NW–SE de máximo acortamiento regional. Los perfiles sísmicos de reflexión muestran que la acreción magmática acomodó la mayor parte de la extensión del Mioceno medio y superior producida en este margen. A continuación, el margen de Palomares sufre una inversión tectónica que genera fallas inversas N40ºE, pliegues y fallas de salto en dirección con una orientación N10ºE que afloran tanto en la parte emergida como en la sumergida. Estas estructuras compresivas producen deflexiones en cañones submarinos y producen escarpes submarinos indicando que tienen un carácter activo, lo que es congruente con los mecanismos focales de terremotos recientes que a su vez coinciden con el elipsoide de esfuerzos actual ($\sigma 1$ con una orientación NW–SE). Las principales estructuras son las crestas antiformales de Abubacer y Cabrera y las fallas inversas asociadas junto con los segmentos del sistema de fallas sinistro de Palomares (tanto en tierra como en mar). La falla inversa de Abubacer acomoda la mayor parte de la inversión en la zona sumergida (hasta 1,5 km de desplazamiento). Esta falla muestra una geometría planar hasta que se anastomosa en un despegue horizontal en la zona de transición dúctil-frágil (aproximadamente a 10 km de profundidad). El conjunto de estructuras que afloran en el margen de Palomares, tanto en tierra como en mar, se ajustan bien con un modelo de convergencia oblicua en donde el acortamiento NW–SE se reparte entre fallas inversas *"en-echelon"* y sus pliegues asociados y fallas de salto

en dirección a lo largo del margen NNE–SSW.

12.5 Inversión Neógena del Mediterráneo Occidental

La inversión tectónica del margen de Palomares se inicia durante la transición Tortoniense–Mesiniense y continúa hasta nuestros días. Las estructuras de inversión de este margen son coetaneas con las observadas en el margen Argelino. La inversión compresiva que se produce en el Mediterráneo occidental a partir del final del Mioceno está produciendo un nuevo límite de placas transpresivo en los márgenes meridionales de las cuencas Algero–Balear y de Alborán. Este límite de placas se ha propagado hacia el oeste desde el margen Argelino. Este proceso se inicia hace aproximadamente 7 Ma y migra hacia la cresta de Alborán (hace aproximadamente 5 Ma) y finaliza en el margen meridional de la cuenca occidental de Alborán.

Part IV – References

Abad, I., Nieto, F., Peacor, D.R., Velilla, N., 2003. Prograde and retrograde diagenetic and metamorphic evolution in metapelitic rocks of Sierra Espuña (Spain). Clay Minerals, 38, 1-23.

Aguirre, J., 1998. El Plioceno del SE de la Península Ibérica (provincia de Almería). Síntesis estratigráfica, sedimentaria, bioestratigráfica y paleogeográfica. Revista de la Sociedad Geológica de España, 11, 295-315.

Aguirre, J., Sánchez-Almazo, I.M., 2004. The Messinian post-evaporitic deposits of the Gafares area (Almería-Níjar basin, SE Spain). A new view of the "Lago-Mare" facies. Sedimentary Geology, 168, 71-95.

Alfaro, P., Bartolomé, R., Borque, M.J., Estévez, A., García-Mayordomo, J., García-Tortosa, F.J., Gil, A.J., Gràcia, E., Lo Iacono, C., Perea, H., 2012. The Bajo Segura Fault Zone: Active blind thrusting in the Eastern Betic Cordillera (SE Spain). Journal of Iberian Geology, 38, 271-284.

Alvado, J.C., Sédimentation, deformation et manifestations magmatiques associées au couloir de décrochement de Palomares: le bassin de Vera (SE de l´Espagne), Doctoral Thesis, 23-232, Univ. Paris, 1986.

Alvarez-Marrón, J., 1999. Pliocene to Holocene structure of the eastern Alboran sea (western Mediterranean). Proceedings of the Ocean Drilling Program, Scientific results, 161, 345-355.

Augier, R., Booth-Rea, G., Agard, P., Martínez-Martínez, J.M., Jolivet, L., Azañón, J.M., 2005. Exhumation constraints for the lower Nevado-Filabride Complex (Betic Cordillera, SE Spain): a Raman thermometry and Tweequ multiequilibrium thermobarometry approach. Bulletin De La Societe Geologique De France, 176, 403-416.

Azañón, J.M., García Dueñas, V., Martínez Martínez, J.M., Crespo Blanc, A., 1994. Alpujarride tectonic sheets in the central Betics and similar eastern allochthonous units (SE Spain). Comptes Rendus de l'Académie des Sciences de Paris, 318, 667-674.

Azañón, J.M., Crespo Blanc, A., García Dueñas, V., 1997. Continental collision, crustal thinning and nappe-forming during the Pre-Miocene evolution of the Alpujárride Complex (Alborán Domain, Betics). Journal of Structural Geology, 19, 1055-1071.

Azañón, J.M., Crespo Blanc, A., 2000. Exhumation during a continental collision inferred from the tectonometamorphic evolution of the Alpujarride Complex in the central Betics (Alboran Domain, SE Spain). Tectonics, 19, 549-565.

Azañón, J.M., Azor, A., Booth-Rea, G., Torcal, F., 2004a. Relation between active tectonics, shallow earthquakes and the drainage pattern in the NE border of the Granada Basin. European Geophysical Union (EGU), Nize.

Azañón, J.M., Azor, A., Booth-Rea, G., Torcal, F., 2004b. Small-scale faulting, topographic steps and seismic risk in the Alhambra (Granada, SE Spain). Journal of Quaternary Science, 19, 219-227.

Azañón, J.M., Booth-Rea, G., Martínez-Martínez, J.M., Teixidó, T., Peña, J.A., 2007. Repeated activity of the Malaha fault affecting a Roman to Medieval archaeological site (Granada basin, Spain). EGU 2007, Viena.

Azdimousa, A., Bourgois, J., Poupeau, G., Montigny, R., 1998. Histoire thermique du massif de Kétama (Maroc): sa place en Afrique du Nord et dans les Cordillères bétiques. Comptes Rendus de l'Académie des Sciences - Series IIA - Earth and Planetary Science, 326, 847-853.

Azdimousa, A., Jabaloy, A., Asebriy, L., Booth-Rea, G., González-Lodeiro, F., Bourgois, J., 2007. Lithostratigraphy and structure of the Temsamane unit (eastern external Rif, Morocco). Revista de la Sociedad Geológica de España, 20, 187-200.

Azor, A., Keller, E.A., Yeats, R.S., 2002. Geomorphic indicators of active fold growth: South Mountain-Oak Ridge anticline, Ventura basin, southern California. Geological Society of America Bulletin, 114, 745-753.

Bakker, H.E., De Jong, K., Helmers, H., Bierman, C., 1989. The geodynamic evolution of the Internal Zone of the Betic Cordilleras (South-East Spain): a model based on structural analysis and geothermobarometry. Journal of

Metamorphic Geology, 7, 359-381.

Balanyá, C.J., García-Dueñas, V., Azañón, J.M., Sánchez-Gómez, M., 1998. Reply [to "Comment on 'Alternating contractional and extensional events in the Alpujarride nappes of the Alboran Domain (Betics, Gibraltar Arc)'"]. Tectonics, 17, 977-981.

Balanyá, J.C., García-Dueñas, V., 1987. Les directions structurales dans le Domaine d'Alborán de part et d'autre du Détroit de Gibraltar. Comptes Rendus de l'Académie des Sciences de Paris, 304, Série II, 929-932.

Balanyá, J.C., Azañón, J.M., Sánchez Gómez, M., García Dueñas, V., 1993. Pervasive ductile extension, isothermal decompression and thinning of the Jubrique unit in the Paleogene (Alpujárride Complex, western Betics Spain). Comptes Rendus de l'Académie des Sciences de Paris, 316, 1595-1601.

Balanyá, J.C., García-Dueñas, V., Azañón, J.M., Sánchez-Gómez, M., 1997. Alternating contractional and extensional events in the Alpujarride nappes of the Alboran Domain (Betics, Gibraltar Arc). Tectonics, 16, 226-238.

Balanyá, J.C., Crespo-Blanc, A., Azpiroz, M.D., Expósito, I., Luján, M., 2007. Structural trend line pattern and strain partitioning around the Gibraltar Arc accretionary wedge: Insights as to the mode of orogenic arc building. Tectonics, 26.

Ballesteros, M., Rivera, J., Muñoz, A., Muñoz-Martín, A., Acosta, J., Carbó, A., Uchupi, E., 2008. Alboran Basin, southern Spain - Part II: Neogene tectonic implications for the orogenic float model. Marine and Petroleum Geology, 25, 75-101.

Barragán, G., Evolución Geodinámica de la Depresión de Vera, , Doctoral Thesis, 300, Universidad de Granada, 1997.

Behr, W.M., Platt, J.P., 2012. Kinematic and thermal evolution during two-stage exhumation of a Mediterranean subduction complex. Tectonics, 31, TC4025.

Béjar, M., Herráiz, E., Martínez-Díaz, J.J., Lopéz, C., Capote, R., Tsige, M., 2006. Interpretación sismotectónica de la serie sísmica de Gérgal (2002, Mw 4.8) mediante datos sismológicos y de interferometría de RADAR (INSAR). Geogaceta, 39.

Bell, J.W., Amelung, F., King, G.C.P., 1997. Preliminary late Quaternary slip history of the Carboneras fault, southeastern Spain. Journal of Geodynamics, 24, 51-66.

Billi, A., Faccenna, C., Bellier, O., Minelli, L., Neri, G., Piromallo, C., Presti, D., Scrocca, D., Serpelloni, E., 2011. Recent tectonic reorganization of the Nubia-Eurasia convergent boundary heading for the closure of the western Mediterranean. Bulletin De La Societe Geologique De France, 182, 279-303.

Bokelmann, G., Maufroy, E., Buontempo, L., Morales, J., Barruol, G., 2011. Testing oceanic subduction and convective removal models for the Gibraltar arc: Seismological constraints from dispersion and anisotropy. Tectonophysics, 502, 28-37. Booth-Rea, G., Tectónica cenozoica en el Dominio Cortical de Alborán, Doctoral Thesis, 253, Universidad de Granada, 2001.

Booth-Rea, G., Azáñon, J.M., Goffe, B., Vidal, O., Martínez-Martínez, J.M., 2002. High-pressure, low-temperature metamorphism in Alpujarride Units of southeastern Betics (Spain). Comptes Rendus Geoscience, 334, 857-865.

Booth-Rea, G., Azañón, J.M., García-Dueñas, V., Augier, R., 2003a. Uppermost-Tortonian to present depocentre migration related with segmentation of the Palomares Fault Zone (PFZ), SE Betics, Spain. Comptes Rendus Geoscience, 335, 751-761.

Booth-Rea, G., Azañón, J.M., Martínez-Martínez, J.M., 2003b. Metamorfismo de AP/BT en metapelitas de la unidad de Ragua (complejo Nevado-Filábride, Béticas). Resultados termobarométricos del estudio de equilibrios locales. Geogaceta, 34, 87-90.

Booth-Rea, G., Azañón, J.M., García-Dueñas, V., Sánchez-Gómez, M., 2003c. A "core-complex-type structure" formed by superposed ductile and brittle extension followed by folding and high-angle normal faulting. The Santi Petri dome (western Betics, Spain). Comptes Rendus Geoscience, 335, 265-274.

Booth-Rea, G., Azañón, J.M., Azor, A., García-Dueñas, V., 2004a. Influence of strike-slip

fault segmentation on drainage evolution and topography. A case study: the Palomares fault zone (southeastern Betics, Spain). Journal of Structural Geology, 26/9, 1615-1632.

Booth-Rea, G., Martínez-Martínez, J.M., Azañón, J.M., Augier, R., 2004b. HP/LT metamorphism in metapelites of the two lowermost tectonic units of the Internal Betics, southern Spain: insights from multiequilibrium thermobarometric results., 32th International Geology Congress (IGC), Florence, Italy.

Booth-Rea, G., Azañón, J.M., García-Dueñas, V., 2004c. Extensional tectonics in the northeastern Betics (SE Spain): case study of extension in a multilayered upper crust with constrating rheologies. Journal of Structural Geology, 26, 2039-2058.

Booth-Rea, G., Azañón, J.M., Martínez-Martínez, J.M., Vidal, O., García-Dueñas, V., 2005. Contrasting structural and P-T evolution of tectonic units in the southeastern Betics: Key for understanding the exhumation of the Alboran Domain HP/LT crustal rocks (western Mediterranean). Tectonics, 24, 23 pp.

Booth-Rea, G., Ranero, C., Martínez-Martínez, J.M., Grevemeyer, I., 2007. Crustal types and Tertiary tectonic evolution of the Alborán sea, western Mediterranean. Geochemistry Geophysics Geosystems, 8.

Booth-Rea, G., Giaconia, F., Martínez-Martínez, J.M., Azañón, J.M., 2012a. The Almenara detachment (southeastern Betics). GeoTemas, 13, 1615-1618.

Booth-Rea, G., Jabaloy-Sánchez, A., Azdimousa, A., Asebriy, L., Vílchez, M.V., Martínez-Martínez, J.M., 2012b. Upper-crustal extension during oblique collision: the Temsamane extensional detachment (eastern Rif, Morocco). Terra Nova, 24, 505-512.

Bourgois, J., Mauffret, A., Ammar, A., Demnati, A., 1992. Multichannel Seismic Data Imaging of Inversion Tectonics of the Alboran Ridge (Western Mediterranean-Sea). Geo-Marine Letters, 12, 117-122.

Bousquet, J.C., Montenat, C., 1974. Présence de décrochements nord-est - sud-ouest plio-quaternaires, dans les Cordillères bétiques orientales (Espagne). Extension et signification générale. Comptes Rendus de l'Académie des Sciences de Paris, 278, 2617-2620.

Bousquet, J.C., 1979. Quaternary strike-slip faults in southeastern Spain. Tectonophysics, 52, 277-286.

Brachert, T.C., Krautworst, U.M.R., Stueckrad, O.M., 2002. Tectono-climatic evolution of a Neogene intramontane basin (Late Miocene Carboneras subbasin, southeast Spain): revelations from basin mapping and biofacies analysis. Basin Research, 14, 503-521.

Braga, C., Martín, J.M., Quesada, C., 2003. Patterns and average rates of late Neogene–Recent uplift of the Betic Cordillera, SE Spain. Geomorphology, 50, 3-26.

Braga, J.C., Martín, J.M., Betzler, C., Brachert, T.C., 1996. Miocene temperate carbonates in the Agua Amarga basin (Almería, SE Spain). Revista de la Sociedad Geológica de España, 9, 285-296.

Braga, J.C., Martin, J.M., Riding, R., Aguirre, J., Sanchez-Almazo, I.M., Dinares-Turell, J., 2006. Testing models for the Messinian salinity crisis: The Messinian record in Almeria, SE Spain. Sedimentary Geology, 188, 131-154.

Brocklehurst, S.H., Whipple, K.X., 2002. Glacial erosion and relief production in the Eastern Sierra Nevada, California. Geomorphology, 42, 1-24.

Brookfield, M.E., 1998. The evolution of the great river systems of southern Asia during the Cenozoic India-Asia collision: rivers draining southwards. Geomorphology, 22, 285-312.

Buforn, E., Udías, A., Mezcua, J., 1988. Seismicity and focal mechanisms in South Spain. Bulletin of the Seismological Society of America, 78, 2008-2024.

Buforn, E., Sanz de Galdeano, C., Udías, A., 1995. Seismotectonics of the Ibero-Maghrebian region. Tectonophysics, 248, 247-261.

Buforn, E., Bezzeghoud, M., UdÍas, A., Pro, C., 2004. Seismic Sources on the Iberia-African Plate Boundary and their Tectonic Implications. Pure and Applied Geophysics, 161, 623-646.

Bull, W.B., McFadden, L., 1977. Tectonic geomorphology North and South of the Garlock fault, California, in: Doering, D.O. (Ed.), Geomorphology in Arid Regions. State University of New York, Binghamton pp. 115-138.

Bull, W.B., 1977. Tectonic geomorphology of the Mojave Desert, California. U.S. Geological Survey Contract Report 14-0-001-G-394. Office of Earthquakes, Volcanoes, and Engineering, Menlo Park, California, p. 188.

Bull, W.B., 2007. Tectonic Geomorphology of Mountains: A New Approach to Paleoseismology. Wiley-Blackwell, Oxford.

Buontempo, L., Bokelmann, G.H.R., Barruol, G., Morales, J., 2008. Seismic anisotropy beneath southern Iberia from SKS splitting. Earth and Planetary Science Letters, 273, 237-250.

Burbank, D.W., Anderson, R.S., 2001. Tectonic Geomorphology. Blackwell Science.

Calvo, M., Vegas, R., Osete, M.L., 1997. Paleomagnetic results from Upper Miocene and Pliocene rocks from the Internal Zone of the eastern Betic Cordilleras (southern Spain). Tectonophysics, 277, 271-283.

Campos, J., Maldonado, A., Campillo, A.C., 1992. Post-Messinian Evolutional Patterns of the Central Alboran Sea. Geo-Marine Letters, 12, 173-178.

Candy, I., Black, S., Sellwood, B.W., 2005. U-series isochron dating of immature and mature calcretes as a basis for constructing Quaternary landform chronologies for the Sorbas basin, southeast Spain. Quaternary Research, 64, 100-111.

Candy, I., Black, S., 2009. The timing of Quaternary calcrete development in semi-arid southeast Spain: Investigating the role of climate on calcrete genesis. Sedimentary Geology, 218, 6-15.

Carminati, E., Wortel, M.J.R., Spakman, W., Sabadini, R., 1998. The role of slab detachment processes in the opening of the western-central Mediterranean basins: some geological and geophysical evidence. Earth and Planetary Science Letters, 160, 651-665.

Clark, M.K., Schoenbohm, L.M., Royden, L.H., Whipple, K.X., Burchfiel, B.C., Zhang, X., Tang, W., Wang, E., Chen, L., 2004. Surface uplift, tectonics, and erosion of eastern Tibet from large-scale drainage patterns. Tectonics, 23, 1-21.

Comas, M.C., García Dueñas, V., Jurado, M.J., 1992. Neogene tectonic evolution of the Alboran Sea from Mcs data. Geo-Marine Letters, 12, 157-164.

Comas, M.C., Dañobeitia, J.J., Alvárez Marrón, J., Soto, J.I., 1997. Crustal reflections and structure in the Alboran Basin. Preliminary results of the ESCI-Alborán survey. Revista de la Sociedad Geológica de España, 8, 529-542.

Comas, M.C., Platt, J.P., Soto, J.I., Watts, A.B., 1999. The origin and tectonic history of the Alborán Basin: insights from Leg 161 results, in: Zahan, R., Comas, M.C., Klaus, A. (Eds.), Proceedings of the Ocean Drilling Program, Scientific Results, pp. 555-579.

Coppier, G., Ott d´Estevou, O., Montenat, C., 1990. Kinematics and paleogeographic evolution of the eastern Almeria basins, in: Montenat, C. (Ed.), Les Bassins Neogenes du Domaine Betique Orientale (Espagne). IGAL, Paris, pp. 189-193.

Coulon, C., Mergatsi, M., Fourcade, S., Maury, R.C., Bellon, H., Louni-Hacini, A., Cotten, J., Coutelle, A., Hermitte, D., 2002. Post-collisional transition from calc-alcaline to alkaline volcanism during the Neogene in Oranie (Algeria): magmatic expression of a slab breakoff. Lithos, 62, 87-110.

Crespo-Blanc, A., Campos, J., 2001. Structure and kinematics of the South Iberian paleomargin and its relationship with the Flysch Trough units: extensional tectonics within the Gibraltar Arc fold-and-thrust belt (western Betics). Journal of Structural Geology, 23, 1615-1630.

Crespo-Blanc, A., de Lamotte, D.F., 2006. Structural evolution of the external zones derived from the Flysch trough and the South Iberian and Maghrebian paleomargins around the Gibraltar arc: A comparative study. Bulletin De La Societe Geologique De France, 177, 267-282.

Crespo Blanc, A., Orozco, M., García-Dueñas, V.,

1994. Extension versus compression during the Miocene tectonic evolution of the Betic chain. Late folding of normal fault systems. Tectonics, 13, 78-88.

Chalouan, A., Michard, A., 1990. The Ghomarides nappes, Rif coastal range, Morocco: a variscan chip in the Alpine belt. Tectonics, 9, 1565-1583.

Chen, Y.C., Sung, Q.C., Cheng, K.Y., 2003. Along-strike variations of morphotectonic features in the Western Foothills of Taiwan: tectonic implications based on stream-gradient and hypsometric analysis. Geomorphology, 56, 109-137.

Dahlstro, C.D.A., 1970. Structural Geology in Eastern Margin of Canadian Rocky-Mountains. American Association of Petroleum Geologists Bulletin, 54, 843-&.

Davis, G.H., Bump, A.P., Garcia, P.E., Ahlgren, S.G., 2000. Conjugate Riedel deformation band shear zones. Journal of Structural Geology, 22, 169-190.

de Jong, G., 1993. The tectono-metamorphic evolution of the Veleta Complex and the development of the contact with the Mulhacen Complex (Betic Zone, SE Spain). Geologie en Mijnbouw, 71, 227-237.

de Jong, K., 2003. Very fast exhumation of high-pressure metamorphic rocks with excess 40Ar and inherited 87Sr, Betic Cordilleras, southern Spain. Lithos, 70, 91-110.

de Larouzière, F.D., Bolze, J., Bordet, P., Hernandez, J., Montenat, C., Ottd´Estevou, P., 1988. The Betic segment of the lithospheric Trans-Alboran shear zone during the Late Miocene. Tectonophysics, 152, 41-52.

Dercourt, J., Zonenshain, L.P., Ricou, L.E., Kazmin, V.G., Le Pichon, X., Knipper, A.L., Grandjacquet, C., Sborshikov, I.M., Geyssant, J., Lepvrier, C., Perchersky, D.H., Boulin, J., Sibuet, J.C., Savostin, L.A., Sorokhtin, O., Westphal, M., Bazhenov, M.L., Lauer, J.P., Biju-Duval, B., 1986. Geologic evolution of the Tethys belt from the Atlantic to the Pamirs since the Lias. Tectonophysics, 123, 241-315.

Déverchère, J., Yelles, K., Domzig, A., de Lepinay, B.M., Bouillin, J.P., Gaullier, V., Bracene, R., Calais, E., Savoye, B., Kherroubi, A., Le Roy, P., Pauc, H., Dan, G., 2005. Active thrust faulting offshore Boumerdes, Algeria, and its relations to the 2003 Mw 6.9 earthquake. Geophysical Research Letters, 32.

Dewey, J.F., Helman, M.L., Turco, E., Hutton, D.H.W., Knott, S.D., 1989. Kinematics of the western Mediterranean., in: Coward, M.P., Dietrich, D., Park, R.G. (Eds.), Alpine Tectonics. Special Publication Geological Society of London, London, pp. 265-283.

Díaz, J., Gallart, J., Villaseñor, A., Mancilla, F., Pazos, A., Córdoba, D., Pulgar, J.A., Ibarra, P., Harnafi, M., 2010. Mantle dynamics beneath the Gibraltar Arc (western Mediterranean) from shear-wave splitting measurements on a dense seismic array. Geophysical Research Letters, 37.

Docherty, C., Banda, E., 1995. Evidence for the eastward migration of the Alboran Sea based on regional subsidence analysis: A case for basin formation by delamination of the subcrustal lithosphere? Tectonics, 14, 804-818.

Domzig, A., Yelles, K., Le Roy, C., Deverchere, J., Bouillin, J.P., Bracene, R., de Lepinay, B.M., Le Roy, P., Calais, E., Kherroubi, A., Gaullier, V., Savoye, B., Pauc, H., 2006. Searching for the Africa-Eurasia Miocene boundary offshore western Algeria (MARADJA'03 cruise). Comptes Rendus Geoscience, 338, 80-91.

Duebendorfer, E.M., Black, R.A., 1992. Kinematic role of transverse structures in continental extension: An example from the Las Vegas Valley shear zone, Nevada. Geology, 20, 1107-1110.

Duggen, S., Hoernle, K., van den Bogaard, P., Rupke, L., Phipps Morgan, J., 2003. Deep roots of the Messinian salinity crisis. Nature, 422, 602-606.

Duggen, S., Hoernle, K., van den Bogaard, P., Harris, C., 2004a. The role of subduction in forming the western Mediterranean and causing the Messinian Salinity Crisis. Earth and Planetary Science Letters, 218, 91-108.

Duggen, S., Hoernle, K., van den Bogaard, P., Harris, C., 2004b. Magmatic evolution of the Alboran region: The role of subduction in forming the western Mediterranean and

causing the Messinian Salinity Crisis. Earth and Planetary Science Letters, 218, 91-108.

Duggen, S., Hoernle, K., Van den Bogaard, P., Garbe-Schonberg, D., 2005. Post-Collisional Transition from Subduction- to Intraplate-type Magmatism in the Westernmost Mediterranean: Evidence for Continental-Edge Delamination of Subcontinental Lithosphere. Journal of Petrology, 46, 1155-1201.

Duggen, S., Hoernle, K., Klügel, A., Geldmacher, J., Thirlwall, M., Hauff, F., Lowry, D., Oates, N., 2008. Geochemical zonation of the Miocene Alborán Basin volcanism (westernmost Mediterranean): geodynamic implications. Contributions to Mineralogy and Petrology, 156, 577-593.

Dula, W.F., 1991. Geometric Models of Listric Normal Faults and Rollover Folds. The American Association of Petroleum Geologists Bulletin, 75, 1609-1625.

Dumont, J.F., Santana, E., Vilema, W., 2005. Morphologic evidence of active motion of the Zambapala Fault, Gulf of Guayaquil (Ecuador). Geomorphology, 65, 223-239.

Durand-Delga, M., Rossi, P., Olivier, P., Puglisi, D., 2000. Situation structurale et nature ophiolitique des roches basiques jurassiques associées aux flyschs maghrébins du Rif (Maroc) et de Sicile (Italie). Comptes Rendus de l'Académie des Sciences de Paris, 331, 29-38.

Echeverria, A., Khazaradze, G., Garate, J., Asensio, E., Masana, E., Suriñach, E., 2011. Present-day GPS crustal deformation rates in the Eastern Betics (SE Spain). In: Abstracts, G.R. (Ed.), EGU General Assembly 2011, Vienna.

El Bakkali, S., Gourgaud, A., Bourdier, J.L., Bellon, H., Gundogdu, N., 1998. Post-collision neogene volcanism of the Eastern Rif (Morocco): magmatic evolution trough time. Lithos, 45, 523-543.

Epard, J.L., Groshong, R.H., 1993. Excess area and depth to detachment. American Association of Petroleum Geologists Bulletin, 77, 1291-1302.

Esteban, J.J., Sanchez-Rodriguez, L., Seward, D., Cuevas, J., Tubia, J.M., 2004. The late thermal history of the Ronda area, southern Spain. Tectonophysics, 389, 81-92.

Faccenna, C., Piromallo, C., Crespo-Blanc, A., Jolivet, L., Rossetti, F., 2004. Lateral slab deformation and the origin of the western Mediterranean arcs. Tectonics, 23, doi:10.1029/2002TC001488.

Faulds, J.E., Varga, R.J., 1998. The role of accommodation zones and transfer zones in the regional segmentation of extended terranes. Special Papers-Geological Society of Aamerica, 1-46.

Faulkner, D.R., Lewis, A.C., Rutter, E.H., 2003. On the internal structure and mechanics of large strike-slip fault zones: field observations of the Carboneras fault in southeastem Spain. Tectonophysics, 367, 235-251.

Favre, P., Stampfli, G., Wildi, W., 1991. Jurassic sedimentary record and tectonic evolution of the northwestern corner of Africa. Palaeogeography, palaeoclimatology, palaeoecology, 87, 53-73.

Fernández-Ibánez, F., Peréz-Peña, J.V., Azor, A., Soto, J.I., Azañón, J.M., 2010. Normal faulting driven by denudational isostatic rebound. Geology, 38, 643-646.

Fernández-Ibáñez, F., Soto, J.I., Zoback, M.D., Morales, J., 2007. Present-day stress field in the Gibraltar Arc (western Mediterranean). Journal of Geophysical Research-Solid Earth, 112.

Fernández, J., Soria, J., Viseras, C., 1996. Stratigraphic architecture of the Neogene basins in the central sector of the Betic Cordillera (Spain): Tectonic control and base-level changes, in: Friend, P.F.D.C.J. (Ed.), Tertiary Basins of Spain: The Stratigraphic Record of Crustal Kinematics. Cambridge University Press, Cambridge, pp. 353-365.

Fortuin, A.R., Krijgsman, W., 2003. The Messinian of the Nijar Basin (SE Spain): sedimentation, depositional environments and paleogeographic evolution. Sedimentary Geology, 160, 213-242.

Fortuin, A.R., Dabrio, C.J., 2008. Evidence for Late Messinian seismites, Nijar Basin, south-east Spain. Sedimentology, 55, 1595-1622.

Galindo-Zaldívar, J., González-Lodeiro, F.,

Jabaloy, A., 1989. Progressive extensional shear structures in a detachment contact in the Western Sierra Nevada (Betic Cordilleras, Spain). Geodinamica Acta, 3, 73-85.

Galindo-Zaldívar, J., Jabaloy, A., González-Lodeiro, F., 1996. Reactivation of the Mecina Detachment in the western sector of Sierra Nevada (Betic Cordilleras, SE Spain). Comptes Rendus de l'Académie des Sciences Series IIa, 323, 615-622.

García-Casco, A., Sánchez-Navas, A., Torres-Roldán, R.L., 1993. Disequilibrium decomposition and breakdown of muscovite in High P-T gneisses, Betic alpine belt (Southern Spain). American Mineralogist, 78, 158-177.

García-Casco, A., Torrés-Roldán, R., 1999. Natural metastable reactions involving garnet, staurolite and cordierite: implications for petrogenetic grids and the extensional collapse of the Betic-Rif belt. Contributions to Mineralogy and Petrology, 136, 131-153.

García-Castellanos, D., Villasenor, A., 2011. Messinian salinity crisis regulated by competing tectonics and erosion at the Gibraltar arc. Nature, 480, 359-U108.

García-Dueñas, V., Martínez-Martínez, J.M., Orozco, M., Soto, J., 1988. Plis-nappes, cisillements syn- à post-métamorphiques et cisaillements ductiles-fragiles en distension dans les Nevado-Filabrides (Cordillères bétiques, Espagne). Comptes Rendus de l'Académie des Sciences de Paris, 307, Série II, 1389-1395.

García-Dueñas, V., Martínez-Martínez, J.M., 1988. Sobre el adelgazamiento mioceno del Dominio Cortical de Alborán, el Despegue Extensional de Filabres (Béticas orientales). Geogaceta, 5, 53-55.

García-Dueñas, V., Balanyá, J.C., Martínez-Martínez, J.M., 1992. Miocene extensional detachments in the outcropping basement of the Northern Alboran Basin (Betics) and their tectonic implications. Geo-Marine Letters, 12, 88-95.

García-Hernández, M., López-Garrido, A.C., Rivas, P., Sanz de Galdeano, C., Vera, J.A., 1980. Mesozoic paleogeographic evolution of the External Zones of the Betic Cordillera. Geologie en Mijnbouw, 59, 155-168.

García, A.F., Zhu, Z., Ku, T.L., Sanz de Galdeano, C., Chadwick, O.A., Montero, J.C., 2003. Tectonically driven landscape development within the eastern Alpujarran Corridor, Betic Cordillera, SE Spain (Almeria). Geomorphology, 50, 83-110.

García, A.F., Zhu, Z., Ku, T.L., Chadwick, O.A., Montero, J.C., 2004. An incision wave in the geologic record, Alpujarran Corridor, southern Spain (Almeria). Geomorphology, 60, 37-72.

Garrido, C.J., Gueydan, F., Booth-Rea, G., Precigout, J., Hidas, K., Padrón-Navarta, J.A., Marchesi, C., 2011. Garnet lherzolite and garnet-spinel mylonite in the Ronda peridotite: Vestiges of Oligocene backarc mantle lithospheric extension in the western Mediterranean. Geology, 39, 927-930.

Giaconia, F., Booth-Rea, G., Martínez-Martínez, J.M., Azañón, J.M., Pérez-Peña, J.V., Pérez-Romero, J., Villegas, I., 2012a. Geomorphic evidence of active tectonics in the Sierra Alhamilla (eastern Betics, SE Spain). Geomorphology, 145-146, 90-106.

Giaconia, F., Booth-Rea, G., Martínez-Martínez, J.M., Azañón, J.M., Pérez-Peña, J.V., 2012b. Geomorphic analysis of the Sierra Cabrera, an active pop-up in the constrictional domain of conjugate strike-slip faults: The Palomares and Polopos fault zones (eastern Betics, SE Spain). Tectonophysics, 580, 27-42.

Giaconia, F., Booth-Rea, G., Martínez-Martínez, J.M., Azañón, J.M., Pérez-Romero, J., Villegas, I., 2013a. Mountain front migration and drainage captures related to fault segment linkage and growth: the Polopos transpressive fault zone (southeastern Betics, SE Spain). Journal of Structural Geology, 46, 76-91.

Giaconia, F., Booth-Rea, G., Martínez-Martínez, J.M., Azañón, J.M., 2013b. Late Miocene Extensional tectonics in the evolution of the eastern Betics, an example from the Neogene-Quaternary Sorbas basin (SE Spain). In: 2013, A.E.R.C. (Ed.), Exploring the Mediterranean: New Concepts In An Ancient Seaway, Barcelona.

Giaconia, F., Booth-Rea, G., Ranero, C.R., Grácia, E., Bartolomé, R., Calahorrano, A., Lo

Iacono, C., Vendrell, M.G., Cameselle, A.L., Costa, S., Gómez de la Peña, L., Martínez-Loriente, S., Perea, H., Miñas, M., Submitted. Compressional tectonic inversion of the Algero–Balearic basin: latemost Miocene to present oblique convergence at the Palomares margin (western Mediterranean). Tectonics.

Gibbs, A.D., 1984. Structural evolution of extensional basin margins. Journal of the Geological Society of London, 141, 609-620.

Gill, R.C.O., Aparicio, A., El Azzouzi, M., Hernandez, J., Thirlwall, M.F., Bourgois, J., Marriner, G.F., 2004. Depleted arc volcanism in the Alboran Sea and shoshonitic volcanism in Morocco: geochemical and isotopic constraints on Neogene tectonic processes. Lithos, 78, 363-388.

Goffé, B., Michard, A., García-Dueñas, V., González-Lodeiro, F., Monié, P., Campos, J., Galindo-Zaldívar, J., Jabaloy, A., Martínez-Martínez, J.M., Simancas, F., 1989. First evidence of high-pressure, low-temperature metamorphism in the Alpujarride nappes, Betic Cordillera (SE Spain). European Journal of Mineralogy, 1, 139-142.

Goldsworthy, M., Jackson, J., 2000. Active normal fault evolution in Greece revealed by geomorphology and drainage patterns. Journal of the Geological Society, 157, 967-981.

Gómez-Pugnaire, M.T., Fernández-Soler, J.M., 1987. High-Pressure metamorphism in metabasite from the Betic Cordilleras (SE Spain) an its evolution during the Alpine orogeny. Contributions to Mineralogy and Petrology, 95, 231-244.

González-Casado, J.M., Casquet, C., Martínez-Martínez, J.M., García-Dueñas, V., 1995. Retrograde evolution of quartz segregations from the Dos Picos shear zone in the Nevado-Filábride Complex (Betic chains, Spain). Evidence from fluid inclusions and quartz c-axis fabrics. Geologische Rundschau, 84, 175-186.

Gràcia, E., Pallàs, R., Soto, J.I., Comas, M., Moreno, X., Masana, E., Santanach, P., Diez, S., García, M., Dañobeitia, J.J., and HITS Team, 2006. Active faulting offshore SE Spain (Alboran Sea): Implications for earthquake hazard assessment in the Southern Iberian Margin. Earth and Planetary Science Letters, 241, 734-749.

Gràcia, E., Ranero, C.R., Bartolome, R., and GASSIS cruise party, 2011. New seismic imaging across the Gibraltar Arc from the Alboran Sea to Gulf of Cadiz (South Iberia): First results of the TOPOMED-GASSIS cruise. In: American Geophysical Union, F.M. (Ed.), Eos Trans AGU, San Francisco (USA).

Gràcia, E., Bartolome, R., Lo Iacono, C., Moreno, X., Stich, D., Martínez-Diaz, J.J., Bozzano, G., Martínez-Loriente, S., Perea, H., Masana, E., Dañobeitia, J.J., Tello, O., Sanz, J.L., Carreño, E., and EVENT-SHELF Team, 2012. Acoustic and seismic imaging of the Adra Fault (NE Alboran Sea): in search of the source of the 1910 Adra earthquake. Natural Hazards and Earth System Sciences, 12, 3255-3267.

Gutscher, M.-A., Dominguez, S., Westbrook, G., Le Roy, P., Rosas, F., Duarte, J.C., Terrinha, P., Miranda, J.M., Graindorge, D., Gailler, A., 2012. The Gibraltar subduction: A decade of new geophysical data. Tectonophysics, 574-575, 72-91.

Gutscher, M.A., Klaeschen, D., Flueh, E., Malavieille, J., 2001. Non-Coulomb wedges, wrong-way thrusting, and natural hazards in Cascadia. Geology, 29, 379-382.

Hack, J.T., 1973. Stream profile analysis and stream-gradient index. Journal of Research of the Us Geological Survey, 1, 421-429.

Harvey, A.M., Wells, S.G., 1987. Response of Quaternary Fluvial Systems to Differential Epeirogenic Uplift - Aguas and Feos River Systems, Southeast Spain. Geology, 15, 689-693.

Harvey, A.M., Miller, S.Y., Wells, S.G., 1995. Quaternary soil and river terrace sequences in the Aguas/Feos river systems: Sorbas basin, southeast Spain. Mediterranean Quaternary River Environments, 263-292.

Harvey, A.M., Foster, G., Hannam, J., Mather, A.E., 2003. The Tabernas alluvial fan and lake system, southeast Spain: applications of mineral magnetic and pedogenic iron oxide analyses towards clarifying the Quaternary sediment sequences. Geomorphology, 50, 151-171.

Haughton, P., 2001. Contained turbidites used to track sea bed deformation and basin migration, Sorbas Basin, south-east Spain. Basin Research, 13, 117-139.

Hernandez, J., de Larouzière, F.D., Bolze, J., Bordet, P., 1987. Le magmatisme Néogène bético-rifain et le couloir de décrochement trans-Alborán. Bulletin De La Societe Geologique De France, (8) III, 257-267.

Hilley, G.E., Arrowsmith, J.R., 2008. Geomorphic response to uplift along the Dragon's Back pressure ridge, Carrizo Plain, California. Geology, 36, 367-370.

Hodgson, D.M., Haughton, P.D.W., 2004. Impact of syndepositional faulting on gravity current behaviour and deep-water stratigraphy: Tabernas-Sorbas Basin, SE Spain. Geological Society, London, Special Publications, 222, 135-158.

Hoernle, K., Duggen, S., Geldmacher, J., Klügel, A., Party, S.B.S., 2003. METEOR Cruise No. 51, Leg 1, Vulkosa: Vulcanismus Ostatlantik-Alboran in Meteor Berichte 03-1 Ostatlantik-Mittelmeer-Schwarzes Meer, Cruise No. 51, 2001. GEOMAR Res. Cent., Kiel, Germany.

Holbrook, J., Schumm, S.A., 1999. Geomorphic and sedimentary response of rivers to tectonic deformation: a brief review and critique of a tool for recognizing subtle epeirogenic deformation in modern and ancient settings. Tectonophysics, 305, 287-306.

Hovius, N., 2000. Macroscale process systems of mountain belt erosion, in: Summerfield, M.A. (Ed.), Geomorphology and Global Tectonics. Wiley and Sons, Chichester, pp. 77-105.

Hsü, K.J., Ryan, W.B.F., Cita, M.B., 1973. Late Miocene desiccation of the Mediterranean. Nature, 242, 240-244.

Hsü, K.J., Montadert, L., Bernoulli, D., Cita, M.B., Erickson, A.L., Garrison, R.E., Kidd, R.B., Melières, F., Múller, C., Wright, R., 1977. History of the Messinian salinity crisis. Nature, 267, 399-403.

Huibregtse, P., van Alebeek, H., Zall, M., Biermann, C., 1998. Paleostress analysis of the northern Nijar and southern Vera basins: constraints for the Neogene displacement history of major strike-slip faults in the Betic Cordilleras, SE Spain. Tectonophysics, 300, 79-101.

Iribarren, L., Vergés, J., Camurri, F., Fullea, J., Fernandez, M., 2007. The structure of the Atlantic–Mediterranean transition zone from the Alboran Sea to the Horseshoe Abyssal Plain (Iberia–Africa plate boundary). Marine Geology, 243, 97-119.

Jackson, J., Leeder, M., 1994. Drainage Systems and the Development of Normal Faults - an Example from Pleasant Valley, Nevada. Journal of Structural Geology, 16, 1041-1059.

Jackson, J., Norris, R., Youngson, J., 1996. The structural evolution of active fault and fold systems in central Otago, New Zealand: evidence revealed by drainage patterns. Journal of Structural Geology, 18, 217-234.

Johnson, C., Harbury, N., Hurford, A.J., 1997. The role of extension in the Miocene denudation of the Nevado-Filábride Complex, Betic Cordillera (SE Spain). Tectonics, 16, 189-204.

Johnson, C., 1997. Resolving denudational histories in orogenic belts with apatite fission-track thermochronology and structural data: An example from southern Spain. Geology, 623-626.

Jolivet, L., Augier, R., Robin, C., Suc, J.-P., Rouchy, J.M., 2006. Lithospheric-scale geodynamic context of the Messinian salinity crisis. Sedimentary Geology, 188-189, 9-33.

Jonk, R., Biermann, C., 2002. Deformation in Neogene sediments of the Sorbas and Vera Basins (SE Spain): constraints on simple-shear deformation and rigid body rotation along major strike-slip faults. Journal of Structural Geology, 24, 963-977.

Keller, E.A., 1986. Investigation of active tectonics: use of surficial earth processes, in: Wallace, R.E. (Ed.), Active Tectonics. National Academy Press, Washington D.C., pp. 136-147.

Keller, E.A., Pinter, N., 2002. Active Tectonics: Earthquakes, Uplift, and Landscape. Prentice Hall, New Jersey.

Keller, J.V.A., Hall, S.H., Dart, C.J., McClay, K.R., 1995. The geometry and evolution

of a transpressional strike-slip system: the Carboneras fault, SE Spain. Journal of the Geological Society of London, 152, 339-351.

Khazaradze, G., Gárate, J., Suriñach, E., Davila, J.M., Asensio, E., 2008. Crustal deformation in south-eastern Betics from CuaTeNeo GPS network. Geo-Temas, 10, 1023-1026.

Kherroubi, A., Deverchere, J., Yelles, A., Mercier de Lepinay, B., Domzig, A., Cattaneo, A., Bracene, R., Gaullier, V., Graindorge, D., 2009. Recent and active deformation pattern off the easternmost Algerian margin, Western Mediterranean Sea: New evidence for contractional tectonic reactivation. Marine Geology, 261, 17-32.

Kobor, J.S., Roering, J.J., 2004. Systematic variation of bedrock channel gradients in the central Oregon Coast Range: implications for rock uplift and shallow landsliding. Geomorphology, 62, 239-256.

Konc, Z., Structure and Composition of the Subcontinental Lithospheric Mantle in Convergent Settings: Insights from mantle xenoliths hosted in alkaline magmatism, Doctoral Thesis, 209, Universidad de Granada, 2013.

Konc, Z., Garrido, C.J., Tommasi, A., Hidas, K., Vauchez, A., Padrón-Navarta, J.A., Acosta-Vigil, A., Szabó, C., Marchesi, C., Submitted. Deformtaion Record, Seismic Properties and Flow of the Shallow Upper Mantle in the Westernmost Mediterranean: Insights from mantle xenoliths in Plio-Pleistocene Alkali Basalts from the eastern Betic Cordillera (SE Spain). Geochemistry Geophysics Geosystems.

Korup, O., 2006. Rock-slope failure and the river long profile. Geology, 34, 45-48.

Krautworst, U.M.R., Brachert, T.C., 2003. Sedimentary facies during early stages of flooding in an extensional basin: the Breche Rouge de Carboneras (Late Miocene, Almeria/SE Spain). International Journal of Earth Sciences, 92, 610-623.

Krijgsman, W., Hilgen, F.J., Raffi, I., Sierro, F.J., Wilson, D.S., 1999. Chronology, causes and progression of the Messinian salinity crisis. Nature, 400, 652-655.

Krijgsman, W., Fortuin, A.R., Hilgen, F.J., Sierro, F.J., 2001. Astrochronology for the Messinian Sorbas basin (SE Spain) and orbital (precessional) forcing for evaporite cyclicity. Sedimentary Geology, 140, 43-60.

Larouzière, F.D., Bolze, J., Bordet, P., Hernandez, J., Montenat, C., Ottd´Estevou, P., 1988. The Betic segment of the lithospheric Trans-Alboran shear zone during the Late Miocene. Tectonophysics, 152, 41-52.

Lave, J., Avouac, J.P., 2001. Fluvial incision and tectonic uplift across the Himalayas of central Nepal. Journal of Geophysical Research-Solid Earth, 106, 26561-26591.

Le Pourhiet, L., Huet, B., May, D.A., Labrousse, L., Jolivet, L., 2012. Kinematic interpretation of the 3D shapes of metamorphic core complexes. Geochemistry Geophysics Geosystems, 13.

Leuchters, W., Grevemeyer, I., Ranero, C.R., Villasenor, A., Booth-Rea, G., Gallart, J., 2011. Seismotectonics and Seismic Structure of the Alboran Sea, Western Mediterranean - Constraints from Local Earthquake Monitoring and Seismic Refraction and Wide-Angle Profiling. In: Union, A.G. (Ed.), Fall Meeting 2011,

Li, Q., Ruano, P., Pedrera, A., Galindo-Zaldívar, J., 2012. Estructura de la cuenca sedimentaria de Tabernas-Sorbas mediante prospección gravimétrica y magnética (Zonas Internas, Cordillera Bética Oriental). Geogaceta, 52, 117-120.

Lis Mancilla, F.d., Stich, D., Berrocoso, M., Martín, R., Morales, J., Fernandez-Ros, A., Páez, R., Pérez-Peña, A., 2013. Delamination in the Betic Range: Deep structure, seismicity, and GPS motion. Geology, 41, 307-310.

Lonergan, L., 1993. Timing and Kinematics of deformation in the Malaguide Complex, Internal Zone of the Betic Cordillera, Southeast Spain. Tectonics, 12, 460-476.

Lonergan, L., Mangerajetzky, M.A., 1994. Evidence for Internal Zone Unroofing from Foreland Basin Sediments, Betic Cordillera, Se Spain. Journal of Structural Geology, 151, 515-529.

Lonergan, L., Platt, J., 1995. The Malaguide-Alpujarride boundary: a major extensional contact in the Internal Zone of the eastern Betic Cordillera, SE Spain. Journal of Structural Geology, 17, 1665-1671.

Lonergan, L., White, N., 1997. Origin of the Betic-Rif mountain belt. Tectonics, 16, 504-522.

Lonergan, L., Johnson, C., 1998. Reconstructing orogenic exhumation histories using synorogenic detrital zircons and apatites: an example from the Betic Cordillera, SE Spain. Basin Research, 10, 353-364.

López Sánchez-Vizcaíno, V., Rubatto, D., Gómez-Pugnaire, M.T., Trommsdorff, V., Müntener, O., 2001. Middle Miocene high-pressure metamorphism and fast exhumation of the Nevado-Filábride complex, SE Spain. Terra Nova, 13, 327-332.

Luján, M., Storti, F., Balanyá, J.C., Crespo-Blanc, A., Rossetti, F., 2003. Role of decollement material with different rheological properties in the structure of the Aljibe thrust imbricate (Flysch Trough, Gibraltar Arc): an analogue modelling approach. Journal of Structural Geology, 25, 867-881.

Luján, M., Crespo-Blanc, A., Balanyá, J.C., 2006. The Flysch Trough thrust imbricate (Betic Cordillera): A key element of the Gibraltar Arc orogenic wedge. Tectonics, 25.

Maher, E., Harvey, A.M., France, D., 2007. The impact of a major Quaternary river capture on the alluvial sediments of a beheaded river system, the Rio Alias SE Spain. Geomorphology, 84, 344-356.

Maillard, A., Mauffret, A., 2013. Structure and present-day compression in the offshore area between Alicante and Ibiza Island (Eastern Iberian Margin). Tectonophysics, 591, 116-130.

Malekzade, Z., Abbassi, M.R., Bellier, O., Authemayou, C., 2007. Strain Partitioning in West-Central Zagros Fold and Thrust Belt: Implication for Seismic Hazard Analysis. Journal of Seismology and Earthquakes Engineering, 9, 85-98.

Marchesi, C., Garrido, C.J., Bosch, D., Bodinier, J.L., Hidas, K., Padrón-Navarta, J.A., Gervilla, F., 2012. A Late Oligocene Suprasubduction Setting in the Westernmost Mediterranean Revealed by Intrusive Pyroxenite Dikes in the Ronda Peridotite (Southern Spain). Journal of Geology, 120, 237-247.

Marín-Lechado, C., Galindo-Zaldivar, J., Rodriguez-Fernandez, L.R., Serrano, I., Pedrera, A., 2005. Active faults, seismicity and stresses in an internal boundary of a tectonic arc (Campo de Dalias and Nijar, southeastern Betic Cordilleras, Spain). Tectonophysics, 396, 81-96.

Martín, J.M., Braga, J.C., Riding, R., 1993. Siliciclastic stromatolites and thrombolites, late Miocene, SE Spain. Journal of Sedimentary Research, 63.

Martín, J.M., Braga, J.C., 1994. Messinian events in the Sorbas Basin in southeastern Spain and their implications in the recent history of the Mediterranean. Sedimentary Geology, 90, 257-268.

Martín, J.M., Braga, J.C., Betzler, C., 2003. Late Neogene-Recent uplift of the Cabo de Gata volcanic province, Almeria, SE Spain. Geomorphology, 50, 27-42.

Martínez-Díaz, J.J., 2002. Stress field variation related to fault interaction in a reverse oblique-slip fault: the Alhama de Murcia fault, Betic Cordillera, Spain. Tectonophysics, 356, 291-305.

Martínez-Díaz, J.J., Rigo, A., Luis, L., Capote, R., Hernández-Enrile, J.L., Carreño, E., Tsige, M., 2002. Caracterización geológica y sismotectónica del terremoto de Mula (febrero de 1999, Mb: 4,8) mediante la utilización de datos geológicos, sismológicos y de interferometría de RADAR (INSAR). Boletín Geológico y Minero, 113, 22-33.

Martínez-Díaz, J.J., Hernández-Enrile, J.L., 2004. Neotectonics and morphotectonics of the southern Almería region (Betic Cordillera-Spain) kinematic implications. International Journal of Earth Sciences, 93, 189-206.

Martínez-García, P., Comas, M., Soto, J.I., Lonergan, L., Watts, A.B., 2013. Strike-slip tectonics and basin inversion in the WesternMediterranean: the Post-Messinian evolution of the Alboran Sea. Basin Research,

25, 1-27.

Martínez-Martínez, J.M., 1986. Evolución tectóno-metamórfica del Complejo Nevado-Filábride en el sector de unión entre Sierra Nevada y Sierra de los Filabres (Cordilleras Béticas). Cuadernos de Geología beríca, 13, 1-194.

Martínez-Martínez, J.M., Soto, J.I., Balanyá, J.C., 1997. Crustal decoupling and intracrustal flow beneath domal exhumed core complexes, Betic (SE Spain). Terra Nova, 9, 223-227.

Martínez-Martínez, J.M., Azañón, J.M., 1997. Mode of extensional tectonics in the southeastern Betics (SE Spain). Implications for the tectonic evolution of the peri-Alborán orogenic system. Tectonics, 16, 205-225.

Martínez-Martínez, J.M., Soto, J.I., Balanyá, J.C., 2002. Orthogonal folding of extensional detachments: structure and origin of the Sierra Nevada elongated dome (Betics, SE Spain). Tectonics, 21, 3-1–3-20.

Martínez-Martínez, J.M., Soto, J.I., Balanyá, J.C., 2004. Elongated domes in extended orogens: A mode of mountain uplift in the Betics (Southeast Spain), in: Whitney, D.L., Teyssier, C., Siddoway, C.S. (Eds.), Gneiss domes in orogeny. Geological Society of America Special Paper, Boulder, Colorado, pp. 243-266.

Martínez-Martínez, J.M., 2006. Lateral interaction between metamorphic core complexes and less-extended, tilt-block domains: the Alpujarras strike-slip transfer fault zone (Betics, SE Spain). Journal of Structural Geology, 28, 602-620.

Martínez-Martínez, J.M., Booth-Rea, G., Azañón, J.M., Torcal, F., 2006. Active transfer fault zone linking a segmented extensional system (Betics, southern Spain): Insight into heterogeneous extension driven by edge delamination. Tectonophysics, 422, 159-173.

Masana, E., Martínez-Díaz, J.J., Hernández-Enrile, J.L., Santanach, P., 2004. The Alhama de Murcia fault (SE Spain), a seismogenic fault in a diffuse plate boundary: Seismotectonic implications for the Ibero-Magrebian region. Journal of Geophysical Research, 109.

Masana, E., Pallas, R., Perea, H., Ortuno, M., Martínez-Díaz, C., García-Meléndez, E., Santanach, P., 2005. Large Holocene morphogenic earthquakes along the Albox fault, Betic Cordillera, Spain. Journal of Geodynamics, 40, 119-133.

Mather, A.E., Cenozoic drainage evolution of the Sorbas Basin, SE Spain., Doctoral Thesis, 276, University of Liverpool, 1991.

Mather, A.E., 1993. Basin inversion: some consequences for drainage evolution and alluvial architecture. Sedimentology, 40, 1069-1089.

Mather, A.E., 2000a. Impact of headwater river capture on alluvial system development: an example from the Plio-Pleistocene of the Sorbas Basin, SE Spain. Journal of the Geological Society, 157, 957-966.

Mather, A.E., 2000b. Adjustment of a drainage network to capture induced base-level change: an example from the Sorbas Basin, SE Spain. Geomorphology, 34, 271-289.

Mather, A.E., Harvey, A.M., Stokes, M., 2000. Quantifying long-term catchment changes of alluvial fan systems. Geological Society of America Bulletin, 112, 1825-1833.

Mather, A.E., Stokes, A., Griffiths, J.S., 2002. Quaternary landscape evolution: A framework for understanding contemporary erosion, southeast Spain. Land Degradation & Development, 13, 89-109.

Mauffret, A., Maldonado, A., Campillo, A.C., 1992. Tectonic Framework of hte Easter Alboran and West Algerian Basins, Western Mediterranean. Geo-Marine Letters, 12, 104-110.

Mauffret, A., Frizon de Lamotte, D., Lallemant, S., Gorini, C., Maillard, A., 2004. E-W opening of the Algerian Basin (Western Mediterranean). Terra Nova, 16, 257-264.

Mauffret, A., Ammar, A., Gorini, B., Jabour, H., 2007. The Alboran Sea (Western Mediterranean) revisited with a view from the Moroccan Margin. Terra Nova, 19, 195-203.

Mauffret, A., 2007. The Northwestern (Maghreb) boundary of the Nubia (Africa) Plate. Tectonophysics, 429, 21-44.

Mayer, L., 1986. Tectonic geomorphology of

escarpments and mountain fronts, in: Wallace, R.E. (Ed.), Active Tectonics. National Academy Press, Washington DC, pp. 125-135.

Mazzoli, S., Helman, M., 1994. Neogene patterns of relative plate motion for Africa-Europe: some implications for recent central Mediterranean tectonics. Geologische Rundschau, 83, 464-468.

McClay, K., Khalil, S., 1998. Extensional hard linkages, eastern Gulf of Suez, Egypt. Geology, 26, 563-566.

McClusky, S., Reilinger, R., Mahmoud, S., Ben Sari, D., Tealeb, A., 2003. GPS constraints on Africa (Nubia) and Arabia plate motions. Geophysical Journal International, 155, 126-138.

MEDIMAP GROUP, Loubrieu, B., Mascle, J., 2008. Morpho-bathymetry of the Mediterranean Sea, Map CIESM edition.

Meijninger, B.M.L., Vissers, R.L.M., 2006. Miocene extensional basin development in the Betic Cordillera, SE Spain revealed through analysis of the Alhama de Murcia and Crevillente Faults. Basin Research, 18, 547-571.

Menéndez, I., Silva, P.G., Martín-Betancor, M., Pérez-Torrado, F.J., Guillou, H., Scaillet, S., 2008. Fluvial dissection, isostatic uplift, and geomorphological evolution of volcanic islands (Gran Canaria, Canary Islands, Spain). Geomorphology, 102, 189-203.

Merrits, D., Vincent, K., 1989. Geomorphic response of coastal streams to low, intermediate, and high rates of uplift, Medocino triple junction region, northern California. Geological Society of America Bulletin, 101, 1373-1388.

Michard, A., Goffé, B., Bouybaouene, M.L., Saddiqi, O., 1997. Late Hercynian-Mesozoic thinning in the Alboran domain: metamorphic data from the northern Rif, Morocco. Terra Nova, 9, 171-174.

Miller, K.G., Mountain, G.S., Wright, J.D., Browning, J.V., 2011. A 180-Million-Year Record of Sea Level and Ice Volume Variations from Continental Margin and Deep-Sea Isotopic Records. Oceanography, 24, 40-53.

Molin, P., Pazzaglia, F.J., Dramis, F., 2004. Geomorphic expression of active tectonics in a rapidly-deforming forearc, sila massif, calabria, southern Italy. American Journal of Science, 304, 559-589.

Montenat, C., Ott d´Estevou, P., de La Chapelle, G., 1990. Le bassin de Nijar-Carboneras et el couloir du Bas-Andarax, in: Montenat, C. (Ed.), Les bassins Neogenes du Domaine Betique Oriental (Espagne), Paris, pp. 129-164.

Montenat, C., Ott d´Estevou, P., 1990. Easten betic Neogene Basins-A review, in: Montenat, C. (Ed.), Les Bassins Neogenes du Domaine Bétique Orientale (Espagne). Documents et Travaux IGAL, pp. 9-15.

Morel, J.L., Meghraoui, M., 1996. Goringe-Alboran-Tell tectonic zone: A transpression system along the Africa-Eurasia plate boundary. Geology, 24, 755-758.

Moreno, X., Masana, E., Gràcia, E., Bartolome, C., Piqué-Serra, O., 2008. Estudio paleosismológico de la Falla de Carboneras: Evidencias tierra-mar de actividad tectónica reciente. GeoTemas, 10, 1035-1038.

Muñoz, A., Ballesteros, M., Montoya, I., Rivera, J., Acosta, J., Uchupi, E., 2008. Alboran Basin, southern Spain—Part I: Geomorphology. Marine and Petroleum Geology, 25, 59-73.

Nash, D.J., Smith, R.F., 1998. Multiple calcrete profiles in the Tabernas Basin, southeast Spain: Their origins and geomorphic implications. Earth Surface Processes and Landforms, 23, 1009-1029.

Necea, D., Fielitz, W., Matenco, L., 2005. Late Pliocene-Quaternary tectonics in the frontal part of the SE Carpathians: Insights from tectonic geomorphology. Tectonophysics, 410, 137-156.

Negro, F., Agard, P., Goffe, B., Saddiqi, O., 2007. Tectonic and metamorphic evolution of the Temsamane units, External Rif (northern Morocco): implications for the evolution of the Rif and the Betic-Rif arc. Journal of the Geological Society, 164, 829-842.

Nieto, F., Velilla, N., Peacor, D.R., Ortega-Huertas,

M., 1994. Regional retrograde alteration of sub-greenschist facies chlorite to smectite. Contributions to Mineralogy and Petrology, 115, 243-252.

Nijhuis, H.J., Plurifacial alpine metamorphism in the southeastern Sierra de los Filabres, South of Lubrín, SE Spain, Doctoral Thesis, Univ. Amsterdam, 1964.

Nocquet, J.-M., Calais, E., 2004. Geodetic measurements of crustal deformation in the Western Mediterranean and Europe, Geodynamics of Azores-Tunisia. Springer, pp. 661-681.

O'Callaghan, J.F., Mark, D.M., 1984. The Extraction of Drainage Networks from Digital Elevation Data. Computer Vision Graphics and Image Processing, 28, 323-344.

Ollier, C., 1981. Tectonics and Landforms. Longman, London.

Ott d'Estevou, P., Montenant, C., 1990. Le Bassin de Sorbas-Tabernas, in: Montenant, C. (Ed.), Les Bassins Neogenes du Domaine Bétique Oriental (Espagne). IGAL, CNRS, Paris, pp. 101-128.

Ott d´Estevou, P., Montenat, C., 1985. Evolution structurale de la zone bétique orientale (Espagne) du Tortonien à l´Holocène. Comptes Rendus de l'Académie des Sciences, 300, 363-368.

Ott d´Estevou, P., Montenat, C., Alvado, J.C., 1990. Le Bassin de Vera - Garrucha, in: Montenat, C. (Ed.), Les Bassins Neogenes du Domaine Betique Oriental (Espagne). IGAL, Paris, pp. 165-187.

Ouchi, S., 1985. Response of alluvial rivers to slow active tectonic movement. Geological Society of America Bulletin, 96, 504-515.

Padrón-Navarta, J.A., López Sánchez-Vizcaíno, V., Garrido, C.J., Gómez-Pugnaire, M.T., 2011. Metamorphic Record of High-pressure Dehydration of Antigorite Serpentinite to Chlorite Harzburgite in a Subduction Setting (Cerro del Almirez, Nevado–Filábride Complex, Southern Spain). Journal of Petrology, 52, 2047-2078.

Pedrera, A., Marín-Lechado, C., Galindo-Zaldívar, J., Rodríguez-Fernández, L.R., Ruiz-Constán, A., 2006. Fault and fold interaction during the development of the Neogene-Quaternary Almería-Níjar basin (SE Betic Cordilleras). Tectonics of the Western Mediterranean and North Africa, 262, 217-230.

Pedrera, A., Galindo-Zaldivar, J., de Galdeano, C.S., Lopez-Garrido, A.C., 2007. Fold and fault interactions during the development of an elongated narrow basin: The Almanzora Neogene-Quaternary Corridor (SE Betic Cordillera, Spain). Tectonics, 26, -.

Pedrera, A., Galindo-Zaldivar, J., Ruiz-Bustos, A., Rodriguez-Fernandez, J., Ruiz-Constan, A., 2009a. The role of small-scale fold and fault development in seismogenic zones: example of the western Huercal-Overa Basin (eastern Betic Cordillera, Spain). Journal of Quaternary Science, 24, 581-592.

Pedrera, A., Pérez-Peña, J.V., Galindo-Zaldívar, J., Azañón, J.M., Azor, A., 2009b. Testing the sensitivity of geomorphic indices in areas of low-rate active folding (eastern Betic Cordillera, Spain). Geomorphology, 105, 218-231.

Pedrera, A., Galindo-Zaldivar, J., Marin-Lechado, C., Garcia-Tortosa, F.J., Ruano, P., Garrido, A.C.L., Azanon, J.M., Pelaez, J.A., Giaconia, F., 2012. Recent and active faults and folds in the central-eastern Internal Zones of the Betic Cordillera. Journal of Iberian Geology, 38, 191-208.

Perea, H., Gràcia, E., Alfaro, P., Bartolomé, R., Lo Iacono, C., Moreno, X., Masana, E., Team, E.-S., 2012. Quaternary active tectonic structures in the offshore Bajo Segura basin (SE Iberian Peninsula - Mediterranean Sea). Natural Hazards and Earth System Sciences, 12, 3151-3168.

Pérez-Peña, J.V., Azañón, J.M., Booth-Rea, G., Azor, A., Delgado, J., 2009a. Differentiating geology and tectonics using a spatial autocorrelation thechnique for the hypsometric integral. Journal of Geophysical Research, 114, 1-15.

Pérez-Peña, J.V., Azañón, J.M., Azor, A., 2009b. CalHypso: An ArcGIS extension to calculate hypsometric curves and their statistical moments. Applications to drainage basin analysis in SE Spain. Computers &

Geosiences, 35, 1214-1223.

Pérez-Peña, J.V., Azañón, J.M., Azor, A., Delgado, J., Gonzalez-Lodeiro, F., 2009c. Spatial analysis of stream power using GIS: SLk anomaly maps. Earth Surface Processes and Landforms, 34, 16-25.

Pérez-Peña, J.V., Azor, A., Azañon, J.M., Keller, E.A., 2010. Active tectonics in the Sierra Nevada (Betic Cordillera, SE Spain): Insights from geomorphic indexes and drainage pattern analysis. Geomorphology, 119, 74-87.

Pesquer, D.A., Grevemeyer, I., Ranero, C.R., Gallart, J., 2008. Seismic structure of the passive continental margin of SE Spain and the SW Balearic promontory, western Mediterranean sea. In: Transactions, E. (Ed.), AGU Fall Meeting 2008,

Piller, W.E., Harzhauser, M., Mandic, O., 2007. Miocene Central Paratethys stratigraphy - current status and future directions. Stratigraphy, 4, 151-168.

Platt, J.P., Van der Eeckhout, B., Janzen, E., Konert, G., Simon, O.J., Weijermars, R., 1983. The structure and tectonic evolution of the Aguilón fold-nappe, Sierra Alhamilla, Betic Cordilleras, SE Spain. Journal of Structural Geology, 5, 519-535.

Platt, J.P., Behrmann, J.H., 1986. Structures and fabrics in a crustal-scale shear zone, Betic Cordilleras, SE Spain. Journal of Structural Geology, 5, 519-538.

Platt, J.P., Vissers, R.L.M., 1989. Extensional collapse of thickened continental lithosphere: A working hipothesis for the Alboran Sea and Gibraltar Arc. Geology, 17, 540-543.

Platt, J.P., Allerton, S., Kirker, A., Platzman, E., 1995. Origin of the Western Subbetic Arc (South Spain) - Paleomagnetic and Structural Evidence. Journal of Structural Geology, 17, 765-775.

Platt, J.P., Allerton, S., Kirker, A., Mandeville, C., Mayfield, A., Platzman, E.S., Rimi, A., 2003. The ultimate arc: Differential displacement, oroclinal bending, and vertical axis rotation in the External Betic-Rif arc. Tectonics, 22, pp. 29.

Platt, J.P., Anczkiewicz, R., Kelley, S.P., Soto, J.I., Thirlwall, M., 2004. Two phases of continental subduction in the Betic orogen, Western Mediterranean. Geological Society of America Annual Meeting, Denver.

Platt, J.P., Kelley, S.P., Carter, A., Orozco, M., 2005. Timing of tectonic events in the Alpujárride Complex, Betic Cordillera, southern Spain. Journal of the Geological Society of London, 162, 1-12.

Platt, J.P., Anczkiewicz, R., Soto, J.I., Kelley, S.P., Thirlwall, M., 2006. Early Miocene continental subduction and rapid exhumation in the western Mediterranean. Geology, 34, 981-984.

Polyak, B.G., Fernandez, M., Khutorskoy, M.D., Soto, J.I., Basov, I.A., Comas, M.C., Khain, V.Y., Alonso, B., Agapova, G.V., Mazurova, I.S., Negredo, A., Tochitsky, V.O., delaLinde, J., Bogdanov, N.A., Banda, E., 1996. Heat flow in the Alboran Sea, western Mediterranean. Tectonophysics, 263, 191-218.

Puga, E., Díaz de Federico, A., Nieto, J.M., 2002. Tectonostratigraphic subdivision and petrological characterisation of the deepest complexes of the Betic zone: a review. Geodinamica Acta, 15, 23-43.

Ramsey, L.A., Walker, R.T., Jackson, J., 2008. Fold evolution and drainage development in the Zagros mountains of Fars province, SE Iran. Basin Research, 20, 23-48.

Ranalli, G., 1995. Rheology of the Earth, Second edition ed. Chapman & Hall.

Reicherter, K.R., Reiss, S., 2001. The Carboneras Fault Zone (Southeastern Spain) revisited with ground penetrating radar - Quaternary structural styles from high-resolution images. Geologie en Mijnbouw - Netherlands Journal of Geosciences, 80, 129-138.

Riding, R., Braga, J.C., Martín, M.J., Sánchez Almazo, I.M., 1998. Mediterranean Messinian Salinity Crisis: constraints from a coeval marginal basin, Sorbas, southeastern Spain. Marine Geology, 146, 1-20.

Rockwell, T.K., Keller, E.A., Johnson, D.L., 1984. Tectonic Gemorphology of alluvial fans and mountain fronts near Ventura, California. , in: Morisawa, M., Hack, T.J. (Eds.), Tectonic

Geomorphology State University of New York, Binghamton, pp. 183-207.

Rodriguez-Fernandez, J., Sanz de Galdeano, C., Serrano, F., 1990. Le Couloir des Alpujarras, in: Montenat, C. (Ed.), Les Bassins Neogenes du Domaine Bétique Oriental (Espagne). IGAL, CNRS, Paris, pp. 87-100.

Rodríguez-Fernández, J., Sanz de Galdeano, C., 2006. Late orogenic intramontane basin development: the Granada basin, Betics (southern Spain). Basin Research, 18, 85-102.

Rodríguez-Fernández, J., Roldán, F.J., Azañón, J.M., García-Cortés, A., In Press. El colapso gravitacional del frente orogénico alpino en el Dominio Subbético durante el Mioceno medio-superior: el complejo extensional subbético. Boletín Geológico y Minero de España.

Rodríguez Fernández, J., Comas, M.C., Soria, J., Martín Pérez, J.A., Soto, J.I., 1999. The Sedimentary Record of the Alboran Basin: an Attempt at Sedimentary Sequence Correlation and Subsidence Analysis, in: Zahn, R., Comas, M.C., Klaus, A. (Eds.), Proceedings of the Ocean Drilling Program, Scientific Results, pp. 69-76.

Rosenbaum, G., Lister, G.S., Duboz, C., 2002. Relative motions of Africa, Iberia and Europe during Alpine Orogeny. Tectonophysics, 359, 117-129.

Rouchy, J.M., Taberner, C., Blancvalleron, M.M., Sprovieri, R., Russell, M., Pierre, C., Distefano, E., Pueyo, J.J., Caruso, A., Dinaresturell, J., Gomiscoll, E., Wolff, G.A., Cespuglio, G., Ditchfield, P., Pestrea, S., Combourieunebout, N., Santisteban, C., Grimalt, J.O., 1998. Sedimentary and Diagenetic Markers of the Restriction in a Marine Basin - The Lorca Basin (Se Spain) During the Messinian. Sedimentary Geol., 121, 23-55.

Ruegg, G., 1964. Geologische onderzoekingen in het bekken van Sorbas, S Spanje. Amsterdan Geological Institute, Univ. of Amsterdan.

Rutter, E.H., Faulkner, D.R., Burgess, R., 2012. Structure and geological history of the Carboneras Fault Zone, SE Spain: Part of a stretching transform fault system. Journal of Structural Geology, 1-19.

Salvini, F., Billi, A., Wise, D.U., 1999. Strike-slip fault-propagation cleavage in carbonate rocks: the Mattinata Fault Zone, Southern Apennines, Italy. Journal of Structural Geology, 21, 1731-1749.

Sallarès, V., Gailler, A., Gutscher, M.-A., Graindorge, D., Bartolomé, R., Gràcia, E., Díaz, J., Dañobeitia, J.J., Zitellini, N., 2011. Seismic evidence for the presence of Jurassic oceanic crust in the central Gulf of Cadiz (SW Iberian margin). Earth and Planetary Science Letters, 311, 112-123.

Sanz de Galdeano, C., Rodriguez-Fernandez, J., López-Garrido, A.C., 1985. A strike-slip fault corridor within the Alpujarras Mountains (Betic Cordilleras, Spain). Geologische Rundschau, 74, 641-655.

Sanz de Galdeano, C., 1987. Strike-slip faults in the Southern border of the Vera Basin (Almeria, Betic Cordilleras). Estudios geológicos, 39, 157-165.

Sanz de Galdeano, C., Shanov, S., Galindo-Zaldivar, J., Radulov, A., Nikolov, G., 2010. A new tectonic discontinuity in the Betic Cordillera deduced from active tectonics and seismicity in the Tabernas Basin. Journal of Geodynamics, 50, 57-66.

Sanz de Galdeano, C., García-Tortosa, F.J., Peláez, J.A., Alfaro, P., Azañón, J.M., Galindo-Zaldívar, J., López Casado, C., López Garrido, A.C., Rodríguez-Fernández, J., Ruano, P., 2012. Main active faults in the Granada and Guadix-Baza Basins (Betic Cordillera). Journal of Iberian Geology, 38, 209-223.

Scotney, P., Burgess, R., Rutter, E.H., 2000. 40Ar/39Ar age of the Cabo de Gata volcanic series and displacements on the Carboneras fault zone, SE Spain. Journal of the Geological Society of London, 157, 1003-1008.

Schumm, S., Dumont, J., Holbrook, J., 2000. Active Tectonics and Alluvial Rivers. Cambridge University Press, Cambridge.

Seeber, L., Gornitz, V., 1983. River Profiles Along the Himalayan Arc as Indicators of Active Tectonics. Tectonophysics, 92, 335-367.

Serpelloni, E., Vannucci, G., Pondrelli, S., Argnani, A., Casula, G., Anzidei, M., Baldi,

P., Gasperini, P., 2007. Kinematics of the Western Africa-Eurasia plate boundary from focal mechanisms and GPS data. Geophysical Journal International, 169, 1180-1200.

Sibson, R.H., 1986. Rupture interaction with fault jogs, in: Das, S., Boatwright, J. (Eds.), Earthquake Source Mechanics. American Geophysical Union Monograph, pp. 157-167.

Sierro, F.J., Hilgen, F.J., Krijgsman, W., Flores, J.A., 2001. The Abad composite (SE Spain): a Messinian reference section for the Mediterranean and the APTS. Palaeogeography, palaeoclimatology, palaeoecology, 168, 141-169.

Silva, P.G., Goy, J.L., Zazo, C., Bardaji, T., 2003. Fault-generated mountain fronts in southeast Spain: geomorphologic assessment of tectonic and seismic activity. Geomorphology, 50, 203-225.

Simon, O.J., Geological investigations in the Sierra de Almagro, southeastern Spain., Doctoral Thesis, 164 p, Amsterdam University, 1963.

Small, E.E., Anderson, R.S., 1995. Geomorphically Driven Late Cenozoic Rock Uplift in the Sierra-Nevada, California. Science, 270, 277-280.

Snyder, N.P., Whipple, K.X., Tucker, G.E., Merritts, D.J., 2000. Landscape response to tectonic forcing: Digital elevation model analysis of stream profiles in the Mendocino triple junction region, northern California. Geological Society of America Bulletin, 112, 1250-1263.

Soto, J.I., Estructura y evolución metamórfica del Complejo Nevado-Filábride en la terminación oriental de la Sierra de los Filabres (Cordilleras Béticas), Doctoral Thesis, Univ. de Granada, 1991.

Soto, J.I., Comas, M.C., Azañón, J.M., Martínez-Martínez, J.M., Sánchez-Gómez, M., Party, B.c.T.-L.S., 2000. Structure of the Palomares and Mazarron Margins (SE Spain). In: Commission, I.O. (Ed.), International Conference and Eight Post-Cruise Meeting of the Training-Trough-Research Programme, Granada, Spain.

Soto, J.I., Fernández-Ibáñez, F., Fernandez, M., García-Casco, A., 2008. Thermal structure of the crust in the Gibraltar Arc: Influence on active tectonics in the western Mediterranean. Geochemistry Geophysics Geosystems, 9.

Stapel, G., Moeys, R., Biermann, C., 1996. Neogene evolution of the Sorbas basin (SE Spain) determined by paleostress analysis. Tectonophysics, 255, 291-305.

Stich, D., Ammon, C.J., Morales, J., 2003a. Moment tensor solutions for small and moderate earthquakes in the Ibero-Maghreb region. Journal of Geophysical Research, 108, 20.

Stich, D., Batllo, J., Morales, J., Macia, R., Dineva, S., 2003b. Source parameters of the M-W=6.1 1910 Adra earthquake (southern Spain). Geophysical Journal International, 155, 539-546.

Stich, D., Serpelloni, E., de Lis Mancilla, F., Morales, J., 2006. Kinematics of the Iberia-Maghreb plate contact from seismic moment tensors and GPS observations. Tectonophysics, 426, 295-317.

Stokes, M., Mather, A.E., 2000. Response of Plio-Pleistocene alluvial systems to tectonically induced base-level changes, Vera Basin, SE Spain. Journal of the Geological Society of London, 157, 303-316.

Stokes, M., Mather, A.E., Belfoul, A., Farik, F., 2008. Active and passive tectonic controls for transverse drainage and river gorge development in a collisional mountain belt (Dades Gorges, High Atlas Mountains, Morocco). Geomorphology, 102, 2-20.

Stokes, M., 2008. Plio-Pleistocene drainage development in an inverted sedimentary basin: Vera basin, Betic Cordillera, SE Spain. Geomorphology, 100, 193-211.

Strahler, A.N., 1952. Hypsometric (Area-Altitude) Analysis of Erosional Topography. Geological Society of America Bulletin, 63, 1117-1142.

Strzerzynski, P., Deverchere, J., Cattaneo, A., Domzig, A., Yelles, K., de Lepinay, B.M., Babonneau, N., Boudiaf, A., 2010. Tectonic inheritance and Pliocene-Pleistocene inversion of the Algerian margin around Algiers: Insights from multibeam and seismic reflection data

(vol 8, TC2008, 2010). Tectonics, 29.

Sylvester, A.G., 1988. Strike-slip faults. Geological Society of America Bulletin, 100, 1666-1703.

Tubía, J.M., Gil Ibarguchi, J.I., 1991. Eclogites of the Ojén nappe: a record of subduction in the Alpujárride complex (Betic Cordilleras, southern Spain). Journal of the Geological Society of London, 148, 801-804.

Tubía, J.M., Cuevas, J., Navarro-Vilá, F., Alvarez, F., Aldaya, F., 1992. Tectonic evolution of the Alpujárride Complex (Betic Cordillera, Southern Spain). Journal of Structural Geology, 14, 193-203.

Turner, S.P., Platt, J.P., George, R.M.M., Kelley, S.P., Pearson, D.G., Nowell, G.M., 1999. Magmatism Associated with Orogenic Collapse of the Betic-Alboran Domain, Se Spain. Journal of Petrology, 40, 1011-1036.

van der Beek, P., Champel, B., Mugnier, J.L., 2002. Control of detachment dip on drainage development in regions of active fault-propagation folding. Geology, 30, 471-474.

Vázquez, M., Jabaloy, A., Barbero, L., Stuart, F.M., 2011. Deciphering tectonic- and erosion-driven exhumation of the Nevado–Filábride Complex (Betic Cordillera, Southern Spain) by low temperature thermochronology. Terra Nova, 23, 257-263.

Vázquez, M., Asebriy, L., Azimousa, A., Jabaloy, A., Booth-Rea, G., Barbero, L., Mellini, M., González-Lodeiro, F., In press. Evidence of extensional metamorphism associated to Cretaceous rifting of the North-Maghrebian passive margin: The Tanger-Ketama Unit (External Rif, northern Morocco). Geologica Acta, 11.

Vera, J.A., 2001. Evolution of the South Iberian Continental Margin. Peri-Tethys Memoir 6: Peri-Tethyan Rift/Wrench Basins and Passive Margins, 186, 109-143.

Vernant, P., Chery, J., 2006. Mechanical modelling of oblique convergence in the Zagros, Iran. Geophysical Journal International, 165, 991-1002.

Völk, H.R., Geologie et stratigraphie du Bassin Neogene de Vera, Doctoral Thesis, 121, Amsterdam University, 1966.

Völk, H.R., 1967. Relations between Neogene sedimentation and late orogenic movements in the Eastern Betic Cordilleras (SE Spain). Geologie en Mijnbouw, 46, 471-474.

Walcott, R.C., Summerfield, M.A., 2008. Scale dependence of hypsometric integrals: An analysis of southeast African basins. Geomorphology, 96, 174-186.

Walker, R., Jackson, J., 2002. Offset and evolution of the Gowk fault, S.E. Iran: a major intra-continental strike-slip system. Journal of Structural Geology, 24, 1677-1698.

Walsh, J.J., Watterson, J., 1991. Geometric and kinematic coherence and scale effects in normal fault systems. Geological Society, London, Special Publications, 56, 193-203.

Watts, A.B., Platt, J.P., Buhl, P., 1993. Tectonic evolution of the Alboran Sea basin. Basin Research, 5, 153-177.

Wegmann, K.W., Pazzaglia, F.J., 2002. Holocene strath terraces, climate change, and active tectonics: The Clearwater River basin, Olympic Peninsula, Washington State. Geological Society of America Bulletin, 114, 731-744.

Weijermars, R., Roep, T.B., Van den Eeckhout, B., Postma, G., Kleverlaan, K., 1985. Uplift history of a Betic fold nappe inferred from Neogene-Quaternary sedimentation and tectonics (in the Sierra Alhamilla and Almería, Sorbas and Tabernas Basins of the Betic Cordilleras, SE Spain). Geologie en Mijnbouw, 64, 397-411.

Weijermars, R., 1987. The Palomares brittle-ductile Shear Zone of southern Spain. Journal of Structural Geology, 9, 139-157.

Wells, S.G., Bullard, T.F., Menges, C.M., Drake, P.G., Karas, P.A., Kelson, K.I., Ritter, J.B., Wesling, J.R., 1988. Regional variations in tectonic geomorphology along a segmented convergent plate boundary pacific coast of Costa Rica. Geomorphology, 1, 239-265.

Whipple, K.X., Tucker, G.E., 1999. Dynamics of the stream-power river incision model: Implications for height limits of mountain ranges, landscape response timescales, and research needs. Journal of Geophysical

Research-Solid Earth, 104, 17661-17674.

Whitfield, E., Harvey, A.M., 2012. Interaction between the controls on fluvial system development: tectonics, climate, base level and river capture – Rio Alias, Southeast Spain. Earth Surface Processes and Landforms, 37, 1387-1397.

Wood, J., 1966. An introduction to the lower Messinian temperate water facies of the Sorbas basin (Abad Member and Azagador Member), in: Eds Mather, A.E.S., M. (Ed.), 2n Cortijo Urra Field Meeting, SE Spain: Field Guide, University of Plymouh, UK, pp. 14-23.

Yelles, A., Domzig, A., Deverchere, J., Bracene, R., de Lepinay, B.M., Strzerzynski, P., Bertrand, G., Boudiaf, A., Winter, T., Kherroubi, A., Le Roy, P., Djellit, H., 2009. Plio-Quaternary reactivation of the Neogene margin off NW Algiers, Algeria: The Khayr al Din bank. Tectonophysics, 475, 98-116.

Zeck, H.P., 1996. Betic-RIF Orogeny - Subduction of Mesozoic Tethys Lithosphere Under Eastward Drifting Iberia, Slab Detachment Shortly Before 22Ma, and Subsequent Uplift and Extensional Tectonics. Tectonophysics, 254, 1-16.

Zeck, H.P., 1999. Alpine kinematic evolution in the W Mediterranean: A W-ward directed subduction regime followed by slab roll-back and slab detachment, in: al., D.e. (Ed.), The Mediterranean Basin: Tertiary Extension Within the Alpine Orogen. Geol. Soc. Spec. Publ., pp. 109-120.

Zhang, K., Liu, K.Y., Yang, J.C., 2004. Asymmetrical valleys created by the geomorphic response of rivers to strike-slip fault. Quaternary Research, 62, 310-315.

Part V – Appendix

ISSN (print): 1698-6180. ISSN (online): 1886-7995
www.ucm.es/info/estratig/journal.htm

Journal of Iberian Geology 38 (1) 2012: 225-238
http://dx.doi.org/10.5209/rev_JIGE.2012.v38.n1.39214

Active tectonics in the central and eastern Betic Cordillera through morphotectonic analysis: the case of Sierra Nevada and Sierra Alhamilla

Tectónica activa en la Cordillera Bética Oriental y Central mediante análisis morfotectónico: el caso de Sierra Nevada y Sierra Alhamilla

J. M. Azañón*[1,2], J. V. Pérez-Peña[1], F. Giaconia[2], G. Booth-Rea[1,2], J. M. Martínez-Martínez[1,2], M. J. Rodríguez-Peces[3]

[1] *Departamento de Geodinámica, Campus de Fuentenueva s/n, Universidad de Granada, 18071 Granada, Spain.*
[2] *Instituto Andaluz de Ciencias de la Tierra (UGR-CSIC), Granada, Spain*
[3.] *Departamento de Geodinámica, Universidad Complutense de Madrid, C/ J. Antonio Novais 12, 28040 Madrid, Spain*

**corresponding author: jazanon@ugr.es*

Received: 11/07/2011 / Accepted: 05/03/2012

Abstract

Quaternary activity of folds and faults can be assessed by the analysis of drainage network and the evaluation of geomorphic indexes. These analyses are especially productive in semiarid areas where tectonic rates are low-to-moderate and Quaternary dating is limited. In this work, we have revisited the most relevant GIS-based methodologies used to assess tectonic activity by using morphometric analyses and we discuss the tectonic implications in two key areas of the central and eastern Betic Cordillera (Sierra Nevada and Sierra Alhamilla regions). In the Sierra Nevada area, the use of geomorphic indexes in the mountain range and in the neighboring Granada and Guadix-Baza basins suggests that all are part of the same SW-directed extensional system. The Granada basin (except in its NE border) subsided during the Late Pleistocene as it is located in the hanging wall of the extensional system. On the other hand, the Sierra Nevada mountain range, the NE border of the Granada basin and the Guadix-Baza basin are located in the active uplifted foot wall of the system. Thus, the higher fluvial incision rates in the Guadix-Baza basin can be directly correlated with the most recent uplift history of Sierra Nevada mountain range. In the Sierra Alhamilla region, a geomorphic study shows Late Pleistocene activity along the North Alhamilla Reverse Fault and the dextral transpressive South Gafarillos Fault, two segments of the Polopos Fault Zone, previously considered as an inactive fault.

Keywords: Betic Cordillera, active tectonics, drainage networks, tectonic geomorphology

Resumen

La actividad cuaternaria de pliegues y fallas puede ser estimada mediante el análisis de las redes de drenaje y el cálculo de índices geomorfológicos. Este tipo de análisis es especialmente útil en zonas semiáridas con tasas de bajas y moderadas de actividad tectónica, y con escasas dataciones cuaternarias. En este trabajo hemos hecho una revisión de los principales trabajos que utilizan

metodologías desarrolladas con SIG para la evaluación de actividad tectónica por medio de análisis morfométricos y discutimos sus aportaciones en dos áreas claves de la Cordillera Bética central y este (Sierra Nevada y Sierra Alhamilla). En la región de Sierra Nevada, el cálculo de índices geomorfológicos tanto en la sierra como en las cuencas neógenas de Granada y Guadix-Baza pone de manifiesto que los tres son parte del mismo sistema extensional. La cuenca de Granada (excepto su borde NE) está situada sobre el bloque de techo del sistema extensional y por tanto sometida a subsidencia, mientras que Sierra Nevada, la cuenca de Guadix-Baza y el borde NE de la propia cuenca de Granada están situados en el bloque de muro del sistema, sometido a un levantamiento activo. De este modo, las altas tasas de incisión registradas en la Cuenca de Guadix-Baza tienen una correlación directa con la historia más reciente del levantamiento de Sierra Nevada. En la región de Sierra Alhamilla, un estudio geomorfológico pone de manifiesto la activación en el Pleistoceno Superior de la falla inversa del borde norte de Sierra Alhamilla y del segmento sur de la falla transpresiva dextral de Gafarillos, ambos segmentos de la falla de Polopos, la cual había sido previamente considerada como inactiva.

Palabras clave: Cordillera Bética, tectónica activa, redes de drenaje, geomorfología tectónica.

1. Introduction

Active tectonics is one of the fastest growing disciplines in Earth Sciences due to the recent development of new geochronological and geodetic tools which facilitate the acquisition of accurate rates (uplift rates, incision rates, erosion rates, slip rates on faults, *etc*.) at variable (10^3-10^6 years) time-scales (*e.g*., Schumm *et al*., 2000; Burbank and Anderson, 2001; Keller and Pinter, 2002; Bull, 2007; 2009).

Tectonic geomorphology is a relatively new discipline within active tectonics. It provides valuable tools to assess tectonic activity of structures with low-to-medium deformation rates, especially when there is a lack of Quaternary dating. In the field of tectonic geomorphology and landscape evolution, the use of Geographic Information Systems (GIS) is relatively recent. The availability of Digital Elevation Models (DEM) has produced a revolution in this field. DEM have replaced old topographic maps, allowing for better and faster analysis of topographic parameters. One of the most important features of DEM is the possibility of extracting river networks with stream gradients and catchment areas.

The analysis of drainage networks is a powerful tool to detect recent tectonic activity and uplift (e.g. Ouchi, 1985; Clark *et al.*, 2004) as river channels are very sensitive to changes in the parameters that control their shape and gradient (*e.g*. Whipple and Tucker, 1999; Korup, 2006). Rivers tend to develop equilibrium profiles in relative short times (10^3-10^6 yr), and therefore, anomalies in the river network systems, once other factors as lithology or climate are discarded, are normally due to recent tectonic activity. Therefore, geomorphic indexes based on river parameters as gradient, relief, properties of watersheds, etc., can provide relevant information of the Quaternary activity of tectonic structures. The technologies that GIS provide to perform statistical analyses, as well as the great availability of high-precision DEM, have allowed the advance in the field of geomorphic indexes. Within this methodological framework it is possible to calculate effectively traditional geomorphic indexes as well as re-formulate them in order to achieve a better morphometric analyses.

In this work we summarize some of these new GIS-based methodologies that analyze drainage networks through the calculation of geomorphic indexes. We show that the application of such methodologies in areas of low-to-medium tectonic rates (0.1 – 2 mm/yr), as the central and eastern Betic Cordillera, allow evaluating recent tectonic activity that otherwise would be imperceptible. We revisit some of the new geomorphic analyses carried out in two areas of the Betic Cordillera, namely the Sierra Nevada and the Sierra Alhamilla areas (Fig. 1). The first area comprises the Sierra Nevada mountain range and the Granada and Guadix-Baza Neogene basins. The new morphometric analyses suggest that the present-day relief of this area is the result of the recent tectonic activity of an extensional system involving not only Sierra Nevada mountain range, but also the Granada and Guadix-Baza Neogene to Quaternary basins. In the Sierra Alhamilla area, the use of geomorphic indices allows estimating active tectonic rates for Pleistocene structures.

2. Summary of GIS-based methodologies for landscape analysis

2.1. SLk index and SLk anomaly maps

The original SL index was defined by Hack (1973) as:

$$SL = (\Delta H / \Delta L) \bullet L$$

where SL is the stream length-gradient index in a particular channel reach, $\Delta H/\Delta L$ is the channel slope, and L is the total channel length from the central point of the river reach where the SL is calculated to the highest point on the channel. The SL index highlights anomalies in river longitudinal profiles, providing criteria to evaluate and quantify these slope changes (Hack, 1973; Kel-

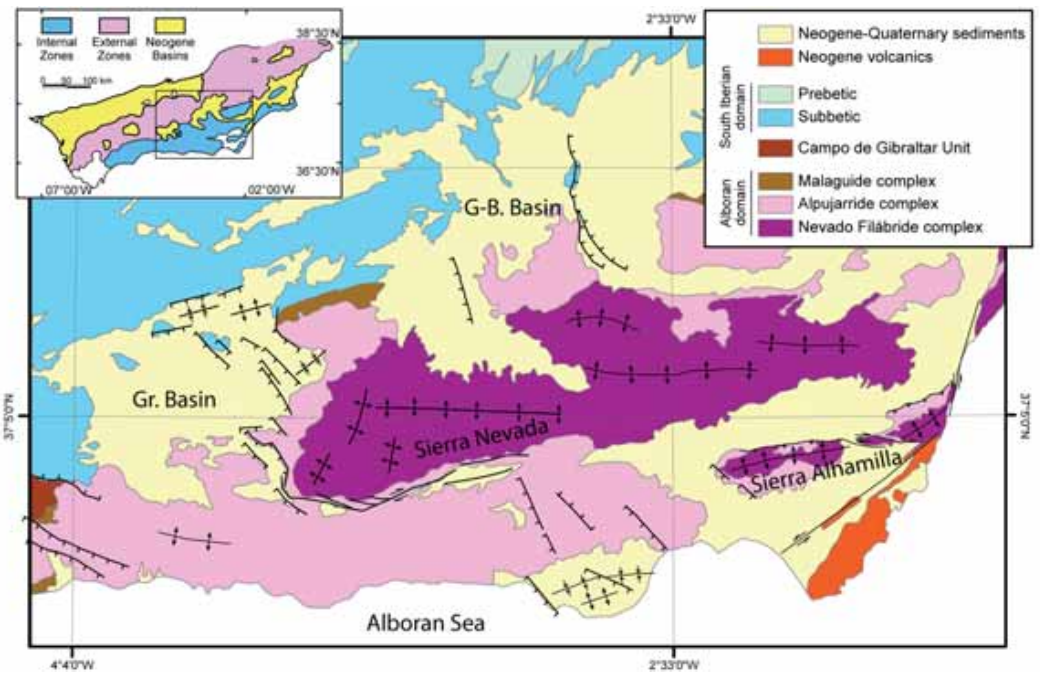

Fig. 1.- General tectonic sketch of the central and eastern Betic Cordillera. The inset shows the location within the Betic Cordillera. (Gr. Basin stands for Granada basin; G-B. Basin stands for Guadix-Baza basin).

Fig. 1.- Esquema tectónico general de los sectores central y oriental de la Cordillera Bética. El recuadro muestra la localización respecto de la Cordillera Bética. (Gr. Basin corresponde a Cuenca de Granada; G-B. Basin corresponde a Cuenca de Guadix-Baza).

ler and Pinter, 2002; Pérez-Peña *et al.*, 2009a).The SL index is very sensitive to changes in channel slope. These changes are mainly due to lithologic, tectonic, or climatic factors. Perez-Peña *et al.* (2009a) proposed a re-defined SLk index, by using the graded river gradient (K) to normalize the SL index. These authors also proposed a new GIS-based methodology to create SLk anomaly maps by using geostatistical kriging. This methodology has been used to evaluate the activity of tectonic structures (faults and folds) in some recent studies in the Betic Cordillera with good results (Pérez-Peña *et al.*, 2009a; Pedrera *et al.*, 2009; Giaconia *et al.*, 2012).

2.2. Hypsometry analysis through GIS

The hypsometric curve represents the distribution of area and altitude within the selected basins (Strahler, 1952). This curve is obtained by plotting the proportion of the total basin height (relative height) against the proportion of total basin area (relative area) (Strahler, 1952; Keller and Pinter, 2002; Pérez-Peña *et al.*, 2009b). The shape of the hypsometric curve is related to the degree of dissection of the basin (*e.g.* its erosional stage). The hypsometric integral (*HI*) is defined as the area below the hypsometric curve and it varies from 0 to 1. HI values of 1 depict drainage basins in a youthful geomorphic stage and they are related with convex hypsometric curves, HI values near 0 are typical of mature basins reaching the peneplain stage and they relate with concave hypsometric curves. Perez-Peña *et al.* (2009c) proposed a GIS-based methodology for the analysis of the hypsometry by using local indices of spatial autocorrelation (LISA). They extracted the HI values for regular squares (not for drainage basins) and observed that the raw estimation of HI values did not present a clear view of grouped high or low values. However, when they applied Moran's I autocorrelation index and Gi* hot-spot statistical analysis (Moran, 1950; Ord and Getis, 1995), the HI values grouped in cluster of high and low values. They proved that the clusters were closely related with the activity of tectonic structures.

2.3. V_f and S_{mf} indexes

Valley width to valley height ratio (V_f) (Bull and McFadden, 1977) is a geomorphic index conceived to discriminate between V-shaped valleys (V_f values close to 0) and U-shaped flat-floored valleys (high V_f values). Deep V-shaped valleys are associated with linear active incision, and related to areas subjected to active tectonics, while flat-floored valleys are characteristic of sectors with less river incision and low tectonic activity (e.g. Keller and Pinter, 2002). This index has been applied to evaluate the relative degree of tectonic activity of several mountain fronts located in the eastern and central Betic Cordillera (Silva *et al.*, 2003; García-Tortosa *et al.*, 2008; Pedrera *et al.*, 2009; Pérez-Peña *et al.*, 2010).

Mountain-front sinuosity was defined by Bull (1977) as:

$$S_{mf} = L_{mf} / L_s$$

where S_{mf} is the mountain front sinuosity; L_{mf} is the length of the mountain front along the foot of the mountain, *i.e*., the topographic break in the slope, and Ls is the length of the mountain front measured along a straight line. This index has been used to evaluate the relative tectonic activity along mountain fronts (Bull and McFadden, 1977; Keller and Pinter, 2002; Silva *et al.*, 2003; Bull, 2007; Pérez-Peña *et al.*, 2010; Giaconia *et al.*, 2012). In active mountain fronts, uplift will prevail over erosional processes, yielding straight fronts with low values of S_{mf}. Along less active fronts, erosional processes will generate irregular or sinuous fronts with high values of S_{mf}. Some studies have proposed that values of the S_{mf} index lower than 1.4 are indicative of tectonically active fronts (Silva *et al.*, 2003).

2.4. Erosion analysis through GIS

GIS technologies offer exceptional tools to analyze the erosion processes within an area. Pérez-Peña *et al.* (2009d) proposed a methodology to reconstruct the morphology of theGuadix-Baza basin prior to the entrenchment of the river network. The methodology proposed in their work consists of reconstructing the morphology of a glacis surface formed on top of the sedimentary sequence prior to river entrenchment. These authors used a raster Digital Elevation Model (DEM) with a 20-m resolution to isolate the pixels (cells) representing the glacis and to reconstruct its initial morphology. This reconstructed model was compared with the present-day morphology of the Guadix–Baza basin to estimate the volume of sediments eroded since the basin was captured by the Guadalquivir River system. With this methodology it is possible to obtain not only the erosion rates for the sedimentary basin, but also a view of how erosion evolved in the basin since its capture (Pérez-Peña *et al.*, 2009d).

This methodology can be also applied to drainage basins in mountain ranges by interpolating the altitudes from present-day lateral divides of the basins (Menéndez *et al.*, 2008). This surface is known as ridgeline surface and can be deemed as a theoretical pre-incision surface. Therefore, the altitude differences between this surface and the present-day relief can be deemed as a proxy of the erosion within the drainage basin (Menéndez *et al.*, 2008; Pérez-Peña *et al.*, 2010).

3. Geological and tectonic setting.

3.1. The Sierra Nevada area

The Sierra Nevada mountain range (Fig. 1) has been considered as an orogenic dome or core-complex structure (Martínez-Martínez *et al.*, 2004) exhumed since the Late Miocene in an extensional tectonic regime. The Pliocene-Quaternary tectonic evolution of this range is responsible for the formation of a large-scale open antiformal ridge coincident with the whole extent of the Sierra Nevada and coeval normal faulting. Some authors have considered this antiformal ridge as related to a blind-thrust buried under the northern E–W oriented mountain front of the Sierra Nevada (Galindo-Zaldívar *et al.*, 2003). Normal faulting in this model is related to NNW-SSE extension sub-perpendicular to the maximum Africa-Iberia present-day shortening. Nevertheless, other authors (Martínez-Martínez *et al.*, 2006; Pérez-Peña *et al.*, 2010) consider that the present-day topography of the Sierra Nevada is the consequence of the interference of two orthogonal sets of Miocene-Pliocene large-scale open folds trending roughly E–W and NNE–SSW. These authors interpreted the NNE-SSW fold, as well as the normal NW-SE faults of the western border of Sierra Nevada, as related to the westward migration of a rolling hinge behind the active extensional loci. These normal faults limit the Neogene-Quaternary Granada sedimentary basin, and they clearly indicate activity in Quaternary-Holocene times (Calvache and Viseras, 1997; Alfaro *et al.*, 2001). Some authors have proposed slip rates of 0.6-0.8 mm/yr for these normal faults in the Quaternary (Sanz de Galdeano, 1996; Keller *et al.*, 1996). However, recent studies have proposed higher slip rates for them (Reinhardt *et al.*, 2007). These authors dated Quaternary sediments using radiometric methods and proposed that 50 m of a fault-related base-level fall must have occurred in the last 21 ka.

The Sierra Nevada is bounded west and northwards by two of the largest Neogene-Quaternary basins in the central Betic Cordillera, the Granada and Guadix-Baza basins respectively (Fig. 1). These two basins have quite similar sedimentary records (Rodríguez-Fernández *et al.*, 2012), and both changed in Quaternary times from an internal to an external drainage to the Atlantic Ocean via the Guadalquivir River (the biggest river in south Spain). Despite these similarities, the Quaternary geomorphic evolution and the present-day topography of the Guadix-Baza and Granada basins are quite different. The differences are probably linked to the recent tectonics of the Sierra Nevada extensional dome. The Guadix-Baza basin's present-day topography consists of a high plateau with a mean altitude of 1000 m, strongly dissected by the river network (Pérez-Peña *et al.*, 2009d; García-Tortosa *et al.*, 2011) (Fig. 1). Its Late Quaternary evolution is mostly dominated by erosional processes that followed its capture by the Guadalquivir River (Azañón *et al.*, 2005). In contrast, the Late Quaternary evolution of the Granada

basin is dominated by active normal faulting along its northeastern border, where the maximum relief is concentrated. The remainder of the basin has a mean altitude of ≈ 700 m, being scarcely incised by the fluvial network (Pérez-Peña *et al.*, 2009d).

3.2. The Sierra Alhamilla area

The Neogene to Quaternary sedimentary basins in the southeastern Betic Cordillera, like the Sorbas-Tabernas and the Almería-Níjar basins, initiated as extensional sedimentary depocentres formed in the hinterland of the Gibraltar orogenic arc during the middle to late Miocene (García-Dueñas *et al.*, 1992; Martínez-Martínez and Azañón, 1997; Comas *et al.*, 1999; Booth-Rea *et al.*, 2005; Booth-Rea *et al.*, 2007). However, late Miocene to present convergence between Nubia and Iberia (Dewey *et al.*, 1989; McClusky *et al.*, 2003; Serpelloni *et al.*, 2007) has resulted in tectonic inversion of the extensional basins and development of folds, reverse and strike-slip fault systems including dextral and sinistral faults (Weijermars *et al.*, 1985; Montenat and Ott d'Estevou, 1990; Comas *et al.*, 1999; Booth-Rea *et al.*, 2004). The most important sinistral strike-slip faults active during the latest Miocene and Quaternary are the Carboneras (Bell *et al.*, 1997; Gràcia *et al.*, 2006), the Alhama de Murcia (Martínez-Díaz, 2002; Masana *et al.*, 2004), the Palomares (Bousquet, 1979; Booth-Rea *et al.*, 2004), and the Terreros sinistral fault-zones (Booth-Rea *et al.*, 2004), all of them with NNE/SSW to NE/SW trends. Dextral faults conjugate to these are not as large and show a WNW/ESE orientation, like the Gafarillos fault zone (Fig. 1, Ott d'Estevou and Montenant, 1990; Stapel *et al.*, 1996; Barragán, 1997; Huibregtse *et al.*, 1998; Jonk and Biermann, 2002).

Most of the Pliocene and Quaternary sedimentary cover in the eastern basins of the Betic Cordillera is related to releasing jogs of strike-slip faults (e.g. Montenat and Ott d'Estevou, 1990) or in synclines between E/W to ENE/WSW–elongated antiformal ridges, where the metamorphic basement is bounded by folded extensional detachments (Martínez-Martínez and Azañón, 1997; Martínez-Martínez *et al.*, 2002; Booth-Rea *et al.*, 2005). This basement is made up of several metamorphic complexes belonging to the Alboran domain, a terrain that collided with the South Iberian and Maghrebian passive margins during the Miocene, forming the Gibraltar arc and the Betic and Rif cordilleras (Balanyá and García-Dueñas, 1987; Martínez-Martínez and Azañón, 1997; Platt *et al.*, 2003; Booth-Rea *et al.*, 2007). The Sierra Alhamilla anticlinorium is an example of these elongated antiformal ridges where metamorphic rocks crop out, surrounded by Miocene to Quaternary sediments of the Sorbas-Tabernas and Níjar-Almería basins (Fig. 1). Most of the deformation leading to the development of the Alhamilla anticlinorium occurred during the late Miocene, being sealed by Messinian carbonates (Weijermars *et al.*, 1985). This, for example, occurred with the Gafarillos dextral fault zone to the northeast of the Alhamilla anticlinorium (Fig. 1). Thus, most authors have considered that this dextral strike-slip system, conjugate to the NE-SW sinistral Cabrera and Palomares faults has been inactive since the Messinian (Ott d'Estevou and Montenant, 1990; Stapel *et al.*, 1996; Huibregtse *et al.*, 1998; Jonk and Biermann, 2002). Here we show how the use of geomorphic indexes in the Sierra Alhamilla anticlinorium area has unveiled the presence of active segments of both reverse and strike-slip faults that form the Polopos Fault Zone (PFZ) (Giaconia *et al.*, 2012).

The main late Miocene to Quaternary tectonic structures in the Sierra Alhamilla region are the transpressive dextral-reverse Polopos Fault Zone that includes the dextral Gafarillos fault segments to the east of the ridge and their continuation towards the west as the North Alhamilla reverse fault (NARF) in the northern limb of the Alhamilla anticlinorium (Ott d'Estevou and Montenant, 1990; Stapel *et al.*, 1996; Huibregtse *et al.*, 1998; Jonk and Biermann, 2002). The southwestern side of the Alhamilla ridge, in the Almería-Níjar basin, Pliocene-Quaternary high-angle normal faults occur with NW-SE to NNW-SSE strike (Fig. 1, Martínez-Martínez and Azañón, 1997; Marín-Lechado *et al.*, 2005; Pedrera *et al.*, 2006; Sanz de Galdeano *et al.*, 2010).

4. New geomorphic analyses

4.1. Morphotectonic analyses in a central Betic region: The Sierra Nevada area

4.1.1. Geomorphic indexes in Sierra Nevada

The fault-bounded mountain fronts of western Sierra Nevada have been studied through the S_{mf} index (Fig. 2). The values of this geomorphic index for western Sierra Nevada (Fig. 2) indicate active fronts, in which the tectonic activity prevails over the erosion forces (Martín-Rojas *et al.*, 2001; El Hamdouni *et al.*, 2008). Pérez-Peña *et al.* (2010) also calculated the S_{mf} index for the south and northern border of Sierra Nevada, combining their values with the V_f index. Their results indicate that the more recent uplift is concentrated along its western mountain front, where S_{mf} and V_f present the lowest values (Fig. 2). The southern mountain front of Sierra Nevada is characterized by low values of S_{mf} and V_f, with

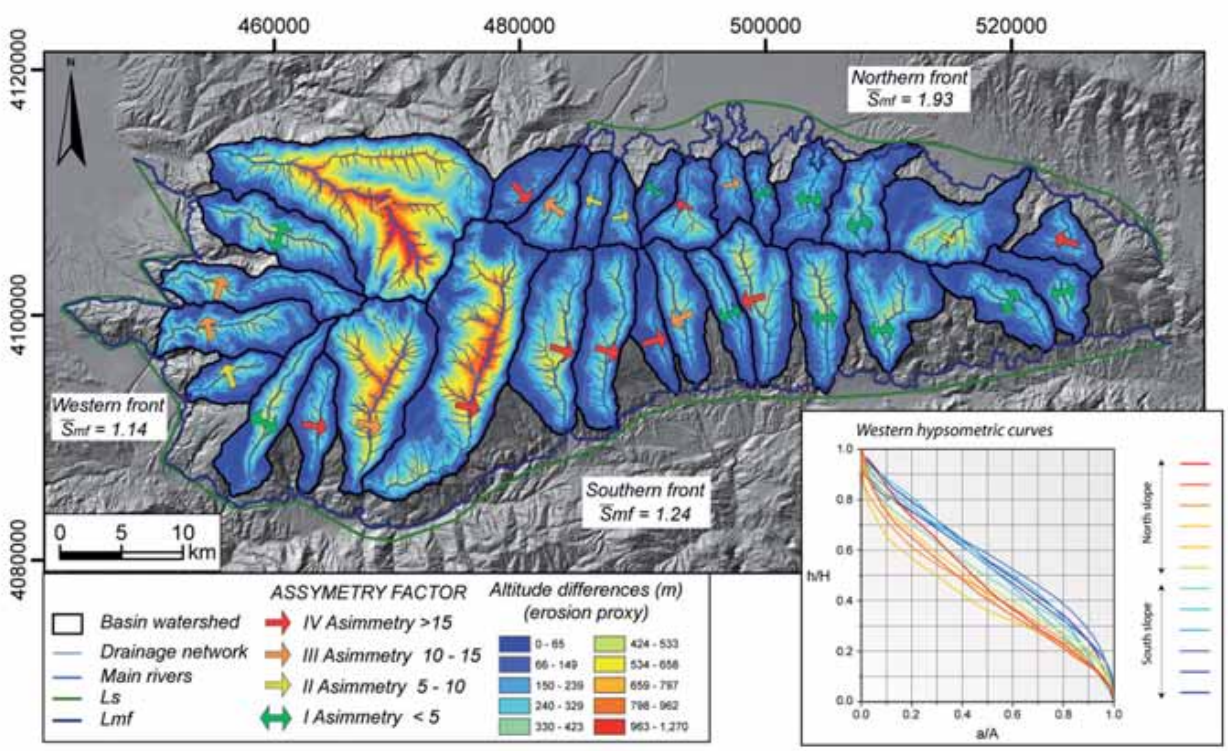

Fig. 2.- Digital elevation model (DEM) with the drainage network and the calculated geomorphic indexes in the Sierra Nevada mountain range. The arrows show the direction of basin asymmetry and the colors its magnitude (see Pérez-Peña *et al.*, 2010 for further details). The western, southern, and northern mountain fronts are depicted. S_{mf} values indicate that western and southern fronts are tectonically active whereas the northern front is inactive. Altitude differences between basin ridgeline-surfaces and present day topography show that the erosion is more prominent in the western part of the mountain range. The inset shows the differences between northern and southern hypsometric curves from the western sector of the Sierra Nevada.

Fig. 2.- Modelo digital del terreno con la red de drenaje y los índices geomorfológicos calculados en Sierra Nevada. Las flechas indican el sentido de la asimetría de las subcuencas y los colores la magnitud (ver Pérez-Peña *et al.*, 2010 para más detalles). Se representan los frentes montañosos occidental, meridional y septentrional. Los valores de S_{mf} indican que los frentes meridional y occidental son tectónicamente activos mientras que el frente norte es inactivo. Las diferencias entre la topografía actual y una superficie extrapolada a partir de las trazas de las divisorias locales muestran que la erosión es más prominente en el sector occidental de Sierra Nevada. El recuadro muestra las diferencias entre las curvas hipsométricas del sector occidental de Sierra Nevada.

S_{mf} values increasing eastward. Nevertheless, the northern mountain front, which corresponds to the contact between the Guadix-Baza basin and the northern limb of the E–W antiformal ridge, has the highest S_{mf} and V_f values, thus suggesting low rates of tectonic activity, and thus pointing to an inactive northern fold limb during the Quaternary (Fig. 2).

In the same study, Perez-Peña *et al.* (2010) point that other geomorphic indicators, including hypsometric curves (Fig. 2), longitudinal/ridge-line river profiles, and drainage patterns, depict N–S variations. They relate these N–S variations as due to the fact that the local base-level is ≈1100 m in the northern mountain front of the Sierra Nevada and ≈600 m in the southern front, *i.e.*, the southern slope streams have more erosional power than the northern ones. These differences in base-level altitudes could be the response to a differential tectonic uplift of the northern mountain front with respect to the southern one.

All the geomorphic indicators show that the western part of Sierra Nevada range is more active than the eastern part. Vazquez *et al.* (2011) showed, by using U/Th-He and Fission Tracks dating, a westward migration of the locus of extension in Sierra Nevada. Thus, the western sector of this range has been exhumed later than the eastern one. On the other hand, NE-SW open folds, outcropping in the western termination, are responsible of changes in the asymmetry of subbasins (Fig. 2, Pérez-Peña *et al.*, 2010), which is a clear evidence of Pleistocene activity of these folds. Analysis of erosion in the Sierra Nevada range, which can be approximated by means of the altitude differences between ridgeline surfaces and present-day topography, is also compatible with the aforementioned geomorphic results, showing the highest volume of erosion in the western sector (Fig. 2).

4.1.2. Geomorphic analyses in the Granada and Guadix-Baza basins

Through the morphometric analysis of the drainage network of the Granada and Guadix-Baza basin it is possible to have a new view of the Quaternary evolution of both basins and, consequently, of their tectonic activity. In the Granada basin (Fig. 3), there is a lack of Quaternary ages, making it difficult to evaluate the Quaternary activity of the active structures within the basin. Pérez-Peña *et al.* (2009a) studied the SLk index in the NE border of the Granada basin, and they proposed that the NW-SE normal faults presented evidences of Quaternary activity (Figs. 3 and 4). Their SLk anomaly map (Fig. 4) showed several anomalies, some of them clearly related with the Quaternary activity of the NW-SE normal faults. In the SLk anomaly map presented by these authors, the anomalies 1, 5, 3, and 4 match with the aforementioned normal fault systems. Some of them have a lithological component, but anomaly 3 in figure 4 presents high SLk values within the same materials in an area with documented present-day fault activity (Azañón *et al.*, 2004).

The hypsometry analysis in the Granada basin reveals also the same pattern; a NE border being uplifted by the activity of the NW-SE normal fault (Pérez-Peña *et al.*, 2009c) (Fig. 5). The use of LISA to the HI value distribution shows that the NE border of the Granada basin is affected by differential uplift related with the NW-SE normal faults, thus having a different drainage pattern system than the rest of the basin (Pérez-Peña *et al.*, 2009c). This drainage pattern, which presents deep incised V-shaped valleys, is similar to the Guadix-Baza drainage system.

The Quaternary landscape evolution of the Guadix-Baza Neogene basin is conditioned by erosional processes. Pérez-Peña *et al.* (2009d) studied the erosion rates within this basin to elucidate its Quaternary landscape evolution. The great differences in the erosion rates obtained between the Guadix and Baza sub-basins are the consequence of three factors: the position of the capture point near the Guadix sub-basin, the greater area of the Baza sub-basin, and the Quaternary activity of the Baza fault, which affected the normal propagation of the erosion wave eastwards (See Figure 6 in Pérez-Peña *et al.*, 2009d). The activity of the Baza fault (Alfaro *et al.*, 2008; García-Tortosa *et al.*, 2008, 2011) has been also corroborated by other authors through morphometric analyses. García-Tortosa *et al.* (2008) applied geomorphic indexes to the Baza fault and considered this fault as one of the most active faults of the Betic Cordillera. The activity of this N-S active normal fault contrasts with the absence of faults in the southern border of the basin. This border, despite being the limit with the Sierra Nevada mountain range, does not present significant tectonic activity in Quaternary times (Pérez-Peña *et al.*, 2010).

4.2. Morphotectonic analyses in an eastern Betic region: The Sierra Alhamilla area.

4.2.1. Geomorphic response to the Polopos fault zone

Fault segmentation and fluvial terrace mapping along the Polopos fault zone have shown that both its reverse and dextral strike-slip fault segments cut Pleistocene sediments (Giaconia *et al.*, 2012). This Quaternary to present activity is reflected by the geomorphic indexes study. The low S_{mf} index values occurring in the Sierra Alhamilla northern front, especially eastwards, support the late Pleistocene activity of the North Alhamilla re-

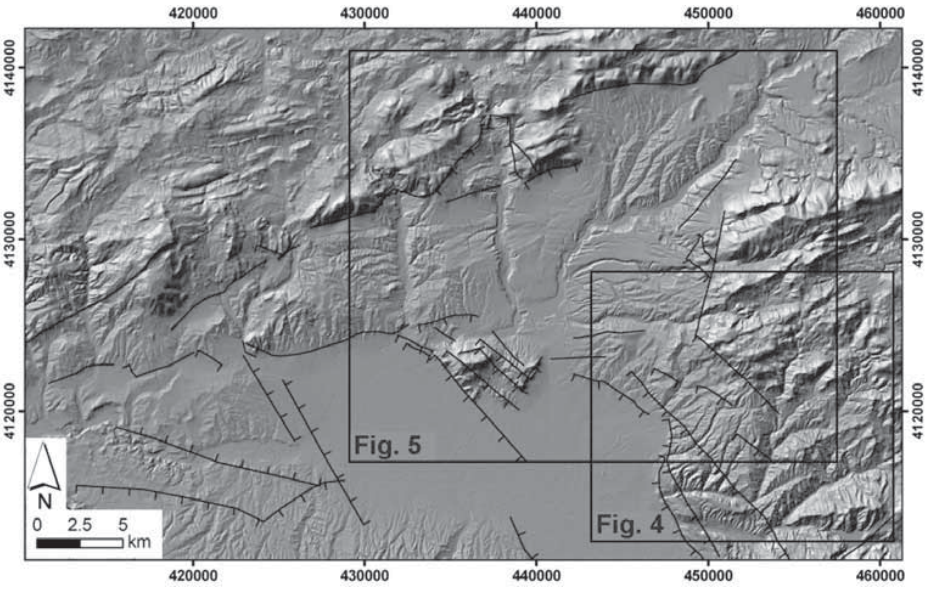

Fig. 3.- Digital elevation model (DEM) of the NE border of the Granada basin. The higher river entrenchment can be observed in the footwall of the main NW-SE normal faults.

Fig. 3.- Modelo digital del terreno del borde NE de la Cuenca de Granada. Los principales encajamientos de las partes altas de los cauces fluviales pueden observarse en el bloque de muro de las principales fallas normales NW-SE.

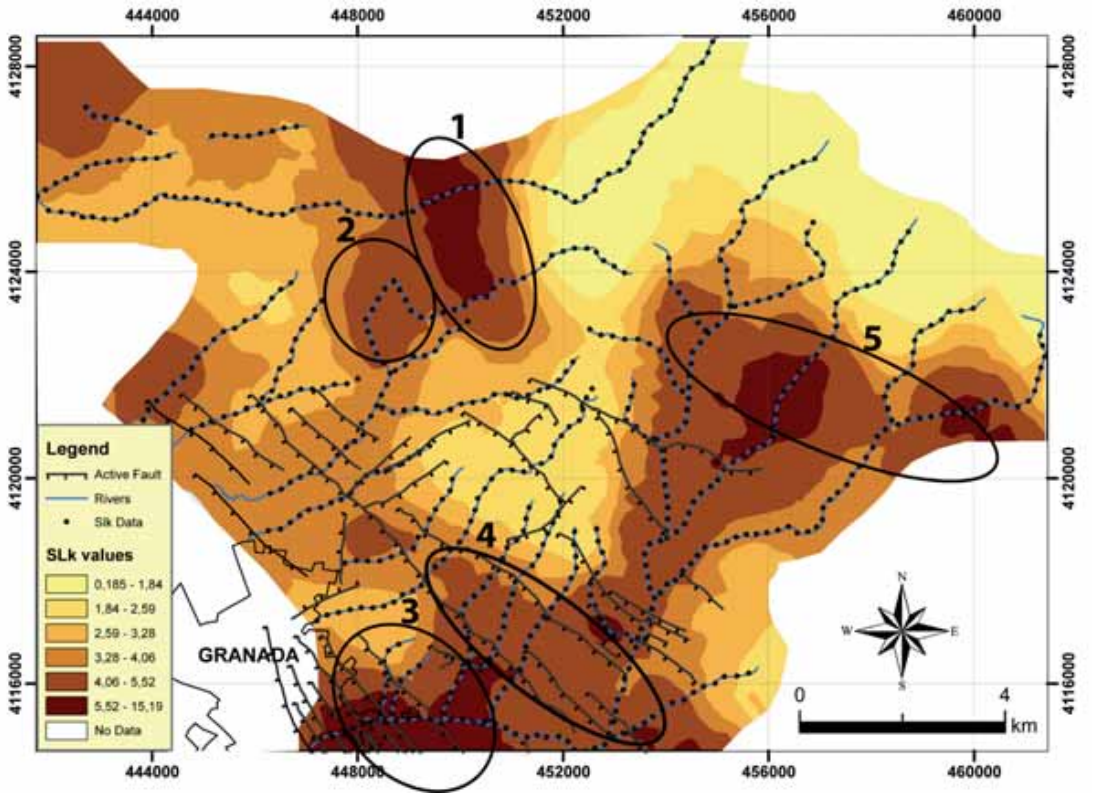

Fig. 4.- SLk map for the NE border of the Granada basin. The main anomalies are highlighted and numbered. Modified from Pérez-Peña *et al.* (2009c)

Fig. 4.- Mapa de SLk del borde NE de la Cuenca de Granada. Se resaltan y numeran las principales anomalías. Modificada de Pérez-Peña *et al.* (2009c)

verse fault (mountain fronts Nc, Nd and Ne in figure 6, values are shown in table 1). Taking into account the integration between the S_{mf} and the V_f indices proposed by Silva *et al.* (2003) and the absence of geological marker useful to determine slip-rates, we are able to assign an uplift-rate ranging between 0.5 and 0.05 m/ky for the southern hanging-wall block of this fault. In addition, the occurrence of the SLk anomaly 1 in figure 7 confirms such uplift.

The eastern part of the Sierra Alhamilla northern front shows low values of S_{mf} and V_f (V_f in figure 6, values are shown in table 1 and 2, respectively) that allow us to assign an uplift rate higher than 0.5 m/ky for the southern hanging-wall block of the north Alhamilla reverse fault-south Gafarillo fault (NARF-SGF) system. This uplift is supported also by the high SLk anomaly 2 and 3 in figure 7, which is located just to the south of this fault system, and by the southward basin asymmetries recognized here (Fig. 6). The occurrence of streams with convex longitudinal profiles and basins with convex and complex hypsometric curves in the northern slope support the Quaternary- to present-activity of this fault system (Fig. 7). The relative uplift of the southern block of the NARF-SGF fault system changes local base-levels causing the occurrence of younger basins. In addition, in response to reverse displacement along this fault system, foot-reju-

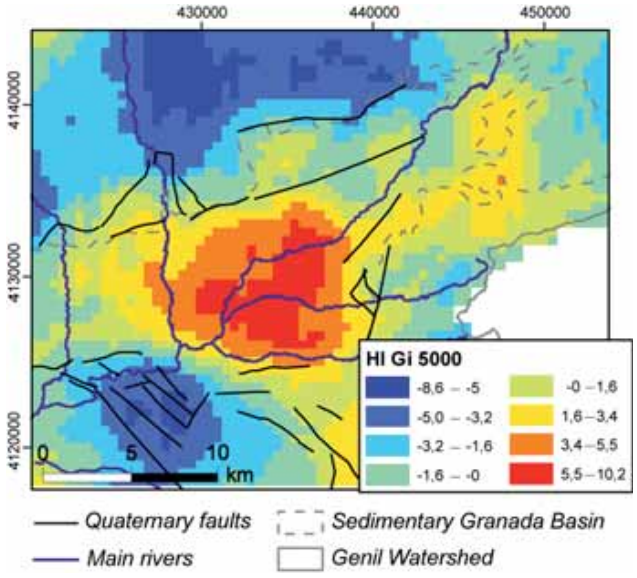

Fig. 5.- Getis-Ord*-statistic estimation for the HI value distribution in the NE border of the Granada basin. The figure shows how the clusters of high values are related with the footwall of active normal faults. . Modified from Pérez-Peña *et al.* (2009c)

Fig. 5.- Estimación estadística Getis-Ord* para la distribución de valores de la integral hipsométrica en el borde NE de la Cuenca de Granada. La figura muestra cómo las agrupaciones con altos valores de IH están relacionadas con los bloques de muro de las fallas normales. Modificada de Pérez-Peña *et al.* (2009c)

Front	Smf	Front	Smf
Sa	1.20	W	1.06
Sb	1.30	Na	1.47
Sc	1.01	Nb	1.22
Sd	1.70	Nc	1.44
Se	1.14	Nd	1.40
Sf	1.96	Ne	1.23
Sg	1.01	Nf	1.10
Sh	1.30	E	1.38

Table 1.- Table reporting the S_{mf} (mountain front sinuosity) values for each front shown in the map.

Tabla 1.- Valores del S_{mf} (sinuosidad del frente montañoso) para cada uno de los frentes que se muestran en el mapa.

Stream	Vf	Stream	Vf
1	0.59	22	0.92
3	0.25	23	1.22
4	0.90	24	1.22
7	0.87	27	1.22
9	0.34	29	1.44
11	0.14	30	1.44
12	0.46	32	1.40
13	0.78	33	1.10
14	1.08	34	1.10
17	0.84	35	1.10
20	0.27	36	1.38
21	0.22	37	1.23

Table 2.- Table reporting the *Vf* (valley floor width-to-height ratio) values for each stream shown in the map.

Tabla 2.- Valores del *Vf* (relación entre anchura-altura de los valles fluviales) para cada uno de los valles que se muestran en el mapa.

venation processes should occur in basins above the fault trace, thus generating complex hypsometric curve shapes.

4.2.2. Geomorphic response to the Pliocene-Quaternary high-angle normal faulting

The low S_{mf} and V_f values obtained for the Sierra Alhamilla southern front (Sa, Sc and Se in figure 6, values are shown in table 1) support the recent to present activity of the NW-SE- to NNW-SSE-striking high-angle normal fault system that affects the southern slope of the ridge and the Almería-Níjar basin. The integration of these two indices allows us to assign an uplift rate to these faults higher than 0.5 m/ky.

The Quaternary activity of this fault system is confirmed by the occurrence of basins with S-shaped, convex and complex hypsometric curve shapes at the southern slope (Fig. 6). In response to NE-SW normal displacement, the relative uplift of southern slope sectors with respect to the sedimentary basin has changed the streams local base-level thus, producing younger drainage basins or head-rejuvenation processes that generate complex hypsometric curve shapes (Fig. 6). According to these observations, longitudinal stream profiles in the southern slope locally show concave-convex profiles with knick-points and high SLk anomalies 4, 5 and 6 occur (Fig. 7). An analogous scenario can be described for the eastern part of the Sierra Alhamilla southern slope where a Pliocene-Quaternary high-angle normal fault having a N-S strike and an eastwards normal displacement occurs. This fault producing a relative uplift of its western foot-wall block causes the occurrence of low S_{mf} and V_f values, basins with complex hypsometric curve and the high SLk anomaly 7 shown in figure 7.

5. Discussion

5.1. New tectonic model for the Sierra Nevada area

The geomorphic indexes for the Sierra Nevada suggest that the more recent uplift is concentrated along its western mountain front, where S_{mf} and V_f present the lowest values. Higher incision rates in this western sector can be due to tectonic uplift in the hanging wall of the NW-SE normal faults. These normal faults belong to the same system as the one in the NE border of the Granada basin. The N-S variations in the geomorphic indices are caused by the differences in the base level for the river incision that, in turn, are due to a differential uplift of both mountain fronts. The southern front of the Sierra Nevada has been interpreted as a transfer fault that links two areas of active extension (the Granada-Padul basins, and the western Sierra de Gador) (Fig. 8; Martínez-Martinez *et al.*, 2006; Pérez-Peña *et al.*, 2010). The northern mountain front of Sierra Nevada corresponds to an unconformity between the Neogene-Quaternary sedimentary infill of the Guadix-Baza basin and the metamorphic rocks of Sierra Nevada. This mountain front and the Neogene Guadix-Baza basin are located in the foot wall of the mentioned system.

The Quaternary landscape evolution of the Granada and Guadix-Baza basins are very different, and are strongly conditioned by tectonics. The Granada basin has a mean altitude of 600 m, being scarcely incised by the fluvial network, except in the NE margins of the basin near the fault-bounded mountain front. The Guadix-Baza basin has a mean altitude of 1000 m, with the fluvial network deeply incised (down to 200 m) into the Neogene-Quaternary infill. These topographic and geomorphic differences are probably due to the different tectonic location of the two basins: The Granada basin, except its NE border, is located in the hanging wall of the NW-SE extensional system bounding Sierra Nevada to the west, being thus subjected in a great extent to Quater-

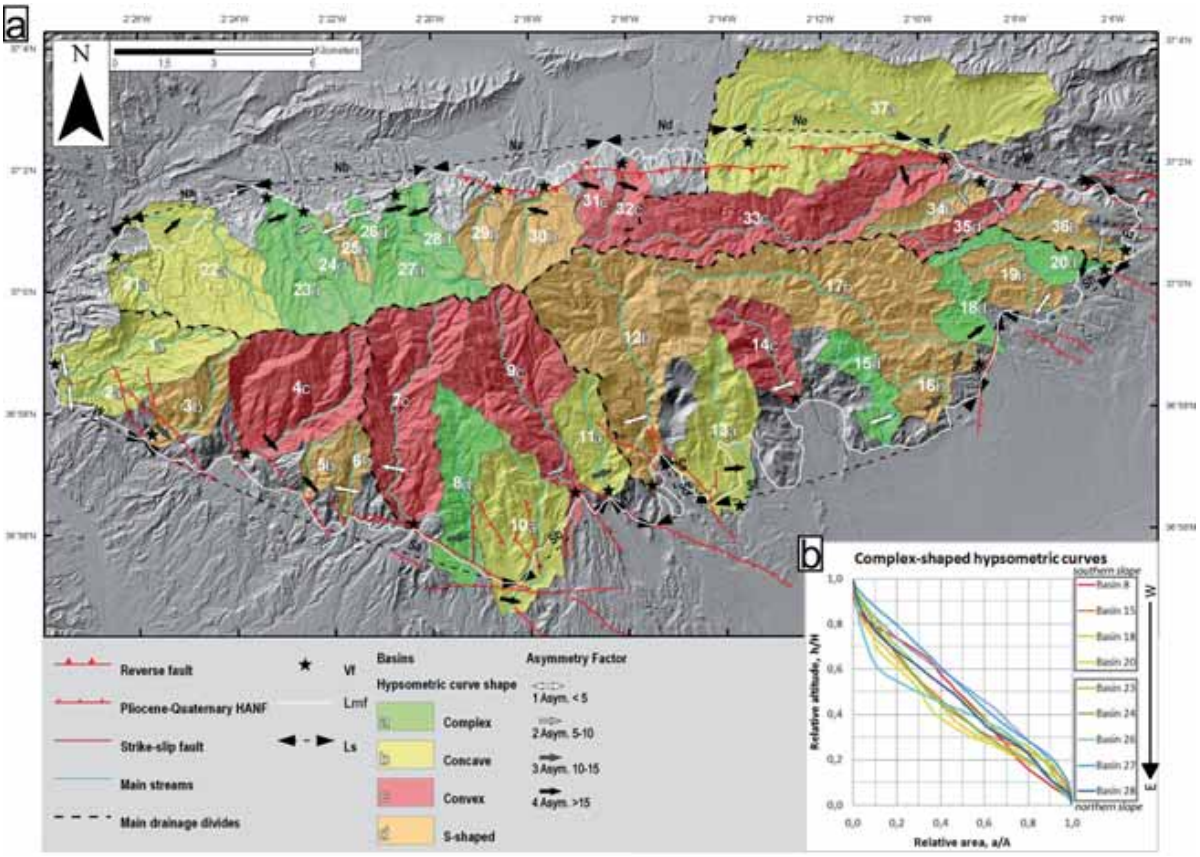

Fig. 6.- a) Drainage basin distribution map where the main drainage divides, streams, watersheds of main streams and drainage basins (classified depending on their hypsometric curve shapes) and Quaternary active tectonics (after Martínez-Martínez *et al.*, 1997) are shown. The following geomorphic indices are reported: the basin asymmetry factor, the mountain front sinuosity (S_{mf}, together with the mountain front, L_{mf}, and its length measured along a straight line, L_S), and finally the valley floor width-to-height ratio (V_f). b) Complex hypsometric curves associated with "rejuvenation" processes, at the foot or head of the streams.

Fig. 6.- a) Distribución de la red de drenaje, subcuencas y principales cauces fluviales (clasificados en función de la forma de su curva hipsométrica) y su relación con la tectónica activa cuaternaria en la Sierra Alhamilla (Martínez-Martínez *et al.*, 1997). Se muestran los valores de los siguientes índices geomorfológicos: factor de asimetría de las subcuencas, sinuosidad de los frentes montañosos (S_{mf}) y, finalmente, la relación entre anchura y altura de los valles fluviales (V_f). b) Curvas hipsométricas complejas asociadas con los procesos de "rejuvenecimiento" en los pies o cabeceras de los valles fluviales.

nary subsidence. On the contrary, the Guadix-Baza basin is located in the footwall of the above-mentioned extensional system, being part together with Sierra Nevada of a single block affected by tectonic uplift during the Quaternary (Fig. 8).

Traditional tectonic models of the Sierra Nevada area do not mention the important differences between the eastern and western part of the range or between its northern and southern mountain fronts (Galindo-Zaldívar *et al.*, 2003). Some authors have proposed recent models for this area (Martínez-Martínez *et al.*, 2004, 2006) explaining the mentioned differences within the mountain range, but they still do not explain the significant contrast between the landscapes of the Granada and Guadix-Baza basins. The evolution of these two basins has traditionally considered very similar (Fernández *et al.*, 1996; Rodríguez-Fernández and Sanz de Galdeano, 2006), with the only difference of the normal faulting affecting mainly to the Granada basin (Sanz de Galdeano *et al.*, 2003; Azañón *et al.*, 2004). Despite the fact that the Granada and Guadix-Baza basins present a similar evolution from Tortonian to Middle-Pleistocene, their Quaternary landscape evolution is rather different. The activity of the NW-SE normal faults in the Granada basin is not enough to explain the contrast in landscape, geomorphology, and drainage network incision respect to the Guadix-Baza basin. However, the tectonic model, based on Martínez-Martínez *et al.* (2006), is compatible with the results obtained through the combination of geomorphic analyses. They are part of the same extensional system causing extension in the Granada basin and the western part of Sierra de Gador. This exten-

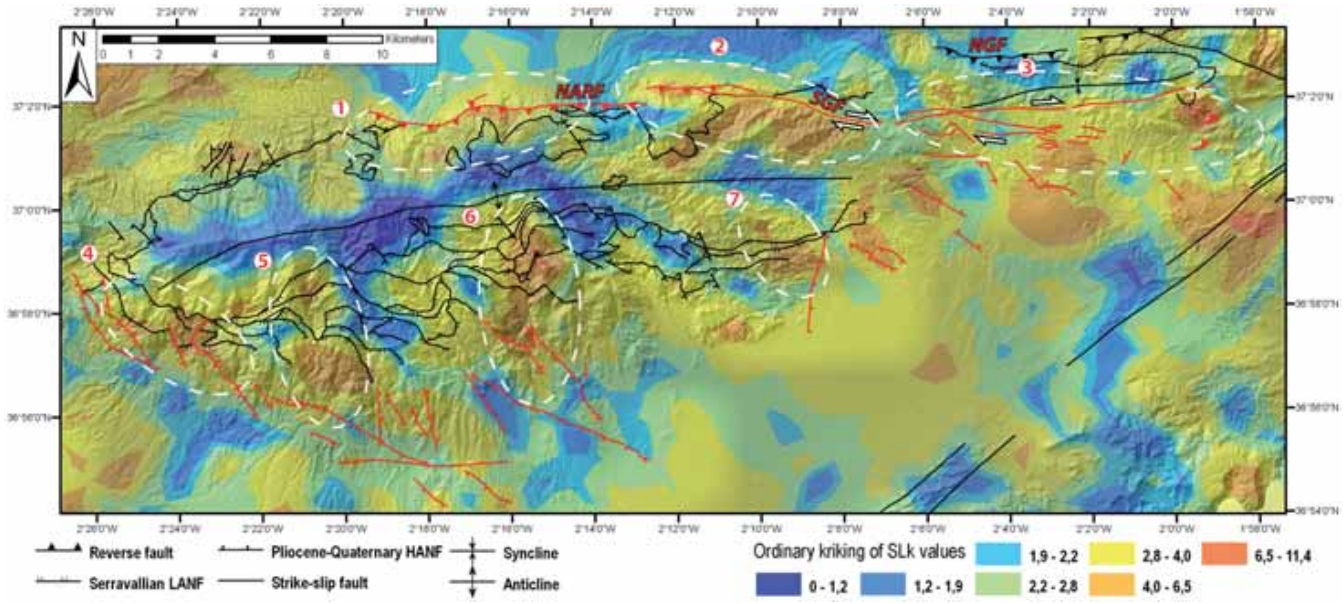

Fig. 7.- *SLk* map and main tectonic structures of Sierra Alhamilla: the North Alhamilla Reverse Fault (NARF) and the South Gafarillos Fault (SGF) after Martínez-Martínez *et al.*(1997). Active faults during the Quaternary are shown in red.

Fig. 7.- Mapa SLk y principales estructuras tectónicas de la Sierra Alhamilla: la falla inversa del N de Alhamilla (NARF) y la falla del Sur de Gafarillos (SGF) según Martínez-Martínez *et al.* (1997). Se muestran en rojo las fallas con actividad cuaternaria.

sional system, connected by a transfer zone to the south of Sierra Nevada, and the active NE-SW active folding in Sierra Nevada are compatible with the present-day NW-SE trend in the regional compressional stress. This model can help to elucidate the recent tectonic evolution of the whole system including Sierra Nevada mountain range and the Granada and Guadix-Baza Neogene basins. Uplift in the Sierra Nevada mountain range and the Guadix-Baza basin is a coetaneous process to the active extensional subsidence in the Granada basin.

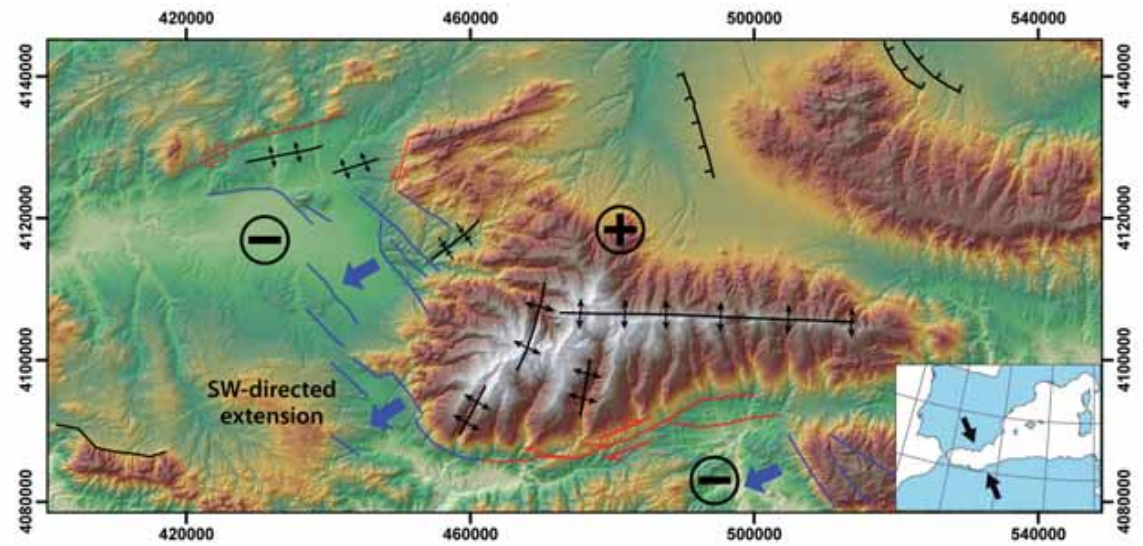

Fig. 8.- General sketch showing the tectonic configuration of the Sierra Nevada area. The uplifted block is located eastwards and it includes the Sierra Nevada mountain range, the Guadix-Baza basin and the NE border of the Granada basin. The Granada basin lies on the hanging wall of the extensional system, thus being affected by active sinking.

Fig. 8.- Esquema general que muestra la configuración tectónica del área de Sierra Nevada. El bloque levantado se sitúa hacia el este e incluye a Sierra Nevada, la Cuenca de Guadix-Baza y el borde NE de la Cuenca de Granada. La Cuenca de Granada está en el bloque de techo de un sistema extensional activo que produce su subsidencia.

5.2. Morphometric contribution to the tectonic scenario in the Sierra Alhamilla

The qualitative and quantitative geomorphic analyses carried out in Sierra Alhamilla suggest that it has been tectonically active during the Pleistocene and the Holocene, and probably up to present-day. The tectonic structures that control the hillslope and drainage network of the Sierra Alhamilla and surrounding Neogene to Quaternary sedimentary basins are the Polopos fault system and the NW-SE- to NNW-SSE-striking high-angle normal fault system, to the north and to the south of the ridge, respectively. In both cases the relative uplift of one of the two fault blocks (the foot-wall in the case of the normal faults and the hanging-wall in that of the reverse faults) induces a set of geomorphic responses. Typically they are: regular mountain fronts that show low values of S_{mf} and V_f, highly asymmetric drainage basins that give information about tectonic tilting, streams with convex longitudinal profiles and drainage basins with convex and complex hypsometric curves in response to head- or foot-rejuvenation processes, and finally high Slk anomalies near to the fault and on the uplifted fault block.

6. Conclusion

This work summarizes some of the new GIS-based methods for the landscape analysis recently used in two areas of the Betic Cordillera (central and eastern sectors). Through the application of such geomorphic analyses it is possible to understand tectonic activity and Quaternary landscape evolution, both necessary to establish coherent tectonic models. In the Betic Cordillera, the present-day landscape is mainly conditioned by the recent tectonic activity, and has to be considered as the key to estimate differential uplift, folding, subsidence and displacement rates.

Through the application of new GIS-based methodologies for drainage network and landscape analysis it is possible to reach a better understanding of the recent tectonic activity. These morphometric analyses are especially valuable in areas of low-to-medium tectonic rates (0.1 - 2 mm/yr) with scarce chronological dating. In this work, on the basis of these morphometric analyses, new and more complete tectonic models have been proposed for Sierra Nevada and Sierra Alhamilla regions (central and eastern Betic Cordillera respectively). The evolution of Sierra Nevada mountain range is closely related with the landscape of the Granada and Guadix-Baza basins. The Granada basin is located in the hanging wall of a NW-SE directed extensional system, whereas the Guadix-Baza basin, the NE border of the Granada basin, and the Sierra Nevada mountain range are located in the footwall, thus being affected by active uplift in the Upper-Pleistocene. In the Sierra Alhamilla area, the use of geomorphic analyses allow estimating tectonic activity and infer tectonic rates for structures that were thought to be inactive in the Upper-Pleistocene.

Acknowledgments

This study was supported by research projects CGL2008-03249/BTE, CGL-2011-29920, TOPOIBERIA CONSOLIDER-INGENIO2010 and CTM2007-66179-C02-01/MAR from the Spanish Ministry of Science and Innovation and MMA083/2007 from the Spanish Ministry of Environment. We thank Dr. José A. Álvarez and an anonymous reviewer for their constructive revisions that helped to improve the scientific quality of this paper.

References

Alfaro, P., Galindo Zaldívar, J., Jabaloy Sánchez, A., López Garrido, A.C., Sanz de Galdeano, C. (2001): Evidence for the activity and paleoseismicity of the Padul fault (Betic Cordillera, SE Spain). *Acta Geológica Hispánica* 36, 283-295.

Alfaro, P., Delgado, J., Sanz de Galdeano, C., Galindo-Zaldívar, J., García-Tortosa, F.J., López-Garrido, A.C., López-Casado, C., Marín-Lechado, C., Gil, A., Borque, M.J. (2008): The Baza Fault: a major active extensional fault in the central Betic Cordillera (south Spain). *International Journal of Earth Sciences (Geol Rundsch)* 97, 1353-1365. doi:10.1007/s00531-007-0213-z.

Azañón, J. M., Azor, A., Booth-Rea, G., Torcal, F. (2004): Small-scale faulting, topographic steps and seismic ruptures in the Alhambra (Granada, southeast Spain), *Journal of Quaternary Science* 19, 219-227. doi:10.1002/jqs.838.

Azañón, J.M., Azor, A., Pérez-Peña, J.V., Carrillo, J.M. (2005): Late Quaternary large-scale rotational slides induced by river incision: The Arroyo de Gor area (Guadix basin, SE Spain). *Geomorphology* 69, 152-168. doi:10.1016/j.geomorph.2004.12.007.

Balanyá, J.C., García-Dueñas, V. (1987): Les directions structurales dans le Domaine d'Alborán de part et d'autre du Détroit de Gibraltar. *Comptes Rendus de l'Académie des Sciences de Paris* 304, 929-932.

Barragán, G. (1997): *Evolución Geodinámica de la Depresión de Vera*. PhD Thesis, Universidad de Granada: 300 p.

Bell, J.W., Amelung, F., King, G.C.P. (1997): Preliminary late Quaternary slip history of the Carboneras fault, southeastern Spain. *Journal of Geodynamics* 24, 51-66. doi:10.1016/S0264-3707(96)00029-4.

Booth-Rea, G., Azañón, J.M., Azor, A., García-Dueñas, V. (2004): Influence of strike-slip fault segmentation on drainage evolution and topography. A case study: the Palomares fault zone (southeastern Betics, Spain). *Journal of Structural Geology* 26, 1615-1632. doi:10.1016/j.jsg.2004.01.007.

Booth-Rea, G., Azañón, J.M., Martínez-Martínez, J.M., Vidal, O., García-Dueñas, V. (2005): Contrasting structural and P-T evolutions of tectonic units in the southeastern Betics: key for understanding the exhumation of the Alboran Domain HP/LT crustal rocks (Western Mediterranean). *Tectonics* 24, TC2009. doi:10.1029/2004TC001640.

Booth-Rea, G., Ranero, C., Martínez-Martínez, J.M., Grevemeyer, I. (2007): Crustal types and Tertiary tectonic evolution of the Alborán sea, western Mediterranean. *Geochemistry Geophysics Geosystems* 8, Q10004. doi:10.1029/2007GC001639.

Bousquet, J.C. (1979): Quaternary strike-slip faults in southeastern Spain. *Tectonophysics* 52, 277-286. doi:10.1016/0040-1951(79)90232-4.

Bull, W.B. (1977): Tectonic geomorphology of the Mojave Desert, California. *U.S. Geological Survey Contract Report 14-08-001-G-394*, 376 p.

Bull, W.B. (2007): *Tectonic Geomorphology of Mountains: A New Approach to Paleoseismology.* Wiley-Blackwell, Oxford: 326 p.

Bull, W.B. (2009): *Tectonically Active Landscapes.* Wiley-Blackwell, Oxford: 326 p.

Bull, W.B., McFadden, L.D. (1977): Tectonic geomorphology north and south of the Garlock fault, California. In: D. O. Doehering (ed.), *Geomorphology in arid regions. Proccedings at the Eighth Annual Geomorphology Simposium.* State University of New York. Binghamton, NY: 115-138.

Burbank, D.W., Anderson, R.S. (2001): *Tectonic Geomorphology.* Blackwell Science, Oxford: 247 p.

Calvache, M.L., Viseras, C. (1997): Long-term control mechanisms of stream piracy processes in Southeast Spain. *Earth Surface Processes and Landforms* 22, 93-105. doi:10.1002/(SICI)1096-9837(199702).

Clark, M.K., Schoenbohm, L.M., Royden, L.H., Whipple, K.X., Burchfiel, B.C., Zhang, X., Tang, W., Wang, E., Chen, L. (2004): Surface uplift, tectonics, and erosion of eastern Tibet from large-scale drainage patterns. *Tectonics* 23, TC1006. doi:10.1029/2002TC001402.

Comas, M.C., Platt, J.P., Soto, J.I., Watts, A.B. (1999): The Origin and Tectonic History of the Alborán Basin: Insights from Leg 161 Results. In: R. Zahan, M. C. Comas , A. Klaus (eds.), *Proceedings of the Ocean Drilling Program, Scientific Results:* 555-579.

Dewey, J.F., Helman, M.L., Turco, E., Hutton, D.H.W., Knott, S.D. (1989): Kinematics of the western Mediterranean. In: M. P. Coward, D. Dietrich , R. G. Park (ed.), *Alpine Tectonics.* Special Publication Geological Society of London. London: 265-283. doi:10.1144/GSL.SP.1989.045.01.15.

El Hamdouni, R., Irigaray, C., Fernandez, T., Chacon, J., Keller, E.A. (2008): Assessment of relative active tectonics, southwest border of the Sierra Nevada (southern Spain). *Geomorphology* 96, 150-173. doi:10.1016/j.geomorph.2007.08.004.

Fernández, J., Viseras, C., Soria, J. (1996): Stratigraphic architecture of the Neogene basins in the central sector of the Betic Cordillera (Spain): tectonic control and base-level changes. In: Friend, P.F., Dabrio, C. (eds.), *Tertiary Basins of Spain: The Stratigraphic Record of Crustal Kinematics*. Cambridge Univ. Press, Cambridge: 353-365.

Galindo-Zaldívar, J., Gil, A.J., Borque, M.J., González Lodeiro, F., Jabaloy Sánchez, A., Marín-Lechado, C., Ruano, P., Sanz de Galdeano, C. (2003): Active faulting in the internal zones of the central Betic Cordilleras (SE, Spain). *Journal of Geodinamics* 36, 239-250. doi:10.1016/S0264-3707(03)00049-8.

García-Dueñas, V., Balanyá, J.C., Martínez-Martínez, J.M. (1992): Miocene extensional detachments in the outcropping basement of the Northern Alboran Basin (Betics) and their tectonic implications. *Geo-Marine Letters* 12, 88-95. doi:10.1007/BF02084917.

García-Tortosa, F.J., Alfaro, P., Galindo-Zaldívar, J., Gibert, L., López-Garrido, A.C., Sanz de Galdeano, C., Ureña, M. (2008): Geomorphologic evidence of the active Baza Fault (Betic Cordillera, South Spain). *Geomorphology* 97, 374-391. doi:10.1016/j.geomorph.2007.08.007.

García-Tortosa, F.J., Alfaro, P., Sanz de Galdeano, C., Galindo-Zaldívar, J. (2011). Glacis geometry as a geomorphic marker of recent tectonics: The Guadix–Baza basin (South Spain). *Geomorphology* 125, 517-529. doi:10.1016/j.geomorph.2010.10.021.

Gràcia, E., Pallas, R., Soto, J.I., Comas, M., Moreno, X., Masana, E., Santanach, P., Diez, S., Garcia, M., Danobeitia, J. (2006): Active faulting offshore SE Spain (Alboran Sea): Implications for earthquake hazard assessment in the Southern Iberian Margin. *Earth and Planetary Science Letters* 241, 734-749. doi:10.1016/j.epsl.2005.11.009.

Giaconia, F., Booth-Rea, G., Martínez-Martínez, J.M., Azañón, J.M., Pérez-Peña, J.V., Pérez-Romero, J., Villegas I. (2012): Geomorphologic evidence of active tectonics in Sierra Alhamilla (eastern Betics, SE Spain). *Geomorphology* 145-146, 90-106. doi:10.1016/j.geomorph.2011.12.043.

Hack, J.T. (1973): Stream profile analysis and stream-gradient index. *Journal of Research of the U.S. Geological Survey* 1, 421-429.

Huibregtse, P., van Alebeek, H., Zall, M., Biermann, C. (1998): Paleostress analysis of the northern Nijar and southern Vera basins: constraints for the Neogene displacement history of major strike-slip faults in the Betic Cordilleras, SE Spain. *Tectonophysics* 300, 79-101. doi:10.1016/S0040-1951(98)00235-2.

Jonk, R., Biermann, C. (2002): Deformation in Neogene sediments of the Sorbas and Vera Basins (SE Spain): constraints on simple-shear deformation and rigid body rotation along major strike-slip faults. *Journal of Structural Geology* 24, 963-977. doi:10.1016/S0191-8141(01)00107-9.

Keller, E.A., Pinter, N. (2002): *Active Tectonics. Earthquakes, Uplift, and Landscape.* Prentice Hall, New Jersey: 362 p.

Keller, E.A., Sanz de Galdeano, C., Chacon, J. (1996): Tectonic geomorphology and earthquake hazard of Sierra Nevada, Southern Spain. *1ª Conferencia Internacional Sierra Nevada*, Granada, 201-218.

Korup, O. (2006): Rock-slope failure and the river long profile. *Geology* 34, 45-48. doi:10.1130/G21959.1.

Marín-Lechado, C., Galindo-Zaldivar, J., Rodriguez-Fernandez, L.R., Serrano, I., Pedrera, A. (2005): Active faults, seismicity and stresses in an internal boundary of a tectonic arc (Campo de Dalias and Nijar, southeastern Betic Cordilleras, Spain). *Tectonophysics* 396, 81-96. doi:10.1016/j.tecto.2004.11.001.

Martínez-Díaz, J.J. (2002): Stress field variation related to fault interaction in a reverse oblique-slip fault: the Alhama de Murcia fault, Betic Cordillera, Spain. *Tectonophysics* 356, 291-305. doi:10.1016/S0040-1951(02)00400-6.

Martínez-Martínez, J.M., Azañón, J.M. (1997): Mode of extensional tectonics in the southeastern Betics (SE Spain). Implications for the tectonic evolution of the peri-Alborán orogenic system. *Tectonics* 16, 205-225. doi:10.1029/97TC00157.

Martínez-Martínez, J.M., Soto, J.I., Balanyá, J.C. (2002): Orthogonal folding of extensional detachments: structure and origin of the Sierra Nevada elongated dome (Betics, SE Spain). *Tectonics* 21, 1012. doi:10.1029/2001TC001283.

Martínez-Martínez, J.M., Soto, J.I., Balanyá, J.C. (2004): Elongated domes in extended orogens: A mode of mountain uplift in the Betics (southeast Spain). In: D. L. Whitney, C. Teyssier , C. S. Siddoway (ed.), *Gneiss domes in orogeny.* Geological Society of America. Boulder, Colorado: 243-266.

Martínez-Martínez, J.M., Booth-Rea, G., Azañón, J.M., Torcal, F. (2006): Active transfer fault zone linking a segmented extensional system (Betics, southern Spain): Insight into heterogeneous extension driven by edge delamination. *Tectonophysics* 422, 159-173. doi:10.1016/j.tecto.2006.06.001.

Martín-Rojas, I., Martín-Martín, M., Sanz de Galdeano, C. (2001): Índices geomorfológicos de los frentes montañosos del borde occidental de Sierra Nevada (Granada - España). In: C. Sanz de Galdea-

no, J. Pelaez Montilla , A. C. López Garrido (eds.), *La cuenca de Granada. Estructura, tectónica activa, sismicidad, geomorfología y dataciones existentes.* Universidad de Granada, Granada: 59-66.

Masana, E., Martínez-Díaz, J.J., Hernández-Enrile, J.L., Santanach, P. (2004): The Alhama de Murcia fault (SE Spain), a seismogenic fault in a diffuse plate boundary: Seismotectonic implications for the Ibero-Magrebian region. *Journal of Geophysical Research* 109, B01301. doi:10.1029/2002JB002359.

McClusky, S., Reilinger, R., Mahmoud, S., Ben Sari, D., Tealeb, A. (2003): GPS constraints on Africa (Nubia) and Arabia plate motions. *Geophysical Journal International* 155, 126-138. doi:10.1046/j.1365-246X.2003.02023.x.

Menéndez, I., Silva, P.G., Martín-Betancor, M., Pérez-Torrado, F.J., Guillou, H., Scaillet, S. (2008). Fluvial dissection, isostatic uplift, and geomorphological evolution of volcanic islands (Gran Canaria, Canary Islands, Spain). *Geomorphology* 102, 189-203. doi:10.1016/j.geomorph.2007.06.022.

Montenat, C., Ott d´Estevou, P. (1990): Easten betic Neogene Basins-A review. In: C. Montenat (ed.), *Les Bassins Neogenes du Domaine Bétique Orientale (Espagne).* Documents et Travaux IGAL, 9-15.

Moran, P.A.P. (1950): Notes on continuous stochastic phenomena. *Biometrika* 37(1-2), 17-23.

Ott d'Estevou, P., Montenant, C. (1990): Le Bassin de Sorbas-Tabernas. In: C. Montenant (ed.), *Les Bassins Neogenes du Domaine Bétique Oriental (Espagne).* IGAL, CNRS. Paris: 101-128.

Ord, J. K., Getis, A. (1995): Local spatial autocorreltacion statistics. Distributional issues and application. *Geographical analysis* 27, 286-306. doi:10.1111/j.1538-4632.1995.tb00912.x.

Ouchi, S. (1985): Response of alluvial rivers to slow active tectonic movement. *Geological Society of America Bulletin* 96, 504-515. doi:10.1130/0016-7606(1985)96<504:ROARTS>2.0.CO;2.

Pedrera, A., Marin-Lechado, C., Galindo-Zaldivar, J., Rodriguez-Fernandez, L.R., Ruiz-Constan, A. (2006): Fault and fold interaction during the development of the Neogene-Quaternary Almeria-Nijar basin (SE Betic Cordilleras). In: C. Moratti, A. Chaluan (eds.), *Tectonics of the Western Mediterranean and North Africa.* Geological Society, London, Special Publications, 217-230. doi:10.1144/GSL.SP.2006.262.01.13.

Pedrera, A., Pérez-Peña, J.V., Galindo-Zaldívar, J., Azañón, J.M., Azor, A. (2009): Testing the sensitivity of geomorphic indices in areas of low-rate active folding (eastern Betic Cordillera, Spain). *Geomorphology* 105, 218-231. doi:10.1016/j.geomorph.2008.09.026.

Pérez-Peña, J.V., Azañón, J.M., Azor, A., Delgado, J., González-Lodeiro, F. (2009a): Spatial analysis of stream power using GIS: SLk anomaly maps. *Earth Surface Processes and Landforms* 34, 16-25. doi:10.1002/esp.1684.

Pérez-Peña, J.V., Azañón, J.M., Azor, A. (2009b): CalHypso: An ArcGIS extension to calculate hypsometric curves and their statistical moments. Applications to drainage basin analysis in SE Spain. *Computers & Geosciences* 35, 1214-1223. doi:10.1016/j.cageo.2008.06.006.

Pérez-Peña, J.V., Azañón, J.M., Booth-Rea, G., Azor, A., Delgado, J. (2009c): Differentiating geology and tectonics using a spatial autocorrelation technique for the hypsometric integral. *Journal of Geophysical Research-Earth Surface* 114, F02018. doi:10.1029/2008JF001092.

Pérez-Peña, J.V., Azañón, J.M., Azor, A., Tuccimei, P., Della Seta, M., Soligo, M. (2009d): Quaternary landscape evolution and erosion rates for an intramontane Neogene basin (Guadix-Baza basin, SE Spain). *Geomorphology* 106, 206-218. doi:10.1016/j.geomorph.2008.10.018.

Pérez-Peña, J.V., Azor, A., Azañón, J.M., Keller, E.A. (2010): Active tectonics in the Sierra Nevada (Betic Cordillera, SE Spain): Insights from geomorphic indexes and drainage pattern analysis. *Geomorphology* 119, 74-87. doi:10.1016/j.geomorph.2010.02.020.

Platt, J.P., Allerton, S., Kirker, A., Mandeville, C., Mayfield, A., Platzman, E.S., Rimi, A. (2003): The ultimate arc: Differential displacement, oroclinal bending, and vertical axis rotation in the External Betic-Rif arc. *Tectonics* 22, 1017. doi:10.1029/2001TC001321.

Reinhardt, L.J., Bishop, P., Hoey, T.B., Dempster, T.J., Sanderson, D.C.W. (2007): Quantification of the transient response to base-level fall in a small mountain catchment: Sierra Nevada, southern Spain. *Journal of Geophysical Research-Earth Surface* 112, F03S05. doi:10.1029/2006JF000524.

Rodríguez-Fernández, J., Sanz de Galdeano, C. (2006): Late orogenic intramontane basin development: the Granada basin, Betics (southern Spain). *Basin Research* 18, 85-102. doi:10.1111/j.1365-2117.2006.00284.x.

Rodríguez-Fernández, J., Azor, A., Azañón, J.M. (2012): The Betic intramontane basins (SE spain): stratigraphy, subsidence, and tectonic history. In: Busby, C., Azor, A. (eds.), *Tectonics of Sedimentary Basins: Recent Advances*, Blackwell Publishing Ltd, 23, 461-479.

Sanz de Galdeano, C. (1996): Datos sobre las deformaciones neógenas y cuaternarias del sector del Padul (Granada). *1ª Conferencia Internacional Sierra Nevada*, Granada, 219-231.

Sanz de Galdeano, C., Peláez-Montilla, J.A., Casado C.L. (2003): Seismic potential of the main active faults in the Granada basin (southern Spain), *Pure and Applied Geophysics* 160, 1537-1556. doi:10.1007/s00024-003-2359-3.

Sanz de Galdeano, C., Shanov, S., Galindo-Zaldivar, J., Radulov, A., Nikolov, G. (2010): A new tectonic discontinuity in the Betic Cordillera deduced from active tectonics and seismicity in the Tabernas Basin. *Journal of Geodynamics* 50, 57-66. doi:10.1016/j.jog.2010.02.005.

Schumm, S.A., Dumont, J.F., Holbrook, J.M. (2000): *Active tectonics and alluvial rivers.* Cambridge University Press, Cambridge: 276 p.

Serpelloni, E., Vannucci, G., Pondrelli, S., Argnani, A., Casula, G., Anzidei, M., Baldi, P., Gasperini, P. (2007): Kinematics of the Western Africa-Eurasia plate boundary from focal mechanisms and GPS data. *Geophysical Journal International* 169, 1180-1200. doi:10.1111/j.1365-246X.2007.03367.x.

Silva, P.G., Goy, J.L., Zazo, C., Bardají, T. (2003): Fault-generated mountain fronts in southeast Spain: geomorphologic assessment of tectonic and seismic activity. *Geomorphology* 50, 203-225. doi:10.1016/S0169-555X(02)00215-5.

Stapel, G., Moeys, R., Biermann, C. (1996): Neogene evolution of the Sorbas basin (SE Spain) determined by paleostress analysis. *Tectonophysics* 255, 291-305. doi:10.1016/0040-1951(95)00190-5.

Strahler, A.N. (1952): Hypsometric (area-altitude) analysis of erosional tophography. *Geological Society of America Bulletin* 63, 1117-1142. doi:10.1130/0016-7606(1952)63[1117:HAAOET]2.0.CO;2.

Vázquez, M., Jabaloy, A., Barbero, L., Stuart, F. (2011): Deciphering tectonic- and erosion-driven exhumation of the Nevado–Filábride Complex (Betic Cordillera, Southern Spain) by low temperature thermochronology. *Terra Nova*, 23, 257-263. doi:10.1111/j.1365-3121.2011.01007.x.

Weijermars, R., Roep, T.B., Van den Eeckhout, B., Postma, G., Kleverlaan, K. (1985): Uplift history of a Betic fold nappe inferred from Neogene-Quaternary sedimentation and tectonics (in the Sierra Alhamilla and Almería, Sorbas and Tabernas Basins of the Betic Cordilleras, SE Spain). *Geologie en Mijnbouw* 64, 397-411.

Whipple, K.X., Tucker, G.E. (1999): Dynamics of the stream-power river incision model: Implications for height limits of mountain ranges, landscape response timescales, and research needs. *Journal of Geophysical Research-Solid Earth* 104, 17661-17674. doi:10.1029/1999JB900120.

ISSN (print): 1698-6180. ISSN (online): 1886-7995
www.ucm.es/info/estratig/journal.htm

Journal of Iberian Geology 38 (1) 2012: 191-208
http://dx.doi.org/10.5209/rev_JIGE.2012.v38.n1.39213

Recent and active faults and folds in the central-eastern Internal Zones of the Betic Cordillera

Las fallas y pliegues recientes y activos de la parte centro-oriental de las Zonas Internas de la Cordillera Bética

A. Pedrera*[1], J. Galindo-Zaldívar[2, 3], C. Marín-Lechado[1], F.J. García-Tortosa[4], P. Ruano[2, 3], A.C. López Garrido[3], J.M. Azañón[2, 3], J.A. Peláez[5], and F. Giaconia[2]

[1] *Instituto Geológico y Minero de España- Ríos Rosas 23, 28003 Madrid, Spain.*
[2] *Departamento de Geodinámica, Universidad de Granada 18071-Granada, Spain.*
[3] *Instituto and Andaluz de Ciencias de la Tierra, CSIC- Universidad de Granada, 18071-Granada, Spain.*
[4] *Dpto. de Geología, Universidad de Jaén, Campus Las Lagunillas 23071 Jaén, Spain.*
[5] *Dpto de Física, Universidad de Jaén, Campus Las Lagunillas 23071 Jaén, Spain.*

**Corresponding author: a.pedrera@igme.es*

Received: 05/07/2011 / Accepted: 25/01/2012

Abstract

The most recent tectonic structures of the central-eastern Internal Zones of the Betic Cordillera (from 3.1ºW to 1.7ºW and to the south of 37.525ºN) include fault and folds developed from the Late Miocene onwards, which are related to N-S/NW-SE directed continental collision and moderate thickening of a crust that is relatively hot at depth. In this setting, E-W to WSW-ENE folds, with locally associated E-W transpressive right-lateral and reverse faults, favoured the emersion of the northern Alborán basin palaeomargin and the progressive intramontane basin disconnection. The NNE-SSW to NE-SW trending regional left-lateral Palomares and Carboneras fault zones are dominant structures in the easternmost part of the cordillera. In addition, NW-SE to WNW-ESE trending normal and oblique-slip normal faults are widespread. The collision is still active and continues to drive active folds and faults, some probably being the likely source of moderate-sized earthquakes. The Campo de Dalías and surrounding sectors, deformed by active ENE-WSW folds and NW-SE to WNW-ESE oblique-slip normal faults, are probably the sites with the largest concentration of significant earthquakes during recent years. Moderate-magnitude earthquakes (Mw 5.0 to 6.5) have occurred there at fairly regular intervals, in 1804, 1910, and 1994. Toward the east, NW-SE trending normal faults extending from Almería to the Tabernas basin deform the Quaternary rocks with associated moderate seismicity (the 2002 Gergal Mw 4.7 earthquake, and possibly the 1894 Nacimiento earthquake, felt with intensity VII). In the Sorbas-Vera basin, the Palomares fault zone is also responsible for moderate-sized earthquakes (1518 Vera earthquake). In the Almanzora corridor, NW-SE to WNW-ESE trending Lúcar-Somontín faults also could be considered one of the possible source of moderate-magnitude seismicity (1932 Lúcar, Mw 4.8 earthquake felt

with intensity VIII). Toward the east, between Albox and Partaloa, several small reverse faults and associated compressive structures deform Quaternary alluvial and fluvial sediments. Although some of these folds reveal a slow and progressive deformation from the Middle Pleistocene onwards, some of these reverse fault segments that deform the western Huércal-Overa basin could host the 1972 NW Partaloa, mbLg 4.8 earthquake, felt with intensity VII.

Keywords: Active Tectonics; Earthquakes; Tectonic Evolution; Gibraltar Arc.

Resumen

Las estructuras tectónicas más recientes que deforman la parte centro-oriental de las Zonas Internas de Cordillera Bética (entre 3.1º y 1.7ºO y al sur de 37.525ºN) son fallas y pliegues que comenzaron a formarse aproximadamente en el Mioceno superior en un contexto de colisión continental N-S/NO-SE y moderado engrosamiento cortical. En este marco tectónico, pliegues y fallas transpresivas dextras e inversas de direcciones E-O/OSO-ENE favorecieron la emersión del borde norte de la paleocuenca de Alborán y la progresiva desconexión de pequeñas cuencas intramontañosas. Además, comenzaron a formarse las grandes zonas de falla de Palomares y Carboneras, con direcciones NNE-SSO y NE-SO respectivamente y movimientos sinistros, que también han condicionado la evolución de la Cordillera Bética oriental desde el Mioceno superior. Algunas fallas con salto normal/normal-oblicuo y trazas NO-SE/ONO-ESE también se han desarrollado ampliamente en toda la zona de estudio. La colisión, aún activa, permite que algunos pliegues y fallas continúen propagándose en la actualidad, eventualmente causando terremotos con magnitudes moderadas. El Campo de Dalías y los sectores adyacentes, deformados por pliegues activos de direcciones ENE-OSO y fallas NO-SE/ONO-ESE normales-oblicuas, probablemente representan la zona con mayor concentración de terremotos importantes (Mw 5.0-6.5) con eventos recurrentes en 1804, 1910 y 1994. Al este del Campo de Dalías, una amplia zona de falla normal se extiende en dirección NO-SE desde Almería hasta la cuenca de Tabernas. Esta zona de falla muestra evidencias de funcionamiento durante el Cuaternario y tiene sismicidad moderada asociada a su terminación septentrional (el terremoto de Gergal en 2002 con Mw 4.7; y posiblemente el terremoto de Nacimiento en 1894 con intensidad VII). La zona de falla de Palomares es también responsable de terremotos moderados en la Cuenca de Sorbas-Vera (terremoto de Vera en 1518). En la parte central del corredor del Almanzora, alguno de los segmentos de falla normal que se extienden entre Lúcar y Somontín podría ser responsable del terremoto de Lúcar, en 1932 (Mw 4.8 e intensidad VIII). Al este, entre Albox y Partaloa, se han descrito fallas inversas y pliegues asociados que deforman sedimentos cuaternarios. Aunque algunas de estas estructuras muestran evidencias de funcionamiento lento y progresivo durante el Cuaternario, el terremoto de Partaloa en 1972 (mbLg 4.8 e intensidad VII) pudo ser causado por la actividad de cualquiera de estos segmentos de falla inversa que deforman la parte occidental de la cuenca de Huércal-Overa.

Palabras clave: Sismicidad, Tectónica Activa; Terremotos; Evolución Tectónica; Arco de Gibraltar.

1. Introduction

The recent and active tectonic structures of the Betic Cordillera have attracted attention of Earth scientists since the 1970s (Andrieux *et al.*, 1971; Biju Duval *et al.*, 1977; Groupe de Recherche Neotectonique, 1977; Bousquet and Montenat, 1974; Bousquet and Phillip, 1976; Bousquet, 1979), and since then, much geological and geomorphological research has been focused on their identification in order to establish the mechanisms responsible for the tectonic evolution of the orogen (*e.g*., Sanz de Galdeano, 1983; Ott d'Estevou and Montenat, 1985; Sanz de Galdeano, 1990) and to estimate their seismogenic potential (*e.g*., Sanz de Galdeano and López Casado, 1988; Sanz de Galdeano *et al.*, 1995). While the location, geometry, and kinematics of the main structures are well established, the processes involved in their development and the present-day activity of some of these structures are still under debate. It is widely accepted that compressional and extensional structures have deformed the Internal Zones of the Betic Cordillera since the Late Miocene. This region exhibits a variety of deformational styles, dominated by folds, right-lateral and normal faults in the central Betics (*e.g.,* Galindo-Zaldívar *et al.*, 2003), and by large left-lateral strike-slip faults in the eastern sector of the cordillera that also interact with folds and normal/normal-oblique faults (*e.g.,* Martínez-Díaz, 2002; Masana *et al.*, 2004; Booth-Rea *et al.*, 2003; Pedrera *et al.*, 2010a). The present study attempts to sketch a coherent picture of these recent tectonic structures that deform the central-eastern (from the longitude 3.1ºW to 1.7ºW and to the south of 37.525ºN) Internal Zones of the Betic Cordillera (Fig. 1). Special attention is placed on the faults and folds that have been active during Quaternary times, which are potential sources of future earthquakes.

2. Geological setting

The Betic Cordillera, together with the Rif, constitutes the westernmost part of the Alpine Mediterranean belt in the convergent Eurasian and African plate boundary (Fig. 1A). The Alpine evolution of the orogen is determined by the interaction between the two major plates and the intermediate placed Alborán Domain (Internal

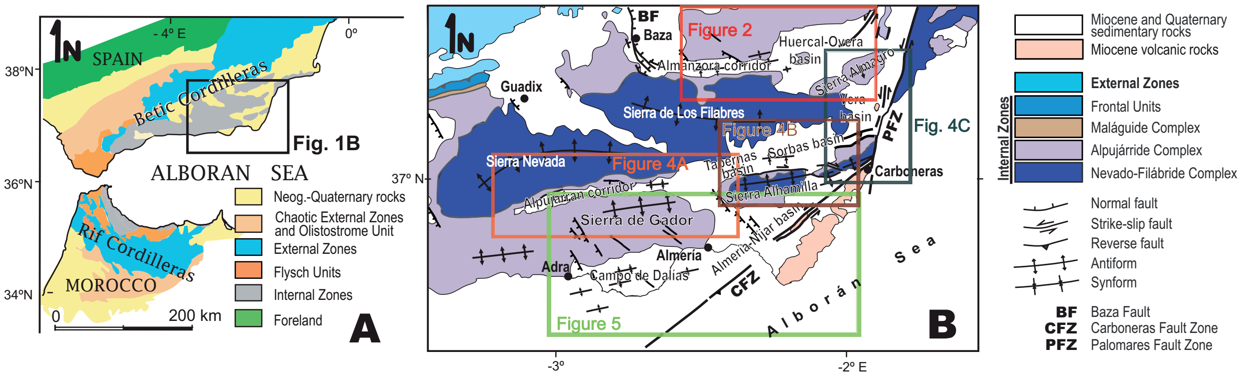

Fig. 1.- (A) Simplified geological map of the Betic and Rif Cordilleras including the location of figure 1B. (B) Geological sketch map of the central-eastern Betic Cordillera with the positions of the neotectonic maps of figures 2, 4A, 4B, 4C, 5.

Fig. 1.- (A) Mapa geológico simplificado de las Cordilleras Bético-Rifeñas con la posición de la figura 1B. (B) Mapa geológico simplificado del sector central y oriental de la Cordillera Bética con la localización de los mapas neotectónicos de la figuras 2, 4A, 4B, 4C, 5.

Zones of the Betic and Rif Cordillera) (*e.g.,* Andrieux *et al.*, 1971; Sanz de Galdeano, 1990). In a framework of continuous N-S to NW-SE convergence, subduction and subsequent collision, with the destruction of Mesozoic oceanic basins (*e.g.,* Martín-Algarra, 1987) and slab roll-back, reasonably explain the latest Oligocene to middle Miocene evolution of the Betic-Rif cordilleras and the development of the large Alborán basin (*e.g.,* Lonergan and White, 1997). Therefore, during the early and middle Miocene the metamorphic rocks of the Alborán Domain were exhumed at the footwall of extensional brittle-ductile detachments (Aldaya *et al.*, 1984; Galindo-Zaldívar, 1986; García-Dueñas and Martínez-Martínez, 1988; Jabaloy *et al.*, 1993) and the Alborán basin was formed, floored by thinned continental crust, exhibiting a large arched sedimentary depocenter: theWest Alborán basin (Comas *et al.*, 1992, 1999; Soto *et al.*, 1996; Chalouan and Michard, 2004). Roughly since the late Miocene, the subduction shifted to N-S/NW-SE continental collision, the crust started to thicken, and the northern margin of the Alborán basin progressively emerged. Consequently, intramontane sedimentary basins gradually became isolated from the original Alborán basin, some completely emerging (*e.g.,* Braga *et al.*, 2003). This continent collision is still active at a rate of 4-5 mm/yr (Argus *et al.*, 1989; DeMets *et al.*, 1990, 1994) and continues driving the development of active folds and faults (*e.g.,* Sanz de Galdeano *et al.*, 1995; Galindo-Zaldívar *et al.*, 2003). Therefore, current displacement of the Earth's surface reveals the oblique convergence between the Iberian and African plates, showing a movement of the Eurasian plate and the Betic Cordillera toward the SSW/SW with respect to the African plate (Stich *et al.*, 2006; Fadil *et al.*, 2006; Tahayt *et al.*, 2008; Vernant *et al.*, 2010), which is roughly in accordance with the present-day stress setting (*e.g.*, Fernández-Ibáñez *et al.*, 2007; Pedrera *et al.*, 2011).

In the Betic Cordillera, the structures that formed since the late Miocene up to now have been classically designated as recent or neotectonic. These structures determine the spatial distribution of the uplifted areas subjected to erosion and the sedimentary basins. Below, we describe the recent and active structures that, from north to south, deform the Almanzora corridor and the Huércal-Overa basin, the Alpujarran corridor and the Tabernas, Sorbas, and Vera basins, and the Campo de Dalías and the Almería-Níjar basin (Fig. 1B).

3. The Almanzora corridor and the Huércal-Overa basin

The Almanzora corridor and the Huércal-Overa basin are located between the Sierra de Los Filabres and Sierra de Las Estancias (Figs 1 and 2). Both basins are essentially filled by Serravallian-lower Tortonian continental/fluvial-deltaic sediments, and became a marine realm during the late Tortonian. The marine-continental transition started in Messinian times. Continental sedimentation along rivers and alluvial fans together with erosion occurred during the Pliocene and Quaternary.

3.1. Late Miocene tectonic structures

Compressive and extensional structures deformed the late Miocene-Quaternary sediments of the Almanzora corridor and the Huércal-Overa basin (Briend, 1981; Briend *et al.*, 1990; Mora-Gluckstadt, 1993; Poisson *et al.*, 1999;

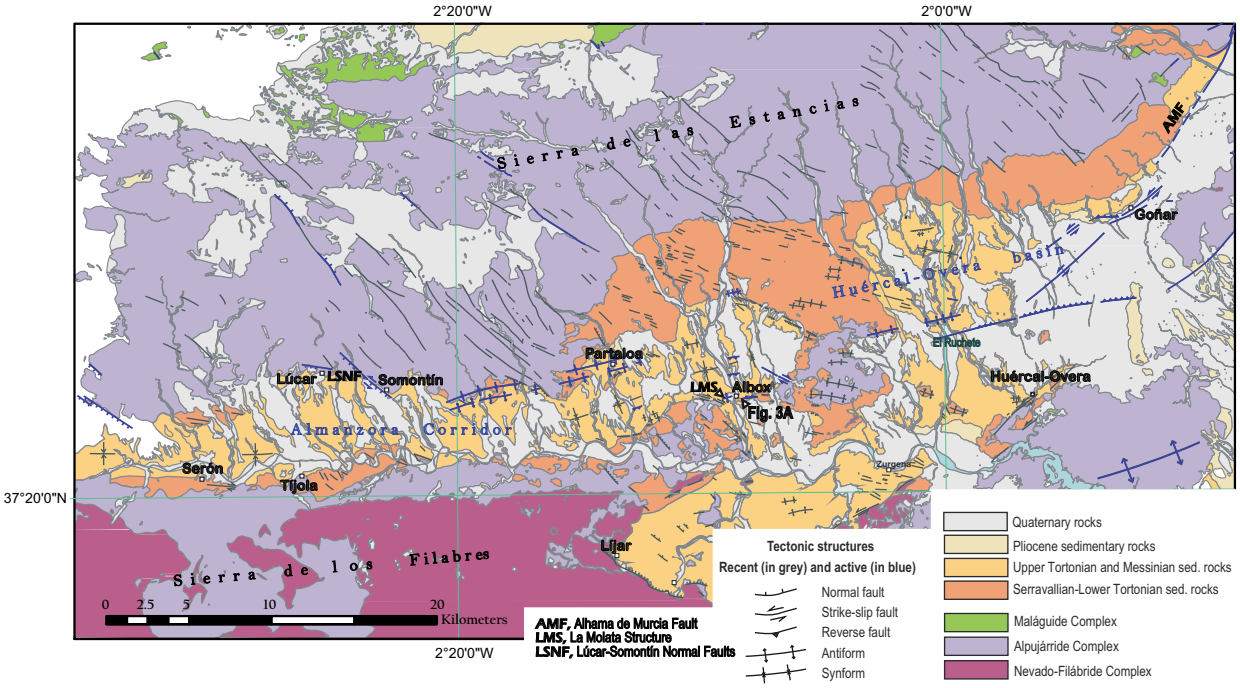

Fig. 2.- Geological map of the Almanzora corridor and the Huércal-Overa basin with traces of the recent (in grey) and active (blue) tectonic structures. The location of figure 3A is marked.

Fig. 2.- Mapa geológico del Corredor del Almanzora y la Cuenca de Huércal-Overa que incluye las trazas de las estructuras tectónicas recientes (en gris) y activas (en azul). La posición de la figura 3A está indicada.

Augier, 2004; Augier *et al.*, 2005; Meijninger and Vissers, 2006; Pedrera *et al.*, 2007; Pedrera *et al.*, 2010a). The study area was deformed by a succession of kilometric scale folds with orientations ranging from E-W to ENE-WSW: the Sierra de Los Filabres and Sierra de Almagro antiforms, Almanzora corridor synform and Sierra de Las Estancias antiform (Booth-Rea *et al.*, 2003, 2004; Pedrera *et al.*, 2007, 2009b). The antiforms coincide with the ranges where the metamorphic rocks crop out, while the synforms correspond to the sedimentary basins. Folding started there with the Sierra de los Filabres antiform nucleation during Serravallian-early Tortonian, as revealed by the syntectonic angular unconformities founded in its northern limb (Pedrera *et al.*, 2007). Large-scale folds continued growing and propagating to the north, forming the Almanzora corridor in the late Tortonian (Pedrera *et al.*, 2007). Moreover, the sedimentary rocks have been deformed since late Tortonian by ENE-WSW minor folds (Pedrera *et al.*, 2007; Pedrera *et al.*, 2010a). To the east, these minor folds progressively change their trend from ENE-WSW to WNW-ESE (Pedrera *et al.*, 2010a). In addition, the late Miocene sediments are quite deformed by several sets of faults. The most abundant set is formed by WNW-ESE to NW-SE normal faults that show a widespread distribution in the basins (Briend, 1981; Briend *et al.*, 1990; Mora-Gluckstadt, 1993; Poisson *et al.*, 1999; Augier, 2004; Augier *et al.*, 2005; Meijninger and Vissers, 2006; Pedrera *et al.*, 2007; Pedrera *et al.*, 2010a). Subvertical strike-slip dextral faults, E-W to ESE-WNW oriented, deformed the Tortonian sediments that crop out mainly in the southern Almanzora corridor boundary (Fig. 2; Poisson *et al.*, 1999; Pedrera *et al.*, 2007).

3.2. Active tectonic structures

The westernmost part of the Almanzora corridor is affected by a set of NW-SE faults that deform up to the Quaternary glacis and constitute the western end of the corridor. These fault segments are related to the normal Baza fault (Alfaro *et al.*, 2008; García-Tortosa *et al.*, 2008; Sanz de Galdeano *et al.*, this volume), which extends more than 30 km along the Baza basin, showing a N-S to NW-SE variable strike, and dipping to the NE (Fig. 1B). In the central part of the corridor, the Lúcar fault — formed by a set of ENE-WSW oriented and 40º-75º south dipping normal faults— locally deforms the Quaternary sediments. Close to Somontín, the Quaternary sediments are deformed by a NW-SE oriented high-dipping fault

that generates a steep scarp. The fault surface shows horizontal striation with a left-lateral sense of motion overprinted on the normal striation. The eastern Almanzora corridor (Somontín-Partaloa sector) and the western Huércal-Overa basin are both deformed by widespread small-scale contractional tectonic structures, which include WNW-ESE trending dextral faults and ENE-WSW oriented open folds, fault-propagation folds, and reverse faults (Figs. 2 and 3A; Briend *et al.*, 1990; Pedrera *et al.*, 2009a and 2009b). Using a geomorphological approach, García-Meléndez (2000) and García-Meléndez *et al.* (2004) defined the Albox fault as an ENE-WSW to E-W fault zone with reverse-dextral kinematics that runs from the eastern Huércal-Overa basin as far as the Almanzora corridor to the west. The La Molata fault-propagation fold is one of the best-exposed outcrops (Fig. 2, Pedrera *et al.*, 2009a. This fold and its related faults have propagated progressively, as evidenced by the syn-tectonic geometry of the growth strata. Strain rates calculated across the structure give a constant ~0.007 mm/yr horizontal shortening and ~0.014 mm/yr vertical displacement from the mid-Pleistocene to the present (Pedrera *et al.*, 2009a). The central and eastern part of the Huércal-Overa basin is deformed by ENE-WSW trending reverse faults with a splay geometry, belonging to the southern end of the Alhama de Murcia left-lateral transcurrent fault (AMF) (Martínez-Díaz *et al.*, this volume). These faults deform the Quaternary alluvial fan deposits in the eastern Huércal-Overa basin (Groupe de Recherche Néotectonique, 1977; Briend, 1981) and have been recently characterized with geomorphological, structural, and paleoseismologic studies (García-Meléndez *et al.*, 2003; Soler *et al.*, 2003; Masana *et al.*, 2005; Meijninger and Vissers, 2006; Ortuño *et al.*, 2009). Thus, paleoseismologic studies near Goñar (Fig. 2) in the eastern Huércal-Overa basin, identify at least two paleoearthquakes associated with the AMF during the last 150 ka and estimate a minimum vertical slip rate of ~0.02 mm/yr in the southern fault termination since the Middle Pleistocene (Ortuño *et al.*, 2009). In addition, a palaeoseismologic study in El Ruchete sector (Fig. 2) identified fault segments with short-term slip-rates ranging from 0.01 to 0.4 mm/yr and two possible paleoearthquakes deposits associated with them (Masana *et al.*, 2005). This reverse fault segment probably belongs to the horsetail reverse splay of the AMF (Fig. 2).

The drainage network of the Almanzora River, highly controlled by the above structures, reflects the activity of the faults and folds since the Messinian (Stokes, 2008; Stokes and Mather, 2000, 2003; Pedrera *et al.*, 2009c). The presence of normal faults condition small changes in the direction of the north Almanzora River tributary stream. In addition, the role of the above-described active folds in the landscape evolution and drainage development was characterized in the folded eastern Almanzora corridor and western Huércal-Overa basin (Pedrera *et al.*, 2009c).

4. The Alpujarran corridor, the Tabernas basin, and the Sorbas-Vera basin

The Alpujarran corridor is an E-W elongated valley formed by a roughly synformal structure located between the Sierra Nevada to the north and the Sierras Lújar-Contraviesa-Gádor to the south. Eastwards the corridor extends to the Tabernas basin, which continues into the Sorbas-Vera basin, between Sierra de Los Filabres to the north and Sierra Alhamilla and Sierra Cabrera to the south (Figs. 1 and 4). These basins are partially filled with lower Miocene to Quaternary deposits and constitute a zone of crustal weakness where recent and active deformation structures are nucleated (Ott d'Estevou *et al.*, 1990; Rodríguez-Fernández, 1982). Researchers agree on the presence throughout this area of a main right-lateral fault zone (*e.g.,* Sanz de Galdeano *et al.*, 1985; Galindo-Zaldívar, 1986; Sanz de Galdeano, 1989; Jabaloy *et al.*, 1992; Galindo-Zaldívar *et al.*, 2003; Martínez-Díaz and Hernández-Enrile, 2004; Martínez-Martínez, 2006; Martínez-Martínez *et al.*, 2006; Sanz de Galdeano *et al.*, 2010). However, controversy persists concerning the deep continuity of the structures, the relationships of the exposes faults with seismicity, the driving mechanisms, and in some cases the age of fault activity. On the other hand, there is a general consensus regarding the features of the major left-lateral Palomares fault zone (PFZ), which developed since the late Tortonian in the eastern part of the Sorbas-Vera basin (*e.g.,* Bousquet and Phillip, 1976; Bousquet, 1979; Montenat *et al.*, 1987; Weijermars, 1987; Ott d'Estevou *et al.,* 1990; Silva *et al.*, 1993; Booth-Rea *et al.*, 2003).

4.1. Miocene tectonic structures

After the end of metamorphism in the Internal Zones, a set of top-to-the west low-angle normal faults thinned the crust and exhumed the Nevado-Filábride complex, up to the middle Miocene (*e.g.,* Aldaya *et al.*, 1984; Galindo Zaldívar, 1986; García-Dueñas and Martínez-Martínez, 1988; Jabaloy *et al.*, 1993). Afterwards, the crustal-thinning process shifted to crustal thickening and relief formation, when the Sierra Nevada and Sierra de los Filabres started to emerge (Braga *et al.*, 2003) as large antiforms that folded the extensional detachments

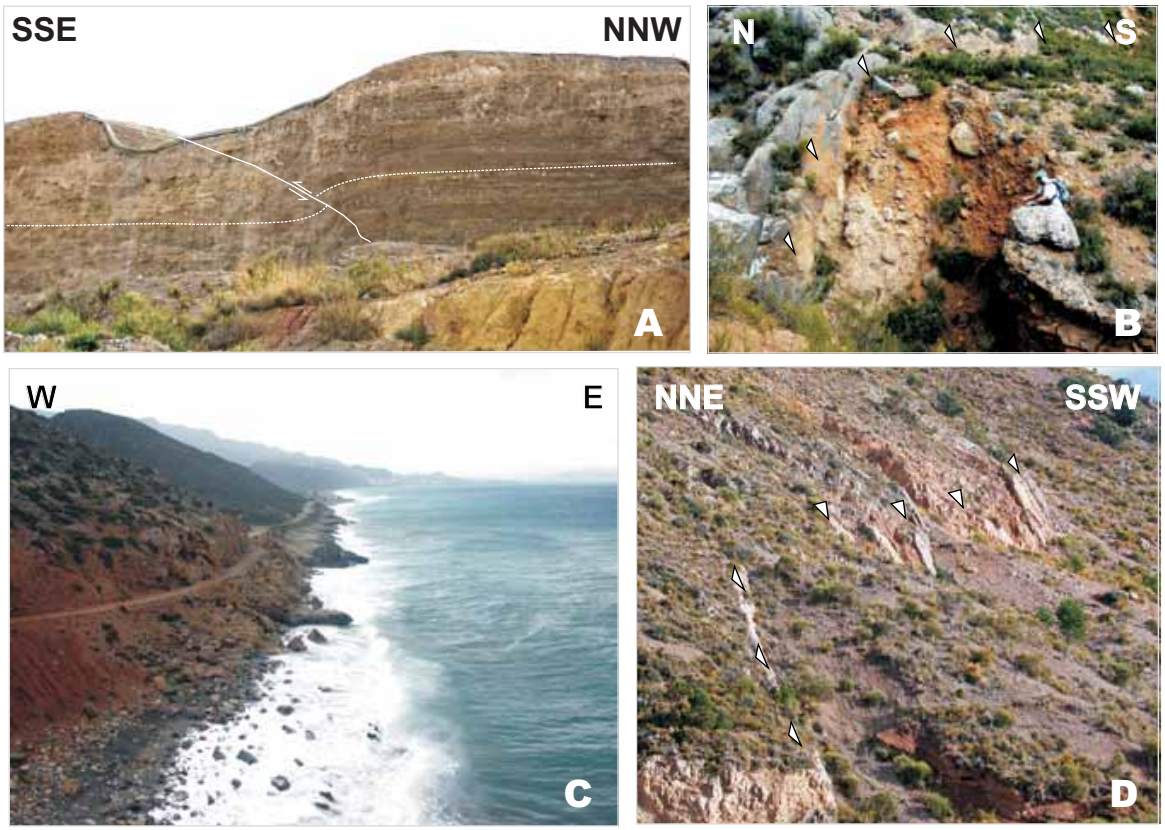

Fig. 3.- Field view of several active tectonic structures placed in the central-eastern Betic Cordillera. (A) ENE-WSW trending reverse fault and associated antiform that deform Quaternary conglomerates near Albox in the Huércal-Overa basin. (B) Laujar de Andarax normal fault: E-W oriented normal fault dipping toward the south affecting Quaternary sedimentary rocksin the northern Alpujarran corridor margin. (C) Rectilinear coast line that coincides with a fault segment of the left-lateral Palomares fault zone, which controls the eastern termination of the Sierra Cabrera. (D) Balanegra fault zone: NW-SE oriented normal fault segment that deforms Quaternary sediments in the western termination of the Sierra de Gádor, close to the village of Berja.

Fig. 3.- Ejemplos de algunas estructuras activas situadas en el área de estudio. (A) Falla inversa y pliegue asociado de direcciones ENE-OSO que deforman conglomerados cuaternarios en las proximidades de Albox, en la Cuenca de Huércal-Overa. (B) Falla normal de Laujar de Andarax: segmento que afecta a sedimentos cuaternarios con dirección aproximada E-O y buzamiento hacia el Sur. (C) Tramo de costa rectilíneo asociado a un segmento de la Falla de Palomares que controla la terminación oriental de Sierra Cabrera. (D) Zona de falla de Balanegra: segmento de dirección NO-SE que deforma sedimentos cuaternarios en la terminación occidental de la Sierra de Gador, cerca de Berja.

(Martínez-Martínez *et al.*, 1995; Martínez-Martínez and Azañón, 1997; Galindo-Zaldívar *et al.*, 2003; Pedrera *et al.*, 2009b). The deformation also propagated southward since the late Tortonian with the development of E-W kilometre-sized folds (Weijermars, 1985) that determined the isolation of the Alpujarra-Tabernas-Sorbas corridor (Fig. 4). A major E-W right-lateral fault zone composed by subvertical fault segments runs within the corridor (Sanz de Galdeano *et al.*, 1985), developing foliated cataclasites and fault-bound lenses (Sanz de Galdeano *et al.*, 1985). Faults segments with intermediate to low dips and oblique-slip including normal and reverse components have been also described, as in the Ugijar area (Fig. 4A; Galindo-Zaldívar, 1986).

Eastwards, E-W strike-slip faults segments are also well developed running along the southern part of the western Tabernas basin (Sanz de Galdeano *et al.*, 2010) and the northern boundary of Sierra Alhamilla antiform, the so-called Lucainena fault (Sanz de Galdeano, 1989) (Fig. 4A, B). The Lucainena fault branches into two segments to the east (Sanz de Galdeano, 1989). The northern segment, which runs near Gafarillos village, changes it orientation from E-W to NW-SE and cross-cut upper Tortonian sediments and the metamorphic rocks of the Sierra Cabrera (Sanz de Galdeano, 1989). This fault segment is usually called the Gafarillos fault (Stapel, 1996; Huibregtse *et al.*, 1998; Jonk and Bierman, 2002) or North Gafarillos fault (Giaconia *et al.*, 2012). The southern

fault segment runs from Los Guardianes, near Polopos village, to the southern boundary of Sierra Cabrera antiform with an ENE-WSW trend, being called the Polopos fault (Keller *et al.*, 1995) or the South Gafarillos fault (Fig. 4; Giaconia *et al.*, 2012).

The E-W right-lateral faults along the Alpujarras, the E-W oriented right-lateral faults of the southern Tabernas basin, and the dextral-reverse faults in the southern Sorbas basin have been traditionally interpreted as transpressive faults developed under N/S to NNW/SSE compression (*e.g.,* Sanz de Galdeano *et al.*, 1985, 1989; Stapel, 1996; Huibregtse *et al.*, 1998; Jonk and Bierman, 2002). However, Martínez-Martínez (2006) and Martínez-Martínez *et al.* (2006) propose a different interpretation for the Alpujarra right-lateral faults. They consider this fault zone to be part of a WSW-directed extensional system connecting two normal fault systems that thinned the Betic hinterland since the middle Miocene to the present.

In the absence of accurate, deep geophysical data, the deep continuity of the right-lateral faults has been considered to have a crustal (Sanz de Galdeano *et al.*, 1985) or at least shallow crustal character (Martínez-Díaz and Hernández-Enrile, 2004; Martínez-Martínez *et al.*, 2006), although Galindo-Zaldívar (1986) suggests that fault structures of the central Alpujarras corridor are restricted to the shallowest part of the crust.

Toward the east, the Palomares fault zone (PFZ), which is formed by several N10ºE to N20ºE left-lateral fault segments, deforms the eastern sector of the Vera basin (Fig. 4C) (Bousquet and Phillip, 1976; Bousquet, 1979; Weijermars, 1987). The Miocene sediments of the Vera basin are involved within the fault zone. Therefore, two depocenters filled by latest Tortonian to Quaternary sediments are linked to the movement of Arteal and Palomares fault segments (Fig. 4C; Booth-Rea *et al.*, 2003). Thus, the PFZ is considered a transcurrent deformation zone

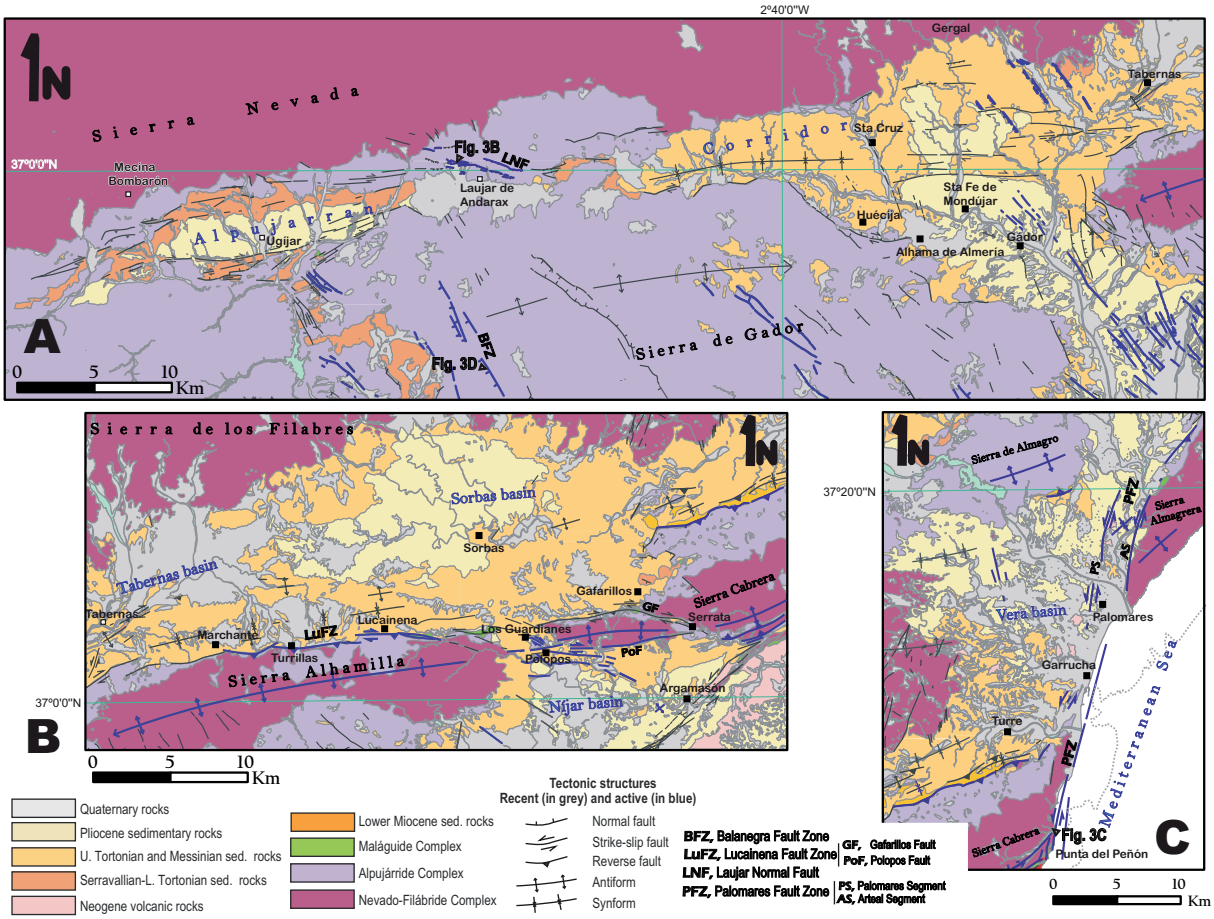

Fig. 4.- (A) Geological map of the Alpujarran corridor, (B) Tabernas/Sorbas basin, and (C) Vera basin showing traces of the recent (in grey) and active (blue) tectonic structures. The locations of figures 3B and C are marked.

Fig. 4.- Mapa geológico del Corredor de las Alpujarras, (B) la Cuenca de Tabernas/Sorbas y (C) la Cuenca de Vera con las trazas de las estructuras tectónicas recientes (en gris) y activas (en azul). La posición de la figuras 3B y C están indicadas.

active during most of the Neogene and Quaternary (*e.g.,* Montenat *et al.*, 1987; Ott d'Estevou *et al.* 1990; Silva *et al.*, 1993; Ruano *et al.*, 2007). Both ends are characterized by a change in the fault segments direction, which acquire a splay geometry that may be consistent with the development of reverse faults and antiforms since upper Miocene (Sierra Cabrera and Sierra Almagrera).

4.2. Active tectonic structures

The major dextral fault zone of the Alpujarra-Tabernas-Sorbas basins may have continued its activity up to the Quaternary (Sanz de Galdeano *et al.*, 1985; Martínez-Díaz and Hernández-Enrile, 2004; Martínez-Martínez *et al.*, 2006). Moreover, most of the dextral faults appear to be covered by the thin Plio-Quaternary sediments in the western Ugijar basin (Galindo-Zaldívar, 1986). Eastwards, the southern border of the Sorbas basin shows evidence of recent dextral oblique-reverse faulting (Sanz de Galdeano, 1989; Martínez-Díaz and Hernández-Enrile, 2004; Giaconia *et al.*, 2012).

A clear evidence of Quaternary faulting is found in the eastern Alpujarran corridor, in the Laujar de Andarax zone (García-Tortosa and Sanz de Galdeano, 2007). This consists of an E-W trending fault zone formed by southward-dipping normal faults segments affecting Quaternary deposits (Fig. 3B and 4A). Quaternary faults with related seismic activity are also found along a NW-SE zone that stretches from Almería to the Tabernas basin and separates Sierra Alhamilla from Sierra de Gádor (Sanz de Galdeano *et al.*, 2010). Seismicity is concentrated in the basement at the north-western edge, near Gergal, and this may correspond to the area of propagation of the fault zone.

The dextral-reverse Polopos fault deforms the Messinian and locally Quaternary sedimentary rocks of the Níjar basin with (Sanz de Galdeano, 1989). A recent geomorphic analysis confirms that active tectonics influences the streams and hillslopes of the Sierra Alhamilla antiform related to the Polopos fault and identify Quaternary contractional deformation associated to the Lucainena fault zone to the east of Marchante (the North Alhamilla Reverse Fault of Giaconia *et al.*, 2012).

The PFZ deforms Pleistocene conglomerates, close to Palomares village, developing an impressive fault-mirror with subhorizontal striations (Bousquet and Phillip, 1976). Pliocene-Quaternary sedimentary depocenters reveal that deformation along the PFZ fault zone migrated towards the eastern Arteal fault segment, which bounds the western mountain front of Sierra Almagrera (Booth-Rea *et al.*, 2003). In addition, the Quaternary activity of the PFZ favoured stream dissection, headward erosion of streams transverse to the active fault segments, and the asymmetry of the drainage network (Booth-Rea *et al.*, 2004; Stokes, 2008). The almost straight coastline from Palomares to Punta del Peñón is controlled by the PFZ (Figs. 3C and 4C), therefore the Late Pleistocene-Holocene marine terraces are uplifted along the coast (Goy and Zazo, 1986). In addition, Pleistocene conglomerates located in the Punta del Peñón contain numerous pebbles striated under the left-lateral shear of the PFZ. At its southern end, the PFZ splays into a horsetail formed by ENE-WSW reverse faults (Fig. 3C and 4C). South-dipping reverse faults form the north boundary of the Sierra Cabrera (Booth-Rea *et al.*, 2004), locally affecting Quaternary sediments (Sanz de Galdeano, 1987), and north-dipping reverse faults constitute the southern edge of the Sierra (Keller *et al.*, 1995).The CuaTeNeo (Cuantificiación de la Tectónica actual y Neotectónica) GPS non-permanent network was installed in 1996 to quantify the deformation in the Eastern Betic Cordillera. The network consists of 15 monuments covering an area of 120x50 km in Murcia and Almería (Colomina *et al.*, 1998; Khazaradze *et al.*, 2007 and 2008). In the northern part of the GPS network, the stations placed westward of the AMF and the PFZ show insignificant motions with respect to the stable part of the Eurasian plate. The GPS sites placed close to coast, eastward of the AMF and the PFZ, move 1-1.5 mm/yr toward the NNW revealing a strain accumulation (Echeverria *et al.*, 2011; Frontera *et al.*, 2011).

5. The Campo de Dalías and the Almería-Níjar basin

The Campo de Dalías and the Almería-Níjar basin are located at the boundary between the Alborán Sea and the Betic Cordillera. In both basins, the Tortonian and Pliocene marine sedimentary rocks, which belonged to the Northern Alborán basin, have emerged in Quaternary times (Fig. 5).

5.1. Late Miocene tectonic structures

The Carboneras fault zone (CFZ) is a major regional left-lateral fault that extends onshore along the Almería-Níjar basin (Bousquet and Montenant 1974; Ott d'Estevou and Montenant; 1985, Keller *et al.,* 1995; Scotney *et al.,* 2000; Faulkner *et al.*, 2003) and continues offshore along the Almería Gulf in a NE-SW direction (Fig. 5; De Larouzière *et al.*, 1988; Gràcia *et al.*, 2006. The upper Miocene sediments, together with metamorphic and volcanic basement rocks, crop out along the highly deformed CFZ (Bousquet and Montenant 1974; Rutter *et al.*, 1986;

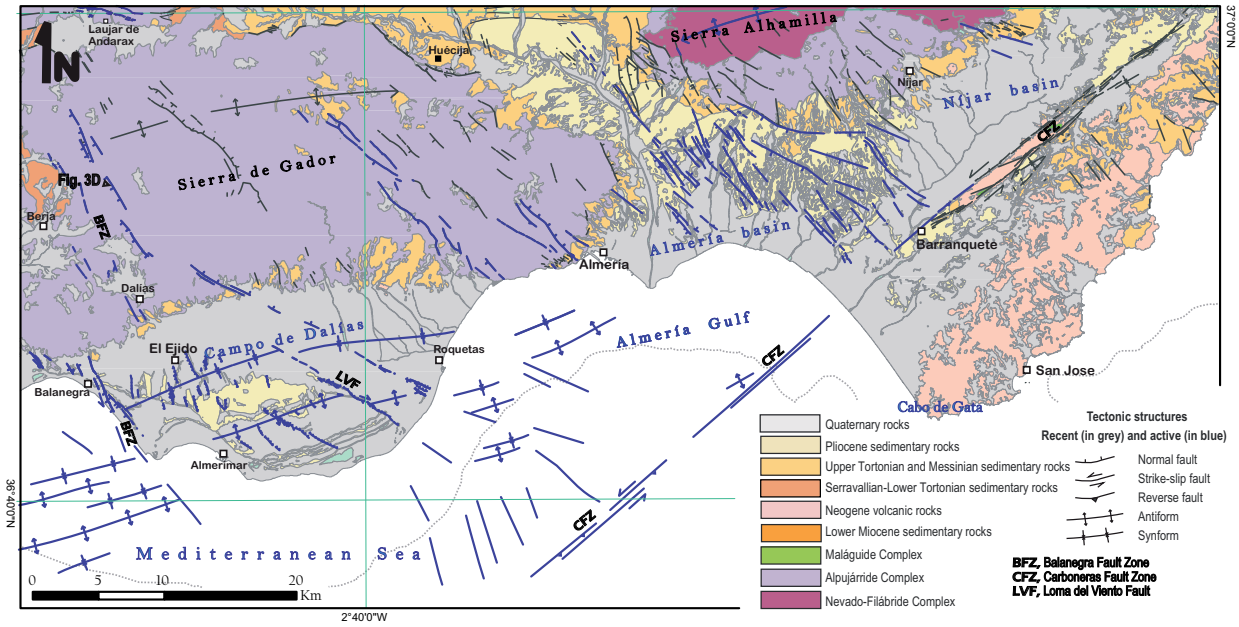

Fig. 5.- Geological map of the Campo de Dalías and the Almería/Níjar Basin with the traces of the recent (in grey) and active (blue) tectonic structures. The location of figure 3D is marked.

Fig. 5.- Mapa geológico del Campo de Dalías y de la Cuenca de Almería/Níjar con las trazas de las estructuras tectónicas recientes (en gris) y activas (en azul). La posición de la figura 3D está indicada.

Van de Poel, 1991; Keller *et al.*, 1995). The nucleation of the crustal-scale CFZ is closely linked to the Miocene volcanism, which modified the thermal structure and the strength of the lithosphere (Pedrera *et al.*, 2010b). Northwards of the CFZ, the sedimentary rocks are widely deformed by folds with a hundreds of meters amplitude and consistently showing an ENE-WSW strike onshore and offshore (Figs. 4B and 5). These folds deformed the sediments before the Messinian generating a cartographic unconformity between the highly folded upper Tortonian rocks and the less deformed post-Messinian sediments (Weijermars *et al.*, 1985).

To the north, the highest reliefs in the area are linked to culminations on the hinge line of the Sierra Alhamilla and Sierra the Gádor antiforms, which have an ENE-WSW orientation, 10 km of maximum amplitude, and are 25 to 30 km long respectively, and more than 1300 m high. The lower Tortonian-Serravallian conglomerates and the upper Tortonian sediments that surround the ranges are folded, revealing the fold geometry and the age of the deformation. In the Sierra Alhamilla, the late Tortonian rocks dip 20º in the southern slopes, yet are vertical or even overturned on the northern slopes as a consequence of the northward fold vergence and the activity of the E-W oriented high-angle reverse to right-lateral Lucainena fault zone (Weijermars *et al.*, 1985; Sanz de Galdeano, 1989).

The Níjar basin is intensely deformed by high-angle dipping normal faults since the Late Miocene (Martínez-Díaz and Hernández-Enrile, 2004; Marín-Lechado *et al.*, 2005; Pedrera *et al.*, 2006; Sanz de Galdeano *et al.*, 2010). They have a consistent NNW-SSE to NW-SE strike. Although the normal faults have a widespread distribution, their presence predominates in western Níjar, extending toward the Tabernas basins and very locally toward the Sorbas basin. The Níjar basin depocenter is associated with this NW-SE oriented normal fault activity. The maximum sedimentary thickness, established from gravity data, reaches more than 1 km in the western sector of the basin (Pedrera *et al.*, 2006). The fault surfaces dip towards the SW and usually deform the Tortonian and Messinian sediments, showing variable geometries from listric to domino-like systems. To the south-eastern part of the Almería Níjar basin, NW-SE normal faults dipping mainly to the NE deform the Pliocene sediments, sometimes showing syn-sedimentary features (Marín-Lechado *et al.*, 2005; Pedrera *et al.*, 2006).

5.2. Active tectonic structures

ENE-WSW open to gentle N-vergent folds affect the Pliocene and Quaternary sediments that extend along the continental shelf of the Almería Gulf, the Campo de

Dalías (Marín-Lechado *et al.*, 2006) and the Níjar basin (Fig. 5; Sanz de Galdeano, 1989; Huibregtse *et al.*, 1998; Pedrera *et al.*, 2006). These folds indicate the continuity of the contractional deformation after the major Messinian unconformity. In addition, normal to normal-oblique faults deform alluvial sediments up to the Pliocene and the Quaternary, generating fault scarps. In the Almería-Níjar basin, NNW-SSE to NW-SE normal faults are responsible for high slopes and sharp topography in the western part of the Sierra Alhamilla antiform and deform its southern limb. Therefore, from Gergal to Cabo de Gata, they control the Andarax valley geometry and the rectilinear coast line (*e.g.,* Martínez-Díaz and Hernández-Enrile, 2004; Marín-Lechado *et al.*, 2005; Pedrera *et al.*, 2006; Sanz de Galdeano *et al.*, 2010). From a geomorphological point of view, abrupt changes in the channels slope are probably associated to the activity of these normal faults (Giaconia, 2012).

Onshore recent tectonic activity of the CFZ is well observed near Barranquete, in the SW sector, where N30º-45ºE subvertical left-lateral fault surfaces deform Quaternary sediments (*e.g.,* Boorsma, 1992; Pedrera *et al.*, 2006). There, detailed geochronological and paleoseismic studies have been carried out (Moreno, 2011). Slip-rates, paleoseismologic, and seismic potential behaviour of the CFZ derived from onshore-offshore results have been recently described in detail by Moreno (2011) . A GPS station on the southern fault block is moving 1.5±0.7 mm/yr toward the NNE with respect to northward stations. This can be interpreted as being mainly caused by the left-lateral strike slip motion along the CFZ (Khazaradze *et al.*, 2010).

The Campo de Dalías is widely deformed by subvertical oblique-slip faults that have directions between NW-SE and WNW-ESE and that have been active since the Pleistocene (Martínez-Díaz, 1998; Martínez-Díaz and Hernández-Enrile, 2004; Marín-Lechado *et al.*, 2004, 2005; Pedrera *et al.*, 2012). The Balanegra fault zone extends from the western end of the Sierra de Gádor toward the Alborán Sea, controlling the western termination of the Sierra de Gádor antiform and the NW-SE oriented straight morphology of the coast line (Figs. 3D and 5; Martínez-Díaz and Hernández-Enrile, 2004; Marín-Lechado *et al.*, 2005 and 2010; Fernández-Ibáñez *et al.*, 2006). Other prominent fault is the WNW-ESE oriented Loma del Viento fault (Figs. 3D and 5), which deforms the central part of the Campo de Dalías with dextral-normal kinematics since Pleistocene (Marín-Lechado *et al.*, 2004; Martínez-Díaz and Hernández-Enrile, 2004; Pedrera *et al.*, 2012). The Loma del Viento fault is formed by six onshore segments and some of them are hard-linked (Pedrera *et al.*, 2012). Fault slip enhances toward the linkage sectors with an estimated long-term slip rate of 0.07±0.03mm/yr since the Pleistocene (Fig. 5; Pedrera *et al.*, 2012). The normal to normal-oblique faults continue toward the Alborán Sea, as deduced from NW-SE trending lineaments detected by bathymetric studies (Fig. 5; Gràcia *et al.*, 2006).

A non-permanent GPS network was installed in the Campo de Dalías to control the crustal deformation associated with active folds and faults. GPS measurements were made in 2006 and 2011, and the data are being processed. In addition, two precision levelling profiles were installed along the southern part of the Balanegra fault zone and measured in 2006, 2007, 2009, and 2010 to estimate the short-term fault-slip rate (Marín-Lechado *et al.*, 2010).

6. Seismicity and Earthquake Sources

The sector of the Betic Cordillera addressed in this paper is affected by distributed seismicity of low to moderate magnitude, which is limited to the upper crust (*e.g.,* Stich *et al.*, 2003, 2010; Fernández-Ibáñez and Soto, 2008). Earthquakes larger than Mw 5 rarely occur (Table 1). These major earthquakes can cautiously be associated with possible source faults, on the basis of damage descriptions in the cases of pre-instrumentally registered events and the estimated location and source analysis derived from the moment tensor solution in the case of the most recent earthquakes (Table 1). In the Campo de Dalías and surrounding sectors, large events occurred close to the village of Dalías (August 25, 1804, with felt intensity VIII-IX in the scale EMS-98 used throughout this paper, and Mw 6.4 macroseismic magnitude) and close to Adra, where a Mw 6.1 earthquake and Mw 5.5 aftershock occurred on June 16, 1910. The source parameters of the main Adra shock was established after analysing six analogue seismogram recordings (M_0=1.50·10^{-18} Nm, Mw=6.1, oblique strike-slip event at 16 km in depth; Stich *et al.*, 2003). Recently, two related events occurred to the south of Berja (December 23, 1993, Mw 5.3, m_{bLg}), and of Guardias Viejas (January 4, 1994, Mw 4.9). Both reveal strike-slip, slightly oblique fault plane solutions with a N120ºE oriented dextral nodal plane (Stich *et al.*, 2001), very similar to that found for the June 16, 1910 Adra earthquake. Stich *et al.* (2001) analysed the complete 1993-1994 seismic series and later seismicity in the area up to 1998, recognizing 39 multiplet clusters with N120-130ºE and N60-70ºE lineaments. These earthquakes could be assigned to the Balanegra fault zone (Marín-Lechado *et al.*, 2005), which is formed by N120ºE

Date	Latitude (N)	Longitude (W)	Intensity (EMS-98 scale)	Magnitude	Location	Possible source
01/01/1406	37.25	1.87	VII-VIII	M_S 5.0[1]	Vera. Al	Palomares Fault
01/11/1487	36.83	2.47	VIII	M_S 5.4[1]	Almería	NW-SE normal faults
09/11/1518	37.23	1.87	VIII-IX	M_S 6.0[1]	Vera. Al	Palomares Fault
22/09/1522	36.97	2.67	VIII-IX	M_W 6.5[2]	W Alhama de Almería. Al	Carboneras Fault; NW-SE normal faults
31/12/1658	36.83	2.47	VIII	M_S 5.4[1]	Almería	NW-SE normal faults
---/---/1686	36.85	2.95	VI-VII	M_S 4.5[1]	Berja. Al	Balanegra Fault Zone -western Gádor
25/08/1804	36.77	2.83	VIII-IX	M_W 6.4[2]	Dalías. Al	Balanegra or Loma del Viento Fault
25/08/1804*	36.77	2.83	VII	M_S 4.7[1]	Dalías. Al	Balanegra or Loma del Viento Fault
29/08/1804*	36.77	2.83	VII	M_S 4.7[1]	Dalías. Al	Balanegra or Loma del Viento Fault
10/06/1863	37.37	1.93	VI-VII	M_S 4.5[1]	Huércal-Overa	Reverse faults Huércal Overa (South termination AMF)
11/06/1894	37.12	2.67	VII	M_S 4.7[1]	Nacimiento. Al	NW-SE normal faults
13/05/1895	37.00	1.90	VI-VII	M_S 4.5[1]	Carboneras. Al	Palomares Fault
16/06/1910	36.67 36.84[2]	3.37 3.00[2]	VIII	M_W 6.1[3] M_W 6.7[2]	Adra. Al	Balanegra Fault Zone
16/06/1910*	36.67	3.37	VII	M_W 5.5[3]	Adra. Al	Balanegra Fault Zone
22/04/1912	37.03	2.95	VII	M_S 4.7[1]	Ocaña. Al	
05/03/1932	37.42 37.51[2]	2.45 2.45[2]	VIII	m_D 4.8 M_W 5.7[2]	Lúcar. Al	Lúcar-Somontín Faults
16/03/1972	37.42	2.24	VII	m_{bLg} 4.8	NW Partaloa. Al	Reverse faults eastern Almanzora
13/09/1984	36.98	2.34	V	m_{bLg} 5.0	SE Tabernas. Al	
23/12/1993	36.78	2.94	VII	m_{bLg} 5.0	S Berja	Strike-slip, slightly oblique Balanegra Fault
04/01/1994*	36.57	2.82	VII	m_{bLg} 4.9	N Alborán	Strike-slip slightly oblique Balanegra Fault
04/02/2002	37.09	2.53	V	m_{bLg} 5.1 M_W 4.6	S Gergal. Al	NW-SE normal faults.

** Foreshock;*
1 From maximum intensity, using the D'Amico et al. (1999) relationship; 2 Mezcua et al. (2004), using the procedure by Bakun and Wentworth (1997); 3 Stich et al. (2003a)

Table 1.- Significant historic and instrumental earthquakes in the study area.
Tabla 1.- Terremotos históricos e instrumentales en la zona de estudio.

to N160ºE trending oblique-slip segments. Instrumental seismicity is concentrated in the basement at the northwestern end of the fault zone, where the 2002 Gergal earthquake Mw 4.7 was located (Sanz de Galdeano *et al.*, 2010). In addition, the 1894 Nacimiento earthquake (VII) could be tentatively associated with these normal faults. The 1522 Almería earthquake (VIII-IX), for which the exact epicentre is unknown, has been associated with the offshore segment of the CFZ (Reicherter and Hübscher, 2006). Vera was destroyed in 1518 (VIII-IX) by an earthquake that could be hosted by the left-lateral Palomares fault (Bousquet, 1979; Weijermars, 1987). Toward the north, two moderate earthquakes were registered in the Almanzora corridor: the April 5, 1932 Lúcar earthquake (VIII, m_D 4.8) and the April 16, 1972 NW Partaloa earthquake (VII, m_{bLg} 4.8). The Lúcar earthquake could tentatively be associated with the Lúcar and Somontín fault zone, which extends from the Almanzora basin towards the Sierra de la Estancias, crossing the village of Lúcar. The village of Partaloa is located above a sector deformed by active ENE-WSW reverse faults and associated folds (Pedrera *et al.*, 2007, 2009a, 2009c).

7. Discussion and Conclusions

This work compiles the available information on the late Miocene to Quaternary faults and folds in the central-eastern Internal Zones of the Betic Cordillera. Some of these features have probably been the source of moderate-sized earthquakes throughout history and therefore are potential sources of future earthquakes.

7.1. Late Miocene geodynamic evolution

Regarding the evolution of the tectonic structures over time, folding started in the present position of the Sierra

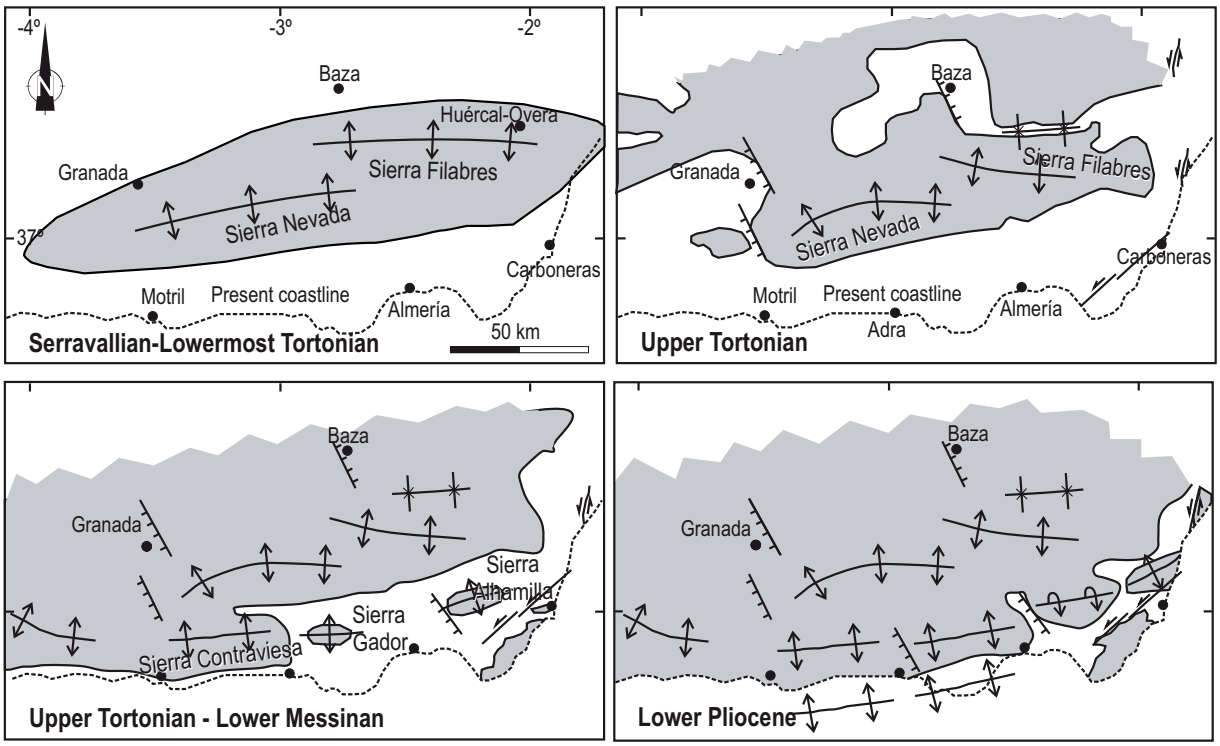

Fig. 6.- Paleogeographic and tectonic evolution of the central-eastern Betic Cordillera from the Serravallian-lowermost Tortonian onward. Evolution of the emergent land reconstructed from the facies distributions in the Neogene basins (Braga *et al.*, 2003). Note that the progressive emergence of the sierras coincides with the traces of the antiforms.

Fig. 6-. Reconstrucción paleogeográfica y evolución tectónica del sector central y oriental de la Cordillera Bética desde el Serravaliense-Tortoniense inferior. La distribución espacial y temporal de tierras emergidas/sumergidas se estableció a partir del análisis de facies (modificado de Braga *et al.*, 2003). Es preciso remarcar la coincidencia entre la posición de las sierras y la traza de las antiformas.

Nevada and Sierra de Los Filabres during the Serravallian-early Tortonian (Fig. 6). Therefore, stratigraphic and sedimentological studies indicate that a large E-W island started to emerge there at this time (Braga *et al.*, 2003). These large-scale antiforms underwent progressive lateral growth from east to west, folding the previous extensional detachments and therefore favouring the final exhumation of the Nevado-Filábride rocks. Fission-track analyses revealed that cooling to nearly surface temperatures occurred first in the Sierra de Los Filabres during the mid-Serravallian (12 Ma) and later in Sierra Nevada, located to the west (9-8 Ma; Johnson *et al.* 1997). The erosion of these ranges supplied sediments to the nearby basins. Progressive unconformities found in the Serravallian-lower Tortonian conglomerate formation located in the Almanzora corridor are coeval with the Sierra de Los Filabres antiform growth. Since the late Tortonian, folding continues and propagates northwards (Sierra de Las Estancias) and southwards (the Sierra de Gádor, the Sierra Alhamilla and the Sierra Cabrera). In addition, the Almanzora corridor, the Huércal-Overa basin, the Alpujarran corridor, and the Tabernas basin acquired their elongate shape.

The origin of the E-W to ENE-WSW trending large-scale open folds is still under debate. The folds have been interpreted as caused by isostatic rebound in response to extensional denudation along the regional extensional detachments (*e.g.,* Martínez-Martínez *et al.*, 2002; Augier *et al.*, 2005; Meigninger and Vissers, 2006). Alternatively, we consider them as contractional folds developed above upper-crustal detachments developed in a collisional framework (*e.g.,* Weijermars *et al.*, 1985; Montenat and Ott d'Estevou, 1990; Sanz de Galdeano and Vera, 1992; Martínez-Martínez *et al.*, 1995; Galindo-Zaldívar *et al.*, 2003; Sanz de Galdeano and Alfaro, 2004; Pedrera *et al.*, 2009b). In any case, these folds contribute to the uplift of the northern boundary of the Alborán Basin gradually disconnecting the now emerged intramontane basins (Comas *et al.*, 1992, 1999) and inducing the development of the present-day relief (Fig. 6; Braga *et al.*, 2003; Sanz de Galdeano and Alfaro, 2004. In addition, melts in the deep crust and middle to upper Miocene volcanism also

conditioned the relief and the deformation mode (Duggen *et al.*, 2008; Soto *et al.*, 2008).

Coevally to large-scale open fold development, E-W transpressive right-lateral and reverse faults nucleated along the Alpujarra, the Tabernas, and the Sorbas basins while the NNE-SSW/NE-SW left-lateral Palomares and Carboneras fault zones occurred in the easternmost part of the cordillera (Fig. 6). Thus, the Polopos fault has been interpreted as a conjugate fault system to the Carboneras and Palomares left-lateral fault zones (Giaconia *et al.*, 2012). Coeval to the relief growth, NW-SE to E-W normal and oblique slip normal faults developed.

During the Messinian, Pliocene and Quaternary, compression contributed to the progression of the moderate crustal thickening and to the regional progressive emersion of the marine basins with the final capture by the drainage network of the endorheic basins. Active folds caused the emersion of the northern Alborán Sea (Marín-Lechado *et al.*, 2006). In addition, there was continued activity of some segments of the strike-slip faults. Moreover, normal and normal-oblique faults have remained active during the Quaternary to the present in this part of the cordillera.

7.2. Active Tectonics

The present study summarized the most prominent active faults of the central-eastern Internal Zones of the Betic Cordillera (from 3.1ºW to 1.7ºW and to the south of 37.525ºN) providing detailed maps of the fault and fold traces (Fig. 7). The Campo de Dalías and surrounding sectors are probably the sites with the greatest concentra-

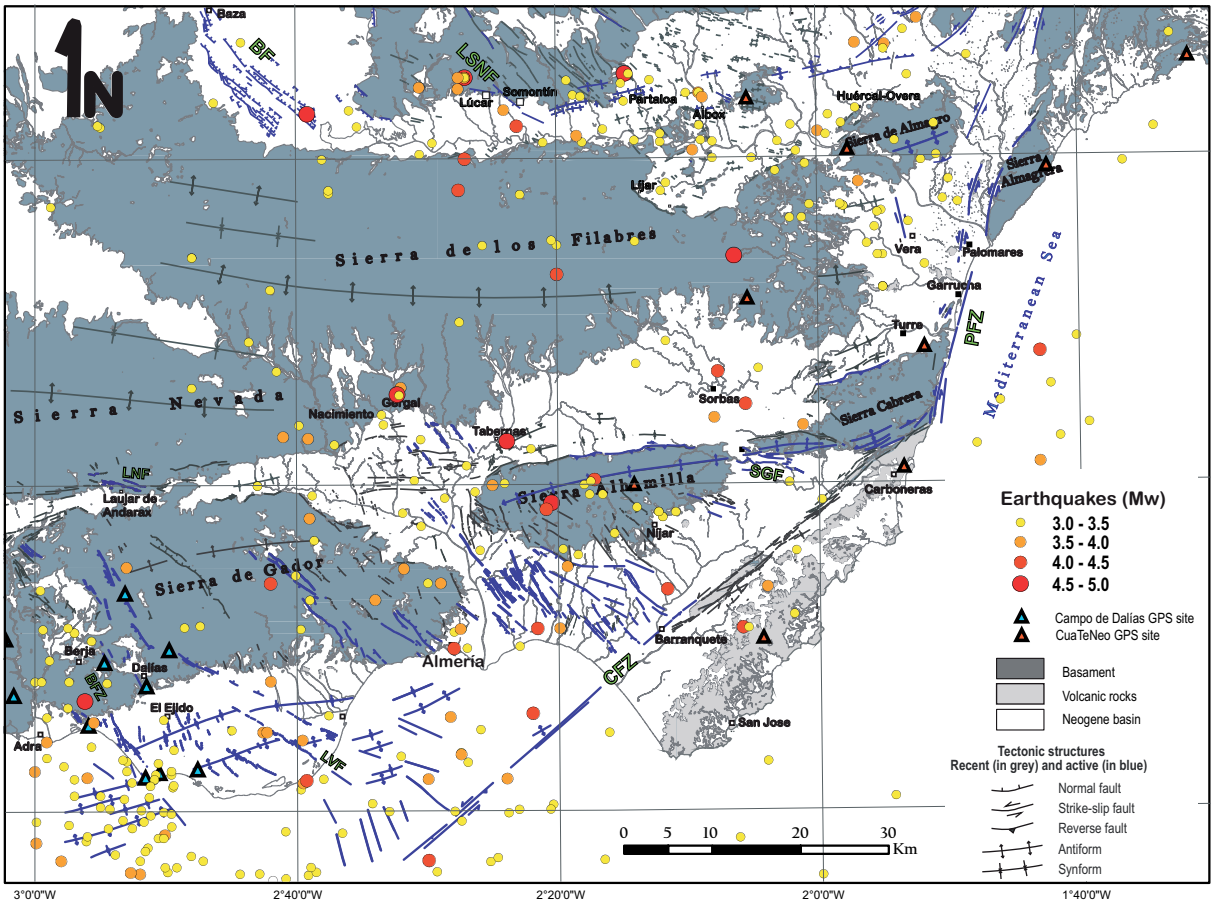

Fig. 7.- Seismotectonic map of the study area showing traces of recent and active tectonic structures and the location of the seismicity with $M_W \geq 3$ for the period 1926-2011 from the Instituto Geográfico Nacional catalogue (http//:www.ign.es). The non-permanent GPS sites of the networks CuaTeNeo and Campo de Dalías are marked.

Fig. 7.- Mapa sismotectónico del area de estudio con la traza de las principales estructuras tectónicas (recientes y activas) y la posición de la sismicidad $M_W \geq 3$ comprendida entre 1926-2011 (catalogo del IGN, Instituto Geográfico Nacional, http//:www.ign.es). Se ha incluido la posición (no permanente) de los GPS pertenecientes a las redes CuaTeNeo y Campo de Dalías.

tion of large earthquakes during the recent history. Moderate-sized earthquakes (Mw 5.0 to 6.0-6.5) have occurred in this area at fairly regular intervals, in 1804, 1910, and 1993 probably associated to the Balanegra fault zone activity (Marín-Lechado *et al.*, 2010). Despite the absence of clear historic earthquakes associated with the Loma del Viento fault, it is reasonable to consider it as a potential seismic fault (Pedrera *et al.*, 2012). There, we have designed a multidisciplinary control of the potential earthquakes sources. We have mapped the active faults and folds in detail. In addition, we performed a 3D geological model by incorporating borehole and geophysical data to establish the geometry of the tectonic structures. The sector is monitored with a non-permanent GPS network and high-precision levelling profiles (Fig. 7). The geometric knowledge of these structures combined with geodetic measurements of tectonic-strain accumulation yield improved models of nucleation, linkage, and propagation of active faults, as well as their seismic implications.

The NW-SE trending Quaternary faults extending from Almería to the Tabernas basin and separating Sierra Alhamilla from Sierra de Gádor have related seismicity (Fig. 7). These NW-SE normal faults have higher seismic potential than does the E-W dextral system (the 2002, Mw 4.7 Gergal earthquake and the 1894 Nacimiento earthquake, VII).

Toward the north in the Almanzora corridor, the Lúcar-Somontín NW-SE to WNW-ESE trending Quaternary faults could also cautiously be considered as possible sources of moderate-magnitude seismicity (the April 5, 1932 Lúcar m_D 4.8 earthquake, VIII). Toward the east, between Albox and Partaloa, several small reverse faults and associated compressive structures deforming Quaternary alluvial and fluvial sediments (Fig. 7) have been described?. The syn-folding fan geometry observed in the one of these structures (La Molata structure, Pedrera *et al.*, 2009a) suggests a slow and progressive deformation from middle Pleistocene onward. They do not show scarps or erosive deposits, such as clastic wedges, indicative of abrupt deformation events related to earthquakes, suggesting that the La Molata structure is most likely connected with aseismic slip during Quaternary fault-related fold growth. Nevertheless, some of these reverse fault segments could have associated moderate-sized events such as the April 16, 1972 NW Partaloa, m_{bLg} 4.8 earthquake (VII). Regarding the proximity between the villages Lúcar and Partaloa, further seismic studies of the main shock parameters are necessary to identify viable source structures.

The PFZ is very favourably oriented (N10-20ºE trend) with respect to the present-day stress field for left-lateral strike-slip displacement. The angle between the fault strike and the maximum principal stress is around 30º. Therefore, this fault probably nucleates moderate-sized earthquakes (1518 Vera earthquake). Unlike the Palomares fault, the CFZ is almost orthogonal to the present-day maximum horizontal compressive stress. Although not very suitably oriented to act as a strike-slip fault, it could act as a high-angle reverse or reverse-oblique fault despite its sub-vertical geometry. Paleoseismic data, high resolution seismic profiles and sediment coring indicate Quaternary activity of some fault segments (Reicherter and Hübscher, 2006; Moreno *et al.*, 2009). The ongoing GPS results derived from the CuaTeNeo network will decisively contribute to understand the relationship between the strain accumulation and seismic potential of the Carboneras and Palomares fault zones (Fig. 7).

Acknowledgements

This study was supported by the projects TOPO-IBERIA CONSOLIDER-INGENIO CSD2006-00041, CGL2010-21048, CGL-2008-03474-E, P09-RNM-5388 of the Spanish Ministry of Science and Education, project CGL-2011-29920, as well as by Research Groups RNM-148, RNM-325, and RNM-370 of the Junta de Andalucía Regional Government. We thank Carlos Sanz de Galdeano for constructive reading of the manuscript. We appreciate the revisions of Reinoud Vissers and Pedro Alfaro that notably improved the quality of the paper.

References

Aldaya, F., Campos, J., García-Dueñas, V., González-Lodeiro, F., Orozco, M. (1984): El contacto Alpujárrides-Nevado-Filábrides en la vertiente meridional de Sierra Nevada. Implicaciones tectónicas. In: J. López Ruiz (ed.), *El borde Mediterráneo español: evolución del orógeno bético y geodinámica de las depresiones neógenas*, CSIC-Universidad de Granada, Granada: 18–20.

Alfaro, P., Delgado, J., Sanz de Galdeano, C., Galindo-Zaldívar, J., García-Tortosa, F.J., López Garrido, A.C., López Casado, C., Marín, C., Gil, A.J., Borque, M.J. (2008): The Baza Fault: a major active extensional fault in the central Betic Cordillera (south Spain). *International Journal of Earth Sciences* 97, 1353–1365. doi: 10.1007/s00531-007-0213-z

Andrieux, J., Fontbote, J.M., Mattauer, M. (1971): Sur un modele expiicatif de 1'Arc de Gibraltar. *Earth Planet. Sci. Lett.* 12, 191–198.

Argus, D. F., Gordon, R. G., DeMets, C., Stein, S. (1989): Closure of the Africa-Eurasia-North America plate motion circuit and tectonics of the Gloria fault. *J.Geophys. Res.* 94, 5585–5602.

Augier, R. (2004): *Evolution tardi-orogénique des Cordilères Bétiques (Espagne): Apports d'un étude intégrée.* PhD Thesis, Univ. Pierre et Marie Curie, Paris: 400 pp.

Augier, R., Jolivet, L., Robin, C. (2005): Late Orogenic doming in the eastern Betic Cordilleras: Final exhumation of the Nevado-Filábride complex and its relation to basin genesis. *Tectonics* 24, TC4003. doi:10.1029/2004TC001687.

Bakun, W. H., and Wentworth, C. M. (1997): Estimating earthquake location and magnitude from seismic intensity data. *Bulletin of the Seismological Society of America* 87, 1502 1521.

Biju Duval, B., Dercourt, J., Le Pichon, X. (1977): From the Tethys to the Mediterranean seas: a plate tectonic model of the evolution of the western alpine system. In: B. Biju DuvaI and L. Montadert (ed.), *Structural History of the Mediterranean Basin*, Technip, Paris: 143-164.

Booth-Rea, G, Azañón, J.M., Azor, A., García-Dueñas, V. (2004): Influence of strike-slip fault segmentation on drainage evolution and topography. A case study: the Palomares Fault Zone (southeastern Betics, Spain). *Journal of Structural Geology* 26, 1615-1632. doi: 10.1016/j.jsg.2004.01.007

Booth-Rea, G., Azañón, J.M., García-Dueñas, V., Augier, R. (2003): Uppermost Tortonian to Quaternary depocentre migration related with segmentation of the strike-slip Palomares Fault Zone, Vera basin, SE Spain. *Comptes Rendus Geoscience* 335, 751–761. doi:10.1016/S1631-0713(03)00121-4

Boorsma, L.J. (1992): Syn-tectonic sedimentation in a Neogene strike-slip basin containing a stacked Gilbert-type delta (SE Spain). *Sed. Geol.* 81: 105–123.

Bousquet, J.C. (1979): Quaternary strike-slip faults in southeastern Spain. *Tectonophysics* 52, 277–286.

Bousquet, J.C., Montenat, C. (1974): Présence de décrochements Nord-Est, Sud-Ouest plioquaternaires dans les Cordillères bétiques orientales (Espagne). Extension et signification générale. *C. R. Acad. Sci.* 278, 2617–2620.

Bousquet, J.C., Phillip, H. (1976): Observations microtectóniques sur la compresion nord-sud quaternaire des Cordillères bétiques orientales (Espagne meridionale-Arc de Gibraltar). *Bull Soc. Geol. France* 28, 711–724.

Braga, J.C., Martín, J.M., Quesada, C. (2003): Patterns and average rates of late Neogene-Recent uplift of the Betic Cordillera, SE Spain. *Geomorphology* 50, 3–26.

Briend, M. (1981): *Evolution morpho-tectonique du bassin Néogène de Huércal Overa (Cordilleres betiques orientales, Espagne).* Ph. Thesis, Inst. Géol., Albertde-Lapparent. Paris. Doc. Trav. IGAL: 208 pp.

Briend, M., Montenat, C., Ott d'Estevou, P. (1990): Le Bassin de Huércal Overa. In: C. Montenat (ed.), *Les Bassins Néogeènes du Domaine Beétique Orientale (Espagne)*. Documents et Travaux du Institut Géologique Albert-de-Lapparent 12-13, Paris: 239-259.

Chalouan, A., Michard, A. (2004): The Alpine Rif Belt (Morocco): a case of mountain building in a subduction-subduction-transform fault triple junction. *Pure Appl.* Geophys. 161, 489-519. doi: 10.1007/s00024-003-2460-7

Colomina, I., Fleta, J., Giménez, J., Goula, X., Masana, E., Ortiz, M. À., Santanach, P., Soro, M., Suriñach, E., Talaya, J., Térmens, A. (1998): The CuaTeNeo GPS network to quantify horizontal movements in the Southeastern part of the Iberian Peninsula. *1ª Asamblea Hispano-Portuguesa de Geodesia y Geofísica, 9ª Asamblea Nacional de Geodesia y Geofísica*, Aguadulce, Almería: 199-204.

Comas, M.C., García-Dueñas, V., Jurado, M.J. (1992): Neogene tectonic evolution of the Alborán Basin from MCS data. *Geo-Mar. Lett.* 12, 157-164.

Comas, M.C., Platt, J.P., Soto, J.I., Watts, A.B. (1999): The origin and tectonic history of the Alborán Basin: Insights from ODP Leg 161 results. In: Zahn, R., Comas, M.C., Klaus, A. (eds), *Proceedings of the Ocean Drilling Program, Scientific Results 161*, College Station, TX (Ocean Drilling Program), 555-580.

D Amico,V., D. Albarello, and Mantovanil, E. (1999): A distribution-free analysis of magnitud-intensity relationships: an application to the Mediterranean region. *Phys. Chem. Earth* 24,517-521.

De Larouzière, F.D., Bolze, J., Bordet, P., Hemandez, J., Montenat, Ch., Ott d'Estevou, P. (1988): The Betic segment of the lithospheric Trans-Alborán shear zone during the Late Miocene. *Tectonophysics* 152, 41-52.

DeMets, C., Gordon, R.G., Argus, D.F., Stein, S. (1990): Current plate motions. *Geophysical Journal International* 101, 425-478.

DeMets, C., Gordon, R.G., Argus, D.F., Stein, S. (1994): Effect of recent revisions to the geomagnetic reversal time scale on estimates of current plate motions. *Geophys. Res. Lett.* 21, 2191-2194.

Duggen, S., Hoernle, K., Klügel, A., Geldmacher, J., Thirlwall, M., Hauff, F., Lowry, D., Oates, N. (2008): Geochemical zonation of the Miocene Alborán Basin volcanism westernmost Mediterranean, geodynamic implications. *Contrib. Mineral. Petrol*. 156, 577–593. doi:10.1007/s00410-008r-r0302-4.

Echeverria, A., Khazaradze, G., Garate, J., Asensio, E., Masana, E., Suriñach, E. (2011): Present-day GPS crustal deformation rates in the Eastern Betics (SE. Spain). *Geophysical Research Abstracts* 13, EGU2011, EGU *General Assembly 2011, Viena: -8005*

Fadil, A., Vernant, P., McClusky, S., Reilinger, R., Gomez, F., Ben Sari, D., Moura- bit, T., Feigl, K.L., Barazangi, M. (2006): Active Tectonics of the western Mediterranean: GPS evidence for roll back of a delaminated subcontinental lithospheric slab beneath the Rif Mountains, Morocco. *Geology* 34, 529–532, doi:10.1130/ G22291.1.

Faulkner, D.R., Lewis, A.C., Rutter, E.H. (2003): On the internal structure and mechanics of large strike-slip fault zones: field observations of the Carboneras fault in southeastern Spain. *Tectonophysics* 367, 235-251.

Fernández-Ibáñez, F., Pérez-Peña, J.V., Azañón J.M., González-Lodeiro, F. (2006): Morphological and structural characterization of western Sierra de Gádor (Betic Cordillera). *Geogaceta* 40, 71-76.

Fernández-Ibáñez, F., Soto, J.I., Zoback, M.D., Morales, J. (2007): Present-day stress field in the Gibraltar Arc (western Mediterranean). *J. Geophys. Res.* 112, B08404, doi:10.1029/2006JB004683.

Fernández-Ibáñez, F., Soto, J.I. (2008): Crustal rheology and seismicity in the Gibraltar Arc western Mediterranean. *Tectonics* 27, TC2007, doi:10.1029/2007TC002192.

Frontera, T., Concha, A., Blanco, P., Echeverria, A., Goula, X., Arbiol, R., Khazaradze, G., Pérez, F., Suriñach, E. (2011): DInSAR coseismic deformation of the May 2011 Mw 5.1 Lorca earthquake (Southern Spain). *Solid Earth Discussions* 3, 2, 963-974.

Galindo Zaldívar, J. (1986): Etapas de fallamiento neógenas en la mitad occidental de la depresión de Ugijar (Cordilleras Béticas). *Estudios Geológicos* 42, 1-10.

Galindo-Zaldívar, J., Gil, A.J., Borque, M.J., González-Lodeiro, F, Jabaloy, A., Marín-Lechado, C., Ruano, P., Sanz de Galdeano, C. (2003): Active faulting in the internal zones of the central Betic Cordilleras (SE, Spain). *Journal of Geodynamics* 36, 239-250. doi:10.1016/S0264-3707(03)00049-8

García-Dueñas, V., Martínez-Martínez, J.M. (1988): Sobre el adelgazamiento mioceno del Dominio de Alborán: El despegue de los Filabres (Béticas orientales). *Geogaceta* 5, 53-55.

García-Meléndez, E., 2000. *Geomorfología y Neotectónica del Cuaternario de la cuenca de Húercal-Overa y corredor del Almanzora. Análisis y Cartografía mediante Teledetección y SIG. Unpublished PhD Thesis.* Universidad de Salamanca, Salamanca: 528 pp.

García-Meléndez, E., Goy, J.L., Zazo, C. (2003): Neotectonic and Plio-Quaternary landscape development within the eastern Huércal-Overa Basin (Betic Cordilleras, southeastern Spain). *Geomorphology* 50, 111–133.

García-Meléndez, E., Goy, J.L., Zazo, C. (2004). Quaternary tectonic activity in the Húercal-Overa Basin (Almería, Southeast Spain): deformations associated with the Albox fault. *Geogaceta* 36, 63–66.

García-Tortosa, F.J., Alfaro, P., Galindo-Zaldívar, J., Gibert, L., López Garrido, A.C., Sanz de Galdeano, C., Ureña, M. (2008): Geomorphologic evidence of the active Baza fault (Betic Cordillera, South Spain). *Geomorphology* 97, 374-391. doi:10.1016/j.geomorph.2007.08.007,

García-Tortosa, F.J., Sanz de Galdeano, C. (2007): Evidencias geomorfológicas de actividad tectónica cuaternaria en el frente montañoso del borde sur de Sierra Nevada: la falla normal de Laujar de Andarax. *Cuaternario y Geomorfología* 21, 101-112.

Giaconia, F., Booth-Rea, G., Martínez-Martínez, J. M., Azañón, J. V. Pérez-Peña., M. Pérez-Romero J., Villegas, I. (2012): Geomorphic evidence of active tectonics in the Sierra Alhamilla (eastern Betics, SE Spain). *Geomorphology* 145-146, 90–106. doi: 10.1016/j.geomorph.2011.12.043.

Goy, J.L., Zazo, C. (1986): Synthesis of the Quaternary in the Almería littoral, neotectonic activity and its morphologic features, Eastern Betics, Spain. *Tectonophysics* 130, 259-270.

Gràcia, E., Pallàs, R., Soto, J. I., Comas M., Moreno X., Masana, E., Santanach P., Diez S., García, M., Dañobeitia, J., HITS scientific party. (2006): Active faulting offshore SE Spain (Alborán Sea): Implications for earthquake hazard assessment in the Southern Iberian Margin. *Earth and Planetary Science Letters* 241, 734-749. doi:10.1016/j.epsl.2005.11.009

Groupe de Recherche Neotectonique (1977): L'histoire tectonique récente (Tortonien á Quaternaire) de l'Arc de Gibraltar: résultats de l'analyse structurale en Espagne. *Bull Soc. Geol. France* 7.

Huibregtse, P., Alebeek, H.V., Zaal, M., Biermann, C. (1998): Paleostress analysis of the northern Níjar and southern Vera basins: constraints for the Neogene displacement history of major strike-slip faults in the Betic Cordilleras, SE Spain. *Tectonophysic*s 300, 79-101.

Jabaloy, A., Galindo Zaldívar, J., González Lodeiro, F. (1992): The Mecina Extensional System: Its relation with the Post-Aquitanian piggy-back basins and the paleostresses (Betic Cordilleras, Spain). *Geo-Mar. Lett.* 12, 96-103.

Jabaloy, A., Galindo-Zaldívar, J., González-Lodeiro, F. (1993): The Alpujárride/Nevado-Filábride extensional shear zone (Betic Cordilleras, SE Spain). *Journal of Structural Geology* 15, 555-569.

Jonk, R., Biermann, C. (2002): Deformation in Neogene sediments of the Sorbas and Vera Basins (SE Spain): constraints on simple-shear deformation and rigid body rotation along major strike-slip faults. *J. Struct. Geol.* 24, 963-977.

Johnson, C., Harbury, N., Hurford A.J. (1997): The role of extension in the Miocene denudation of the Nevado-Filábride Complex, Betic Cordillera (SE Spain), *Tectonics* 16, 189-204.

Khazaradze, G., Asensio, E., Moreno, X., Masana, E. (2010): Present-day crustal motion along the Carboneras fault in the Betic Cordilleras, Spain. *American Geophysical Union, Fall Meeting 2010, abstract*, San Francisco, California: G22A-08

Khazaradze, G., Gárate, J., Suriñach, E., Davila, J.M., Asensio, E. (2008): Crustal deformation in south-eastern Betics from CuaTeNeo GPS network. *GeoTemas* 10, 1-4.

Khazaradze, G., Suriñach, E., Gárate, J., Davila J. M. (2007): Crustal deformation in Eastern Betics from CuaTeNeo GPS network. *Geophysical Research Abstracts Vol. 9, EGU2007, EGU General Assembly 2007*, Viena: 05314

Keller, J.V.A., Hall, S.H., Dart, C.J., McClay, K.R. (1995): The geometry and evolution of a transpressional strike-slip system: the Carboneras fault, SE Spain. *J. Geol. Soc. London* 152, 339-351.

Lonergan, L., White, N. (1997): Origin of the Betic-Rif mountain belt. *Tectonics* 16, 504-522.

Marín-Lechado, C.; Galindo-Zaldívar, J.; Gil, A.J.; Borque, M.J.; De Lacy, C.; Pedrera, A.; López-Garrido, A.C.; Alfaro, P.; García-Tortosa, F.J.; Ramos, M.I.; Rodríguez-Caderot, G.; Rodríguez-Fernández, J.; Ruiz-Costán, A.: Sanz De Galdeano, C. (2010): Levelling Profiles and a GPS Network to Monitor the Active Folding and Faulting Deformation in the Campo de Dalías (Betic Cordillera, Southeastern Spain). *Sensors* 10, 3504-3518. doi:10.3390/s100403504

Marín-Lechado, C., Galindo-Zaldívar, J., Rodríguez-Fernández, L. R., González-Lodeiro, F. (2004): Faulted hybrid joints: an example from the Campo de Dalías (Betic Cordilleras, Spain). *Journal of Structural Geology* 26, 2025–2037. doi:10.1016/j.jsg.2004.03.006

Marín-Lechado, C., Galindo-Zaldívar, J., Rodríguez-Fernández, L.R., Pedrera A. (2006): Mountain front development by folding and crustal thickening in the Internal Zone of the Betic Cordillera-Alborán Sea Boundary. *Pure Appl. Geophys.* 164, 1-21, doi: 10.1007/s00024-006-0157-4.

Marín-Lechado, C., Galindo-Zaldívar, J., Rodríguez-Fernández, L. R., Serrano I., Pedrera, A. (2005): Active faults, seismicity and stresses in an internal boundary of a tectonic arc (Campo de Dalías and Níjar, southeastern Betic Cordilleras, Spain). *Tectonophysics* 396, 81-96.

Martín-Algarra, A. (1987): Evolution geológica alpina del contacto entre las Zonas Internas y las Zonas Externas de la Cordillera Bética (Sector Occidental). Ph.D. Thesis. Universidad de Granada, Granada: 1368 pp.

Martínez-Díaz, J.J. (1998): Neotectónica y Tectónica Activa del sector centrooccidental de Murcia y Sur de Almería, Cordillera Bética (España). Ph.D. Thesis, Universidad Complutense de Madrid, 466 p.

Martínez-Díaz, J.J. (2002): Stress field variation related to fault interaction in a reverse oblique-slip fault: the Alhama de Murcia fault, Betic Cordillera, Spain. *Tectonophysics* 356, 291-305.

Martínez-Díaz, J.J., Hernández-Enrile, J.L. (2004): Neotectonics and morphotectonics of the southern Almería region (Betic Cordillera–Spain) kinematic implications. *Int. J.* Earth Sci. 93, 189–206. doi: 10.1007/s00531-003-0379-y.

Martínez-Díaz, J.J., Masana, E. Ortuno, M. (2012): Active Tectonics of the Alhama De Murcia Fault, Betic Cordillera, Spain. *Journal of Iberian Geology* doi.: xxxxxxxxx

Martínez-Martínez, J.M. (2006): Lateral interaction between metamorphic core complexes and less-extended, tilt-block domains: the Alpujarras strike-slip transfer fault zone (Betics, SE Spain). *Journal of Structural Geology* 28, 602-620. doi: 10.1016/j.jsg.2006.01.012.

Martínez-Martínez, J. M., Azañón J. M. (1997): Mode of extensional tectonics in the southeastern Betics (SE Spain): Implications for the tectonic evolution of the peri-Alborán orogenic system, *Tectonics* 16, 205–225.

Martínez-Martínez, J.M., Booth-Rea, G., Azañón, J.M., Torcal, F. (2006): Active transfer fault zone linking a segmented extensional system (Betics, southern Spain): Insight into heterogeneous extensión driven by edge delamination. *Tectonophysics* 422, 159-173. doi:10.1016/j.tecto.2006.06.001.

Martínez-Martínez J.M., Soto J.I., Balanyá J.C. (1995): Large scale structures in the Nevado-Filábride complex and crustal seismic fabrics of the deep reflection seismic profile ESCI-Béticas 2. *Revista de la Sociedad Geológica de España* 8, 477-489.

Martínez-Martínez, J.M., Soto, J.I., Balanyá, J.C. (2002): Orthogonal folding of extensional detachments: structure and origin of the Sierra Nevada elongated dome (Betics, SE Spain). *Tectonics* 21, 1012,. doi:10.1029/2001TC001283.

Masana, E, Martínez-Díaz, J.J., Hernández-Enrile, J.L., Santanach, P. (2004): The Alhama de Murcia fault (SE Spain), a seismogenic fault in diffuse plate boundary. Seismotectonic implications for the Ibero-Magrebian region. *J. Geophys. Res.* 109, 1-17. doi:10.1029/2002JB002359

Masana, E., Pallàs, R., Perea, H., Ortuño, M., Martínez-Díaz, J.J., García-Meléndez, E., Santanach, P. (2005): Large Holocene morphogenic earthquakes along the Albox fault, Betic Cordillera, Spain. *J. Geodynamics* 40, 119-133. doi: 10.1016/j.jog.2005.07.002

Meijninger, B.M.L., Vissers, R.M.L. (2006): Miocene extensional basin development in the Betic Cordillera, SE Spain, revealed through analysis of the Alhama de Murcia and Crevillente Faults. *Basin Research* 18, 547-571. doi: 10.1111/j. 1365-2117.2006.00308.x.

Mezcua, J., Rueda, J., Blanco, R. M. (2004): Reevaluation of historic earthquakes in Spain, *Seismol. Res. Lett.* 75, 75–81. doi: 10.1785/gssrl.75.1.75

Montenat, C., P. Ott d'Estevou (1990): Eastern Betic Neogene basins-A review. In: C. Montenat (ed.), *Les Bassins Néogeènes du Domaine Beétique Orientale (Espagne)*. Documents et Travaux du Institut Géologique Albert-de-Lapparent 12-13, Paris: 9-15.

Montenat, C., Ott d'Estevou, P., Masse, P. (1987): Tectonic-sedimentary characters of the Betic Neogene basins evolving in a crustal transcurrent shear zone (SE Spain). *Bulletin Centre de Recherché Exploration Production. Elf-Aquitaine* 11, 1-22.

Mora-Gluckstadt, M. (1993): *Tectonic and sedimentary analysis of the Huércal Overa region, South East Spain, Betic Cordillera.* PhD. Thesis, University of Oxford, Oxford: 300 pp.

Moreno, X. (2011): *Neotectonic and Paleoseismic Onshore-Offshore integrated study of the Carboneras Fault (Eastern Betics, SE Iberia).* PhD. Thesis, University of Barcelona, Barcelona.

Moreno, X.; Masana, E.; Gracia, E.; Bartolome, R.; Lo Iacono, C.; Rodés, A.; Pallàs, R. (2009): An integrated multiscale paleoseismic and neotectonic approach of the Carboneras Fault Zone, SE Spain, and its marine continuation in the Alborán Sea. *American Geophysical Union, Fall Meeting 2009, abstract*. San Francisco, California: T21D-1853.

Ortuño, M.C., Masana, E., Buylaert, J. P., Canora, C., Cunha, P., García-Meléndez, E., Martínez-Díaz, J., Murrey, A., Sohbati, R., Štěpančíková, P. (2009): Paleoseismic activity at the southern termination of Alhama de Murcia fault (Southeastern Betics, Spain): geomporphic and trenching evidence along a slow moving fault. *American Geophysical Union, Fall Meeting 2009, abstract*. San Francisco, California: T21D-1851.

Ott d'Estevou, Ph., Montenat, Ch. (1985): Evolution structurale de la zone betique orientale (Espagne) du Tortonien a l'Holocene. *C.R. Acad. Sci. Paris* 300, II, 8, 363-368.

Ott d'Estevou, P., Montenat, Ch., Alvado, J.C. (1990): Le Bassin de Vera-Garrucha. In: C. Montenat (ed.), *Les Bassins Néogeènes du Domaine Beétique Orientale (Espagne)*. Documents et Travaux du Institut Géologique Albert-de-Lapparent 12-13, Paris: 165-187.

Pedrera, A., Galindo-Zaldívar, J., Ruiz-Bustos, A., Rodríguez-Fernández, J., Ruíz- Constán, A. (2009a): The role of small-scale fold and fault development in seismogenic zones: example of the Western Huércal-Overa basin (Eastern Betic Cordillera, Spain). *J. Quat. Sci.* 24, 581–592, doi:10.1002/jqs.1246.

Pedrera, A., Galindo-Zaldívar, J., Ruiz-Constán, A., Duque, C., Marín-Lechado, C., Serrano, I. (2009b): Recent large fold nucleation in the upper crust: Insight from gravity, magnetic, magnetotelluric and seismicity data (Sierra de Los Filabres–Sierra de Las Estancias, Internal Zones, Betic Cordillera). *Tectonophysics* 463, 1-4, 145-160. doi:10.1016/j.tecto.2008.09.037

Pedrera, A., Galindo-Zaldívar, J., Sanz de Galdeano, C., López-Garrido, A.C. (2007): Fold and fault interactions during the development of an elongated narrow basin: The Almanzora Neogene-Quaternary Corridor (SE Betic Cordillera, Spain). *Tectonics* 26, TC6002. doi: 10.1029/2007TC002138.

Pedrera, A., Galindo-Zaldívar, J., Tello, A., Marín-Lechado, C. (2010a): Intramontane basin development related to contractional and extensional structure interaction at the termination of a major sinistral fault: The Huércal-Overa Basin (Eastern Betic Cordillera). *Journal of Geodynamics* 49, 271–286. doi:10.1016/j.jog.2010.01.008

Pedrera, A., Mancilla, F., Ruiz-Constán, A., Galindo-Zaldívar, J., Morales, J., Arzate, J., Marín-Lechado, C., Ruano, P., Buontempo, L., Anahnah, F., Stich, D. (2010b): Crustal-scale transcurrent fault development in a weak-layered crust from an integrated geophysical research: Carboneras Fault Zone, eastern Betic Cordillera, Spain, *Geochem. Geophys. Geosyst.* 11, Q12005. doi:10.1029/2010GC003274.

Pedrera, A., Marín-Lechado, C., Galindo-Zaldívar, J., Rodríguez-Fernández, L.R., Ruiz-Constán, A. (2006) Fault and fold interaction during the development of the Neogene-Quaternary Almería-Níjar basin (SE Betic Cordilleras). In: Moratti, G., Chalouan, A. (eds*). Tectonics of the Western Mediterranean and North Africa.* Geological Society, London, Special Publications, 262, 217–230.

Pedrera, A., Marín-Lechado, C., Stich, D., Ruiz-Constán, A., Galindo-Zaldívar, J., Rey-Moral, C., Mancilla, F. (2012): Nucleation, linkage and active propagation of a segmented Quaternary normal-dextral fault: the Loma del Viento fault (Campo de Dalías, Eastern Betic Cordillera, SE Spain). *Tectonophysics* 522–523, 208–217. doi: oi:10.1016/j.tecto.2011.12.001.

Pedrera, A., Pérez-Peña, J.V., Galindo-Zaldívar, J., Azañón, J.M., Azor, A. (2009c): Testing the sensitivity of geomorphic indices in areas of low-rate active folding (eastern Betic Cordillera, Spain). *Geomorphology* 105, 218–231. doi:10.1016/j.geomorph.2008.09.026

Pedrera, A., Ruiz-Constán, A., Galindo-Zaldívar, J., Chalouan, A., Sanz de Galdeano, C., Marín-Lechado, C., Ruano, P., Benmakhlouf, M., Akil, M., López-Garrido, A.C., Chabli, A., Ahmamou, M., González-Castillo, L. (2011): Is there an active subduction beneath the Gibraltar orogenic arc? Constraints from Pliocene to present-day stress field. *Journal of Geodynamics* 52, 2, 83-96. doi:10.1016/j.jog.2010.12.003

Poisson, A.M., Morel, J.L., Andrieux, J., Coulon, M., Wernli, R. Guernet, C. (1999): The origin and development of Neogene basins in the SE Betic Cordillera (SE Spain): a case study of the Tabernas-Sorbas and Huércal Overa Basins. *J. Petrol. Geol.* 22, 97-114.

Reicherter, K., Hübscher, C. (2006): Off-Shore evidence for the 1522 Almería earthquake (M>6.5) in the Alborán Sea (southern Spain), *Journal of Seismology* 11, 15-26. doi: 10.1007/s10950-006-9024-0.

Rodríguez-Fernández, J. (1982): *El Mioceno del sector central de las Cordilleras Béticas.* PhD. Thesis, Universidad de Granada, 224 pp.

Ruano, P., Galindo-Zaldívar, J., Pedrera, A., Marín-Lechado, C. (2007): Paleostresses and recent tectonic activity of the Palomares-Carboneras strike-slip faults (Eastern Betic Cordilleras, SE Spain). *Procceding of IUGG 2007*, Perugia.

Rutter, E.H., Maddock, R.H., Hall, S.H., White, S.H. (1986): Comparative microstructures of natural and experimentally produced clay-bearing fault gouges. In: Y. Wang-Chi (ed.), *International Structure of Fault Zones*, Pure Appl. Geophys. 124, 3-30.

Sanz de Galdeano, C. (1983): Los accidentes y fracturas principales de las Cordilleras Béticas. *Estudios Geológicos* 39, 157-165.

Sanz de Galdeano, C. (1987): Strike-slip faults in the Southern Border of the Vera Basin (Almería, Betic Cordilleras). *Estudios Geológicos* 43, 435–443.

Sanz de Galdeano C. (1989): Las fallas de desgarre del borde Sur de la cuenca de Sorbas Tabernas (norte de Sierra Alhamilla, Almería, Cordilleras Béticas). *Bol. Geol. y Min.* 101, 73-85.

Sanz de Galdeano, C. (1990): Geologic evolution of the Betic Cordilleras in the western Mediterranean, Micoene to present. *Tectonophysics* 172: 107-119.

Sanz de Galdeano, C., Alfaro, P. (2004): Tectonic significance of the

present relief of the Betic Cordillera, *Geomorphology* 63, 3-4, 175-190. doi:10.1016/j.geomorph. 2004.04.002.

Sanz de Galdeano, C., Lopez Casado, C. (1988): Fuentes sísmicas en al ámbito Bético-Rifeño. *Rev. Geofis. Madrid* 44, 175-198.

Sanz de Galdeano, C., López-Casado, C., Delgado, J., Peinado, M.A. (1995): Shallow seismicity and active faults in the Betic Cordillera. A preliminary approach to seismic sources associated with specific faults. *Tectonophysics* 248, 293-302.

Sanz de Galdeano C., Rodríguez Fernández, J., López Garrido A.C. (1985): A strike-slip fault corridor within the Alpujarra Mountains (Betic Cordilleras, Spain). *Geol. Rundsch.* 74, 3, 641-655. doi:10.1111/j.1365-2117.2006.00284

Sanz de Galdeano C., Shanov S., Galindo-Zaldívar J., Radulov A., Nikolov G. (2010): A new tectonic discontinuity in the Betic Cordillera deduced from active tectonics and seismicity in the Tabernas Basin. *Journal of Geodynamics* 50, 57-66. doi:10.1016/j.jog.2010.02.005

Sanz de Galdeano, C., García-Tortosa, F.J., Peláez, J.A., Alfaro, P., Azañón, J.M., Galindo- Zaldívar, J., López Casado, C., López,-Garrido, A.C., Rodríguez-Fernández, J., Ruano, P. (2012): Main active faults in the Granada and Guadix-Baza basins. *Journal of Iberian Geology* doi, xxxxxxxxxxxxxxxxxxxxx

Sanz de Galdeano, C., Vera, J. A. (1992): Stratigraphic record and palaeogeographical context of the Neogene basins in the Betic Cordillera, Spain. *Basin Res.* 4, 21–36.

Scotney, P., Burgess, R., Rutter, E.H. (2000): 40Ar/39Ar age of the Cabo the Gata volcanic series and displacements on the Carboneras fault zone, SE Spain. *J. Geol. Soc. London* 157, 1003-1008.

Silva, P.G., Goy, J.L., Somoza, L., Zazo, C., Bardají, T. (1993): Landscape response to strike-slip faulting linked to collisional settings: Quaternary tectonics and basin formation in the Eastern Betics, southeast Spain. *Tectonophysics* 224, 289-303.

Soler, R., Masana, E., Santanach, P. (2003): Evidencias geomorfológicas y estructurales del levantamiento tectónico reciente en la terminación sudoccidental de la falla de Alhama de Murcia (Cordillera Bética Oriental). *Revista de la Sociedad Geológica de España* 16, 123-133.

Soto, J.I., Comas, M.C., de la Linde, J. (1996): Espesor de sedimentos en la cuenca de Alborán mediante una conversión sísmica corregida. *Geogaceta* 20, 382–385.

Soto, J.I., Fernández-Ibáñez, F., Fernàndez, M., García-Casco, A. (2008): Thermal structure of the crust in the Gibraltar Arc: influence on active tectonics in the western Mediterranean. *Geochem. Geophys. Geosyst.* 9, Q10011. doi:10.1029/2008GC002061.

Stapel, G., Moeys, R., Biermann, C. (1996): Neogene evolution of the Sorbas basin (SE Spain) determined by paleostress analysis. *Tectonophysics* 255, 291-305.

Stich, D., Ammon, C.J., Morales, J. (2003): Moment tensor solutions for small and moderate earthquakes in the Ibero-Maghreb region. *J. Geophys. Res.* 108, 2148. doi: 10.1029/2002JB002057

Stich, D., Martín, R. Morales, J. (2010): Moment tensor inversion for Iberia–Maghreb earthquakes 2005–2008. *Tectonophysics* 483, 3-4, 390-398. doi:10.1016/j.tecto.2009.11.006

Stich, D., Aguacil, G., Morales, J. (2001): The relative locations of multiplets in the vicinity of the western Almería (southern Spain) earthquake series of 1993-1994. *Geophys. J. Int.* 146, 801- 812.

Stich, D., Serpelloni, E., Mancilla, F., Morales, J. (2006): Kinematics of the Iberia-Maghreb plate contact from seismic moment tensors and GPS observations. *Tectonophysics* 42, 295-317. doi: 10.1016/j.tecto.2006.08.004.

Stokes, M (2008): Plio-Pleistocene drainage development in an inverted sedimentary basin: Vera basin, Betic Cordillera, SE Spain. *Geomorphology* 100, 193–211. doi:10.1016/j.geomorph.2007.10.026

Stokes, M., Mather, A.E. (2000): Response of Plio-Pleistocene alluvial systems to tectonically induced base-level changes, Vera Basin, SE Spain. *Journal of the Geological Society of London* 157, 303–316.

Stokes, M., Mather, A.E. (2003): Tectonic origin and evolution of a transverse drainage: the Río Almanzora, Betic Cordillera, SE Spain. *Geomorphology* 50, 59–81.

Tahayt, A., Mourabit, T., Rigo, A., Feigl, K.L., Fadil, A., McClusky, S., Reilinger, R., Serroukh, M., Ouazzani-Touhami, A., Ben Sari, D., Vernant, P. (2008): Present-day movements of tectonic blocks in the Betic-Rif Arc from GPS measurements 1999–2005. *Comptes Rendus Geoscience* 340, 400–413, doi:10.1016/j.crte.2008.02.003.

Van de Poel, H.M. (1991): Messinian stratigraphy of the Níjar Basin (S.E. Spain) and the origin of its gypsum-ghost limestones. *Geologie en Mijnbouw* 70, 215-234.

Vernant, P., Fadil, A., Mourabit, T., Ouazar, D., Koulali, A., Davila, J.M., Garate, J., McClusky, S., Reilinger, R.E. (2010): Geodetic constraints on active tec- tonics of the Western Mediterranean: implications for the kinematics and dynamics of the Nubia-Eurasia plate boundary zone. *J. Geodyn.* 49, 123–129, doi:10.1016/j.jog.2009.10.007.

Weijermars, R. (1985): Uplift and subsidence history of the Alborán Basin and a profile of the Alborán Diapir (W-Mediterranean). *Geol. Mijnbouw* 64, 349-356.

Weijermars, R. (1987): The Palomares brittle ductile shear zone of Southern Spain, *Journal Structural Geology* 9, 139-157.

Journal of the Geological Society, London, Vol. **170**, 2013, pp. 47–55. doi: 10.1144/jgs2011-131.

Backarc basin inversion and subcontinental mantle emplacement in the crust: kilometre-scale folding and shearing at the base of the proto-Alborán lithospheric mantle (Betic Cordillera, southern Spain)

KÁROLY HIDAS[1*], GUILLERMO BOOTH-REA[1,2], CARLOS J. GARRIDO[1], JOSÉ MIGUEL MARTÍNEZ-MARTÍNEZ[1,2], JOSÉ ALBERTO PADRÓN-NAVARTA[3,4], ZOLTÁN KONC[1], FLAVIO GIACONIA[1,2], ERWIN FRETS[1] & CLAUDIO MARCHESI[1]

[1]*Instituto Andaluz de Ciencias de la Tierra, CSIC & UGR, Avenida de las Palmeras 4, 18100 Armilla (Granada), Spain*

[2]*Department of Geodynamics, University of Granada, Fuentenueva s/n, 18002 Granada, Spain*

[3]*Géosciences Montpellier, Université Montpellier-2 & CNRS, CC 60, Place E. Bataillon, 34095 Montpellier, France*

[4]*Research School of Earth Sciences, The Australian National University, Building 61, Mills Road, Canberra, ACT 0200, Australia*

**Corresponding author (e-mail: karoly.hidas@csic.es)*

Abstract: To constrain the latest evolutionary stages and mechanisms of exhumation and emplacement of subcontinental peridotites in the westernmost Mediterranean, we present here a detailed structural study of the transition from granular spinel peridotite to plagioclase tectonite in the western Ronda Peridotite (Betic Cordillera, southern Spain). We show that the plagioclase tectonite foliation represents an axial surface particularly well developed in the reverse limb of a downward facing moderately plunging and moderately inclined synform at the base of the Ronda massif. The fold limbs are cut by several mylonitic and ultramylonitic shear zones with top-to-the-SW sense of shear. After restoring the middle to late Miocene vertical-axis palaeomagnetic rotation and the early Miocene tectonic tilting of the massif, these studied structures record southward-directed kinematics. We propose a geodynamic model in which folding and shearing of an attenuated mantle lithosphere occurred by backarc basin inversion during late Oligocene (23–25 Ma) southward collision of the Alborán Domain with the palaeo-Maghrebian passive margin, leading to the intracrustal emplacement of peridotites in the earliest Miocene (21–23 Ma).

One of the most peculiar features of the arcuate Betic–Rif orogenic belt (western Mediterranean) is the occurrence of massive outcrops of subcontinental lithospheric mantle (i.e. the Ronda and Beni Bousera peridotite massifs; Fig. 1a). Several contrasting models have been proposed to explain the exhumation of these massifs and its relationship to the geodynamic evolution of the western Mediterranean, including the rollback of an eastward subducted oceanic lithosphere slab (Royden 1993; Lonergan & White 1997; Wortel & Spakman 2000; Gutscher *et al*. 2002; Spakman & Wortel 2004; Bokelmann & Maufroy 2007; Bokelmann *et al*. 2011), convective removal (Platt & Vissers 1989) or delamination (García-Dueñas *et al*. 1992; Seber *et al*. 1996; Calvert *et al*. 2000; Duggen *et al*. 2003; Tubía *et al*. 2004) of overthickened continental lithospheric mantle, or transpressional emplacement during oblique plate convergence (Mazzoli & Martín Algarra 2011). Most of these models agree that extension affected the orogenic wedge during the latest Oligocene to Early Miocene, explaining the majority of geological and geophysical observations in the area (Calvert *et al*. 2000), but only a few of them try to account for the presence of the Ronda Peridotite massif (the largest outcrop of subcontinental lithospheric mantle on Earth; *c*. 450 km^2), which was exhumed from diamond facies (>140 km, Davies *et al*. 1993) and emplaced into middle crustal HP–LT to LP–HT metamorphic units (e.g. Tubía & Cuevas 1986; Tubía 1994; Zeck 1997; Argles *et al*. 1999; Esteban *et al*. 2011).

The polybaric and polythermal history of the Ronda exhumation is preserved as a protracted record in different tectonometamorphic domains (Fig. 1b: garnet, spinel and plagioclase peridotite; e.g. Obata 1980; Van der Wal & Vissers 1996) of which plagioclase peridotite developed at the lowest pressure related to the latest evolutional stages of the massif. However, previous structural studies have not satisfactorily integrated the LP–HT structures of this domain into the evolution of the Betic–Rif chain and into the emplacement of the Ronda massif, because plagioclase peridotite has been interpreted as formed either by delamination-derived diapiric asthenospheric flow (Tubía 1994; Tubía *et al*. 2004) or by ductile extensional shear zones affecting partially molten lithosphere prior to its intracrustal emplacement (Van der Wal & Vissers 1996).

The main issues we discuss include the understanding of (1) the transition from a kilometre-scale partially melted domain (represented by the Ronda recrystallization front; e.g. Van der Wal & Bodinier 1996; Lenoir *et al*. 2001; Soustelle *et al*. 2009) to the formation of late, ductile structures in the plagioclase peridotite domain (Van der Wal & Vissers 1996), and (2) the relation of this transition to the exhumation and crustal emplacement of the massif. Here we present new structural data from this transition indicating massif-scale rotation of the compositional layering that evolved continuously from the spinel to the plagioclase facies and developed contemporaneously with the plagioclase tectonite foliation, recording kilometre-scale folding of the shallow subcontinental lithospheric mantle. After restoring the clockwise vertical-axis rotation and the counterclockwise horizontal-axis tectonic tilting of the massif (García-Dueñas *et al*. 1992; Crespo-Blanc & Campos 2001; Villasante-Marcos *et al*. 2003), our detailed structural mapping shows that the fold formed before crustal emplacement of the Ronda Peridotite during southward thrusting in the backarc setting of the Alborán Domain (western Mediterranean basin).

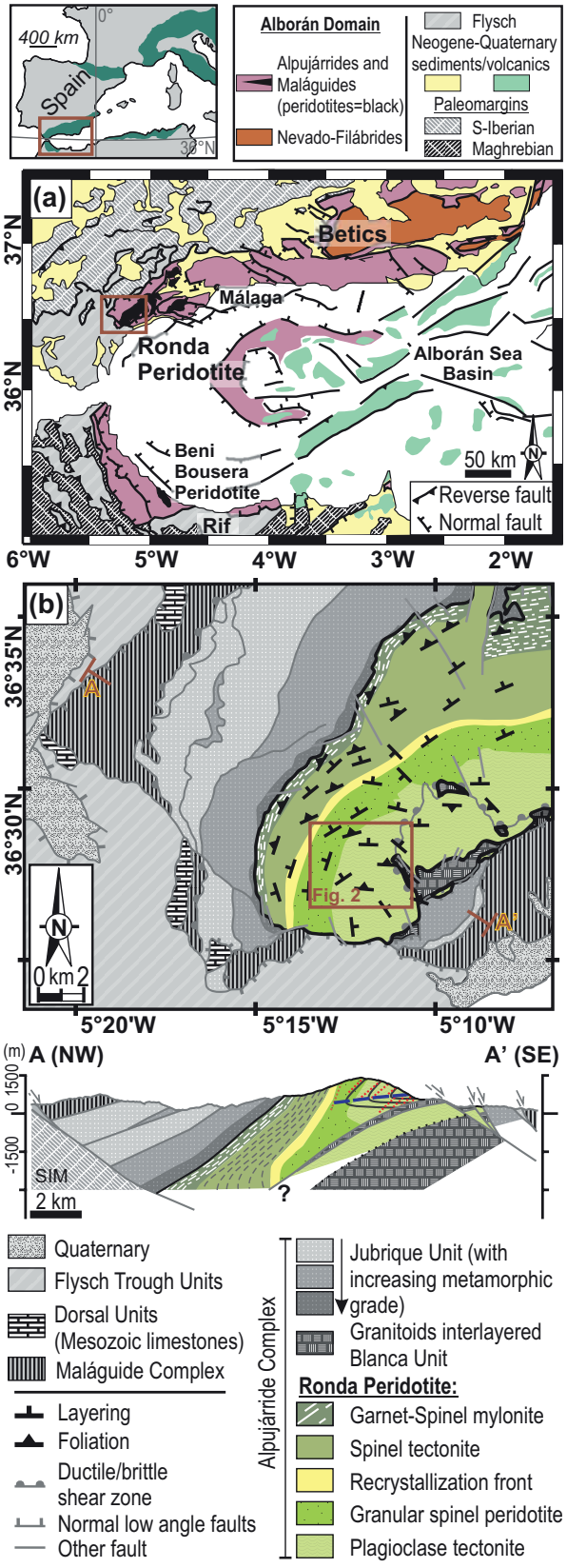

Structure of the Ronda Peridotite massif

The Ronda massif is a coherent lithospheric mantle section zoned into several kilometre-scale petrological, geochemical and structural domains (Obata 1980; Van der Wal & Bodinier 1996; Van der Wal & Vissers 1996; Lenoir *et al*. 2001; Esteban *et al*. 2007; Precigout *et al*. 2007; Soustelle *et al*. 2009). Results of the extensive earlier studies provide a basis to summarize the temporal and structural evolution of the domains from older to younger structures and from the top to the bottom of the massif (from NNW to SSE) as follows.

(1) The garnet–spinel (grt–sp) mylonite and spinel tectonite domains represent the vestiges of Proterozoic lithospheric mantle, with the grt–sp mylonites interpreted either as younger structures formed by high-pressure shearing of an older spinel tectonite domain (Van der Wal & Vissers 1996), or as formed coevally with spinel tectonites by increasing strain localization and cooling at the top of the massif (Precigout *et al*. 2007; Garrido *et al*. 2011).

(2) The granular spinel peridotite domain is composed of coarse granular spinel peridotites formed by annealing of the spinel tectonites during thermal erosion and partial melting (>1250 °C, 1.5 GPa) above the upwelling asthenosphere, at the base of the extremely attenuated lithospheric section (Van der Wal & Bodinier 1996; Van der Wal & Vissers 1996; Lenoir *et al*. 2001; Vauchez & Garrido 2001; Bodinier *et al*. 2008; Soustelle *et al*. 2009). The transition from the spinel tectonite to the granular spinel peridotite domain is a narrow (*c*. 200–400 m wide) and continuous (*c*. 20 km long) transitional zone referred to as the recrystallization front, which is considered as a former isotherm overlying partially molten granular peridotites (Van der Wal & Bodinier 1996; Lenoir *et al*. 2001).

(3) The youngest, underlying plagioclase tectonite domain overprints the granular spinel peridotite domain and records the latest stages of evolution of the Ronda Peridotite under progressive cooling (800–900 °C) and decompression (0.5–0.7 GPa; Obata 1980).

Structure of the transition from granular spinel peridotite to plagioclase tectonite

Our study focuses on the westernmost Ronda Peridotite massif where granular spinel peridotite grades into plagioclase tectonite (Fig. 1b). We selected this area because the transition here is well exposed and unaffected by the late mantle imbrications overthrusting crustal

Fig. 1. (**a**) Simplified geological map (modified after Comas *et al*. 1999; Booth-Rea *et al*. 2007) with the main tectonic domains forming the Betic–Rif orogenic belt (see inset for location). The figure also highlights the Ronda Peridotite in southern Spain and Beni Bousera Peridotite in northern Morocco. The rectangle indicates the area shown in (**b**). (**b**) Simplified geological map and cross-section of the westernmost Alborán Domain in the Betic chain with the tectonometamorphic domains and internal structures of the western Ronda Peridotite (mapped by Darot 1973; Obata 1980; Van der Wal & Vissers 1996; Lenoir *et al*. 2001; Precigout *et al*. 2007; Soustelle *et al*. 2009). The Ronda Peridotite is outlined in black. The A–A' cross-section is modified after García-Dueñas *et al*. (1992) and Sánchez-Gómez *et al*. (2002), showing the appearance of the reconstructed fold (continuous black curves) in the southeastern part of the massif with fold axial-plane trace (dashed blue line; flat lying dashed line in printed version) and axial planar S_2 tectonite foliation (dotted lines). SIM, South Iberian margin. Study area is shown enlarged in Fig. 2.

rocks. These imbricated structures were previously interpreted as crustal lenses deformed synchronously with the ductile deformation of the plagioclase tectonite domain (e.g. Van der Wal & Vissers 1996) but more recent studies have shown that intercalation of peridotites among layers of crustal Blanca Units is postkinematic to peridotite deformation and, in addition, is strongly modified by superimposed extensional faulting (Sánchez-Gómez *et al*. 2002).

The oldest structures in the western Ronda Peridotite occur in the garnet–spinel mylonite and the underlying spinel tectonite domains (Van der Wal & Vissers 1996; Precigout *et al*. 2007; Soustelle *et al*. 2009) as garnet pyroxenite compositional layering (S_0) and high-temperature (high-*T*) ductile peridotite foliation (S_1) with a NE–SW-trending stretching lineation (L_1) defined by spinel aggregates and, in the garnet–spinel mylonite, by elongated orthopyroxene (Darot 1973; Balanyá *et al*. 1997; Precigout *et al*. 2007; Soustelle *et al*. 2009). The S_1 foliation is subparallel to the S_0 compositional layering and dips generally 70–80° to the WNW (Van der Wal & Vissers 1996; Soustelle *et al*. 2009; Fig. 1b). In the most intensely foliated spinel tectonites, the S_0 compositional layering exhibits boudins and metre-scale isoclinal folds with axial planes parallel to the S_1 foliation (Van der Wal & Vissers 1996; Garrido & Bodinier 1999). The S_1 spinel tectonite foliation disappears at the recrystallization front, which is interpreted as a peridotite solidus isotherm that annealed and melted the spinel tectonite domain giving way to underlying apparently undeformed granular spinel peridotite (Van der Wal & Bodinier 1996; Van der Wal & Vissers 1996; Lenoir *et al*. 2001). As a result of melting and decompression the S_0 compositional layering is represented by spinel pyroxenite in the granular spinel peridotite domain (Seiland Facies of Obata 1980) and by plagioclase–spinel pyroxenite in the plagioclase tectonite domain (Garrido & Bodinier 1999; Bodinier *et al*. 2008). In the study area only these pyroxenites were considered as the markers of S_0 compositional layering. In addition to S_0, two newly developed structures characterize the lower part of the granular spinel peridotite and the plagioclase tectonite domains (study area, Fig. 2a): (1) a higher-temperature peridotite foliation S_2 (hereafter referred as high-*T* structure); (2) a lower-temperature and/or higher strain (hereafter referred as low-*T* structure) mylonitic to ultramylonitic foliation (S_m) developed in shear zones that cut the high-*T* structures.

At the highest topographic levels of our study area (Fig. 2a), located immediately below the recrystallization front (see Fig. 1b), the S_0 compositional layering is marked by spinel pyroxenite dipping 70–80° to the NW, thus being subparallel to the garnet pyroxenite S_0 of the overlying spinel tectonite domain (Fig. 1b; Van der Wal & Vissers 1996). Down-section, at the transition from the granular spinel peridotite to the plagioclase tectonite domain, the S_0 compositional layering rotates gradually clockwise, at the base of the massif having a dip of 40–60° to the ENE (Fig. 2a). The first occurrence of the new high-*T* S_2 foliation is found close to the recrystallization front in the northwestern part of the study area (Fig. 2a), where plagioclase-free spinel lherzolite shows foliation dipping 60–80° to the north that crosscuts the spinel pyroxenite S_0 (Fig. 3a). Further to the SSE in the plagioclase tectonite domain the S_2 foliation becomes increasingly penetrative in porphyroclastic lherzolite that shows plagioclase rims around spinel (Fig. 3b and e) and it is slightly weaker in more refractory peridotite that lacks plagioclase. In both cases the S_2 foliation crosscuts S_0 compositional layering and former isoclinal folds (Fig. 3c), and shows a fairly uniform dip of 50–70° to the NNE (Fig. 2a) with stretching lineation (L_2) trending NE–SW in the foliation plane (Fig. 2a inset).

The younger low-*T* structure in the study area is marked by the development of mylonitic to ultramylonitic microstructures in shear zones (Fig. 3d) with olivine grain sizes <200 μm (10–50 μm for ultramylonites; Fig. 3f). Although Van der Wal & Vissers (1996) interpreted the whole plagioclase tectonite domain as a shear zone, they reported only high-*T* ductile S_2 structure in this domain and did not recognize the low-*T* ultramylonite bands. These shear zones first occur as thinner (<10 cm) and discontinuous bands at the base of the granular spinel peridotite domain and as much wider shear zones (up to 5–10 m width; Fig. 3d) in the plagioclase tectonite domain (Fig. 2a). In the eastern part of the study area, a thick ultramylonite shear zone (10 m wide; Fig. 3d) can be tracked westward for 2 km where it progressively narrows to less than 1 m (Fig. 2a). The strike of the low-*T* S_m mylonitic foliation is subparallel to that of the high-*T* S_2 foliation but it dips more gently, 30–50° to the NNE (Fig. 2a inset). Elongated orthopyroxene porphyroclasts and spinel denote a NE–SW-trending lineation L_m, subparallel to the high-*T* L_2 lineation of plagioclase tectonite (Fig. 2a inset). Microstructure of the low-*T* mylonites implies top-to-the-SW sense of shear (Fig. 3f) in accordance with the sigmoidal character of S_2 foliation in the shear zones (Fig. 3d inset).

Origin and significance of plagioclase tectonites

Our detailed mapping of the granular peridotite and the plagioclase tectonite domains clearly shows large-scale gradual rotation of the S_0 compositional layering (Fig. 2a) that cannot be accounted for solely by shearing as suggested by Van der Wal & Vissers (1996). Instead, the S_0 compositional layering forms two limbs of a kilometre-scale fold with a high-*T* axial-plane foliation (S_2) (Fig. 2a inset), which is well developed in the reverse limb (Fig. 2a and b). The fold axial surface dips 50° to the north (average orientation of the S_2 foliation) and the fold axis plunges *c*. 45° to the NE (intersection between the layering in both limbs and between the S_2 foliation and the layering; Fig. 2a inset). This single fold has only two major limbs, which means that the fold asymmetry or fold vergence cannot be reconstructed. However, cleavage vergence, defined here as the horizontal direction of the sense of acute angle towards which the S_2 foliation needs to be rotated so that it becomes parallel to S_0 layering (see Bell 1981, and references therein), further clarifies internal fold geometry. As reported by Van der Wal & Vissers (1996) elsewhere in the plagioclase tectonite domain, we also observed in our study area a NW cleavage vergence to the north and a SE cleavage vergence to the SE (Fig. 2a and b). Local vergence changes related to minor folds at a scale of 10–100 m are also present, of which the largest one is shown in the southeastern part of the study area (Fig. 2b). Because the Ronda Peridotite is a coherent lithospheric mantle section (Obata 1980; Van der Wal & Vissers 1996) that is also continuous with its overlying crustal envelope (Tubía 1994; Balanyá *et al*. 1997; Argles *et al*. 1999; Platt *et al*. 2003), the polarity in the northern side of the massif is upwards. It follows that the kilometre-scale fold at the base of the mantle section is a non-cylindrical, moderately plunging, moderately inclined, downward facing synform (i.e. anticline) (Fig. 2b). It should be noted that its fold axis is subparallel to the trace of the stretching L_2 lineation in the S_2 peridotite foliation plane (Fig. 2a inset) but this geometry is similar to that observed in large-scale folding of other orogenic peridotites, such as the central part of the Lanzo Peridotite Massif in the Alps (Nicolas & Boudier 1975; Boudier 1978). In fact, the parallelism between fold axis and mineral lineation is a common feature in rocks deformed by folding associated with shearing (e.g. Bell 1978, and references therein), where the fold is formed initially by flattening but the increase of simple shear component progressively rotates the fold axis within its own axial plane until it lies parallel to lineation (compare a sheath fold). In the study area, high-*T* (S_2–L_2) and low-*T* (S_m–L_m) structures show a similar orientation (Fig. 2a inset), which

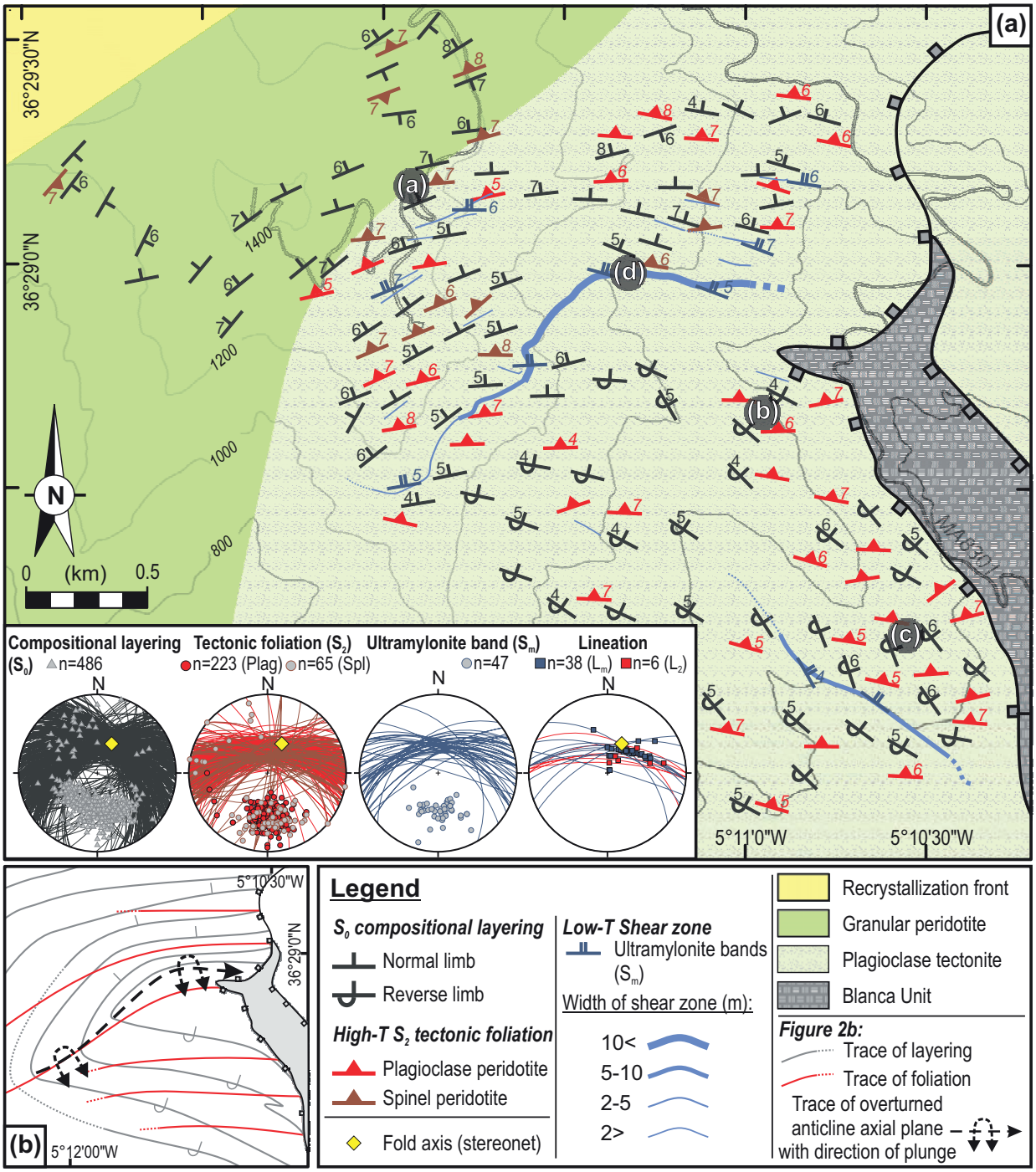

Fig. 2. (**a**) Structural map of the study area. White letters in black shaded circles refer to the location of outcrops shown in Figure 3. Numbers beside the symbols of layering, high-*T* and low-*T* foliation indicate the dip values where, for example, 4 should be read as a 40° dip. Inset in the bottom left corner shows lower hemisphere, equal angle (Wulff) stereographic projections of all field measurements as traces of planes and their poles for compositional layering (S_0), high-*T* tectonite foliation (S_2), and low-*T* shear zone foliation (S_m). In the second pole figure from the left (high-*T* S_2), grey circles (pale circles in the printed version) are the poles of plagioclase-free foliation, whereas red circles (dark circles in the printed version) are the poles of plagioclase tectonite foliation. Stretching lineations in high-*T* (L_2) and low-*T* (L_m) structures are plotted on their corresponding foliation planes (S_2 and S_m, respectively). Diamond symbol in pole figures corresponds to the fold axis. *n*, number of data; Plag, plagioclase tectonite foliation; Spl, plagioclase-free tectonite foliation. (**b**) Interpretative map of the large-scale folding of the S_0 compositional layering with the S_2 axial plane foliation in the study area. The changes from NW to SE cleavage vergence in normal and reverse limbs of the fold that corresponds to the 'north-vergent' and 'south-vergent' domains of Van der Wal & Vissers (1996), interpreted by them as shear zones with opposite kinematics, should be noted. Also noteworthy is a small inversion in cleavage vergence in the southeastern part of the study area, which is interpreted as a minor fold developed on the reverse limb of the fold.

indicates that they must record similar kinematics. Therefore, low-*T* shear zones are interpreted to have formed synkinematically with the folding by increasing strain localization upon cooling at the brittle–ductile transition of peridotite (Boullier & Gueguen 1975).

Van der Wal & Vissers (1996) concluded that the high-*T* foliation S_2 in the plagioclase tectonite domain developed in two diachronous kilometre-scale shear zones with opposite kinematics: an older 'south-vergent' shear zone, as wide as the entire plagioclase tectonite domain, with top-to-the-north sense of shear that was overprinted by a younger and narrower 'north-vergent' shear zone recording top-to-the-south sense of shear. At the borders of the oppositely directed shear zones, they observed minor folds (*c*. 100 m length scale) with the high-*T* S_2 foliation as axial plane (see Van der Wal & Vissers 1996, p. 36, fig. 11) that they suggested to form as shear folds owing to strain gradients preserved in the margins of shear zones with opposite kinematics. In contrast, our structural data show that the local change in cleavage vergence corresponds to changes from the normal to the reverse limbs of the large-scale fold (Fig. 2a and b) instead of two opposite shear senses in diachronous shear zones. Small-scale folds described by Van der Wal & Vissers (1996) are explained here as minor folds developed on the normal limb of the kilometre-scale anticline. The presence of undeformed granular spinel peridotite lenses within foliated plagioclase tectonite, and the occurrence of crustal lenses of the underlying Blanca unit within the younger, north-vergent shear zones were claimed by Van der Wal & Vissers (1996) as further support for increasing strain localization and their relation with the emplacement of the Ronda Peridotite. However, later studies have demonstrated that these crustal lenses represent brittle imbrications of the plagioclase tectonite overthrusting crustal rocks, and that they are unrelated to the ductile high-*T* deformation of peridotite (Sánchez-Gómez *et al*. 2002; Fig. 1b, cross-section). In our study area crustal lenses are not present in the SE-vergent domains, supporting that such crustal lenses are due to brittle tectonics (Sánchez-Gómez *et al*. 2002) unrelated to the processes that resulted in the ductile S_2 peridotite foliation. Alternative models for the origin of plagioclase tectonites are that they represent an upwelling asthenospheric mantle diapir at the base of a thinned continental lithosphere during mantle extrusion in a transform-fault context (Tubía 1994) or triggered by sublithospheric delamination (Tubía *et al*. 2004). However, mapping of structures related to 3D mantle diapirs below a fast palaeo-spreading ridge in the Oman ophiolite shows that diapirs are composed of coarse-granular peridotite formed by high-temperature deformation producing steep peridotite lineations and warped vertical foliation trajectories (Ceuleneer *et al*. 1988; Nicolas & Boudier 1995; Jousselin *et al*. 1998). Formation of the Ronda plagioclase tectonites decoupled from their overlying peridotite domains in high-temperature asthenospheric flow is further inconsistent with (1) the kilometre-scale folding of high-*T* structures from the spinel to the plagioclase lherzolite facies (Fig. 2a) indicating that the S_0 compositional layering was folded upon cooling and decompression in a coherent lithospheric mantle section, (2) subhorizontal lineations of the high-*T* plagioclase tectonite foliation with respect to the palaeo-horizontal recrystallization

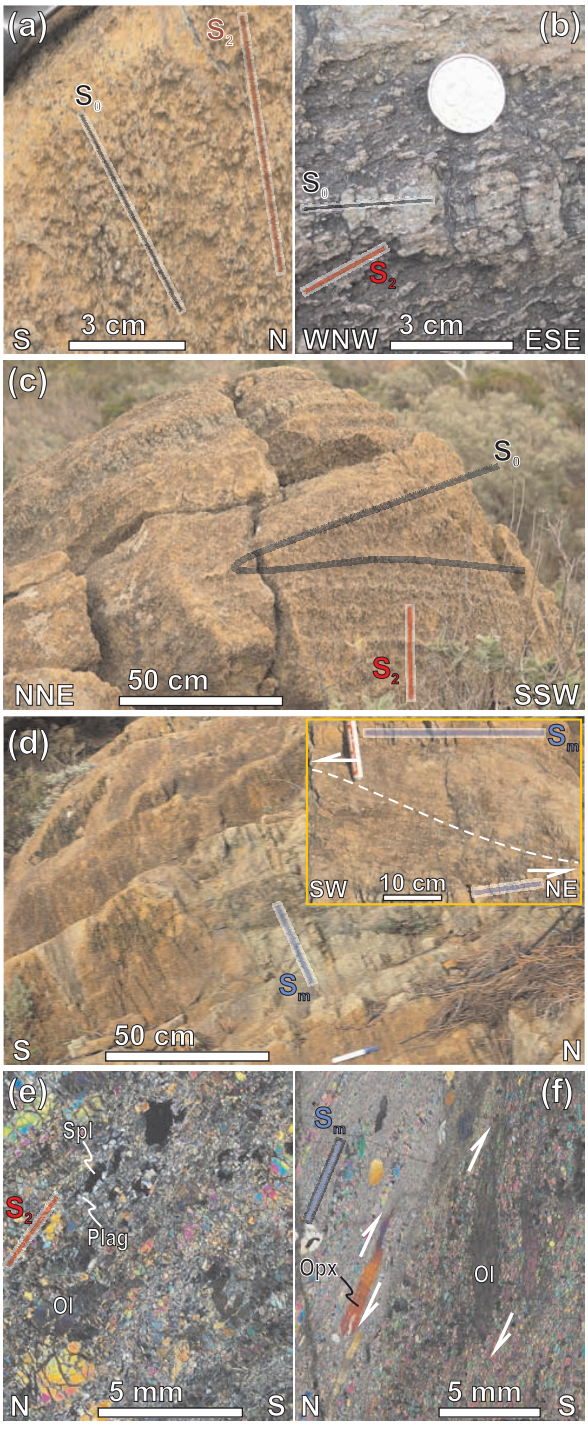

Fig. 3. (**a**–**d**) Field views of the main structural features of the study area discussed in the text. Outcrop locations are shown in Figure 2. (**a**) Crosscutting relationship between high-*T* S_2 tectonite foliation and S_0 compositional layering observed in plagioclase-free spinel lherzolite indicating that large-scale folding initiated in the spinel lherzolite facies. (**b**) Crosscutting relationship between high-*T* S_2 foliation and S_0 compositional layering observed in plagioclase tectonite. (**c**) Metre-scale unsheared isoclinal folding of the S_0 compositional layering crosscut by high-*T* S_2 plagioclase tectonite foliation indicating that isoclinal folds, similar to those observed in the overlying domains by Van der Wal & Vissers (1996) and Garrido & Bodinier (1999), formed earlier than the plagioclase tectonite foliation and are not related to the kilometre-scale folded structure studied here. (**d**) A 10 m wide shear zone developed in peridotite with low-*T* S_m shear zone foliation. Inset shows sigmoidal character of high-*T* S_2 foliation (white dashed line) between low-*T* ultramylonite bands (S_m). (**e**, **f**) Cross-polarized light photomicrographs of plagioclase tectonite (**e**) and mylonitic–ultramylonitic shear zone (**f**). White arrows in (**f**) and inset of (**d**) indicate top-to-the-SW sense of shear in the low-*T* structures.

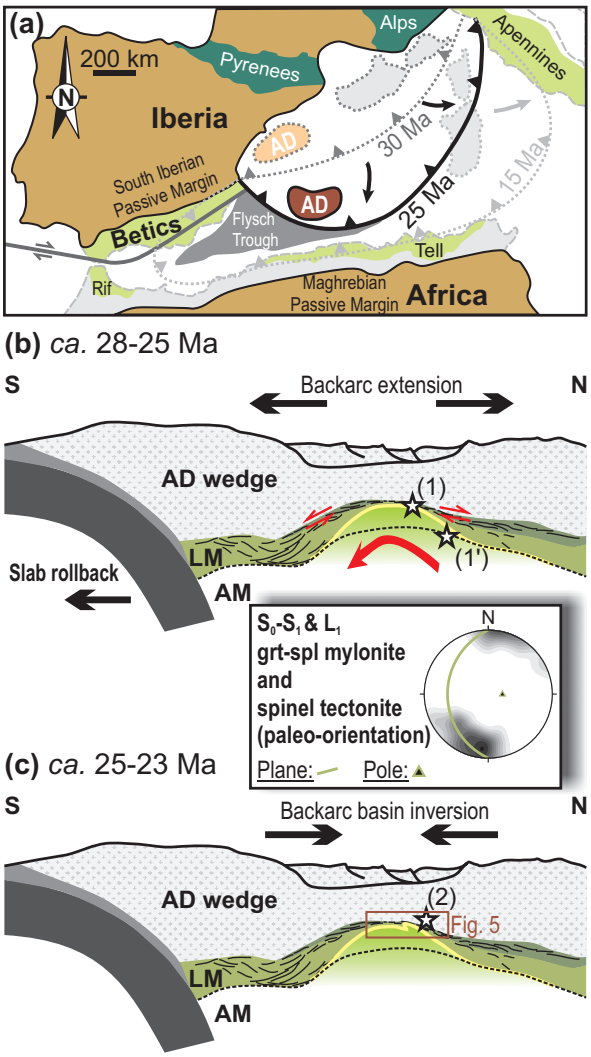

Fig. 4. (**a**) Geodynamic reconstruction (modified after Booth-Rea *et al*. 2007 and Marchesi *et al*. 2012) showing the tectonic scenario proposed for the westernmost Mediterranean for the Late Oligocene–Early Miocene. AD, Alborán Domain including Ronda Peridotite. (**b**) North–south cross-section for the Late Oligocene backarc extension (modified after Garrido *et al*. 2011). In the figure, (1) denotes the formation of grt–spl mylonites owing to backarc extension and (1') refers to partial melting at the base of the lithosphere induced by asthenospheric upwelling. (**c**) North–south cross-section for the Late Oligocene–Early Miocene backarc basin inversion that led to kilometre-scale folding indicated by (2) and shown in detail in Figure 5 (area outlined). Shading of the lithospheric mantle is the same as for Ronda Peridotite in Figure 1b. AD wedge, Alborán crustal units; AM, asthenospheric mantle; LM, lithospheric mantle. Lower hemisphere, equal angle (Wulff) stereographic projection shows the palaeo-orientation of the S_0 compositional layering and the S_1 tectonite foliation (simplified to a single plane, as they are essentially parallel to each other) as a trace of plane and its pole, along with L_1 mineral lineation as grey shaded density contours (contours from 0.0 to 11.1) in the grt–sp mylonite and spinel tectonite domains of the Ronda Peridotite (Darot 1973; Van der Wal & Vissers 1996; Precigout *et al*. 2007; Soustelle *et al*. 2009). The palaeo-orientation was approximated by undoing the late brittle rotations (tectonic tilting: García-Dueñas *et al*. 1992; palaeomagnetic rotation: Villasante-Marcos *et al*. 2003).

front and the overlying spinel tectonite foliations that would represent the lithospheric domain, and (3) the presence of low-*T* shear zones showing similar structures to the high-*T* plagioclase tectonites, which cannot occur in high-temperature asthenospheric flow. Diapiric models do not account for the geochemical signatures of peridotites and pyroxenites in the different tectonic domains (Garrido & Bodinier 1999) and the similar Re–Os ages of the different domains indicating a provenance from the same section of old subcontinental lithospheric mantle (Marchesi *et al*. 2010).

Geodynamic implications

The Alpine history of the Ronda Peridotite is related to strong Oligocene (Balanyá *et al*. 1997; Argles *et al*. 1999) thinning of the Alpujárride–Maláguide Eocene (Platt *et al*. 2005) orogenic wedge (Alborán crustal domain). Marchesi *et al*. (2012) showed that late Oligocene intrusive mantle pyroxenites in the Ronda massif were in equilibrium with andesite-like melts and have a geochemical signature similar to Neogene subduction-related lavas of the western and central Mediterranean. Rather than convective removal or delamination of a previously generated lithospheric root, these data support thinning of the Alborán Domain orogenic wedge and its convective thermal erosion induced by slab rollback in a backarc basin situated several hundred kilometres further east (south of the Balearic Islands) during the Palaeogene (Fig. 4a; Lonergan & White 1997; Rosenbaum *et al*. 2002; Faccenna *et al*. 2004; Booth-Rea *et al*. 2007; Garrido *et al*. 2011). In this setting, the 21–23 Ma intracrustal emplacement of the Ronda Peridotite (Priem *et al*. 1979; Esteban *et al*. 2011) occurred after the collision with the Maghrebian passive margin (*c*. 23–25 Ma; Booth-Rea *et al*. 2005), providing a common origin for the peridotite bodies in the Betic–Rif and in the Kabylian belt in Algeria (Caby *et al*. 2001; Bruguier *et al*. 2009). Lonergan (1993) also proposed initial south-directed migration of the Alborán Domain to explain the southward-directed thrusting of the Maláguide–Alpujárride nappe-stack after undoing palaeomagnetic rotations in the eastern Betics. During the early Miocene the system propagated westward, resulting in the oblique collision with the South Iberian passive margin and the high-pressure metamorphism of the Nevado–Filábride units between 15 and 17 Ma (López Sánchez-Vizcaíno *et al*. 2001; Platt *et al*. 2006). All these time constraints are in agreement with the 25 ± 1 Ma Lu–Hf ages obtained for the formation of overlying garnet pyroxenites in the Beni Bousera massif, which is the counterpart to the Ronda Peridotite in northern Morocco (Blichert-Toft *et al*. 1999; Pearson & Nowell 2004) as well as with the 19 ± 5 Ma U–Pb ages of crystallization of late granites that crosscut the Ronda Peridotite (Sánchez-Rodríguez & Gebauer 2000). Garrido *et al*. (2011) have proposed a similar scenario to account for the poly-metamorphic, tectonic and igneous history of the Ronda Peridotite. Those workers considered that the Ronda grt–sp mylonite domain was formed in the Oligocene during decompression and cooling of garnet peridotites from 2.4–2.7 GPa at 1020–1100 °C (*c*. 85 km) to 2 GPa at 800–900 °C (*c*. 65 km) as a result of early exhumation and thinning of the Alborán Domain.

Structural and palaeomagnetic studies have shown that after its emplacement the Ronda Peridotite underwent important brittle tectonic tilting (*c*. 50° anticlockwise rotation around a horizontal N70°E-directed axis with respect to its present-day position; García-Dueñas *et al*. 1992; Crespo-Blanc & Campos 2001) and vertical-axis *c*. 35° clockwise rotation (Villasante-Marcos *et al*. 2003). To discuss the kinematic evolution of the Ronda Peridotite in a geodynamic framework one should consider these brittle rotations and restore the present-day structures to their original

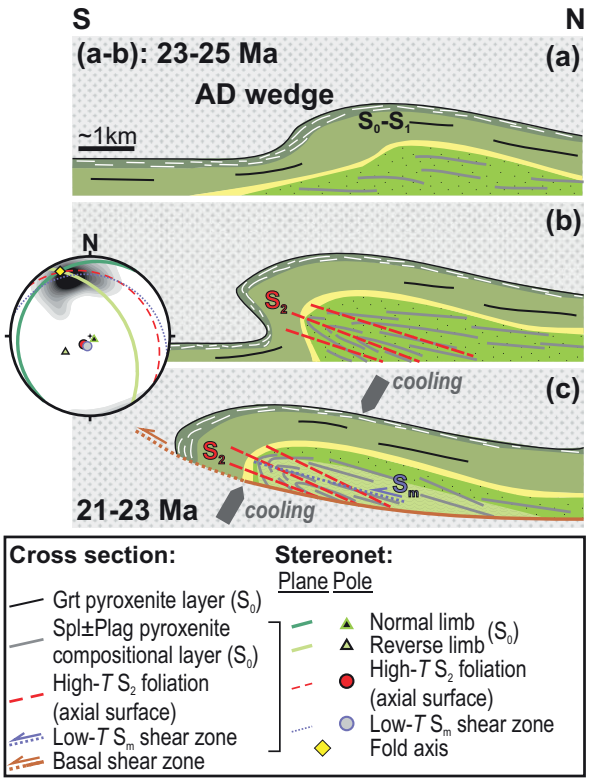

Fig. 5. (**a**–**c**) Proposed scenario in north–south cross-sections for the initiation and development of Late Oligocene massif-scale folding and Early Miocene intracrustal emplacement of the Ronda Peridotite. Shading follows that of the Ronda Peridotite introduced in Figure 1b. Lower hemisphere, equal angle (Wulff) stereographic projection shows the average palaeo-orientations of normal and reverse limbs (S_0 compositional layering), S_2 tectonite foliation, S_m shear zone foliation as traces of planes and their poles along with subparallel stretching lineations of L_2 and L_m as grey shaded density contours (contours from 0.0 to 11.1) in the study area. The palaeo-orientation was approximated by undoing the late brittle rotations (tectonic tilting: García-Dueñas *et al*. 1992; palaeomagnetic rotation: Villasante-Marcos *et al*. 2003). Grt, garnet; Plag, plagioclase; Spl, spinel.

palaeo-orientation. Feinberg *et al*. (1996) and Villasante-Marcos *et al*. (2003) showed that the massif was already tilted when the palaeomagnetic rotation took place in the middle to late Miocene. Consequently, we restored first the younger palaeomagnetic rotation and then the older tectonic tilting of the massif by rotating the structural data anticlockwise 35° around a vertical axis (Villasante-Marcos *et al*. 2003) and then clockwise 50° around a horizontal N35°E axis, the latter one corresponding to the present-day N70°E horizontal axis (García-Dueñas *et al*. 1992; Crespo-Blanc & Campos 2001) corrected for the later palaeomagnetic rotation. The present-day WNW-dipping S_0–S_1 planar structures and NE–SW-trending L_1 lineation of the grt–sp mylonite and spinel tectonite domains (Fig. 1b) currently record top-to-the-north kinematics (Darot 1973; Balanyá 1991; Balanyá *et al*. 1993; Tubía 1994). Undoing the late brittle rotations results in a palaeo-orientation of the S_0–S_1 planar structures dipping 25° to the west associated with a north–south-trending L_1 lineation (Fig. 4b stereogram) and sub-horizontal north-directed kinematics. This kinematics and the decompressive *P*–*T* path of the grt–sp mylonite (Garrido *et al*. 2011) are consistent with late Palaeogene thinning of a thick subcontinental lithospheric mantle in a backarc setting along an extensional detachment (Fig. 4b). This early thinning and exhumation was followed in the Late Oligocene–Early Miocene by heating and melting of the base of the extremely attenuated subcontinental lithosphere under spinel peridotite facies conditions (*c*. 1.5 GPa; Lenoir *et al*. 2001).

Restoring the late brittle rotations for our structural data from the granular spinel peridotite and the younger plagioclase tectonite domains results in a subhorizontal, slightly inclined anticline with a fold axis plunging 5° to the NNW and a NE-dipping axial surface (Fig. 5 stereogram). Our study shows that the high-T S_2 foliation already occurs in plagioclase-free spinel lherzolite (Fig. 3a) at the base of the granular spinel peridotites. The existence of the same high-T S_2 foliation in the underlying plagioclase tectonite domain (Fig. 2a) implies that the axial plane foliation developed continuously from the spinel to the plagioclase facies. These observations indicate that the fold started to form in the spinel lherzolite facies (Fig. 5a) in the deep, hottest part of the melted mantle domain below the recrystallization front (Fig. 2a), and developed a kilometre-scale anticline during progressive cooling and decompression at the base of the massif in the plagioclase tectonite domain (Fig. 5b and c). Folding further developed along a low-angle basal thrust-zone that continuously juxtaposed hot peridotite over colder metamorphic units during decompression (Fig. 5c). Upon cooling near the brittle–ductile peridotite transition, low-T shear zones (S_m), synkinematic to the high-T S_2 plagioclase tectonite foliation, developed in the reverse limb of the fold (Fig. 5c). This scenario resulted in a geometry where peridotites were conductively cooled from above and progressively cooled in the basal plagioclase tectonites with the hottest domain preserved in the centre of the massif. This above-and-below cooling would also account for the preservation of the metastable high-pressure grt–sp mylonites and the freezing of the melting recrystallization front in the core of the Ronda Peridotite massif (Fig. 5c). Furthermore, restoring the shear sense to its palaeo-orientation in the low-T structures, which are considered as formed synkinematically to folding, implies a top-to-the-south kinematics for the latest stages of the ductile evolution of the Ronda Peridotite, which is opposite to the higher-pressure northward-directed kinematics of the overlying grt–sp mylonite and spinel tectonite domains (compare the stereograms in Figs 4b and 5a). This southward kinematics can be accounted for by an inversion from a backarc extension during slab rollback to a contractional basin during Late Oligocene–Early Miocene collision of the Alborán orogenic wedge with the Maghrebian passive margin (Fig. 4a and c). We propose that orogenic shortening and southward thrusting initiated a ductile fold recording the early Miocene intracrustal emplacement of the Ronda Peridotite (Figs 4c and 5a–c).

Conclusions

The transition from the granular spinel peridotite to the plagioclase tectonite domain of the Ronda Peridotite records kilometre-scale folding and shearing at the base of the subcontinental lithospheric mantle section that initiated during decompression and cooling of the massif from spinel to plagioclase lherzolite facies. Newly developed foliation in plagioclase lherzolite from the plagioclase tectonite domain represents the axial-plane foliation of an anticline. Synkinematic mylonitic–ultramylonitic shear zones were formed at the peridotite plastic–brittle transition mainly in the reverse limb of this fold. Palaeo-orientation of the present-day structures, inferred from restoring the Miocene tectonic tilting and vertical-axis clockwise palaeomagnetic rotation of the massif, indicates a subhorizontal inclined anticline and a top-to-the-south sense of shear for the

synkinematic shear zones. This geometry and the reconstructed kinematics suggest an Early Miocene inversion in the Alborán backarc extension prior to the intracrustal emplacement of the Ronda Peridotite massif. We propose a geodynamic model in which folding and shearing of an attenuated mantle lithosphere occurred by backarc basin inversion during southward collision of the Alborán Domain with the palaeo-Maghrebian passive margin (23–25 Ma), leading to the intracrustal emplacement of peridotites in the earliest Miocene (21–23 Ma).

We acknowledge the constructive reviews by G. Gutiérrez-Alonso and J. Platt, as well as the editorial work of JGS Subject Editor E. Bozkurt, which substantially improved the paper. This work was supported by grants from the International Lithosphere Program (CC4-MEDYNA), the Spanish Ministry of Science and Innovation (MICINN, grants CGL2010-14848 and AI-HF2008-073) and Junta de Andalucía (grants RNM-131 and 2009RNM4495) to C.J.G.

References

Argles, T.W., Platt, J.P. & Waters, D.J. 1999. Attenuation and excision of a crustal section during extensional exhumation: The Carratraca Massif, Betic Cordillera, southern Spain. *Journal of the Geological Society, London*, **156**, 149–162.

Balanyá, J.C. 1991. *Estructura del dominio de Alborán en la parte Norte del Arco de Gibraltar*. PhD thesis, University of Granada.

Balanyá, J.C., Azañón, J.M., Sánchez-Gómez, M. & García-Dueñas, V. 1993. Pervasive ductile extension, isothermal decompression and thinning of the Jubrique unit in the Paleogene (Alpujárride Complex, western Betics Spain). *Comptes Rendus de l'Académie des Sciences, Série II*, **316**, 1595–1601.

Balanyá, J.C., García-Dueñas, V., Azañón, J.M. & Sánchez-Gómez, M. 1997. Alternating contractional and extensional events in the Alpujarride Nappes of the Alboran domain (Betics, Gibraltar arc). *Tectonics*, **16**, 226–238.

Bell, A.M. 1981. Vergence: an evaluation. *Journal of Structural Geology*, **3**, 197–202.

Bell, T.H. 1978. Progressive deformation and reorientation of fold axes in a ductile mylonite zone: the Woodroffe thrust. *Tectonophysics*, **44**, 285–320.

Blichert-Toft, J., Albarède, F. & Kornprobst, J. 1999. Lu–Hf isotope systematic of garnet pyroxenites from Beni Bousera, Morocco: implications for basalt origin. *Science*, **283**, 1303–1306.

Bodinier, J.L., Garrido, C.J., Chanefo, I., Bruguier, O. & Gervilla, F. 2008. Origin of pyroxenite–peridotite veined mantle by refertilization reactions: evidence from the Ronda peridotite (Southern Spain). *Journal of Petrology*, **49**, 999–1025.

Bokelmann, G. & Maufroy, E. 2007. Mantle structure under Gibraltar constrained by dispersion of body waves. *Geophysical Research Letters*, **34**, 5.

Bokelmann, G., Maufroy, E., Buontempo, L., Morales, J. & Barruol, G. 2011. Testing oceanic subduction and convective removal models for the Gibraltar arc: seismological constraints from dispersion and anisotropy. *Tectonophysics*, **502**, 28–37.

Booth-Rea, G., Azañón, J.M., Martínez-Martínez, J.M., Vidal, O. & García-Dueñas, V. 2005. Contrasting structural and *P–T* evolution of tectonic units in the southeastern Betics: Key for understanding the exhumation of the Alboran Domain HP/LT crustal rocks (western Mediterranean). *Tectonics*, **24**, TC2009, doi: 10.1029/2004TC001640.

Booth-Rea, G., Ranero, C.R., Martínez-Martínez, J.M. & Grevemeyer, I. 2007. Crustal types and Tertiary tectonic evolution of the Alboran sea, western Mediterranean. *Geochemistry, Geophysics, Geosystems*, **8**, Q10005, doi: 10.1029/2007GC001639.

Boudier, F. 1978. Structure and petrology of the Lanzo peridotite massif (Piedmont Alps). *Geological Society of America Bulletin*, **89**, 1574–1591.

Boullier, A.M. & Gueguen, Y. 1975. SP-mylonites—origin of some mylonites by superplastic flow. *Contributions to Mineralogy and Petrology*, **50**,93–104.

Bruguier, O., Hammor, D., Bosch, D. & Caby, R. 2009. Miocene incorporation of peridotite into the Hercynian basement of the Maghrebides (Edough massif, NE Algeria): implications for the geodynamic evolution of the Western Mediterranean. *Chemical Geology*, **261**, 171–183.

Caby, R., Hammor, D. & Delor, C. 2001. Metamorphic evolution, partial melting and Miocene exhumation of lower crust in the Edough metamorphic core complex, west Mediterranean orogen, eastern Algeria. *Tectonophysics*, **342**, 239–273.

Calvert, A., Sandvol, E., *et al.* 2000. Geodynamic evolution of the lithosphere and upper mantle beneath the Alboran region of the western Mediterranean: constraints from travel time tomography. *Journal of Geophysical Research*, **105**, 10871–10898.

Ceuleneer, G., Nicolas, A. & Boudier, F. 1988. Mantle flow patterns at an oceanic spreading center—the Oman peridotites record. *Tectonophysics*, **151**, 1–26.

Comas, M.C., Platt, J.P., Soto, J.I. & Watts, A.B. 1999. The origin and tectonic history of the Alboran Basin: insights from Leg 161 results. *In*: Zahn, R., Comas, M.C. & Klaus, A. (eds) *Proceedings of the Ocean Drilling Program. Scientific Results*. Ocean Drilling Program, College Station, TX, **161**, 555–580.

Crespo-Blanc, A. & Campos, J. 2001. Structure and kinematics of the South Iberian paleomargin and its relationship with the Flysch Trough units: extensional tectonics within the Gibraltar Arc fold-and-thrust belt (western Betics). *Journal of Structural Geology*, **23**, 1615–1630.

Darot, M. 1973. *Méthodes d'analyse structurale et cinématique. Application à l'étude du massif ultrabasique de la Sierra Bermeja*. PhD thesis, University of Nantes.

Davies, G.R., Nixon, P.H., Pearson, D.G. & Obata, M. 1993. Tectonic implications of graphitized diamonds from the Ronda, peridotite massif, southern Spain. *Geology*, **21**, 471–474.

Duggen, S., Hoernle, K., van den Bogaard, P., Rupke, L. & Phipps Morgan, J. 2003. Deep roots of the Messinian salinity crisis. *Nature*, **422**, 602–606.

Esteban, J.J., Cuevas, J., Tubía, J.M., Liati, A., Seward, D. & Gebauer, D. 2007. Timing and origin of zircon-bearing chlorite schists in the Ronda peridotites (Betic Cordilleras, Southern Spain). *Lithos*, **99**, 121–135.

Esteban, J.J., Cuevas, J., Tubía, J.M., Sergeev, S. & Larionov, A. 2011. A revised Aquitanian age for the emplacement of the Ronda peridotites (Betic Cordilleras, southern Spain). *Geological Magazine*, **148**, 183–187.

Faccenna, C., Piromallo, C., Crespo-Blanc, A., Jolivet, L. & Rossetti, F. 2004. Lateral slab deformation and the origin of the western Mediterranean arcs. *Tectonics*, **23**, TC1012.

Feinberg, H., Saddiqi, O. & Michard, A. 1996. New constraints on the bending of the Gibraltar Arc from paleomagnetism of the Ronda peridotites (Betic Cordilleras, Spain). *In*: Morris, A. & Tarling, D.H. (eds) *Paleomagnetism and Tectonics of the Mediterranean Region*. Geological Society, London, Special Publications, **105**, 43–52.

García-Dueñas, V., Balanyá, J.C. & Martínez-Martínez, J.M. 1992. Miocene extensional detachments in the outcropping basement of the northern Alboran Basin (Betics) and their tectonic implications. *Geo-Marine Letters*, **12**, 88–95.

Garrido, C.J. & Bodinier, J.L. 1999. Diversity of mafic rocks in the Ronda peridotite: evidence for pervasive melt–rock reaction during heating of subcontinental lithosphere by upwelling asthenosphere. *Journal of Petrology*, **40**, 729–754.

Garrido, C.J., Gueydan, F., Booth-Rea, G., Precigout, J., Hidas, K., Padrón-Navarta, J.A. & Marchesi, C. 2011. Garnet lherzolite and garnet–spinel mylonite in the Ronda peridotite: vestiges of Oligocene backarc mantle lithospheric extension in the western Mediterranean. *Geology*, **39**, 927–930.

Gutscher, M.A., Malod, J., Rehault, J.P., Contrucci, I., Klingelhoefer, F., Mendes-Victor, L. & Spakman, W. 2002. Evidence for active subduction beneath Gibraltar. *Geology*, **30**, 1071–1074.

Jousselin, D., Nicolas, A. & Boudier, F. 1998. Detailed mapping of a mantle diapir below a paleo-spreading center in the Oman ophiolite. *Journal of Geophysical Research—Solid Earth*, **103**, 18153–18170.

Lenoir, X., Garrido, C.J., Bodinier, J.L., Dautria, J.M. & Gervilla, F. 2001. The recrystallization front of the Ronda peridotite: evidence for melting and thermal erosion of subcontinental lithospheric mantle beneath the Alboran basin. *Journal of Petrology*, **42**, 141–158.

Lonergan, L. 1993. Timing and kinematics of deformation in the Malaguide Complex, internal zone of the Betic Cordillera, southeast Spain. *Tectonics*, **12**, 460–476.

Lonergan, L. & White, N. 1997. Origin of the Betic–Rif mountain belt. *Tectonics*, **16**, 504–522.

López Sánchez-Vizcaíno, V., Rubatto, D., Gómezpugnaire, M.T., Trommsdorff, V. & Müntener, O. 2001. Middle Miocene high-pressure metamorphism and fast exhumation of the Nevado–Filábride Complex, SE Spain. *Terra Nova*, **13**, 327–332.

Marchesi, C., Griffin, W.L., Garrido, C.J., Bodinier, J.-L. & Pearson, N.J. 2010. Persistence of mantle lithospheric Re–Os signature during asthenospherization of the subcontinental lithospheric mantle: insights from *in situ* isotopic analysis of sulfides from the Ronda peridotite (Southern Spain). *Contributions to Mineralogy and Petrology*, **159**, 315–330.

Marchesi, C., Garrido, C.J., Bosch, D., Bodinier, J.L., Hidas, K., Padrón-Navarta, J.A. & Gervilla, F. 2012. A Late Oligocene suprasubduction setting in the westernmost Mediterranean revealed by intrusive pyroxenite dykes in the Ronda Peridotite (southern Spain). *Journal of Geology*, **120**, 237–247.

Mazzoli, S. & Martín Algarra, A. 2011. Deformation partitioning during transpressional emplacement of a 'mantle extrusion wedge': the Ronda peridotites, western Betic Cordillera, Spain. *Journal of the Geological Society, London*, **168**, 373–382.

Nicolas, A. & Boudier, F. 1975. Kinematic interpretation of folds in Alpine-type peridotites. *Tectonophysics*, **25**, 233–260.

Nicolas, A. & Boudier, F. 1995. Mapping oceanic ridge segments, Oman ophiolite. *Journal of Geophysical Research—Solid Earth*, **100**, 6179–6197.

Obata, M. 1980. The Ronda peridotite—garnet-lherzolite, spinel-lherzolite, and plagioclase-lherzolite facies and the *P–T* trajectories of a high temperature mantle intrusion. *Journal of Petrology*, **21**, 533–572.

Pearson, D.G. & Nowell, G.M. 2004. Re-Os and Lu-Hf isotope constraints on the origin and age of pyroxenites from the Beni Bousera Peridotite Massif: implications for mixed peridotite-pyroxenite mantle sources. *Journal of Petrology*, **45**, 439–455.

Platt, J.P. & Vissers, R.L.M. 1989. Extensional collapse of thickened continental lithosphere: a working hypothesis for the Alboran Sea and Gibraltar arc. *Geology*, **17**, 540–543.

Platt, J.P., Whitehouse, M.J., Kelley, S.P., Carter, A. & Hollick, L. 2003. Simultaneous extensional exhumation across the Alboran Basin: implications for the causes of late orogenic extension. *Geology*, **31**, 251–254.

Platt, J.P., Kelley, S.P., Carter, A. & Orozco, M. 2005. Timing of tectonic events in the Alpujárride Complex, Betic Cordillera, southern Spain. *Journal of the Geological Society, London*, **162**, 451–462.

Platt, J.P., Anczkiewicz, R., Soto, J.-I., Kelley, S.P. & Thirlwall, M. 2006. Early Miocene continental subduction and rapid exhumation in the western Mediterranean. *Geology*, **34**, 981–984.

Precigout, J., Gueydan, F., Gapais, D., Garrido, C.J. & Essaifi, A. 2007. Strain localisation in the subcontinental mantle—a ductile alternative to the brittle mantle. *Tectonophysics*, **445**, 318–336.

Priem, H.N.A., Boelrijk, N.A.I.M., Hebeda, E.H., Oen, I.S., Verdurmen, E.A.T. & Verschure, R.H. 1979. Isotopic dating of the emplacement of the ultramafic masses in the Serrania de Ronda, Southern Spain. *Contributions to Mineralogy and Petrology*, **70**, 103–109.

Rosenbaum, G., Lister, G.S. & Duboz, C. 2002. Relative motions of Africa, Iberia and Europe during Alpine orogeny. *Tectonophysics*, **359**, 117–129.

Royden, L.H. 1993. Evolution of retreating subduction boundaries formed during continental collision. *Tectonics*, **12**, 629–638.

Sánchez-Gómez, M., Balanyá, J.C., García-Dueñas, V. & Azañón, J.M. 2002. Intracrustal tectonic evolution of large lithosphere mantle slabs in the western end of the Mediterranean orogen (Gibraltar arc). *Journal of the Virtual Explorer*, **8**, 23–34.

Sánchez-Rodríguez, L. & Gebauer, D. 2000. Mesozoic formation of pyroxenites and gabbros in the Ronda area (southern Spain), followed by Early Miocene subduction metamorphism and emplacement into the middle crust: U–Pb sensitive high-resolution ion microprobe dating of zircon. *Tectonophysics*, **316**, 19–44.

Seber, D., Barazangi, M., Tadili, B.A., Ramdani, M., Ibenbrahim, A. & BenSari, D. 1996. Three-dimensional upper mantle structure beneath the intraplate Atlas and interplate Rif mountains of Morocco. *Journal of Geophysical Research—Solid Earth*, **101**, 3125–3138.

Soustelle, V., Tommasi, A., Bodinier, J.L., Garrido, C.J. & Vauchez, A. 2009. Deformation and reactive melt transport in the mantle lithosphere above a large-scale partial melting domain: the Ronda Peridotite Massif, southern Spain. *Journal of Petrology*, **50**, 1235–1266.

Spakman, W. & Wortel, R. 2004. A tomographic view on western Mediterranean geodynamics. *In*: Cavazza, W., Roure, F., Spakman, W., Stampfli, G.M. & Ziegler, P.A. (eds) *The TRANSMED Atlas—the Mediterranean Region from Crust to Mantle*. Springer, Berlin, 31–52.

Tubía, J.M. 1994. The Ronda Peridotites (Los Reales nappe)—an example of the relationship between lithospheric thickening by oblique tectonics and late extensional deformation within the Betic Cordillera (Spain). *Tectonophysics*, **238**, 381–398.

Tubía, J.M. & Cuevas, J. 1986. High-temperature emplacement of the Los Reales peridotite nappe (Betic Cordillera, Spain). *Journal of Structural Geology*, **8**, 473–&.

Tubía, J.M., Cuevas, J. & Esteban, J.J. 2004. Tectonic evidence in the Ronda peridotites, Spain, for mantle diapirism related to delamination. *Geology*, **32**, 941–944.

Van der Wal, D. & Bodinier, J.L. 1996. Origin of the recrystallisation front in the Ronda peridotite by km-scale pervasive porous melt flow. *Contributions to Mineralogy and Petrology*, **122**, 387–405.

Van der Wal, D. & Vissers, R.L.M. 1996. Structural petrology of the Ronda peridotite, SW Spain: deformation history. *Journal of Petrology*, **37**, 23–43.

Vauchez, A. & Garrido, C.J. 2001. Seismic properties of an asthenospherized lithospheric mantle: constraints from lattice preferred orientations in peridotite from the Ronda massif. *Earth and Planetary Science Letters*, **192**, 235–249.

Villasante-Marcos, V., Osete, M.L., Gervilla, F. & García-Dueñas, V. 2003. Palaeomagnetic study of the Ronda peridotites (Betic Cordillera, southern Spain). *Tectonophysics*, **377**, 119–141.

Wortel, M.J.R. & Spakman, W. 2000. Subduction and slab detachment in the Mediterranean–Carpathian region. *Science*, **290**, 1910–1917.

Zeck, H.P. 1997. Mantle peridotites outlining the Gibraltar Arc—centrifugal extensional allochthons derived from the earlier Alpine, westward subducted nappe pile. *Tectonophysics*, **281**, 195–207.

Received 5 December 2011; revised typescript accepted 12 July 2012.
Scientific editing by Erdin Bozkurt.